

لجنة الميكانيك  
تقدم لكم..

# [المكتبة التخصصية]



<http://www.Mech.MuslimEngineer.Net>



[FB.com/Groups/Mid.Group](https://www.facebook.com/Groups/Mid.Group)



0789434018



MechFet

# Fundamentals of Machine Elements

SI Version

Third Edition



Steven R. Schmid  
Bernard J. Hamrock  
Bo O. Jacobson



Fundamentals of

# Machine Elements

SI Version  
Third Edition

This page intentionally left blank



Fundamentals of

# Machine Elements

SI Version

Third Edition

Steven R. Schmid  
Bernard J. Hamrock  
Bo O. Jacobson



CRC Press  
Taylor & Francis Group  
Boca Raton London New York

CRC Press is an imprint of the  
Taylor & Francis Group, an **informa** business

CRC Press  
Taylor & Francis Group  
6000 Broken Sound Parkway NW, Suite 300  
Boca Raton, FL 33487-2742

© 2014 by Taylor & Francis Group, LLC  
CRC Press is an imprint of Taylor & Francis Group, an Informa business

No claim to original U.S. Government works  
Version Date: 20140501

International Standard Book Number-13: 978-1-4822-4750-3 (eBook - PDF)

This book contains information obtained from authentic and highly regarded sources. Reasonable efforts have been made to publish reliable data and information, but the author and publisher cannot assume responsibility for the validity of all materials or the consequences of their use. The authors and publishers have attempted to trace the copyright holders of all material reproduced in this publication and apologize to copyright holders if permission to publish in this form has not been obtained. If any copyright material has not been acknowledged please write and let us know so we may rectify in any future reprint.

Except as permitted under U.S. Copyright Law, no part of this book may be reprinted, reproduced, transmitted, or utilized in any form by any electronic, mechanical, or other means, now known or hereafter invented, including photocopying, microfilming, and recording, or in any information storage or retrieval system, without written permission from the publishers.

For permission to photocopy or use material electronically from this work, please access [www.copyright.com](http://www.copyright.com) (<http://www.copyright.com/>) or contact the Copyright Clearance Center, Inc. (CCC), 222 Rosewood Drive, Danvers, MA 01923, 978-750-8400. CCC is a not-for-profit organization that provides licenses and registration for a variety of users. For organizations that have been granted a photocopy license by the CCC, a separate system of payment has been arranged.

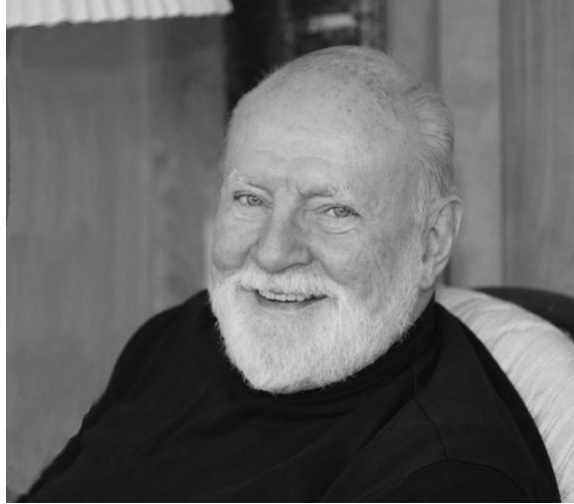
**Trademark Notice:** Product or corporate names may be trademarks or registered trademarks, and are used only for identification and explanation without intent to infringe.

Visit the Taylor & Francis Web site at  
<http://www.taylorandfrancis.com>

and the CRC Press Web site at  
<http://www.crcpress.com>



## Dedication



This book is dedicated to Professor Bernard J. Hamrock, a great friend and mentor. Those who have had the pleasure of knowing him understand that his is a rare intellect: a world-class researcher who fundamentally changed machine design with his contributions to contact mechanics and lubrication theory; a gifted instructor and research advisor; a prolific author of exceptional papers and books; and a valuable colleague to all who have come to know him.

Professor Hamrock's professional accomplishments are exceeded only by his personal ones: A beloved husband, his love for his wife, Rosemary, is unwavering, as is his dedication as a father and grandfather; friendly to all, and a trusted friend when needed. He is by no means the stereotypical bookish professor. A football athlete in his youth, he maintains a love of the Buckeyes, of his world travels and his wine sommeliering. Those who know Bernie are grateful for the experience.

Steven R. Schmid  
Notre Dame, Indiana

This page intentionally left blank





# Contents

## Part I — Fundamentals

### 1. Introduction

- 1.1 What is Design? 4
- 1.2 Design of Mechanical Systems 4
- 1.3 Design as a Multidisciplinary Endeavor 5
- 1.4 Design of Machine Elements 6
- 1.5 Computers in Design 12
- 1.6 Catalogs and Vendors 13
- 1.7 Units 13
- 1.8 Unit Checks 14
- 1.9 Significant Figures 15
- 1.10 Summary 16

### 2. Load, Stress, and Strain

- 2.1 Introduction 22
- 2.2 Critical Section 22
- 2.3 Load Classification and Sign Convention 23
- 2.4 Support Reactions 24
- 2.5 Static Equilibrium 24
- 2.6 Free-Body Diagram 26
- 2.7 Supported Beams 27
- 2.8 Shear and Moment Diagrams 27
- 2.9 Stress 34
- 2.10 Stress Element 34
- 2.11 Stress Tensor 35
- 2.12 Plane Stress 35
- 2.13 Mohr's Circle 37
- 2.14 Three-Dimensional Stresses 39
- 2.15 Octahedral Stresses 40
- 2.16 Strain 41
- 2.17 Strain Tensor 42
- 2.18 Plane Strain 42
- 2.19 Summary 44

### 3. Introduction to Materials and Manufacturing

- 3.1 Introduction 54
- 3.2 Ductile and Brittle Materials 54
- 3.3 Classification of Solid Materials 55
- 3.4 Stress-Strain Diagrams 58
- 3.5 Properties of Solid Materials 60
- 3.6 Stress-Strain Relationships 67
- 3.7 Two-Parameter Materials Charts 68
- 3.8 Effects of Manufacturing 74
- 3.9 Summary 83

### 4. Stresses and Strains

- 4.1 Introduction 90
- 4.2 Properties of Beam Cross Sections 90
- 4.3 Normal Stress and Strain 94
- 4.4 Torsion 98
- 4.5 Bending Stress and Strain 99
- 4.6 Transverse Shear Stress and Strain 104
- 4.7 Summary 109

### 5. Deformation

- 5.1 Introduction 116
- 5.2 Moment-Curvature Relation 116
- 5.3 Singularity Functions 117
- 5.4 Method of Superposition 120
- 5.5 Strain Energy 120
- 5.6 Castigliano's Theorem 123
- 5.7 Summary 126

## 6. Failure Prediction for Static Loading

- 6.1 Introduction 134
- 6.2 Stress Concentration 134
- 6.3 Fracture Mechanics 140
- 6.4 Modes of Crack Growth 141
- 6.5 Fracture Toughness 141
- 6.6 Failure Prediction for Uniaxial Stress State 143
- 6.7 Failure Prediction for Multiaxial Stress State 144
- 6.8 Summary 152

## 7. Fatigue and Impact

- 7.1 Introduction 160
- 7.2 Fatigue 160
- 7.3 Cyclic Stresses 162
- 7.4 Strain Life Theory of Fatigue 162
- 7.5 Fatigue Strength 163
- 7.6 Fatigue Regimes 168
- 7.7 Stress Concentration Effects 169
- 7.8 The Modified Endurance Limit 171
- 7.9 Cumulative Damage 175
- 7.10 Influence of Nonzero Mean Stress 176
- 7.11 Influence of Multi-Axial Stress States 180
- 7.12 Fracture Mechanics Approach to Fatigue 182
- 7.13 Linear Impact Stresses and Deformations 183
- 7.14 Summary 186

## 8. Lubrication, Friction, and Wear

- 8.1 Introduction 196
- 8.2 Surface Parameters 196
- 8.3 Conformal and Nonconformal Surfaces 197
- 8.4 Hertzian Contact 198
- 8.5 Bearing Materials 203
- 8.6 Lubricant Rheology 205
- 8.7 Regimes of Lubrication 211
- 8.8 Friction 214
- 8.9 Wear 216
- 8.10 Summary 220

## Part II — Machine Elements

### 9. Columns

- 9.1 Introduction 228
- 9.2 Equilibrium Regimes 228
- 9.3 Concentrically Loaded Columns 229
- 9.4 End Conditions 231
- 9.5 Euler's Buckling Criterion 232
- 9.6 Johnson's Buckling Criterion 232
- 9.7 AISC Criteria 234
- 9.8 Eccentrically Loaded Columns 234
- 9.9 Summary 238

### 10. Stresses and Deformations in Cylinders

- 10.1 Introduction 244
- 10.2 Tolerances and Fits 244
- 10.3 Pressurization Effects 245
- 10.4 Rotational Effects 250
- 10.5 Press Fits 252
- 10.6 Shrink Fits 254
- 10.7 Summary 256



## 11. Shafting and Associated Parts

- 11.1 Introduction 264
- 11.2 Design of Shafts for Static Loading 264
- 11.3 Fatigue Design of Shafts 267
- 11.4 Additional Shaft Design Considerations 271
- 11.5 Critical Speed of Rotating Shafts 272
- 11.6 Keys, Roll Pins, Splines and Set Screws 275
- 11.7 Retaining Rings and Pins 278
- 11.8 Flywheels 279
- 11.9 Couplings 285
- 11.10 Summary 288

## 12. Hydrodynamic and Hydrostatic Bearings

- 12.1 Introduction 298
- 12.2 The Reynolds Equation 299
- 12.3 Thrust Slider Bearings 303
- 12.4 Journal Slider Bearings 314
- 12.5 Squeeze Film Bearings 321
- 12.6 Hydrostatic Bearings 322
- 12.7 Summary 327

## 13. Rolling-Element Bearings

- 13.1 Introduction 337
- 13.2 Historical Overview 337
- 13.3 Bearing Types and Selection 338
- 13.4 Geometry 341
- 13.5 Kinematics 346
- 13.6 Separators 348
- 13.7 Static Load Distribution 349
- 13.8 Elastohydrodynamic Lubrication 359
- 13.9 Fatigue Life 361
- 13.10 Variable Loading 367
- 13.11 Summary 369

## 14. General Gear Theory; Spur Gears

- 14.1 Introduction 380
- 14.2 Types of Gears 380
- 14.3 Gear Geometry 381
- 14.4 Gear Ratio 386
- 14.5 Contact Ratio and Gear Velocity 387
- 14.6 Tooth Thickness and Backlash 389
- 14.7 Gear Trains 390
- 14.8 Gear Manufacture and Quality 392
- 14.9 Gear Materials 395
- 14.10 Loads Acting on a Gear Tooth 400
- 14.11 Bending Stresses in Gear Teeth 400
- 14.12 Contact Stresses in Gear Teeth 406
- 14.13 Elastohydrodynamic Film Thickness 407
- 14.14 Gear Design Synthesis 409
- 14.15 Summary 412

## 15. Helical, Bevel, and Worm Gears

- 15.1 Introduction 422
- 15.2 Helical Gears 422
- 15.3 Bevel Gears 427
- 15.4 Worm Gears 436
- 15.5 Summary 442

## **16. Fasteners, Connections, and Power Screws**

- 16.1 Introduction 448
- 16.2 Thread Terminology, Classification, and Designation 448
- 16.3 Power Screws 450
- 16.4 Threaded Fasteners 454
- 16.5 Riveted Fasteners 464
- 16.6 Welded, Brazed, and Soldered Joints 467
- 16.7 Adhesive Bonding 474
- 16.8 Integrated Snap Fasteners 476
- 16.9 Summary 479

## **17. Springs**

- 17.1 Introduction 492
- 17.2 Spring Materials 492
- 17.3 Helical Compression Springs 495
- 17.4 Helical Extension Springs 502
- 17.5 Helical Torsion Springs 504
- 17.6 Leaf Springs 506
- 17.7 Gas Springs 508
- 17.8 Belleville Springs 509
- 17.9 Wave Springs 509
- 17.10 Summary 512

## **18. Brakes and Clutches**

- 18.1 Introduction 520
- 18.2 Thermal Considerations 520
- 18.3 Thrust Pad Clutches and Brakes 522
- 18.4 Cone Clutches and Brakes 525
- 18.5 Block or Short-Shoe Brakes 526
- 18.6 Long-Shoe, Internal, Expanding Rim Brakes 528
- 18.7 Long-Shoe, External, Contracting Rim Brakes 532
- 18.8 Symmetrically Loaded Pivot-Shoe Brakes 533
- 18.9 Band Brakes 535
- 18.10 Slip Clutches 536
- 18.11 Summary 538

## **19. Flexible Machine Elements**

- 19.1 Introduction 548
- 19.2 Flat Belts 548
- 19.3 Synchronous Belts 551
- 19.4 V-Belts 551
- 19.5 Wire Ropes 555
- 19.6 Rolling Chains 559
- 19.7 Summary 566

## **Appendix A: Physical and Mechanical Properties of Materials 573**

## **Appendix B: Stress-Strain Relationships 583**

## **Appendix C: Stress Intensity Factors for Some Common Crack Geometries 591**

## **Appendix D: Shear, Moment, and Deflection of Selected Beams 597**

## **Appendix E: Dimensions of Threaded Fasteners 601**

## **Index 605**

## Preface

The nature of the engineering profession is changing. It was once commonplace that students had significant machinery exposure before studying mechanical engineering, and it always was assumed that students would receive practical experience in internships or some form of co-operative employment during their college years, if not sooner. Students were historically drawn from much less diverse groups than today; students from a few decades ago (such as the authors) naturally gained experience with machinery from working on their car or tractor, and this experience was especially helpful for courses in design of machine elements. The demographics have changed, permanently and irrevocably, and the characteristics of incoming students have also changed. This has been exacerbated by the advances in technology that make maintenance of most machinery a discipline for only the specially trained. However, with a broad perspective, it has become clear that the demographics change has been an extremely positive development for the profession.

Design presents a number of challenges and opportunities to instructors. As a topic of study it is exciting because of its breadth and unending ability to provide fascinating opportunities for research, analysis, and creativity. Literally every discipline and sub-discipline in engineering has strong ties to design, and most universities have used design and manufacturing as the basis of a capstone course that culminates a mechanical engineering bachelor's degree. To students of engineering, it is, at first, an intimidating field so enormous that any semester or academic year sequence in machine design can do nothing but scratch the surface of the subject. This perception is absolutely true; like so many other areas of specialization within engineering, design truly is an area where lifelong learning is necessary.

Machine design is a challenge to both instructors and students. There are a number of courses, such as statics, dynamics, solid and fluid mechanics, etc., where topics for study are broken down into small portions and where closed-form, quantitative problems are routinely solved by students and by faculty during lectures. Such problems are important for learning concepts, and they give students a sense of security in that absolute answers can be determined. Too often, machine design is presented in a similar fashion. While, in practice, such closed-form solutions do exist, they are relatively rare. Usually, multiple disciplines are blended, and the information available is insufficient to truly optimize a desired outcome. In practice, engineers need to apply good judgment after they have researched a problem as best they can, given budgetary and time restrictions. They must then state or decide upon a solution, if not an answer. These difficult open-ended problems are much more demanding than closed-form solutions, and require a different mindset. Instead of considering a number as valid or invalid (usually by checking against the answer provided in the book or by the instructor), an open-ended problem can be evaluated only with respect to whether the result is reasonable and if good scientific methods were used. As experimental philosophers, design engineers should not hesitate proving their designs with prototypes or demonstrations. Of course, many students are taught that three weeks of modeling can save a day in the laboratory. (Sadly, this statement is not always recognized as ironic.)

This book is intended to provide the undergraduate student with a clear and thorough understanding of both the theory and application of the fundamentals of machine elements. It is expected that this book will also be used as a

reference by practicing engineers. The book is not directed toward lower level undergraduate students — familiarity with differential and integral calculus is often needed to comprehend the material presented. The design of machine elements involves a great deal of geometry as well. Therefore, the ability to sketch the various configurations that arise, as well as to draw a free-body diagram of the loads acting on a component, are also needed. The material covered in this text is appropriate as a third- or fourth-year engineering course for students who have studied basic engineering sciences, including physics, engineering mechanics, and materials and manufacturing processes.

The book is divided into two parts. Part I (Chapters 1 to 8) presents the fundamentals, and Part II (Chapters 9 to 19) uses the fundamentals in considering the design of various machine elements. The material in Part I is sequential; material presented in early chapters is needed in subsequent chapters. This building-block approach provides the foundation necessary to design the various machine elements considered in Part II.

## Learning Tools

The following pedagogical devices are used in each chapter to improve understanding and motivate the student:

- Each chapter will open with a photograph that clearly depicts the machine elements or topics covered in the chapter. Chapters will also have an opening quotation that is related to the chapter; the goal is to pique the reader's interest in the subject matter and start each chapter with a positive and entertaining feature to draw the students into the topic.
- In the margin to the side of the illustration, the contents, examples, case studies, and design procedures present in the chapter are listed.
- After the illustration, each chapter has a brief abstract that indicates the contents at a very high level. Part of this abstract will include a list of machine elements covered in the chapter, the typical applications of the machine elements in the chapter, and the alternate machine elements that can be considered by designers.
- A list of symbols and subscripts is then presented to help students with nomenclature as they read the chapter.
- Figures and tables have been redrawn in this edition to use modern graphical procedures of three-dimensional sketches, thick boundary lines, and sans-serif fonts in illustrations.
- Examples are printed with a light gray background to differentiate them from the text. Examples demonstrate the mathematical procedures covered and are useful for students performing quantitative problems.
- Design procedures are printed with a light color background to differentiate them from the text and examples. The design procedures are useful guides to common design problems and aide students with all levels of Bloom's taxonomy of learning.

- Case studies are printed with a light color background and are placed just before the chapter-ending summary. Case studies are mostly qualitative descriptions of important modern applications of the chapter's machine elements, but at a depth that requires an understanding of the chapter material. Case studies are intended to reference the chapter's subject matter and place it in the proper design framework so that students have no doubt that the chapter is relevant and important.
- After the summary, the chapter has a list of key words that the student can use for study or to help with jargon when necessary.
- A summary of equations is contained after the key words, and is intended to help students as they work on chapter-ending problems. The summary of equations is also a useful handout for instructors to copy and give to the students for exams.
- Every chapter includes lists of recommended readings consisting of modern as well as classic books and other resources that are especially timeless and relevant.
- The styles of the chapter-ending problems have been designed to cover every stage in modern learning taxonomies. Chapter-ending problems are organized as:
  1. Questions. These address the "remembering" task of learning taxonomies.
  2. Qualitative Problems. These are carefully designed to take an understanding of machine elements gleaned from the book and lecture and applying them to a new situation.
  3. Quantitative Problems. These problems focus on numerical analysis, with some extension to evaluating designs and results. Historically, machine element texts have provided only such analysis problems. Answers to the majority of quantitative problems are given. Solutions to the homework problems can be found in the Instructor's Solutions Manual, available to instructors who adopt the text. In addition, most problems have worksheets, where a partial solution is provided.
  4. Synthesis, Design, and Projects. These are open-ended, often team-based exercises that require creation of new designs or principles and that go beyond normal analysis problems.

Engineering educators will recognize that the end-of-chapter problems are designed to accommodate taxonomies of learning, allowing students of all backgrounds to develop an understanding, familiarity, and mastery of the subject matter.

The qualitative problems and synthesis, design, and projects class of problems also promote a useful method of active learning. In addition to conventional lecture format classes, an instructor can incorporate these problems in "seminar" sessions, active learning, or else for group projects. The authors have found this approach to be very useful and appreciated by students.

Certain users will recognize a consistent approach and pedagogy as the textbook *Manufacturing Engineering and Technology*, and will find that the texts complement each other. This is by intent, and it is hoped that the engineering student will realize quickly that *to do manufacturing or design, one needs to know both*.

## Web Site

A web site containing other book-related resources can be found at [www.crcpress.com/product/isbn/9781482247480](http://www.crcpress.com/product/isbn/9781482247480). The web site provides reported errata, web links to related sites of interest, password-protected solutions to homework problems for instructors, a bulletin board, and information about ordering books and supplements. The web site also contains presentation files for instructors and students, using full-color graphics whenever possible.

## Contents

Chapter 1 introduces machine design and machine elements and covers a number of topics, such as safety factors, statistics, units, unit checks, and significant figures. In designing a machine element it is important to evaluate the kinematics, loads, and stresses at the critical section. Chapter 2 describes the applied loads (normal, torsional, bending, and transverse shear) acting on a machine element with respect to time, the area over which the load is applied, and the location and method of application. The importance of support reaction, application of static force and moment equilibrium, and proper use of free-body diagrams is highlighted. Shear and moment diagrams applied to beams for various types of singularity function are also considered. Chapter 2 then describes stress and strain separately.

Chapter 3 focuses on the properties of solid engineering materials, such as the modulus of elasticity. (Appendix A gives properties of ferrous and nonferrous metals, ceramics, polymers, and natural rubbers. Appendix B explores the stress-strain relationships for uniaxial, biaxial, and triaxial stress states.) Chapter 4 describes the stresses and strains that result from the types of load described in Chapter 2, while making use of the general Hooke's law relationship developed in Appendix B. Chapter 4 also considers straight and curved members under these four types of load.

Certainly, ensuring that the design stress is less than the yield stress for ductile materials and less than the ultimate stress for brittle materials is important for a safe design. However, attention must also be paid to displacement (deformation) since a machine element can fail by excessive elastic deformation. Chapter 5 attempts to quantify the deformation that might occur in a variety of machine elements. Some approaches investigated are the integral method, the singularity function, the method of superposition, and Castigliano's theorem. These methods are applicable for distributed loads.

Stress raisers, stress concentrations, and stress concentration factors are investigated in Chapter 6. An important cause of machine element failure is cracks within the microstructure. Therefore, Chapter 6 covers stress levels, crack-producing flaws, and crack propagation mechanisms and also presents failure prediction theories for both uniaxial and multiaxial stress states. The loading throughout Chapter 6 is assumed to be static (i.e., load is gradually applied and equilibrium is reached in a relatively short time). However, most machine element failures involve loading conditions that fluctuate with time. Fluctuating loads induce fluctuating stresses that often result in failure by means of cumulative damage. These topics, along with impact loading, are considered in Chapter 7.

Chapter 8 covers lubrication, friction, and wear. Not only must the design stress be less than the allowable stress and the deformation not exceed some maximum value, but also lubrication, friction, and wear (tribological considerations) must be properly understood for machine elements to be successfully designed. Stresses and deformations for con-



centrated loads, such as those that occur in rolling-element bearings and gears, are also determined in Chapter 8. Simple expressions are developed for the deformation at the center of the contact as well as for the maximum stress. Chapter 8 also describes the properties of fluid film lubricants used in a number of machine elements. Viscosity is an important parameter for establishing the load-carrying capacity and performance of fluid-film lubricated machine elements. Fluid viscosity is greatly affected by temperature, pressure, and shear rate. Chapter 8 considers not only lubricant viscosity, but also pour point and oxidation stability, greases and gases, and oils.

Part II (Chapters 9 to 20) relates the fundamentals to various machine elements. Chapter 9 deals with columns, which receive special consideration because yielding and excessive deformation do not accurately predict the failure of long columns. Because of their shape (length much larger than radius) columns tend to deform laterally upon loading, and if deflection becomes critical, they fail catastrophically. Chapter 9 establishes failure criteria for concentrically and eccentrically loaded columns.

Chapter 10 considers cylinders, which are used in many engineering applications. The chapter covers tolerancing of cylinders; stresses and deformations of thin-walled, thick-walled, internally pressurized, externally pressurized, and rotating cylinders; and press and shrink fits.

Chapter 11 considers shafting and associated parts, such as keys, snap rings, flywheels, and couplings. A shaft design procedure is applied to static and cyclic loading; thus, the material presented in Chapters 6 and 7 is directly applied to shafting. Chapter 11 also considers critical speeds of rotating shafts.

Chapter 12 presents the design of hydrodynamic bearings — both thrust and journal configurations — as well as design procedures for the two most commonly used slider bearings. The procedures provide an optimum pad configuration and describe performance parameters, such as normal applied load, coefficient of friction, power loss, and lubricant flow through the bearing. Similar design information is given for plain and nonplain journal bearings. The chapter also considers squeeze film and hydrostatic bearings, which use different pressure-generating mechanisms.

Rolling-element bearings are presented in Chapter 13. Statically loaded radial, thrust, and preloaded bearings are considered, as well as loaded and lubricated rolling-element bearings, fatigue life, and dynamic analysis. The use of the elastohydrodynamic lubrication film thickness is integrated with the rolling-element bearing ideas developed in this chapter.

Chapter 14 covers general gear theory and the design of spur gears. Stress failures are also considered. The transmitted load is used to establish the design bending stress in a gear tooth, which is then compared with an allowable stress to establish whether failure will occur. Chapter 14 also considers fatigue failures. The Hertzian contact stress with modification factors is used to establish the design stress, which is then compared with an allowable stress to determine whether fatigue failure will occur. If an adequate protective elastohydrodynamic lubrication film exists, gear life is greatly extended.

Chapter 15 extends the discussion of gears beyond spur gears as addressed in Chapter 14 to include helical, bevel, and worm gears. Advantages and disadvantages of the various types of gears are presented.

Chapter 16 covers threaded, riveted, welded, and adhesive joining of members, as well as power screws. Riveted and threaded fasteners in shear are treated alike in design and failure analysis. Four failure modes are presented:

bending of member, shear of rivet, tensile failure of member, and compressive bearing failure. Fillet welds are highlighted, since they are the most frequently used type of weld. A brief stress analysis for lap and scarf adhesively bonded joints is also given.

Chapter 17 treats the design of springs, especially helical compression springs. Because spring loading is most often continuously fluctuating, Chapter 16 considers the design allowance that must be made for fatigue and stress concentration. Helical extension springs are also covered in Chapter 16. The chapter ends with a discussion of torsional and leaf springs.

Brakes and clutches are covered in Chapter 18. The brake analysis focuses on the actuating force, the torque transmitted, and the reaction forces in the hinge pin. Two theories relating to clutches are studied: the uniform pressure model and the uniform wear model.

Chapter 19 deals with flexible machine elements. Flat belts and V-belts, ropes, and chains are covered. Methods of effectively transferring power from one shaft to another while using belts, ropes, and chains are also presented. Failure modes of these flexible machine elements are considered.

## What's New in This Edition

This third edition represents a major revision from the second edition. In addition to the pedagogy enhancements mentioned above, the contents have been greatly expanded and organized to aid students of all levels in design synthesis and analysis approaches. Design synthesis is generally taught or expected of students only after a machine elements course in most college curricula. This book attempts to provide guidance through design procedures for synthesis issues, but it also exposes the reader to a wide variety of machine elements.

Users of the second edition will immediately recognize that this third edition has been completely re-typeset using a space-saving, two-column approach, and all figures redrawn to match the new column widths. The space-saving typesetting format has saved over 300 pages from the previous edition, while the content has been expanded considerably. This was, in fact, a goal: too many textbooks are difficult to use because they give the impression of completeness, but this is often illusory. Large margins and gaps between topics artificially produce heavy tomes. Our goal was to create a book with good coverage that can be more easily carried by students.

In every chapter opening box, the reader is directed toward other machine elements that can serve the same purpose, which can also help in synthesis. As an example, a student designing a gear set for power transmission between two shafts may thus be reminded that a belt drive is perhaps an alternative worthy of consideration.

The book has been designed to compliment the well-known manufacturing textbooks *Manufacturing Processes for Engineering Materials* and *Manufacturing Engineering and Technology* by Kalpakjian and Schmid. Students who use both texts in their engineering studies will recognize similarities in organization, graphical styles, and, it is hoped, clarity.

The classes of chapter-ending problems have been introduced above, but they have been carefully designed to aid students to develop a deep understanding of each chapter's subject matter. They have been developed using learning taxonomies that require ever-sophisticated cognitive effort. That is, students are required to remember (Questions), apply knowledge to fairly simple and straightforward questions (Qualitative Problems), extend the knowledge to ana-

lytical problems (Quantitative Problems), and finally asked to extend their analytical abilities to open-ended and synthesis problems requiring creativity in their solution (Synthesis and Design Problems).

A major effort has been made to expand coverage in all areas. Specific changes to this edition include:

- In Chapter 1, additional design considerations have been listed in Section 1.4, additional examples and case studies have been added, and life cycle engineering has been included.
- Chapter 3 now includes a description of hardness and common hardness tests used for metals; this clarifies the use of these concepts in gear design. In addition, the manufacturing discussion has been expanded.
- The use of retaining rings in Chapter 11 necessitated the inclusion of flat groove stress concentration factors in Chapter 6.
- Chapter 7, on fatigue design, has been significantly expanded. The staircase method for determining endurance limits has been added in Design Procedure 7.2, the fatigue strength concentration factor descriptions are longer with more mathematical models, and Haigh diagrams are included to show the effects of mean stress. Additional material data has been included for the fracture mechanics approaches to fatigue design.
- In Chapter 8, a streamlined discussion of typical surface finishes in machine elements, and manufacturing processes used to produce them, has been prepared. In addition, a discussion of the commonly used bearing materials has been added.
- Chapter 11 has been expanded considerably. In addition to an expanded discussion of keys and set screws, the chapter presents new treatment of spline, pin, and retaining ring design, and has a new section on the design of shaft couplings.
- Hydrodynamic bearings are increasingly important because of their widespread use in transportation and power industries; while the discussion of thrust and journal bearings has been retained, the analysis is simplified and more straightforward. The discussion of squeeze film and hydrostatic bearings has been expanded.
- Chapter 13 has been extensively rewritten to reflect the latest International Standards Organization standards that unify the approach used to design rolling element bearings. This has allowed a simplification of bearing selection and analysis, as will be readily apparent. Further, this remains the only machine element book that accurately depicts the wide variety of bearings available. This treatment now includes the topic of toroidal bearings, a novel design that is now widely available, and leads to compact and high load carrying designs. Life adjustment factors and effects of variable loading have been expanded, and an industrially relevant case study on windmill bearings has been exhaustively researched and included in the chapter.
- The treatment of spur gear design in Chapter 14 has been modified to reflect the latest advances in materials, including powder metal materials that have become extremely popular for automotive applications. The importance of lubrication in gears has been emphasized.

Further, a design synthesis approach for spur gear design has been included in Section 14.14.

- Geometry factors for bevel gears in Chapter 15 have been simplified without loss in accuracy. Also, a design synthesis approach for worm gears has been included.
- The discussion of fasteners and welds in Chapter 16 has been expanded considerably. The importance of the heat affected zone for weld quality is discussed, and the classes of welds and their analysis methods are described. This includes the treatment of modern welding approaches such as friction stir welding as well as laser and electron beam welding.
- Gas springs and wave springs have been added to the discussion of Chapter 17.
- Chapter 18 has been reorganized, starting with fundamental principles that apply to all brake and clutch systems, especially thermal effects. Additional automotive examples have been added.
- Chapter 19 has been essentially rewritten to reflect the latest standards and manufacturer's recommendations on belt design, chains, and wire ropes. In addition, silent chains have been included into the chain discussion.
- The appendices have been expanded to provide the student with a wide variety of material properties, geometry factors for fracture analysis, and new summaries of beam deflection. While it is recognized that modern students have such information readily available via the Internet, making such material available in the textbook is useful for reference purposes.

This text has been under preparation for over four years, and required meticulous efforts at maintaining a consistent approach, careful statement of design procedures wherever they were useful, and expansion of chapter-ending problems. We hope the student of machine element design will enjoy and benefit from this text.

Steven R. Schmid  
The University of Notre Dame

Bernard J. Hamrock  
The Ohio State University

Bo O. Jacobson  
Lund University

## Acknowledgments

Many people helped to produce this textbook. Jonathan Plant, who was the editor of the first edition, was extremely supportive during the preparation of this edition. Professor Serope Kalpakjian (ret.) of the Illinois Institute of Technology made numerous comments and helpful suggestions, and also assisted in review of the manuscript. Professor William Dornfeld kindly used draft versions of this textbook in a number of semesters and made very constructive comments and suggestions. Dr. Michael Kotsalas of the Timken company was of great assistance in modernizing the chapters in bearing design. A number of faculty members from the mechanical engineering departments at Notre Dame and Ohio State University provided comments about the text. In particular, the authors would like to thank Professors John Renaud, Anthony Luscher, Si Lee, Necip Berme, and Bharat Bhushan. Special thanks are also due to Triodyne, Inc. personnel, especially Ralph L. Barnett, whose insights were invaluable. A number of resources from Triodyne were kindly made available in the preparation of the text.

Many reviewers have been associated with this project. The authors would like to acknowledge them for their time, expertise, and advice. The list of reviewers are Timothy Rodts, Michael Giordano, Matthew Prygoski, and Amy Libardi, University of Notre Dame; Miguel Angel Sellés Cantó, Escola Politècnica Superior d' Alcoi, Universitat Politècnica de València; Peder Klit, Technical University of Denmark; Robert W. Ellis, Lawrence Technological University; James Adams, Metal Powder Industries Federation; Thomas Kurfess, Georgia Institute of Technology; Paul K. Wright, University of California at Berkeley; Jian Cao, Northwestern University; K. Scott Smith, University of North Carolina at Charlotte; William G. Ovens, Rose-Hulman Institute of Technology; John D. Reid, University of Nebraska–Lincoln; Steven Y. Liang, Georgia Institute of Technology; Steven A. Velinsky, University of California–Davis; Thierry Blanchet, Rensselaer Polytechnic Institute; K.V.C. Rao, Michigan Technological University; Alexander G. Liniecki, San Jose State University; Jesa Kreiner, California State University–Fullerton; Clarence Maday, North Carolina State University; J. Darrell Gibson, Rose-Hulman Institute of Technology; Terry F. Lehnhoff, University of Missouri–Rolla; Yu Michael Wang, University of Maryland; B.K. Rao, Idaho State University; W. Brent Hall, University of Illinois–Urbana-Champaign; N. Duke Perreira, Lehigh University; Gordon Pennock, Purdue University; Richard E. Dippery, Kettering University; Anthony Luscher, Ohio State University; Michael Peterson, Colorado State University; Gary McDonald, The University of Tennessee at Chattanooga; Wayne D. Milestone, University of Wisconsin–Madison; and Dean Taylor, Cornell University.

The authors also acknowledge the use of tables and illustrations from the following publishers: American Gear Manufacturers Association, American Society of Mechanical Engineers, American Society for Testing and Materials, BHRA Fluid Engineering, Butterworths, Elsevier Science Publishing Company, Engineering Sciences Data Unit, Ltd., Heinemann (London), Hemisphere Publishing Corporation, Macmillan Publishing Company, Inc., Mechanical Technology Incorporated, Metal Powder Industries Federation, Non-Ferrous Founders Society, Oxford University Press, Inc., Penton Publishing Inc., Society of Automotive Engineers, Society of Tribologists and Lubrication Engineers, VCH Publishers, John Wiley & Sons, and Wykeham Publications (London), Ltd. The specific sources are identified in the text.

## About the Authors

**Steven R. Schmid** received his B.S. degree in Mechanical Engineering from the Illinois Institute of Technology in 1986. He then joined Triodyne, Inc., where his duties included investigation of machinery failures and consultation in machine design. He earned his Master's degree from Northwestern University in 1989 and his Ph.D. in 1993, both in mechanical engineering. In 1993 he joined the faculty at the University of Notre Dame, where he is currently a Professor of Aerospace and Mechanical Engineering and teaches and conducts research in the fields of design and manufacturing. Dr. Schmid received the American Society of Mechanical Engineers Newkirk Award and the Society of Manufacturing Engineers Parsons Award in 2000. He was also awarded the Kaneb Center Teaching Award in 2000, 2003, and 2010, and served as a Kaneb fellow in 2003. Dr. Schmid holds professional engineering (P.E.) and certified manufacturing engineer (C.Mfg.E.) licenses. He is co-author (with S. Kalpakjian) of *Manufacturing Engineering and Technology* (2014) and *Manufacturing Processes for Engineering Materials* (2008), both published by Prentice Hall. He was awarded the ASME Foundation Swanson Fellowship in 2012, and is a Fellow of the American Society of Mechanical Engineers.

**Bernard J. Hamrock** joined the staff of Ohio State University as a professor of Mechanical Engineering in 1985 and is now Professor Emeritus. Prior to joining Ohio State University he spent 18 years as a research consultant in the Tribology Branch of the NASA Lewis Research Center in Cleveland, Ohio. He received his Ph.D. and Doctor of Engineering degrees from the University of Leeds, Leeds, England. Professor Hamrock's research has resulted in a book with Duncan Dowson, *Ball Bearing Lubrication*, published in 1982 by Wiley Interscience, three separate chapters for handbooks, and over 150 archival publications. His second book, *Fundamentals of Fluid Film Lubrication* was published in 1993 by McGraw-Hill, and a second edition, with co-authors Steven Schmid and Bo Jacobson, in 2004. His awards include the 1976 Melville Medal from the American Society of Mechanical Engineers, the NASA Exceptional Achievement Medal in 1984, the 1998 Jacob Wallenberg Award given by The Royal Swedish Academy of Engineering Sciences, and the 2000 Mayo D. Hersey Award from the American Society of Mechanical Engineers.

**Bo O. Jacobson** received his Ph.D. and D.Sc. degrees from Lund University in Sweden. From 1973 until 1987 he was Professor of Machine Elements at Luleå Technology University in Sweden. In 1987 he joined SKF Engineering & Research Centre in the Netherlands, while retaining a professorship at Chalmers University from 1987 to 1991 and at Luleå Technical University from 1992 to 1997. In 1997 he was appointed Professor of Machine Elements at Lund University, Sweden. Professor Jacobson was a NRC Research Fellow at NASA Lewis Research Center from 1981 to 1982. He has published four compendia used at Swedish universities. His text *Rheology and Elastohydrodynamic Lubrication* was published by Elsevier in 1991, and his book *Rolling Contact Phenomena* (with J. Kalker) was published in 2000 by Springer. Professor Jacobson has more than 100 archival publications. His awards include the prestigious Gold Medal given by the Institution of Mechanical Engineers, England, and the Wallenberg Award in 1984.



# Part I □ Fundamentals

## Outline

Chapter 1	Introduction
Chapter 2	Load, Stress, and Strain
Chapter 3	Introduction to Materials and Manufacturing
Chapter 4	Stresses and Strains
Chapter 5	Deformation
Chapter 6	Failure Prediction for Static Loading
Chapter 7	Fatigue and Impact
Chapter 8	Lubrication, Friction, and Wear

This page intentionally left blank



# Chapter 1

## Introduction



The i8 concept car, a hybrid sports car requiring three liters per 100 km and acceleration from 0 to 100 km/hr in under five seconds.  
Source: Courtesy of BMW.

*The invention all admir'd, and each, how he  
To be th' inventor miss'd; so easy it seem'd,  
Once found, which yet unfound most would have thought  
Impossible*

John Milton

### Contents

- 1.1 What is Design? 4
- 1.2 Design of Mechanical Systems 4
- 1.3 Design as a Multidisciplinary Endeavor 5
- 1.4 Design of Machine Elements 6
- 1.5 Computers in Design 12
- 1.6 Catalogs and Vendors 13
- 1.7 Units 13
- 1.8 Unit Checks 14
- 1.9 Significant Figures 15
- 1.10 Summary 16

### Examples

- 1.1 Safety Factor of Wire Rope in an Elevator 8
- 1.2 Length of Electrical Connections in a Supercomputer 13
- 1.3 Astronomical Distances 13
- 1.4 Unit Checks 14
- 1.5 Significant Figures 15

### Design Procedures

- 1.1 The Safety Hierarchy 9
- 1.2 Procedure for Unit Checks 14

### Case Studies

- 1.1 *Mason v. Caterpillar Tractor Co.* 9
- 1.2 Sustainable Manufacturing in the Production of Nike Athletic Shoes 11
- 1.3 Loss of the Mars Climate Orbiter 14
- 1.4 Design and Manufacture of the Invisalign Orthodontic Product 15

Design is arguably the most important specialization in modern industrial society. Integral to most engineering curricula, and also making up its own specialization in many schools, design is critical for wealth generation, development of economic activity, and the creation of jobs. This chapter introduces design synthesis, where a new machine or system is produced to address a need or to satisfy customer requirements. Design analysis is also discussed, which involves the use of engineering disciplines to determine critical dimensions, select acceptable materials, and even optimize designs. To bring high-quality products to market quickly, it is important to integrate multiple disciplines early in the design process, including solid and fluid mechanics, materials selection, marketing, manufacturing, safety, and environmental concerns. Many times, constraints are applied to mechanical designs, such as those mandated by governmental codes or industrial standards. It has been observed that simultaneous higher quality and lower costs arise when manufacturing can exploit automation, but automation can only be justified for larger production runs than most products can justify. One method of achieving the benefits of large-scale manufacture is to use standard sizes and types of machine elements in design, but this requires some sophistication with respect to significant figures, measurement units, and specification of dimensions.



## Symbols

$n_s$	safety factor
$n_{sx}$	safety factor involving quality of materials, control over applied load, and accuracy of stress analysis
$n_{sy}$	safety factor involving danger to personnel and economic impact
$\sigma_{all}$	allowable normal stress, Pa
$\sigma_d$	design normal stress, Pa

## 1.1 What is Design?

Design means different things to different people. A clothing manufacturer believes that incorporating different materials or colors into a new dress constitutes design. A potter paints designs onto china to complement its surroundings. An architect designs ornamental facades for residences. An engineer chooses a bearing from a catalog and incorporates it into a speed-reducer assembly. These design activities, although they appear to be fundamentally different, share a common thread: they all require significant creativity, practice, and vision to be done well.

“Engineering,” wrote Thomas Tredgold, “is the art of directing the great sources of power in nature for the use and convenience of man” [Florman 1987]. It is indeed significant that this definition of engineering is more than 60 years old — few people now use the words “engineering” and “art” in the same sentence, let alone in a definition. However, many products are successful for nontechnical reasons, reasons that cannot be proved mathematically. On the other hand, many problems are mathematically tractable, but usually because they have been inherently overconstrained. Design problems are, almost without exception, open-ended problems combining hard science and creativity. Engineering is indeed an art, even though *parts* of engineering problems lend themselves well to analysis.

For the purposes of this textbook, **design** is the transformation of concepts and ideas into useful machinery. A **machine** is a combination of mechanisms and other components that transforms, transmits, or uses energy, load, or motion for a specific purpose. If Tredgold’s definition of engineering is accepted, design of machinery is the fundamental practice in engineering.

A machine comprises several different machine elements properly designed and arranged to work together as a whole. Fundamental decisions regarding loading, kinematics, and the choice of materials must be made during the design of a machine. Other factors, such as strength, reliability, deformation, tribology (friction, wear, and lubrication), cost, and space requirements also need to be considered. The objective is to produce a machine that not only is sufficiently rugged to function properly for a reasonable time, but also is economically feasible. Further, nonengineering decisions regarding marketability, product liability, ethics, politics, etc. must be integrated early in the design process. Since few people have the necessary tools to make all these decisions, machine design in practice is a discipline-blending human endeavor.

This textbook emphasizes one of the disciplines necessary in design — mechanical engineering. It therefore involves calculation and consideration of forces, energies, temperatures, etc., — concepts instilled into an engineer’s psyche.

To “direct the great sources of power in nature” in machine design, the engineer must recognize the functions of the various machine elements and the types of load they transmit. A **machine element** may **function** as a normal load

transmitter, a torque transmitter, an energy absorber, or a seal. Some common load transmitters are rolling-element bearings, hydrodynamic bearings, and rubbing bearings. Some torque transmitters are gears, shafts, chains, and belts. Brakes and dampers are energy absorbers. All the machine elements in Part II can be grouped into one of these classifications.

Engineers must produce safe, workable, good designs, as stated in the first fundamental canon in the *Code of Ethics for Engineers* [ASME 2012]:

Engineers shall hold paramount the safety, health, and welfare of the public in the performance of their professional duties.

Designing reasonably safe products involves many design challenges to ensure that components are large enough, strong enough, or tough enough to survive the loading environment. One subtle concept, but of huge importance, is that the engineer has a duty to protect the welfare of the general public. Welfare includes economic well-being, and it is well known that successful engineering innovations lead to wealth and job creation. However, products that are too expensive are certain to fail in a competitive marketplace. Similarly, products that do not perform their function well will fail. Economics and functionality are always pressing concerns, and good design inherently means safe, economical, and functional design.

## 1.2 Design of Mechanical Systems

A **mechanical system** is a synergistic collection of machine elements. It is synergistic because as a design it represents an idea or concept greater than the sum of the individual parts. For example, a mechanical clock, although merely a collection of gears, springs, and cams, also represents the physical realization of a time-measuring device. Mechanical system design requires considerable flexibility and creativity to obtain good solutions. Creativity seems to be aided by familiarity with known successful designs, and mechanical systems are often collections of well-designed components from a finite number of proven classes.

Designing a mechanical system is a different type of problem than selecting a component. Often, the demands of the system make evident the functional requirements of a component. However, designing a large mechanical system, potentially comprising thousands or even millions of machine elements, is a much more open, unconstrained problem.

To design superior mechanical systems, an engineer must have a certain sophistication and experience regarding machine elements. Studying the design and selection of machine elements affords an appreciation for the strengths and limitations of classes of components. They can then be more easily and appropriately incorporated into a system. For example, a mechanical system cannot incorporate a worm gear or a Belleville spring if the designer does not realize that these devices exist.

A toolbox analogy of problem solving can be succinctly stated as, “If your only tool is a hammer, then every problem is a nail.” The purpose of studying machine element design is to fill the toolbox so that problem solving and design synthesis activities can be flexible and unconstrained.

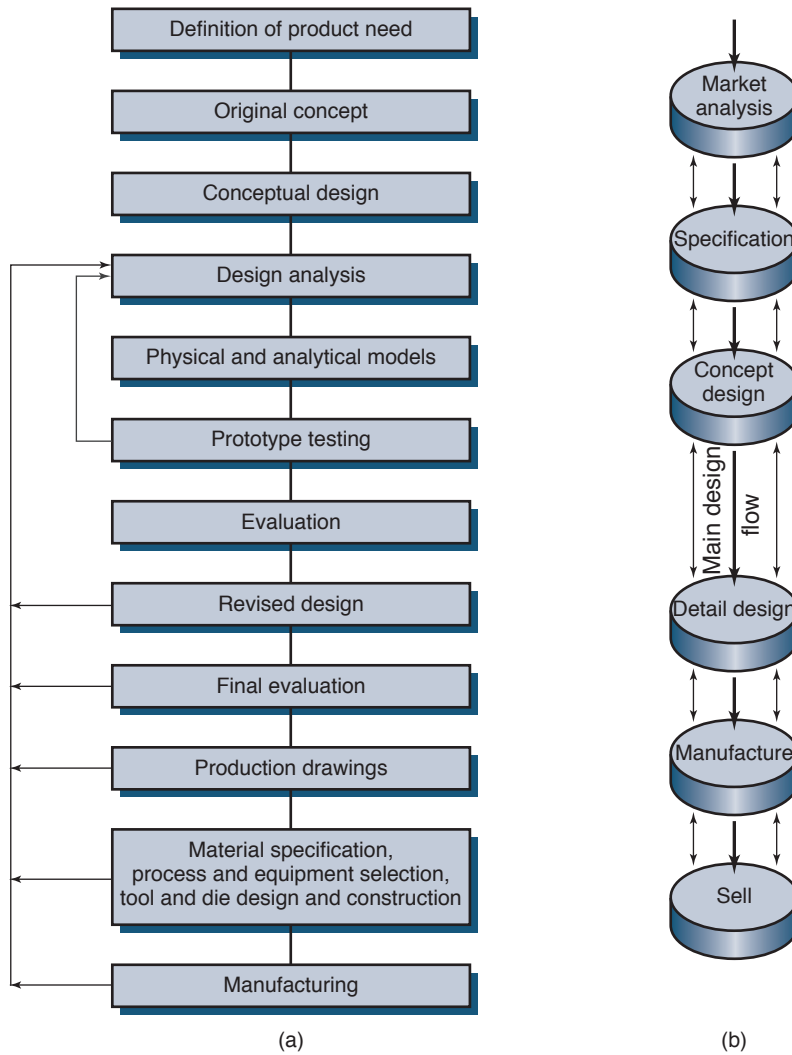


Figure 1.1: Approaches to product development. (a) Classic approach, with large design iterations typical of the over-the-wall engineering approach. *Source:* Adapted from Kalpakjian and Schmid [2003]. (b) A more modern approach, showing a main design flow with minor iterations representing concurrent engineering inputs. *Source:* Adapted from Pugh [1996].

### 1.3 Design as a Multidisciplinary Endeavor

The quality revolution that transformed the manufacturing sector in the early 1980s has forever changed the approach companies and engineers take toward product development. A typical design process of the recent past (Fig. 1.1a) shows that the skills involved in machine element design played an essential role in the process. This approach was commonly used in the United States in the post-World War II era.

The term *over-the-wall engineering* (OTW) has been used to describe this design approach. Basically, someone would apply a particular skill and then send the product “over the wall” to the next step in development. A product design could sometimes flow smoothly from one step to the next and into the marketplace within weeks or months. This was rarely the case, however, as usually a problem would be discovered. For example, a manufacturing engineer might ask that workpieces be more easily clamped into a milling machine fixture. The design engineer would then alter the design and send the product back downstream. A materials

scientist might then point out that the material chosen had drawbacks and suggest a different choice. The design engineer would make the alteration and resubmit the design. This process could continue *ad infinitum*, with the result that the product would take a long time to develop. It is not surprising that modifications to this approach started being developed in the 1970s and 1980s.

Figure 1.1b shows a more modern design approach. Here, there is still the recognized general flow of information from product conception through introduction into the marketplace, but there is immediate involvement of many disciplines in the design stage. Different disciplines are involved simultaneously instead of sequentially as with the OTW approach. Some tasks are extremely technical, such as design analysis (the main focus of this book) or manufacturing. Others are nontechnical, such as market analysis. **Concurrent engineering** is the philosophy of involving many disciplines from the beginning of a design effort and keeping them involved throughout product development. Thus, redundant efforts are minimized and higher quality products are developed more quickly. Although design iterations still occur, the iteration loops are smaller and incur much less wasted time, effort, and expense. Also, design shortcomings can be

corrected before they are incorporated. For example, service personnel can inform design engineers of excessive component failures in previous designs during the conceptual design stage for a new model, and shortcomings can be corrected instead of persisting. No such mechanism for correcting design shortcomings ever existed in conventional design approaches or management structures.

Another important concept in design is the time to market. Bringing high-quality products to market quickly is normal practice in the consumer electronics industry, where rapid change shortened useful market life to a few months. Minimizing time to market is now recognized as essential for controlling development costs. Further, new products introduced before their competitors' products usually enjoy a larger share of the market and profits. Thus, manufacturers who could ship products weeks or even days faster than their competitors had a distinct sales advantage. Saving development time through concurrent engineering made companies much more competitive in the global marketplace.

Concurrent engineering has profoundly affected design engineers. They can no longer work alone and must participate in group discussions and design reviews. They need good communications skills. Designing machinery has become a cooperative endeavor.

Clearly, many disciplines now play a role in product development, but design engineers cannot merely focus on their discipline and rely on experts for the rest. They need familiarity with other disciplines, at least from a linguistics standpoint, to integrate them into the design process. Thus, modern engineers may need to speak the language of materials science, law, marketing, etc., even if they are not experts in these fields.

## 1.4 Design of Machine Elements

Specifying a mechanical system is only the beginning of the design synthesis process. Particular machine element classes need to be chosen, possibly leading to further design iterations. Designing a proper machine element usually involves the following steps:

1. Selecting a suitable type of machine element from consideration of its function
2. Estimating the size of the machine element that is likely to be satisfactory
3. Evaluating the machine element's performance against design requirements or constraints
4. Modifying the design and dimensions until the performance is near to whichever optimum is considered most important

The last two steps in the process can be handled fairly easily by someone who is trained in analytical methods and understands the fundamental principles of the subject. The first two steps, however, require some creative decisions and, for many, represent the most difficult part of design.

After a suitable type of machine element has been selected for the required function, the specific machine element is designed by analyzing kinematics, load, and stress. These analyses, coupled with proper material selection, will enable a stress-strain-strength evaluation in terms of a safety factor (as discussed in Section 1.4.1). A primary question in designing any machine element is whether it will fail in service. Most people, including engineers, commonly associate **failure** with the actual breaking of a machine element. Although

breaking is one type of failure, a design engineer must have a broader understanding of what really determines whether a part has failed.

A machine element is considered to have failed:

1. When it becomes completely inoperable
2. When it is still operable but is unable to perform its intended function satisfactorily
3. When serious deterioration has made it unreliable or unsafe for continued use, necessitating its immediate removal from service for repair or replacement

The role of the design engineer is to predict the circumstances under which failure is likely to occur. These circumstances are stress-strain-strength relationships involving the bulk of the solid members and such surface phenomena as friction, wear, lubrication, and environmental deterioration.

The principles of design are universal. An analysis is equally valid regardless of the size, material, and loading. However, an analysis by itself should not be looked on as an absolute and final truth. An analysis is limited by the assumptions imposed and by its range of applicability. Thus, designers often must check and verify if they have addressed considerations such as:

- Have all alternative designs been thoroughly investigated?
- Can the design be simplified and the number of its components minimized without adversely affecting its intended functions and performance?
- Can the design be made smaller and lighter?
- Are there unnecessary features to the product or some of its components, and if so, can they be eliminated or combined with other features?
- Have modular design and building-block concepts been considered for a family of similar products and for servicing and repair, upgrading, and installing options?
- Are the specified dimensional tolerances and surface finish unnecessarily tight, thereby significantly increasing product cost, and can they be relaxed without any adverse effects?
- Will the product be difficult or excessively time consuming to assemble and disassemble for maintenance, servicing, or recycling of some or all of its components?
- Is the use of fasteners minimized, including their quantity and variety?
- Have environmental considerations been taken into account and incorporated into product design, as well as material and process selection?
- Have green design and life-cycle engineering principles been applied, including recycling considerations?

Design analysis attempts to predict the strength or deformation of a machine element so that it can safely carry the imposed loads for as long as required. Assumptions have to be made about the material properties under different loading types (axial, bending, torsion, and transverse shear, as well as various combinations) and classes (static, sustained, impact, or cyclic). These loading constraints may vary throughout the machine as they relate to different machine elements, an important factor for the design engineer to keep in mind.

### 1.4.1 Safety in Mechanical Design

The code of Hammurabi, a Babylonian doctrine over 3000 years old, had this requirement:

If a builder build a house for a man and do not make its construction firm, and the house which he has built collapse and cause the death of the owner of the house, that builder shall be put to death.

It could be argued that engineers are getting off a lot easier these days. Modern legal doctrines do not call for the death of manufacturers of unsafe products or of the engineers who designed them. Regardless of the penalty, however, engineers have a moral and legal obligation to produce reasonably safe products. A number of fundamental concepts and tools are available to assist them in meeting this challenge.

#### Safety Factor

If 500 tension tests are performed on a specimen of one material, 500 different yield strengths will be obtained if the precision and accuracy of measurement are high enough. With some materials, a wide range of strengths can be achieved; in others, a reasonable guaranteed minimum strength can be found. However, this strength does not usually represent the stress that engineers apply in design.

Using results from small-scale tension tests, a design engineer prescribes a stress somewhat less than the semi-empirical strength of a material. The **safety factor** can be expressed as

$$n_s = \frac{\sigma_{all}}{\sigma_d} \quad (1.1)$$

where  $\sigma_{all}$  is the allowable normal stress and  $\sigma_d$  is the design normal stress. If  $n_s > 1$ , the design is adequate. The larger  $n_s$ , the safer the design. If  $n_s < 1$ , the design may be inadequate and redesign may be necessary. In later chapters, especially Chapter 6, more will be said about  $\sigma_{all}$  and  $\sigma_d$ . The rest of this section focuses on the left side of Eq. (1.1).

It is difficult to accurately evaluate the various factors involved in engineering design problems. One factor is the shape of a part. For an irregularly shaped part, there may be no design equations available for accurate stress computation. Sometimes the load is uncertain. For example, the loading applied to a bicycle seat and frame depends on the size of the rider, speed, and size of bumps encountered. Another factor is the consequences of part failure; life-threatening consequences require more consideration than non-life-threatening consequences.

Engineers use a safety factor to ensure against such uncertain or unknown conditions. The engineering student is often asked, What safety factor was used in the design, and which value should be used? Safety factors are sometimes prescribed by code, but usually they are rooted in design experience. That is, design engineers have established through a product's performance that a safety factor is sufficient. Future designs are often based on safety factors found adequate in previous products for similar applications.

Particular design experience for specific applications does not form a basis for the rational discussion of illustrative examples or for the guidance of engineering students. The Pugsley [1966] method for determining the safety factor is a potential approach for obtaining safety factors in design, although the reader should again be warned that safety factor selection is somewhat nebulous in the real world and the Pugsley method can be unconservative; that is, it predicts safety factors that are too low for real applications. Pugsley

Table 1.1: Safety factor characteristics A, B, and C.

Characteristic <sup>a</sup>		B			
A	C	vg	g	f	p
vg	vg	1.1	1.3	1.5	1.7
	g	1.2	1.45	1.7	1.95
	f	1.3	1.6	1.9	2.2
	p	1.4	1.75	2.1	2.45
g	vg	1.3	1.55	1.8	2.05
	g	1.45	1.75	2.05	2.35
	f	1.6	1.95	2.3	2.65
	p	1.75	2.15	2.55	2.95
f	vg	1.5	1.8	2.1	2.4
	g	1.7	2.05	2.4	2.75
	f	1.9	2.3	2.7	3.1
	p	2.1	2.55	3.0	3.45
p	vg	1.7	2.15	2.4	2.75
	g	1.95	2.35	2.75	3.15
	f	2.2	2.65	3.1	3.55
	p	2.45	2.95	3.45	3.95

<sup>a</sup> vg = very good, g = good, f = fair, and p = poor.

A = quality of materials, workmanship, maintenance, and inspection.

B = control over load applied to part.

C = accuracy of stress analysis, experimental data or experience with similar parts.

Table 1.2: Safety factor characteristics D and E.

Characteristic E <sup>a</sup>		D		
		ns	s	vs
ns		1.0	1.2	1.4
s		1.0	1.3	1.5
vs		1.2	1.4	1.6

<sup>a</sup> vs = very serious, s = serious, and

ns = not serious

D = danger to personnel

E = economic impact

systematically determined the safety factor from

$$n_s = n_{sx} n_{sy} \quad (1.2)$$

where

$n_{sx}$  = safety factor involving characteristics A, B, and C

A = quality of materials, workmanship, maintenance, and inspection

B = control over load applied to part

C = accuracy of stress analysis, experimental data, or experience with similar devices

$n_{sy}$  = safety factor involving characteristics D and E

D = danger to personnel

E = economic impact

Table 1.1 gives  $n_{sx}$  values for various A, B, and C conditions. To use this table, estimate each characteristic for a particular application as being very good (vg), good (g), fair (f), or poor (p). Table 1.2 gives  $n_{sy}$  values for various D and E conditions. To use this table, estimate each characteristic for a particular application as being very serious (vs), serious (s), or not serious (ns). Substituting the values of  $n_{sx}$  and  $n_{sy}$  into Eq. (1.2) yields a proposed safety factor.

Although a simple procedure to obtain safety factors, the Pugsley method illustrates the concerns present in safety factor selection. Many parameters, such as material strength and applied loads, may not be well known, and confidence in the engineering analysis may be suspect. For these reasons the safety factor has sometimes been called an "ignorance factor," as it compensates for ignorance of the total environment, a situation all design engineers encounter to some extent. Also,



the Pugsley method is merely a guideline and is not especially conservative; most engineering safety factors are much higher than those resulting from Eq. (1.2), as illustrated in Example 1.1.

### Example 1.1: Safety Factor of Wire Rope in an Elevator

**Given:** A wire rope is used on an elevator transporting people to the 20th floor of a building. The design of the elevator can be 50% overloaded before the safety switch shuts off the motor.

**Find:** What safety factor should be used?

**Solution:** The following values are assigned:

- A = vg, because life threatening
- B = f to p, since large overloads are possible
- C = vg, due to being highly regulated
- D = vs, people could die if the elevator fell from the 20th floor
- E = vs, possible lawsuits

From Tables 1.1 and 1.2 the safety factor is

$$n_s = n_{sx}n_{sy} = (1.6)(1.6) = 2.56$$

Note that the value of  $n_{sx} = 1.6$  was obtained by interpolation from values in Table 1.1. By improving factors over which there is some control,  $n_{sx}$  can be reduced from 1.6 to 1.0 according to the Pugsley method, thus reducing the required safety factor to 1.6.

Just for illustrative purposes, the safety factor for this situation is prescribed by an industry standard [ANSI 2010] and cannot be lower than 7.6 and may need to be as high as 11.9. The importance of industry standards is discussed in Section 1.4.2, but it is clear that the Pugsley method should be used only with great caution.

### Product Liability

When bringing a product to the market, it is probable that safety will be a primary consideration. A design engineer must consider the **hazards**, or injury producers, and the **risk**, or likelihood of obtaining an injury from a hazard, when evaluating the safety of a system. Unfortunately, this is mostly a qualitative evaluation, and combinations of hazard and risk can be judged acceptable or unacceptable.

The ethical responsibilities of engineers to provide safe products are clear, but the legal system also enforces societal expectations through a number of legal theories that apply to designers and manufacturers of products. Some of the more common legal theories are the following:

- **Caveat Emptor.** Translated as “Let the buyer beware,” this is a doctrine founded on Roman laws. In the case of a defective product or dangerous design, the purchaser or user of the product has no legal recourse to recover losses. In a modern society, such a philosophy is incompatible with global trade and high-quality products, and is mentioned here only for historical significance.
- **Negligence.** In negligence, a party is liable for damages if they failed to act as a reasonable and prudent party would have done under like or similar circumstances. For negligence theory to apply, the injured party, or *plaintiff*, must demonstrate:

1. That a standard of care was violated by the accused party, or *defendant*.
2. That this violation was the *proximate cause* of the accident.
3. That no contributory negligence of the plaintiff caused the misfortune.

- **Strict liability.** Under the strict liability doctrine, the actions of the plaintiff are not an issue; the emphasis is placed on the machine. To recover damages under the strict liability legal doctrine, the plaintiff must prove that:

1. The product contained a defect that rendered it unreasonably dangerous. (For example, an inadequately sized or cracked bolt fastening a brake stud to a machine frame.)
2. The defect existed at the time the machine left the control of the manufacturer. (The manufacturer used the cracked bolt.)
3. The defect was a proximate cause of the accident. (The bolt broke, the brake stud fell off the machine, the machine’s brake didn’t stop the machine, resulting in an accident.) Note that the plaintiff does not need to demonstrate that the defect was the proximate cause; the actions of the plaintiff that contribute to his or her own accident are not considered under strict liability.

- **Comparative fault.** Used increasingly in courts throughout the United States, juries are asked to assess the relative contributions that different parties had in relation to an accident. For example, a jury may decide that a plaintiff was 75% responsible for an accident, and reduce the monetary award by that amount.

- **Assumption of risk.** Although rarely recognized, the *assumption of risk* doctrine states that a plaintiff has limited recourse for recovery of loss if they purposefully, knowingly, and intentionally conducted an unsafe act.

One important requirement for engineers is that their products must be reasonably safe for their intended uses as well as their *reasonably foreseeable misuses*. For example, a chair must be made structurally sound and stable enough for people to sit on (this is the intended use). In addition, a chair should be stable enough so that someone can stand on the chair to change a light bulb, for example. It could be argued that chairs are designed to be sat upon, and that standing on a chair is a misuse. This may be true, but represents a reasonably foreseeable misuse of the chair, and must therefore be considered by designers. In the vast majority of states, misuses of a product that are not reasonably foreseeable do not have to be considered by the manufacturers.

The legal doctrines and ethical requirements that designers produce safe products are usually consistent. Sometimes, the legal system does result in requirements that engineers cannot meet. For example, in the famous *Barker vs. Lull* case in New Jersey, the court ruled that product manufacturers have a nondelegable duty to warn of the unknowable.

*Liability proofing* is the practice of incorporating design features with the intent of limiting product liability exposure without other benefits. This can reduce the safety of machinery. For example, one approach to liability proofing is to place a very large number of warnings onto a machine, with the unfortunate result that all of the warnings are ignored by machine operators. The few hazards that are not obvious and

can be effectively warned against are then “lost in the noise” and a compromise of machine safety can occur.

### Case Study 1.1: *Mason v. Caterpillar Tractor Co.*

Wilma Mason brought action under negligence theory against Caterpillar Tractor Company and Patton Industries for damages after her husband received fatal injuries while trying to repair a track shoe on a Caterpillar tractor. Mr. Mason was repairing the track shoe with a large sledgehammer, when a small piece of metal from the track shoe shot out, striking him, and causing fatal injuries. The plaintiff alleged that the tractor track was defective because the defendants failed to use reasonable methods of heat treatment, failed to use a sufficient amount of carbon in the steel, and failed to warn the decedent of “impending danger.”

The Trial and Appellate courts both granted summary judgements in favor of the defendants. They ruled that the plaintiff failed to show evidence of a product defect that existed when the machine left the control of the manufacturer. Mr. Mason used a large, 10-kg sledgehammer with a full swing, striking a raised portion of the track shoe. There was no evidence that the defendants were even aware that the track shoes were being repaired or reassembled by sledgehammers. It was also noted by the court that the decedent wore safety glasses, indicating his awareness of the risk of injury.

### Safety Hierarchy

A design rule that is widely accepted in general is the **safety hierarchy**, which describes the steps that a manufacturer or designer should use when addressing hazards. The safety hierarchy is given in Design Procedure 1.1. Eliminating hazards through design can imply a number of different approaches. For example, a mechanical part that is designed so that its failure is not reasonably foreseeable is one method of eliminating a hazard or risk of injury. However, design of a system that eliminates injury producers or moves them away from people also represents a reasonable approach.

This book emphasizes mechanical analysis and design of parts to reduce or eliminate the likelihood of failure. As such, it should be recognized that this approach is one of the fundamental, necessary skills required by engineers to provide reasonably safe products.

### Design Procedure 1.1: The Safety Hierarchy

A designer should attempt the following, in order, in attempting to achieve reasonable levels of safety:

1. Eliminate hazards through design.
2. Reduce the risk or eliminate the hazard through safeguarding technology.
3. Provide warnings.
4. Train and instruct.
5. Provide personal protective equipment.

There is a general understanding that primary steps are more efficient in improving safety than later steps. That is, it is more effective to eliminate hazards through design than to use guards, which are more effective than warnings, etc. Clearly, the importance of effective design cannot be overstated.

### Failure Mode and Effects Analysis and Fault Trees

Some common tools available to design engineers are **failure mode and effects analysis** (FMEA) and **fault tree analysis**. FMEA addresses component failure effects on the entire system. It forces the design engineer to exhaustively consider reasonably foreseeable failure modes for every component and its alternatives.

FMEA is flexible, allowing spreadsheets to be tailored for particular applications. For example, an FMEA can also be performed on the steps taken in assembling components to identify critical needs for training and/or warning.

In fault tree analysis, statistical data are incorporated into the failure mode analysis to help identify the most likely (as opposed to possible) failure modes. Often, hard data are not available, and the engineer’s judgment qualitatively identifies likely failure modes.

As discussed above, machine designers are legally required to provide reasonably safe products and to consider the product’s intended uses as well as foreseeable misuses. FMEA and fault tree analysis help identify unforeseeable misuses as well. For example, an aircraft designer may identify aircraft-meteorite collision as a possible loading of the structure. However, because no aircraft accidents have resulted from meteorite collisions and the probability of such occurrences is extremely low, the design engineer ignores such hypotheses, recognizing they are not reasonably foreseeable.

### Load Redistribution, Redundancy, Fail Safe, and the Doctrine of Manifest Danger

One potential benefit of failure mode and effects analysis and fault tree analysis is that they force the design engineer to think of minimizing the effects of individual component failures. A common goal is that the failure of a single component should not result in a catastrophic accident. The design engineer can ensure this by designing the system so that, upon a component failure, loads are redistributed to other components without exceeding their nominal strengths — a philosophy known as **redundancy** in design. For example, a goose or other large bird sucked into an aircraft engine may cause several components to fail and shut down the engine. This type of accident is not unheard of and is certainly reasonably foreseeable. Thus, modern aircraft are designed with sufficient redundancy to allow a plane to fly and land safely with one or more engines shut down.

Many designs incorporate redundancy. Redundant designs can be *active* (where two or more components are in use but only one is needed) or *passive* (where one component is inactive until the first component fails). An example of an active redundant design is the use of two deadbolt locks on a door: both bolts serve to keep the door locked. A passive redundant design example would entail adding a chain lock on a door having a deadbolt lock: if the deadbolt lock fails, the chain will keep the door closed.

An often-used philosophy is to design machinery with **fail-safe** features. For example, a brake system (see Chapter 18) can be designed so that a pneumatic cylinder pushes the brake pads or shoes against a disk or drum, respectively. Alternatively, a spring could maintain pressure against the

disk or drum and a pneumatic system could work against the spring to release the brake. If the pressurized air supply were interrupted, such a design would force brake actuation and prevent machinery motion. This alternative design is fail safe as long as the spring is far more reliable than the pneumatic system.

The **doctrine of manifest danger** is a powerful tool used by machinery designers to prevent catastrophic losses. If danger becomes manifest, troubleshooting is straightforward and repairs can be quickly made. Thus, if a system can be designed so that imminent failure is detectable or so that single-component failure is detectable before other elements fail in turn, a safer design results. A classic application of the doctrine of manifest danger is in the design of automotive braking systems, where the brake shoe consists of a friction material held onto a metal backing plate by rivets. By making the rivets long enough, an audible and tactile indication is given to the car driver when the brake system needs service. That is, if the friction material has worn, the rivets will contact the disk or drum, indicating through noise and vibration that maintenance is required, and this occurs long before braking performance is compromised.

## Reliability

Safety factors are a way of compensating for variations in loading and material properties. Another approach that can be extremely successful in certain circumstances is the application of **reliability** methods.

As an example, consider the process of characterizing a material's strength through tension tests (see Section 3.4). Manufacturing multiple tension test specimens from the same extruded billet of aluminum would result in little difference in measured strength from one test specimen to another. Thus, aluminum in general (as well as most metals) is a *deterministic* material, and deterministic methods can be used in designing aluminum structures if the load is known. For example, in a few hundred tensile tests, a guaranteed minimum strength can be defined that is below the strength of any test specimen and that would not vary much from one test population to another. This guaranteed minimum strength is then used as *the* strength for design analysis. Such deterministic methods are used in most solid mechanics and mechanics courses. That is, all specimens of a given material have a single strength and the loading is always well defined.

Most ceramics, however, would have a significant range of any given material property, including strength. Thus, ceramics are *probabilistic*, and an attempt to define a minimum strength for a population of ceramic test specimens would be an exercise in futility. There would not necessarily be a guaranteed minimum strength. One can only treat ceramics in terms of a likelihood or probability of strength exceeding a given value. There are many such probabilistic materials in engineering practice.

Some loadings, on the other hand, are well known and never vary much. Examples are the stresses inside intravenous (IV) bags during sterilization, the load supported by counterweight springs, and the load on bearings supporting centrifugal fans. Other loads can vary significantly, such as the force exerted on automotive shock absorbers (depends on the size of the pothole and the speed at impact) or on wooden pins holding a chair together (depends on the weight of the seated person or persons) or the impact force on the head of a golf club.

For situations where a reasonable worst-case scenario cannot be defined, reliability methods are sometimes a reasonable design approach. In reliability design methods, the goal is to achieve a reasonable likelihood of survival under

the loading conditions during the intended design life. This approach has its difficulties as well, including the following:

1. To use statistical methods, a reasonable approximation of an infinite test population must be defined. That is, mean values and standard deviations about the mean, and even the nature of the distribution about the mean, must be known. However, they are not usually very well characterized after only a few tests. After all, if only a few tests were needed to quantify a distribution, deterministic methods would be a reasonable, proper, and less mathematically intensive approach. Thus, characterization can be expensive and time consuming, since many experiments are needed.
2. Even if strengths and loadings are known well enough to quantify their statistical distributions, defining a desired reliability is as nebulous a problem as defining a desired safety factor. A reliability of 99% might seem acceptable, unless that were the reliability of an elevator you happened to be occupying. A reliability of 100% is not achievable, or else deterministic methods would be used. A reliability of 99.999...% should be recognized as an extremely expensive affair, and as indicative of overdesign as a safety factor of 2000.
3. The mathematical description of the data has an effect on reliability calculations. A quantity may be best described by a Gaussian or normal distribution, a lognormal distribution, a binary distribution, a Weibull distribution, etc. Often, one cannot know beforehand which distribution is best. Some statisticians recommend using a normal distribution until it is proved ineffective.

The implications are obvious: Reliability design is a complicated matter and even when applied does not necessarily result in the desired reliability if calculated from insufficient or improperly reduced data.

This textbook will emphasize deterministic methods for the most part. The exceptions are the treatments of rolling-element bearings and gears and reliability in fatigue design. For more information on reliability design, refer to the excellent text by Lewis [1995] among others.

## 1.4.2 Government Codes and Industry Standards

In many cases, engineers must rely on government codes and industry-promulgated standards for design criteria. Some of the most common sources for industry standards are:

1. ANSI, the American National Standards Institute
2. ASME, the American Society of Mechanical Engineers
3. ASTM, the American Society for Testing and Materials
4. AGMA, the American Gear Manufacturers Association
5. AISI, the American Iron and Steel Institute
6. AISC, the American Institute of Steel Construction
7. ISO, the International Standards Organization
8. NFPA, the National Fire Protection Association
9. UL, Underwriters Laboratories



Government codes are published annually in the Code of Federal Regulations (CFR) and periodically in the Federal Register (FR) at the national level. States and local municipalities have codes as well, although most relate to building standards and fire prevention.

Code compliance is important for many reasons, some of which have already been stated. However, one essential goal of industry standards is conformability. For example, bolt geometries are defined in ANSI standards so that bolts have fixed thread dimensions and bolt diameters. Therefore, bolts can be mass produced, resulting in inexpensive, high-quality threaded fasteners. Also, maintenance is simplified in that standard bolts can be purchased anywhere, making replacement parts readily available.

### 1.4.3 Manufacturing

Design and manufacturing are difficult to consider apart from one another. The tenet of “form follows function” suggests that shapes are derived only from applied loads in the design environment. However, this is not always the case, and the shapes of products are often natural progressions from arbitrary beginnings.

**Design for manufacturability (DFM)** is a well-established and important tool for design engineers. Manufacturability plays a huge role in the success of commercial products. After all, a brilliant concept that cannot be manufactured cannot be a successful design (per the definition in Section 1.1). Also, because most manufacturing costs are determined by decisions made early in the design process, market success depends on early consideration of a complete product lifecycle, including manufacturing. Individual components should be designed to be easily fabricated, assembled, and constructed (*design for assembly, DFA*). Although manufacturing and assembly are outside the scope of this text, Fig. 1.2 shows their effect on design.

Engineers must wear many hats. Some predominant concerns of a design engineer have been discussed, but many more exist, including:

1. *Environmental or sustainable design*: This issue addresses whether products can be produced that are less harmful to the environment. Biodegradable or easily recycled materials may need to be selected to satisfy this concern.
2. *Economics*: Deciding whether a product will be profitable is of utmost concern.
3. *Legal considerations* - Violating patents and placing unreasonably dangerous products into the marketplace are not only ethically wrong but have legal ramifications as well.
4. *Marketing*: The features of a product that attract consumers and the product's presentation to the marketplace play a significant role in a product's success.
5. *Serviceability*: If a part breaks, can repairs be done in the field, or must customers send the product back to the manufacturer at excessive expense? Unless such concerns are incorporated into design, long-term customer loyalty is compromised.
6. *Quality*: Approaches such as *total quality engineering* and *Taguchi methods* have been successfully applied to make certain that no defects are shipped.

These are merely a few of the concerns faced by design engineers.

The design process may appear so elaborate and involved that no one can master it. In actuality, one important skill makes the design process flow smoothly: effective communication. Communication between diverse disciplines involved in product design ensures that all voices are heard and all design constraints are satisfied early, before significant costs are incurred. Effective communication skills, written and oral, are the most important trait of a good engineer. Although this text emphasizes the more analytical and technical sides of design, it is important to remember that design is not merely an analytical effort but one of human interaction.

### 1.4.4 Life Cycle Engineering

**Life cycle engineering (LCE)** involves consecutive and inter-linked stages of a product or a service, from the very beginning to its disposal or recycling; it includes the following:

1. Extraction of natural resources
2. Processing of raw materials
3. Manufacturing of products
4. Transportation and distribution of the product to the customer
5. Use, maintenance, and reuse of the product
6. Recovery, recycling, reuse, or disposal of its components

All of these factors are applicable to any type of product. Each product can have its own metallic and nonmetallic materials, processed into individual components and assembled; thus, each product has its own life cycle. Moreover, (a) some products are intentionally made to be disposable, particularly those made of paper, cardboard, inexpensive plastic, and glass, but nonetheless are all recyclable, and (b) numerous other products are completely reusable.

A major aim of LCE is to consider reusing and recycling the components of a product, beginning with the earliest stage of product design. This is also called **green design** or **green engineering**. These considerations also include environmental factors, optimization, and numerous technical factors regarding each component of a product.

As is now universally acknowledged, the natural resources on Earth are limited, thus clearly necessitating the need and urgency to conserve materials and energy. The concept of **sustainable design** emphasizes the need for conserving resources, particularly through proper maintenance and reuse. While profitability is important to an organization, sustainable design is meant to meet purposes such as (a) increase the life cycle of products, (b) eliminate harm to the environment and the ecosystem, and (c) ensure our collective well-being, especially for the benefit of future generations.

### Case Study 1.2: Sustainable Manufacturing in the Production of Nike Athletic Shoes

Among numerous examples from industry, the production of Nike shoes clearly has indicated the benefits of sustainable manufacturing. The athletic shoes are assembled using adhesives. Up to around 1990, the adhesives used contained petroleum-based solvents, which pose health hazards

**Rapid prototyping**, also called *3D printing* or *additive manufacturing*, is another computer-driven technology that produces parts from geometry data files in hours or even minutes. Rapid prototyping has been especially helpful in design visualization and rapid detection of design errors. For example, a casting with an excessively thin wall is easily detected when a solid model is held in the hand, a subtlety that is difficult to discern when viewing a part drawing on a computer screen. Significant developments have occurred in rapid prototyping in recent years. Currently, a wide variety of polymers can be used, as well as metals and ceramics.

**Finite element analysis (FEA)** is the most prevalent computational method for solid and fluid mechanics analysis, as well as heat transfer. The finite element computational method solves complex shapes, such as those found in machinery, and replaces the complex shape with a set of simple elements interconnected at a finite set of node points. In FEA, a part geometry is sectioned into many subsections or *elements*. The stiffness of each element is known and is expressed in terms of a stiffness matrix for that element. By combining all the stiffness matrices, applying kinematic and stress boundary conditions, and solving for unknown stresses or displacements, complicated geometries and loading conditions can be easily analyzed.

## 1.6 Catalogs and Vendors

Manufacturing concerns are inseparable from design. Clearly, many machine elements are mass produced because there is an economic justification for large production runs using hard automation. Hard automation generally results in higher quality, tighter tolerance parts than soft automation or hand manufacture, and usually results in less expensive parts as well. In fact, many industry standards mentioned in Section 1.4.2 exist to prescribe geometries that can be mass produced in order to achieve quality and cost benefits. For example, a centerless grinder can produce many high-quality 15-mm-diameter bushings, whereas a single 15-mm bushing is difficult to manufacture and would be very expensive by comparison. Therefore, the practice of machine design often involves selecting mass-produced components from suppliers, often as summarized in catalogs or web sites.

Mechanical designers know the importance of good vendor identification and readily available and up-to-date catalog information. The Internet has brought a huge variety of machine element catalogs to every designer's desktop, and it will be assumed that students are well-aware of Internet search tools and can quickly retrieve product catalogs if desired. Often in this textbook, portions of a manufacturer's catalog will be provided so that data are convenient for problem solving, but it should be recognized that the complete product portfolios are usually much larger than the abstracted data presented.

## 1.7 Units

The solutions to engineering problems must be given in specific and consistent units that correspond to the specific parameter being evaluated. Two systems of units are generally used in practice:

1. **Système International d'Unités (SI units):** Force is measured in newtons, length in meters (sometimes millimeters are more convenient for certain applications), time in seconds, mass in kilograms, and temperature in

degrees Celsius. In addition, absolute temperature is measured in degrees Kelvin, where the temperature in Kelvin is the temperature in Celsius plus 273.15°.

2. **English units:** Force is measured in pounds force, length in inches, time in seconds, mass in pounds mass, and temperature in degrees Fahrenheit.

In Chapter 8 an additional measure, viscosity, is given in the centimeter-gram-seconds (cgs) system.

The SI units, prefixes, and symbols used throughout the text are shown in Table 1.3 as well as inside the front cover. The primary units of this text are SI.

Basic SI units, some definitions, and fundamental and other useful conversion factors are given in Table 1.4, which is also inside the front cover. Note that many units can be quite confusing. For example, a ton in the United States and Canada refers to a weight of 2000 lb, while in the United Kingdom it is a term for weight or mass equivalent to 2240 lb. Sometimes, a weight is reported in short tons (2000 lb) or long tons (2240 lb). The metric equivalent, called a metric ton or a tonne, is 1000 kg. As another example, a horsepower in English units is 550 ft-lb/s or 746 W. However, in metric countries, a horsepower is defined as 736 W. Keeping track of units is a necessary task for design analysis, as illustrated in Case Study 1.3.

### Example 1.2: Length of Electrical Connections in a Supercomputer

**Given:** A supercomputer has a calculation speed of 1 gigaflop =  $10^9$  floating-point operations per second. Performance can be limited if the electrical connections within the supercomputer are so long that electron travel times are greater than the calculation's speed.

**Find:** Determine the critical length of electrical wire for such connections if the electron speed for coaxial cables is 0.9 times the speed of light ( $3 \times 10^8$  m/s).

**Solution:** If the speed is determined only by the cable length,

$$l = \frac{(0.9)(3 \times 10^8)}{10^9} = 0.27 \text{ m} = 27 \text{ cm}$$

The mean cable length must be less than 27 cm.

### Example 1.3: Astronomical Distances

**Given:** The distance from Earth to  $\alpha$ -Centauri is 4 light-years.

**Find:** How many terameters away is  $\alpha$ -Centauri? Note that the speed of light is  $3 \times 10^8$  m/s.

**Solution:** Note that 1 year = (365)(24)(3600) s =  $(3.1536 \times 10^7)$  s. The distance from Earth to  $\alpha$ -Centauri is

$$(4)(3.1536 \times 10^7 \text{ s})(3 \times 10^8 \text{ m/s}) = 3.784 \times 10^{16} \text{ m}$$

From Table 1.3b,  $1 \text{ T} = 10^{12}$ . Therefore, the distance is 37,840 Tm.

Table 1.3: SI units and prefixes.

(a) SI units			
Quantity	Unit	SI symbol	Formula
<b>SI base units</b>			
Length	meter	m	-
Mass	kilogram	kg	-
Time	second	s	-
Temperature	kelvin	K	-
<b>SI supplementary unit</b>			
Plane angle	radian	rad	-
<b>SI derived units</b>			
Energy	joule	J	N-m
Force	newton	N	kg-m/s <sup>2</sup>
Power	watt	W	J/s
Pressure	pascal	Pa	N/m <sup>2</sup>
Work	joule	J	N-m

(b) SI prefixes

Multiplication factor	Prefix	SI symbol for prefix
1,000,000,000,000 = 10 <sup>12</sup>	tera	T
1,000,000,000 = 10 <sup>9</sup>	giga	G
1,000,000 = 10 <sup>6</sup>	mega	M
1000 = 10 <sup>3</sup>	kilo	k
100 = 10 <sup>2</sup>	hecto	h
10 = 10 <sup>1</sup>	deka	da
0.1 = 10 <sup>-1</sup>	deci	d
0.01 = 10 <sup>-2</sup>	centi	c
0.001 = 10 <sup>-3</sup>	milli	m
0.000 001 = 10 <sup>-6</sup>	micro	μ
0.000 000 001 = 10 <sup>-9</sup>	nano	n
0.000 000 000 001 = 10 <sup>-12</sup>	pico	p

## Case Study 1.3: Loss of the Mars Climate Orbiter

On December 11, 1998, the Mars Climate Orbiter was launched to start its nearly 10-month journey to Mars. The Mars Climate Orbiter was a \$125 million satellite intended to orbit Mars and measure the atmospheric conditions on that planet over a planetary year. It was also intended to serve as a communications relay for the Mars Climate Lander, which was due to reach Mars in December 1999. The Mars Climate Orbiter was destroyed on September 23, 1999 as it was maneuvering into orbit.

The cause for the failure was quickly determined: the manufacturer, Lockheed Martin, programmed the entry software in English measurements. However, the navigation team at NASA's Jet Propulsion Laboratory in Pasadena, California assumed the readings were in metric units. As a result, trajectory errors were magnified instead of corrected by mid-course thruster firings. This painful lesson demonstrated the importance of maintaining and reporting units with all calculations.

## 1.8 Unit Checks

Unit checks should always be performed during engineering calculations to make sure that each term of an equation is in the same system of units. The importance of knowing the units of the various parameters used in an equation cannot be overemphasized. In this text, a symbol list giving the units of each parameter is provided at the beginning of each chapter. If no units are given for a particular phenomenon, it is dimensionless. This symbol list can be used as a partial check during algebraic manipulations of an equation.

Table 1.4: Conversion factors and definitions.

Definitions	
Acceleration of gravity	1 g = 9.8066 m/s <sup>2</sup> (32.174 ft/s <sup>2</sup> )
Energy	Btu (British thermal unit) = amount of energy required to raise 1 lbm of water 1°F (1 Btu = 778.2 ft-lb) kilocalorie = amount of energy required to raise 1 kg of water 1K (1 kcal = 4187 J)
Length	1 mile = 5280 ft 1 nautical mile = 6076.1 ft
Power	1 horsepower = 550 ft-lb/s
Pressure	1 bar = 10 <sup>5</sup> Pa
Temperature	Fahrenheit: $t_F = \frac{9}{5}t_C + 32$ Rankine: $t_R = t_F + 459.67$ Kelvin: $t_K = t_C + 273.15$ (exact)
Kinematic viscosity	1 poise = 0.1 kg/m-s 1 stoke = 0.0001 m <sup>2</sup> /s
Volume	1 cubic foot = 7.48 gal
Useful conversion factors	
1 in.	= 0.0254 m = 25.4 mm
1 lbm	= 0.4536 kg
1° R	= $\frac{5}{9}$ K
1 ft	= 0.3048 m
1 lb	= 4.448 N
1 lb	= 386.1 lbm-in./s <sup>2</sup>
1 ton	= 2000 lb (shortton) or 2240 lb (long ton)
1 tonne	= 1000 kg (metric ton)
1 kgf	= 9.807 N
1 lb/in. <sup>2</sup>	= 6895 Pa
1 ksi	= 6.895 MPa
1 Btu	= 1055 J
1 ft-lb	= 1.356 J
1 hp	= 746 W = 2545 Btu/hr <sup>a</sup>
1 kW	= 3413 Btu/hr
1 quart	= 0.000946 m <sup>3</sup> = 0.946 liter
1 kcal	= 3.968 Btu

<sup>a</sup> Note that in countries using the metric system, a horsepower is defined as 75 kpm/s, or 736 W.

## Design Procedure 1.2: Procedure for Unit Checks

It is generally advisable to carry units throughout calculations. However, an expression can generally be evaluated by:

1. Establish units of specific terms of an equation while making use of Table 1.3a.
2. Place units of terms into both sides of an equation and reduce.
3. The unit check is complete if both sides of an equation have the same units.

## Example 1.4: Unit Checks

**Given:** The centrifugal force,  $P$ , acting on a car going through a curve with a radius,  $r$ , at a velocity,  $v$ , is  $m_a v^2 / r$ , where  $m_a$  is the mass of the car. Assume a 1.3-tonne car drives at 100 km/hr through a 100-m-radius bend.

**Find:** Calculate the centrifugal force.

**Solution:** Rewriting using metric units gives

$$m_a = 1.3 \text{ tonne} = 1300 \text{ kg}$$

$$v = 100 \text{ km/hr} = \frac{(100 \text{ m})(1000)}{3600 \text{ s}} = 27.78 \text{ m/s}$$

The centrifugal force is

$$P = \frac{m_a v^2}{r} = \frac{(1300 \text{ kg})(27.78 \text{ m/s})^2}{100 \text{ m}}$$

This results in  $P = 10,030 \text{ kg-m/s}^2$  or  $10,030 \text{ N}$ .

## 1.9 Significant Figures

The accuracy of a number is specified by how many significant figures it contains. Throughout this text, four significant figures will be used unless otherwise limited. For example, 8201 and 30.51 each have four significant figures. When numbers begin or end with a zero, however, it is difficult to tell how many significant figures there are. To clarify this situation, the number should be reported by using *scientific notation* involving powers of 10. Thus, the number 8200 can be expressed as  $8.200 \times 10^3$  to represent four significant figures. Also, 0.005012 can be expressed as  $5.012 \times 10^{-3}$  to represent four significant figures.

### Example 1.5: Significant Figures

**Given:** A car with a mass of 1502 kg is accelerated by a force of 14.0 N.

**Find:** Calculate the acceleration with the proper number of significant figures.

**Solution:** Newton's equation gives that acceleration equals the force divided by the mass

$$a = \frac{P}{m_a} = \frac{14.0}{1502} = 0.00932091 \text{ m/s}^2$$

Since force is accurate to three figures, the acceleration can only be calculated with the accuracy of

$$\pm \frac{0.5}{140} = \pm 0.004 = \pm 0.4\%$$

Therefore, the acceleration is  $0.00932 \text{ m/s}^2$ .

### Case Study 1.4: Design and Manufacture of the Invisalign Orthodontic Product

Widespread healthcare and improved diet and living habits have greatly extended the expected lifetime of people within the last century. Modern expectations are not only that life will be extended, but also that the *quality* of life will be maintained late in life. One important area where this concern manifests itself is with teeth; straight teeth lead to a healthy bite with low tooth stresses, and they also lend themselves to easier cleaning and therefore are more resistant to decay. Thus, straight teeth, in general, last longer with less pain. Of course, there are aesthetic reasons that people wish to have straight teeth as well.



(a)

(b)

Figure 1.3: The Invisalign® product. (a) An example of an Aligner; (b) a comparison of conventional orthodontic braces and a transparent Aligner. *Source:* Courtesy of Align Technology, Inc.

Orthodontic braces have been available to straighten teeth for over 50 years. These involve metal, ceramic, or plastic brackets that are adhesively bonded to teeth, with fixtures for attachment to a wire that then forces compliance on the teeth and straightens them to the desired shape within a few years. Conventional orthodontic braces are a well-known and wholly successful approach to long-term dental health. However, there are many drawbacks to conventional braces, including:

- They are aesthetically unappealing.
- The sharp wires and brackets can cause painful oral irritation to the teeth and gums.
- They trap food, leading to premature tooth decay.
- Brushing and flossing of teeth are far more difficult with braces in place, and therefore they are less effective for most individuals.
- Certain foods must be avoided because they will damage the braces.

One innovative solution is the Invisalign product produced by Align Technology. Invisalign consists of a series of Aligners, each of which the patient wears for approximately two weeks. Each Aligner (see Fig. 1.3) consists of a precise geometry which incrementally moves teeth to their desired positions. Because they are inserts that can be removed for eating, brushing, and flossing, most of the drawbacks of conventional braces are eliminated. Further, since they are produced from transparent plastic, they do not seriously affect the patient's appearance.

The Invisalign product uses an impressive combination of advanced technologies, and the production process is shown in Fig. 1.4. The treatment begins with an orthodontist creating a polymer impression of the patient's teeth or a direct digital image of the teeth using a 3D intra oral scanner (Fig. 1.4a). In case of physical impressions, the impressions are then used to create a three-dimensional CAD representation of the patient's teeth, as shown in Fig. 1.4b. Proprietary computer-aided design software then assists in the development of a treatment strategy for moving the teeth in optimal fashion.

Specially produced software called ClinCheck then produces a digital video of the incremental movements which can be reviewed by the treating orthodontist and modified if necessary.



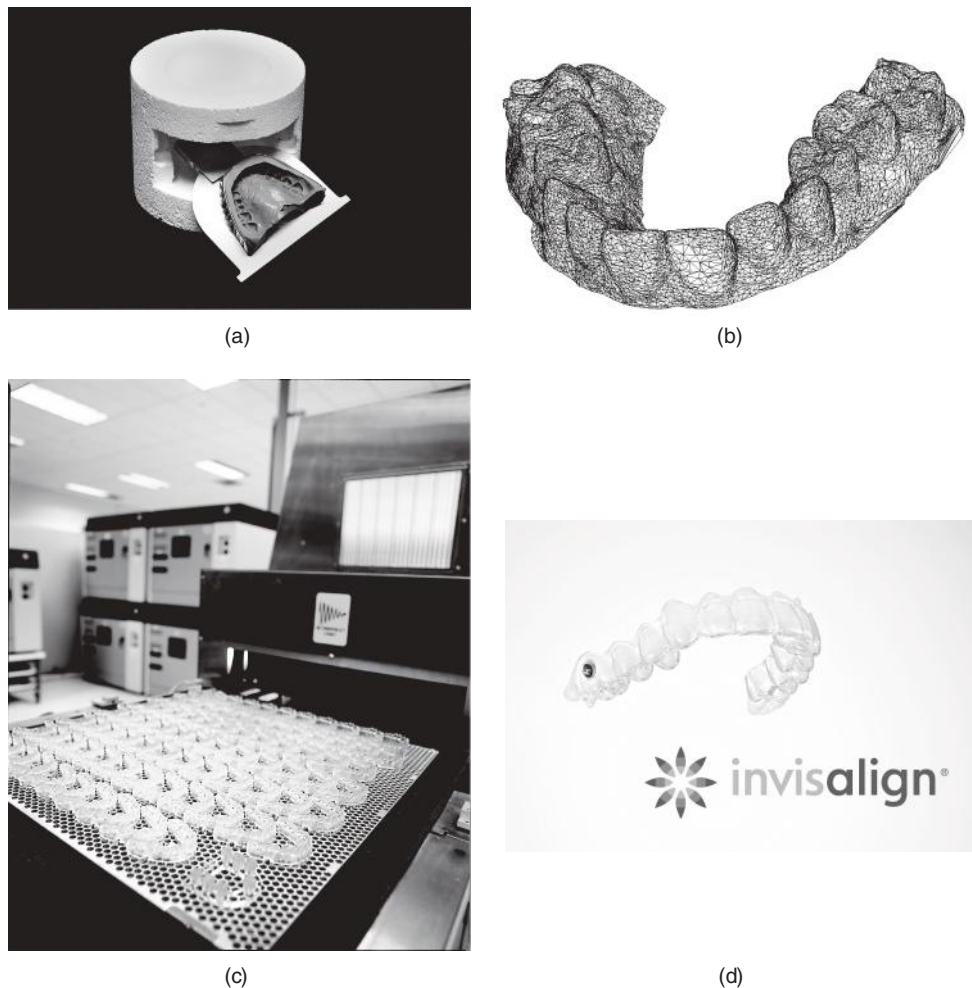


Figure 1.4: The process used in application of Invisalign orthodontic treatment. (a) Impressions are made of the patient's teeth by the orthodontist and shipped to Align Technology, Inc. These are used to make plaster models of the patient's teeth. (b) High-resolution, three-dimensional representations of the teeth are produced from the plaster models. The correction plan is then developed using computer tools. (c) Rapid-prototyped molds of the teeth at incremental positions are produced through stereolithography. (d) An Aligner is produced by molding a transparent plastic over the stereolithography part. Each Aligner is used for approximately two weeks. The patient is left with a beautiful smile. *Source:* Courtesy of Align Technology, Inc.

Once a treatment plan has been designed, the computer-based information needs to be used to produce the Aligners. This is done through a novel application of rapid prototyping technology. Stereolithography is a process that uses a focused laser to cure a liquid photopolymer. The laser only cures a small depth of the polymer, so a part can be built on a tray that is progressively lowered into a vat of photopolymer as layers or slices of the desired geometry are traced and rastered by the laser.

A number of materials are available for stereolithography, but these have a characteristic yellow-brown shade to them and are therefore unsuitable for direct application as an orthodontic product. Instead, the stereolithography machine produces patterns of the desired incremental positions of the teeth (Fig. 1.4c). A sheet of clear polymer is then molded over these patterns to produce the Aligners. These are sent to the treating orthodontist and new Aligners are given to the patient as needed, usually every two weeks or so.

The Invisalign product has proven to be very popular for patients who wish to have straight teeth without almost

anyone knowing they are in treatment. It depends on advanced engineering technologies, precise force delivery through custom engineered shapes, CAD and manufacturing, and rapid prototyping and advanced polymer manufacturing processes.

## Summary

This chapter introduced the concept of design as it applies to machines and machine elements. The most important goal of the design process is to ensure that the design does not fail. To avoid failure, the design engineer must predict the circumstances under which failure is first likely to occur. These circumstances or criteria can involve the material properties and applied loads, as well as surface phenomena, including friction, wear, lubrication, and environmental deterioration.

The concept of failure was quantified by using a safety factor, which is the ratio of the allowable stress established for the material to the maximum design stress that will oc-

cur. Besides the simple safety factor, other failure models, such as failure mode and effects analysis and fault tree analysis, among many others, were presented. The ethical requirements in producing safe designs were stated, along with strategies for achieving this constraint, including the Safety Hierarchy and Doctrine of Manifest Danger. Design was found to be a cooperative endeavor where multidisciplinary approaches are invaluable.

## Key Words

**artificial intelligence (AI)** attempts to duplicate how the human mind works in computer processes

**computer-aided design (CAD)** application of computer technology to planning, performing, and implementing the design process

**concurrent engineering** design approach wherein all disciplines involved with a product are in the development process from beginning to end

**design** transformation of concepts and ideas into useful machinery

**English units** system of units where:

- force is measured in pounds force (lbf)
- length in inches (in.)
- time in seconds (s)
- mass in pounds mass (lbm)
- temperature in degrees Fahrenheit (°F)

**expert systems** computer programs that solve specialized problems on an expert level

**fail-safe** design approach where no catastrophic loss can occur as a result of a component failure

**failure** the condition of a machine element when it is completely inoperable, cannot perform its intended function adequately, or is unreliable for continued safe use

**failure mode and effects analysis (FMEA)** systematic consideration of component failure effects on the entire system

**fault tree analysis** statistical data used to identify the most likely failure modes

**finite element analysis (FEA)** computational method used for solving for stress, strain, temperature, etc. in complex shapes, such as those found in machinery; replaces the complex shape with a set of simple elements interconnected at a finite set of node points

**machine** combination of mechanisms and other components that transform, transmit, or use energy, load, or motion for a specific purpose

**machine element function** normal load transmitter, torque transmitter, energy absorber, or seal

**manifest danger** design approach where needed service is made apparent before catastrophic failure

**mechanical system** synergistic collection of machine elements

**rapid prototyping** parts produced quickly from computer geometry description files

**redundancy** additional capacity or incorporation of backup systems so that a component failure does not lead to catastrophic loss

**safety factor** ratio of allowable stress to design stress

**SI units** system of units where:

- force is measured in newtons (N)
- length in meters (m)
- time in seconds (s)
- mass in kilograms (kg)
- temperature in degrees Kelvin (K)

## Recommended Readings

### General Engineering

- Florman, S.C. (1976) *The Existential Pleasures of Engineering*, St. Martin's Press.
- Petroski, H. (1992) *To Engineer Is Human*, Vintage Books.

### General Design

- Haik, Y., (2003) *Engineering Design Process*, Thomson.
- Hyman, B. (2003) *Fundamentals of Engineering Design*, 2nd ed., Prentice-Hall.
- Lindbeck, J.R., (1995) *Product Design and Manufacture*, Prentice-Hall.
- Otto, K., and Wood, K., (2000) *Product Design: Techniques in Reverse Engineering and New Product Development*, Prentice-Hall.
- Ullman, D.G., (2009) *The Mechanical Design Process*, McGraw-Hill.
- Vogel, C.M., and Cagan, J. (2012) *Creating Breakthrough Products*, 2nd ed., Prentice-Hall.

### Manufacturing/Design for Manufacture

- Boothroyd, G., Dewhurst, P., and Knight, W. (2010) *Product Design for Manufacture and Assembly*, 3rd ed., Taylor & Francis.
- Boothroyd, G. (2005) *Assembly Automation and Product Design*, 2nd ed., Taylor & Francis.
- DeGarmo, E.P., Black, J.T., and Kohser, R.A. (2011) *DeGarmo's Materials and Processes in Manufacturing*, 9th ed., Prentice-Hall.
- Dieter, G.E. and Schmidt, L. (2008) *Engineering Design*, 4th ed., McGraw-Hill.
- Kalpakjian, S., and Schmid, S.R. (2008) *Manufacturing Processes for Engineering Materials*, 5th ed., Prentice-Hall.
- Kalpakjian, S., and Schmid, S.R. (2010) *Manufacturing Engineering and Technology*, 6th ed., Pearson.
- Wright, P.K. (2001) *21st Century Manufacturing*, Prentice-Hall.

### Concurrent Engineering

- Anderson, D.M. (2010) *Design for Manufacturability & Concurrent Engineering*, CIM Press.
- Nevins, J.L., and Whitney, D.E. (Eds.) (1989) *Concurrent Design of Products and Processes*, McGraw-Hill.
- Prasad, B. (1996) *Concurrent Engineering Fundamentals*, Prentice-Hall.
- Pugh, S. (1996) *Creating Innovative Products Using Total Design*, Addison-Wesley.
- Pugh, S. (1991) *Total Design*, Addison-Wesley.

## References

- ANSI (2010) A17.1 "Minimum Safety Requirements for Passenger Elevators," American National Standards Institute.
- ASME (2012) *Code of Ethics for Engineers*, Board on Professional Practice and Ethics, American Society of Mechanical Engineers.
- Boothroyd, G. (1992) *Assembly Automation and Product Design*, Marcel Dekker.
- Florman, S.C. (1987) *The Civilized Engineer*, St. Martin's Press.
- Kalpakjian, S. and Schmid, S.R. (2003) *Manufacturing Processes for Engineering Materials*, 4th ed., Prentice-Hall.
- Kalpakjian, S., and Schmid, S.R. (2010) *Manufacturing Engineering and Technology*, 6th ed., Pearson.
- Lewis, E.E. (1995) *Introduction to Reliability Engineering*, 2nd ed., Wiley.
- Petroski, H. (1992) *To Engineer Is Human*, Vintage Books.
- Pugh, S. (1996) *Creating Innovative Products Using Total Design*, Addison-Wesley.
- Pugsley, A.G. (1966) *The Safety of Structures*, Edward Arnold.

## Questions

- 1.1 What is design?
- 1.2 What is *over-the-wall engineering*?
- 1.3 What is failure?
- 1.4 Define *safety factor*.
- 1.5 Explain the terms "product liability," "negligence," and "strict liability."
- 1.6 What is the Safety Hierarchy?
- 1.7 Give two examples of standards promulgating bodies.
- 1.8 What is a life cycle?
- 1.9 How do you define a product's life cycle?
- 1.10 Name two unit systems.

## Qualitative Problems

- 1.11 Describe the differences between a safety factor and reliability.
- 1.12 Explain why it is said that design casts the largest shadow.
- 1.13 List factors that you feel should be considered when selecting a safety factor.
- 1.14 List some of the concerns that must be considered by a product designer.
- 1.15 What are the advantages and disadvantages of the Pugsley method for estimating safety factor?
- 1.16 Journal bearings on train boxcars in the early 19th century used a "stink additive" in their lubricant. If the bearing got too hot, it would attain a noticeable odor, and an oiler would give the bearing a squirt of lubricant at the next train stop. What design philosophy does this illustrate? Explain.
- 1.17 Explain why engineers must work with other disciplines, using specific product examples.
- 1.18 A car is being driven at 150 km/hr on a mountain road where the posted speed limit is 100 km/hr. At a tight turn, one of the tires fails (a blowout) causing the driver

to lose control and results in an accident involving property losses and injuries but no loss of life. Afterward, the driver decides to file a lawsuit against the tire manufacturer. Explain which legal theories give him a viable argument to make a claim.

- 1.19 Give three examples of fail-safe and three examples of fail-unsafe products.
- 1.20 List three measures that are known within (a) one; (b) two; (c) three; and (d) more than three significant figures.

## Quantitative Problems

- 1.21 A hand-held drilling machine has a bearing to take up radial and thrust load from the drill. Depending on the number of hours the drill is expected to be used before it is scrapped, different bearing arrangements will be chosen. A rubbing bushing has a 50-hr life. A small ball bearing has a 300-hr life. A two-bearing combination of a ball bearing and a cylindrical roller bearing has a 10,000-hr life. The cost ratios for the bearing arrangements are 1:5:20. What is the optimum bearing type for a simple drill, a semiprofessional drill, and a professional drill?
- 1.22 Using the hand-held drill described in Problem 1.21, if the solution with the small ball bearing was chosen for a semiprofessional drill, the bearing life could be estimated to be 300 hr until the first spall forms in the race. The time from first spall to when the whole rolling-contact surface is covered with spalls is 200 hr, and the time from then until a ball cracks is 100 hr. What is the bearing life
  - (a) If high precision is required?
  - (b) If vibrations are irrelevant?
  - (c) If an accident can happen when a ball breaks?
- 1.23 The dimensions of skis used for downhill competition need to be determined. The maximum force transmitted from one foot to the ski is 2500 N, but the snow conditions are not known in advance, so the bending moment acting on the skis is not known. Estimate the safety factor needed.
- 1.24 A crane has a loading hook that is hanging in a steel wire. The allowable normal tensile stress in the wire gives an allowable force of 100,000 N. Estimate the safety factor that should be used.
  - (a) If the wire material is not controlled, the load can cause impact, and fastening the hook in the wire causes stress concentrations. (If the wire breaks, people can be seriously hurt and expensive equipment can be destroyed.)
  - (b) If the wire material is extremely well controlled, no impact loads are applied and the hook is fastened in the wire without stress concentrations. (If the wire breaks, no people or expensive equipment can be damaged.)



**1.25** Calculate the following:

- The velocity of hair growth in meters per second, assuming hair grows 0.75 in. in one month.
- The weight of a 1-in. diameter steel ball bearing in meganewtons.
- The mass of a 1-kg object on the surface of the moon.
- The equivalent rate of work in watts of 4 horsepower.

**1.26** The unit for dynamic viscosity in the SI system is newton-seconds per square meter, or pascal-seconds ( $\text{N}\cdot\text{s}/\text{m}^2 = \text{Pa}\cdot\text{s}$ ). How can that unit be rewritten using the basic relationships described by Newton's law for force and acceleration?

**1.27** The unit for dynamic viscosity in Problem 1.26 is newton-seconds per square meter ( $\text{N}\cdot\text{s}/\text{m}^2$ ) and the kinematic viscosity is defined as the dynamic viscosity divided by the fluid density. Find at least one unit for kinematic viscosity.

**1.28** A square surface has sides 1 m long. The sides can be split into decimeters, centimeters, or millimeters, where  $1 \text{ m} = 10 \text{ dm}$ ,  $1 \text{ dm} = 10 \text{ cm}$ , and  $1 \text{ cm} = 10 \text{ mm}$ . How many millimeters, centimeters, and decimeters equal 1 m? Also, how many square millimeters, square centimeters, and square decimeters equal a square meter?

**1.29** A volume is 1 tera ( $\text{mm}^3$ ) large. Calculate how long the sides of a cube must be to contain that volume.

**1.30** A ray of light travels at a speed of  $300,000 \text{ km/s} = 3 \times 10^8 \text{ m/s}$ . How far will it travel in 1 ps, 1 ns, and 1  $\mu\text{s}$ ?

**1.31** Two smooth flat surfaces are separated by a  $10\text{-}\mu\text{m}$ -thick lubricant film. The viscosity of the lubricant is  $0.100 \text{ Pa}\cdot\text{s}$ . One surface has an area of  $1 \text{ dm}^2$  and slides over the plane surface with a velocity of  $1 \text{ km/hr}$ . Determine the friction force due to shearing of the lubricant film. Assume the friction force is the viscosity times the surface area times the velocity of the moving surface and divided by the lubricant film thickness.

**1.32** A firefighter sprays water on a house. The nozzle diameter is small relative to the hose diameter, so the force on the nozzle from the water is

$$F = v \frac{dm_a}{dt}$$

where  $v$  is the water velocity and  $dm_a/dt$  is the water mass flow per unit time. Calculate the force the firefighter needs to hold the nozzle if the water mass flow is 3 tons/hr and the water velocity is 100 km/hr.

**1.33** The mass of a car is 1346 kg. The four passengers in the car weigh 643 N, 738 N, 870 N, and 896 N. It is raining and the additional mass due to the water on the car is 1.349 kg. Calculate the total weight and mass of the car, including the passengers and water, using four significant figures.

**1.34** During an acceleration test of a car the acceleration was measured to be  $1.4363 \text{ m/s}^2$ . Because slush and mud adhered to the bottom of the car, the mass was estimated to be  $1400 \pm 100 \text{ kg}$ . Calculate the force driving the car and indicate the accuracy.

## Design and Projects

**1.35** Design transport containers for milk in 1- and 4-liter sizes.

**1.36** Design a kit of tools for campers so they can prepare and eat meals. The kit should have all of the implements needed, and be lightweight and compact.

**1.37** An acid container will damage the environment and people around it if it leaks. The cost of the container is proportional to the container wall thickness. The safety can be increased either by making the container wall thicker or by mounting a reserve tray under the container to collect the leaking acid. The reserve tray costs 10% of the thick-walled container cost. Which is less costly, to increase the wall thickness or to mount a reserve tray under the container?

This page intentionally left blank

## Chapter 2

# Load, Stress, and Strain



Collapse of the Tacoma Narrows bridge in 1940. Source: AP Photos.

*The careful text-books measure  
(Let all who build beware!)  
The load, the shock, the pressure  
Material can bear.  
So when the buckled girder  
Lets down the grinding span,  
The blame of loss, or murder,  
Is laid upon the man.  
Not on the stuff - The Man!*

Rudyard Kipling, *Hymn of Breaking Strain*

This chapter addresses fundamental problems essential to design: determining the location in a part that is likely to fail, and how to analyze stresses and strains that occur at the critical location. The concept of the critical section is discussed, and the terminology of different loads is defined. The concepts of equilibrium and free-body diagrams are then presented, leading to the production of shear and bending moment diagrams for beams. There are numerous methods of producing such diagrams, and three of the most common and powerful techniques are presented. Stress and strain are discussed next, with an emphasis that they are tensors. The common circumstances of plane stress and plane strain are defined. The ability to determine stress states based on orientation is demonstrated through stress transformation equations and Mohr's circle diagrams, and the procedure for finding principal stresses for a generalized three-dimensional stress state is given. The useful concept of octahedral stresses is presented, and the chapter ends by briefly describing the use of strain gages and rosettes to experimentally determine strains.

### Contents

2.1	Introduction	22
2.2	Critical Section	22
2.3	Load Classification and Sign Convention	23
2.4	Support Reactions	24
2.5	Static Equilibrium	24
2.6	Free-Body Diagram	26
2.7	Supported Beams	27
2.8	Shear and Moment Diagrams	27
2.9	Stress	34
2.10	Stress Element	34
2.11	Stress Tensor	35
2.12	Plane Stress	35
2.13	Mohr's Circle	37
2.14	Three-Dimensional Stresses	39
2.15	Octahedral Stresses	40
2.16	Strain	41
2.17	Strain Tensor	42
2.18	Plane Strain	42
2.19	Summary	44

### Examples

2.1	Critical Section of a Simple Crane	22
2.2	Classification of Load Types	24
2.3	Loads on a Lever Assembly	24
2.4	Static Equilibrium of a Ladder	25
2.5	Equilibrium of a Suspended Sphere	26
2.6	Free-Body Diagram of an External Rim Brake	27
2.7	Shear and Moment Diagrams by Method of Sections	28
2.8	Shear and Moment Diagrams by Direct Integration	28
2.9	Shear and Moment Diagrams Using Singularity Functions	30
2.10	Shear and Moment Expressions Using Singularity Functions	32
2.11	Stress in Beam Supports	34
2.12	Stresses in Stress Element	35
2.13	Stress Transformation	37
2.14	Mohr's Circle	38
2.15	Three-Dimensional Mohr's Circle	39
2.16	Octahedral Stresses	41
2.17	Calculation of Strain	42
2.18	Strain Gage Rosette	44

### Design Procedures

2.1	Establish Critical Section and Loading	22
2.2	Drawing Shear and Moment Diagrams by the Method of Sections	28
2.3	Working with Singularity Functions	30
2.4	Shear and Moment Diagrams by Singularity Functions	30
2.5	Mohr's Circle	37

## Symbols

$A$	area, $\text{m}^2$
$d$	diameter, $\text{m}$
$g$	gravitational acceleration, $9.807 \text{ m/s}^2$
$l$	length, $\text{m}$
$M$	moment, $\text{N}\cdot\text{m}$
$m_a$	mass, $\text{kg}$
$n$	any integer
$P$	force, $\text{N}$
$q$	load intensity function, $\text{N/m}$
$R$	reaction force, $\text{N}$
$r$	radius of Mohr's circle, $\text{m}$
$\mathbf{S}$	stress tensor
$\mathbf{S}'$	principal stress tensor
$\mathbf{T}$	strain tensor
$T$	torque, $\text{N}\cdot\text{m}$
$V$	transverse shear force, $\text{N}$
$W$	normal applied load, $\text{N}$
$w_o$	load per unit length, $\text{N/m}$
$x, y, z$	Cartesian coordinate system, $\text{m}$
$x', y', z'$	rotated Cartesian coordinate system, $\text{m}$
$\gamma$	shear strain
$\delta$	elongation, $\text{m}$
$\epsilon$	normal strain
$\theta$	deviation from initial right angle or angle of force application, $\text{deg}$
$\mu$	coefficient of friction
$\sigma$	normal stress, $\text{Pa}$
$\tau$	shear stress, $\text{Pa}$
$\tau_{1/2}$	principal shear stresses in triaxial stress state, $\text{Pa}$
$\tau_{2/3}, \tau_{1/3}$	
$\phi$	angle of oblique plane, $\text{deg}$

## Subscripts

$a$	axial
$b$	biaxial stress
$c$	center
$e$	von Mises
$r$	roller
$t$	triaxial stress; transverse
$x, y, z$	Cartesian coordinates
$x', y', z'$	rotated Cartesian coordinates
$\theta$	angle representing deviation from initial right angle
$\sigma$	normal stress
$\tau$	shear stress
$\phi$	angle of oblique plane
$1, 2, 3$	principal axes

## 2.1 Introduction

The focus of this text is the design and analysis of machines and machine elements. Since machine elements carry **loads**, it follows that an analysis of loads is essential in machine element design. Proper selection of a machine element often is a simple matter of calculating the stresses or deformations expected in service and then choosing a proper size so that critical stresses or deformations are not exceeded. The first step in calculating the stress or deformation of a machine element is to accurately determine the load. Load, stress, and strain in all its forms are the foci of this chapter, and the information developed here is used throughout the text.

## 2.2 Critical Section

To determine when a machine element will fail, the designer evaluates the stress, strain, and strength at the critical section. The **critical section**, or the location in the design where the largest internal load is developed and failure is most likely, is often not intuitively known beforehand. Design Procedure 2.1 lists the common steps in determining the critical section and loading. The first and second steps arise from system design. The third step is quite challenging and may require analysis of a number of locations or failure modes before the most critical is found. For example, a beam subjected to a distributed load might conceivably exceed the maximum deflection at a number of locations; thus, the beam deflection would need to be calculated at more than one position.

In general, the critical section will often occur at locations of geometric nonuniformity, such as where a shaft changes its diameter along a fillet, or at an interface between two different materials. Also, locations where load is applied or transferred are often critical locations. Finally, areas where the geometry is most critical are candidates for analysis. This topic will be expanded upon in Chapter 6.

### Design Procedure 2.1: Critical Section and Loading

To establish the critical section and the critical loading, the designer:

1. Considers the external loads applied to a machine (e.g., a gyroscope)
2. Considers the external loads applied to an element within the machine (e.g., a ball bearing)
3. Locates the critical section within the machine element (e.g., the inner race)
4. Determines the loading at the critical section (e.g., contact stresses)

### Example 2.1: Critical Section of a Simple Crane

**Given:** A simple crane, shown in Fig. 2.1a, consists of a horizontal beam loaded vertically at one end with a load of 10 kN. The beam is pinned at the other end. The force at the pin and roller must not be larger than 30 kN to satisfy other design constraints.

**Find:** The location of the critical section and also whether the load of 10 kN can be applied without damage to the crane.

**Solution:** The forces acting on the horizontal beam are shown in Fig. 2.1b. Summation of moments about the pin (at  $x = 0$ ) gives

$$(1.0)P = (0.25)W_r,$$

so that  $W_r$  is found to be 40 kN. Summation of vertical forces gives

$$-W_p + W_r - 10 \text{ kN} = 0,$$

which results in  $W_p = 30 \text{ kN}$ . The critical section is at the roller, since  $W_r > W_p$ . Also, since  $W_r > W_{\text{all}}$ , failure will occur. To avoid failure, the load at the end of the horizontal beam must be reduced.

## Load Classification and Sign Convention

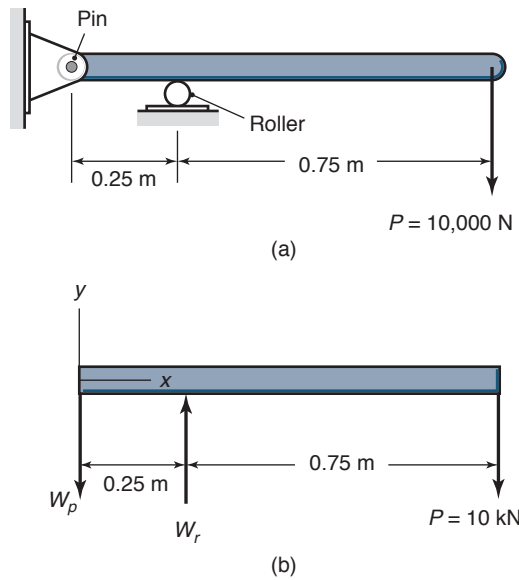


Figure 2.1: A schematic of a simple crane and applied forces considered in Example 2.1. (a) Assembly drawing; (b) free-body diagram of forces acting on the beam.

## 2.3 Load Classification and Sign Convention

Any applied load can be classified with respect to time in the following ways:

1. **Static load** — Load is gradually applied and equilibrium is reached in a relatively short time. The structure experiences no dynamic effects.
2. **Sustained load** — Load, such as the weight of a structure, is constant over a long time.
3. **Impact load** — Load is rapidly applied. An impact load is usually attributed to an energy imparted to a system.
4. **Cyclic load** — Load can vary and even reverse its direction and has a characteristic period with respect to time.

The load can also be classified with respect to the area over which it is applied:

1. **Concentrated load** — Load is applied to an area much smaller than the loaded member, such as presented for nonconformal surfaces in Section 8.4. An example would be the contact between a caster and a support beam on a mechanical crane, where the contact area is around 100 times smaller than the surface area of the caster. For these cases, the applied force can be considered to act at a point on the surface.
2. **Distributed load** — Load is spread along a large area. An example would be the weight of books on a bookshelf.

Loads can be further classified with respect to location and method of application. Also, the coordinate direction must be determined before the sign of the loading can be established:

1. **Normal load** — The load passes through the centroid of the resisting section. Normal loads may be tensile

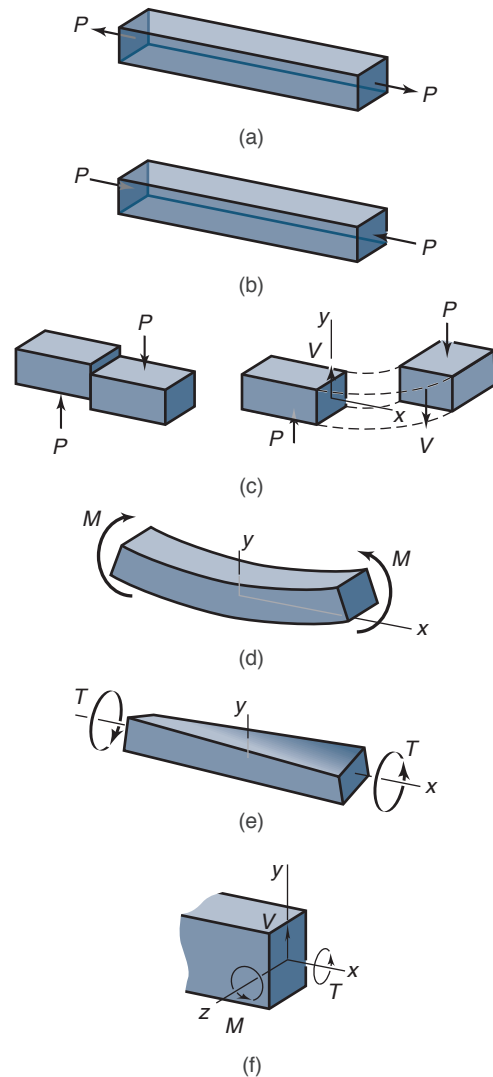


Figure 2.2: Load classified as to location and method of application. (a) Normal, tensile; (b) normal, compressive; (c) shear; (d) bending; (e) torsion; (f) combined.

(Fig. 2.2a) or compressive (Fig. 2.2b). The established sign convention has tensile loads being positive and compressive loads being negative.

2. **Shear load** — The separated bar in Fig. 2.2c illustrates the action of positive shearing. The figure has been redrawn to show the surface of interest on the right side. A shear force is positive if the force direction and the normal direction are both positive or both negative. The shear force,  $V$ , shown on the left surface of Fig. 2.2c is in the positive  $y$ -direction, which is upward, and the normal to the surface is in the positive  $x$ -direction. Thus, the shear force is positive. On the right surface of Fig. 2.2c the shear force is also positive, since the direction of the shear force and the normal to the surface are both negative. A shear force is negative if the force direction and the normal direction have different signs. If the positive  $y$ -coordinate had been chosen to be upward (negative) rather than downward (positive) in Fig. 2.2c, the shear force would be negative rather than positive. Thus, to establish whether a shear force is positive or negative, the positive  $x$ - and  $y$ -coordinates must be designated.

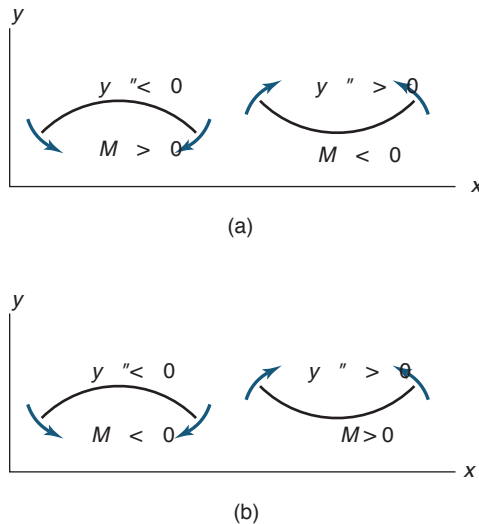


Figure 2.3: Sign conventions used in bending. (a) Positive moment leads to a tensile stress in the positive  $y$ -direction; (b) positive moment acts in a positive direction on a positive face. The sign convention shown in (b) will be used in this book.

3. *Bending load* — This commonly occurs when load is applied transversely to the longitudinal axis of the member. Figure 2.2d shows a member that is subject to equal and opposite moments applied at its ends. The moment results in normal stresses in a cross section transverse to the normal axis of the member, as described further in Section 4.5.2.

The sign convention used in bending stress analysis should be briefly discussed. Two common sign conventions are used in engineering practice, as illustrated in Fig. 2.3. The difference between these two sign conventions is in the sign of the moment applied, and each sign convention has its proponents and critics. The proponents of the sign convention shown in Fig. 2.3a prefer that the stresses that arise in the beam follow the rule that, for a positive moment, a positive distance from the neutral axis results in a positive (tensile) stress. On the other hand, the sign convention shown in Fig. 2.3b allows certain mnemonic methods for its memorization, such as a positive moment results in a deformed shape that “holds water” or has a positive second derivative. Perhaps the best reason for using the sign convention in Fig. 2.3b is that the convention for bending moments is the same as for applied shear forces — that a positive force or moment acting on a face with a positive outward pointing normal acts in a positive direction when using a right-handed coordinate system.

It should be recognized that sign conventions are arbitrary, and correct answers can be obtained for problems using any sign convention, as long as the sign convention is applied consistently within a problem. In this book, the bending sign convention of Fig. 2.3b will be used, but this should not be interpreted as mandatory for solution of problems.

4. *Torsion load* — Such a load subjects a member to twisting motion, as shown in Fig. 2.2e. The twist results in a distribution of shear stresses on the transverse cross section of the member. Positive torsion occurs in Fig. 2.2e. The right-hand rule is applicable here.

5. *Combined load* — Figure 2.2f shows a combination of two or more of the previously defined loads (e.g., shear, bending, and torsion acting on a member). Note that positive shear, bending, and torsion occur in this figure.

## Example 2.2: Classification of Load Types

**Given:** A diver jumping on a diving board.

**Find:**

- a) The load type when the diver lands on the diving board
- b) The load type when the diver stands motionless waiting for the signal to jump
- c) The load type on the diving board just as the diver jumps
- d) The load type of the diving board assembly against the ground when no dynamic loads are acting

**Solution:**

- a) Impact load — as the diver makes contact with the diving board.
- b) Static load — when the diver is motionless.
- c) Cyclic load — when the diving board swings up and down just after the dive
- d) Sustained load — when gravity acts on the diving board structure, pressing it against the ground

## Example 2.3: Loads on a Lever Assembly

**Given:** The lever assembly shown in Fig 2.4a.

**Find:** The normal, shear, bending, and torsional loads acting at section B.

**Solution:** Figure 2.4b shows the various loads acting on the lever, all in the positive direction. To the right of the figure, expressions are given for the loading at section B of the lever shown in Fig. 2.4a.

## 2.4 Support Reactions

Reactions are forces developed at supports. For two-dimensional problems (i.e., bodies subjected to coplanar force systems), the types of support most commonly encountered, along with the corresponding reactions, are shown in Table 2.1. (Note the direction of the forces on each type of support and the reaction they exert on the attached member.) One way to determine the support reaction is to imagine the attached member as being translated or rotated in a particular direction. If the support prevents translation in a given direction, a force is developed on the member in that direction. Likewise, if the support prevents rotation, a moment is applied to the member. For example, a roller prevents translation only in the contact direction, perpendicular (or normal) to the surface; thus, the roller cannot develop a coupled moment on the member at the point of contact.

## 2.5 Static Equilibrium

Equilibrium of a body requires both a balance of forces, to prevent the body from translating (moving) along a straight or curved path, and a balance of moments, to prevent the body from rotating. From statics, it is customary to present



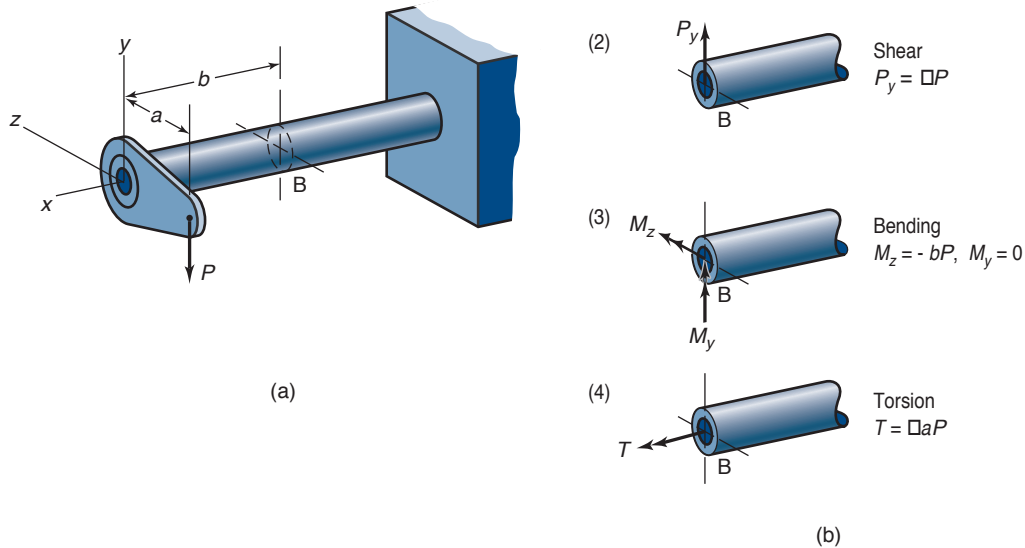


Figure 2.4: Lever assembly and results. (a) Lever assembly; (b) results showing (1) normal, tensile, (2) shear, (3) bending, and (4) torsion on section B of lever assembly.

Table 2.1: Four types of support with their corresponding reactions.

Type of support	Reaction

these equations as

$$\sum P_x = 0, \quad \sum P_y = 0, \quad \sum P_z = 0, \quad (2.1)$$

$$\sum M_x = 0, \quad \sum M_y = 0, \quad \sum M_z = 0. \quad (2.2)$$

Often, in engineering practice, the loading on a body can be represented as a system of coplanar forces. If this is the case, and the forces lie in the  $x$ - $y$  plane, the equilibrium conditions of the body can be specified by only three equations:

$$\sum P_x = 0, \quad \sum P_y = 0, \quad \sum M_z = 0. \quad (2.3)$$

Note that the moment,  $M_z$ , is a vector perpendicular to the plane that contains the forces. Successful application of the equilibrium equations requires complete specification of all the known and unknown forces acting on the body.

### Example 2.4: Static Equilibrium of a Ladder

**Given:** A painter stands on a ladder that leans against the wall of a house. Assume the painter is at the midheight of the ladder. The ladder stands on a horizontal surface with a coefficient of friction of 0.3 and leans at an angle of  $20^\circ$  against the house, which also has a coefficient of friction of 0.3.

**Find:** Whether the painter and ladder are in static equilibrium and what critical coefficient of friction,  $\mu_{cr}$ , will not provide static equilibrium.

**Solution:** Figure 2.5 shows a diagram of the forces acting on the ladder due to the weight of the painter as well as the weight of the ladder. The mass of the ladder is  $m_l$  and the mass of the painter is  $m_p$ . If the ladder starts to slide, the friction force will counteract the motion.

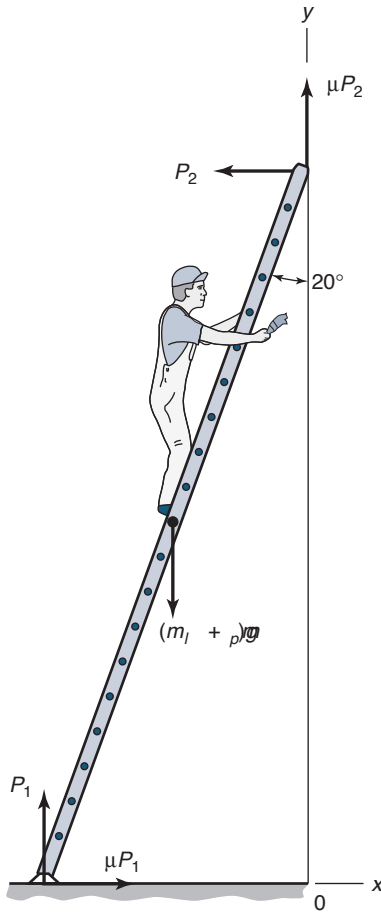


Figure 2.5: Ladder in contact with a house and the ground while having a painter on the ladder.

Summation of horizontal forces gives

$$\sum P_x = \mu_{cr} P_1 - P_2 = 0, \quad (a)$$

or  $P_2 = \mu_{cr} P_1$ . Summation of vertical forces results in

$$P_1 (1 + \mu_{cr}^2) = (m_l + m_p) g.$$

Therefore,

$$P_1 = \frac{(m_l + m_p) g}{1 + \mu_{cr}^2}. \quad (b)$$

Making use of Eq. (a) gives

$$P_2 = \frac{\mu_{cr} (m_l + m_p) g}{1 + \mu_{cr}^2}. \quad (c)$$

Applying moment equilibrium about point 0 results in

$$P_1 l \sin 20^\circ - P_2 l \cos 20^\circ - (m_l + m_p) g \frac{l}{2} \sin 20^\circ = 0, \quad (d)$$

where  $l$  is the ladder length. Substituting Eqs. (b) and (c) into Eq. (d) gives

$$0 = \frac{(m_l + m_p) g l \sin 20^\circ}{1 + \mu_{cr}^2} - \frac{\mu_{cr} (m_l + m_p) g l \cos 20^\circ}{1 + \mu_{cr}^2} - (m_l + m_p) g \frac{l}{2} \sin 20^\circ,$$

or

$$0 = \frac{1}{1 + \mu_{cr}^2} - \frac{\mu_{cr}}{\tan 20^\circ (1 + \mu_{cr}^2)} - \frac{1}{2}.$$

Through algebraic manipulation,

$$0.5 = \frac{\tan 20^\circ - \mu_{cr}}{\tan 20^\circ (1 + \mu_{cr}^2)}$$

$$0.5 \tan 20^\circ + 0.5 \mu_{cr}^2 \tan 20^\circ = \tan 20^\circ - \mu_{cr}$$

$$\mu_{cr}^2 + \frac{\mu_{cr}}{0.5 \tan 20^\circ} - 1 = 0$$

so that

$$\mu_{cr} = 0.1763.$$

Since  $\mu$  is given as 0.3, the ladder will not move, so that the painter and ladder are in static equilibrium. The critical coefficient where the ladder starts to slide is 0.1763.

## 2.6 Free-Body Diagram

An entire machine, any individual machine element, or any part of a machine element can be represented as a free body. Static equilibrium is assumed at each level. The best way to account for the forces and moments in the equilibrium equations is to draw the free-body diagram. For the equilibrium equations to be correctly applied, the effects of all the applied forces and moments must be represented in the free-body diagram.

A **free-body diagram** is a sketch of a machine, a machine element, or part of a machine element that shows all acting forces, such as applied loads and gravity forces, and all reactive forces. The reactive forces are supplied by the ground, walls, pins, rollers, cables, or other means. The sign of the reaction may not be known, but it can be assigned arbitrarily or guessed. If, after the static equilibrium analysis, the sign of the reactive force is positive, the initial direction is correct; if it is negative, the direction is opposite to that initially guessed.

### Example 2.5: Equilibrium of a Suspended Sphere

**Given:** A steel sphere, shown in Fig. 2.6a, has a mass of 10 kg and hangs from two wires. A spring attached to the bottom of the sphere applies a downward force of 150 N.

**Find:** The forces acting on the two wires. Also, draw a free-body diagram showing the forces acting on the sphere.

**Solution:** Figure 2.6b shows the free-body diagram of the forces acting on the sphere. Summation of the vertical forces gives

$$2P \cos 60^\circ - m_a g - 150 = 0.$$

or

$$P = \frac{(10)(9.807) + 150}{2 \cos 60^\circ} = 248.1 \text{ N.}$$

## Shear and Moment Diagrams

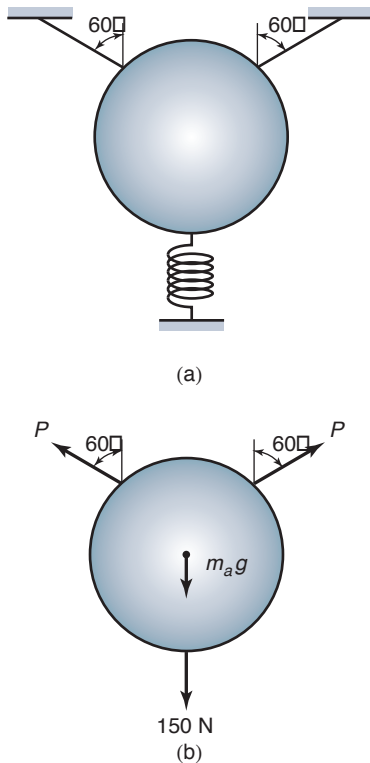


Figure 2.6: Sphere and applied forces. (a) Sphere supported with wires from top and spring at bottom; (b) free-body diagram of forces acting on sphere.

### Example 2.6: Free-Body Diagram of an External Rim Brake

**Given:** The external rim brake shown in Fig. 2.7a.

**Find:** Draw a free-body diagram of each component of the system.

**Solution:** Figure 2.7b shows each brake component as well as the forces acting on them. The static equilibrium of each component must be preserved, and the friction force acts opposite to the direction of motion on the drum and in the direction of motion on both shoes. The  $4W$  value in Fig. 2.7b was obtained from the moment equilibrium of the lever. Details of brakes are considered in Chapter 18, but in this chapter it is important to be able to draw the free-body diagram of each component.

## 2.7 Supported Beams

A **beam** is a structural member designed to support loading applied perpendicular to its longitudinal axis. In general, beams are long, often straight bars having a constant cross-section. Often, they are classified by how they are supported. Three major types of support are shown in Fig. 2.8:

1. A **simply supported beam** (Fig. 2.8a) is pinned at one end and roller-supported at the other.
2. A **cantilevered beam** or **cantilever** (Fig. 2.8b) is fixed at one end and free at the other.
3. An **overhanging beam** (Fig. 2.8c) has one or both of its ends freely extending past its supports.

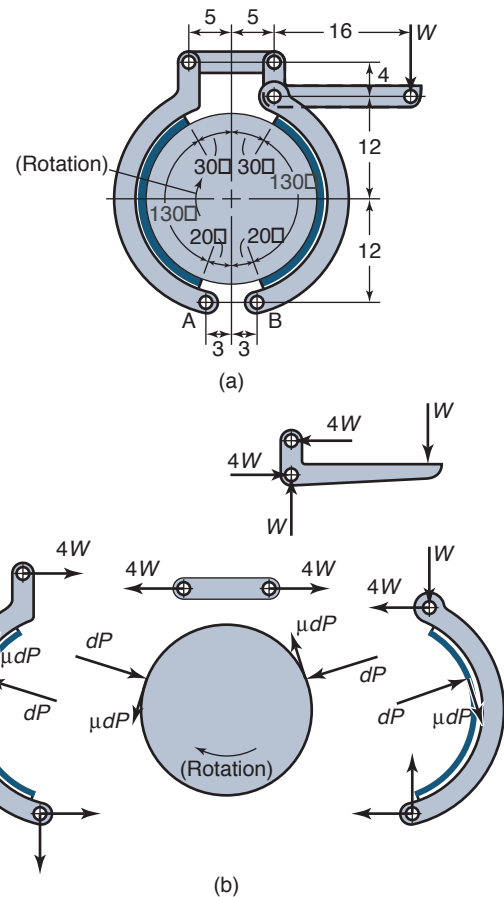


Figure 2.7: External rim brake and applied forces, considered in Example 2.6. (a) External rim brake; (b) external rim brake with forces acting on each part. (Linear dimensions are in millimeters.)

Two major parameters used in evaluating beams are strength and deflection, as discussed in Chapter 5. Shear and bending are the two primary modes of beam loading. However, if the height of the beam is large relative to its width, elastic instability can become important and the beam can twist under loading (see *unstable equilibrium* in Section 9.2.3).

## 2.8 Shear and Moment Diagrams

Designing a beam on the basis of strength requires first finding its maximum shear and moment. This section describes three common and powerful approaches for developing shear and moment diagrams. Usually, any of these methods will be sufficient to analyze any statically determinate beam, so the casual reader may wish to emphasize one method and then continue to the remaining sections.

### 2.8.1 Method of Sections

One way to obtain shear and moment diagrams is to apply equilibrium to sections of the beam taken at convenient locations. This allows expression of the transverse shear force,  $V$ , and the moment,  $M$ , as functions of an arbitrary position,  $x$ , along the beam's axis. These shear and moment functions can then be plotted as shear and moment diagrams from which the maximum values of  $V$  and  $M$  can be obtained.

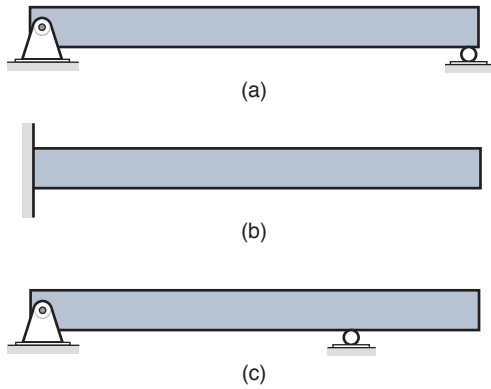


Figure 2.8: Three types of beam support. (a) Simply supported; (b) cantilevered; (c) overhanging.

## Design Procedure 2.2: Drawing Shear and Moment Diagrams by the Method of Sections

The procedure for drawing shear and moment diagrams by the method of sections is as follows:

1. Draw a free-body diagram and determine all the support reactions. Resolve the forces into components acting perpendicular and parallel to the beam's axis.
2. Choose a position,  $x$ , between the origin and the length of the beam,  $l$ , thus dividing the beam into two segments. The origin is chosen at the beam's left end to ensure that any  $x$  chosen will be positive.
3. Draw a free-body diagram of the two segments and use the equilibrium equations to determine the transverse shear force,  $V$ , and the moment,  $M$ .
4. Plot the shear and moment functions versus  $x$ . Note the location of the maximum moment. Generally, it is convenient to show the shear and moment diagrams directly below the free-body diagram of the beam.
5. Additional sections can be taken as necessary to fully quantify the shear and moment diagrams.

## Example 2.7: Shear and Moment Diagrams by Method of Sections

**Given:** The bar shown in Fig. 2.9a.

**Find:** Draw the shear and moment diagrams.

**Solution:** For  $0 \leq x < l/2$ , the free-body diagram of the bar section is as shown in Fig. 2.9b. The unknowns  $V$  and  $M$  are positive. Applying the equilibrium equations gives

$$\sum P_y = 0 \rightarrow V = -\frac{P}{2}, \quad (a)$$

$$\sum M_z = 0 \rightarrow M = \frac{P}{2}x. \quad (b)$$

For  $l/2 \leq x < l$ , the free-body diagram is shown in Fig. 2.9c. Again,  $V$  and  $M$  are shown in the positive direction.

$$\sum P_y = 0 \rightarrow \frac{P}{2} - P + V = 0, \quad \text{or} \quad V = P/2. \quad (c)$$

$$\sum M_z = 0 \rightarrow M + P\left(x - \frac{l}{2}\right) - \frac{P}{2}x = 0.$$

Therefore,

$$M = \frac{P}{2}(l - x). \quad (d)$$

The shear and moment diagrams in Fig. 2.9d can be obtained directly from Eqs. (a) to (d).

## 2.8.2 Direct Integration

Note that if  $q(x)$  is the load intensity function in the  $y$ -direction, the transverse shear force is

$$V(x) = - \int_{-\infty}^x q(x) dx, \quad (2.4)$$

and the bending moment is

$$M(x) = - \int_{-\infty}^x V(x) dx = \int_{-\infty}^x \int_{-\infty}^x q(x) dx dx. \quad (2.5)$$

For simple loading cases, direct integration is often the most straightforward method of producing shear and moment diagrams. Since the integral of a curve is its area, graphically producing a shear or moment diagram follows directly from the loading. The only complication arises from point loadings and their use in developing a shear diagram. With concentrated loadings, the shear diagram will take a "jump" equal in magnitude to the applied load. The sign convention used for moment diagrams is important; recall that the sign convention described in Fig. 2.3b is used in this textbook.

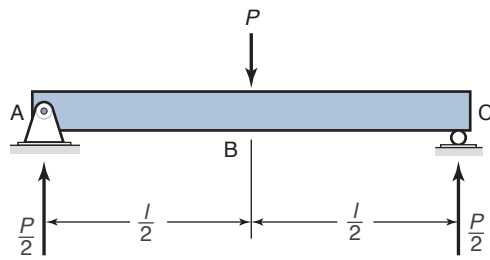
## Example 2.8: Shear and Moment Diagrams by Direct Integration

**Given:** The beam shown in Fig. 2.10a. From static equilibrium, it can be shown that  $R_A = 12$  kN and  $R_B = 4$  kN in the directions shown.

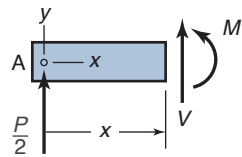
**Find:** The shear and moment diagrams by direct integration. Determine the location and magnitude of the largest shear force and moment.

**Solution:** The shear diagram will be constructed first. Consider the loads on the beam and work from left to right to construct the shear diagram. The following steps are followed to construct the shear diagram:

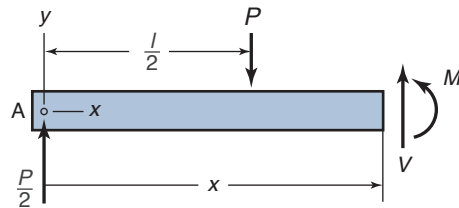
1. At the left end (at  $x = 0$ ), there is a downward acting force. As discussed above, this means that the shear diagram will see a jump in its value at  $x = 0$ . From Eq. (2.4), a downward acting load leads to an upward acting shear force (that is, its sign is opposite to the loading). Thus, the diagram jumps upward by a magnitude of 4 kN.
2. Moving to the right, this value is unchanged until  $x = 2$  m, where a 12 kN concentrated load acts upward. This results in a downward jump as shown.



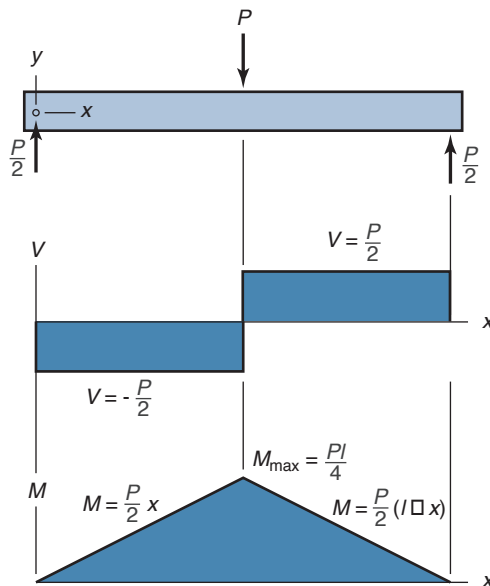
(a)



(b)

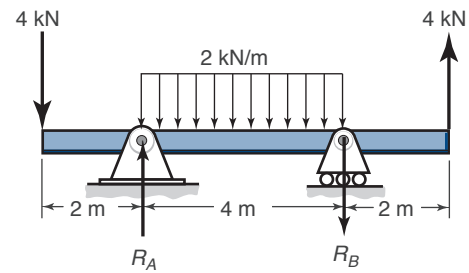


(c)

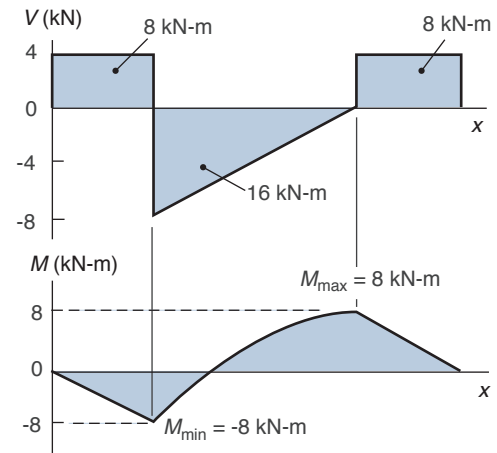


(d)

Figure 2.9: Simply supported beam. (a) Midlength load and reactions; (b) free-body diagram for  $0 < x < l/2$ ; (c) free-body diagram for  $l/2 \leq x < l$ ; (d) shear and moment diagrams.



(a)



(b)

Figure 2.10: Beam for Example 2.8. (a) Applied loads and reactions; (b) shear diagram with areas indicated, and moment diagram with maximum and minimum values indicated.

3. The constant distributed loading to the right of  $x = 2$  m will result in a shear force that changes linearly with respect to  $x$ . From Eq. (2.4), the magnitude of the total change is the integral of the applied load, or just its area. Thus, the total change due to the  $2\text{ kN/m}$  distributed load from  $x = 2$  to  $x = 6$  is  $8\text{ kN}$ , and since the distributed load acts downward, this change is upward in the shear diagram because of the sign convention used in Eq. (2.4). Therefore, the value of the shear force at  $x = 6$  is  $(-8\text{ kN}) + 8\text{ kN} = 0$ . The line from  $x = 2$  to  $x = 6$  is shown.
4. At  $x = 6$ , there is a concentrated force associated with the downwards acting force  $R_B$ , so there is an upward jump of  $4\text{ kN}$ .
5. At  $x = 8$ , the upward acting force leads to a downward jump of  $4\text{ kN}$ , returning the shear to zero.

The bending moment is obtained from repeated application of Eq. (2.5). However, note that the integral of the shear force is the area under the shear force curve. The shear diagram just developed consists of rectangles and triangles, where the area is calculated from geometry. The areas have been indicated in the shear diagram. For example, the shear diagram up to  $x = 2$  consists of a rectangle with a height of  $V = 4\text{ kN}$  and a base of  $x = 2\text{ m}$ . Thus, its area is  $8\text{ kN-m}$ .

The moment diagram is then constructed using the following steps.

1. At a starting value of  $M = 0$  at  $x = 0$ , the diagram will be constructed from left to right. From  $x = 0$  to  $x = 2$  m, the value of the shear diagram is positive and constant. Integrating this curve results in a linear profile. Since the shear diagram is positive, the moment that results must be negative according to Eq. (2.5), and at  $x = 2$  m, the value is 8 kN-m. This linear profile is shown in the figure.
2. From  $x = 2$  m to  $x = 6$  m, the shear diagram is linear with respect to  $x$ , so that the moment diagram will be quadratic. At  $x = 6$  m, it is known that the moment will have a value of 8 kN-m by summing the areas of the shear diagram segments. The slope of the moment curve is equal to the value of the shear curve, as seen by taking the derivative of Eq. (2.5). Thus, the slope is initially large and at  $x = 6$  it is zero.
3. From  $x = 6$  m to  $x = 8$  m, the moment diagram has a linear profile and ends at  $M = 0$ . This can be seen by summing the areas in the shear diagram, remembering that areas below the abscissa are considered negative.

The shear and moment diagrams are shown in Fig. 2.10b. It can be seen that the largest magnitude of shear stress is at  $x = 2$  m and has a value of  $|V|_{\max} = 8$  kN. The largest magnitude of bending moment is  $|M|_{\max} = 8$  kN-m.

### 2.8.3 Singularity Functions

If the loading is simple, the method for obtaining shear and moment diagrams described in Sections 2.8.1 or 2.8.2 can be used. Often, however, this is not the situation. For more complex loading, methods such as **singularity functions** can be used. A singularity function in terms of a variable,  $x$ , is written as

$$f_n(x) = \langle x - a \rangle^n. \quad (2.6)$$

where  $n$  is any integer (positive or negative) including zero, and  $a$  is a reference location on a beam. Singularity functions are denoted by using angular brackets. The advantage of using a singularity function is that it permits writing an analytical expression directly for the transverse shear and moment over a range of discontinuities.

Table 2.2 shows six singularity and load intensity functions along with corresponding graphs and expressions. Note in particular the inverse ramp example. A unit step is constructed beginning at  $x = a$ , and the ramp beginning at  $x = a$  is subtracted. To have the negative ramp discontinued at  $x = a + b$ , a positive ramp beginning at this point is constructed; the summation results in the desired loading.

### Design Procedure 2.3: Singularity Functions

Some general rules relating to singularity functions are:

1. If  $n > 0$  and the expression inside the angular brackets is positive (i.e.,  $x \geq a$ ), then  $f_n(x) = (x - a)^n$ . Note that the angular brackets to the right of the equal sign in Eq. (2.6) are now parentheses.
2. If  $n > 0$  and the expression inside the angular brackets is negative (i.e.,  $x < a$ ), then  $f_n(x) = 0$ .

3. If  $n < 0$ , then  $f_n(x) = 0$ .

4. If  $n = 0$ , then  $f_n(x) = 1$  when  $x \geq a$  and  $f_n(x) = 0$  when  $x < a$ .

5. If  $n \geq 0$ , the integration rule is

$$\int_{-\infty}^x \langle x - a \rangle^n = \frac{\langle x - a \rangle^{n+1}}{n + 1}.$$

Note that this is the same as if there were parentheses instead of angular brackets.

6. If  $n < 0$ , the integration rule is

$$\int_{-\infty}^x \langle x - a \rangle^n dx = \langle x - a \rangle^{n+1}.$$

7. When  $n \geq 1$ , then

$$\frac{d}{dx} \langle x - a \rangle^n = n \langle x - a \rangle^{n-1}.$$

### Design Procedure 2.4: Shear and Moment Diagrams by Singularity Functions

The procedure for drawing the shear and moment diagrams by making use of singularity functions is as follows:

1. Draw a free-body diagram with all the applied distributed and concentrated loads acting on the beam, and determine all support reactions. Resolve the forces into components acting perpendicular and parallel to the beam's axis.
2. Write an expression for the load intensity function  $q(x)$  that describes all the singularities acting on the beam. Use Table 2.2 as a reference, and make sure to "turn off" singularity functions for distributed loads and the like that do not extend across the full length of the beam.
3. Integrate the negative load intensity function over the beam length to get the shear force. Integrate the negative shear force distribution over the beam length to get the moment, in accordance with Eqs. (2.4) and (2.5).
4. Draw shear and moment diagrams from the expressions developed.

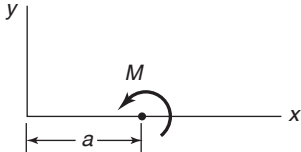
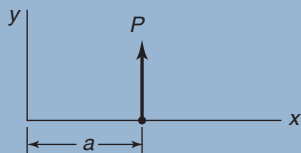
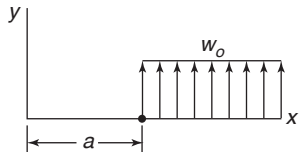
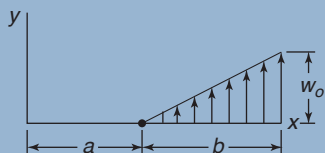
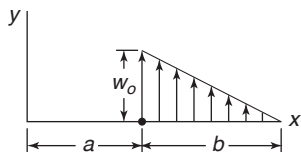
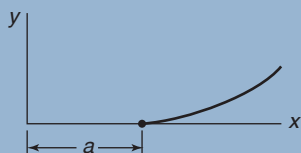
### Example 2.9: Shear and Moment Diagrams Using Singularity Functions

**Given:** The same conditions as in Example 2.7.

**Find:** Draw the shear and moment diagrams by using a singularity function for a concentrated force located midway on the beam.



Table 2.2: Singularity and load intensity functions with corresponding graphs and expressions.

Singularity	Graph of $q(x)$	Expression for $q(x)$
Concentrated moment		$q(x) = M \langle x - a \rangle^{-2}$
Concentrated force		$q(x) = P \langle x - a \rangle^{-1}$
Unit step		$q(x) = w_0 \langle x - a \rangle^0$
Ramp		$q(x) = \frac{w_0}{b} \langle x - a \rangle^1$
Inverse ramp		$q(x) = w_0 \langle x - a \rangle^0 - \frac{w_0}{b} \langle x - a \rangle^1$
Parabolic shape		$q(x) = \langle x - a \rangle^2$

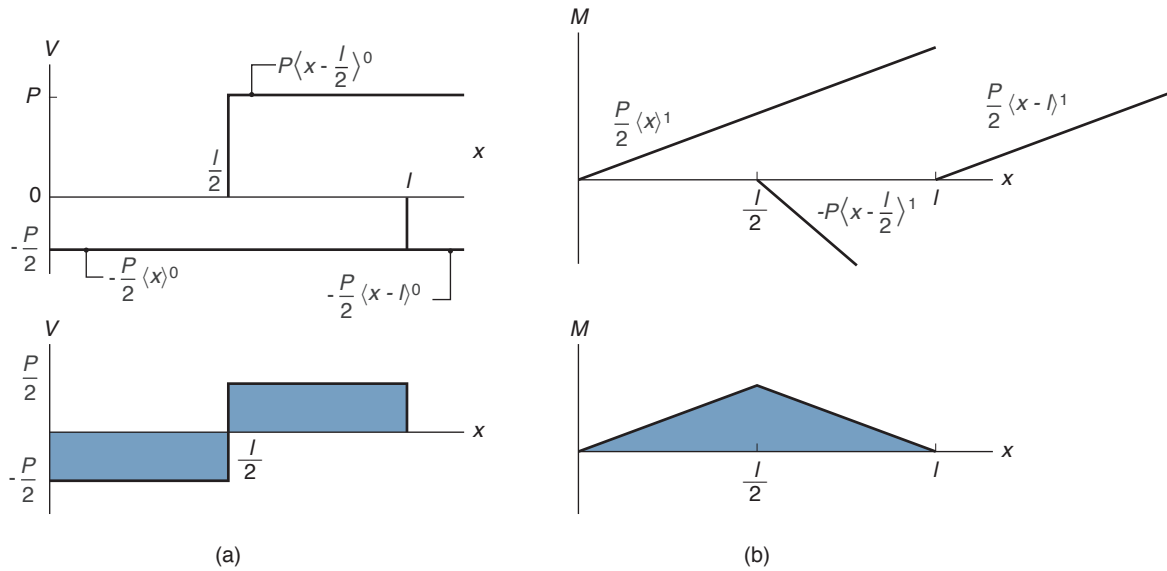


Figure 2.11: (a) Shear and (b) moment diagrams for Example 2.9.

**Solution:** The load intensity function for the simply supported beam shown in Fig. 2.9a is

$$q(x) = \frac{P}{2} \langle x \rangle^{-1} - P \left\langle x - \frac{l}{2} \right\rangle^{-1} + \frac{P}{2} \langle x - l \rangle^{-1}$$

The shear expression is

$$V(x) = - \int_{-\infty}^x \left[ \frac{P}{2} \langle x \rangle^{-1} - P \left\langle x - \frac{l}{2} \right\rangle^{-1} + \frac{P}{2} \langle x - l \rangle^{-1} \right] dx$$

or

$$V(x) = -\frac{P}{2} \langle x \rangle^0 + P \left\langle x - \frac{l}{2} \right\rangle^0 - \frac{P}{2} \langle x - l \rangle^0$$

Figure 2.11a shows the resulting shear diagrams. The diagram at the top shows individual shear, and the diagram below shows the composite of these shear components. The moment expression is

$$M(x) = - \int_{-\infty}^x \left[ -\frac{P}{2} \langle x \rangle^0 + P \left\langle x - \frac{l}{2} \right\rangle^0 - \frac{P}{2} \langle x - l \rangle^0 \right] dx$$

or

$$M(x) = \frac{P}{2} \langle x \rangle^1 - P \left\langle x - \frac{l}{2} \right\rangle^1 + \frac{P}{2} \langle x - l \rangle^1$$

Figure 2.11b shows the moment diagrams. The diagram at the top shows individual moments; the diagram at the bottom is the composite moment diagram. The slope of  $M_2$  is twice that of  $M_1$  and  $M_3$ , which are equal. The resulting shear and moment diagrams are the same as those found in Example 2.7.

### Example 2.10: Shear and Moment Expressions Using Singularity Functions

**Given:** A simply supported beam shown in Fig. 2.12a where  $P_1 = 8$  kN,  $P_2 = 5$  kN,  $w_o = 4$  kN/m, and  $l = 12$  m.

**Find:** The shear and moment expressions as well as their corresponding diagrams while using singularity functions.

**Solution:** The first task is to solve for the reactions at  $x = 0$  and  $x = l$ . The force representation is shown in Fig. 2.12b. Note that  $w_o$  is defined as the load per unit length for the central part of the beam. In Fig. 2.12b it can be seen that the unit step  $w_o$  over a length of  $l/2$  produces a resultant force of  $w_o l/2$  and that the positive ramp over the length of  $l/4$  can be represented by a resultant vector of

$$w_o \left( \frac{l}{4} \right) \left( \frac{1}{2} \right) \quad \text{or} \quad \frac{w_o l}{8}$$

Also, note that the resultant vector acts at

$$x = \left( \frac{2}{3} \right) \left( \frac{l}{4} \right) = \frac{l}{6}$$

From force equilibrium

$$0 = R_1 + P_1 + P_2 + R_2 - \frac{w_o l}{2} - \frac{w_o l}{8} \quad (a)$$

$$R_1 + R_2 = -P_1 - P_2 + \frac{5w_o l}{8} \quad (b)$$

Making use of moment equilibrium and the moment of the triangular section load gives

$$\frac{(P_1 + 2P_2)l}{4} - \frac{w_o l^2}{4} - \frac{w_o l}{8} \left( \frac{l}{6} \right) + R_2 l = 0$$

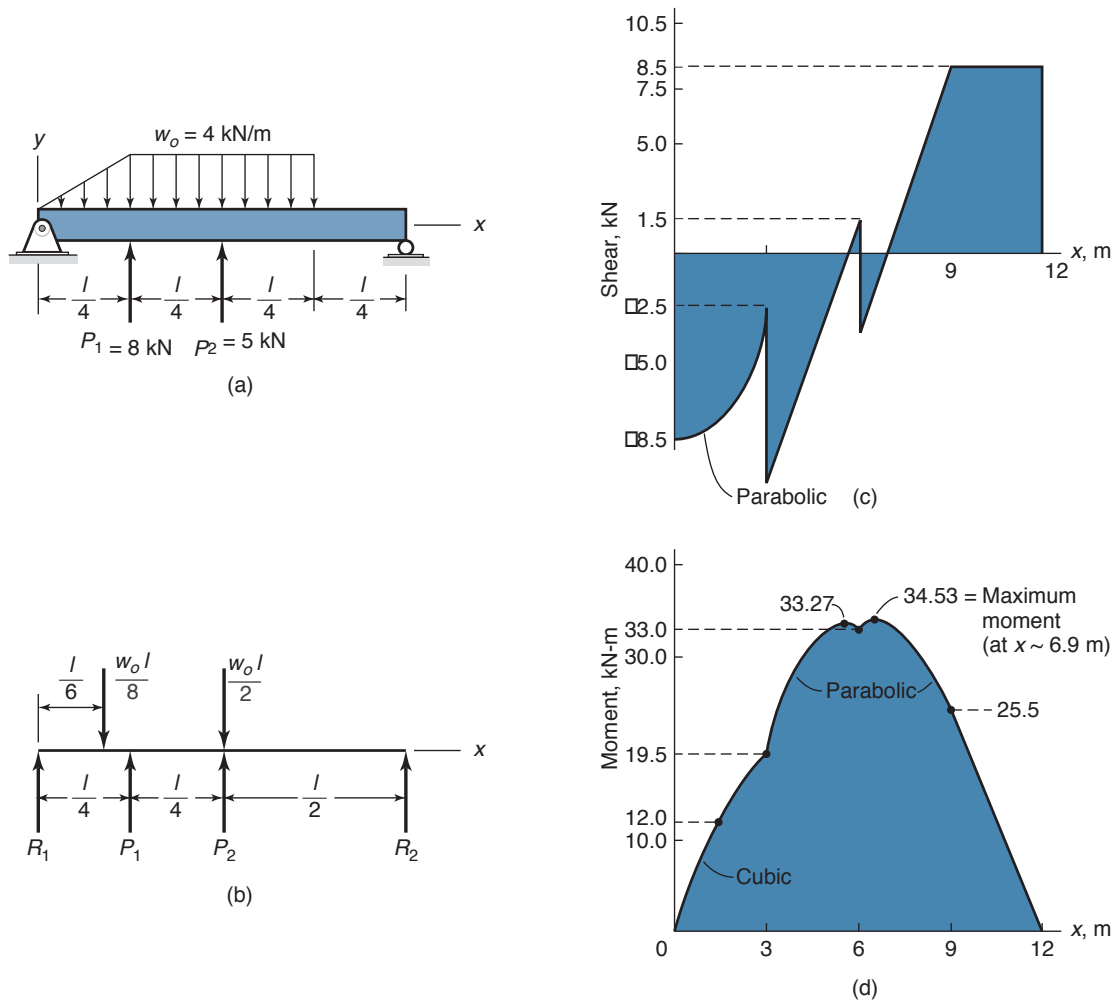


Figure 2.12: Simply supported beam examined in Example 2.10. (a) Forces acting on beam when  $P_1 = 8$  kN,  $P_2 = 5$  kN;  $w_o = 4$  kN/m;  $l = 12$  m; (b) free-body diagram showing resulting forces; (c) shear and (d) moment diagrams.

or

$$R_2 = \frac{13w_o l}{48} - \frac{P_1 + 2P_2}{4} \quad (c)$$

Substituting Eq. (c) into Eq. (b) gives

$$R_1 = -\frac{3P_1}{4} - \frac{P_2}{2} + \frac{17w_o l}{48} \quad (d)$$

Substituting the given values for  $P_1$ ,  $P_2$ ,  $w_o$ , and  $l$  gives

$$R_1 = 8.5 \text{ kN} \quad \text{and} \quad R_2 = 8.5 \text{ kN} \quad (e)$$

The load intensity function can be written as

$$\begin{aligned} q(x) = & R_1 \langle x \rangle^{-1} - \frac{w_o}{l/4} \langle x \rangle^1 + \frac{w_o}{l/4} \left\langle x - \frac{l}{4} \right\rangle^1 \\ & + P_1 \left\langle x - \frac{l}{4} \right\rangle^{-1} + P_2 \left\langle x - \frac{l}{2} \right\rangle^{-1} \\ & + w_o \left\langle x - \frac{3l}{4} \right\rangle^0 + R_2 \langle x - l \rangle^{-1} \end{aligned}$$

Note that a unit step beginning at  $l/4$  is created by initiating a ramp at  $x = 0$  acting in the negative direction and summing it with another ramp starting at  $x = l/4$  acting in the positive

direction, since the slopes of the ramps are the same. The second and third terms on the right side of the load intensity function produce this effect. The sixth term on the right side of the equation turns off the unit step. Integrating the load intensity function gives the shear force as

$$\begin{aligned} V(x) = & -R_1 \langle x \rangle^0 + \frac{2w_o}{l} \langle x \rangle^2 - \frac{2w_o}{l} \left\langle x - \frac{l}{4} \right\rangle^2 \\ & - P_1 \left\langle x - \frac{l}{4} \right\rangle^0 - P_2 \left\langle x - \frac{l}{2} \right\rangle^0 \\ & - w_o \left\langle x - \frac{3l}{4} \right\rangle^1 - R_2 \langle x - l \rangle^0 \end{aligned}$$

Integrating the shear force gives the moment, and substituting the values for  $w_o$  and  $l$  gives

$$\begin{aligned} M(x) = & 8.5 \langle x \rangle^1 + \frac{2}{9} \langle x \rangle^3 - \frac{2}{9} \langle x - 3 \rangle^3 + 8 \langle x - 3 \rangle^1 \\ & + 5 \langle x - 6 \rangle^1 + 2 \langle x - 9 \rangle^2 + 8.5 \langle x - 12 \rangle^1 \end{aligned}$$

The shear and moment diagrams are shown in Fig. 2.12c and d, respectively.

## 2.9 Stress

One of the fundamental problems in engineering is determining the effect of a loading environment on a part. This determination is an essential part of the design process; one cannot choose a dimension or a material without first understanding the intensity of force inside the component being analyzed. **Stress** is the term used to define the intensity and direction of the internal forces acting at a given point. Strength, on the other hand, is a property of a material and will be covered in later chapters.

For normal loading on a load-carrying member in which the external load is uniformly distributed over a cross-section, the magnitude of the average normal stress can be calculated from

$$\sigma_{\text{avg}} = \frac{\text{Average force}}{\text{Cross-sectional area}} = \frac{P}{A}. \quad (2.7)$$

Thus, the unit of stress is force per unit area. Consider a small area  $\Delta A$  on the cross section, and let  $\Delta P$  represent the internal forces acting on this small area. The average intensity of the internal forces transmitted by the area  $\Delta A$  is obtained by dividing  $\Delta P$  by  $\Delta A$ . If the internal forces transmitted across the section are assumed to be continuously distributed, the area  $\Delta A$  can be made increasingly smaller and will approach a point on the surface in the limit. The corresponding force  $\Delta P$  will also become increasingly smaller. The stress at the point on the cross section to which  $\Delta A$  converges is

$$\sigma = \lim_{\Delta A \rightarrow 0} \frac{\Delta P}{\Delta A} = \frac{dP}{dA}. \quad (2.8)$$

The stress at a point acting on a specific plane is a vector and thus has a magnitude and a direction. Its direction is the limiting direction  $\Delta P$  as area  $\Delta A$  approaches zero. Similarly, the shear stress can be defined in a specific plane. Thus, a stress must be defined with respect to a direction.

### Example 2.11: Stress in Beam Supports

**Given:** As shown in Fig. 2.13a, a 3-m-long beam is supported at the left end by a 6-mm-diameter steel wire and at the right end by a 10-mm-diameter steel cylinder. The bar carries a mass  $m_{a1} = 200$  kg and the bar's mass is  $m_{a2} = 50$  kg.

**Find:** Determine the stresses in the wire and in the cylinder.

**Solution:** The wire and cylinder areas are  $A_B = 28.27 \text{ mm}^2$  and  $A_C = 78.54 \text{ mm}^2$ . Figure 2.13b shows a free-body diagram of the forces acting on the bar. Moment equilibrium about point C gives

$$3R_B = 2(200)(9.81) + 1.5(50)(9.81) = 4660 \text{ N}$$

or  $R_B = 1553 \text{ N}$ . From force equilibrium,

$$R_B - m_{a1}g - m_{a2}g + R_C = 0$$

$$R_C = g(m_{a1} + m_{a2}) - R_B = 9.81(200 + 50) - 1553 = 900 \text{ N}$$

The stresses at points B and C are, from Eq. (2.7),

$$\sigma_B = \frac{R_B}{A_B} = \frac{1553}{28.27} = 54.93 \text{ N/mm}^2 = 54.93 \text{ MPa}$$

$$\sigma_C = -\frac{R_C}{A_C} = -\frac{900}{78.54} = -11.46 \text{ N/mm}^2 = -11.46 \text{ MPa}$$

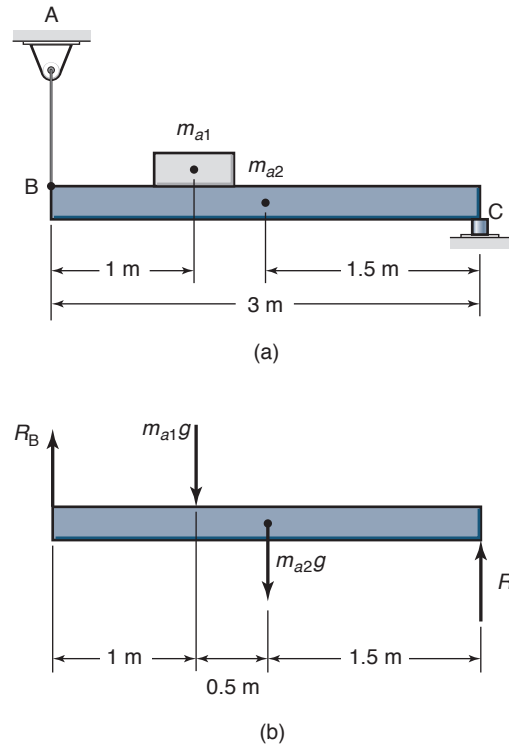


Figure 2.13: Figures used in Example 2.11. (a) Load assembly drawing; (b) free-body diagram.

## 2.10 Stress Element

Figure 2.14 shows a stress element with the origin of stress placed inside the element. Across each of the mutually perpendicular surfaces there are three stresses, yielding a total of nine stress components. Of the three stresses acting on a given surface, the normal stress is denoted by  $\sigma$  and the shear stress by  $\tau$ . A normal stress will receive a subscript indicating the direction in which the stress acts (e.g.,  $\sigma_x$ ). A shear stress requires two subscripts, the first to indicate the plane of the stress and the second to indicate its direction (e.g.,  $\tau_{xy}$ ). The **sign convention for normal stress** distinguishes positive for tension and negative for compression. A positive shear stress points in the positive direction of the coordinate axis denoted by the second subscript if it acts on a surface with an outward normal in the positive direction. The **sign convention for shear stress** is directly associated with the coordinate directions. If both the normal from the surface and the shear are in the positive direction or if both are in the negative direction, the shear stress is positive. Any other combinations of the normal and the direction of shear will produce a negative shear stress. The surface stresses of an element have the following relationships:

1. The normal and shear stress components acting on opposite sides of an element must be equal in magnitude but opposite in direction.
2. Moment equilibrium requires that the shear stresses be symmetric, implying that the subscripts can be reversed in order, or

$$\tau_{xy} = \tau_{yx}, \quad \tau_{xz} = \tau_{zx}, \quad \tau_{yz} = \tau_{zy}, \quad (2.9)$$

thus reducing the nine different stresses acting on the

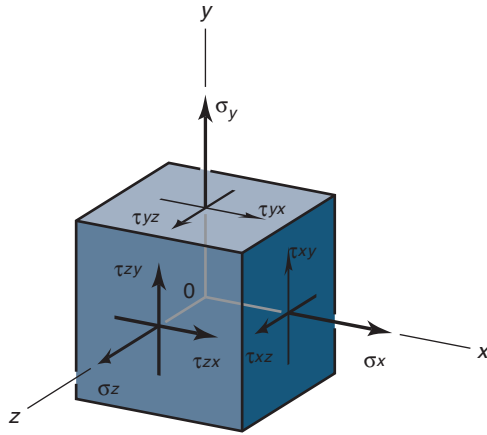


Figure 2.14: Stress element showing general state of three-dimensional stress with origin placed in center of element.

element to six: three normal stresses  $\sigma_x, \sigma_y, \sigma_z$  and three shear stresses  $\tau_{xy}, \tau_{yz}, \tau_{xz}$ .

The general laws of stress transformation, given in Appendix B (Section B.1), enable the determination of stresses acting on any new orthogonal coordinate system.

## Example 2.12: Stresses in Stress Element

**Given:** The stress element shown in Fig. 2.14 is put into a pressure vessel and pressurized to 10 MPa. An additional shear stress of 5 MPa acting on the bottom surface is directed in the positive  $x$ -direction.

**Find:** Are the stresses positive or negative?

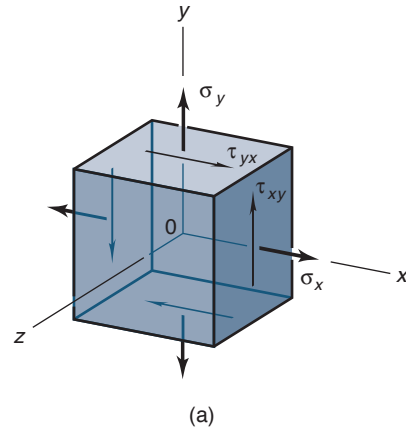
**Solution:** The normal stress here is thus  $\sigma = -10$  MPa. A positive pressure results in a negative normal stress by definition; since the element is loaded in compression by the pressure, it has a negative value. For the shear stress,  $\tau_{zx}$ , a positive shear stress is directed in the positive coordinate direction when the normal to the surface is directed in the positive coordinate direction. A shear stress acting on a surface with the normal in the negative coordinate direction is positive when the stress is directed in the negative coordinate direction. The shear stress in this problem acts on a surface with the normal in the negative  $y$ -direction, but the stress is directed in the positive  $x$ -direction. Thus, the shear is negative.

## 2.11 Stress Tensor

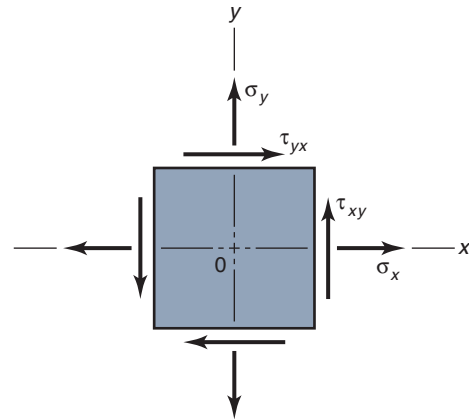
In engineering practice, it is common to encounter scalar quantities, those that have numerical value. Vectors, such as force, have a magnitude as well as a direction. Stress requires six quantities for its definition; thus, stress is a *tensor*. From the stress element of Fig. 2.14 and Eq. (2.9) the stress tensor is

$$\mathbf{S} = \begin{pmatrix} \sigma_x & \tau_{xy} & \tau_{xz} \\ \tau_{xy} & \sigma_y & \tau_{yz} \\ \tau_{xz} & \tau_{yz} & \sigma_z \end{pmatrix}, \quad (2.10)$$

which is a symmetrical tensor. A property of a symmetrical tensor is that there exists an equivalent tensor with an orthog-



(a)



(b)

Figure 2.15: Stress element showing two-dimensional state of stress. (a) Three-dimensional view; (b) plane view.

onal set of axes 1, 2, and 3 (called *principal axes*) with respect to which the tensor elements are all zero except for those in the principal diagonal; thus,

$$\mathbf{S}' = \begin{pmatrix} \sigma_1 & 0 & 0 \\ 0 & \sigma_2 & 0 \\ 0 & 0 & \sigma_3 \end{pmatrix}, \quad (2.11)$$

where  $\sigma_1, \sigma_2$ , and  $\sigma_3$  are principal stresses and will be discussed further below. Note that no shear stresses occur in Eq. (2.11).

## 2.12 Plane Stress

Many cases of stress analysis can be simplified to the case of **plane stress**, where the stresses all occur inside one plane. This is a common and valuable simplification, as the third direction can thus be neglected, and all stresses on the stress element act on two pairs of faces rather than three, as shown in Fig. 2.15. This two-dimensional stress state is sometimes called **biaxial** or **plane stress**.

In comparing the two views of the plane stress element shown in Fig. 2.15, note that all stresses shown in Fig. 2.15b act on surfaces perpendicular to the paper, with the paper being designated as either the  $x$ - $y$  plane or the  $z$  plane. The stresses shown in Fig. 2.15 all have positive values in accordance with the conventions presented in Section 2.10.



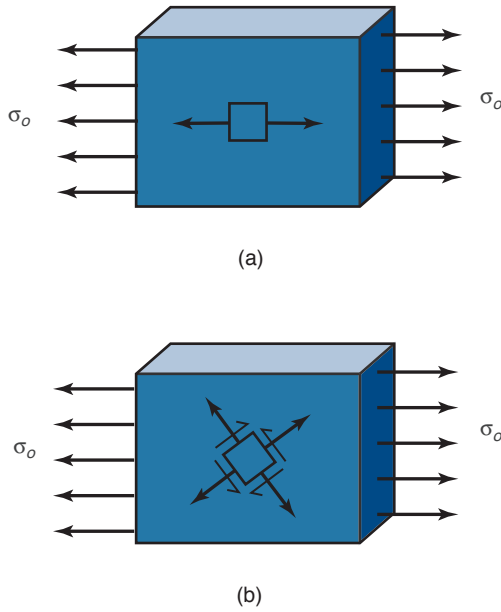


Figure 2.16: Illustration of equivalent stress states. (a) Stress element oriented in the direction of applied stress; (b) stress element oriented in different (arbitrary) direction.

The magnitude of stress depends greatly on the coordinate system orientation. For example, consider the stress element shown in Fig. 2.16a. When a uniform stress is applied to the element, the stress state is clearly  $\sigma_x = \sigma_o$ ,  $\sigma_y = 0$ , and  $\tau_{xy} = 0$ . However, if the original orientation of the element were as shown in Fig. 2.16b, this would no longer be the case, and all stress components in the plane would be nonzero. A profound question can be raised at this point: How does the material know the difference between these stress states? The answer is that there is no difference between the stress states of Fig. 2.16, so that they are *equivalent*. Obviously, it is of great importance to be able to transform stresses from one orientation to another, and the resultant stress transformation equations will be of great use throughout the remainder of the text.

Consider if, instead of the stresses acting as shown in Fig. 2.15b, they act in an oblique plane at angle  $\phi$  as shown in Fig. 2.17. The stresses  $\sigma_x$ ,  $\sigma_y$ , and  $\tau_{xy}$  can then be determined in terms of the stresses on an inclined surface whose normal stress makes an angle  $\phi$  with the  $x$ -axis.

Note from Fig. 2.17 that if the area of the inclined surface is  $A$  (length of the surface times the thickness into the paper), the area of the horizontal side of the triangular element will be  $A \sin \phi$ , and the area of the vertical side,  $A \cos \phi$ . From force equilibrium

$$\begin{aligned} \sigma_\phi A &= \tau_{xy} \sin \phi A \cos \phi + \tau_{yx} \cos \phi A \sin \phi \\ &\quad + \sigma_x \cos \phi A \cos \phi + \sigma_y \sin \phi A \sin \phi. \end{aligned}$$

This reduces to

$$\sigma_\phi = 2\tau_{xy} \sin \phi \cos \phi + \sigma_x \cos^2 \phi + \sigma_y \sin^2 \phi. \quad (2.12)$$

By using trigonometric identities for the double angle, Eq. (2.12) can be written as

$$\sigma_\phi = \frac{\sigma_x + \sigma_y}{2} + \frac{\sigma_x - \sigma_y}{2} \cos 2\phi + \tau_{xy} \sin 2\phi. \quad (2.13)$$

Similarly, from force equilibrium, the shear stress in the oblique plane can be expressed as

$$\tau_\phi = \tau_{xy} \cos 2\phi - \frac{\sigma_x - \sigma_y}{2} \sin 2\phi. \quad (2.14)$$

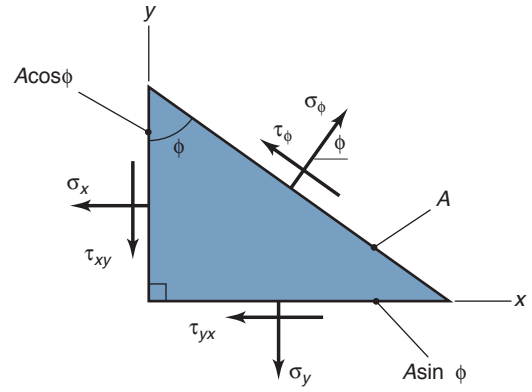


Figure 2.17: Stresses in an oblique plane at an angle  $\phi$ .

Equations (2.13) and (2.14) have maximum and minimum values that are of particular interest in stress analysis. The angle  $\phi_\sigma$ , which gives the extreme value of  $\sigma_\phi$ , can be determined by differentiating  $\sigma_\phi$  with respect to  $\phi$  and setting the result equal to zero, giving

$$\frac{d\sigma_\phi}{d\phi} = -(\sigma_x - \sigma_y) \sin 2\phi_\sigma + 2\tau_{xy} \cos 2\phi_\sigma = 0$$

or

$$\tan 2\phi_\sigma = \frac{2\tau_{xy}}{\sigma_x - \sigma_y}. \quad (2.15)$$

where  $\phi_\sigma$  is the angle where normal stress is extreme. Equation (2.15) has two roots,  $180^\circ$  apart, and for the double-angle nature of the left side of Eq. (2.15) this suggests roots of  $\phi_\sigma$  being  $90^\circ$  apart. One of these roots corresponds to the maximum value of normal stress, the other to the minimum value.

Substituting Eq. (2.15) into Eqs. (2.13) and (2.14) gives the following after some algebraic manipulation:

$$\sigma_{1,2} = \frac{\sigma_x + \sigma_y}{2} \pm \sqrt{\tau_{xy}^2 + \frac{(\sigma_x - \sigma_y)^2}{4}}, \quad (2.16)$$

$$\tau_{\phi_\sigma} = 0. \quad (2.17)$$

At this stress element orientation, where the normal stresses are extreme, the shear stress is zero. The axes that define this orientation are called the **principal axes**, and the normal stresses from Eq. (2.16) are called the **principal normal stresses**. Principal stresses are given numerical subscripts to differentiate them from stresses at any other orientation. A common convention is to order the principal stresses according to

$$\sigma_1 \geq \sigma_2 \geq \sigma_3. \quad (2.18)$$

In plane stress, one of the principal stresses is always zero.

Another orientation of interest is the one where the shear stress takes an extreme value. Differentiating Eq. (2.14) with respect to  $\phi$  and solving for  $\tau$  gives the orientation  $\phi_\tau$ , with resulting extreme shear stress of

$$\tau_{\max}, \tau_{\min} = \tau_1, \tau_2 = \pm \sqrt{\left(\frac{\sigma_x - \sigma_y}{2}\right)^2 + \tau_{xy}^2} \quad (2.19)$$

and

$$\sigma_{\phi_\tau} = \frac{\sigma_x + \sigma_y}{2}. \quad (2.20)$$

The shear stresses from Eq. (2.19) are called **principal shear stresses**. Thus, on the stress element oriented to

## Mohr's Circle

achieve a maximum shear stress, the normal stresses on the two faces are equal. Also, it can be shown that

$$|\phi_r - \phi_\sigma| = \frac{\pi}{4}. \quad (2.21)$$

In summary, for a plane stress situation where  $\sigma_x$ ,  $\sigma_y$ , and  $\tau_{xy}$  are known, the normal and shear stresses  $\sigma_\phi$  and  $\tau_\phi$  can be determined for any oblique plane at angle  $\phi$  from Eqs. (2.13) and (2.14). Also, the principal normal and shear stresses  $\sigma_1$ ,  $\sigma_2$ ,  $\tau_1$ , and  $\tau_2$  can be determined from Eqs. (2.16) and (2.19).

If the principal normal stresses  $\sigma_1$  and  $\sigma_2$  are known, the normal and shear stresses at any oblique plane at angle  $\phi$  can be determined from the following equations:

$$\sigma_\phi = \frac{\sigma_1 + \sigma_2}{2} + \frac{\sigma_1 - \sigma_2}{2} \cos 2\phi \quad (2.22)$$

$$\tau_\phi = \frac{\sigma_1 - \sigma_2}{2} \sin 2\phi. \quad (2.23)$$

In Eq. (2.23) a second subscript is not needed because  $\tau_\phi$  represents a shear stress acting on any oblique plane at angle  $\phi$  as shown in Fig. 2.17.

### Example 2.13: Stress Transformation

**Given:** A thin, square steel plate is oriented in the  $x$ - and  $y$ -directions. A tensile stress,  $\sigma$ , acts on the four sides. Thus,  $\sigma_x = \sigma_y = \sigma$ .

**Find:** The normal and shear stresses acting on the diagonal of the plate.

**Solution:** From Eq. (2.13),

$$\sigma_\phi = \frac{\sigma_x + \sigma_y}{2} + \frac{\sigma_x - \sigma_y}{2} \cos 2\phi + \tau_{xy} \sin 2\phi$$

Thus,

$$\sigma_{45^\circ} = \frac{\sigma + \sigma}{2} + \frac{\sigma - \sigma}{2} \cos 90^\circ + \tau_{xy} \sin 90^\circ = \sigma$$

Similarly, from Eq. (2.14)

$$\tau_\phi = \tau_{xy} \cos 2\phi - \frac{\sigma_x - \sigma_y}{2} \sin 2\phi$$

Therefore,

$$\tau_{45^\circ} = \tau_{xy} \cos 90^\circ - \frac{\sigma - \sigma}{2} \sin 90^\circ = 0$$

## 2.13 Mohr's Circle

**Mohr's circle** for a triaxial state of stress at a point was first constructed in 1914 by a German engineer, Otto Mohr, who noted that Eqs. (2.13) and (2.14) define a circle in a  $\sigma$ - $\tau$  plane. This circle is used extensively as a convenient method of graphically visualizing the state of stress acting in different planes passing through a given point. The approach used in this text is first to apply Mohr's circle to a two-dimensional stress state; a three-dimensional stress state is discussed in Section 2.14. Indeed, Mohr's circle is most useful for stress visualization in plane stress situations.

Figure 2.18 shows a typical Mohr's circle diagram. A number of observations can be made:

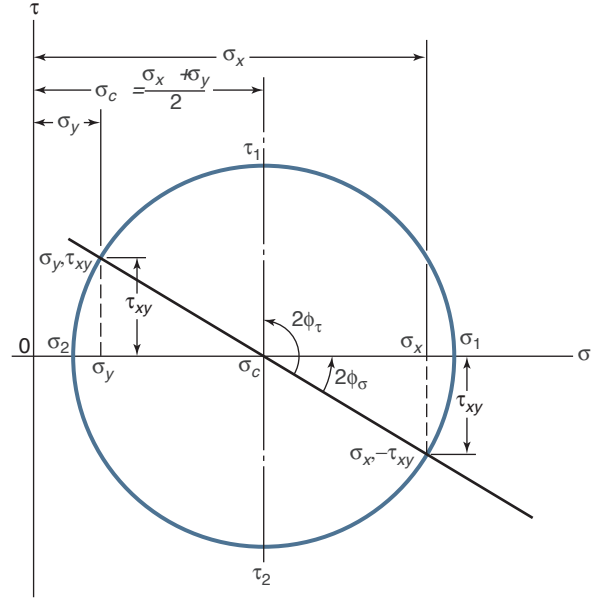


Figure 2.18: Mohr's circle diagram of Eqs. (2.13) and (2.14).

1. Normal stresses are plotted along the abscissa ( $x$ -axis), and shear stresses are plotted on the ordinate ( $y$ -axis).
2. The circle defines all stress states that are equivalent.
3. The biaxial stress state for any direction can be scaled directly from the circle.
4. The principal normal stresses (i.e., the extreme values of normal stress) are at the locations where the circle intercepts the  $x$ -axis.
5. The maximum shear stress equals the radius of the circle.
6. A rotation from a reference stress state in the real plane of  $\phi$  corresponds to a rotation of  $2\phi$  from the reference points in the Mohr's circle plane.

### Design Procedure 2.5: Mohr's Circle

The steps in constructing and using Mohr's circle in two dimensions are as follows:

1. Calculate the plane stress state for any  $x$ - $y$  coordinate system so that  $\sigma_x$ ,  $\sigma_y$ , and  $\tau_{xy}$  are known.
2. The center of the Mohr's circle can be placed at

$$\left( \frac{\sigma_x + \sigma_y}{2}, 0 \right). \quad (2.24)$$

3. Two points diametrically opposite to each other on the circle correspond to the points  $(\sigma_x, -\tau_{xy})$  and  $(\sigma_y, \tau_{xy})$ . Using the center and either point allows one to draw the circle.
4. The radius of the circle can be calculated from stress transformation equations or through geometry by using the center and one point on the circle. For example, the radius is the distance between points  $(\sigma_x, -\tau_{xy})$  and the center, which directly leads to

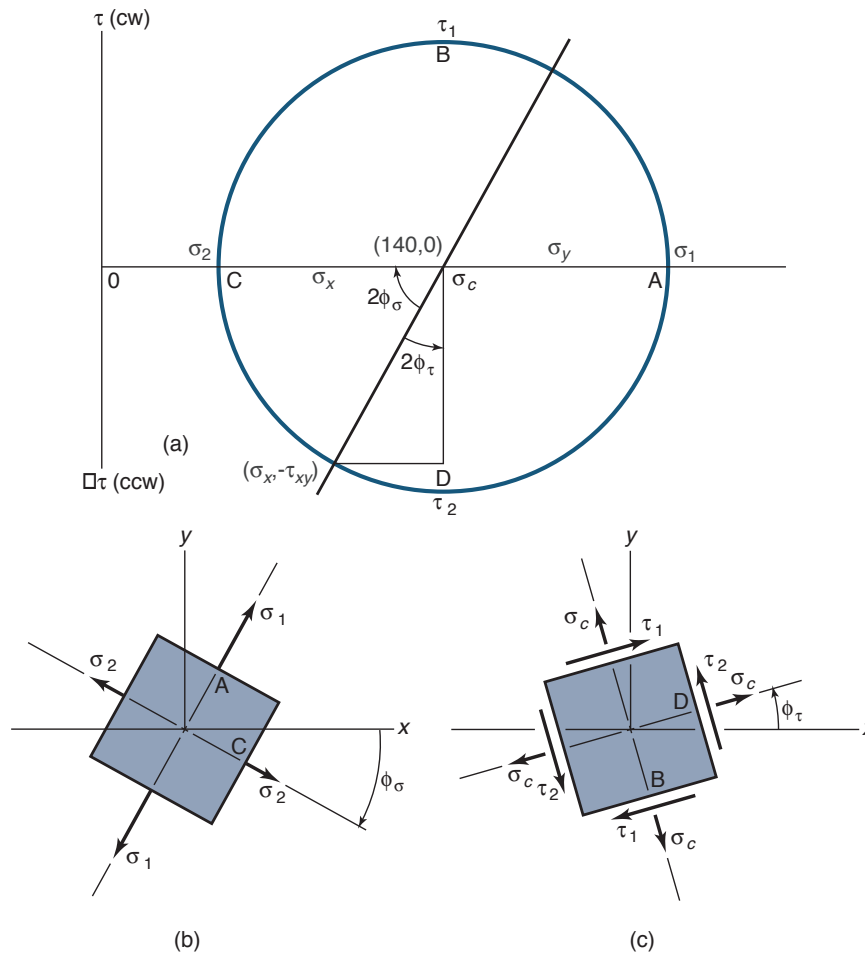


Figure 2.19: Results from Example 2.14. (a) Mohr's circle diagram; (b) stress element for principal normal stress shown in  $x$ - $y$  coordinates; (c) stress element for principal shear stresses shown in  $x$ - $y$  coordinates.

$$r = \sqrt{\left(\frac{\sigma_x - \sigma_y}{2}\right)^2 + \tau_{xy}^2} \quad (2.25)$$

5. The principal stresses have the values  $\sigma_{1,2} = \text{center} \pm \text{radius}$ .
6. The maximum shear stress equals the radius.
7. The principal axes can be found by calculating the angle between the  $x$ -axis in the Mohr's circle plane and the point  $(\sigma_x, -\tau_{xy})$ . The principal axes in the real plane are rotated one-half this angle in the same direction relative to the  $x$ -axis in the real plane.
8. The stresses in an orientation rotated  $\phi$  from the  $x$ -axis in the real plane can be read by traversing an arc of  $2\phi$  in the same direction on the Mohr's circle from the reference points  $(\sigma_x, -\tau_{xy})$  and  $(\sigma_y, \tau_{xy})$ . The new points on the circle correspond to the new stresses  $(\sigma_{x'}, -\tau_{x'y'})$  and  $(\sigma_{y'}, \tau_{x'y'})$ , respectively.

## Example 2.14: Mohr's Circle

**Given:** The plane stresses  $\sigma_x = 90$  MPa,  $\sigma_y = 190$  MPa, and  $\tau_{xy} = 80$  MPa.

**Find:** Draw the Mohr's circle and find the principal normal and shear stresses in the  $x$ - $y$  plane. Determine the stress state when the axes are rotated  $15^\circ$  counterclockwise.

**Solution:** This solution will demonstrate the eight-step approach given in Design Procedure 2.5, with the first step already done in the problem statement. Step 2 advises to calculate the center of the circle and place it at  $(\sigma_c, 0)$ , where

$$\sigma_c = \frac{\sigma_x + \sigma_y}{2} = \frac{(90 + 190)}{2} = 140 \text{ MPa}.$$

According to Step 3, either point  $(\sigma_x, -\tau_{xy})$  or  $(\sigma_y, \tau_{xy})$  can be used to draw the circle. This has been done with the point  $(\sigma_x, -\tau_{xy}) = (90 \text{ MPa}, -80 \text{ MPa})$  to draw the circle as shown in Fig. 2.19. From Step 4 and from the triangle defined by the  $x$ -axis and the point  $(\sigma_x, -\tau_{xy})$ , the radius can be calculated as

$$r = \sqrt{(90 - 140)^2 + (-80)^2} = 94.3 \text{ MPa}.$$

From Step 5 the principal stresses have the values  $\sigma_{1,2} = 140 \pm 94.3$ , or  $\sigma_1 = 234.3$  MPa and  $\sigma_2 = 45.7$  MPa. From Step 6, the maximum shear stress equals the radius, or  $\tau_{\max} = 94.3$  MPa. The principal stress orientation can be determined, if desired, from trigonometry. In the Mohr's circle plane (Fig. 2.19a), the point  $(\sigma_x, -\tau_{xy})$  makes an angle of  $2\phi = \tan^{-1}(80/50) = 58^\circ$  with the  $x$ -axis. To reach the point on the  $x$ -axis, an arc of this angle is needed in the clockwise direction on the Mohr's circle. Thus, the principal plane is  $\phi = 29^\circ$  clockwise from the  $x$ -axis. Finally, the stresses at an angle of  $15^\circ$  can be obtained From Eqs. (2.13) and (2.14) using

$$\sigma_{y'} = 140 + (94.3) \cos 28^\circ = 223.2 \text{ MPa},$$

$$\tau_{x'y'} = (94.3) \sin 28^\circ = 44.3 \text{ MPa}.$$

Figure 2.19b shows an element of the principal normal stresses as well as the appropriate value of  $\phi_\sigma$ . Figure 2.19c shows an element of the principal shear stresses as well as the appropriate value of  $\phi_\tau$ . The stress at the center of the Mohr's circle diagram is also represented in Fig. 2.19c along with the principal shear stresses.

## 2.14 Three-Dimensional Stresses

The general laws of strain transformation, given in Appendix B, enable the determination of strains acting on any orthogonal coordinate system. Considering the general situation shown in Fig. 2.14, the stress element has six faces, implying that there are three principal directions and three principal stresses  $\sigma_1$ ,  $\sigma_2$ , and  $\sigma_3$ . Six stress components ( $\sigma_x$ ,  $\sigma_y$ ,  $\sigma_z$ ,  $\tau_{xy}$ ,  $\tau_{xz}$ , and  $\tau_{yz}$ ) are required to specify a general state of stress in three dimensions, in contrast to the three stress components ( $\sigma_x$ ,  $\sigma_y$ , and  $\tau_{xy}$ ) that were used for two-dimensional (plane or biaxial) stress. Determining the principal stresses for a three-dimensional situation is much more difficult. The process involves finding the three roots to the cubic equation

$$\begin{aligned} 0 = & \sigma^3 - (\sigma_x + \sigma_y + \sigma_z) \sigma^2 + \\ & (\sigma_x \sigma_y + \sigma_x \sigma_z + \sigma_y \sigma_z - \tau_{xy}^2 - \tau_{yz}^2 - \tau_{zx}^2) \sigma \\ & - (\sigma_x \sigma_y \sigma_z + 2\tau_{xy} \tau_{yz} \tau_{zx} - \sigma_x \tau_{yz}^2 - \sigma_y \tau_{zx}^2 - \sigma_z \tau_{xy}^2). \end{aligned} \quad (2.26)$$

In most design situations many of the stress components are zero, greatly simplifying evaluation of this equation.

If the principal orientation of an element associated with a three-dimensional stress state, as well as the principal stresses, is known, this condition is called **triaxial stress**. Figure 2.20 shows a Mohr's circle for a triaxial stress state. It consists of three circles, two externally tangent and inscribed within the third circle. The principal shear stresses shown in Fig. 2.20 are determined from

$$\tau_{1/2} = \frac{\sigma_1 - \sigma_2}{2}, \quad \tau_{2/3} = \frac{\sigma_2 - \sigma_3}{2}, \quad \tau_{1/3} = \frac{\sigma_1 - \sigma_3}{2}. \quad (2.27)$$

The principal normal stresses must be ordered as described in Eq. (2.18). From Eq. (2.27), the maximum principal shear stress is  $\tau_{1/3}$ .

A Mohr's circle can be generated for triaxial stress states, but this is often unnecessary. In most circumstances it is not necessary to know the orientations of the principal stresses; it is sufficient to know their values. Thus, Eq. (2.26) is usually all that is needed.

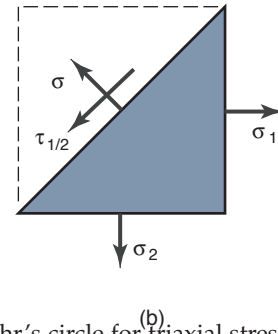
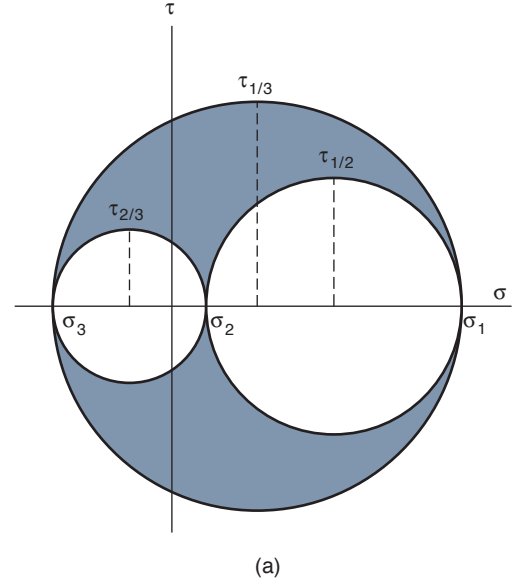


Figure 2.20: Mohr's circle for triaxial stress state. (a) Mohr's circle representation; (b) principal stresses on two planes.

### Example 2.15: Three-Dimensional Mohr's Circle

**Given:** Assume that the principal normal stresses obtained in Example 2.14 are the same for triaxial consideration with  $\sigma_3 = 0$ . That is,  $\sigma_1 = 234.3$  MPa,  $\sigma_2 = 45.7$  MPa, and  $\sigma_3 = 0$ .

**Find:**

- Determine the principal shear stresses for a triaxial stress state and draw the appropriate Mohr's circle diagram.
- If the shear stress  $\tau_{xy}$  is changed from 80 to 160 MPa, show how the Mohr's circles for the biaxial and triaxial stress states change.

**Solution:**

- From Eq. (2.27), the principal shear stresses in a triaxial stress state are

$$\tau_{1/2} = \frac{\sigma_1 - \sigma_2}{2} = \frac{234.3 - 45.7}{2} = 94.3 \text{ MPa},$$

$$\tau_{2/3} = \frac{\sigma_2 - \sigma_3}{2} = \frac{45.7}{2} = 22.85 \text{ MPa},$$

$$\tau_{1/3} = \frac{\sigma_1 - \sigma_3}{2} = \frac{(234.3 - 0)}{2} = 117.15 \text{ MPa}.$$

Figure 2.21a shows the appropriate Mohr's circle diagram for the triaxial stress state.

(b) If the shear stress in Example 2.14 is doubled ( $\tau_{xy} = 160$  MPa instead of 80 MPa), Eq. (2.19) gives

$$\begin{aligned}\tau_1, \tau_2 &= \pm \sqrt{\tau_{xy}^2 + \left(\frac{\sigma_x - \sigma_y}{2}\right)^2} \\ &= \pm \sqrt{160^2 + \left(\frac{90 - 190}{2}\right)^2} \text{ MPa} \\ &= \pm 167.6 \text{ MPa}.\end{aligned}$$

The principal normal stresses for the biaxial stress state are

$$\begin{aligned}\sigma_1 &= \sigma_c + \tau_1 = 140 + 167.6 = 307.6 \text{ MPa}, \\ \sigma_2 &= \sigma_c - \tau_2 = 140 - 167.6 = -27.6 \text{ MPa}.\end{aligned}$$

Figure 2.21b shows the resultant Mohr's circle diagram for the biaxial stress state. In a triaxial stress state that is ordered  $\sigma_1 = 307.6$  MPa,  $\sigma_2 = 0$ , and  $\sigma_3 = -27.6$  MPa, from Eq. (2.27) the principal shear stresses can be written as

$$\begin{aligned}\tau_{1/2} &= \frac{\sigma_1 - \sigma_2}{2} = \frac{307.6 - 0}{2} \text{ MPa} = 153.8 \text{ MPa}, \\ \tau_{2/3} &= \frac{\sigma_2 - \sigma_3}{2} = \frac{0 + 27.6}{2} \text{ MPa} = 13.8 \text{ MPa}, \\ \tau_{1/3} &= \frac{\sigma_1 - \sigma_3}{2} = \frac{307.6 + 27.6}{2} \text{ MPa} = 167.6 \text{ MPa}.\end{aligned}$$

Figure 2.21c shows the Mohr's circle diagram for the triaxial stress state. From Fig. 2.21b and c, the maximum shear stress in the biaxial stress state,  $\tau_1$ , is equivalent to  $\tau_{1/3}$ , the maximum shear stress in the triaxial stress state. However, comparing Figs. 2.19a and 2.21a shows that the maximum shear stress in the plane (or biaxial) stress state is not equal to that in the triaxial stress state. Furthermore, the maximum triaxial stress is larger than the maximum biaxial stress. Thus, if  $\sigma_1$  and  $\sigma_2$  have the same sign in the biaxial stress state, the triaxial maximum stress  $\tau_{1/3}$  must be used for design considerations. However, if  $\sigma_1$  and  $\sigma_2$  have opposite signs in the biaxial stress state, the maximum biaxial and triaxial shear stresses will be the same and either one can be used in the analysis.

## 2.15 Octahedral Stresses

Sometimes it is advantageous to represent the stresses on an octahedral stress element rather than on a conventional cubic element of principal stresses. Figure 2.22 shows the orientation of one of the eight octahedral planes that are associated with a given stress state. Each **octahedral plane** cuts across a corner of a principal element, so that the eight planes together form an octahedron (Fig. 2.22). The following characteristics of the stresses on a octahedral plane should be noted:

1. Identical normal stresses act on all eight planes. Thus, the normal stresses tend to compress or enlarge the octahedron but do not distort it.
2. Identical shear stresses act on all eight planes. Thus, the shear stresses tend to distort the octahedron without changing its volume.

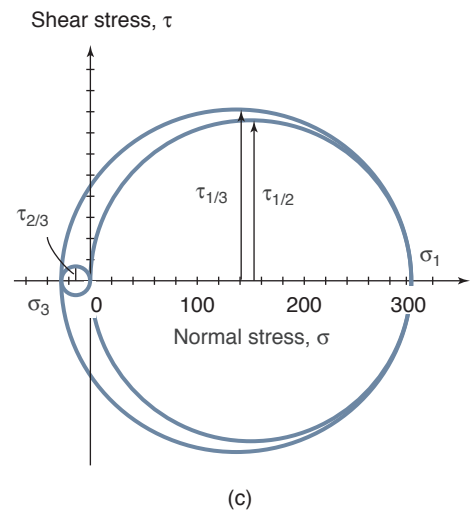
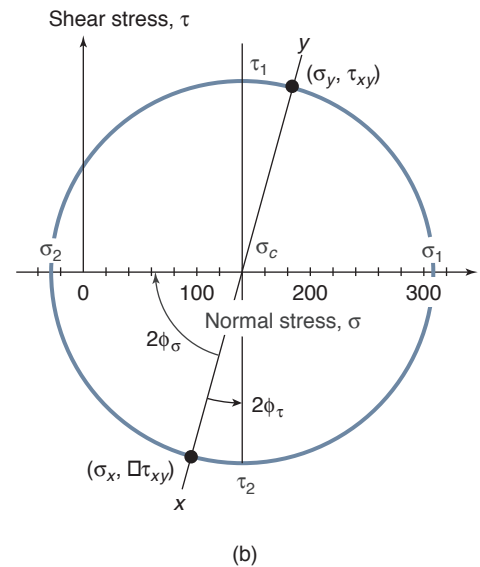
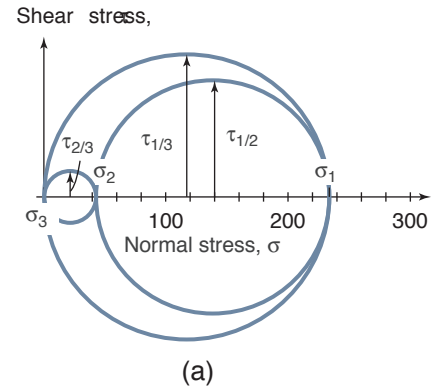


Figure 2.21: Mohr's circle diagrams for Example 2.15. (a) Triaxial stress state when  $\sigma_1 = 234.3$  MPa,  $\sigma_2 = 457$  MPa and  $\sigma_3 = 0$ ; (b) biaxial stress state when  $\sigma_1 = 307.6$  MPa and  $\sigma_2 = -27.6$  MPa; (c) triaxial stress state when  $\sigma_1 = 307.6$  MPa,  $\sigma_2 = 0$ , and  $\sigma_3 = -27.6$  MPa.



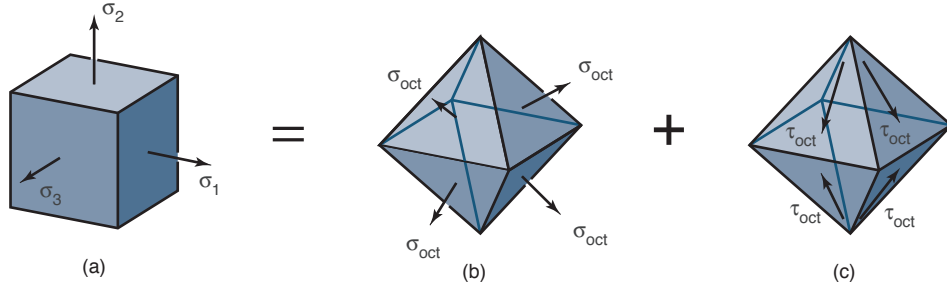


Figure 2.22: Stresses acting on octahedral planes. (a) General state of stress; (b) normal stress; (c) octahedral shear stress.

The fact that the normal and shear stresses are the same for the eight planes is a powerful tool in failure analysis.

The normal octahedral stress can be expressed in terms of the principal normal stresses, or the stresses in the  $x, y, z$  coordinates, as

$$\sigma_{\text{oct}} = \frac{\sigma_1 + \sigma_2 + \sigma_3}{3} = \frac{\sigma_x + \sigma_y + \sigma_z}{3}, \quad (2.28)$$

$$\begin{aligned} \tau_{\text{oct}} &= \frac{1}{3} [(\sigma_1 - \sigma_2)^2 + (\sigma_2 - \sigma_3)^2 + (\sigma_3 - \sigma_1)^2]^{1/2} \\ &= \frac{2}{3} [\tau_{1/2}^2 + \tau_{2/3}^2 + \tau_{1/3}^2]^{1/2}. \end{aligned} \quad (2.29)$$

In terms of octahedral normal stresses,

$$\begin{aligned} 9\tau_{\text{oct}}^2 &= (\sigma_x - \sigma_y)^2 + (\sigma_y - \sigma_z)^2 + (\sigma_z - \sigma_x)^2 \\ &\quad + 6(\tau_{xy}^2 + \tau_{yz}^2 + \tau_{xz}^2). \end{aligned} \quad (2.30)$$

### Example 2.16: Octahedral Stresses

**Given:** Consider the stress state from Example 2.15, where  $\sigma_1 = 234.5$  MPa,  $\sigma_2 = 45.7$  MPa, and  $\sigma_3 = 0$ .

**Find:** Determine the octahedral stresses.

**Solution:** The normal and octahedral stress can be written as

$$\sigma_{\text{oct}} = \frac{\sigma_1 + \sigma_2 + \sigma_3}{3} = \frac{(234.3 + 45.7 + 0)}{3} = 93.3 \text{ MPa}.$$

The shear octahedral stress from Eq. (2.29) can be written as

$$\begin{aligned} \tau_{\text{oct}} &= \frac{2}{3} [\tau_{1/2}^2 + \tau_{2/3}^2 + \tau_{1/3}^2]^{1/2} \\ &= \frac{2}{3} [94.3^2 + 22.9^2 + 117.2^2]^{1/2} \\ &= 101.4 \text{ MPa}. \end{aligned}$$

Just as the direction and intensity of the stress at any given point are important with respect to a specific plane passing through that point, the same is true for strain. Thus, just as for stress, strain is a tensor. Also, just as there are normal and shear stresses, so too there are normal and shear strains. **Normal strain**, designated by the symbol  $\epsilon$ , is used to describe a measure of the elongation or contraction of a linear segment of an element in which stress is applied. The average normal strain is

$$\epsilon_{\text{avg}} = \frac{\delta}{l} = \frac{\text{Average elongation}}{\text{Original length}}. \quad (2.31)$$

Note that strain is dimensionless. Furthermore, the strain at a point is

$$\epsilon = \lim_{\Delta l \rightarrow 0} \frac{\Delta \delta_{\text{avg}}}{\Delta l} = \frac{d\delta_{\text{avg}}}{dl}. \quad (2.32)$$

Figure 2.23 shows the strain on a cubic element subjected to uniform tension in the  $x$ -direction. The element elongates in the  $x$ -direction while simultaneously contracting in the  $y$ - and  $z$ -directions, a phenomenon known as the **Poisson effect**, and discussed further in Section 3.5.2. From Eq. (2.32), the normal strain components can be written as

$$\epsilon_x = \lim_{x \rightarrow 0} \frac{\delta_x}{x}, \quad \epsilon_y = \lim_{y \rightarrow 0} \frac{\delta_y}{y}, \quad \epsilon_z = \lim_{z \rightarrow 0} \frac{\delta_z}{z}. \quad (2.33)$$

Figure 2.24 shows the shear strain of a cubic element due to shear stress in both a three-dimensional view and a two-dimensional (or plane) view. The **shear strain**, designated by  $\gamma$ , is used to measure angular distortion (the change in angle between two lines that are orthogonal in the undeformed state). The shear strain as shown in Fig. 2.24 is defined as

$$\gamma_{yx} = \lim_{y \rightarrow 0} \frac{\delta_x}{y} = \tan \theta_{yx} \approx \theta_{yx}, \quad (2.34)$$

where  $\theta_{yx}$  is the angle representing deviation from initial right angle. Note that a small angle approximation has been used for  $\theta_{yx}$  in Eq. (2.34).

The subscripts used to define the shear strains are like those used to define the shear stresses in Section 2.10. The first subscript designates the coordinate direction perpendicular to the plane in which the strain acts, and the second subscript designates the coordinate direction in which the strain acts. For example,  $\gamma_{yx}$  is the strain resulting from taking adjacent planes perpendicular to the  $y$ -axis and displacing them relative to each other in the  $x$ -direction. The sign conventions for strain follow directly from those developed for stress. A positive stress produces a positive strain and a negative stress produces a negative strain. The shear strain shown in Fig. 2.24 and described in Eq. (2.34) is positive. The strain

## 2.16 Strain

**Strain** is defined as the displacement per length produced in a solid as the result of stress. In designing a machine element, not only must the design be adequate when considering the stress relative to the strength, but it must also be ensured that the displacements and/or deformations are not excessive and are within design constraints. Depending on the application, these deformations may be either highly visible or practically unnoticeable.

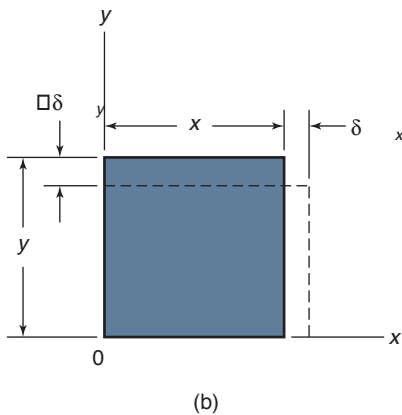
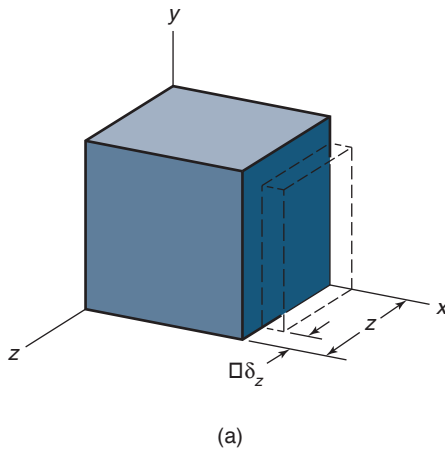


Figure 2.23: Normal strain of cubic element subjected to uniform tension in  $x$ -direction. (a) Three-dimensional view; (b) two-dimensional (or plane) view.

of the cubic element thus contains three normal strains and six shear strains, just as found for stresses. Similarly, symmetry reduces the number of shear strain elements from six to three.

### Example 2.17: Calculation of Strain

**Given:** A 300-mm-long circular aluminum bar with a 50-mm diameter is subjected to a 125-kN axial load. The axial elongation is 0.2768 mm and the diameter is decreased by 0.01522 mm.

**Find:** The transverse and axial strains in the bar.

**Solution:** The axial strain is

$$\epsilon_a = \frac{\delta}{l} = \frac{0.2768}{300} = 9.227 \times 10^{-4}$$

The transverse strain is

$$\epsilon_t = \frac{\delta_t}{d} = \frac{-0.01522}{50} = -3.044 \times 10^{-4}$$

The sign for the transverse strain is negative because the diameter decreased after the bar was loaded. The axial strain is positive because the axial length increased after loading. Note that strain has no dimension, although it is commonly reported in units of m/m or  $\mu\text{m}/\text{m}$ .

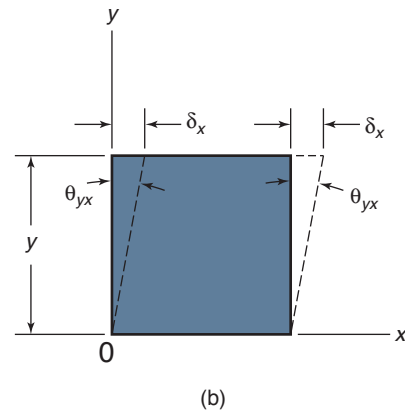
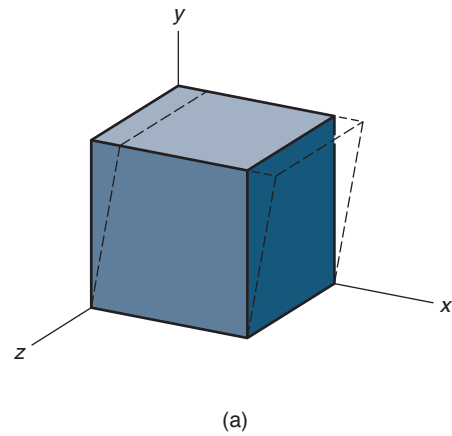


Figure 2.24: Shear strain of cubic element subjected to shear stress. (a) Three-dimensional view; (b) two-dimensional (or plane) view.

## 2.17 Strain Tensor

For strains within the elastic range, the equations relating normal and shear strains with the orientation of the cutting plane are analogous to the corresponding equations for stress given in Eq. (2.10). Thus, the state of strain can be written as a tensor:

$$\mathbf{T} = \begin{pmatrix} \epsilon_x & \frac{1}{2}\gamma_{xy} & \frac{1}{2}\gamma_{xz} \\ \frac{1}{2}\gamma_{xy} & \epsilon_y & \frac{1}{2}\gamma_{yz} \\ \frac{1}{2}\gamma_{xz} & \frac{1}{2}\gamma_{yz} & \epsilon_z \end{pmatrix} \quad (2.35)$$

In comparing Eq. (2.35) with Eq. (2.10) note that  $\epsilon_x$ ,  $\epsilon_y$ , and  $\epsilon_z$  are analogous to  $\sigma_x$ ,  $\sigma_y$ , and  $\sigma_z$ , respectively, but it is half of the shear strain,  $\gamma_{xy}/2$ ,  $\gamma_{yz}/2$ ,  $\gamma_{zx}/2$  that is analogous to  $\tau_{xy}$ ,  $\tau_{yz}$ , and  $\tau_{zx}$ , respectively.

## 2.18 Plane Strain

Instead of the six strains for the complete strain tensor, in plane strain the components  $\epsilon_z$ ,  $\gamma_{xz}$ , and  $\gamma_{yz}$  are zero. Thus, only two normal strain components,  $\epsilon_x$  and  $\epsilon_y$ , and one shear strain component,  $\gamma_{xy}$ , are considered. Figure 2.25 shows the deformation of an element caused by each of the three strains considered in plane strain. The normal strain components  $\epsilon_x$  and  $\epsilon_y$ , shown in Fig. 2.25a and b, are produced by changes in element length in the  $x$ - and  $y$ -directions, respectively. The

shear strain  $\gamma_{xy}$ , shown in Fig. 2.25c, is produced by the relative rotation of two adjacent sides of the element. Figure 2.25c also helps to explain the physical significance that  $\tau$  is analogous to  $\gamma/2$  rather than to  $\gamma$ . Each side of an element changes in slope by an angle  $\gamma/2$  when subjected to pure shear.

The following sign convention is to be used for strains:

1. Normal strains  $\epsilon_x$  and  $\epsilon_y$  are positive if they cause elongation along the  $x$ - and  $y$ -axes, respectively. In Fig. 2.25a and b,  $\epsilon_x$  and  $\epsilon_y$  are positive.
2. Shear strain  $\gamma_{xy}$  is positive when the interior angle of a strain element (A0B in Fig. 2.25c) becomes smaller than  $90^\circ$ .

The principal strains, planes, and directions are directly analogous to those found earlier for principal stresses. The principal normal strains in the  $x$ - $y$  plane, the maximum shear strain in the  $x$ - $y$  plane, and the orientation of the principal axes relative to the  $x$ - and  $y$ -axes are

$$\epsilon_1, \epsilon_2 = \frac{\epsilon_x + \epsilon_y}{2} \pm \sqrt{\left(\frac{1}{2}\gamma_{xy}\right)^2 + \left(\frac{\epsilon_x - \epsilon_y}{2}\right)^2}, \quad (2.36)$$

$$\gamma_{\max} = \pm 2\sqrt{\left(\frac{1}{2}\gamma_{xy}\right)^2 + \left(\frac{\epsilon_x - \epsilon_y}{2}\right)^2}, \quad (2.37)$$

$$2\phi = \tan^{-1} \left( \frac{\gamma_{xy}}{\epsilon_x - \epsilon_y} \right). \quad (2.38)$$

From here there are two important problem classes:

1. If the principal strains are known and it is desired to find the strains acting at a plane oriented at angle  $\phi$  from the principal direction, the equations are

$$\epsilon_\phi = \frac{\epsilon_1 + \epsilon_2}{2} + \frac{\epsilon_1 - \epsilon_2}{2} \cos 2\phi, \quad (2.39)$$

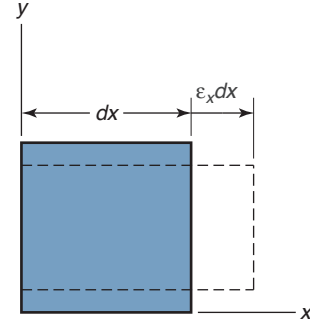
$$\gamma_\phi = (\epsilon_1 - \epsilon_2) \sin 2\phi. \quad (2.40)$$

In Eq. (2.40),  $\gamma_\phi$  represents a shear strain acting on the  $\phi$  plane and directed  $90^\circ$  from the  $\phi$ -axis. Just as for stress, the second subscript is omitted for convenience and no ambiguity results. A Mohr's circle diagram can also be used to represent the state of strain.

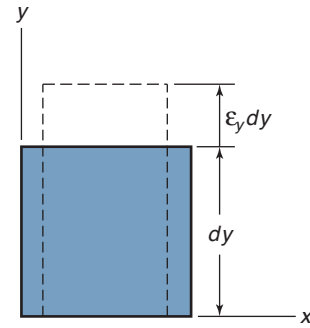
2. The second problem of interest is the case where a normal strain component has been measured in three different but specified directions and it is desired to obtain the strains  $\epsilon_x$ ,  $\epsilon_y$ , and  $\gamma_{xy}$  from these readings. In this case the equation

$$\epsilon_\theta = \epsilon_x \cos^2 \theta + \epsilon_y \sin^2 \theta + \gamma_{xy} \sin \theta \cos \theta \quad (2.41)$$

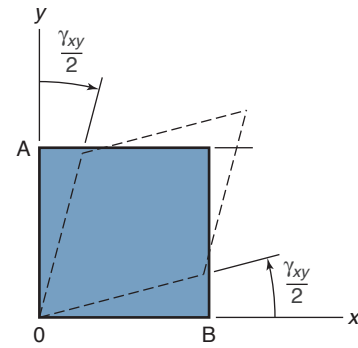
is of great assistance. Here,  $\epsilon_\theta$  is the measured strain in the direction rotated  $\theta$  counterclockwise from the  $x$ -axis, and  $\epsilon_x$ ,  $\epsilon_y$ , and  $\gamma_{xy}$  are the desired strains. Thus, measuring a strain in three different directions gives three equations for the three unknown strains and is sufficient for their quantification. Strain gages are often provided in groups of three, called *rosettes*, for such purposes.



(a)



(b)



(c)

Figure 2.25: Graphical depiction of plane strain element. (a) Normal strain  $\epsilon_x$ ; (b) normal strain  $\epsilon_y$ ; and (c) shear strain  $\gamma_{xy}$ .

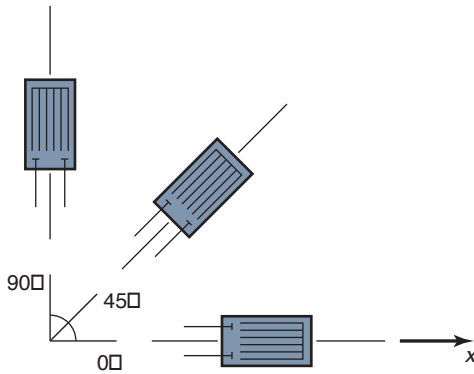


Figure 2.26: Strain gage rosette used in Example 2.18.

### Example 2.18: Strain Gage Rosette

**Given:** A  $0^\circ - 45^\circ - 90^\circ$  strain gage rosette as shown in Fig. 2.25 is attached to a structure with the  $0^\circ$  gage placed along a reference ( $x$ ) axis. Upon loading, the strain in the  $0^\circ$  direction reads  $+50 \mu\text{m/m}$ , the strain gage in the  $45^\circ$  direction reads  $-27 \mu\text{m/m}$ , and the gage in the  $90^\circ$  direction reads 0.

**Find:** The strains  $\epsilon_x$ ,  $\epsilon_y$ , and  $\gamma_{xy}$ .

**Solution:** Equation (2.41) can be applied three times to obtain three equations:

$$\epsilon_{0^\circ} = 50 \mu\text{m/m} = \epsilon_x \cos^2(0^\circ) + \epsilon_y \sin^2(0^\circ) + \gamma_{xy} \sin 0^\circ \cos 0^\circ$$

$$\text{or } \epsilon_x = 50 \mu\text{m/m},$$

$$\epsilon_{90^\circ} = 0 = \epsilon_x \cos^2(90^\circ) + \epsilon_y \sin^2(90^\circ) + \gamma_{xy} \sin 90^\circ \cos 90^\circ$$

$$\text{or } \epsilon_y = 0, \text{ and}$$

$$\epsilon_{45^\circ} = \epsilon_x \cos^2(45^\circ) + \epsilon_y \sin^2(45^\circ) + \gamma_{xy} \sin 45^\circ \cos 45^\circ$$

$$\text{or } \gamma_{xy} = -27 - 50 - 0 = -77 \mu\text{m/m}.$$

## 2.19 Summary

This chapter described how load, stress, and strain affect the design of machine elements. If the proper type of machine element has been selected, a potential cause of failure is the design stress exceeding the strength of the machine element. Therefore, it is important to evaluate the stress, strain, and strength of the machine element at the critical section. To do so first requires a determination of load in all its forms. The applied load on a machine element was described with respect to time, the area over which load is applied, and the location and method of application. Furthermore, the importance of support reactions, application of static force and moment equilibrium, and proper use of free-body diagrams were investigated.

The chapter then focused on shear and moment diagrams applied to a beam. Singularity functions introduced by concentrated moment, concentrated force, unit step, ramp, inverse ramp, and parabolic shape were considered. Various combinations of these singularity functions can exist within a beam. Integrating the load intensity function for the various beam singularity functions over the beam length estab-

lishes the shear force. Integrating the shear force over the beam length determines the moment. From these analytical expressions the shear and moment diagrams can be readily constructed.

Stress defines the intensity and direction of the internal forces at a particular point and acting on a given plane. The stresses acting on an element have normal and shear components. Across each mutually perpendicular surface there are two shear stresses and one normal stress, yielding a total of nine stresses (three normal stresses and six shear stresses). The sign conventions for both the normal and shear stresses were presented. The nine stress components may be regarded as the components of a second-order Cartesian tensor. It was found that the stress tensor is symmetrical, implying that the tensor can be written with zero shear stress and the principal normal stresses along its diagonal.

In many engineering applications, stress analysis assumes that a surface is free of stress or that the stress in one plane is small relative to the stresses in the other two planes. The two-dimensional stress situation is called the biaxial (or plane) stress state and can be expressed in terms of two normal stresses and one shear stress, for example  $\sigma_x$ ,  $\sigma_y$ , and  $\tau_{xy}$ . That the stresses can be expressed in any oblique plane is important in deriving and applying Mohr's circle for a biaxial stress.

The concepts of strain and deflection were also investigated, since these are often design constraints. Just as with stress, strain is a tensor, and transformation equations and Mohr's circle are equally applicable to strain analysis. The concept of strain gage rosettes was introduced as a method to obtain plane strains.

## Key Words

**beam** structural member designed to support loads perpendicular to its longitudinal axis

**bending load** load applied transversely to longitudinal axis of member

**biaxial or plane stress** condition where one surface is comparatively free of stress

**cantilevered beam** support where one end is fixed and the other end is free

**combined load** combination of two or more previously defined loads

**concentrated load** load applied to small nonconformal area

**critical section** section where largest internal stress occurs

**cyclic load** load varying throughout a cycle

**distributed load** load distributed over entire area

**free-body diagram** sketch of part showing all acting forces

**impact load** load rapidly applied

**loads** force, moment, or torque applied to a mechanism or structure

**Mohr's circle** method used to graphically visualize state of stress acting in different planes passing through a given point

**normal load** load passing through centroid of resisting section

## Recommended Readings

**normal strain** elongation or contraction of linear segment of element in which stress is applied

**overhanging beam** support where one or both ends freely extend past support

**principal normal stresses** combination of applied normal and shear stresses that produces maximum principal normal stress or minimum principal normal stress, with a third principal stress between or equivalent to the extremes

**principal shear stresses** combination of applied normal and shear stresses that produces maximum principal shear stress or minimum principal shear stress

**shear load** load collinear with transverse shear force

**shear strain** measure of angular distortion in which shear stress is applied

**sign convention for normal strain** positive if elongation is in direction of positive axes

**sign conversion for normal stress** positive for tension and negative for compression

**sign convention for shear strain** positive if interior angle becomes smaller after shear stress is applied

**sign convention for shear stress** positive if both normal from surface and shear are in positive or negative direction; negative for any other combination

**simply supported beam** support where one end is pinned and the other is roller-supported

**singularity functions** functions used to evaluate shear and moment diagrams, especially when discontinuities, such as concentrated load or moment, exist

**static load** load gradually applied and equilibrium reached in a short time

**strain** dimensionless displacement produced in solid as a result of stress

**stress** intensity and direction of internal force acting at a given point on a particular plane

**sustained load** a load that is constant over a long time

**symmetrical tensor** condition where principal normal stresses exist while all other tensor elements are zero

**torsion load** a load that results in twisting deformation

**triaxial stress** stress where all surfaces are considered

**uniaxial stress** condition where two perpendicular surfaces are comparatively free of stress

## Summary of Equations

Force equilibrium:  $\sum P_x = 0, \sum P_y = 0, \sum P_z = 0$

Moment equilibrium:  $\sum M_x = 0, \sum M_y = 0, \sum M_z = 0$

Transverse shear in beams:  $V(x) = - \int_{-\infty}^x q(x) dx$

Bending moment in beams:  $M(x) = - \int_{-\infty}^x V(x) dx$

Principal stresses in plane stress:

$$\sigma_1, \sigma_2 = \frac{\sigma_x + \sigma_y}{2} \pm \sqrt{\tau_{xy}^2 + \frac{(\sigma_x - \sigma_y)^2}{4}}$$

Mohr's circle

$$\text{Center: } \left( \frac{\sigma_x + \sigma_y}{2}, 0 \right)$$

$$\text{Radius: } r = \sqrt{\left( \frac{\sigma_x - \sigma_y}{2} \right)^2 + \tau_{xy}^2}$$

Octahedral Stresses:

$$\text{Normal: } \sigma_{\text{oct}} = \frac{\sigma_1 + \sigma_2 + \sigma_3}{3} = \frac{\sigma_x + \sigma_y + \sigma_z}{3}$$

Shear:

$$\begin{aligned} \tau_{\text{oct}} &= \frac{1}{3} [(\sigma_1 - \sigma_2)^2 + (\sigma_2 - \sigma_3)^2 + (\sigma_3 - \sigma_1)^2]^{1/2} \\ &= \frac{2}{3} [\tau_{1/2}^2 + \tau_{2/3}^2 + \tau_{1/3}^2]^{1/2} \end{aligned}$$

Principal strains in plane strain:

$$\epsilon_1, \epsilon_2 = \frac{\epsilon_x + \epsilon_y}{2} \pm \sqrt{\left( \frac{1}{2} \gamma_{xy} \right)^2 + \left( \frac{\epsilon_x - \epsilon_y}{2} \right)^2}$$

## Recommended Readings

- Beer, F.P., Johnson, E.R., DeWolf, J., and Mazurek, D. (2011) *Mechanics of Materials*, 6th ed., McGraw-Hill.
- Craig, R.R. (2011) *Mechanics of Materials*, 3rd ed., Wiley.
- Hibbeler, R.C. (2010) *Mechanics of Materials*, 8th ed. Prentice-Hall, Upper Saddle River.
- Popov, E.P. (1968) *Introduction to Mechanics of Solids*, Prentice-Hall.
- Popov, E.P. (1999) *Engineering Mechanics of Solids*, 2nd ed., Prentice-Hall.
- Riley, W.F., Sturges, L.D., and Morris, D.H. (2006) *Mechanics of Materials*, 6th ed., Wiley.
- Shames, I.H., and Pitarresi, J.M. (2000) *Introduction to Solid Mechanics*, 3rd ed., Prentice-Hall.
- Ugural, A.C. (2007) *Mechanics of Materials*, Wiley.

## Questions

- 2.1 What is a concentrated load? What is a distributed load?
- 2.2 What kind of reaction occurs with a roller support? What occurs with a pin?
- 2.3 Define *static equilibrium*.
- 2.4 What is a simply supported beam? What is a cantilever?
- 2.5 Why are singularity functions useful?
- 2.6 Under what conditions does a singularity function *not* equal zero?
- 2.7 Define the terms *stress* and *strain*.
- 2.8 What is a tensor?
- 2.9 Define *normal stress* and *shear stress*.
- 2.10 What is Mohr's circle?
- 2.11 What is a principal stress?
- 2.12 What are the units for stress? What are the units for strain?



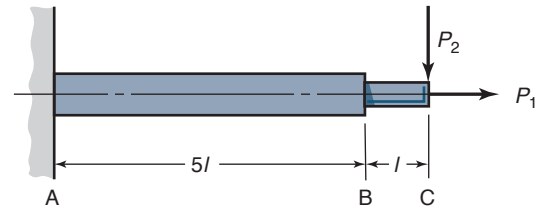
- 2.13 What are octahedral stresses?
- 2.14 What is elongation?
- 2.15 What is a rosette?

## Qualitative Problems

- 2.16 Give three examples of (a) static loads; (b) sustained loads; (c) impact loads; and (d) cyclic loads.
- 2.17 Explain the sign convention for shear forces.
- 2.18 Explain the common sign conventions for bending moments. Which is used in this book?
- 2.19 Without the use of equations, explain a methodology for producing shear and moment diagrams.
- 2.20 Give two examples of scalars, vectors, and tensors.
- 2.21 Explain the difference between plane stress and plain strain. Give an example of each.
- 2.22 Without the use of equations, qualitatively determine the bending moment diagram for a bookshelf.
- 2.23 Explain why  $\tau_{xy} = \tau_{yx}$ .
- 2.24 Define and give two examples of (a) uniaxial stress state; (b) biaxial stress state; and (c) triaxial stress state.
- 2.25 Sketch and describe the characteristics of a three-dimensional Mohr's circle.
- 2.26 What are the similarities and differences between deformation and strain?
- 2.27 The text stated that  $0^\circ$ – $45^\circ$ – $90^\circ$  strain gage rosettes are common. Explain why.
- 2.28 Draw a free body diagram of a book on a table.
- 2.29 If the three principal stresses are determined to be 100 MPa,  $-50$  MPa and 75 MPa, which is  $\sigma_2$ ?
- 2.30 Derive Eq. (2.16).

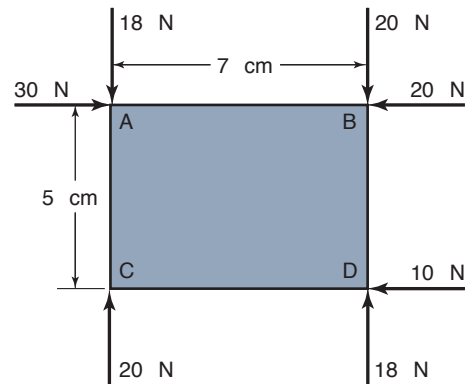
## Quantitative Problems

- 2.31 The stepped shaft A-B-C shown in Sketch *a* is loaded with the forces  $P_1$  and/or  $P_2$ . Note that  $P_1$  gives a tensile stress  $\sigma$  in B-C and  $\sigma/4$  in A-B and that  $P_2$  gives a bending stress  $\sigma$  at B and  $1.5\sigma$  at A. What is the critical section
- (a) If only  $P_1$  is applied?
- (b) If only  $P_2$  is applied?
- (c) If both  $P_1$  and  $P_2$  are applied?



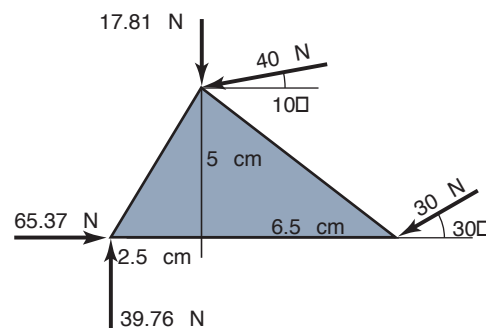
Sketch *a*, used in Problems 2.31 and 2.32.

- 2.32 The stepped shaft in Sketch *a* has loads  $P_1$  and  $P_2$ . Find the load classification if  $P_1$ 's variation is sinusoidal and  $P_2$  is the load from a weight
- (a) If only  $P_1$  is applied
- (b) If only  $P_2$  is applied
- (c) If both  $P_1$  and  $P_2$  are applied
- 2.33 A bar hangs freely from a frictionless hinge. A horizontal force  $P$  is applied at the bottom of the bar until it inclines  $45^\circ$  from the vertical direction. Calculate the horizontal and vertical components of the force on the hinge if the acceleration due to gravity is  $g$ , the bar has a constant cross section along its length, and the total mass is  $m_a$ . *Ans.*  $R_x = \frac{1}{2}m_a g$ ,  $R_y = m_a g$ .
- 2.34 Sketch *b* shows the forces acting on a rectangle. Is the rectangle in equilibrium? *Ans.* No.



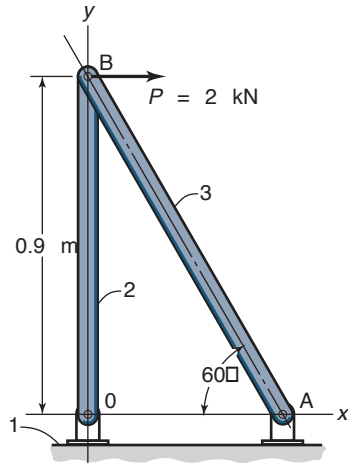
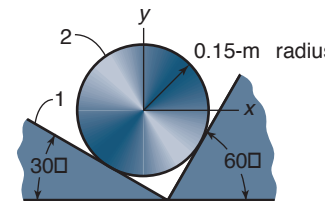
Sketch *b*, used in Problem 2.34

- 2.35 Sketch *c* shows the forces acting on a triangle. Is the triangle in equilibrium? *Ans.* Yes.

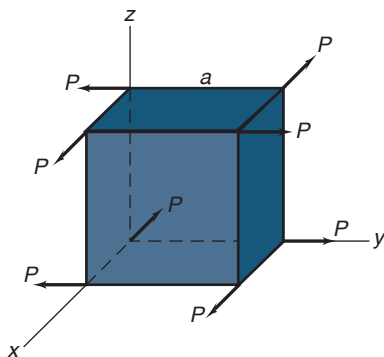


Sketch *c*, used in Problem 2.35

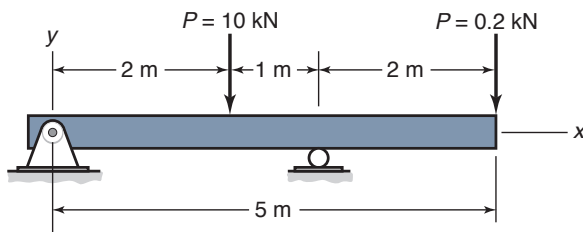
- 2.36 Given the components shown in Sketches *d* and *e*, draw the free-body diagram of each component and calculate the forces.

Sketch *d*, used in Problem 2.36Sketch *e*, used in Problem 2.36

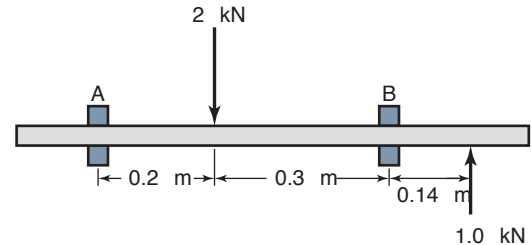
- 2.37 Sketch *f* shows a cube with side lengths  $a$  and eight forces acting at the corners. Is the cube in equilibrium? *Ans.* Yes.

Sketch *f*, used in Problem 2.37

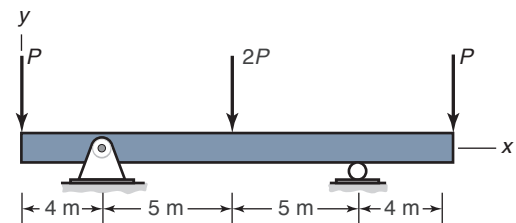
- 2.38 A 5-m-long beam is loaded as shown in Sketch *g*. The beam cross section is constant along its length. Draw the shear and moment diagrams and locate the critical section. *Ans.*  $|V_{\max}| = 6.8 \text{ kN}$ ,  $|M_{\max}| = 6.4 \text{ kN}\cdot\text{m}$ .

Sketch *g*, used in Problem 2.38

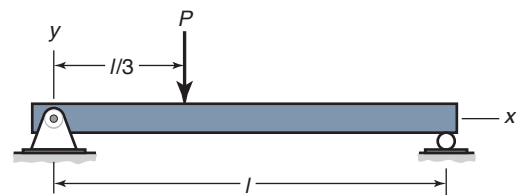
- 2.39 Sketch *h* shows a 0.06-m-diameter steel shaft supported by self-aligning bearings at A and B (which can provide radial but not bending loads on the shaft). Two gears attached to the shaft cause applied forces as shown. The shaft weight can be neglected. Determine the forces at A and B and the maximum bending moment. Draw shear and moment diagrams. *Ans.*  $|M_{\max}| = 296 \text{ Nm}$ .

Sketch *h*, used in Problem 2.39

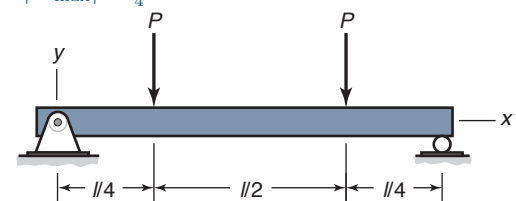
- 2.40 A beam is loaded as shown in Sketch *i*. Determine the reactions and draw the shear and moment diagrams for  $P = 500 \text{ N}$ . *Ans.*  $A_y = B_y = 1000 \text{ N}$ ,  $|M_{\max}| = 2000 \text{ Nm}$ .

Sketch *i*, used in Problem 2.40

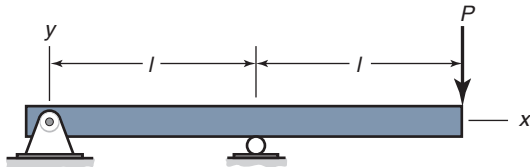
- 2.41 Sketch *j* shows a simply supported beam loaded with a force  $P$  at a position one-third of the length from one of the supports. Determine the largest shear force and bending moment in the beam. Also, draw the shear and moment diagrams. *Ans.*  $|M_{\max}| = \frac{2}{9}Pl$ .

Sketch *j*, used in Problem 2.41

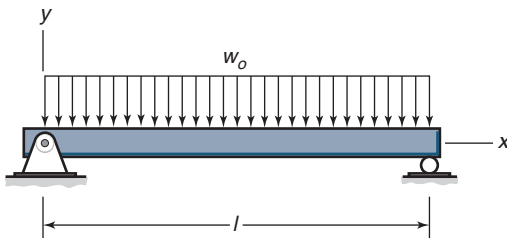
- 2.42 Sketch *k* shows a simply supported beam loaded by two equally large forces  $P$  at a distance  $l/4$  from its ends. Determine the largest shear force and bending moment in the beam, and find the critical location with respect to bending. Also, draw the shear and moment diagrams. *Ans.*  $|M_{\max}| = \frac{1}{4}Pl$ .

Sketch *k*, used in Problem 2.42

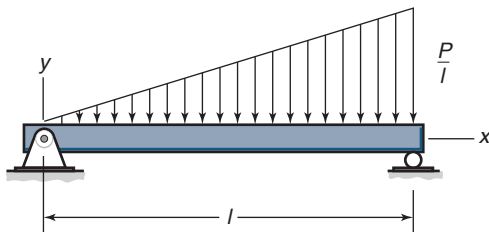
- 2.43 The beam shown in Sketch *l* is loaded by the force  $P$ . Draw the shear and moment diagrams for the beam, indicating maximum values. *Ans.*  $|M|_{\max} = Pl$ .

Sketch *l*, used in Problem 2.43

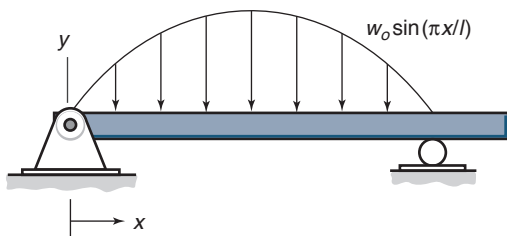
- 2.44 Sketch *m* shows a simply supported beam with a constant load per unit length,  $w_o$ , imposed over its entire length. Determine the shear force and bending moment as functions of  $x$ . Draw a graph of these functions. Also, find the critical section with the largest bending moment. *Ans.*  $M_{\max} = \frac{1}{8}w_o l^2$ .

Sketch *m*, used in Problem 2.44

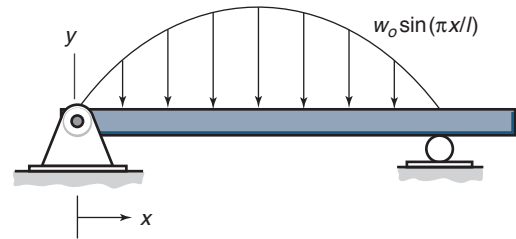
- 2.45 Sketch *n* shows a simply supported beam loaded with a ramp function over its entire length, the largest value being  $P/l$ . Determine the shear force and the bending moment and the critical section with the largest bending moment. Also, draw the shear and moment diagrams. *Ans.*  $|M_{\max}| = \frac{2}{9\sqrt{3}}Pl$ .

Sketch *n*, used in Problem 2.44

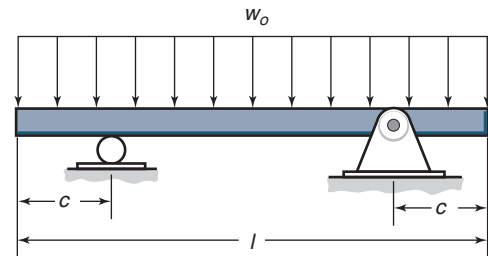
- 2.46 The simply supported beam shown in Sketch *o* has  $P_1 = 5$  kN,  $P_2 = 10$  kN,  $w_o = 5$  kN/m, and  $l = 12$  m. Use singularity functions to determine the shear force and bending moment as functions of  $x$ . Also, draw the shear force and bending moment diagrams. *Ans.*  $|M_{\max}| = 52.5$  kN-m.

Sketch *o*, used in Problem 2.46

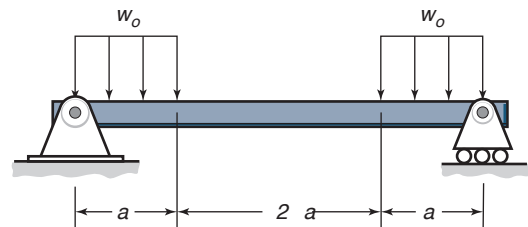
- 2.47 Sketch *p* shows a sinusoidal distributed force applied to a beam. Determine the reactions and largest shear force and bending moment for each section of the beam. *Ans.* Reactions  $= \frac{lw_o}{\pi}$ ,  $|M_{\max}| = \frac{l^2 w_o}{2\pi}$ .

Sketch *p*, used in Problem 2.47

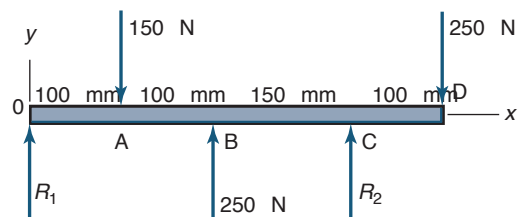
- 2.48 Find the length  $c$  that gives the smallest maximum bending moment for the load distribution shown in Sketch *q*. *Ans.*  $x = 0.207l$ .

Sketch *q*, used in Problem 2.48

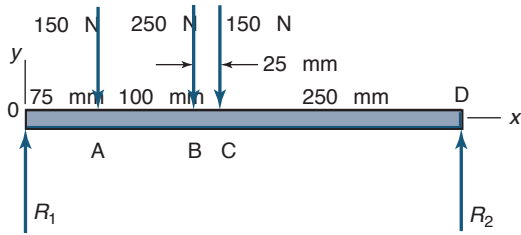
- 2.49 Draw the shear and moment diagrams and give the reaction forces for the load distribution shown in Sketch *r*. *Ans.*  $R = w_o a$ ,  $M_{\max} = \frac{1}{2}w_o a^2$ .

Sketch *r*, used in Problem 2.49

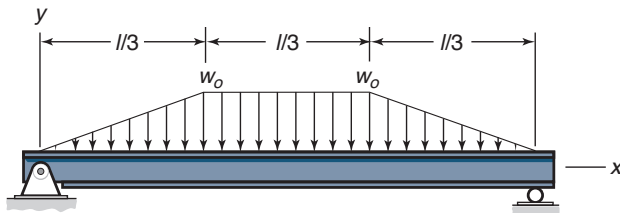
- 2.50 Use singularity functions for the force system shown in Sketch *s* to determine the load intensity, the shear force, and the bending moment in the beam. From a force analysis determine the reaction forces  $R_1$  and  $R_2$ . Also, draw the shear and moment diagrams. *Ans.*  $R_1 = -71$  N,  $R_2 = 221$  N,  $|M|_{\max} = 29.2$  N-m.

Sketch *s*, used in Problem 2.50

- 2.51** Use singularity functions for the force system shown in Sketch *t* to determine the load intensity, the shear force, and the bending moment. Draw the shear and moment diagrams. Also, from a force analysis determine the reaction forces  $R_1$  and  $R_2$ . *Ans.*  $R_1 = 361 \text{ N}$ ,  $R_2 = 189 \text{ N}$ ,  $M_{\max} = 48.2 \text{ N-m}$ .

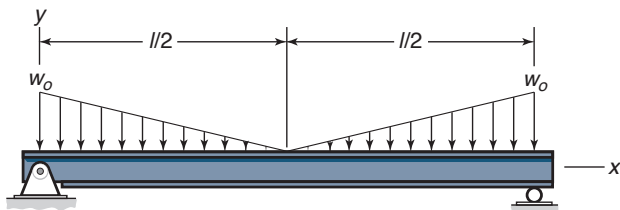
Sketch *t*, used in Problem 2.51

- 2.52** Draw a free-body diagram of the forces acting on the simply supported beam shown in Sketch *u*, with  $w_o = 6 \text{ kN/m}$  and  $l = 10 \text{ m}$ . Use singularity functions to draw the shear force and bending moment diagrams. *Ans.*  $M_{\max} = 63.89 \text{ kN-m}$ .

Sketch *u*, used in Problem 2.52

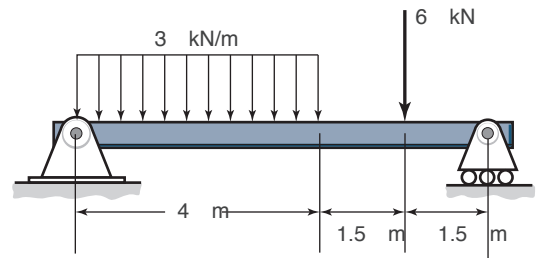
- 2.53** Repeat Example 2.8 using singularity functions.

- 2.54** Sketch *v* shows a simply supported beam with  $w_o = 6 \text{ kN/m}$  and  $l = 10 \text{ m}$ . Draw a free-body diagram of the forces acting along the beam as well as the coordinates used. Use singularity functions to determine the shear force and the bending moment. *Ans.*  $M_{\max} = 25 \text{ kN-m}$ .

Sketch *v*, used in Problem 2.54

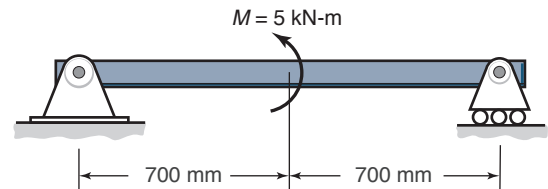
- 2.55** An additional concentrated force with an intensity of 20 kN is applied downward at the center of the simply supported beam shown in Sketch *v*. Draw a free-body diagram of the forces acting on the beam. Assume  $l = 10 \text{ m}$  and  $w_o = 5 \text{ kN/m}$ . Use singularity functions to determine the shear force and bending moments and draw the diagrams. *Ans.*  $M_{\max} = 75 \text{ kN-m}$ .

- 2.56** Draw a free-body diagram of the beam shown in Sketch *w* and use singularity functions to determine the shear force and the bending moment diagrams. Determine the maximum moment. *Ans.*  $|M_{\max}| = 16.19 \text{ kN-m}$ .

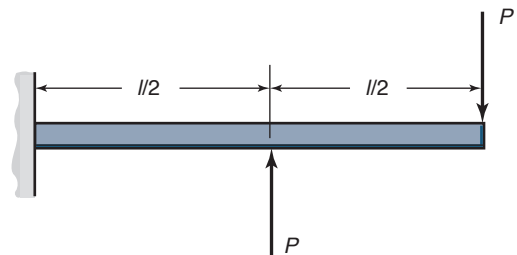
Sketch *w*, used in Problems 2.56 and 2.57

- 2.57** Use direct integration to determine the shear force and bending moment diagrams for the beam shown in Sketch *w*. Determine the maximum moment. *Ans.*  $|M_{\max}| = 16.19 \text{ kN-m}$ .

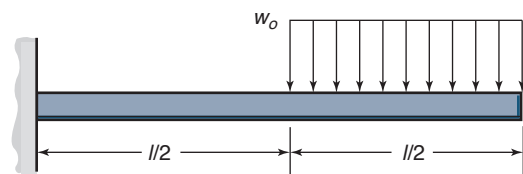
- 2.58** Draw the shear and bending moment diagrams for the beam shown in Sketch *x*. Determine the magnitude and location of the maximum moment. *Ans.*  $|M_{\max}| = 2.5 \text{ kN-m}$ .

Sketch *x*, used in Problem 2.58

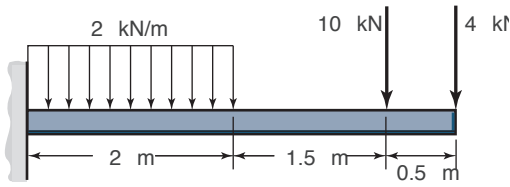
- 2.59** Using singularity functions, draw the shear and moment diagrams for the beam shown in Sketch *y*. Use  $P = 20 \text{ kN}$  and  $l = 4 \text{ m}$ . *Ans.*  $|M_{\max}| = 40 \text{ kN-m}$ .

Sketch *y*, used in Problem 2.59

- 2.60** Determine the location and magnitude of maximum shear stress and bending moment for the beam shown in Sketch *z*. Use  $w_o = 10 \text{ kN/m}$  and  $l = 5 \text{ m}$ . *Ans.*  $|V_{\max}| = 25 \text{ kN}$ ,  $|M_{\max}| = 95.75 \text{ kN-m}$ .

Sketch *z*, used in Problem 2.60

- 2.61** Sketch the shear and bending moment diagrams for the beam shown in Sketch *aa*. Determine the maximum shear force and bending moment. *Ans.*  $|V_{\max}| = 18 \text{ kN}$ ,  $|M_{\max}| = 55 \text{ kN}\cdot\text{m}$ .



Sketch *aa*, used in Problem 2.61

- 2.62** A steel bar is loaded by a tensile force  $P = 20 \text{ kN}$ . The cross section of the bar is circular with a radius of 10 mm. What is the normal tensile stress in the bar? *Ans.*  $\sigma = 63.66 \text{ MPa}$ .

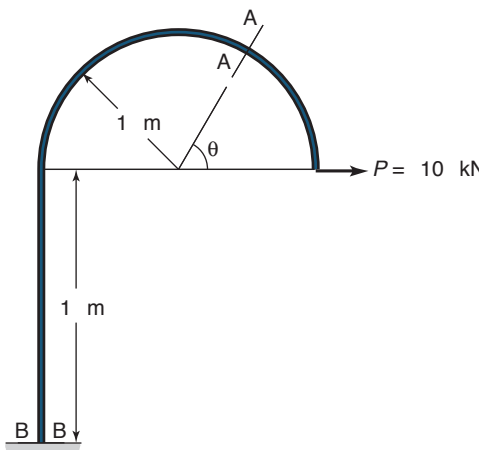
- 2.63** A stainless-steel bar of square cross section is subjected to a tensile force of  $P = 10 \text{ kN}$ . Calculate the required cross section to provide a tensile stress in the bar of 90 MPa. *Ans.*  $l = 10.54 \text{ mm}$ .

- 2.64** What is the maximum length,  $l_{\max}$ , of a copper wire if its weight should not produce a stress higher than 70 MPa when it is hanging vertically? The density of copper is  $8900 \text{ kg/m}^3$ , and the density of air is so small relative to that of copper that it may be neglected. The acceleration of gravity is  $9.81 \text{ m/s}^2$ . *Ans.*  $l_{\max} = 801 \text{ m}$ .

- 2.65** A machine with a mass of 5000 kg will be lifted by a steel rod with an ultimate tensile strength of 860 MPa. A safety factor of 4 is to be used. Determine the diameter needed for the steel rod. *Ans.*  $d = 17.04 \text{ mm}$ .

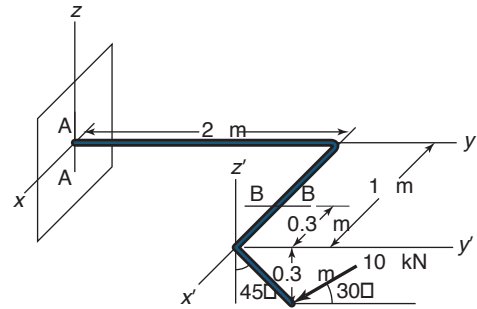
- 2.66** A string on a guitar is made of nylon and has a diameter of 0.5 mm. It is tightened with a force  $P = 12 \text{ N}$ . What is the stress in the string? *Ans.*  $\sigma = 61.12 \text{ MPa}$ .

- 2.67** Determine the normal and shear stresses due to axial and shear forces at sections A and B in Sketch *bb*. The cross sectional area of the rod is  $0.025 \text{ m}^2$  and  $\theta = 30^\circ$ . *Ans.* At section AA,  $\sigma = 200 \text{ kPa}$ ,  $\tau = 346.4 \text{ kPa}$ . At section BB,  $\tau = 400 \text{ kPa}$ .



Sketch *bb*, used in Problem 2.67

- 2.68** Determine the normal and shear stresses in sections A and B of Sketch *cc*. The cross-sectional area of the rod is  $0.00250 \text{ m}^2$ . Ignore bending and torsional effects. *Ans.* In AA,  $\sigma = -3.464 \text{ MPa}$ ,  $\tau = -2.00 \text{ MPa}$ .



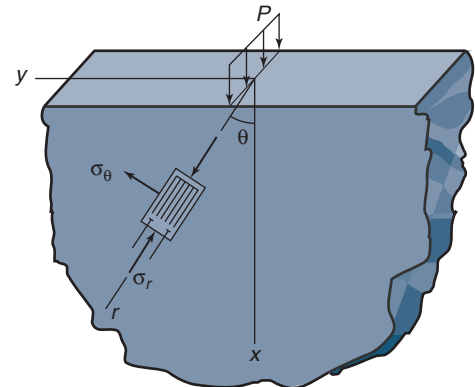
Sketch *cc*, used in Problem 2.68

- 2.69** Sketch *dd* shows a distributed load on a semi-infinite plane. The stress in polar coordinates based on plane stress is

$$\sigma_r = -\frac{2w_o \cos \theta}{\pi r}$$

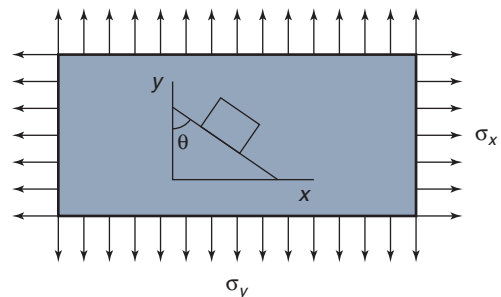
$$\sigma_\theta = \tau_{r\theta} = \tau_{\theta r} = 0$$

Determine the expressions  $\sigma_x$ ,  $\sigma_y$ , and  $\tau_{xy}$  in terms of  $r$  and  $\theta$ . *Ans.*  $\sigma_x = -\frac{2w_o \cos^3 \theta}{\pi r}$ .



Sketch *dd*, used in Problem 2.69

- 2.70** Sketch *ee* shows loading of a thin but infinitely wide and long plane. Determine the angle  $\theta$  needed so that the stress element will have no shear stress. *Ans.*  $\theta = 0$ .



Sketch *ee*, used in Problem 2.70



**2.71** A stress tensor is given by

$$\mathbf{S} = \begin{pmatrix} 200 & 40 & 0 \\ 40 & 25 & 0 \\ 0 & 0 & 0 \end{pmatrix}$$

where all values are in megapascals. Calculate the principal normal stresses and the principal shear stresses.  
*Ans.*  $\sigma_1 = 208.7 \text{ MPa}$ ,  $\sigma_2 = 16.29 \text{ MPa}$ ,  $\sigma_3 = 0$ .

**2.72** A thin, square steel plate is oriented with respect to the  $x$ - and  $y$ -directions. A tensile stress  $\sigma$  acts in the  $x$ -direction, and a compressive stress  $-\sigma$  acts in the  $y$ -direction. Determine the normal and shear stresses on the diagonal of the square. *Ans.*  $\sigma_{45^\circ} = 0$ ,  $\tau_{45^\circ} = -\sigma$ .

**2.73** A thin, rectangular brass plate has normals to the sides in the  $x$ - and  $y$ -directions. A tensile stress  $\sigma$  acts on the four sides. Determine the principal normal and shear stresses. *Ans.*  $\sigma_1 = \sigma_2 = \sigma$ ,  $\tau = 0$ .

**2.74** Given the thin, rectangular brass plate in Problem 2.73, but with the stress in the  $y$ -direction being  $\sigma_y = -\sigma$  instead of  $+\sigma$ , determine the principal normal and shear stresses and their directions. *Ans.*  $\sigma_1 = -\sigma_2 = \sigma$ ,  $\tau = \pm\sigma$ .

**2.75** For the following stress states, sketch the stress element, draw the appropriate Mohr's circle, determine the principal stresses and their directions, and sketch the principal stress elements:

- $\sigma_x = 8$ ,  $\sigma_y = 14$ , and  $\tau_{xy} = 4$ . *Ans.*  $\sigma_1 = 16 \text{ MPa}$ ,  $\sigma_2 = 6 \text{ MPa}$ .
- $\sigma_x = -15$ ,  $\sigma_y = 9$ , and  $\tau_{xy} = 5$ . *Ans.*  $\sigma_1 = 10 \text{ MPa}$ ,  $\sigma_2 = -16 \text{ MPa}$ .
- $\sigma_x = 12$ ,  $\sigma_y = 28$ , and  $\tau_{xy} = 15$ . *Ans.*  $\sigma_1 = 35 \text{ MPa}$ ,  $\sigma_2 = 5 \text{ MPa}$ .
- $\sigma_x = -54$ ,  $\sigma_y = 154$ , and  $\tau_{xy} = -153$ . *Ans.*  $\sigma_1 = 235 \text{ MPa}$ ,  $\sigma_2 = -135 \text{ MPa}$ .

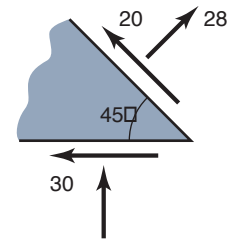
All stresses are in megapascals.

**2.76** Repeat Problem 2.75 for

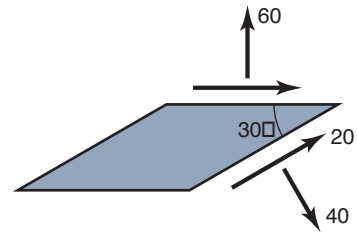
- $\sigma_x = \sigma_y = -10$ , and  $\tau_{xy} = 0$ . *Ans.*  $\tau_{xy} = 0 \text{ MPa}$ .
- $\sigma_x = 0$ ,  $\sigma_y = 30$ , and  $\tau_{xy} = 20$ . *Ans.*  $\sigma_1 = 40 \text{ MPa}$ ,  $\sigma_2 = -10 \text{ MPa}$ .
- $\sigma_x = -20$ ,  $\sigma_y = 40$ , and  $\tau_{xy} = -40$ . *Ans.*  $\sigma_1 = 60 \text{ MPa}$ ,  $\sigma_2 = -40 \text{ MPa}$ .
- $\sigma_x = 30$ ,  $\sigma_y = 0$ , and  $\tau_{xy} = -20$ . *Ans.*  $\sigma_1 = 40 \text{ MPa}$ ,  $\sigma_2 = -10 \text{ MPa}$ .

All stresses are in megapascals.

**2.77** Given the state of stresses shown in the two parts of Sketch *ff* determine the principal stresses and their directions by using Mohr's circle and the stress equations. Show the stress elements. All stresses in Sketch *ff* are in megapascals. *Ans.* (a)  $\sigma_1 = 34 \text{ MPa}$ ,  $\sigma_2 = -38 \text{ MPa}$ .



(a)



(b)

Sketch *ff*, used in Problem 2.77

**2.78** A certain loading on a machine element leads to a stress state of  $\sigma_x = a$ ,  $\sigma_y = a/2$ , and  $\tau_{xy} = a/4$ . What value of  $a$  results in the maximum allowable shear stress of 100 MPa? *Ans.*  $a = 282.8 \text{ MPa}$ .

**2.79** Given the normal and shear stresses  $\sigma_x = 66 \text{ MPa}$ ,  $\sigma_y = 34 \text{ MPa}$ , and  $\tau_{xy} = -63 \text{ MPa}$ , draw the Mohr's circle diagram and the principal normal and shear stresses on the  $x$ - $y$  axis. Determine the triaxial stresses and give the corresponding Mohr's circle diagram. *Ans.*  $\sigma_1 = 115 \text{ MPa}$ ,  $\sigma_2 = 0$ ,  $\sigma_3 = -15 \text{ MPa}$ .

**2.80** Given the normal and shear stresses  $\sigma_x = 0$ ,  $\sigma_y = 10 \text{ MPa}$ , and  $\tau_{xy} = 12 \text{ MPa}$ , draw the Mohr's circle diagram and the principal normal and shear stresses on the  $x$ - $y$  axis. Determine the triaxial stresses and give the corresponding Mohr's circle diagram. *Ans.*  $\sigma_1 = 18 \text{ MPa}$ ,  $\sigma_2 = 0$ ,  $\sigma_3 = -8 \text{ MPa}$ .

**2.81** Given the normal and shear stresses  $\sigma_x = 72 \text{ MPa}$ ,  $\sigma_y = -72 \text{ MPa}$ , and  $\tau_{xy} = -65 \text{ MPa}$ , draw the Mohr's circle diagram and the principal normal and shear stresses on the  $x$ - $y$  axis. Determine the triaxial stresses and give the corresponding Mohr's circle diagram. *Ans.*  $\sigma_1 = 97 \text{ MPa}$ ,  $\sigma_2 = 0$ ,  $\sigma_3 = -97 \text{ MPa}$ .

**2.82** A stress element in plane stress encounters  $\sigma_x = 20 \text{ MPa}$ ,  $\sigma_y = -10 \text{ MPa}$ , and  $\tau_{xy} = 13 \text{ MPa}$ . (a) Determine the three principal stresses and maximum shear stress. (b) Using a Mohr's circle diagram, explain the effect of superimposing a hydrostatic pressure  $p$  on the principal stresses and maximum shear stress. *Ans.* (a)  $\sigma_1 = 24.85 \text{ MPa}$ ,  $\sigma_2 = 0$ ,  $\sigma_3 = -14.85 \text{ MPa}$ .

**2.83** In a three-dimensional stress field, the stresses are found to be  $\sigma_x = 40 \text{ MPa}$ ,  $\sigma_y = 20 \text{ MPa}$ ,  $\sigma_z = 60 \text{ MPa}$ ,  $\tau_{xy} = -20 \text{ MPa}$ ,  $\tau_{yz} = 0$ , and  $\tau_{xz} = 20 \text{ MPa}$ . Draw the stress element for this case. Determine the principal stresses and sketch the corresponding Mohr's circle diagram. *Ans.*  $\sigma_1 = 70.64 \text{ MPa}$ ,  $\sigma_2 = 46.94 \text{ MPa}$ ,  $\sigma_3 = 2.412 \text{ MPa}$ .

**2.84** Given the normal and shear stresses  $\sigma_x = -36$  MPa,  $\sigma_y = 60$  MPa, and  $\tau_{xy} = 20$  MPa, determine or draw the following:

- Two-dimensional Mohr's circle diagram.
- Normal principal stress element in the  $x$ - $y$  plane.
- Shear principal stress.
- Three-dimensional Mohr's circle diagram and corresponding principal normal and shear stresses.  
*Ans.*  $\sigma_1 = 64$  MPa,  $\sigma_2 = 0$ ,  $\sigma_3 = -40$  MPa.

**2.85** The strain tensor in a machine element is

$$\mathbf{T} = \begin{pmatrix} 0.0012 & -0.0001 & 0.0007 \\ -0.0001 & 0.0003 & 0.0002 \\ 0.0007 & 0.0002 & -0.0008 \end{pmatrix}$$

Find the strain in the  $x$ -,  $y$ -, and  $z$ -directions, in the direction of the space diagonal  $\left(\frac{1}{\sqrt{3}}; \frac{1}{\sqrt{3}}; \frac{1}{\sqrt{3}}\right)$ , and in the direction  $\epsilon_x$ ,  $\epsilon_y$ , and  $\epsilon_z$ . *Ans.* In the direction of the diagonal,  $\epsilon = 0.0005$ .

**2.86** A strain tensor is given by

$$\mathbf{T} = \begin{pmatrix} 0.0023 & 0.0006 & 0 \\ 0.0006 & 0.0005 & 0 \\ 0 & 0 & 0 \end{pmatrix}$$

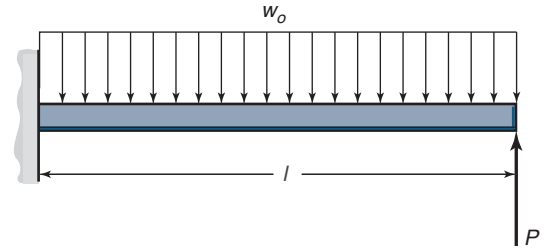
Calculate the maximum shear strain and the principal strains. *Ans.*  $\epsilon_1 = 0.00248$ ,  $\epsilon_2 = 0.00032$ .

## Design and Projects

**2.87** Without using the words "stress" or "strain," define *elastic modulus*.

**2.88** A bookshelf sees a uniform distributed load across its entire length, and is supported by two brackets. Where should the brackets be located? *Hint:* See Problem 2.48.

**2.89** For the beam shown in Sketch *gg*, determine the force  $P$  so that the maximum bending moment in the beam is as small as possible. What is the value of  $|M|_{\max}$ ? *Ans.*  $|M|_{\max} = \frac{1}{2}w_0l^2$

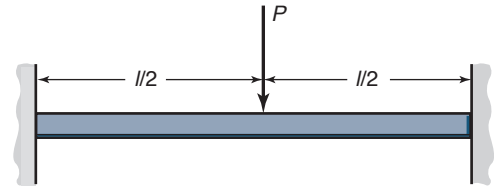


Sketch *gg*, used in Problem 2.89

**2.90** Three- and four-point bending tests are common tests used to evaluate materials.

- Sketch the shear and bending moment diagrams for each test.
- Is there any difference in the stress state for the two tests?
- Which test will cause specimens to fail at a lower bending moment? Why?

**2.91** Sketch *hh* shows a beam that is fixed on both ends with a central load. Can you determine the shear and moment diagrams for this case? If not, explain what additional information you would need and how you would go about solving this problem.



Sketch *hh*, used in Problem 2.91

**2.92** For a  $0^\circ$ - $60^\circ$ - $120^\circ$  strain gage rosette with one base on the  $x$ -axis, derive the strains  $\epsilon_x$ ,  $\epsilon_y$ , and  $\gamma_{xy}$  as a function of  $\epsilon_0$ ,  $\epsilon_{60}$ , and  $\epsilon_{120}$ . *Ans.*  $\epsilon_x = \epsilon_0$ ,  $\epsilon_y = \frac{2}{3}(\epsilon_{60} + \epsilon_{120}) - \frac{1}{3}\epsilon_0$ .

**2.93** A stress tensor is given by

$$\mathbf{S} = \begin{pmatrix} 200 & 40 & -30 \\ 40 & 25 & 10 \\ -30 & 10 & -25 \end{pmatrix}$$

where all values are in megapascals. Calculate the principal normal stresses and the principal shear stresses. *Ans.*  $\sigma_1 = 211.8$  MPa,  $\sigma_2 = 21.46$  MPa,  $\sigma_3 = -33.31$  MPa.

## Chapter 3

# Introduction to Materials and Manufacturing



A hob cuts gear teeth. Source: Courtesy of Sandvik Coromant.

*Give me matter, and I will construct a world out of it.*  
Immanuel Kant

### Contents

- 3.1 Introduction 54
- 3.2 Ductile and Brittle Materials 54
- 3.3 Classification of Solid Materials 55
- 3.4 Stress-Strain Diagrams 58
- 3.5 Properties of Solid Materials 60
- 3.6 Stress-Strain Relationships 67
- 3.7 Two-Parameter Materials Charts 68
- 3.8 Effects of Manufacturing 74
- 3.9 Summary 83

### Examples

- 3.1 Ductility of Materials 55
- 3.2 Thermal Expansion 56
- 3.3 Strength of a Composite Material 58
- 3.4 Design of a Composite Beam 59
- 3.5 Glass Transition Temperature 60
- 3.6 Stiffness of a Fiber Reinforced Polymer 63
- 3.7 Resilience 63
- 3.8 Heat Content of Materials 66
- 3.9 Deformation 67
- 3.10 Material for a Solid Fishing Rod 68
- 3.11 Material for a Tubular Fishing Rod 70
- 3.12 Elastic Strain 70
- 3.13 Design for Wear 70

### Case Study

- 3.1 The Maker Movement 80

Material and manufacturing process selection are essential for design. Being able to exploit a material's potential and characteristics is necessary to ensure that the best material is used for a particular machine element. This chapter will classify, characterize, and guide selection of solid materials in a general sense. Physical and mechanical properties of engineering materials will be examined and two-parameter charts will be used to suggest materials for specific situations. The hardness of materials will be defined, hardness testing will be described, and the importance of hardness will be discussed. A brief summary of the manufacturing processes that are available for each material class will be discussed, with an introduction to their relationship to mechanical design. Processes can be categorized as casting, where a metal is melted, placed in a mold, and cooled to solidification; bulk forming, where a material is forced to take on a new shape; sheet forming, which uses a rolled metal with small thickness to produce a desired shape; material removal processes such as machining, grinding, and other finishing processes; various methods to produce polymer parts; and methods to produce ceramics and composite materials.

## Symbols

$A$	area, m <sup>2</sup>
$\bar{\alpha}$	linear thermal expansion coefficient, (°C) <sup>-1</sup>
$C_p$	specific heat of material, J/(kg·°C)
$C_R$	relative cost
$d$	fiber diameter, m
$E$	modulus of elasticity, Pa
%EL	elongation, percent
$G$	shear modulus, Pa
$g$	gravitational acceleration, 9.807 m/s <sup>2</sup>
$H$	hardness, N/m <sup>2</sup>
HB	Brinell hardness number
HK	Knoop hardness number
HR	Rockwell hardness number
HV	Vickers hardness number
$K$	bulk modulus, Pa
$K_t$	thermal conductivity, W/(m·°C)
$k$	spring rate, N/m
$k_1$	Archard wear constant, (Pa) <sup>-1</sup>
$L$	sliding distance, m
$l$	length, m
$m_a$	mass of body, kg
$P$	force, N
$p$	normal pressure, Pa
$p_l$	limiting pressure, Pa
$Q$	quantity of heat, J
$r$	radius, m
$r_o$	atom size, m
$S$	strength, Pa
$S_u$	ultimate strength, Pa
$S_y$	yield strength, Pa
$t_m$	temperature, °C
$\Delta t_m$	temperature change, °C
$t_h$	thickness, m
$U_r$	modulus of resilience, Pa
$v$	volume fraction
$W$	weight, N
$W_r$	wear rate, m <sup>2</sup>
$\gamma$	shear strain
$\delta$	deformation; deflection, m
$\epsilon$	strain
$\nu$	Poisson's ratio
$\rho$	density, kg/m <sup>3</sup>
$\sigma$	normal stress, Pa
$\tau$	shear stress, Pa
$\tau_f$	fiber-matrix bond strength, Pa

## Subscripts

$a$	axial
all	allowable
$c$	composite; cross sectional
cr	critical
$f$	fiber
fr	at fracture
$g$	glass transition
$i$	inner
$m$	matrix; mean
$t$	transverse
$o$	without load
1,2,3	principal axes

## 3.1 Introduction

The cost of the design stage of a product lifecycle is usually low, typically less than 5% of the total cost. Much higher costs are associated with the materials and manufacturing processes used in a product's production. However, the materials and manufacturing costs are to a great extent set during the design stage. This recognition has been stated as "Design casts the largest shadow."

Recognizing the impact of a design on product cost and quality, design cannot be done without careful consideration of materials and manufacturing. Intelligent material selection requires knowledge of material capabilities and characteristics. Knowledge of manufacturing leads to design of easy-to-manufacture geometries. Selection of material impacts manufacturing, as some processes are incompatible with certain materials. Thus, design, materials selection, and manufacturing are inseparable, and good design requires sophistication regarding materials and manufacturing.

This chapter introduces materials science, distinguishing between ductile and brittle materials in Section 3.2. This is followed by a discussion of the main classes of solids, namely, metals, polymers, ceramics, and composites. Deformation of materials subjected to stress is then discussed, with the behavior of the different material classes discussed in Section 3.3 and important physical and mechanical properties summarized for a wide variety of engineering materials in Section 3.5. Section 3.7 discusses the use of two-material charts in selecting materials for particular loading types, and limits to the utility of these charts is explained. Finally, the chapter closes with a discussion of the major classes of manufacturing processes and their effects on material properties.

## 3.2 Ductile and Brittle Materials

### 3.2.1 Ductile Materials

**Ductility** is a measure of the degree of plastic deformation attained at fracture. Designers often use ductile materials because they can absorb shock (or energy) and, if they become overloaded, will usually exhibit large deformations before failing. Also, stress concentrations (Sections 6.2 and 7.7) can be partially relieved through the deformations that can be achieved by ductile materials.

One way to quantify ductility is by the percent elongation, %EL, given by

$$\%EL = \left( \frac{l_{fr} - l_o}{l_o} \right) \times 100\%, \quad (3.1)$$

where  $l_{fr}$  is the length of the specimen at fracture and  $l_o$  is the original length of the specimen (without load).

A **ductile material** is one with a large percent elongation before failure, arbitrarily defined as 5% or higher for the purposes of this text. Table A.2 shows that the %ELs for low-carbon (AISI 1020), medium-carbon (AISI 1040), and high-carbon steels (AISI 1080) are 37%, 30%, and 25%, respectively. (Note that selected materials from tables in Appendix A also appear on the inside front cover.) Thus, steel is ductile because it far exceeds the 5% elongation described in Eq. (3.1). Also note from Eq. (3.1) that the original length of the specimen,  $l_o$ , is an important value because a significant portion of the plastic deformation at fracture is confined to the neck region. Thus, the magnitude of %EL will depend on the specimen length. The shorter  $l_o$ , the greater the fraction of total elongation from the neck and, consequently, the higher the

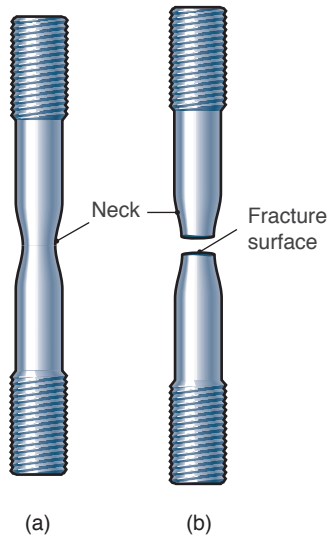


Figure 3.1: Ductile material from a standard tensile test apparatus. (a) Necking; (b) failure.

value of %EL. Therefore,  $l_o$  should be specified when percent elongation values are cited.

Figure 3.1a shows a test specimen of a ductile material in which **necking** (decreasing cross-sectional area and localized deformation) is occurring. Figure 3.1b shows the same specimen just after fracture. Note the considerable amount of plastic deformation at fracture.

### Example 3.1: Ductility of Materials

**Given:** A flat plate is formed into a hollow cylinder with an inner radius of 100 mm and a wall thickness of 60 mm.

**Find:** Determine which temper of AISI 301 stainless steel (see Table A.4) cannot be cold-formed to produce the cylinder. Assume that the midplane of the plate does not experience either tension or compression and will thus not experience any elongation.

**Solution:** The length without load is at the midplane of the plate, or

$$l_o = 2\pi \left( r_i + \frac{t_h}{2} \right) = 2\pi \left( 100 + \frac{60}{2} \right) = 260\pi \text{ mm.}$$

The length at fracture at the outer diameter of the cylinder is

$$l_{fr} = 2\pi r_o = 2\pi(r_i + t_h) = 2\pi(100 + 60) = 320\pi \text{ mm.}$$

Thus, from Eq. (3.1) the percent elongation is

$$\begin{aligned} \%EL &= \left( \frac{l_{fr} - l_o}{l_o} \right) \times 100\% \\ &= \left( \frac{320\pi - 260\pi}{260\pi} \right) \times 100\% \\ &= 23.04\%. \end{aligned}$$

From Table A.4, half-hard, 3/4-hard, and full-hard AISI 301 cannot achieve this strain. However, a lower temper, such as 1/4-, 1/8-, or 1/16-hard, or a fully annealed specimen, would be suitable.



Figure 3.2: Failure of a brittle material from a standard tensile test apparatus.

### 3.2.2 Brittle Material

A **brittle material** produces little (%EL < 5%) or no plastic deformation before failure. Figure 3.2 shows a brittle test specimen at failure. Note that little or no necking occurs prior to failure, in contrast to Fig. 3.1.

## 3.3 Classification of Solid Materials

Engineering materials fall into four major classes: metals, ceramics (including glasses), polymers (including elastomers), and composites. The members of each class generally have the following common features:

1. Similar properties, chemical makeup, and atomic structure
2. Similar processing routes
3. Similar applications

### 3.3.1 Metals

**Metals** are combinations of metallic elements. They have large numbers of nonlocalized electrons (i.e., electrons not bound to particular atoms). Metals are extremely good conductors of electricity and heat and are not transparent to visible light; a polished metal surface has a lustrous appearance. Furthermore, metals are strong and usually deformable, making them extremely important materials in machine design.

Metals are usually ductile and can be made stronger by alloying and by mechanical and heat treatment. High-strength alloys can have a percent elongation as low as 2%, but even this is enough to ensure that the material yields before it fractures. Some cast metals have very low ductility, however. Metals are often used in circumstances where cyclic loading is encountered (see Chapter 7), and they are generally resistant to corrosion. Ductile materials, such as steel, accommodate stress concentrations by deforming in a way that redistributes the load more evenly.

An **isotropic** material has properties that are the same in all directions; a material with directional properties is **anisotropic**. On a microscopic scale, metals form well-defined crystals with ordered packing of atoms. The crystals in a metal are very small and are randomly oriented. Thus,



while a crystal may be anisotropic, a metal should be considered polycrystalline, and the averaged results of many crystals leads to a reasonable assumption of isotropy. However, the crystals, or grains, in a metal may be elongated or oriented, leading to anisotropic behavior, especially with sheet metals. Thus, manufacturing history will determine whether a metal is isotropic or anisotropic.

Most metals are initially cast and then can be further processed to achieve the desired shape. Further processes include secondary casting (such as sand, shell, investment or die casting), bulk forming (forging, extrusion, rolling, drawing), sheet forming (deep drawing, stretch forming, stamping) or machining (milling, turning, grinding, polishing). An additional option for metals is to produce metal powders and form desired shapes through powder metallurgy techniques. Manufacturing processes are addressed in Section 3.8.

### 3.3.2 Ceramics and Glasses

**Ceramics** are compounds of metallic and nonmetallic elements, most frequently oxides, nitrides, and carbides. For example, the ceramic material aluminum oxide (also known as alumina, corundum, or in single crystal form, sapphire), is  $\text{Al}_2\text{O}_3$ . **Glasses** are made up of metallic and nonmetallic elements just as are ceramics, but glasses typically have no clear crystal structure. A typical soda-lime glass consists of approximately 70 wt% silicon dioxide ( $\text{SiO}_2$ ), the balance being mainly soda ( $\text{Na}_2\text{O}$ ) and lime ( $\text{CaO}$ ). Both ceramics and glasses typically insulate against the passage of electricity and heat and are more resistant to high temperatures and harsh chemical environments than are metals and polymers.

Ceramics and glasses, like metals, have high density. However, instead of being ductile like metals, ceramics and glasses are brittle at room temperature. They are typically 15 times stronger in compression than in tension. They are stiff, hard, and abrasion resistant (hence their use for bearings and cutting tools). Thus, they must be considered an important class of engineering material for use in machine elements.

Ceramics are usually obtained by forming a ceramic slurry (a suspension of ceramic powders in water) with binders, and then firing the ceramics to develop a strong bond between particles. Some machining operations are possible with ceramics, but they are often too brittle to be successfully machined. However, grinding and polishing are commonly performed successfully with ceramics.

#### Example 3.2: Thermal Expansion

**Given:** A piece of stabilized zirconia ( $\text{ZrO}_2$ ) has a thermal expansion coefficient of  $12 \times 10^{-6}/^\circ\text{C}$ , and is to be implanted into a steel ring. The fit between the steel and the zirconia is a medium press fit at room temperature. When the temperature fluctuates from room temperature to  $500^\circ\text{C}$ , the zirconia should not loosen.

**Find:** The correct class of steel to be used from those given in Table 3.1.

**Solution:** Since the zirconia should not loosen from the steel when the temperature is increased, a slightly smaller coefficient of thermal expansion, but very close to the zirconia value, is desired for the stainless steel. From Table 3.1, a low- or medium alloy has a coefficient of thermal expansion of  $11 \times 10^{-6}/^\circ\text{C}$  and would therefore be the preferred classes of steel.

### 3.3.3 Polymers and Elastomers

**Polymers** are organic compounds composed of carbon, hydrogen, and other nonmetallic elements. Polymers have large and complex molecular structures.

Polymers, also called **plastics**, are of two basic types: thermoplastics and thermosets. **Thermoplastics** are long-chain molecules, sometimes with branches, where the strength arises from interference between chains and branches. **Thermosets** have a higher degree of cross-linking so that molecular chains are linked together and cannot slide over each other. In general, thermoplastics are more ductile than thermosets, and at elevated temperatures they soften significantly and melt. Thermosets are more brittle, do not soften as much as thermoplastics, and usually degrade chemically before melting.

**Elastomers** have a networked cross-linked structure, but not as extensive as that for more rigid thermosets, so they produce large elastic deformations at relatively light loads. A common example of an elastomer is the material in a rubber band, which displays the typical characteristics of large elastic deformation followed by brittle fracture without any plastic deformation. Further, rubber bands are highly nonlinearly elastic, which is typical of elastomers.

Polymers and elastomers can be extremely flexible with large elastic deformations. Polymers are roughly five times less dense than metals but have nearly equivalent strength-to-weight ratios. Because polymers creep (the time-dependent permanent deformation that occurs under static stress) even at room temperature, a polymer machine element under load may, with time, acquire a permanent set. The properties of polymers and elastomers change greatly with variations in temperature. For example, a polymer that is tough and flexible at  $20^\circ\text{C}$  may be brittle at the  $4^\circ\text{C}$  environment of a household refrigerator and yet creep rapidly at the  $100^\circ\text{C}$  of boiling water.

The mechanical properties of polymers are characterized using the same parameters as for metals (i.e., modulus of elasticity and tensile, impact, and fatigue strengths). However, polymers vary much more in strength, stiffness, etc., than do metals. This variation can be explained by the difference in chain lengths and the amount of polymer that is in a crystalline or amorphous state. Further, a thermoplastic that is deformed plastically will have its molecules aligned in the direction of strain, leading to higher strength and anisotropy. Thus, two polymers with the identical chemical constituents can have very different microstructures and associated variation in mechanical and physical properties. In addition, the mechanical characteristics of polymers, for the most part, are highly sensitive to the rate of deformation, temperature, and chemical nature of the environment (the presence of water, oxygen, organic solvents, etc.). Therefore, the particular values given for polymer mechanical properties should be used with caution.

Polymers are easy to shape: complicated parts performing several functions can be molded from a polymer in a single operation (see Section 3.8.2). However, injection molding operations have high tooling costs and can only be justified for large production runs. Large elastic deflections allow the design of polymer components that snap together, making assembly fast and inexpensive. Polymers are corrosion resistant and have low coefficients of friction.

Thermoplastics and thermosets have very different manufacturing options and strategies. Thermoplastics are generally heated to a temperature above their melting point, formed into a desired shape and then cooled. Examples of common manufacturing processes for thermoplastics include extrusion, injection molding, blow molding, and ther-

### Classification of Solid Materials

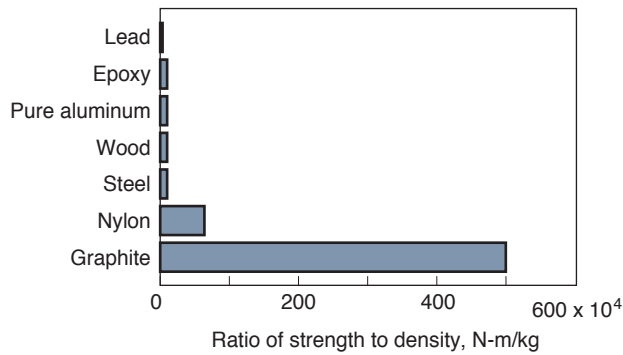


Figure 3.3: Strength/density ratio for various materials.

moforming. Thermosets are blended from their constituents, formed to a desired shape and then cured at elevated temperature and/or pressure to develop cross links. Common manufacturing methods used for thermosets include reaction injection molding, compression molding, and potting (similar to casting).

### 3.3.4 Composites

Figure 3.3 compares a number of materials from a minimum-weight design standpoint (i.e., a larger strength-to-density ratio leads to a lighter design). Fibers can have much better strength-to-weight ratios than conventional extruded bars, molded plastics, and sintered ceramics. However, fibers are often susceptible to corrosion, even in air. For example, graphite fibers will oxidize readily in air and cannot provide their exceptional strength for long.

Many modern technologies require machine elements with demanding combinations of properties that cannot be met by conventional metal alloys, ceramics, and polymeric materials. Present-day technologies require solid materials that have low density, high strength, stiffness and abrasion resistance, and that are not easily corroded. This combination of characteristics is rather formidable, considering that strong materials are usually relatively dense and that increasing stiffness generally decreases impact strength.

**Composite materials** combine the attractive properties of two or more material classes while avoiding some of their drawbacks. A composite is designed to display a combination of the best characteristics of each component material. For example, graphite-reinforced epoxy acquires strength from the graphite fibers while the epoxy protects the graphite from oxidation. The epoxy also helps support shear stresses and provides toughness.

The three main types of composite material are:

1. *Particle reinforced*, which contain particles with approximately the same dimensions in all directions distributed in a matrix, such as concrete.
2. *Discontinuous fiber reinforced*, which use fibers of limited length-to-diameter ratio in a matrix, such as fiberglass.
3. *Continuous fiber reinforced*, where continuous fibers are incorporated, such as seen in graphite tennis rackets.

Figure 3.4 shows a cross section of a continuous fiber-reinforced composite material. Most such composites contain glass, polymer or carbon fibers, and a polymer matrix. These composites cannot be used at elevated temperatures because the polymer matrix softens or degrades, but at room temperature their performance can be outstanding. Some disadvantages

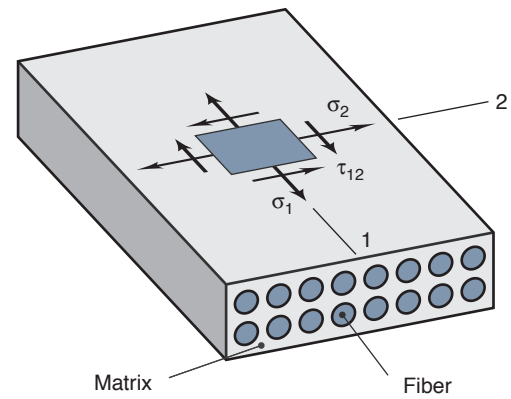


Figure 3.4: Cross section of fiber-reinforced composite material.

of composites are that they are expensive and relatively difficult to form and join.

Composite materials have many characteristics that are different from those of the other three classes of material considered. Whereas metals, polymers, and ceramics are **homogeneous** (properties are not a function of position in the solid), **isotropic** (properties are the same in all directions at a point in the solid), or **anisotropic** (properties are different in all directions at a point in the solid), composites are **non-homogeneous** and **orthotropic**. An orthotropic material has properties that are different in three mutually perpendicular directions at a point in the solid but has three mutually perpendicular planes of material symmetry. Consideration in this text is limited to simple, unidirectional, fiber-reinforced orthotropic composite materials, such as shown in Fig. 3.4.

An important parameter in discontinuous fiber-reinforced composites is the fiber length. Some critical fiber length is necessary for effective strengthening and stiffening of the composite material. The critical length,  $l_{cr}$ , of the fiber depends on the fiber diameter,  $d$ , its ultimate strength,  $S_u$ , and the fiber-matrix bond strength,  $\tau_f$ , according to

$$l_{cr} = \frac{S_u d}{2\tau_f}. \quad (3.2)$$

The two in the denominator of Eq. (3.2) accounts for the fact that the fiber is embedded in the matrix and splits into two parts at failure. For a number of glass- and carbon-fiber-reinforced composites this critical length is about 1 mm, or 20 to 150 times the fiber diameter.

Discontinuous and particle-reinforced composites share many of the manufacturing methods with thermosetting polymers and metals, depending on the matrix materials. Polymer matrix materials are commonly molded or placed onto a form (lay-up) and then cured in an oven. Metal matrix composites use variants of casting or powder metallurgy techniques. Continuous fiber reinforced polymers have unique manufacturing approaches, including tape layup, pultrusion, pulforming, and filament winding.

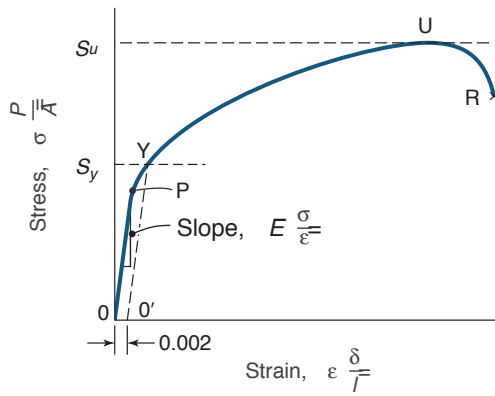


Figure 3.5: Typical stress-strain curve for a ductile material.

### Example 3.3: Strength of a Composite Material

**Given:** A fiber-reinforced plastic contains carbon fibers having an ultimate strength of 1 GPa and a modulus of elasticity of 150 GPa. The fibers are 3 mm long with a diameter of 30  $\mu\text{m}$ .

**Find:** Determine the required fiber-matrix bond strength in order to fully develop the strength of the fiber reinforcement.

**Solution:** From Eq. (3.2), the fiber-matrix bond strength can be expressed as

$$\tau_f = \frac{S_u d}{2l_{cr}} = \frac{(10^9)(30 \times 10^{-6})}{2(0.003)} = 5 \text{ MPa.}$$

## 3.4 Stress-Strain Diagrams

The stress-strain diagram is important in designing machine elements because it yields data about a material's strength without regard to its size or shape. Because stress-strain diagrams differ considerably for the different classes of material, each will be treated separately. The exception is that a stress-strain diagram for composites will not be presented because of the diverse nature of these materials.

### 3.4.1 Metals

Figure 3.5 shows the stress-strain diagram for a ductile metal. Although the stress shown in the figure is tensile, the stress-strain diagrams for most metals are essentially the same for compression and tension.

Figure 3.6 better clarifies the mechanisms and behavior near the yield stress. A number of points presented in Figs. 3.5 and 3.6 need to be defined:

1. **Proportional limit** (point P): Stress at which the stress-strain curve first deviates from linear behavior.
2. **Elastic limit** (point E): Highest stress the material can withstand and still return exactly to its original length when unloaded.
3. **Yield strength** (point Y): The elastic limit is difficult to obtain experimentally, so the yield stress as shown is of-

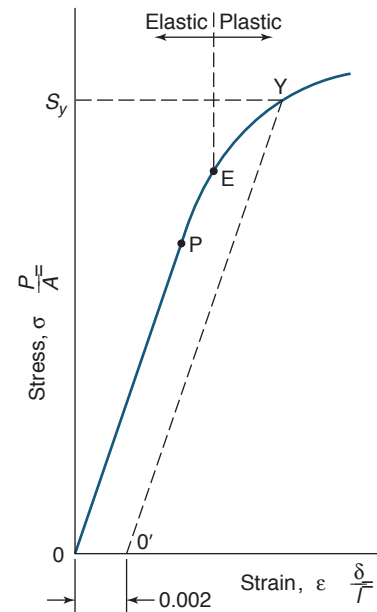


Figure 3.6: Typical stress-strain behavior for ductile metal showing elastic and plastic deformations and yield strength  $S_y$ .

ten used. The yield point is determined by starting a line at a deformation of 0.002 (0.2%) on the  $x$ -axis of Fig. 3.5, and that has a slope equal to the initial elastic modulus. The yield point is the location where this line intercepts the stress-strain curve.

4. **Ultimate strength** (point U): Maximum stress reached in the stress-strain diagram
5. **Fracture stress** (point R): Stress at the time of fracture or rupture.

Note that the elastic limit (point E) is not shown in Fig. 3.5 but is shown in Fig. 3.6 and clarifies behavior near the elastic-plastic demarcation point. In practice, the change in slope is not as pronounced as in Fig. 3.6, and the difference between points E and Y can be more subtle. Note that loading occurs along OPEY; unloading occurs along YO' and is assumed to be linear.

Figure 3.6 can be divided into elastic and plastic regions. The demarcation point is point E, the elastic limit, although Y, the yield point, is often used because it is more easily characterized. Three different phenomena occur during plastic behavior:

1. **Yielding:** A slight increase in stress above the elastic limit (point E) will cause the metal to deform permanently (plastic deformation).
2. **Strain hardening:** After yielding and before reaching the ultimate strength,  $S_u$ , strain hardening occurs. That is, ductile metals become harder and stronger as they plastically deform.
3. **Necking:** Necking, which is a localized deformation and decrease in cross-sectional area, occurs after the ultimate stress is reached and it continues until fracture occurs, as shown in Fig. 3.1.

Thus far, the discussion of stress-strain diagrams has focused on ductile metals. Figure 3.7 compares typical tensile stress-strain diagrams for a brittle and a ductile metal loaded to

Stress-Strain Diagram

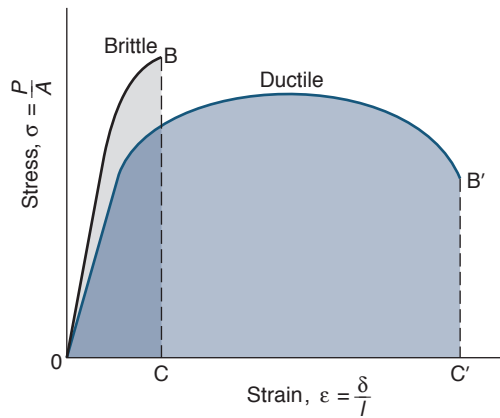


Figure 3.7: Typical tensile stress-strain diagrams for brittle and ductile metals loaded to fracture.

fracture. The brittle metal experiences little or no plastic deformation, whereas the ductile metal attains large strains before fracture occurs. Also, brittle materials have considerably higher (typically 10 times or greater) ultimate strength in compression than in tension. In contrast, ductile materials have essentially the same ultimate strength in compression and in tension.

### 3.4.2 Ceramics

The stress-strain behavior of ceramics is not usually determined by the tensile test used for metals. The reason for this is twofold. First, it is difficult to prepare and test specimens having the required geometry; and second, there is a significant difference in results obtained from tests conducted in compression and in tension. Therefore, a more suitable transverse bending test is most frequently used, in which a specimen having either a circular or rectangular cross section is bent until it fractures. Stress is computed from the specimen thickness, the bending moment, and the moment of inertia of the cross section. The maximum stress, or the stress at fracture, is sometimes called the **modulus of rupture**, and is an important parameter used in characterizing ceramics.

The stress-strain behavior for ceramic materials obtained in the transverse bending test is similar to the tensile test results for metals. A linear relationship exists between stress and strain. In Fig. 3.8, the stress-strain diagram for a ceramic shows that strength depends on whether the loading is compressive or tensile. This is understandable because ceramics are notoriously brittle and, if loaded in tension, imperfections in the material become fracture initiation and propagation sites. In compression, on the other hand, defects such as microcracks are squeezed, so that they do not compromise the material's strength. This kind of behavior can also be seen with cast metals, which have large numbers of voids in their lattices.

Strength for ceramics refers to fracture strength in tension and crushing strength in compression; typically, the compressive strength is many times larger than the tensile strength. Once the crushing strength is reached, the strain increases significantly but the stress decreases. The  $x$  in Fig. 3.8 designates the elastic strain when the fracture strength in tension is reached.

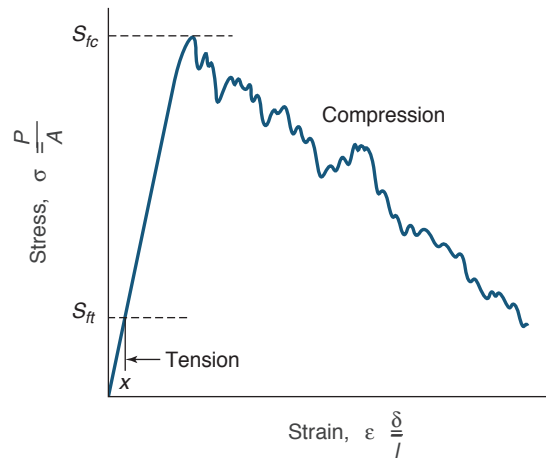


Figure 3.8: Stress-strain diagram for ceramic in tension and in compression.

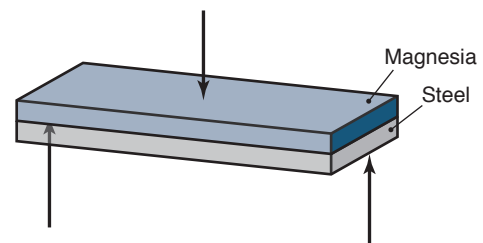


Figure 3.9: Beam loaded in three-point bending used in Example 3.4.

### Example 3.4: Design of a Composite Beam

**Given:** A beam, shown in Fig. 3.9, consists of equal lengths and cross sections of magnesia and AISI 1080 steel. The magnesia and steel sections are bonded together so that they act as a single beam. The beam is simply supported and subjected to three-point bending as shown. Assume that for magnesia,  $E_m = 207$  GPa and  $S_{um} = 105$  MPa and for 1080 steel,  $E_s = 207$  GPa,  $S_{ys} = 380$  MPa, and  $S_{us} = 615$  MPa.

**Find:** Is the beam strongest when the steel is at the bottom (as shown in Fig. 3.9) or at the top?

**Solution:** An important feature of ceramics is that they are typically 15 times stronger in compression than in tension, whereas steels have the same yield stress in compression or tension. In Fig. 3.9, the top member is in compression while the bottom member is in tension. Thus, for the steel at the bottom and magnesia at the top, as shown in Fig. 3.9, the magnesia is in compression with a compressive strength of around  $(15)(105 \times 10^6) = 1575$  MPa and is much stronger than the steel, which is in tension with a strength of 380 MPa. If the magnesia were at the bottom instead of the top, it would be in tension with a strength of 105 MPa and thus would be weaker than the steel, which would be in compression with a strength of 380 MPa. Taking the weakest members of the two beam combinations (since that is where it will fail), we find that the beam is about  $380/105 = 3.642$  times stronger when the steel is at the bottom in Fig. 3.9.



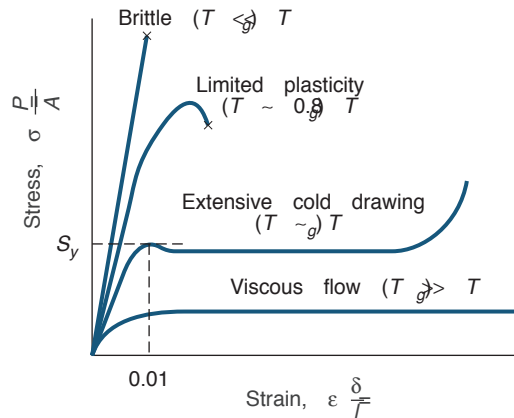


Figure 3.10: Stress-strain diagram for polymer below, at, and above its glass transition temperature,  $T_g$ .

### 3.4.3 Polymers

The testing techniques and specimen configurations used to develop stress-strain diagrams for metals can be used with slight modifications for polymers, especially for highly elastic materials such as rubbers. However, the stress-strain behavior of these materials is unique, and is very sensitive to temperature. For this reason, it also helps to distinguish between thermoplastics and thermosets. Thermosets typically have little plastic deformation, so that their stress-strain diagrams in tension are essentially the same as the brittle materials in Fig. 3.7 or the ceramic in Fig. 3.8. Polymers are slightly stronger ( $\sim 20\%$ ) in compression than in tension.

Thermoplastics behave very differently. Figure 3.10 shows stress-strain behavior for a thermoplastic polymer below, at, and above its glass transition temperature. The **glass transition temperature**,  $T_g$ , is the temperature at which a polymer transforms from a hard and brittle material to a rubbery or leathery solid. For  $T \ll T_g$  the polymer fractures after relatively small strains. For  $T \approx T_g$  the plastic can undergo very large strains. Above the melting temperature (used for manufacturing applications), the material flows like a viscous liquid as shown. Finally, the deformation displayed for  $T \ll T_g$  is fully elastic.

Elastomers, like thermosetting polymers, are brittle, but elastomers can survive large strains before fracture (as can be seen with a rubber band). Elastomers may be elastic, but they are highly nonlinear. After an initial linear zone, the stress-strain diagram becomes markedly nonlinear, having typically a strain of 0.01, as shown in Fig. 3.10. This nonlinearity may be caused either by shear yielding, the irreversible slipping of molecular chains, or by crazing (the formation of low-density, crack-like volumes that scatter light, making the polymer look white).

These stress-strain diagrams for metals, polymers, and ceramics reveal the following characteristics:

1. For brittle solids (ceramics, glasses, brittle polymers, and brittle metals), a yield strength may be difficult to determine and the fracture strength or ultimate strength is used in design.
2. For metals, ductile polymers, and most composites, the ultimate strength is larger than the yield strength by a factor of 1.1 to 4. The reason for this is mainly work hardening or, in the case of composites, load transfer to the reinforcement. Either yield or ultimate strength may be used in design, depending on the particular application and constraints.

### Example 3.5: Glass Transition Temperature

**Given:** A plastic cup is made of polymethylmethacrylate. The room-temperature elongation at fracture is 5% and the glass transition temperature is  $90^\circ\text{C}$ . The cup is sterilized with  $100^\circ\text{C}$  superheated steam at a high pressure, stressing the plastic to 30 MPa.

**Find:** Can the cup be expected to maintain its shape during sterilization?

**Solution:** Since the sterilization temperature is  $10^\circ\text{C}$  above the glass transition temperature, the plastic will deform by more than 5% (see Fig. 3.10). The stress is approximately half the ultimate strength at room temperature. It can therefore be concluded that the cup will deform during sterilization.

## 3.5 Properties of Solid Materials

This section defines the various engineering properties of solid materials needed to select the proper materials for machine elements. All these properties may not be important for each machine element considered in Chapters 9 to 19, but they are important for the wide range of applications of the various machine elements. For each property the relative behaviors of the classes of material are presented as well as the relative behaviors of the various materials within a specific class.

### 3.5.1 Density

**Density** is the mass per unit volume. The SI unit of density is kilograms per cubic meter. Typical densities of solid materials lie between  $10^3$  and  $10^4$   $\text{kg}/\text{m}^3$ . Figure 3.11 illustrates the density ranking of various metals, polymers, and ceramics. Metals, such as lead, copper, and steel, have the highest mass density. Polymers, such as nylon, natural rubber, and polyethylene, have the lowest mass density. Table 3.1 gives values of density at room temperature ( $20^\circ\text{C}$ ).

Metals are dense because they are made of heavy atoms in an efficient packing. Ceramics, for the most part, are also efficiently packed, but have lower densities than metals because they contain oxygen, nitrogen, and carbon atoms. Polymers have low densities because they are mainly made of carbon and hydrogen, and they are never completely crystalline, so that the atoms are not efficiently packed.

Alloying changes the density of metals only slightly. To a first approximation, the highest density of an alloy (metallic solid resulting from combining two or more metals) is given by a linear interpolation between the densities of the alloy concentrations.

### 3.5.2 Modulus of Elasticity, Poisson's Ratio, and Shear Modulus

The **modulus of elasticity** (or **Young's modulus**) is defined as the slope of the linear-elastic part of the stress-strain curve. In Fig. 3.6, the linear portion of the stress-strain curve is between the origin and point P, or at stresses lower than the proportional limit stress. The modulus of elasticity can be written as

$$E = \frac{\sigma}{\epsilon} \quad (3.3)$$

Since strain has no dimension, the modulus of elasticity has the same units as stress, or  $\text{N}/\text{m}^2$ . Figure 3.12 and Table 3.1



Table 3.1: Typical physical properties of common engineering materials.

Material	Elastic modulus, $E$ , (GPa)	Poisson's ratio, $\nu$	Density, $\rho$ , (kg/m <sup>3</sup> )	Thermal conductivity, $K_t$ (W/m $\cdot$ C)	Thermal expansion coefficient, $\alpha$ ( $\mu\text{m}/\text{m}\cdot\text{C}$ )	Specific heat, $C_p$ (J/kg $\cdot$ C)
<b>Metals</b>						
Aluminum	62	0.33	2700	209	23	900
Aluminum alloys	70	0.33	2630-2820	221-239	24	900
Aluminum tin	63	0.33	2700	180	24	960
Babbitt, lead-based	29	0.33	7530	24	20	150
Babbitt, tin-based	52	0.33	7340	56	23	210
Brasses	100	0.33	7470-8940	120	19	390
Bronze, aluminum	117	0.33	8940	50	18	380
Bronze, leaded	97	0.33	9100	47	18	380
Bronze, phosphor	110	0.33	8500	50	18	380
Bronze, porous	60	0.22	8040	30	18	380
Copper	124	0.33	8970	170	18	380
Iron, gray cast	109	0.26	7860	50	11	420
Iron, malleable cast	170	0.26	7860		11	420
Iron, spheroidal graphite	159	0.26	7860	30	11	420
Iron, porous	80	0.20	7460	28	12	460
Iron, wrought	170	0.30	7860	70	12	460
Magnesium alloys	41	0.33	1770	110	27	1000
Nickel alloys	221	0.31	8850	52-63	15	440
Steel, low alloys	196	0.30	7800	35	11	450
Steel, medium and high alloys	200	0.30	7850	30	11	450
Steel, stainless	193	0.30	8030	15	17	500
Steel, high speed	212	0.30	7860	30	11	450
Titanium alloys	110	0.32	4510	8-12	8.4	520
Zinc alloys	50	0.27	7135	110	27	400
<b>Polymers</b>						
Acetal (polyformaldehyde)	2.7	0.35	1400	0.24	90	1460
Nylons (polyamides)	1.9	0.40	1140	0.25	100	1700
Polyethylene, high density	0.9	0.35	940	0.5	126	1800
Phenol formaldehyde	7.0	0.35	1362	0.17	25-40	1600
Rubber, natural	0.004	0.50	930	1.6	80-120	2000
<b>Ceramics</b>						
Alumina (Al <sub>2</sub> O <sub>3</sub> )	390	0.28	961	25	5.0	880
Graphite	27	0.31	2400	125	1.4-4.0	840
Silicon carbide (SiC)	450	0.19	3210	15	4.3	750
Silicon nitride (Si <sub>3</sub> N <sub>4</sub> )	314	0.26	3290	30	3.2	710

give data for the elastic modulus for various metals, polymers, and ceramics at room temperature. The elastic moduli for metals and ceramics are high and quite similar, but those for polymers are considerably lower.

The elastic moduli of most materials depend on two factors: bond strength and bond density per unit area. A bond is like a spring; it has a spring rate,  $k$  (in newtons per meter). The modulus of elasticity,  $E$ , is roughly

$$E = \frac{k}{r_o} \quad (3.4)$$

where  $r_o$  is the atom size (this can be obtained from the mean atomic volume  $4\pi r_o^3/3$ , which is generally known). The wide range of modulus of elasticity in Fig. 3.12 and Table 3.1 is largely caused by the range of  $k$  in materials. The covalent bond is stiff ( $k = 20$  to  $200$  N/m), while the metallic and ionic bonds are somewhat less stiff ( $k = 15$  to  $100$  N/m). Diamond, although not shown in Fig. 3.12 or Table 3.1, has a very high modulus of elasticity because the carbon atom is small (giving a high bond density) and its atoms are linked by extremely strong bonds ( $200$  N/m). Metals have a high modulus of elasticity because close packing gives a high bond density and the bonds are strong, although not as strong as those of diamond. Polymers contain both strong diamond-like covalent bonds and weak hydrogen (or van der Waals) bonds ( $k = 0.5$  to  $2$  N/m); these weak bonds stretch when a polymer is deformed, giving a lower modulus of elasticity. Elastomers have a low modulus of elasticity because they have only an extremely weak restoring force, which is associated with tangled, long-chain molecules when the material is loaded.

In a tension test, there will be axial deformation, but there will also be dimensional changes in the transverse direction, for as a bar extends axially, it contracts transversely. The transverse strain,  $\epsilon_t$ , is related to the axial strain,  $\epsilon_a$ , by **Poisson's ratio**,  $\nu$ , such that

$$\epsilon_t = -\nu\epsilon_a \quad (3.5)$$

The negative sign simply means that the transverse deformation will be in the opposite sense to the axial deformation. Poisson's ratio is dimensionless. Table 3.1 gives quantitative values of Poisson's ratio for various metals, polymers, and ceramics at room temperature. The highest Poisson's ratio approaches 0.5 for rubber, and the lowest is 0.19 for silicon carbide and cemented carbides (although it approaches zero for cork or foams in compression). Poisson's ratio cannot be less than zero (or else the second law of thermodynamics would be violated), nor can it exceed 0.5 (or else a material's volume would increase when compressed).

Shear stress and strain are proportional to each other; that is

$$\tau = G\gamma \quad (3.6)$$

where  $G$  is the **shear modulus** or **modulus of rigidity**. This relation is only true for the linear-elastic region of the shear stress-strain curve (from 0 to  $P$  in Fig. 3.6).  $G$  has units of stress (N/m<sup>2</sup>).

The three material properties  $E$ ,  $G$ , and  $\nu$  are related by the following equation:

$$G = \frac{E}{2(1 + \nu)} \quad (3.7)$$

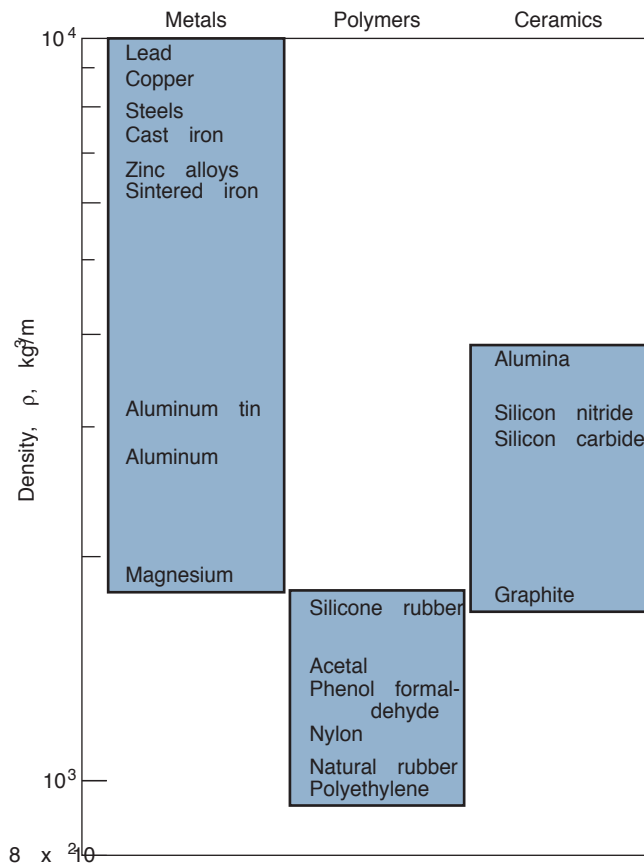


Figure 3.11: Density for various metals, polymers, and ceramics at room temperature (20°C).

Thus, when two parameters are known, the third can easily be determined from Eq. (3.7). That is, if for a particular material, the modulus of elasticity and Poisson's ratio are obtained from Table 3.1, then the shear modulus can be obtained from Eq. (3.7).

The material presented thus far is valid for metals, polymers, or ceramics. To establish the modulus of elasticity for a unidirectional fiber-reinforced composite in the direction of the fibers, it is assumed that the fiber-matrix interfacial bond is good, so that deformation of both matrix and fibers is the same. Under these conditions, the total load sustained by the composite,  $P_c$ , is equal to the loads carried by the matrix,  $P_m$ , and the fiber,  $P_f$ , or

$$P_c = P_m + P_f, \quad (3.8)$$

where subscripts  $c$ ,  $m$ , and  $f$  refer to composite, matrix, and fiber, respectively. Substituting Eq. (3.8) into the definition of stress given by Eq. (2.7) results in

$$\sigma_c = \sigma_m \frac{A_m}{A_c} + \sigma_f \frac{A_f}{A_c}. \quad (3.9)$$

If the composite, matrix, and fiber lengths are equal, Eq. (3.9) becomes

$$\sigma_c = \sigma_m v_m + \sigma_f v_f, \quad (3.10)$$

where  $v_m$  is the volume fraction of the matrix and  $v_f$  is the volume fraction of the fiber in the composite material. Because the same deformation of matrix and fibers was assumed and the composite consists of only matrix and fibers

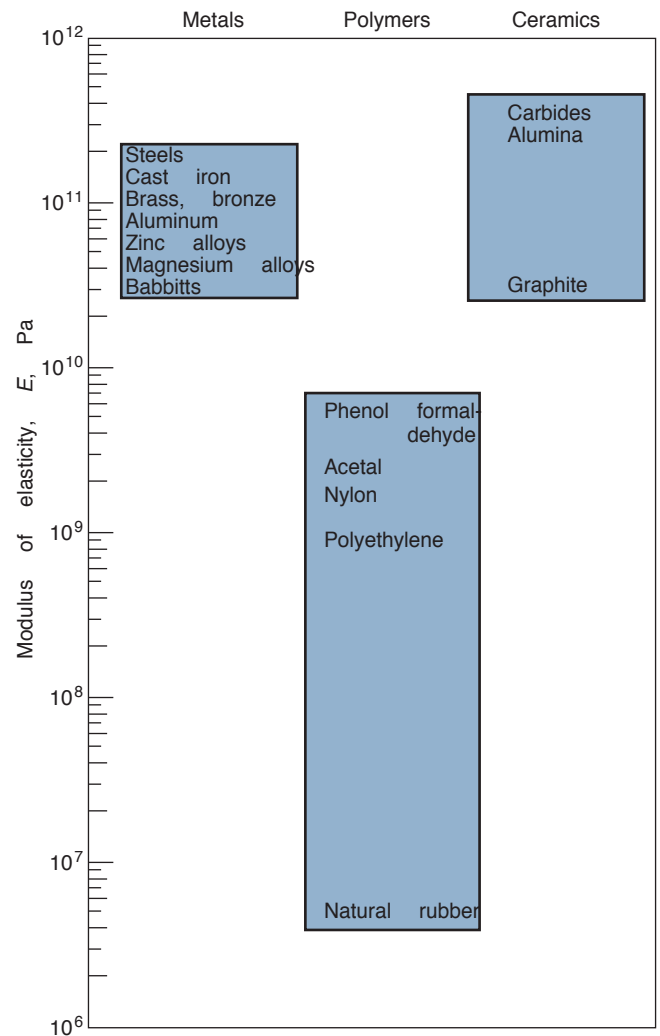


Figure 3.12: Modulus of elasticity for various metals, polymers, and ceramics at room temperature (20°C).

(i.e.,  $v_m + v_f = 1$ ), Eq. (3.10) can be rewritten in terms of the moduli of elasticity as

$$E_c = E_m v_m + E_f v_f \quad (3.11)$$

or

$$E_c = E_m (1 - v_f) + E_f v_f. \quad (3.12)$$

Thus, Eq. (3.12) enables the composite's modulus of elasticity to be determined when the elastic moduli of the matrix and the fiber and the volume fractions of each are known. It can also be shown that the ratio of the load carried by the fibers to that carried by the matrix is

$$\frac{P_f}{P_m} = \frac{E_f v_f}{E_m v_m}. \quad (3.13)$$

Recall that Eqs. (3.8) to (3.13) are only applicable to unidirectional, fiber-reinforced composites.

### Example 3.6: Stiffness of a Fiber Reinforced Polymer

**Given:** A fiber-reinforced plastic contains 10 vol% glass fibers ( $E = 70$  GPa,  $S_u = 0.7$  GPa).

**Find:** Calculate how this fiber percentage has to be changed to give the same elastic properties if the glass fibers are changed to carbon fibers ( $E = 150$  GPa,  $S_u = 1$  GPa). Assume the matrix material has  $E_m = 2$  GPa.

**Solution:** According to Eq. (3.11), the modulus of elasticity for a fiber composite is

$$E_c = E_m v_m + E_f v_f.$$

Therefore, for the glass fiber-reinforced material,

$$E_c = (2 \times 10^9) (0.9) + (70 \times 10^9) (0.1) = 8.8 \text{ GPa}.$$

This composite modulus of elasticity should be maintained for the carbon-reinforced plastic:

$$8.8 \times 10^9 = (2 \times 10^9) x + (150 \times 10^9) (1 - x),$$

which is solved as  $x = 0.954$  or  $1 - x = 0.046$ . Thus, the plastic should contain 4.6 vol% carbon fibers to get the same elastic properties as the glass-fiber-reinforced plastic with 10% glass fibers.

### 3.5.3 Strength

The strength of a machine element depends on the class, treatment, and geometry of the specimen as well as the type of loading that the machine element will experience. This section focuses on the various classes of material and their strength characteristics.

#### Metals

Metals can be divided into ferrous and nonferrous alloys. Ferrous alloys are those in which iron is the primary component, but carbon as well as other alloying elements may be present. Nonferrous alloys are all those alloys that are not iron-based. Recall that the strength of metals is essentially the same in compression or in tension. Tables A.1 through A.12 show the yield strengths for various metals.

#### Polymers

The strength of polymers is determined by a strain of 0.010, as opposed to the nonrecoverable plastic strain of 0.002 used to define yield strength for metals. Polymers are somewhat stronger (~20%) in compression than in tension. Also, when dealing with polymers the strength of interest is the ultimate strength at fracture rather than the yield strength as for metals. The tensile strengths at fracture for selected thermoplastic and thermosetting polymers are given in Table A.13.

#### Ceramics

The strength of interest for ceramics is the fracture strength. Ceramics, being brittle materials, are much stronger in compression (typically 15 times stronger) than in tension. Table A.14 gives fracture strength in tension for selected ceramic materials.

### 3.5.4 Resilience and Toughness

**Resilience** is a material's capacity to absorb energy when it is deformed elastically and then, upon unloading, to release this energy. The **modulus of resilience**,  $U_r$ , is the strain energy per unit volume required to stress a material from an unloaded state to the point of yielding. Mathematically, this is expressed as

$$U_r = \int_0^{\epsilon_y} \sigma d\epsilon, \quad (3.14)$$

where  $\epsilon_y$  is the yield strain, or the strain when the stress is the yield strength,  $S_y$ . For the linear-elastic region, the area below the stress-strain diagram is the modulus of resilience or

$$U_r = \frac{S_y \epsilon_y}{2}. \quad (3.15)$$

Making use of Eq. (3.3) gives

$$U_r = \frac{S_y^2}{2E}. \quad (3.16)$$

An example of a material with high modulus of resilience is high-carbon steel. Resilience is extremely useful in selecting a material for springs (see Chapter 16), or for energy storage, making high-carbon steel alloys primary candidate materials for such applications.

**Toughness** is a material's ability to absorb energy up to fracture. For the static (low-strain rate) situation, toughness can be obtained from the stress-strain curve (e.g., see Fig. 3.5) up to the point of fracture or rupture. **Resilience** is the strain energy per unit volume up to the yield strength of the material (point Y in Fig. 3.5); whereas toughness is energy per unit volume to rupture (point R). While resilience represents energy that can be recovered, toughness is associated with energy that is absorbed by the material during deformation, only some of which may be recovered upon unloading.

For a material to be tough, it must display both strength and ductility; and often, ductile materials are tougher than brittle materials, as demonstrated in Fig. 3.7.

### Example 3.7: Resilience

**Given:** In a mining operation, iron ore is dumped into a funnel-shaped hopper that fills box cars for transport by train. The inside of the hopper wears rapidly because the impact of the ore produces plastic deformation in the hopper surface. A change of surface material is considered.

**Find:** Which is the better choice of hopper surface material, hard steel (AISI 1080) or rubber?

**Solution:** A key parameter to be used in this evaluation is the resilience of the two materials. For AISI 1080 high-carbon steel from Table A.2,  $S_y = 380$  MPa and  $E = 207$  GPa. From Eq. (3.16) the modulus of resilience for AISI 1080 steel is

$$(U_r)_{\text{steel}} = \frac{S_y^2}{2E} = \frac{(380 \times 10^6)^2}{2(207 \times 10^9)} = 348,800 = 0.3488 \text{ MPa}.$$

For natural rubber, from Tables A.13,  $S_u = 30$  MPa and  $E = 0.004$  GPa. Therefore, from Eq. (3.16)

$$(U_r)_{\text{rubber}} = \frac{(30 \times 10^6)^2}{2(4 \times 10^6)} = 112.5 \times 10^6 = 112.5 \text{ MPa}.$$

Rubber is over two orders of magnitude more resilient than steel. Based on this parameter only, it would appear that the inside of the hopper should have a rubber lining.


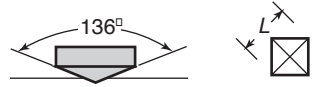
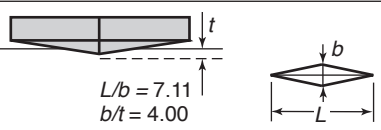
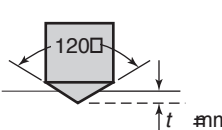
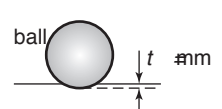
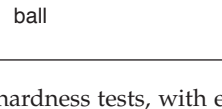
Test	Indenter	Shape of indentation Side view Top view	Load, $P$	Hardness number
Brinell	10-mm steel or tungsten carbide ball		500 kg 1500 kg 3000 kg	$HB = \frac{2P}{(\pi D) (D - \sqrt{D^2 - d^2})}$
Vickers	Diamond pyramid		1-120 kg	$HV = \frac{1.854P}{L^2}$
Knoop	Diamond pyramid		0.025-5 kg	$HK = \frac{14.2P}{L^2}$
Rockwell			kg	
A C D	Diamond cone		60 150 100	HRA HRC HRD
B F G			100 60 150	HRB HRF HRG
E			100	HRE
	$\frac{1}{16}$ - in. diameter steel ball			
	$\frac{1}{8}$ - in. diameter steel ball			

Figure 3.13: General characteristics of selected hardness tests, with equations for calculating hardness. *Source:* Kalpakjian and Schmid [2010].

### 3.5.5 Hardness

Hardness is a commonly used property, since it correlates well to material strength and wear resistance. **Hardness** is usually defined as the resistance of a surface to plastic indentation. There are many particular geometries and loads that are useful for defining hardness. Figure 3.13 summarizes some of the popular hardness tests. Some of these are described below, and further information is contained in Kalpakjian and Schmid [2010].

1. A **Brinell hardness test** involves pressing a steel or tungsten-carbide ball 10 mm in diameter against a surface, with a load of 500, 1500, or 3000 kg (Fig. 3.13). The Brinell hardness number (HB) is defined as the ratio of the applied load in kilograms force to the curved surface area of the indentation given in square millimeters. The harder the material to be tested, the smaller the impression, hence a 1500-kg or 3000-kg load is usually recommended in order to obtain impressions sufficiently large for accurate measurement. Depending on the condition of the material, one of two types of impression develops on the surface after the test (Fig. 3.14) or of any of the other tests described in this section. The impressions in annealed metals generally have a rounded profile (Fig. 3.14a); in cold-worked metals they usually have a sharp profile (Fig. 3.14b). The correct method of measuring the indentation diameter,  $d$ , is shown in the figure.

The indenter, which has a finite elastic modulus, also undergoes elastic deformation under the applied load; as a result, hardness measurements may not be as accurate as expected. One method for minimizing this effect

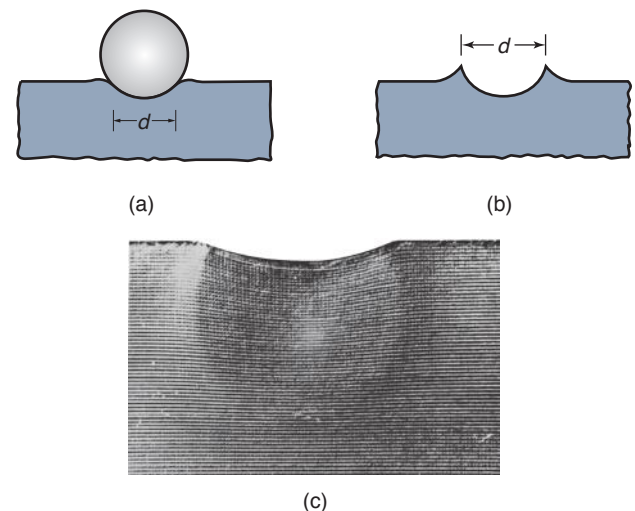


Figure 3.14: Indentation geometry in Brinell hardness testing: (a) annealed metal; (b) work-hardened metal; (c) deformation of mild steel under a spherical indenter. Note that the depth of the permanently deformed zone is about one order of magnitude larger than the depth of indentation. For a hardness test to be valid, this zone should be fully developed in the material. *Source:* Kalpakjian and Schmid [2010].



is to use tungsten-carbide balls because of their higher modulus of elasticity. Carbide balls are usually recommended for Brinell hardness numbers greater than 500.

2. A **Rockwell hardness test**, of which there are many variations, measures the depth of penetration instead of the diameter of the indentation. The indenter is pressed onto the surface, first with a minor load and then with a major load; the difference in the depth of penetration is a measure of the hardness of the material. Some of the more common Rockwell hardness scales and the indenters used are shown in Fig. 3.13, but many more forms have been standardized for particular applications. Rockwell superficial hardness tests have also been developed using the same type of indenters but at lighter loads.
3. The **Vickers test** uses a pyramid-shaped diamond indenter and a load that ranges from 1 kg to 120 kg. The Vickers hardness number is indicated by HV. The impressions obtained are typically less than 0.5 mm on the diagonal. The Vickers test gives essentially the same hardness number regardless of the load, and is suitable for testing materials with a wide range of hardness, including heat-treated steels. More recently, test procedures have been developed to perform Vickers-type tests in atomic force microscopes and nanoindenters, to estimate hardness at penetration depths as low as 20 nm.
4. The **Knoop test** (Fig. 3.13) uses a diamond indenter in the shape of an elongated pyramid, with applied loads ranging generally from 25 g to 5 kg. The Knoop hardness number is indicated by HK. Because of the light loads that are applied, it is a microhardness test; therefore, it is suitable for very small or very thin specimens, and for brittle materials such as carbides, ceramics, and glass. This test is also used for measuring the hardness of the individual grains and components in a metal alloy. The size of the indentation is generally in the range from 0.01 to 0.10 mm; consequently, surface preparation is very important. Because the hardness number obtained depends on the applied load, Knoop test results should always cite the load used.
5. Rebound tests such as the **Scleroscope** and **Leeb tests** are commonly performed. The scleroscope is an instrument in which a diamond-tipped indenter (hammer) enclosed in a glass tube is dropped onto the specimen from a certain height. The hardness is related to the rebound of the indenter: the higher the rebound, the harder the material. The impression made by a scleroscope is very small. Because obtaining reliable results with a scleroscope is difficult, a modern electronic version, called a *Leeb*, or *Equotip*, test, has been developed. In this test, a carbide hammer impacts the surface, and incident and rebound velocities are electronically measured. A Leeb number is then calculated and usually converted to Rockwell or Vickers hardness.
6. The hardness of materials such as rubbers, plastics, and similar soft and elastic nonmetallic materials is generally measured using a **Shore test** with an instrument called a **durometer** (from the Latin *durus*, meaning "hard"). An indenter is pressed against the surface and then a constant load is rapidly applied. The depth of penetration is measured after one second; the hardness is inversely related to the penetration. The hardness numbers in these tests range from 0 to 100.

Because hardness is the resistance to permanent indentation, it can be likened to performing a compression test on a small volume of a material's surface (Fig. 3.14c). Studies have shown that (in the same units) the hardness of a cold-worked metal is about three times its yield stress,  $S_y$ ; for annealed metals, it is about five times  $S_y$ . An additional relationship has been established between the ultimate tensile strength,  $S_u$ , and the Brinell hardness, HB, for steels as measured for a load of 3000 kg:

$$S_u = 3.5HB. \quad (3.17)$$

Note that the units in Eq. (3.17) are important; for the equation to be valid,  $S_u$  must be expressed in MPa and the Brinell hardness measured in kilograms force per square millimeter.

### 3.5.6 Thermal Conductivity

The rate at which heat is conducted through a solid at steady state (meaning that temperature does not vary with time) is a measure of the **thermal conductivity**,  $K_t$ . When two bodies at different temperatures are brought together, the faster-moving molecules of the warmer body collide with the slower-moving molecules of the cooler body and transfer some of their motion to the latter. The warmer body loses energy (drops in temperature) while the cooler one gains energy (rises in temperature). The transfer process stops when the two bodies reach the same temperature. This transfer of molecular motion through a material is called **heat conduction**. Materials differ in how fast they conduct heat. The SI unit of thermal conductivity,  $K_t$ , is watts per meter-Celsius.

Figure 3.15 ranks the thermal conductivity for various metals, polymers, and ceramics. Metals and ceramics in general are good conductors (high  $K_t$ ) and polymers are good insulators (low  $K_t$ ). Table 3.1 quantifies the thermal conductivity values given in Fig. 3.15. In Fig. 3.15 and Table 3.1, unless otherwise stated, the temperature is assumed to be room temperature (20°C).

### 3.5.7 Linear Thermal Expansion Coefficient

Different materials may expand more or less when heated. Thermal strain is proportional to the temperature change, and their ratio is constant over a fairly large temperature range. This observation can be expressed by

$$\epsilon = \bar{\alpha} \Delta t_m, \quad (3.18)$$

where  $\bar{\alpha}$  is called the *linear expansivity* or **linear thermal expansion coefficient**. The SI unit of  $\bar{\alpha}$  is  $(^\circ\text{C})^{-1}$ . Figure 3.16 ranks the linear thermal expansion coefficient for various metals, polymers, and ceramics applied over the temperature range 20 to 200°C. Polymers have the highest thermal expansion coefficient, followed by metals and then ceramics. Table 3.1 gives quantitative values of  $\bar{\alpha}$  for various metals, polymers, and ceramics from 20 to 200°C.

### 3.5.8 Specific Heat Capacity

The nature of a material determines the amount of heat required to change its temperature by a given amount. Imagine an experiment in which a cast iron ball and a babbitt (lead-based white metal) ball of the same size are heated to the temperature of boiling water and then laid on a block of wax. The cast iron ball would melt a considerable amount of wax, but the babbitt ball, in spite of its greater mass, would melt hardly any. It therefore would seem that different materials, in cooling through the same temperature range, release different amounts of heat.



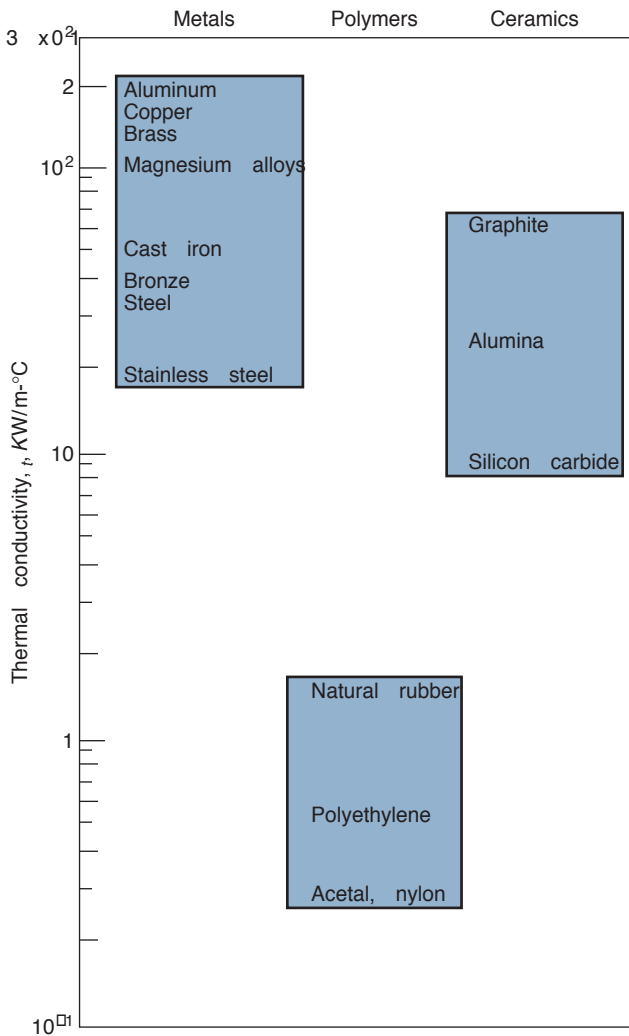


Figure 3.15: Thermal conductivity for various metals, polymers, and ceramics at room temperature ( $20^\circ\text{C}$ ).

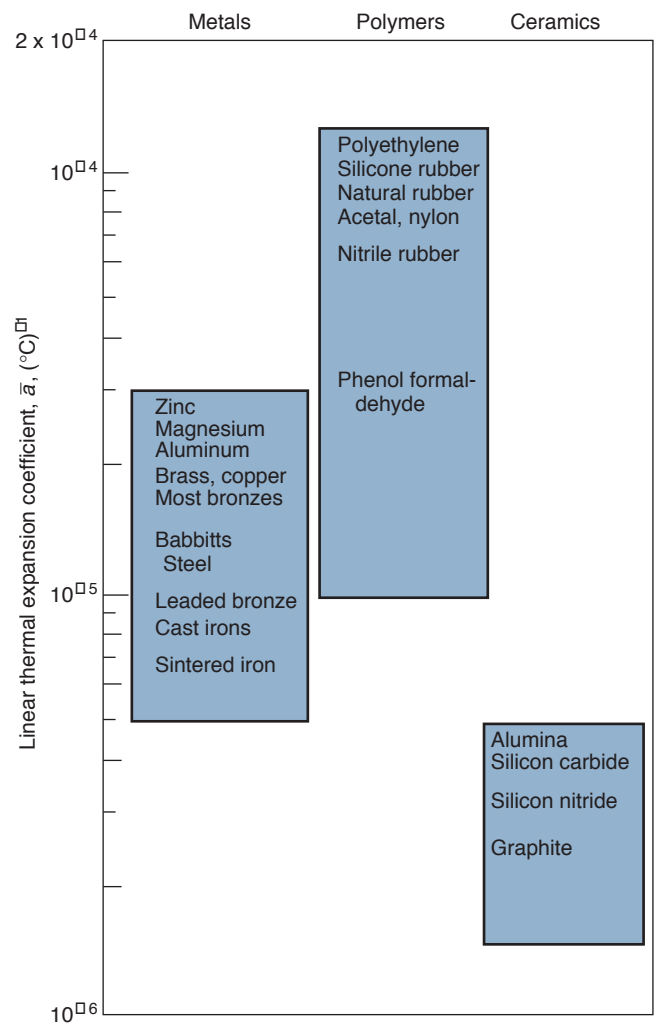


Figure 3.16: Linear thermal expansion coefficient for various metals, polymers, and ceramics at room temperature ( $20^\circ\text{C}$ ).

The quantity of heat energy given up or taken on when a body changes its temperature is given by

$$Q = C_p m_a (\Delta T), \quad (3.19)$$

where

$Q$  = quantity of heat, J  
 $C_p$  = the **specific heat** of the material,  $\text{J}/(\text{kg}^\circ\text{C})$   
 $m_a$  = mass of body, kg  
 $\Delta T$  = temperature change,  $^\circ\text{C}$

Figure 3.17 illustrates the specific heat capacity of various metals, polymers, and ceramics at room temperature ( $20^\circ\text{C}$ ), while Table 3.1 provides quantitative values. Polymers have considerably higher specific heat than metals or ceramics.

### Example 3.8: Heat Content of Materials

**Given:** A thermos is made of two steel bottles, separated by a vacuum, where the inner bottle weighs 200 g and is filled with 500 g of boiling water. The initial temperature of the thermos is  $20^\circ\text{C}$ . The specific heat capacity for water  $C_p = 4180 \text{ J/kg}^\circ\text{C}$ .

**Find:**

- The maximum temperature of the water in the thermos when the heat has spread to the thermos walls
- The maximum temperature if the thermos is preheated by hot water, then emptied and refilled.

**Solution:** From Table 3.1, note that  $C_p$  for steel is  $450 \text{ J/kg}^\circ\text{C}$ .

- Assuming that no heat is dissipated to the surrounding area,

$$(m_a C_p)_{\text{steel}} (T - 20^\circ\text{C}) = (m_a C_p)_{\text{water}} (100^\circ\text{C} - T),$$

## Stress-Strain Relationships

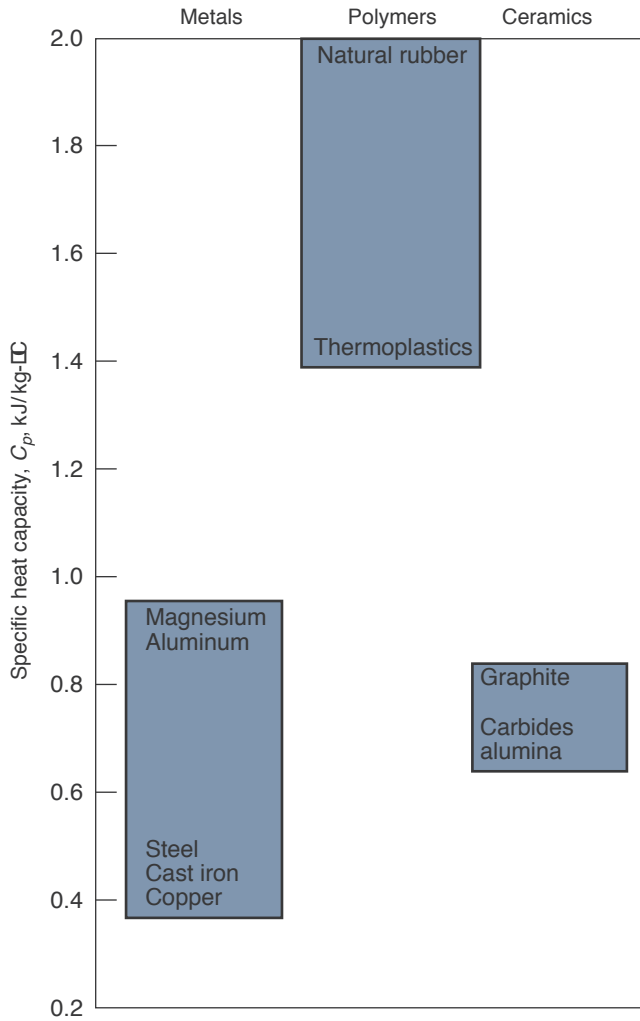


Figure 3.17: Specific heat capacity for various metals, polymers, and ceramics at room temperature (20°C).

or

$$\begin{aligned}
 T &= \frac{100(m_a C_p)_{\text{water}} + 20(m_a C_p)_{\text{steel}}}{(m_a C_p)_{\text{water}} + (m_a C_p)_{\text{steel}}} \\
 &= \frac{100(0.5)(4.180) + 20(0.2)(0.45)}{(0.5)(4.180) + (0.2)(0.45)} \\
 &= 96.7^\circ\text{C}.
 \end{aligned}$$

(b) The only change if the thermos is preheated is that 20°C is replaced with 96.7°C.

$$T = \frac{100(0.5)(4.180) + 96.7(0.2)(0.45)}{(0.5)(4.180) + (0.2)(0.45)} = 99.9^\circ\text{C}.$$

### 3.5.9 Archard Wear Constant

Wear is more difficult than the other properties of solid materials to quantify, partly because it is a surface phenomenon and not a bulk phenomenon, and also because wear involves interactions between two materials. When solids slide

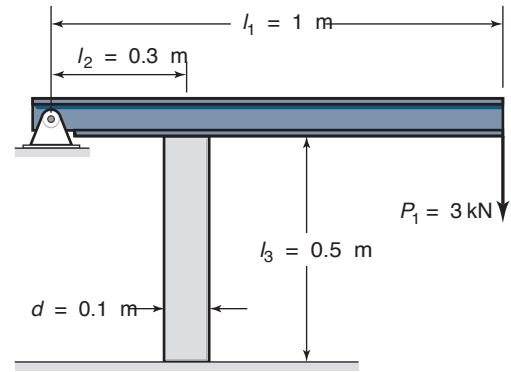


Figure 3.18: Rigid beam assembly use in Example 3.9.

against each other under a normal load, the volume of material lost from the softer surface is characterized by the **Archard wear equation** as:

$$v = k_1 \frac{WL}{3H}, \quad (3.20)$$

where  $v$  is the wear volume,  $W$  is the normal load,  $L$  is the sliding distance, and  $H$  is the hardness.  $k_1$  is the **Archard wear constant**, and is dimensionless if  $H$  is in  $\text{N/m}^2$ . The equations of wear are covered in greater detail in Section 8.9.

## 3.6 Stress-Strain Relationships

As discussed earlier in this chapter, the stress-strain diagrams for most engineering materials exhibit a linear relationship between stress and strain within the elastic limit. Therefore, an increase in stress causes a proportionate increase in strain. First discovered by Robert Hooke in 1678, this linear relationship between stress and strain in the elastic range is known as **Hooke's law**. Thus, for a uniaxial stress state, Hooke's law can be expressed as

$$\sigma = E\epsilon. \quad (3.21)$$

For isotropic materials in a triaxial stress state, the stress and strain are related by the generalized Hooke's law given by:

$$\epsilon_1 = \frac{\sigma_1}{E} - \frac{\nu\sigma_2}{E} - \frac{\nu\sigma_3}{E}, \quad (3.22)$$

$$\epsilon_2 = \frac{\sigma_2}{E} - \frac{\nu\sigma_1}{E} - \frac{\nu\sigma_3}{E}, \quad (3.23)$$

$$\epsilon_3 = \frac{\sigma_3}{E} - \frac{\nu\sigma_1}{E} - \frac{\nu\sigma_2}{E}. \quad (3.24)$$

These equations, and versions for some other common conditions, are derived in Appendix B.

### Example 3.9: Deformation

**Given:** A 1-m-long rigid beam shown in Fig. 3.18 is pinned at its left end, carries a 3-kN vertical load at its right end, and is kept horizontal by a vertical pillar located 0.3 m from the left end. The pillar is a 0.5-m-long steel tube with an outer diameter of 0.1 m and a wall thickness of 5 mm. The modulus of elasticity of the steel is 205 GPa.

**Find:** How much does the right end of the beam deflect due to the 3-kN force?

**Solution:** Moment equilibrium about the hinge pin gives

$$P_1 l_1 - P_2 l_2 = 0,$$

where  $P_2$  is the force in the pillar. Solving for  $P_2$ ,

$$P_2 = \frac{P_1 l_1}{l_2} = \frac{(3000)(1)}{0.3} = 10,000 \text{ N}.$$

Because the beam can rotate only about the hinge pin, the deflection  $\delta_1$  at  $P_1$  can be described by the angle of rotation,  $\alpha$ , and this angle is the same when describing the deflection  $\delta_2$  at  $P_2$ . Thus, for small rotations,  $\delta_1 = l_1 \alpha$  and  $\delta_2 = l_2 \alpha$ . This implies that

$$\delta_1 = \frac{l_1 \delta_2}{l_2}. \quad (a)$$

The compression of the vertical pillar,  $\delta_2$ , can be obtained by using Hooke's law or

$$\delta_2 = \frac{l_3 P_2}{EA} = \frac{l_3 P_2}{\pi E (r_o^2 - r_i^2)}. \quad (b)$$

Substituting Eq. (b) into Eq. (a) gives

$$\begin{aligned} \delta_1 &= \frac{l_1 l_3 P_2}{\pi l_2 E (r_o^2 - r_i^2)} \\ &= \frac{1(0.5)(10,000)}{\pi(0.3)(205 \times 10^9)(0.05^2 - 0.045^2)} \\ &= 5.45 \times 10^{-5} \text{ m} \\ &= 54.5 \mu\text{m}. \end{aligned}$$

## 3.7 Two-Parameter Materials Charts

Material properties limit the performance and life of machine elements. Robust designs seldom derive from consideration of just one property of the solid materials. Thus, the information presented in Section 3.5 on the individual properties of solid materials is not adequate for selecting a material for a particular application. Instead, one or several combinations of properties are needed. Some important property combinations are

- Stiffness versus density ( $E$  versus  $\rho$ )
- Strength versus density ( $S$  versus  $\rho$ )
- Stiffness versus strength ( $E$  versus  $S$ )
- Wear constant versus limiting pressure ( $k_1$  versus  $p_l$ )

A number of other combinations might be useful in material selection, but these are the primary considerations in designing machine elements. Further information using the approach in this section, including additional material parameters and applications, are contained in Ashby [2010].

### 3.7.1 Stiffness versus Density

The modulus of elasticity and density are familiar properties in selecting solid materials. Figure 3.19 shows the full range of elastic modulus,  $E$ , and density,  $\rho$ , for engineering materials. Data for a particular class of material cluster together

and are enclosed by shaded domains. The same class cluster appears on all the diagrams.

Figure 3.19 shows that the moduli of elasticity for engineering materials span five decades from 0.01 to 1000 GPa; the density spans a factor of 200, from less than 100 to 20,000 kg/m<sup>3</sup>.

The chart helps in common problems of material selection for applications in which weight must be minimized. For example, consider a simple tension member where the weight is to be minimized and where the strain cannot exceed a given value,  $\epsilon_{cr}$ . If the material is loaded up to its yield point, the stress is given by  $\sigma = P/A$ . Also, from Hooke's law,

$$\sigma = E \epsilon_{cr}.$$

Equating the stresses gives

$$A = \frac{P}{E \epsilon_{cr}}. \quad (3.25)$$

The weight of the member is

$$W = A g l \rho. \quad (3.26)$$

Substituting Eq. (3.25) into Eq. (3.26) gives

$$\frac{W}{g} = \left( \frac{Pl}{\epsilon_{cr}} \right) \left( \frac{1}{E/\rho} \right). \quad (3.27)$$

Note that the first fraction contains design constraints and the second fraction contains all of the relevant material properties. Thus, the optimum material for minimizing Eq. (3.27) is one that maximizes the quantity  $E/\rho$ . In Fig. 3.19 this is accomplished by considering lines parallel to the  $E/\rho = C$  reference. Those materials with the greatest value in the direction normal to these lines are the optimum materials (i.e., those farthest toward the top and left of the charts). In Fig. 3.19, the reference lines refer to the minimum-weight design subjected to strain requirements under the following conditions:

$E/\rho = C$	Minimum-weight design of stiff tension members
$E^{1/2}/\rho = C$	Minimum-weight design of stiff beams and columns
$E^{1/3}/\rho = C$	Minimum-weight design of stiff plates

### Example 3.10: Material for a Solid Fishing Rod

**Given:** A fishing rod is to be made of a material that gives low weight and high stiffness.

**Find:** From Fig. 3.19 determine which is better, a rod made of plastic (without fiber reinforcement) or a split-cane rod (bamboo fibers glued together).

**Solution:** Figure 3.19 shows that only very special polymers have moduli of elasticity as high as the best wooden fibers. The polymers are also two to three times more dense than wood. A split-cane rod will therefore give a lower weight for a given stiffness than any plastic.

### 3.7.2 Strength versus Density

The weight of an object depends on its volume and its density. Strength, on the other hand, means different things for different classes of solid material. For metals it is the yield strength, which is the same in tension and compression. For

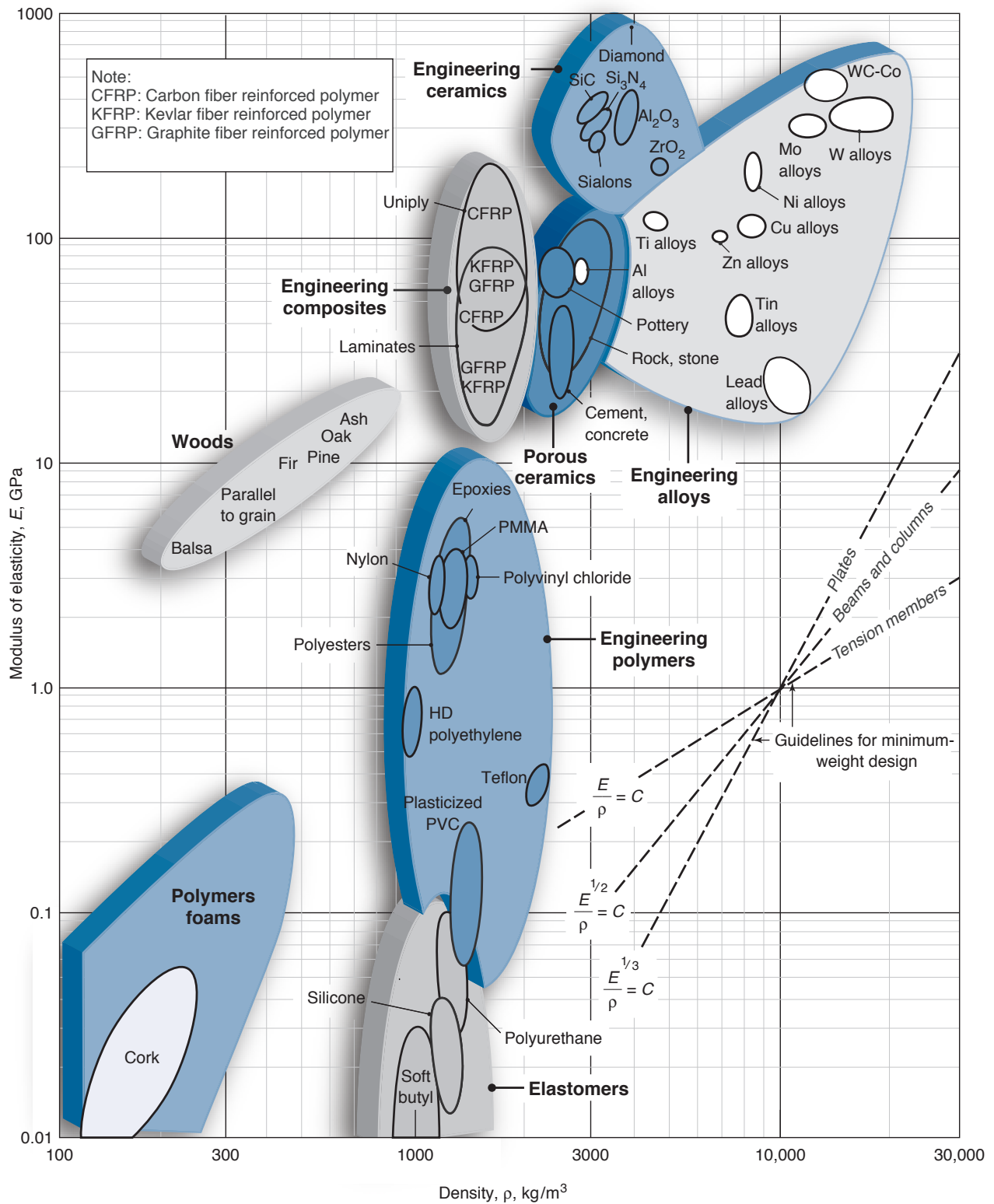


Figure 3.19: Two-parameter material chart containing elastic modulus and density. The diagonal contours show longitudinal wave velocity. The guidelines of constant  $E/\rho$ ,  $E^{1/2}/\rho$  and  $E^{1/3}/\rho$  allow selection of materials for minimum-weight, deflection-limited design. Source: Adapted from Ashby [2010].

brittle ceramics it is the crushing strength in compression, not that in tension, which is about 15 times smaller. For elastomers strength means the fracture strength. For composites it is the tensile failure strength (compressive strength can be lower because of fiber buckling).

Figure 3.20 shows these strengths, for which the symbol  $S$  is used (despite the different failure mechanisms involved), plotted against density,  $\rho$ . The considerable vertical extension of the strength domain for an individual material reflects its wide range of available properties, caused by the degree of alloying, work hardening, grain size, porosity, etc.

Figure 3.20 is useful for determining optimum materials based on strength where deformation under loading is not an issue. Just as before, one chooses a reference line, and materials located at the greatest distance from this line (up and to the left) are superior. The following circumstances correspond to the reference lines in Fig. 3.20:

$\sigma/\rho = C$	Tension members
$\sigma^{2/3}/\rho = C$	Beams and shafts
$\sigma^{1/2}/\rho = C$	Plates

The range of strength for engineering materials spans five decades, from 0.1 MPa (foams used in packaging and energy-absorbing systems) to  $10^4$  MPa (diamond). The range of density is the same as in Fig. 3.19.

### Example 3.11: Material for a Tubular Fishing Rod

**Given:** The fishing rod given in Example 3.10 is manufactured in the form of a tapered tube with a given wall thickness distributed along its length.

**Find:** The material that makes the rod as strong as possible for a given weight.

**Solution:** Figure 3.20 shows that the strongest materials for a given density are diamond and silicon carbide and other ceramics. It is difficult and expensive to use these as fishing rod materials. The best choice is carbon-fiber-reinforced plastic or glass-fiber-reinforced plastic that has 800- to 1000-MPa strength for a density of  $1500 \text{ kg/m}^3$ .

### 3.7.3 Stiffness versus Strength

Figure 3.21 plots modulus of elasticity versus strength. Note that contours of normalized strength,  $S/E$ , etc., appear as a family of straight parallel lines.

The reference lines in Fig. 3.21 are useful for the following circumstances:

$S/E = C$	Design of seals and hinges
$S^{3/2}/E = C$	Elastic components such as knife-edges and diaphragms
$S^2/E = C$	Elastic energy storage per volume (for compact energy adsorption)

### Example 3.12: Elastic Strain

**Given:** The springs in a car suspension can be made of rubber, steel, or a uniply carbon-fiber-reinforced plastic. The geometries of the different suspension springs are quite different, depending on allowable elastic deformations.

**Find:** The maximum elastic strains in the three types of spring if the rubber is polyurethane (PU) and the steel has a strength of 1 GPa.

**Solution:** From Fig. 3.21, PU rubber has a strength of around 30 MPa and a modulus of elasticity of 0.05 GPa. The maximum elastic strain is

$$\left(\frac{S}{E}\right)_{\text{rubber}} = \frac{30}{50} = 0.60$$

Likewise, for steel and carbon-fiber-reinforced plastic

$$\left(\frac{S}{E}\right)_{\text{steel}} = \frac{1}{205} = 0.005$$

$$\left(\frac{S}{E}\right)_{\text{plastic}} = \frac{1}{200} = 0.005$$

The rubber has a maximum elastic strain of 60%, whereas the steel and carbon-fiber-reinforced plastic springs have a maximum elastic strain of 0.5%. Also, from Fig. 3.20 the steel spring will be five times heavier than the carbon-fiber-reinforced plastic spring. It will be seen in Chapter 17 that steel can be made into an effective spring by utilizing a helical shape, or coil.

### 3.7.4 Wear Rate versus Limiting Pressure

Wear presents a new set of problems in attempting to choose a solid material. If the materials are unlubricated, sliding motion is occurring, and if one of the surfaces is steel, the wear rate is defined as

$$W_r = \frac{\text{Volume of material removed}}{\text{Sliding distance}} = \frac{v}{L}. \quad (3.28)$$

The wear rate  $W_r$  thus has the SI unit of square meters. At low limiting pressure,  $p_l$ ,

$$W_r = k_1 A p_l, \quad (3.29)$$

where  $k_1$  is the Archard wear constant,  $A$  is the contact area, and  $p_l$  is the limiting pressure. Figure 3.22 shows the constant  $k_1$  as a function of limiting pressure  $p_l$ . Each class cluster shows the constant value of  $k_1$  at low  $p_l$  and the steep rise as  $p_l$  is approached. Materials cannot be used above their limiting pressure.

### Example 3.13: Design for Wear

**Given:** A polytetrafluoroethylene (PTFE, or Teflon) slider is in contact with high-carbon steel. The sliding distance is 300 m, and the thickness of the Teflon layer allowed to be worn away is 3 mm.

**Find:** How large does the PTFE slider surface have to be so that it will not have excessive wear and the limiting pressure will not be exceeded if the load carried is 10 MN?



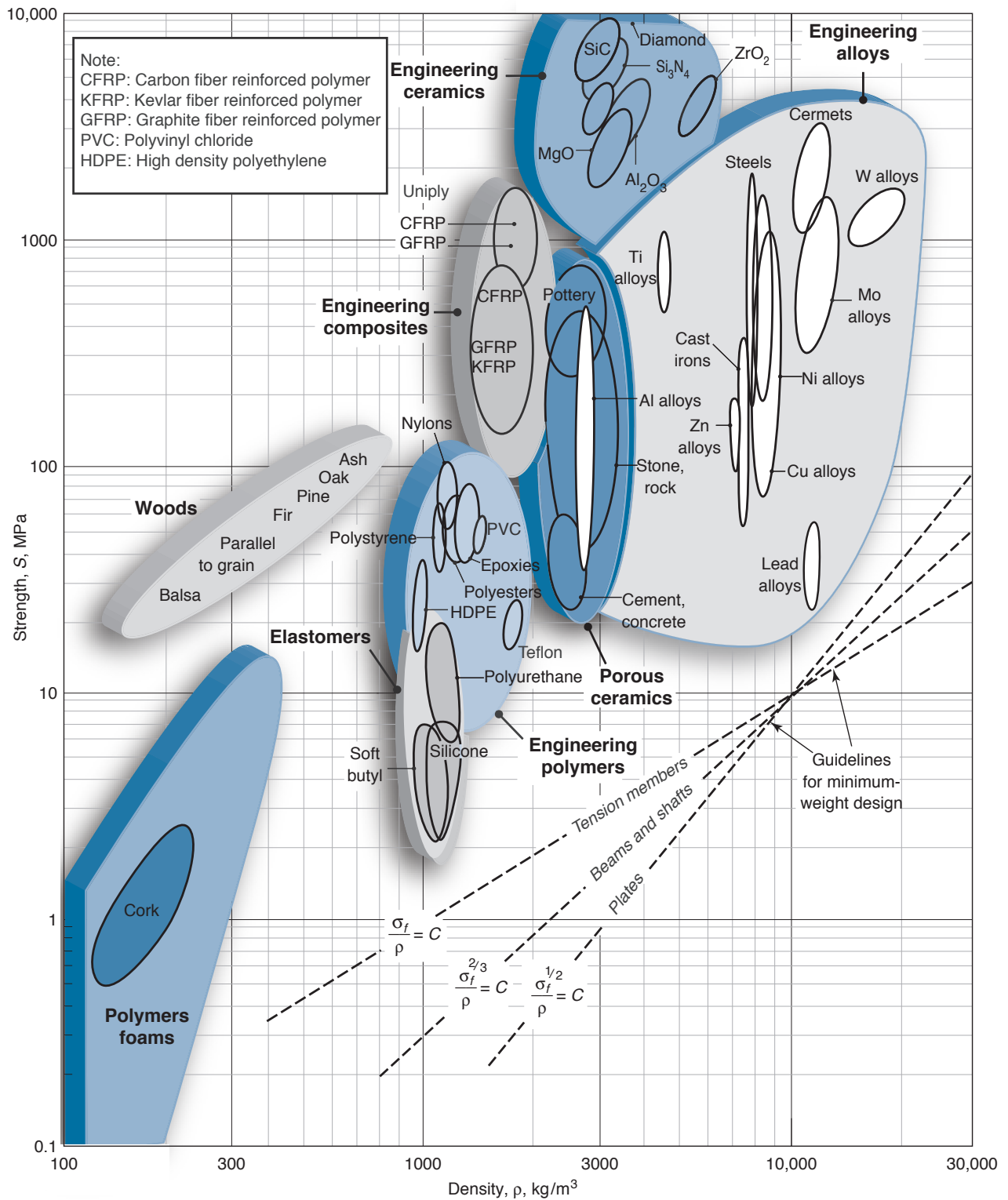


Figure 3.20: Strength versus density. The guidelines of constant  $S/\rho$ ,  $S^{2/3}/\rho$ , and  $S^{1/2}/\rho$  allow selection of materials for minimum-weight, yield-limited design. Source: Adapted from Ashby [2010].

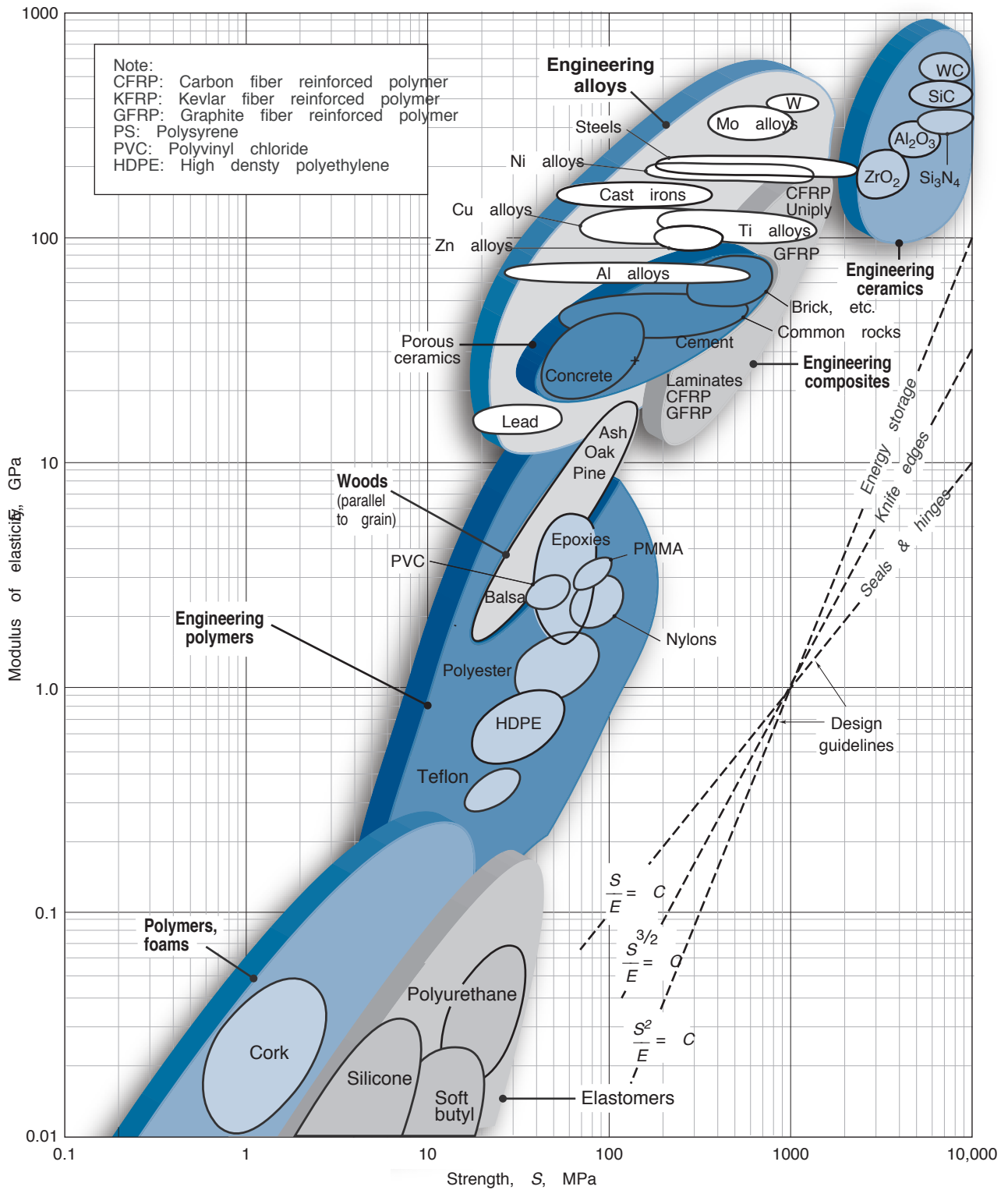


Figure 3.21: A plot of elastic modulus versus strength for engineering materials. The design guidelines help with the selection of materials for such machine elements as springs, knife-edges, diaphragms, and hinges. Source: Adapted from Ashby [2010].

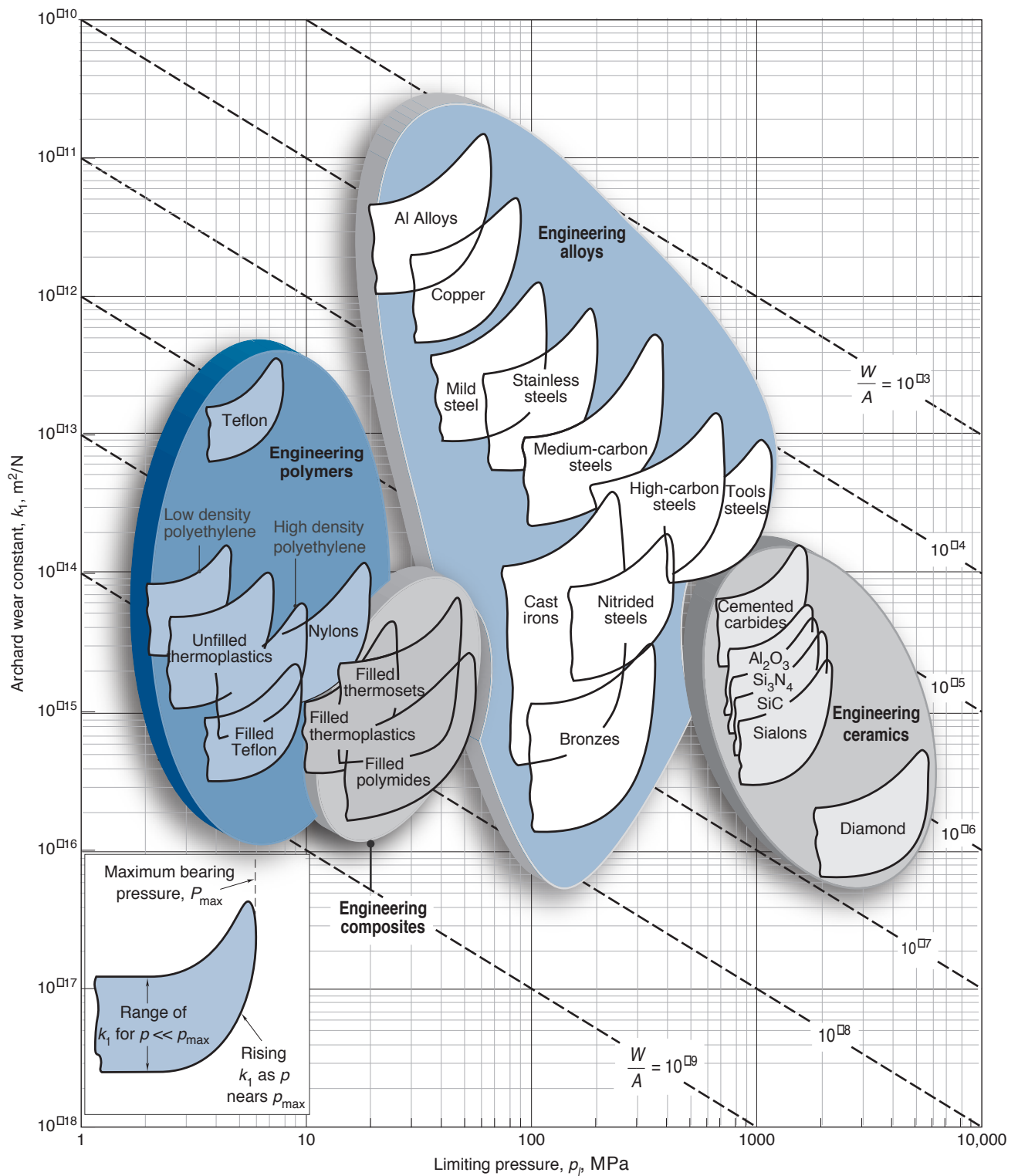


Figure 3.22: Archard wear constant as a function of limiting pressure. Source: Adapted from Ashby [2010].

**Solution:** From Fig. 3.22, the limiting pressure for PTFE on steel is  $p_l = 8$  MPa, and the Archard wear constant is  $k_1 = 2 \times 10^{-13} \text{ m}^2/\text{N}$ . From Eq. (3.29),

$$\frac{W_r}{A} = k_1 p_l = (2 \times 10^{-13}) (8 \times 10^6) = 1.6 \times 10^{-6}.$$

The worn volume of the material is

$$At_h = W_r L,$$

where  $L$  is the sliding distance and  $t_h$  is the wear depth. Therefore,

$$\frac{W_r}{A} = \frac{t_h}{L} = \frac{0.003}{300} = 10^{-5}.$$

The pressure can be written as

$$p = \left( \frac{W_r}{A} \right) \frac{1}{k_1} = \frac{10^{-5}}{2 \times 10^{-13}} = 0.5 \times 10^8 \text{ Pa} = 50 \text{ MPa}.$$

Since  $p \gg p_l$ , the limiting pressure is needed to determine the size of the slider. Thus,

$$p_l A = (10 \times 10^6) \text{ N} = 10^7 \text{ N}.$$

Solving for the area,

$$A = \frac{10^7}{p_l} = \frac{10^7}{8 \times 10^6} = 1.25 \text{ m}^2.$$

The surface area has to be  $1.25 \text{ m}^2$  in order to avoid excessive compressive stress. For these conditions, the wear depth will be only  $0.48 \text{ mm}$ .

### 3.7.5 Young's Modulus versus Relative Cost

In practice, design engineers consider cost much more than it has been considered thus far in this text. Figure 3.23 shows the stiffness of a material versus the relative cost (i.e., the cost per weight of the material divided by the cost per weight of mild steel). The reference lines are useful for the following:

$E/C_R \rho = C$	Minimum-cost design of stiff tension members
$E^{1/2}/C_R \rho = C$	Minimum-cost design of stiff beams and columns
$E^{1/3}/C_R \rho = C$	Minimum-cost design of stiff plates

Figure 3.23 does much to explain why steel and concrete are so valuable as building materials for public works projects where cost is to be minimized. Although a bridge manufactured from teflon is certainly possible, it would be far more costly than a steel-and-concrete bridge.

## 3.8 Effects of Manufacturing

The proper selection of an engineering material is a critical task for successful design. Equally as important for its performance and economic impact is the selection of a manufacturing process or processes for each component. Selection of a manufacturing process has a large effect on the material's microstructure and can dramatically affect the strength, ductility, and other material properties.

This section is a brief introduction to manufacturing process effects on machine element design. Much more informa-

tion is contained in Kalpakjian and Schmid [2010], or Schey [2000].

### 3.8.1 Manufacture of Metals

#### Casting

A wide variety of casting processes are available, all of which involve molten (liquid) metal solidifying within a mold. Castings in general have a microstructure that contains a large number of micropores. In tension, these pores act as stress risers, while in compression, the pores close upon themselves; the main result is a much higher strength in compression than in tension. Castings can have limited ductility because of this microstructure, but ductility can be improved by annealing. The main advantages to castings are low cost, especially for moderate production runs, and highly intricate shapes.

Casting processes are usually classified as expendable mold-expendable pattern; expendable mold-permanent pattern; or permanent mold processes. Some of the most common casting processes are:

- **Expendable mold, expendable pattern.** Investment casting and evaporative pattern casting are common examples of this class of casting process. In investment casting, a pattern is created from a low melting point solid such as a thermoplastic or wax. This pattern is then coated by successive dips into a slurry (ceramic particles suspended in water). Once a desired coating thickness has been developed, the coated pattern is placed in an oven, melting the wax and leaving a cavity. Molten metal is then poured into the cavity, which solidifies in the shape of the original pattern.
- **Expendable mold, permanent pattern.** This class of operations includes sand casting (shown in Fig. 3.24), shell casting, plaster-mold, and ceramic-mold casting. Sand casting is the most prevalent form of casting, with typical applications including machine tool bases, engine blocks, and machine housings. In sand casting and other such processes, a mold is created from a pattern, but the pattern can be reused for many parts.
- **Permanent mold.** Including processes such as die casting, pressure casting, and centrifugal casting, permanent mold processes have high tooling costs and are therefore limited to large production runs. In these operations, the desired part shape is produced into a mold of a metal with a higher melting temperature than the workpiece, or graphite in some applications. Molten metal is injected under high pressure into the mold cavity, so that it fills the mold completely before solidification. Examples of parts produced in permanent mold operations are transmission housings, valve bodies, hand tools, computer housings, toys, and camera frames. Permanent mold processes generally have better surface finish and tolerances than other casting operations.

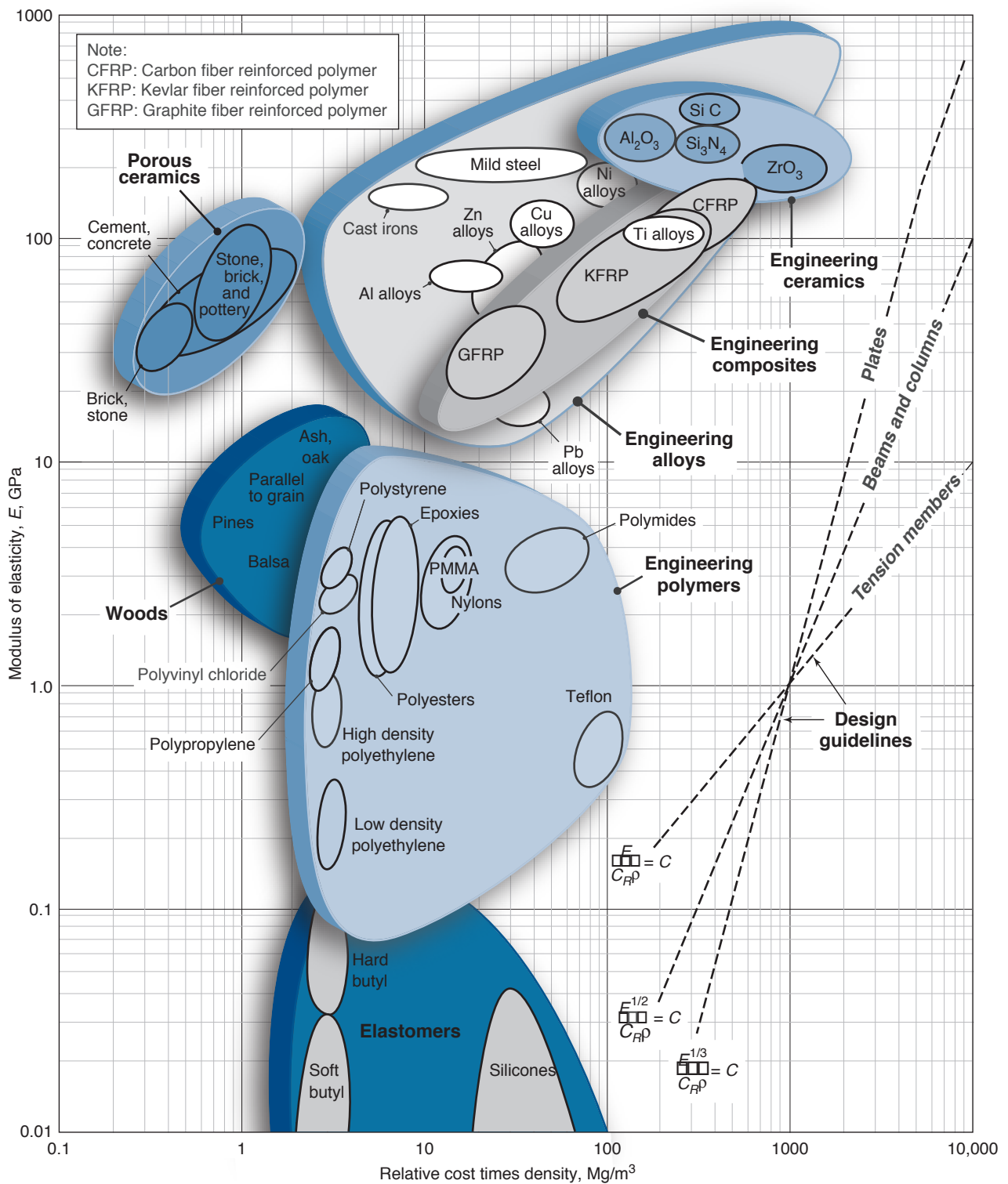


Figure 3.23: Modulus of elasticity as a function of the product of cost and density. The reference lines help with selection of materials for machine elements. Source: After Ashby [2010].



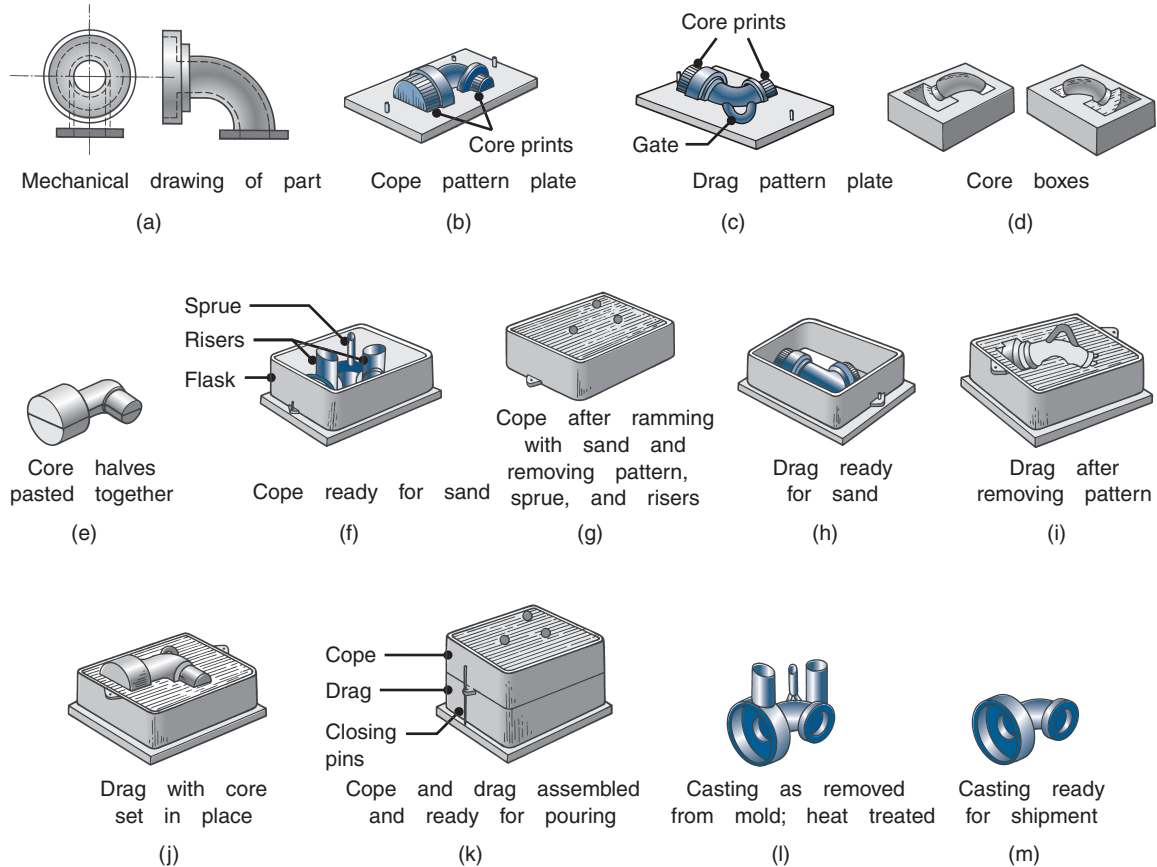


Figure 3.24: Schematic illustration of the sequence of operations for sand casting. (a) A mechanical drawing of the part is used to generate a design for the pattern. Considerations such as part shrinkage and tapers must be built into the drawing. (b, c) Patterns have been mounted on plates equipped with pins for alignment. Note the presence of core prints designed to hold the core in place. (d, e) Core boxes produce core halves, which are pasted together. The cores will be used to produce the hollow area of the part shown in (a). (f) The cope half of the mold is assembled by securing the cope pattern plate to the flask with aligning pins and attaching inserts to form the sprue and risers. (g) The flask is rammed with sand and the plate and inserts are removed. (h) The drag half is produced in a similar manner with the pattern inserted. A bottom board is placed below the drag and aligned with pins. (i) The pattern, flask, and bottom board are inverted; and the pattern is withdrawn, leaving the appropriate imprint. (j) The core is set in place within the drag cavity. (k) The mold is closed by placing the cope on top of the drag and securing the assembly with pins. The flasks then are subjected to pressure to counteract buoyant forces in the liquid, which might lift the cope. (l) After the metal solidifies, the casting is removed from the mold. (m) The sprue and risers are cut off and recycled, and the casting is cleaned, inspected, and heat treated (when necessary). *Source:* Courtesy of the Steel Founders' Society of America.

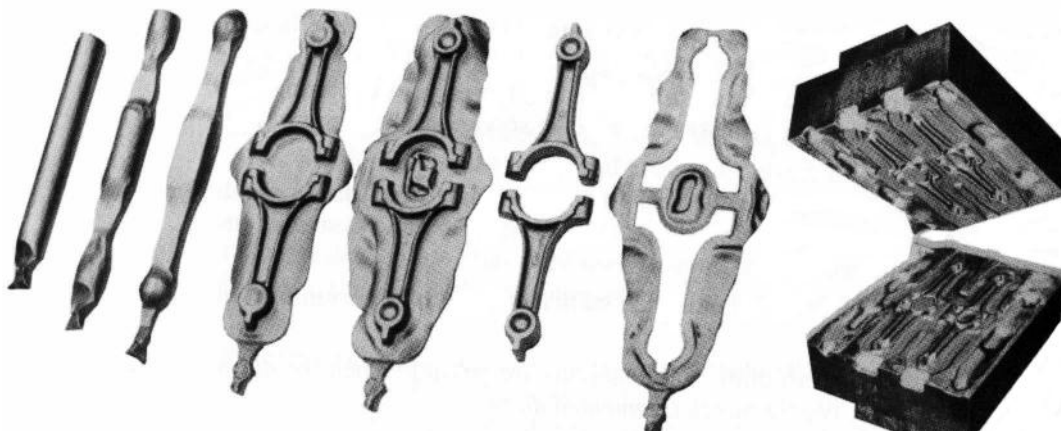
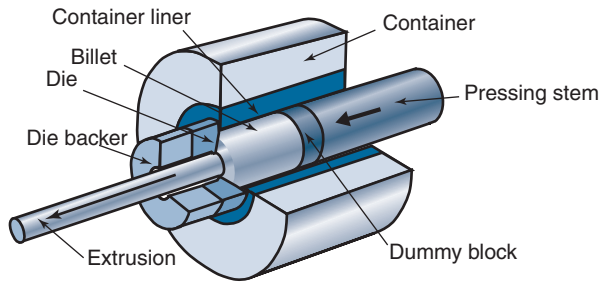
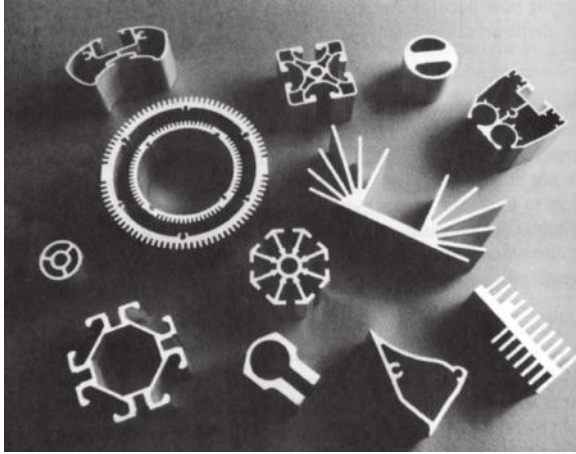


Figure 3.25: An example of the steps in forging a connecting rod for an internal combustion engine, and the die used. *Source:* Schey [2000].



(a)



(b)

Figure 3.26: The extrusion process. (a) Schematic illustration of the forward or direct extrusion process Source: Kalpakjian and Schmid [2010]. (b) Examples of extruded cross sections. Source: Schey [2000].

### Bulk Forming

In bulk forming processes, materials are subjected to large strains in order to achieve the desired shape. Thus, the material must be quite ductile in order to be formed without fracturing. Some of the common bulk forming operations are:

- **Forging.** Forging is controlled deformation of metal through the application of compressive stresses. In *open die forging*, simple die shapes such as flats and rounds are used to obtain a rough shape in the workpiece. In *closed die forging*, as shown in Fig. 3.25, a cavity is carefully prepared in a die, so that the metal will conform to and acquire the cavity shape during forging. Note that the workpiece in forging will develop *flash*, which must be trimmed off; the flash is necessary to ensure that the metal completely fills the die.
- **Extrusion.** In extrusion, shown in Fig. 3.26a, a *billet* is pushed through a die to produce a product with a constant cross-section. Structural shapes are commonly produced through extrusion, and smaller parts can be produced by cutting extrusions to desired lengths.
- **Rolling.** Arguably the most common bulk forming operation, rolling is performed on approximately 90% of metals. In *flat rolling*, a billet is reduced in thickness

through the compressive stress applied by two rollers. Rolling can also be used to produce structural shapes, tubes, rings (such as bearing races), spheres (such as balls in rolling element bearings), and screw threads.

Bulk deformation can take place at elevated temperatures (hot working) to exploit increases in material ductility and decreases in strength and stiffness at elevated temperatures. Cold working has associated with it superior surface finish, improved mechanical properties due to strain hardening, and a more refined microstructure.

### Sheet Forming

One of the main advantages of metals is that they have sufficient ductility to be rolled into thin sheets. These sheets are then used for further processing, allowing the economic production of high-quality parts with large aspect ratios. Since sheet metals are cold-rolled, they will usually have small, elongated grains, some anisotropy, and higher strength than bulk forms of the same material.

The most common sheet forming operations are bending, stretch forming, and deep drawing. In bending, a sheet or tube is forced around a mandrel to a desired shape, or sheet metal is plastically deformed in a die with the desired bend shape. In stretch forming, a sheet is forced between two dies with the desired profile; the sheet-metal plastically deforms to match the die profile. In deep drawing, a cup-shaped part is produced by forcing a sheet or blank into a die cavity; the punch and die have a clearance that is slightly larger than the sheet thickness to avoid shearing the blank. Typical deep drawn parts include cookware, oil pans, and beverage containers.

### Powder Metallurgy (PM)

Metals can be produced in powder form through various approaches. These powders can be further processed by a number of methods, including:

- **Pressing and sintering.** The powder is placed inside a die cavity and compressed under high pressure; the part that is ejected is called a *green compact* and has a strength comparable to chalk. These parts are then *sintered*, or heated in a controlled atmosphere furnace at up to 90% of their absolute melting temperature for up to four hours. In the sintering furnace, the powder particles fuse and develop a strong bond.
- **Metal injection molding.** The powder is mixed with a polymer binder and the mixture is processed by injection molding, as described below. After molding, the part is sintered and perhaps infiltrated by a metal with a lower melting point.
- **Cold and hot isostatic pressing.** The powder is placed in a compliant mold and then placed into a pressurized chamber. The high pressures that result yield a PM part that is strong and has tight tolerances.

PM parts are very porous; they can have up to 20% porosity. As opposed to castings, the pores in PM are not isolated; they are all interconnected. As such, PM parts can be thought of as a sponge, in that once infiltrated by a lubricant, the lubricant is always present. This is one of the main reasons that PM parts are very popular for tribological applications such as gears, cams, bearings, and sleeves.

## Machining

Material removal processes such as metal cutting, grinding, or electrical discharge machining are used to remove material from a bulk form (or near-net shaped form) to achieve desired surface finishes, tolerances, or shapes that are difficult to obtain otherwise. The machining process affects part design in a number of ways, including:

- All machining operations result in feed marks on the workpiece, which can limit the fatigue life. This topic will be discussed in detail in Chapter 7.
- Machining is comparatively expensive and slow.
- Very smooth surfaces or very low tolerances can be produced only through expensive manufacturing operations. Thus, a goal of designers is to specify rough surfaces whenever possible in order to have maximum economy in their designs.
- Machining does not affect the material microstructure. Thus, a brittle material will not become ductile because its surface was machined.
- Machining requires parts to be held in fixtures during machining. Therefore, designers need to incorporate clamping and fixturing locations in their parts to allow machining.
- It is difficult to produce sharp external corners in casting or bulk forming operations, but it is easier to produce sharp external corners in machining.

### 3.8.2 Manufacture of Polymers

Polymers are produced by a wide variety of manufacturing operations; only a few very popular approaches are described here. There are two basic forms of polymers, and these determine the manufacturing strategy that will be used. Thermoplastics are polymers that have a defined melting point; heating them greatly reduces their strength and allows them to flow into desired shapes. Once they are cooled, they regain their strength and hardness. Thermosets chemically degrade when heated long before they melt. The basic strategy used with thermosets is to form the polymer constituents into the desired shape, then through the application of heat and/or pressure, cause these polymers to cure, or set. After the cure cycle, the thermoset part is ready for use.

An innovative set of processes, called *rapid prototyping*, are described in the Case Study at the end of this chapter. Rapid prototyping is experiencing rapid development; some of the latest advanced materials in rapid prototyping are described in Appendix A.15.

#### Thermoplastic Manufacture

Thermoplastics are very common, versatile materials, available in a wide variety of shapes and colors. Thermoplastics are produced from their chemical constituents and are available in bulk, pellet, or powder form for processing into their final desired shape. It should be noted that a “melted” polymer is quite viscous; its consistency can be closer to bread dough or soft taffy than a liquid. This should be understood when trying to visualize the processes described here.

Among the common methods of processing thermoplastics are:

- **Extrusion.** In extrusion, a polymer in pellet or powder form is heated in an extruder, shown in Fig. 3.27.

## Chapter 3 Introduction to Materials and Manufacturing

The polymer is melted in the extruder barrel by the heat input from heating elements as well as the friction between pellets and between pellets and screw. As a result, a liquid polymer is forced out through a die with a desired cavity, resulting in a part with a constant cross section. The polymer is then cooled, usually by forced cool air convection. Polymer tubes, structural members, and rods are produced through extrusion.

- **Injection molding.** Instead of forcing the polymer through a die opening, the polymer is injected into a die cavity. Usually, metal dies are used that incorporate channels for coolant, so that the heat from the polymer is quickly removed. Once solid, the polymer part is ejected and another cycle can begin. Injection molding is extremely popular; a wide variety of automotive, consumer electronic, and home use products are produced by injection molding.
- **Thermoforming.** Thermoforming involves the use of an extruded film that is heated and draped over a (usually) metal die with an intended shape. The soft thermoplastic complies with and cools against the die, and hardens. Plastic packaging, advertising signs, refrigerator liners, and the Invisalign product in Case Study 1.4 are examples of thermoformed products.
- **Blow molding.** In extrusion blow molding, an extruded tube is clamped and expanded by internal pressure against a die-defined cavity. In injection blow molding, a short tubular piece called a *parison* is first injection molded, and then transferred to a blow molding die. Blow molding produces hollow containers such as plastic beverage bottles.

#### Manufacture of Thermosets

Thermosets are also very common. When compared to thermoplastics, thermosets in general have better strength (especially at elevated temperatures) and strength-to-weight ratios. As discussed above, thermosets are manufactured by blending polymer constituents, forming them into the desired shape, and then curing the plastic. Some of the important thermoset manufacturing operations are:

1. **Reaction injection molding.** Similar to injection molding described above, reaction injection molding involves injecting liquid thermoset into a heated die; the elevated temperature then allows curing of the thermoset.
2. **Compression molding.** Compression molding shares many similarities with forging. A powder or clay-like consistency polymer is placed into a heated mold and is compressed to fill the cavity. The polymer then cures into the shape defined by the mold. Compression molded parts have good tolerances and surface finish, and yield a polymer with high molecular weight and crystallinity (and therefore strength) compared to other processes.

### 3.8.3 Manufacture of Ceramics

Ceramics share many processing similarities to PM techniques. Ceramics are processed from powder form, usually by mixing with water and binders. Once formed, a ceramic part will be placed into a furnace, or kiln, to fuse the particles. In all processing techniques, the ceramics will be somewhat porous, and the mechanical properties will depend on this porosity. The most common processes for producing ceramic parts are:



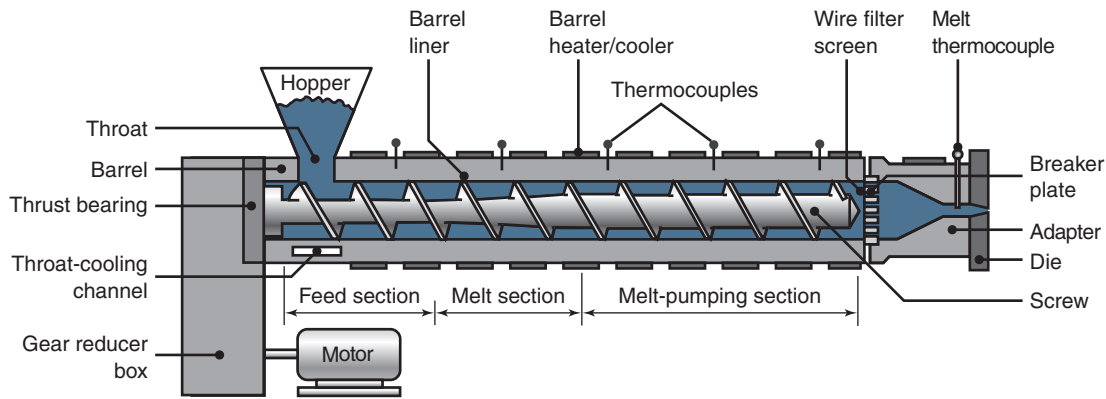


Figure 3.27: Schematic illustration of a typical extruder. Source: Kalpakjian and Schmid [2010].

- **Slip casting.** In slip casting, a ceramic slurry is poured into a permeable mold. Some of the water in the slurry diffuses into the mold, leaving a locally high slurry concentration next to the mold wall. After a few minutes, the slurry is poured from the mold, leaving a coating adhering to the mold. After a few hours, more of the water has been extracted from the slurry and it is removed from the mold. It is very fragile at this step and is fired in a furnace or kiln to fuse the ceramic particles.
- **Dry or wet pressing.** This approach is similar to pressing of metal powders; the resultant compact needs to be fired in a furnace or kiln to develop strength.
- **Doctor-blade process.** In this operation, a claylike consistency of ceramic is spread by a blade. The ceramic can be spread into a sheet or can be formed into a desired shape such as plates or bowls (*jigging*).
- **Pressing and injection molding.** These are similar to the PM and polymer processes of the same name, respectively. The part from these operations needs to be fired to develop strength.

Ceramics and PM parts share many design considerations. Since there is significant shrinkage during sintering or firing, there is a possibility for warpage in large parts, and thin cross sections are likely to fracture. Sharp corners will crumble while the part is in the compact stage, and chamfers are preferable to radii because of tooling design issues.

### 3.8.4 Selection of Manufacturing Processes

Manufacturing process selection is a difficult task and must incorporate design parameters as well as economic considerations. A full discussion of manufacturing process selection is beyond the scope of this text, and the interested reader is again directed to the text by Kalpakjian and Schmid [2010]. However, it should be recognized in the design of machine elements that there are certain trends in processes used. For example:

- Processes that are advantageous for small production runs usually have low capital equipment costs, but high labor costs, whereas hard automation is expensive but has low labor costs. Therefore, the cost per part can be greatly reduced if the parts are produced in quantities large enough to justify purchase of hard automation. In practice, this means that bolts, gears, bearings, etc., are

Table 3.2: Commercially available forms of materials.

Material	Available forms <sup>a</sup>
Aluminum	B, F, I, P, S, T, W
Ceramics	B, p, s, T
Copper and brass	B, f, I, P, s, T, W
Elastomers	b, P, T
Glass	B, P, s, T, W
Graphite	B, P, s, T, W
Magnesium	B, I, P, S, T, w
Plastics	B, f, P, T, w
Precious metals	B, F, I, P, t, W
Steels and stainless steels	B, I, P, S, T, W
Zinc	F, I, P, W

<sup>a</sup> B = bar and rod; F = foil; I = ingot; P = plate and sheet; S = structural shapes; T = tubing; W = wire. Lowercase letters indicate limited availability. Most of the metals are also available in powder form, including prealloyed powders.

mass produced in standard sizes at far greater economy than if produced to order. From a design standpoint, it is therefore important to specify dimensions as standard sizes, such as 50 mm instead of 43.6 mm.

- It should be recognized that product quality and robustness also increase with large production runs.
- Certain materials are commercially available in only some forms (see Table 3.2). The desire to use materials in other forms is not impossible, but is probably not economically advisable.
- Manufacturing processes are determined, to a great extent, by the design requirements of size, strength, tolerance, and surface finish. Figure 3.28 can be used as a guide to help select manufacturing processes based on tolerance and roughness.

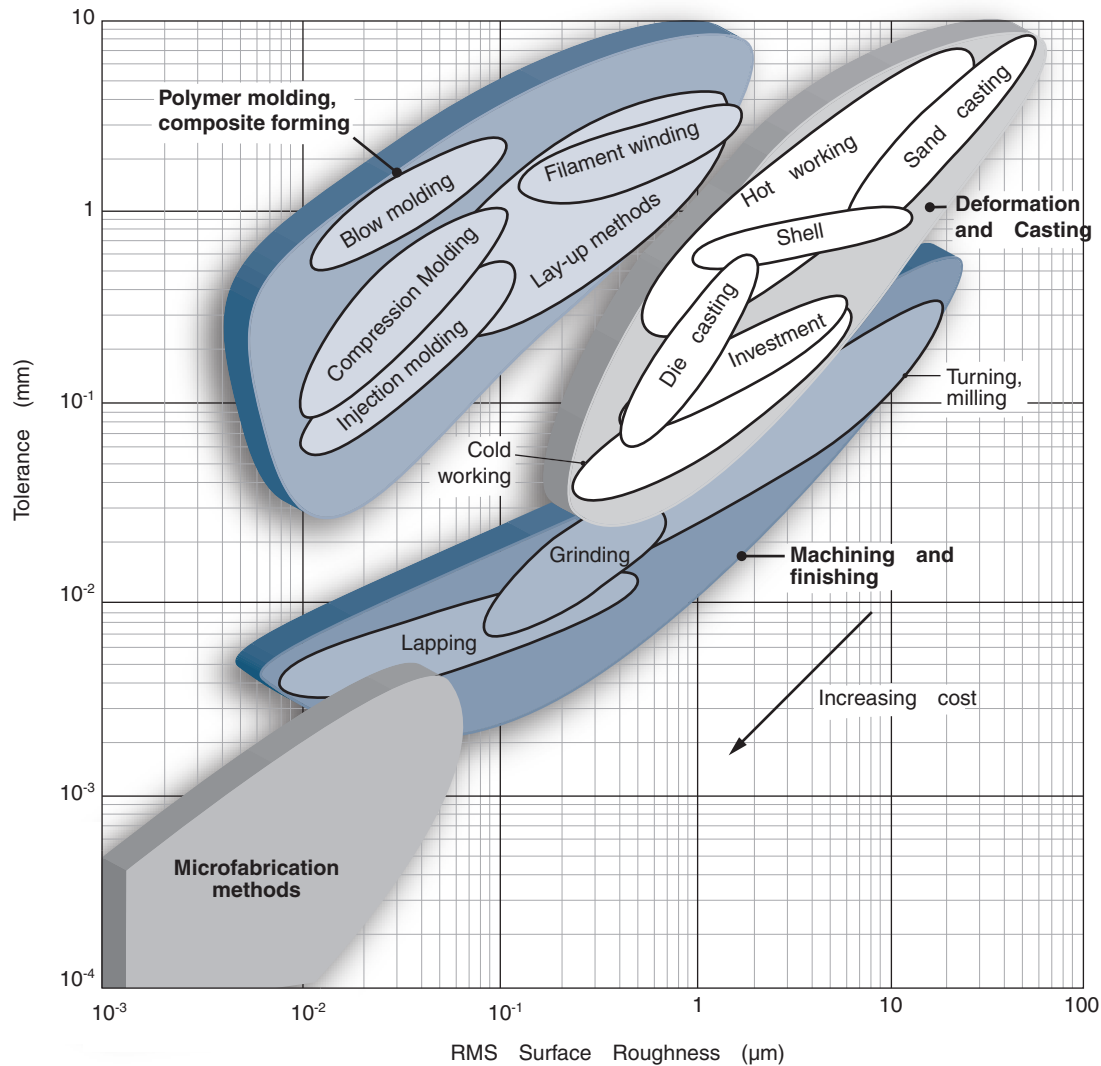


Figure 3.28: A plot of achievable tolerance versus surface roughness for assorted manufacturing operations. The dashed lines indicate cost factors; an increase in precision corresponding to the separation of two neighboring lines gives an increase in cost for a given process, or a factor of two. Source: Adapted from Ashby [2010].

## Case Study: The Maker Movement

Since the 1980s, a large number of manufacturing processes have been developed that use computer representations of parts and computer control to precisely deposit material where desired. These processes are unique in that they create parts layer by layer, using thin slices to get very good part definition. Figure 3.29 summarizes some of the most popular **rapid prototyping** operations, which are also referred to as **3D printing** or **additive manufacturing**. These approaches have the common ability to create individual parts within a few minutes or hours without molds or tools, a capability that is extremely valuable in many circumstances.

Early rapid prototyping machines had significant drawbacks: they were very expensive, materials were initially limited to polymers (and, in some processes, paper), and the mechanical properties that were available were inferior to those that resulted from other manufacturing processes. Also, materials were very expensive; the control of the deposition process placed large demands on the chemical composition and purity of the polymers used.

In the 1990s, a number of technical advances occurred that improved the usefulness of rapid prototyping:

- Materials advances led to the development of polymers with mechanical properties that were comparable to those obtained from other manufacturing processes. While these materials are still relatively expensive, their cost is lower, so that rapid prototyping is more competitive.
- New processes were developed that allowed rapid prototyping to be applied to metals and ceramics, including sand. This led to the direct application of rapid prototyped parts into applications requiring the strength of metals, and also allowed the development of rapid tooling, where tools and dies for other manufacturing processes are produced with the assistance of rapid prototyping operations.
- Computer processors became faster, and CAD software incorporated greater 3D-modeling capability.



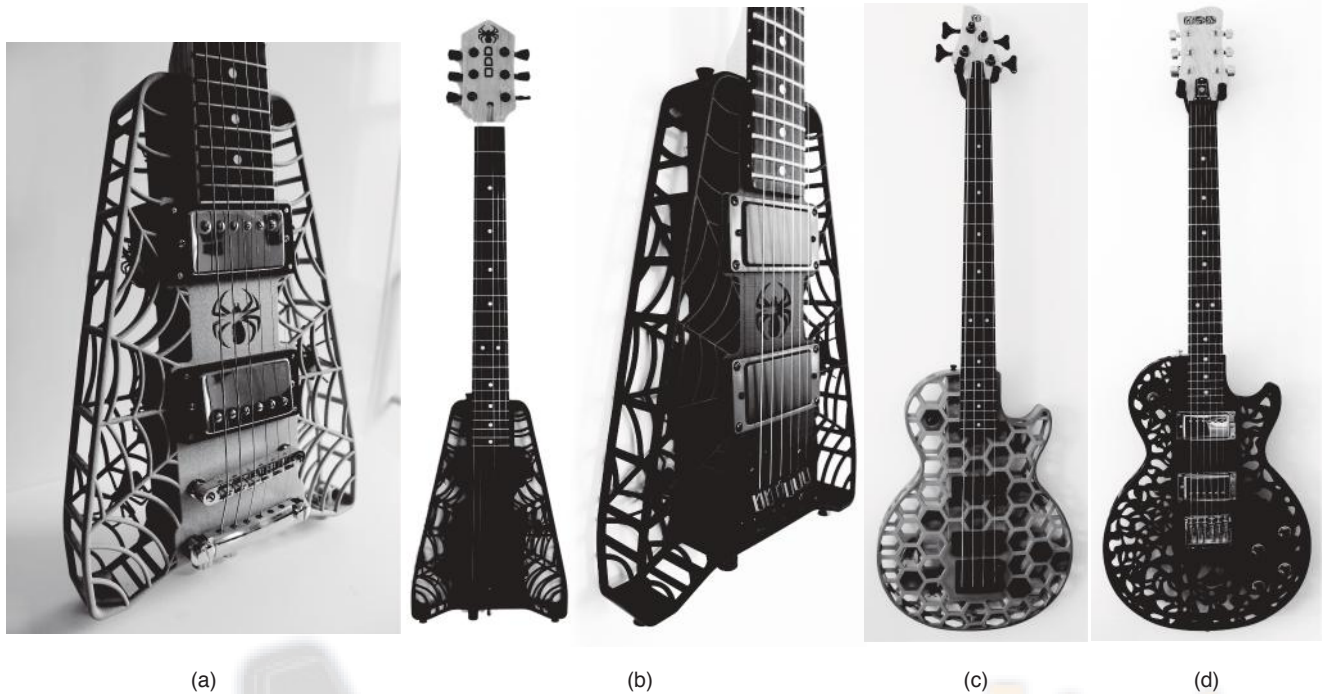


Figure 3.30: Guitars produced through rapid prototyping. (a) Spider design body detail; (b) finished Spider guitars; (c) Hive-b and (d) Atom designs. *Source:* Courtesy of O. Diegel, Massey University.

- New colors and levels of transparency became available, and even multi-colored components could be produced. Variants of three-dimensional printing were developed that used multi-colored binders applied in similar fashion as inkjet printers to achieve full-color prototypes.
- Three-dimensional scanners became more popular and reasonably priced, which allowed the capture of an object's geometry and its import into CAD packages, where the geometry could be modified and then sent directly to a 3D printer. There are currently apps for smart phones that capture the 3D geometry of an object.

These developments are all impressive and led to the great current interest in rapid prototyping operations, and new business models have developed as a result. For example, some businesses will accept a 3D graphics file format by web submission, print the part and mail it to the purchaser by overnight delivery. A clever approach has been used with toys: With care, a 3D scan can be taken of an individual's face or head; a miniaturized model of the head can be added to a toy to produce a superhero doll with an individual's face attached. Creative approaches have been used to design home decorations, clothing, phone and tablet computer cases, musical instruments, etc. Figure 3.30 illustrates some extremely innovative guitar designs that are made possible by the flexible manufacturing offered by rapid prototyping.

While these are interesting and exciting capabilities, much greater interest has developed in rapid prototyping machinery in recent years. The original patents on the fused deposition modeling process have lapsed, and many companies and individuals can now practice this process.

A crowdsourcing community, known as The Maker Movement, has organized, is linked with Internet communication tools, and has developed a number of so-called *Makers*. Such machines are freely available as plans that can be downloaded from the Internet and used to build fully functional 3D printers for only a few hundred dollars. Alternatively, some very inexpensive machines have been marketed based on these crowd-sourced designs, such as the system shown in Fig. 3.31.

Materials researchers have continually improved the mechanical properties and ease of manufacture of polymers. Appendix A summarizes mechanical properties of selected common materials used in rapid prototyping. Also, researchers are able to apply new and innovative materials to rapid prototyping machines, including novel approaches such as printing of food or biological material for producing medical implants.

It has been suggested that the Maker Movement will revolutionize modern society, that design and manufacturing will be an activity performed by anyone with a computer and a 3D printer. This may be true for parts or products that do not need to support significant forces or transmit torque or power. However, as will be seen in Chapters 6 and 7, the design of components for robust performance in highly stressed environments requires a good understanding of engineering principles. Many machine elements have outstanding performance and economy because of mass production; rolling element bearings exemplify this category. And many materials depend on manufacturing processes to develop their full strength; even if a fastener could be produced, it is not necessarily an SAE Grade 8 bolt unless it is properly heat treated, for example.

Regardless, this is an exciting time for the Maker Movement, and this industry is experiencing rapid change and frequent developments that expand the applications and utility of rapid prototyping.

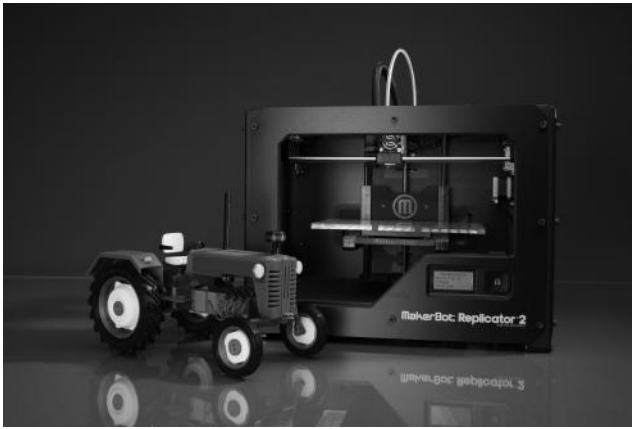


Figure 3.31: A Replicator 2 by MakerBot. This inexpensive 3D printer has a  $6400 \text{ cm}^3$  build volume and can produce parts from a variety of polymers. Shown in the foreground is a model of a tractor produced on a Replicator 2. Source: Courtesy MakerBot Industries, LLC.

### 3.9 Summary

Eight important mechanical properties of solid materials were discussed in this chapter. The differences between ductile and brittle materials were presented. It was found that, at fracture, ductile materials exhibit considerable plastic deformation, whereas brittle materials exhibit little or no yielding before failure.

Four major classes of solid material were described: metals, ceramics and glasses, polymers and elastomers, and composites. The members of each class have common features, such as similar chemical makeup and atomic structure, similar processing routes, and similar applications.

A stress-strain diagram was presented for each class of solid material because they differ significantly. The stress-strain diagrams for metals are essentially the same for compression and tension. This feature is not true for polymers or ceramics. Results of transverse bending tests for ceramics were found to be similar to tensile test results for metals.

A number of solid material properties used in choosing the correct material for a particular application were presented: mass density, modulus of elasticity, hardness, Poisson's ratio, shear modulus, strength, resilience, toughness, thermal conductivity, linear thermal expansion coefficient, specific heat capacity, and Archard wear constant. These parameters were presented for a large selection of materials.

Two-parameter materials charts were also presented. Stiffness versus weight, strength versus weight, stiffness versus strength, and wear constant versus limiting pressure for the various classes of material can give a better idea of the best material for a particular machine element.

An introduction to manufacturing processes and their effects on materials was also presented, with the most common approaches presented for each class of material. These include casting, bulk and sheet forming for metals, many types of molding for polymers, and casting and molding operations for ceramics. Each material can be machined to some extent as well.

The Case Study described the emerging Maker Movement, wherein designers can produce their desired products in a CAD program and have them manufactured directly on a 3D printer. A large number of applications and materials have been used by the Maker Movement.

### Key Words

**anisotropic** material having different properties in all directions at a point in a solid

**Archard wear constant** wear property of a material

**Brinell hardness** a hardness measure that results from a Brinell test, where a steel or tungsten carbide ball is impressed onto a material.

**brittle material** material that fractures at strain below 5%

**ceramics** compounds of metallic and nonmetallic elements

**composite materials** combinations of two or more materials, usually consisting of fiber and thermosetting polymer

**density** mass per unit volume

**ductile material** material that can sustain elongation greater than 5% before fracture

**ductility** degree of plastic deformation sustained at fracture

**elastic limit** stress above which material acquires permanent deformation

**elastomers** polymers with intermediate amount of cross-linking

**fracture stress** stress at time of fracture or rupture

**glasses** compounds of metallic and nonmetallic elements with no crystal structure

**hardness** resistance to surface penetration

**homogeneous** material having properties not a function of position in a solid

**isotropic** material having the same properties in all directions at a point in a solid

**Knoop hardness** a hardness measure that results from a Knoop test, also known as a microhardness test

**metals** combinations of metallic elements

**modulus of elasticity** proportionality constant between stress and strain

**modulus of rupture** stress at rupture from bending test, used to determine strength of ceramics

**necking** decreasing cross-sectional area that occurs after ultimate stress is reached and before fracture

**orthotropic** material having different properties in three mutually perpendicular directions at a point in a solid and having three mutually perpendicular planes of material symmetry

**Poisson's ratio** absolute value of ratio of transverse to axial strain

**polymers** compounds of carbon and other elements forming long-chain molecules

**proportional limit** stress above which stress is no longer linearly proportional to strain

**resilience** capacity of material to release absorbed energy

**Rockwell hardness** a hardness measure that results from a Rockwell test, where the penetration of a cone or ball into a material is measured

**rule of mixtures** linear interpolation between densities of alloy concentration

**specific heat capacity** ratio of heat stored per mass to change in temperature of material

**strain hardening** increase in hardness and strength of ductile material as it is plastically deformed

**thermal conductivity** ability of material to transmit heat

**thermal expansion coefficient** ratio of elongation in material to temperature rise

**thermoplastics** polymers without cross-links

**thermosets** polymers with highly cross-linked structure

**toughness** ability to absorb energy up to fracture

**ultimate strength** maximum stress achieved in stress-strain diagram

**Vickers hardness** a hardness measure that results from a Vickers test, where a diamond pyramid is impressed onto a material

**yield strength** stress level defined by intersection of reference line (with slope equal to initial material elastic modulus and  $x$ -intercept of 0.2%) and material stress-strain curve

**yielding** onset of plastic deformation

**Young's modulus** (see modulus of elasticity)

## Summary of Equations

### Material Properties:

$$\text{Percent elongation: } \%EL = \left( \frac{l_{fr} - l_o}{l_o} \right) \times 100\%$$

$$\text{Elastic modulus: } E = \frac{\sigma_{avg}}{\epsilon_{avg}}$$

$$\text{Poisson's ratio: } \nu = - \frac{\text{Transverse strain}}{\text{Axial strain}}$$

$$\text{Shear modulus: } G = \frac{E}{2(1 + \nu)}$$

$$\text{Modulus of resilience: } U_r = \frac{S_y^2}{2E}$$

$$\text{Heat capacity: } Q = C_p m_a (\Delta T)$$

### Composite Materials:

$$\text{Elastic modulus: } E_c = E_m(1 - v_f) + E_f v_f$$

$$\text{Load sharing: } \frac{P_f}{P_m} = \frac{E_f v_f}{E_m v_m}$$

### Hardness:

$$\text{Brinell hardness: } HB = \frac{2P}{(\pi D) (D - \sqrt{D^2 - d^2})}$$

$$S_u = 3.5HB$$

$$\text{Vickers hardness: } HV = \frac{1.854P}{L^2}$$

$$\text{Knoop hardness: } HK = \frac{14.2P}{L^2}$$

$$\text{Rockwell hardness: } HRA = 100 - 500t, \\ HRB = 130 - 500t, \text{ etc.}$$

$$\text{Archard Wear Law: } v = k_1 \frac{WL}{3H}$$

## Recommended Readings

- Ashby, M.F. (2010) *Materials Selection in Mechanical Design*, 4th ed., Butterworth-Heinemann.
- ASM Metals Handbook, 8th ed. (2009) American Society for Metals.
- Brandt, D.A., and Warner, J.C. (2009) *Metallurgy Fundamentals: Ferrous and Nonferrous*, 5th ed. Goodheart-Wilcox.
- Budinski, K., and Budinski, M. (2009) *Engineering Materials, Properties and Selection*, 9th ed., Prentice-Hall.
- Callister, W.D., and Rethwisch, D.G. (2011) *Fundamentals of Materials Science and Engineering: An Integrated Approach*, 4th ed. Wiley.
- Farag, M.M. (2007) *Selection of Materials and Manufacturing Processes for Engineering Materials*, 2nd ed. Prentice-Hall.
- Flinn, R. A., and Trojan, P. K. (1986) *Engineering Materials and Their Applications*, Houghton Mifflin.
- Kalpajian, S., and Schmid, S.R. (2010) *Manufacturing Engineering and Technology*. 6th ed., Pearson.
- Raman, A. (2006) *Materials Selection and Applications in Mechanical Engineering*, Industrial Press.
- Schey, J.A. (2000) *Introduction to Manufacturing Processes*, 3rd ed., McGraw-Hill.

## References

- Ashby, M.J. (2010) *Materials Selection in Mechanical Design*, 4th ed., Butterworth-Heinemann.
- Kalpajian, S., and Schmid, S.R. (2010) *Manufacturing Engineering and Technology*, 6th. ed., Pearson.
- Schey, J.A. (2000) *Introduction to Manufacturing Processes*, 3rd ed., McGraw-Hill.

## Questions

- 3.1 Define the terms ductile and brittle.
- 3.2 What are the three basic classifications of solids?
- 3.3 What is the difference between a thermoset and a thermoplastic?
- 3.4 What is a composite material?
- 3.5 Define proportional limit. How is this different from elastic limit? How are these different from the yield strength?
- 3.6 How is the yield strength defined?
- 3.7 What is strain hardening?
- 3.8 What is the glass transition temperature for polymers? Does this behavior occur with other materials? Explain.
- 3.9 What is the elastic modulus of a material?
- 3.10 What are the advantageous properties of glass?
- 3.11 What is hardness?
- 3.12 What is ductility, and how is it measured?
- 3.13 What is the difference between thermal expansion and specific heat?
- 3.14 What is casting? What materials can be cast?
- 3.15 Give three examples of bulk metal forming operations.



- 3.16 What is PM?
- 3.17 What is sintering?
- 3.18 What is a thermoplastic? A thermoset?
- 3.19 What are the main manufacturing processes applicable to ceramics?
- 3.20 Why are the molds for producing PM parts larger than the desired shape?

## Qualitative Problems

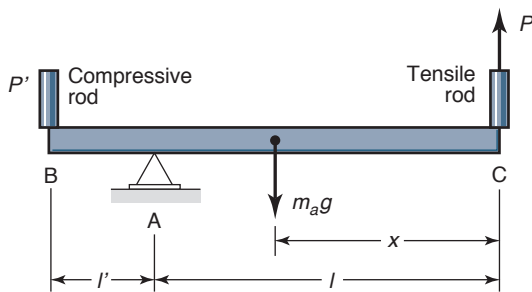
- 3.21 What are the primary functions of the reinforcement in a fiber reinforced polymer? What are the primary functions of the matrix?
- 3.22 Explain why ceramics and cast metals are much stronger in compression than in tension.
- 3.23 Without using the words *stress* or *strain*, define *elastic modulus*.
- 3.24 Sketch typical stress-strain diagrams for metals, ceramics, and polymers.
- 3.25 What is the main difference between resilience and toughness? What is the main similarity between resilience and toughness?
- 3.26 Describe the events that occur when a specimen undergoes a tension test. Sketch a plausible stress-strain curve, and identify all significant regions and points between them. Assume that loading continues up to fracture.
- 3.27 Which hardness tests and scales would you use for very thin strips of metal, such as aluminum foil? Explain.
- 3.28 List the factors that you would consider in selecting a hardness test. Explain your answer.
- 3.29 A statistical sampling of Rockwell C hardness tests is conducted on a material, and it is determined that the material is defective because of insufficient hardness. The supplier claims that the tests are flawed because the diamond-cone indenter was probably dull. Is this a valid claim? Explain.
- 3.30 In a Brinell hardness test, the resulting impression is found to be an ellipse. Give possible explanations for this result.
- 3.31 Which of the properties described in this chapter are important for (a) pots and pans, (b) gears, (c) clothing, (d) paper clips, (e) music wire, (f) beverage cans? Explain your answers.
- 3.32 Identify products that cannot be made of steel, and explain why this is so. (For example, electrical contacts commonly are made of gold or copper because their softness results in low contact resistance, while for steel the contact resistance would be very high.)
- 3.33 What characteristics make polymers advantageous for applications such as gears? What characteristics are drawbacks for such applications?
- 3.34 Review Fig. 3.25 and list reasons why the connecting rod is manufactured in multiple steps, instead of one cavity with one press stroke.
- 3.35 Review Fig. 3.26b and list potential applications for extruded products.

## Quantitative Problems

- 3.36 The design specification for a metal requires a minimum hardness of 80 HRA. If a Rockwell test is performed and the depth of penetration is  $60\text{ }\mu\text{m}$ , is the material acceptable? *Ans. No.*
- 3.37 It can be shown that thermal distortion in precision devices is low for high values of thermal conductivity divided by thermal expansion coefficient. Rank the materials in Table 3.1 according to their suitability to resist thermal distortion.
- 3.38 If a material has a target hardness of 300 HB, what is the expected indentation diameter? Assume the applied load is 3000 kg. *Ans.  $d = 2.95\text{ mm}$ .*
- 3.39 For a material that follows a power law curve for stress-strain behavior, that is,  $\sigma = K\epsilon^n$ , where  $K$  is the strength coefficient and  $n$  is the strain hardening exponent, find the strain at which necking occurs. *Ans.  $\epsilon = n$ .*
- 3.40 A 2-m-long polycarbonate tensile rod has a cross-sectional diameter of 150 mm. It is used to lift a tank weighing 45 tons (45,000 kg) from a 1.8-m-deep ditch onto a road. The vertical motion of the crane's arc is limited to 4.2 m. Will it be possible to lift the tank onto the road? *Ans. Yes.*
- 3.41 Materials are normally classified according to their properties, processing routes, and applications. Give examples of common metal alloys that do not show some of the typical metal features in their applications.
- 3.42 Equation (B.56) in Appendix B gives the relationship between stresses and strains in isotropic materials. For a polyurethane rubber, the elastic modulus at 100% elongation is 7 MPa. When the rubber is exposed to a hydrostatic pressure of 10 MPa, the volume shrinks 0.5%. Calculate Poisson's ratio for the rubber. *Ans.  $\nu = 0.499$ .*
- 3.43 A fiber-reinforced plastic has fiber-matrix bond strength  $\tau_f = 15\text{ MPa}$  and fiber ultimate strength  $S_u = 1\text{ GPa}$ . The fiber length is constant for all fibers at  $l = 1.25\text{ mm}$ . The fiber diameter  $d = 30\text{ }\mu\text{m}$ . Find whether the fiber strength or the fiber-matrix bond will determine the strength of the composite. *Ans. The fiber determines the composite strength.*
- 3.44 Using the same material as in Problem 3.43 but with fiber length  $l = 0.75\text{ mm}$ , calculate if it is possible to increase the fiber stress to  $S_u = 1\text{ GPa}$  by making the fiber rectangular instead of circular, maintaining the same cross-sectional area for each fiber, and if so, give the cross-section dimensions. *Ans.  $h_t = 8.22\text{ }\mu\text{m}$ ,  $w_t = 86.0\text{ }\mu\text{m}$ .*
- 3.45 A copper bar is stressed to its ultimate strength,  $S_u = 150\text{ MPa}$ . The cross-sectional area of the bar before stressing is  $120\text{ mm}^2$ , and the area at the deformed cross section where the bar starts to break at the ultimate strength is  $70\text{ mm}^2$ . How large a force is needed to reach the ultimate strength? *Ans. 18 kN.*

**3.46** AISI 440C stainless steel has ultimate strength  $S_u = 807$  MPa and fracture strength  $S_{fr} = 750$  MPa. At the ultimate strength the cross-sectional area of a tension bar made of AISI 440C is 80% of its undeformed value. At the fracture point the minimum cross-sectional area has shrunk to 70%. Calculate the real stresses at the point of ultimate strength and at fracture. *Ans.* At fracture,  $\sigma = 1071$  MPa; at ultimate strength,  $\sigma = 1009$  MPa.

**3.47** According to Sketch *a*, a beam is supported at point A and at either B or C. At C the silicon nitride tensile rod is lifting the beam end with force  $P = S_{fr}^t$ , where  $A_c$  is the cross-sectional area of the rod. Find the distance A-B such that the silicon nitride rod would be crushed if it took up a compressive force at B instead of a tensile force at C. Note that the strength in compression is fifteen times larger than the strength in tension for silicon nitride. Also, find the reaction forces at A for the two load cases. *Ans.*  $l' = \frac{1}{15}l$ ,  $A_y = \frac{120}{7}P$ .



Sketch *a*, for Problem 3.47

**3.48** Polymers have different properties depending on the relationship between the local temperature and the polymer's glass transition temperature  $T_g$ . The rubber in a bicycle tire has  $T_g = -12^\circ\text{C}$ . Could this rubber be used in tires for an Antarctic expedition at temperatures down to  $-70^\circ\text{C}$ ? *Ans.* No.

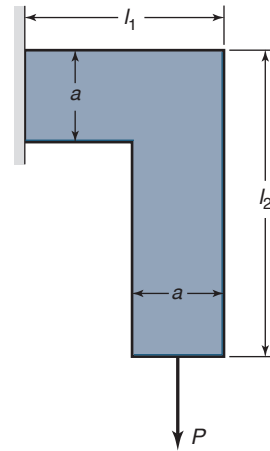
**3.49** What is the modulus of resilience of a highly cold-worked steel with a hardness of 300 HB? Of a highly cold-worked aluminum with a hardness of 120 HB? *Ans.*  $U_{rs} = 1.957$  MPa.

**3.50** Given an aluminum bronze with 25 wt% aluminum and 75 wt% copper, find the density of the aluminum bronze. *Ans.*  $\rho_{\text{bronze}} = 7382$  kg/m<sup>3</sup>

**3.51** The glass-fiber-reinforced plastic in Example 3.6 (Section 3.5.2) is used in an application where the bending deformations, caused by the applied static load, will crack the plastic by overstressing the fibers. Will a carbon-fiber-reinforced plastic also crack if it has the same elastic properties as the glass-fiber-reinforced plastic? *Ans.* Yes.

**3.52** In Problem 3.51, carbon fibers were used to reinforce a polymer matrix. The concentration of fibers was decreased in Example 3.6 (Section 3.5.2) to give the same elastic properties for the carbon-fiber-reinforced polymer as for the glass-fiber-reinforced polymer. If instead, the fiber concentration were kept constant at 10% when the glass fibers were changed to carbon fibers, how much smaller would the deformation be for the same load, and would the fibers be overstressed? The material properties are the same as in Example 3.6.

**3.53** A bent beam, shown in Sketch *b*, is loaded with force  $P = 125,000$  N. The beam has a square cross section  $a^2$ . The length of a side  $a = 30$  mm. The length  $l_1 = 50$  mm and  $l_2 = 100$  mm. The yield strength  $S_y = 350$  MPa (medium-carbon steel). Find whether the stresses in tension and shear are below the allowable stresses. Neglect bending.

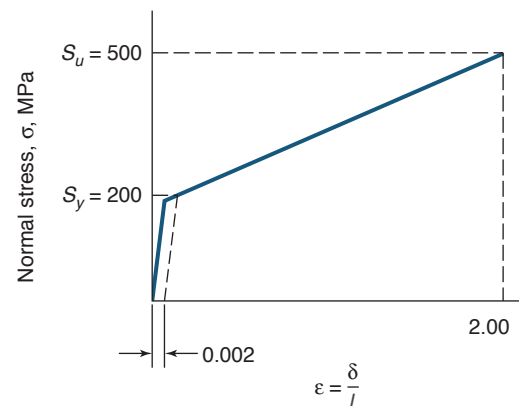


Sketch *b*, for Problem 3.53

**3.54** A steel cube has side length  $l = 0.1$  m, modulus of elasticity  $E = 206$  GPa, and Poisson's ratio  $\nu = 0.3$ . A stress  $\sigma$  is applied to one direction on the cube. Find the compressive stresses needed on the four remaining cube faces to give the same elongation that results from  $\sigma$ . *Ans.*  $\sigma_c = -1.67\sigma$ .

**3.55** For the stressed steel cube in Problem 3.54, calculate the volume ratio ( $v_t/v_c$ ) when  $\sigma = 500$  MPa. *Ans.*  $v_t/v_c = 1.0042$ .

**3.56** A tough material, such as soft stainless steel, has yield strength  $S_y = 200$  MPa, ultimate strength  $S_u = 500$  MPa, and 200% elongation. Find the ratio of the material toughness to the resilience at fracture (the *hyperstatic resilience*), assuming that the stress-strain curve consists of two straight lines according to Sketch *c*. *Ans.* Toughness/resilience = 1080.



Sketch *c*, for Problem 3.56

**3.57** Hooke's law describes the relationship between uniaxial stress and uniaxial strain. What is the ratio of the strain encountered by the most compliant material mentioned in this chapter compared to the stiffest? *Ans.*  $1.125 \times 10^5$ .



- 3.58** According to Archard's wear equation, the wear depth is proportional to the sliding distance and the contact pressure. How will the contact pressure be distributed radially for a disk brake if the wear rate is the same for all radii? *Ans.* Pressure is inversely proportional to radius.
- 3.59** Given a brake pad for a disk brake on a car, and using Archard's wear constant, determine how the wear is distributed over the brake pad if the brake pressure is constant over the pad. *Ans.* Wear rate is proportional to radius.
- 3.60** Derive an expression for the toughness of a material represented by the stress-strain law  $\sigma = K(\epsilon + 0.2)^n$  and whose fracture strain is denoted by  $\epsilon_f$ .

## Design and Projects

- 3.61** List and explain the desirable mechanical properties for (a) an elevator cable, (b) a paper clip, (c) a leaf spring for a truck, (d) a bracket for a bookshelf, (e) piano wire, (f) a wire coat hanger, (g) the clip for a pen, and (h) a staple.
- 3.62** List applications where the following properties would be desirable: (a) high density, (b) low density, (c) high stiffness, (d) low stiffness, (e) high thermal conductivity, and (f) low thermal conductivity.
- 3.63** Give several applications in which both specific strength and specific stiffness are important.
- 3.64** Conduct a literature search and add the following materials to Table 3.1: cork, concrete, ice, sugar, lithium, chromium, and platinum.
- 3.65** A recent development in the automotive industry is to use steel alloys with a high manganese content, called TRIP, TWIP, and martensitic steels. Conduct an Internet search and literature review and write a one-page summary of these materials and their mechanical properties.
- 3.66** Design an actuator to turn on a switch when temperature drops below a certain level. Use two materials with different coefficients of thermal expansion in your design.
- 3.67** Assume that you are in charge of public relations for a large steel-producing company. Outline all of the attractive characteristics of steels that you would like your customers to be informed about.
- 3.68** Assume that you are in competition with the steel industry and are asked to list all of the characteristics of steels that are not attractive. Make a list of these characteristics and explain their relevance to engineering applications.
- 3.69** Aluminum is being used as a substitute material for steel in automobiles. Describe your concerns, if any, in purchasing an aluminum automobile.
- 3.70** Add a column to Table 3.1 and add values of electrical conductivity for the materials given.
- 3.71** Review the technical literature, and produce a figure similar to Fig. 3.24 for investment casting.
- 3.72** Perform an Internet search, and produce a Powerpoint presentation that summarizes applications of rapid prototyping. Whenever possible, indicate the material and machinery used.

This page intentionally left blank

# Chapter 4

## Stresses and Strains



The failed Hyatt Regency Hotel walkway (Kansas City, 1981) that was directly attributable to changes in design that over-stressed structural members. Source: AP Photos.

*I am never content until I have constructed a mechanical model of the subject I am studying. If I succeed in making one, I understand; otherwise I do not.*

William Thomson (Lord Kelvin)

This chapter discusses stresses and strains that arise from common loading conditions discussed in Chapter 2, using the constitutive rules described in Chapter 3. The approaches in this chapter are mainly developed for the analysis of beams and shafts, but are easily adaptable to any machine element, and are usually sufficient for stress analysis and design. The chapter begins with a review of cross-sectional properties such as the centroid of an area, moment of inertia (and the use of the parallel-axis theorem to obtain the moment of inertia), the radius of gyration, section modulus, and mass moment of inertia. After introducing normal stresses and strains due to uniaxial loadings, the chapter considers torsion stresses and strains that are essential for shaft design. Bending stress and strain are then considered for both straight and curved beams, as well as the associated transverse shear stresses. The combination of these stresses due to complicated loadings is then examined.

### Contents

4.1	Introduction	90
4.2	Properties of Beam Cross Sections	90
4.3	Normal Stress and Strain	94
4.4	Torsion	98
4.5	Bending Stress and Strain	99
4.6	Transverse Shear Stress and Strain	104
4.7	Summary	109

### Examples

4.1	Determining the Centroid of an Area	91
4.2	Area and Polar Moment of Inertia	91
4.3	Moment of Inertia and Centroid from Parallel Axis Theorem	92
4.4	Parallel Axis Theorem	93
4.5	Radius of Gyration	93
4.6	Normal Stress, Deformation, and Spring Rate	97
4.7	Elongation and Spring Rate in Tension	97
4.8	Angle of Twist and Spring Rate in Torsion	98
4.9	Power Transmitted by a Shaft	99
4.10	Stress in Bending	101
4.11	Stress in Curved Member	103
4.12	Stress Due to Transverse Shear	105
4.13	Critical Location in a Beam	106

### Case Study

Design of a Shaft for a Coil Slitter 107

## Symbols

$A$	cross sectional area, $m^2$
$A'$	partial cross sectional area, $m^2$
$a$	width, m
$b$	height, m
$c$	distance from neutral axis to outer fiber of solid, m
$d_x, d_y$	distance between two parallel axes, one of which contains centroid of area, m
$E$	modulus of elasticity, Pa
$e$	eccentricity, distance separating centroidal and neutral radii of curved member, m
$G$	shear modulus of elasticity, Pa
$h$	height of triangular cross-sectional area, m
$h_p$	power, W
$I$	area moment of inertia, $m^4$
$I_m$	mass moment of inertia, $kg \cdot m^2$
$J$	polar area moment of inertia, $m^4$
$\bar{J}$	polar area moment of inertia about centroidal coordinates, $m^4$
$k$	spring rate, N/m
$k_a$	angular spring rate, N-m
$l$	length, m
$M$	bending moment, N-m
$m_a$	mass, kg
$P$	force, N
$Q$	first moment about neutral axis, $m^3$
$r$	radius, m
$\bar{r}$	centroidal radius, m
$r_g$	radius of gyration, m
$s$	length of a line segment, m
$T$	torque, N-m
$u$	velocity, m/s
$V$	transverse shear force, N
$w_t$	width, m
$x, y, z$	Cartesian coordinate system, m
$\bar{x}, \bar{y}, \bar{z}$	centroidal coordinate system, m
$x', y'$	coordinates parallel to $x$ - and $y$ -axes
$Z_m$	section modulus, $I/c$ , $m^3$
$\gamma$	shear strain
$\delta$	deformation, m
$\epsilon$	normal strain
$\rho$	density, $kg/m^3$
$\theta$	angle of twist, rad
$\sigma$	normal stress, Pa
$\tau$	shear stress, Pa
$\omega$	angular velocity, rad/s

## Subscripts

$i$	inner
$o$	outer
$x, y, z$	Cartesian coordinates
$\bar{x}, \bar{y}, \bar{z}$	centroidal coordinates
$x', y'$	coordinates parallel to $x$ - and $y$ -axes

## 4.1 Introduction

Normal, torsional, bending, and transverse shear loadings were described in Section 2.3. This chapter describes the stresses and strains resulting from these types of loading while making use of the general Hooke's law relation developed in Chapter 3. The theory developed in this chapter is applicable to any machine element. For the purposes of this

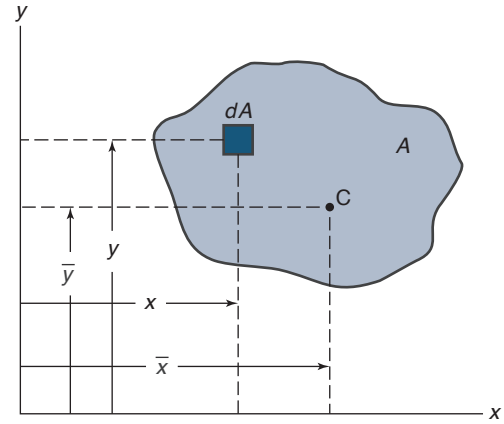


Figure 4.1: Centroid of area. The centroid is at point C with coordinates  $(\bar{x}, \bar{y})$ .

chapter, however, the member is assumed to have a symmetrical cross section and to be made of an isotropic, homogeneous, linear-elastic material. Later in the chapter, a curved member is also considered for bending. More complicated geometries are considered in Chapter 6.

This chapter provides a quick review of stress analysis and more in-depth coverage can be found in the Recommended Readings at the end of the chapter. Section 4.2 describes the approach for calculating important properties of a beam's cross-section, namely its centroid, moment of inertia, section modulus, radius of gyration, and mass moment of inertia. Readers familiar with these topics may wish to proceed to Section 4.3, which introduces the concepts of normal stress and strain, or Section 4.4 which deals with torsion. Bending is discussed in Section 4.5 and the effect of transverse shear in bending is presented in Section 4.6.

## 4.2 Properties of Beam Cross Sections

The centroid of an area, moment of inertia of an area, parallel-axis theorem, radius of gyration, section modulus, and mass moment of inertia are important concepts that need to be defined before proceeding with the remainder of this chapter. These concepts will be used throughout the text.

### 4.2.1 Centroid of Area

The **centroid** of an area (Fig. 4.1), or the *center of gravity* of an area, refers to the point that defines the area's geometric center. Conceptually, this is the point of balance where equal areas exist on each side of the point across arbitrary sections of the body. A finite thickness version of the area would balance on a pin placed at the centroid. Mathematically, it is that point at which the sum of the first moments of area about an axis through it is zero, or

$$\int_A (y - \bar{y}) dA = 0, \quad (4.1)$$

$$\int_A (x - \bar{x}) dA = 0. \quad (4.2)$$

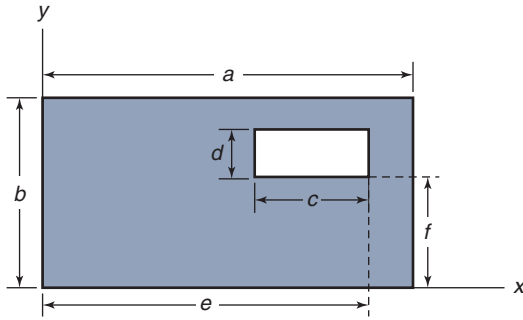


Figure 4.2: Rectangular hole within a rectangular section used in Example 4.1.

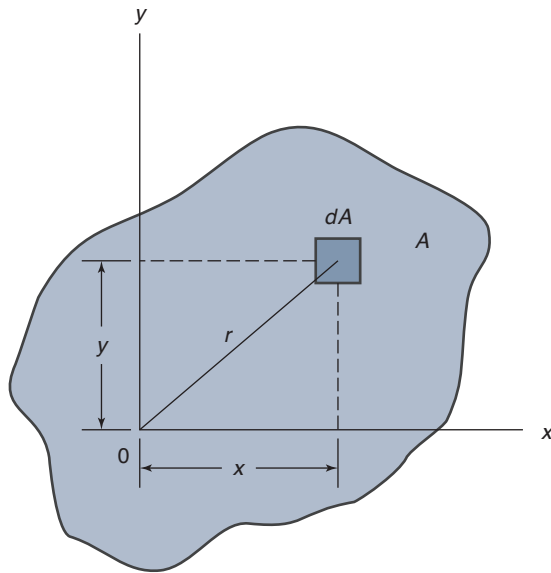


Figure 4.3: Area with coordinates used in describing area moment of inertia.

Solving for  $\bar{x}$  and  $\bar{y}$  gives

$$\bar{y} = \frac{\int_A y dA}{\int_A dA} = \frac{\int_A y dA}{A}, \quad (4.3)$$

$$\bar{x} = \frac{\int_A x dA}{\int_A dA} = \frac{\int_A x dA}{A}. \quad (4.4)$$

A complicated area can usually be divided into simple subareas and Eqs. (4.3) and (4.4) can be applied by making the numerator equal to the sum of the first moment integrals of the separate areas. The denominator is the total area. Thus, the centroid of the composite area is given by

$$\bar{y} = \frac{A_1 \bar{y}_1 + A_2 \bar{y}_2 + \dots}{A_1 + A_2 + \dots}, \quad (4.5)$$

$$\bar{x} = \frac{A_1 \bar{x}_1 + A_2 \bar{x}_2 + \dots}{A_1 + A_2 + \dots}. \quad (4.6)$$

### Example 4.1: Determining the Centroid of an Area

**Given:** Figure 4.2 shows a rectangular part having dimensions  $a \times b$  with a rectangular hole  $c \times d$ . It also shows the coordinates and location of this hole within the rectangular cross section. The dimensions are  $a = 10$  cm,  $b = 5$  cm,  $c = 3$  cm,  $d = 1$  cm,  $e = 9$  cm, and  $f = 3$  cm.

**Find:** The centroid of this part.

**Solution:** In this problem, one could break the section into a number of rectangles to obtain the correct solution. However, a useful approach is demonstrated here, namely treating the hole as a “negative” area. Then, making use of Eqs. (4.5) and (4.6) gives

$$\begin{aligned} \bar{y} &= \frac{A_1 \bar{y}_1 - A_2 \bar{y}_2}{A_1 - A_2} = \frac{ab(b/2) - cd(f + d/2)}{ab - cd} \\ &= \frac{(10)(5)(5/2) - (3)(1)(3 + 1/2)}{(10)(5) - (3)(1)} = 2.436 \text{ cm}, \\ \bar{x} &= \frac{A_1 \bar{x}_1 - A_2 \bar{x}_2}{A_1 - A_2} = \frac{ab(a/2) - cd(e - c/2)}{ab - cd} \\ &= \frac{(10)(5)(10/2) - (3)(1)(9 - 3/2)}{(10)(5) - (3)(1)} = 4.840 \text{ cm}. \end{aligned}$$

### 4.2.2 Area Moment of Inertia

The terms **area moment of inertia** and **second moment of area** are used interchangeably. In Section 4.2.1, the first moment of area,  $\int_A y dA$ , was associated with the centroid and in this section the second moment of area,  $\int_A y^2 dA$ , is used to define the moment of inertia.

Figure 4.3 shows the coordinates that describe the area moments of inertia, which are designated by the symbol  $I$ . The moments of inertia with respect to the  $x$ - and  $y$ -axes, respectively, can be expressed as

$$I_x = \int_A y^2 dA \quad \text{and} \quad I_y = \int_A x^2 dA. \quad (4.7)$$

When the reference axis is normal to the plane of the area, through 0 in Fig. 4.3, the integral is called the **polar moment of inertia**,  $J$ , and can be written as

$$J = \int_A r^2 dA = \int_A (x^2 + y^2) dA = \int_A x^2 dA + \int_A y^2 dA. \quad (4.8)$$

Note from Eq. (4.7) that

$$J = I_x + I_y. \quad (4.9)$$

In defining the polar moment of inertia, the  $x$ - and  $y$ -axes can be any two mutually perpendicular axes intersecting at 0. The unit of moment of inertia and polar moment of inertia is length raised to the fourth power.

### Example 4.2: Area and Polar Moment of Inertia

**Given:** Figure 4.4 shows a circular cross section with radius  $r$  and  $x$ - $y$  coordinates.

**Find:** The area moment of inertia of the circular area about the  $x$ - and  $y$ -axes and the polar moment of inertia about the centroid.



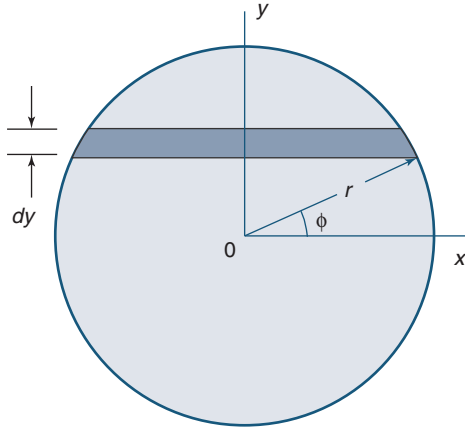


Figure 4.4: Circular cross section used in Example 4.2.

**Solution:** Consider the shaded slice of the circle shown in Fig. 4.4. For any position defined by  $\phi$  between  $\pi/2$  and  $-\pi/2$ , the incremental area is

$$dA = 2r \cos \phi \, dy.$$

From Eq. (4.7), the area moment of inertia of the circular area about the  $x$ -axis is

$$I_x = \int y^2 dA = \int y^2 2r \cos \phi \, dy.$$

But because  $y = r \sin \phi$  and  $dy = r \cos \phi \, d\phi$ ,

$$\begin{aligned} I_x &= 2r^4 \int_{-\pi/2}^{\pi/2} \sin^2 \phi \cos^2 \phi \, d\phi \\ &= \frac{r^4}{2} \int_{-\pi/2}^{\pi/2} \frac{1 - \cos 4\phi}{2} \, d\phi \\ &= \frac{\pi r^4}{4}. \end{aligned}$$

Because of symmetry, the moment of inertia with respect to the  $y$ -axis is

$$I_y = \frac{\pi r^4}{4}.$$

Thus, the area moments of inertia about the  $x$ - and  $y$ -axes are identical and equivalent to  $\pi r^4/4$ . From Eq. (4.9) the polar moment of inertia about the centroid is

$$J_z = I_x + I_y = 2I_x = \frac{\pi r^4}{2}.$$

### 4.2.3 Parallel-Axis Theorem

When an area's moment of inertia has been determined with respect to a given axis through its centroid, the moment of inertia with respect to any parallel axis can be obtained by means of the parallel-axis theorem. Figure 4.5 shows the coordinates and distances to be used in deriving the parallel-axis theorem.

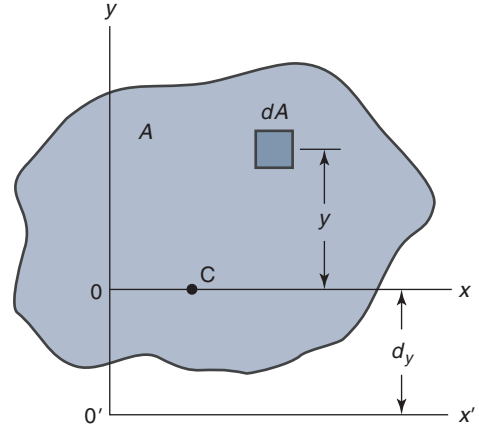


Figure 4.5: Coordinates and distance used in describing the parallel-axis theorem.

The moment of inertia of the area  $A$  about the axis  $x'$  is

$$\begin{aligned} I_{x'} &= \int_A (y + d_y)^2 dA \\ &= \int_A y^2 dA + 2d_y \int_A y dA + d_y^2 \int_A dA, \end{aligned}$$

or

$$I_{x'} = I_x + 2d_y \int_A y dA + Ad_y^2. \quad (4.10)$$

If the  $x$ -axis passes through the centroid of the area,  $\int_A y dA$  is zero and Eq. (4.10) reduces to

$$I_{x'} = I_x + Ad_y^2. \quad (4.11)$$

Similarly, for an axis  $y'$  parallel to the  $y$ -axis that goes through the centroid and is separated by a distance  $d_x$ ,

$$I_{y'} = I_y + Ad_x^2. \quad (4.12)$$

Equations (4.11) and (4.12) are known as the **parallel-axis theorem**, and allow calculation of an area's moment of inertia with respect to any axis.

### Example 4.3: Moment of Inertia and Centroid from Parallel Axis Theorem

**Given:** Figure 4.6 shows a triangular cross section with a circular hole.

**Find:** The area moment of inertia and the centroid.

**Solution:** Assume that the  $y$ -axis starts at the midwidth of the base and is positive in the upward direction. The height of the triangle is

$$h = \frac{6}{2} \tan 60^\circ = 5.196 \text{ cm}.$$

The triangle and circle are defined with an  $a$  and  $b$  subscript, respectively. The centroids and areas of the triangle and the circle can be expressed separately as

$$\bar{y}_a = \frac{h}{3} = \frac{5.196}{3} = 1.732 \text{ cm},$$

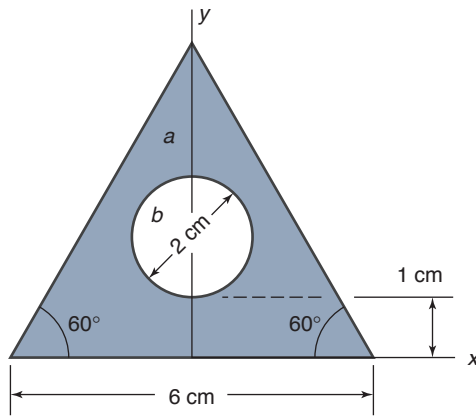


Figure 4.6: Triangular cross section with circular hole, used in Example 4.3.

$$A_a = \frac{1}{2}bh = \frac{1}{2}(6)(5.196) = 15.59 \text{ cm}^2,$$

$$A_b = \frac{\pi d^2}{4} = \frac{\pi(2)^2}{4} = \pi = 3.142 \text{ cm}^2.$$

The centroid of the composite figure is

$$\bar{y} = \frac{\bar{y}_a A_a - \bar{y}_b A_b}{A_a - A_b} = \frac{(1.732)(15.59) - (2)(3.142)}{15.59 - 3.142} = 1.664 \text{ cm}.$$

The moments of inertia of the triangle and circle are

$$I_a = \frac{bh^3}{36} = \frac{6(5.196)^3}{36} = 23.38 \text{ cm}^4,$$

$$I_b = \frac{\pi d^4}{64} = \frac{\pi(2)^4}{64} = 0.7854 \text{ cm}^4.$$

From the parallel-axis theorem, the moment of inertia of the composite area about the centroidal axis is

$$\begin{aligned} I_x &= I_a + (\bar{y} - \bar{y}_a)^2 A_a - I_b - (\bar{y} - \bar{y}_b)^2 A_b \\ &= 23.38 + (1.664 - 1.732)^2(15.59) - 0.7854 \\ &\quad - (1.664 - 2)^2(3.142) \\ &= 2.231 \times 10^{-7} \text{ m}^4. \end{aligned}$$

### Example 4.4: Parallel Axis Theorem

**Given:** Figure 4.7 shows a circular cross section of radius  $r$ , and  $x'$ - $y'$  coordinates.

**Find:** The area moments of inertia  $I_{x'}$ ,  $I_{y'}$  and the polar moment of inertia  $J_{z'}$ , relative to the  $x'$ ,  $y'$ , and  $z'$  axes.

**Solution:** Using Eqs. (4.11) and (4.12) and the results from Example 4.2 gives

$$I_{x'} = I_x + Ad_y^2 = \frac{\pi r^4}{4} + \pi r^2 (4r)^2 = 16.25\pi r^4,$$

$$I_{y'} = I_y + Ad_x^2 = \frac{\pi r^4}{4} + \pi r^2 (3r)^2 = 9.25\pi r^4$$

$$J_{z'} = I_{x'} + I_{y'} = 25.5\pi r^4.$$

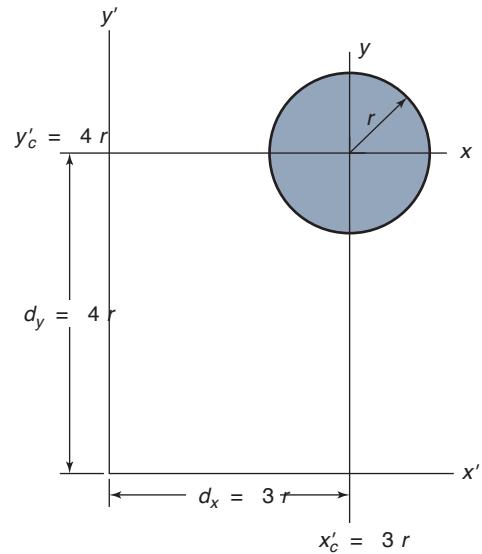


Figure 4.7: Circular cross-sectional area relative to  $x'$ - $y'$  coordinates, used in Example 4.4.

### 4.2.4 Radius of Gyration

An area's **radius of gyration** is the length that, when squared and multiplied by the area, will give the area's moment of inertia with respect to the specific axis, or

$$I = r_g^2 A. \quad (4.13)$$

This is another way of expressing the area's moment of inertia. The radius of gyration can be written as

$$r_g = \sqrt{\frac{I}{A}}. \quad (4.14)$$

The radius of gyration is not the distance from the reference axis to a fixed point in the area (such as the centroid), but it is a useful property of the area and the specified axis.

### Example 4.5: Radius of Gyration

**Given:** The same circular area given in Example 4.4.

**Find:** The radius of gyration with respect to the  $x'$  and  $y'$  axes.

**Solution:** Using Eq. (4.14) and the results from Example 4.4 give

$$r_{gx'} = \sqrt{\frac{I_{x'}}{A}} = \sqrt{\frac{16.25\pi r^4}{\pi r^2}} = 4.03r,$$

$$r_{gy'} = \sqrt{\frac{I_{y'}}{A}} = \sqrt{\frac{9.25\pi r^4}{\pi r^2}} = 3.04r.$$

When the circle is small relative to the distances  $d_x$  and  $d_y$ , the radii of gyration are just a little larger than the centroidal distances  $3r$  and  $4r$ . This is a useful observation that will be applied later in the text, for example in the analysis of spot welds in Section 16.6.

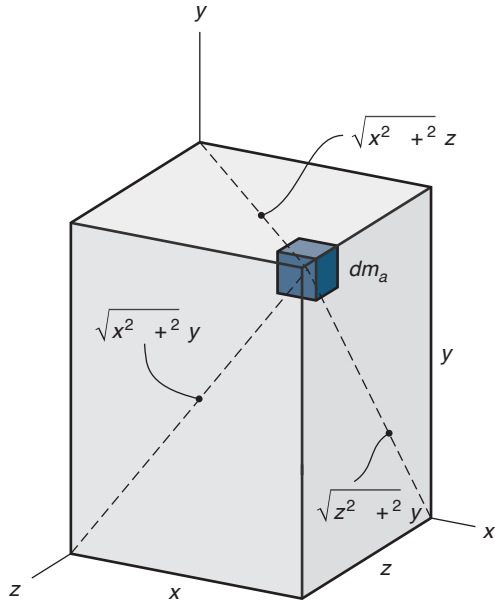


Figure 4.8: Mass element with three-dimensional coordinates.

### 4.2.5 Section Modulus

The **section modulus** is an area's moment of inertia divided by the farthest distance from the centroidal axis to the outer fiber of the solid,  $c$ , or

$$Z_m = \frac{I}{c}. \quad (4.15)$$

The unit of section modulus is length to the third power. The area moment of inertia,  $I$  in Eqs. (4.13) to (4.15), holds for  $I_x$  and  $I_y$  with appropriate changes in  $r_g$  and  $Z_m$ . Thus,  $r_{gx}$  and  $Z_{mx}$  would correspond to the use of  $I_x$ , and  $r_{gy}$  and  $Z_{my}$  would correspond to the use of  $I_y$ .

Table 4.1 gives the centroid, area, and moment of inertia for seven different cross sections. Note that data is presented for moments of inertia about the centroid (using  $\bar{x}$  and  $\bar{y}$  as subscripts) as well as the exterior reference axes (using  $x$  and  $y$  subscripts). Also,  $\bar{J}$  implies that the area polar moment of inertia was taken with the centroidal coordinates;  $J$  (without an overbar) indicates that the area polar moment of inertia was taken with respect to coordinates  $x$  and  $y$ .

### 4.2.6 Mass Moment of Inertia

The **mass moment of inertia** of an element is the product of the element's mass and the square of the element's distance from the axis. Figure 4.8 shows a mass element with three-dimensional coordinates. From this figure, the mass moments of inertia can be expressed with respect to the  $x$ -,  $y$ -, and  $z$ -axes as

$$I_{mx} = \int (y^2 + z^2) dm_a, \quad (4.16)$$

$$I_{my} = \int (x^2 + z^2) dm_a, \quad (4.17)$$

$$I_{mz} = \int (x^2 + y^2) dm_a. \quad (4.18)$$

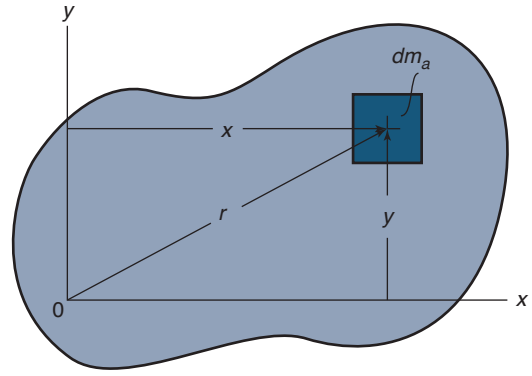


Figure 4.9: Mass element in two-dimensional coordinates and distance from the two axes.

The SI unit of mass moment of inertia is  $\text{kg}\cdot\text{m}^2$ . If, instead of the three-dimensional coordinates given in Fig. 4.8, there is a thin plate (see Fig. 4.9) so that only the  $x$ - $y$  plane needs to be considered, the mass moments of inertia become

$$I_{mx} = \int y^2 dm_a, \quad (4.19)$$

$$I_{my} = \int x^2 dm_a, \quad (4.20)$$

$$J_o = \int r^2 dm_a = \int (x^2 + y^2) dm_a = I_{mx} + I_{my}. \quad (4.21)$$

The polar mass moment of inertia is given in Eq. (4.21) as  $J_o$ . Table 4.2 gives the mass and mass moment of inertia of six commonly used shapes. Just as with Table 4.1, the origin and coordinates are important for the equations relative to a specific shape.

## 4.3 Normal Stress and Strain

The bar shown in Fig. 4.10 supports a force,  $P$ , and is in tension. Such a force increases the length of the bar. For a section some distance away from the ends, an average intensity of the normal force on the cross section, or **average normal stress**,  $\sigma_{\text{avg}}$ , can be written as

$$\sigma_{\text{avg}} = \frac{P}{A}. \quad (4.22)$$

Had the section been cut near the ends, the situation would be more complicated. The stress system would no longer be simple tension uniformly distributed over the cross section because any grips or tooling used to apply the loads invariably result in uneven load distributions. Fortunately, the stresses farther from the load application point are fairly uniform (i.e., stress concentrations, covered in detail in Chapter 6, are reduced as the distance from them increases). This tendency was first noted by Saint-Venant, so it is known as **Saint-Venant's principle**. Its importance should not be underestimated; it makes the application of this chapter's equations possible.<sup>1</sup>

<sup>1</sup>The exact distance that one must travel from a stress concentration before stresses can be considered uniform varies and can range from one characteristic length (diameter, grip length, etc.) to over ten characteristic lengths for some composite materials.

Table 4.1: Centroid, area moment of inertia, and area for common cross sections.

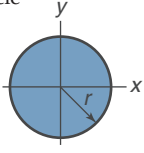
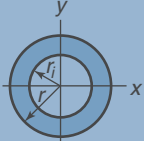
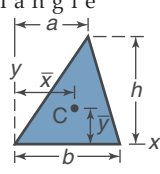
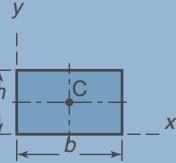
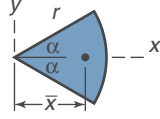
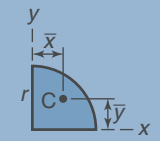
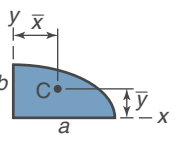
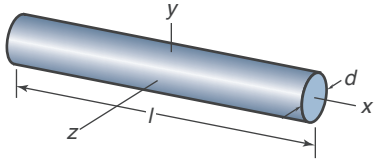
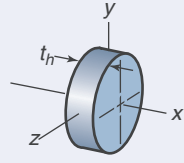
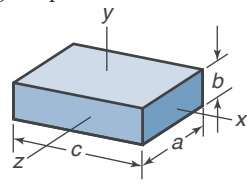
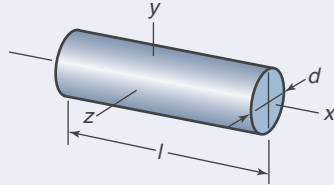
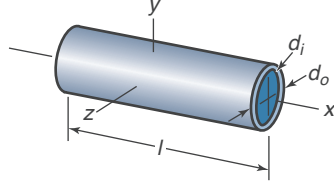
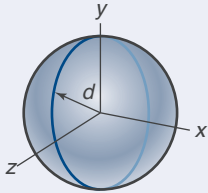
Cross section	Centroid	Area moment of inertia	Area
<b>Circle</b> 	$\bar{x} = 0$ $\bar{y} = 0$	$I_x = I_{\bar{x}} = \frac{\pi}{4} r^4$ $I_y = I_{\bar{y}} = \frac{\pi}{4} r^4$ $J = \frac{\pi}{2} r^4$	$A = \pi r^2$
<b>Hollow circle</b> 	$\bar{x} = 0$ $\bar{y} = 0$	$I_x = I_{\bar{x}} = \frac{\pi}{4} (r^4 - r_i^4)$ $I_y = I_{\bar{y}} = \frac{\pi}{4} (r^4 - r_i^4)$ $J = \frac{\pi}{2} (r^4 - r_i^4)$	$A = \pi (r^2 - r_i^2)$
<b>Triangle</b> 	$\bar{x} = \frac{a + b}{3}$ $\bar{y} = \frac{h}{3}$	$I_x = \frac{bh^3}{12}, I_{\bar{x}} = \frac{bh^3}{36}$ $I_y = \frac{bh(b^2 + ab + a^2)}{12}$ $I_{\bar{y}} = \frac{bh(b^2 - ab + a^2)}{36}$ $J = \frac{bh}{36} (b^2 + h^2 + a^2 - ab)$	$A = \frac{bh}{2}$
<b>Rectangle</b> 	$\bar{x} = \frac{b}{2}$ $\bar{y} = \frac{h}{2}$	$I_x = \frac{bh^3}{12}, I_{\bar{x}} = \frac{bh^3}{12}$ $I_y = \frac{b^3h}{12}, I_{\bar{y}} = \frac{b^3h}{12}$ $J = \frac{bh}{12} (b^2 + h^2)$	$A = bh$
<b>Circular sector</b> 	$\bar{x} = \frac{2r \sin \alpha}{3\alpha}$	$I_x = \frac{r^4}{4} \left( \alpha - \frac{1}{2} \sin 2\alpha \right)$ $I_y = \frac{r^4}{4} \left( \alpha + \frac{1}{2} \sin 2\alpha \right)$ $J = \frac{1}{2} r^4 \alpha$	$A = r^2 \alpha$
<b>Quarter-circle</b> 	$\bar{x} = \bar{y} = \frac{4r}{3\pi}$	$I_x = I_y = \frac{\pi r^4}{16}$ $I_{\bar{x}} = I_{\bar{y}} = \left( \frac{\pi}{16} - \frac{4}{9\pi} \right) r^4$ $J = \frac{\pi r^4}{8}$	$A = \frac{\pi r^2}{4}$
<b>Elliptical quadrant</b> 	$\bar{x} = \frac{4a}{3\pi}$ $\bar{y} = \frac{4b}{3\pi}$	$I_x = \frac{\pi ab^3}{16}, I_{\bar{x}} = \left( \frac{\pi}{16} - \frac{4}{9\pi} \right) ab^3$ $I_y = \frac{\pi a^3 b}{16}, I_{\bar{y}} = \left( \frac{\pi}{16} - \frac{4}{9\pi} \right) a^3 b$ $J = \frac{\pi ab}{16} (a^2 + b^2)$	$A = \frac{\pi ab}{4}$

Table 4.2: Mass and mass moment of inertia of six solids.

Shape	Equations
<p>Rod</p> 	$m_a = \frac{\pi d^2 l \rho}{4}$ $I_{my} = I_{mz} = \frac{m_a l^2}{12}$
<p>Disk</p> 	$m_a = \frac{\pi d^2 t_h \rho}{4}$ $I_{mx} = \frac{m_a d^2}{8}$ $I_{my} = I_{mz} = \frac{m_a d^2}{16}$
<p>Rectangular prism</p> 	$m_a = abc\rho$ $I_{mx} = \frac{m_a (a^2 + b^2)}{12}$ $I_{my} = \frac{m_a (a^2 + c^2)}{12}$ $I_{mz} = \frac{m_a (b^2 + c^2)}{12}$
<p>Cylinder</p> 	$m_a = \frac{\pi d^2 l \rho}{4}$ $I_{mx} = \frac{m_a d^2}{8}$ $I_{my} = I_{mz} = \frac{m_a (3d^2 + 4l^2)}{48}$
<p>Hollow cylinder</p> 	$m_a = \frac{\pi l \rho (d_o^2 - d_i^2)}{4}$ $I_{mx} = \frac{m_a (d_o^2 - d_i^2)}{8}$ $I_{my} = I_{mz} = \frac{m_a (3d_o^2 + 3d_i^2 + 4l^2)}{48}$
<p>Sphere</p> 	$m_a = \frac{\pi d^3 \rho}{6}$ $I_{mx} = I_{my} = I_{mz} = \frac{m_a d^2}{10}$



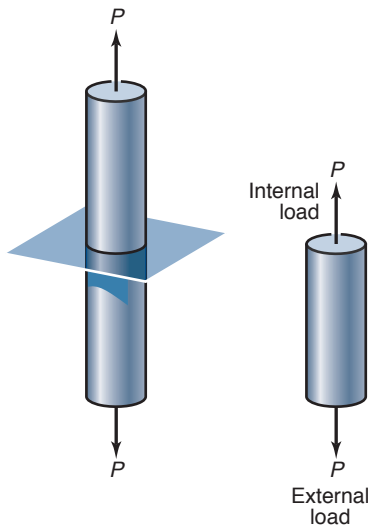


Figure 4.10: Circular bar with tensile load applied.

Consistent with the sign convention presented in Chapter 2, a tensile normal stress is taken as positive and a compressive normal stress is negative. The total length change in a uniform bar caused by an axial load is called the **elastic deformation**,  $\delta$ . The **normal strain** is

$$\epsilon = \frac{\delta}{l} = \frac{\text{Elastic deformation}}{\text{Original length}}. \quad (4.23)$$

Although the strain is dimensionless, it is often expressed in terms of meter per meter, or often  $\mu\text{m}/\text{m}$ . From Hooke's law for a uniaxial normal loading,

$$\sigma = \epsilon E \quad \text{or} \quad \epsilon = \frac{\sigma}{E} \quad (4.24)$$

where  $E$  is the modulus of elasticity described in Section 3.5.2 and is a constant for a given material. Substituting Eqs. (4.22) and (4.24) into Eq. (4.23) gives

$$\delta = \epsilon l = \frac{\sigma l}{E} = \frac{Pl}{AE}. \quad (4.25)$$

Equations (4.24) and (4.25) are valid for either tension or compression. The **spring rate** is the ratio of normal to elastic deflection or, for axial loading,

$$k = \frac{P}{\delta} = \frac{AE}{l}. \quad (4.26)$$

Equations (4.22) to (4.26) hold for any cross section that is constant over the length  $l$ .

### Example 4.6: Normal Stress, Deformation, and Spring Rate

**Given:** A hollow carbon steel shaft 50 mm long must carry a normal force of 5000 N at a normal stress of 100 MPa. The inside diameter is 65% of the outside diameter.

**Find:** The outside diameter, the axial deformation, and the spring rate.

**Solution:** The cross-sectional area can be expressed as

$$\begin{aligned} A &= \frac{\pi}{4} (d_o^2 - d_i^2) = \frac{\pi d_o^2}{4} \left[ 1 - \left( \frac{d_i}{d_o} \right)^2 \right] \\ &= \frac{\pi d_o^2}{4} \left[ 1 - \left( \frac{0.65 d_o}{d_o} \right)^2 \right] = 0.4536 d_o^2. \end{aligned}$$

From Eq. (4.22),

$$A = \frac{P}{\sigma} = \frac{5000}{100 \times 10^6} = 5 \times 10^{-5} \text{ m}^2.$$

Therefore,

$$0.4536 d_o^2 = 5 \times 10^{-5} \text{ m}^2$$

or

$$d_o = 1.05 \times 10^{-2} \text{ m} = 10.5 \text{ mm}.$$

For carbon steel, the modulus of elasticity is 207 GPa (see Table 3.1). From Eq. (4.25), the elastic deformation is

$$\delta = \frac{Pl}{AE} = \frac{(5000)(0.05)}{(5 \times 10^{-5})(207 \times 10^9)} = 24.15 \times 10^{-6} \text{ m},$$

or  $\delta = 24.15 \mu\text{m}$ . From Eq. (4.26), the spring rate is

$$k = \frac{P}{\delta} = \frac{5000}{24.15 \times 10^{-6}} = 2.07 \times 10^8 \text{ N/m}.$$

### Example 4.7: Elongation and Spring Rate in Tension

**Given:** A fisherman catches a salmon with a lure fastened to his 0.45-mm-diameter nylon line. When the fish bites, it is 46 m from the reel. The modulus of elasticity of the line material is 4 GPa, and the salmon pulls with a force of 50 N.

**Find:** The elastic elongation of the line, the spring rate, and the tensile stress in the line.

**Solution:** The cross-sectional area of the line is

$$A = \frac{\pi d^2}{4} = \frac{\pi (0.45)^2}{4} = 0.1590 \text{ mm}^2.$$

The stress being exerted on the line by the salmon is

$$\sigma = \frac{P}{A} = \frac{50}{0.159 \times 10^{-6}} = 0.3144 \text{ GPa}.$$

The elongation of the line is

$$\delta = \epsilon l = \frac{\sigma l}{E} = \frac{(0.3144)(46)}{4} = 3.615 \text{ m}.$$

The spring rate of the line is  $k = P/\delta = 13.83 \text{ N/m}$ .

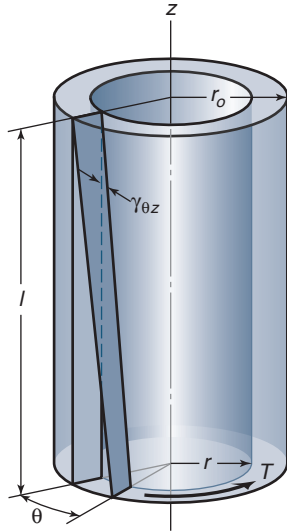


Figure 4.11: Twisting of member due to applied torque.

## 4.4 Torsion

A **shaft** is a slender element that is mainly loaded by axial moment or twist (torque), which causes torsional deformation and associated shear stresses. Thus, **torsion** is a loading that results in twisting of the shaft. Design of shafts will be investigated in detail in Chapter 11; the focus here is on the twisting, or torsion, to which shafts are subjected and the resulting stresses. A major use of the shaft is to transfer or transmit mechanical power from one point to another. Designers are interested primarily in the twisting moment that can be transmitted by the shaft without damaging the material or exceeding deformation constraints. Hence, it is important to be able to calculate the stresses in the shaft and the angle of twist. Solid circular members are of primary concern because most torque-transmitting shafts are of this shape. For cross sections that are not circular, the interested reader is referred to the classic text by Timoshenko and Goodier [1970].

### 4.4.1 Stress and Strain

Figure 4.11 shows the twisting of a member due to an applied torque. The circular shaft deforms such that each plane cross section originally normal to the axis remains plane and normal and does not distort within its own plane. While Fig. 4.11 shows a hollow shaft, a solid shaft is simply a special case where the inner radius equals zero. The shaft is fixed at the top and a torque is applied to the bottom end. The angle of twist is  $\theta$  and the extension strains are assumed to be zero. Thus,  $\epsilon_r = \epsilon_\theta = \epsilon_z = \gamma_{r\theta} = \gamma_{rz} = 0$ , and the only nonzero strain is

$$\gamma_{\theta z} = r \frac{d\theta}{dz} \approx \frac{r\theta}{l}. \quad (4.27)$$

Equation (4.27) can also be obtained from Fig. 4.11 by observing the common surface, as it relates  $l\gamma_{\theta z}$  and  $r\theta$ .

From Hooke's law, the stress is related to the strain by

$$\tau_{\theta z} = G\gamma_{\theta z} = Gr \frac{d\theta}{dz} \approx \frac{Gr\theta}{l}, \quad (4.28)$$

where  $G$  is the shear modulus of elasticity given in Eq. (3.7). In Eq. (4.28), the shear strain,  $\gamma_{\theta z}$ , and the shear stress,  $\tau_{\theta z}$ ,

vary linearly with respect to the rate of twist  $d\theta/dz \approx \theta/l$ . Also, the shear stress does not change in the  $\theta$ -direction (because of symmetry) or in the  $z$ -direction (because the deformation and the stress pattern are uniform along the shaft's length).

The rate of twist  $d\theta/dz$ , or  $\theta/l$  in Eq. (4.28), still must be determined. To do so, the stresses must satisfy equilibrium. The applied twisting moment, or torque, is

$$T = \int_A r (\tau_{\theta z} dA) = \frac{G\theta}{l} \int_A r^2 dA. \quad (4.29)$$

The polar moment of inertia is

$$J = \int_A r^2 dA. \quad (4.30)$$

Substituting Eq. (4.30) into Eq. (4.29) gives the torque and the angle of twist as

$$T = \frac{G\theta J}{l} \quad \text{and} \quad \theta = \frac{Tl}{GJ}. \quad (4.31)$$

Also, substituting Eqs. (4.29) and (4.30) into Eq. (4.28) gives

$$\tau_{\theta z} = \frac{Tr}{J}. \quad (4.32)$$

The maximum stress is

$$\tau_{\max} = \frac{Tc}{J}. \quad (4.33)$$

where  $c$  is the distance from the neutral axis to the outer fiber. The angular spring rate can be expressed as

$$k_a = \frac{T}{\theta} = \frac{JG}{l}. \quad (4.34)$$

### Example 4.8: Angle of Twist and Spring Rate in Torsion

**Given:** A 50-mm-long, hollow circular shaft made of carbon steel must carry a torque of 5000 N-m at a maximum shear stress of 70 MPa. The inside diameter is one-half the outside diameter.

**Find:** The outside diameter, the angle of twist, and the angular spring rate.

**Solution:** From Table 4.1 for a hollow cylinder,

$$J = \frac{\pi}{2} (r_o^4 - r_i^4) = \frac{\pi r_o^4}{2} \left[ 1 - \left( \frac{r_i}{r_o} \right)^4 \right]. \quad (a)$$

From Eq. (4.15), the section modulus is

$$Z_m = \frac{J}{c} = \frac{T}{\tau_{\max}} = \frac{5000}{70 \times 10^6} = 71.43 \times 10^{-6} \text{ m}^3. \quad (b)$$

Note that

$$\frac{r_i}{r_o} = \frac{r_i}{r_o} = 0.5 \quad \text{and} \quad c = \frac{d_o}{2}. \quad (c)$$

Therefore, by making use of Eqs. (a) and (c), Eq. (b) becomes

$$\frac{\pi r_o^3}{2} [1 - (0.5)^4] = 71.43 \times 10^{-6} \text{ m}^3.$$

Solving for  $r_o$ ,

$$r_o^3 = 48.51 \times 10^{-6} \text{ m}^3,$$

## Bending Stress and Strain

so that  $r_o = 0.03647 \text{ m} = 36.47 \text{ mm}$  and  $d_o = 72.94 \text{ mm}$ . Note from Eqs. (b) and (c) that

$$J = cZ_m = \frac{d_o}{2} Z_m = \left( \frac{0.07294}{2} \right) (71.43 \times 10^{-6}),$$

or  $J = 2.605 \times 10^{-6} \text{ m}^4$ . The shear modulus of elasticity for carbon steel is 80 GPa. Making use of Eq. (4.31) gives the angular twist due to torsion as

$$\theta = \frac{Tl}{GJ} = \frac{(5000)(0.050)}{(80 \times 10^9)(2.605 \times 10^{-6})} = 0.00120 \text{ rad.}$$

From Eq. (4.34) the angular spring rate is

$$k_a = \frac{T}{\theta} = \frac{5000}{0.00120} = 4.167 \times 10^6 \text{ N-m/rad.}$$

### 4.4.2 Power Transfer

One of the most common uses of a circular shaft is in power transmission; therefore, no discussion of torsion can exclude this important topic. **Power** is the rate of doing work or

$$h_p = Pu. \quad (4.35)$$

For rotating systems,

$$P = \frac{T}{r}. \quad (4.36)$$

Since  $u = \omega r$ ,

$$h_p = Pu = T\omega, \quad (4.37)$$

where

$P$  = force, N

$u$  = velocity, m/s

$T$  = torque, N-m

$\omega$  = angular velocity, rad/s

The SI unit of work is a joule, or a newton-meter. The SI unit of power is a watt, or a joule per second. Solving Eq. (4.37) for torque yields

$$T = \frac{h_p}{\omega}. \quad (4.38)$$

### Example 4.9: Power Transmitted by a Shaft

**Given:** A shaft carries a torque of 1000 N-m and turns at 900 rpm.

**Find:** The power transmitted in kilowatts.

**Solution:** The angular velocity is

$$\omega = (900 \text{ rpm}) \frac{2\pi}{60} = 94.25 \text{ rad/s}$$

From Eq. (4.37),

$$h_p = T\omega = (1000)(94.25) = 94.25 \text{ kW}$$

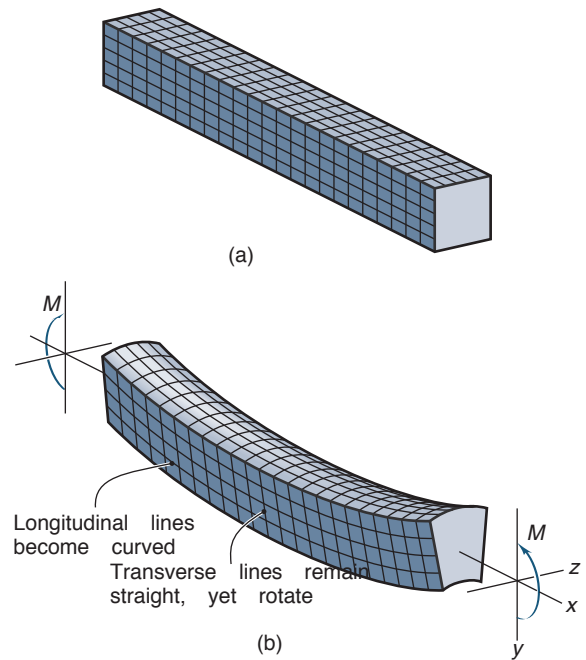


Figure 4.12: Bar made of elastic material to illustrate effect of applied bending moment. (a) Undeformed bar; (b) deformed bar.

## 4.5 Bending Stress and Strain

### 4.5.1 Straight Member

A **beam** is usually a long and slender member that supports predominantly bending loads. Analysis of beam bending is a common concern to engineers. Bending occurs in horizontal members of buildings (joists) subjected to vertical floor loading, in leaf springs on a truck, and in wings of an airplane supporting the weight of the fuselage. In each of these applications the stress and deformation are important design considerations.

Throughout this section the following assumptions are made:

1. The material is Hookian (see Section 3.6).
2. Deformations are small.

Figure 4.12 shows bending occurring in a highly deformable material, such as rubber, which is well-suited for demonstration purposes. The behavior of this bar can be extended to traditional beam materials such as steel, but with much smaller deformations. Figure 4.12a shows an undeformed bar with a square cross section marked by longitudinal and transverse grid lines. In Fig. 4.12b, a moment is applied. The longitudinal lines become curved while the transverse lines remain straight and undergo a rotation. The longitudinal lines have a radius when the bar is deformed, even though initially they were straight. Inspection of Fig. 4.12b suggests that the neutral axis will shift upward when the moment is applied. For elastic bending of stiffer beam materials, strains are low and warping of cross sections and shifting of the neutral axis will be ignored. Figure 4.13 further demonstrates the effect of bending. The bending moment causes the material in the bottom portion of the beam to stretch, or be

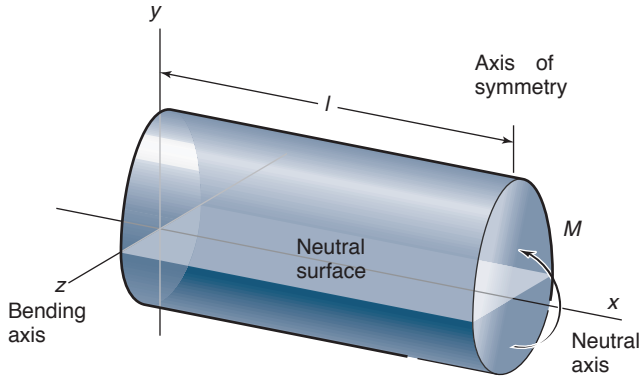


Figure 4.13: Bending occurring in a cantilevered bar, showing neutral surface.

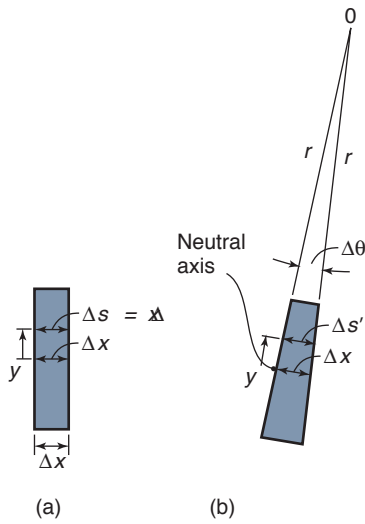


Figure 4.14: Undeformed and deformed elements in bending.

in tension, and that in the top to be in compression. Consequently, between these two regions there must be a surface, called the *neutral surface*, in which the longitudinal fibers of the material will not undergo a change in length. On this neutral surface no bending stress is occurring, and it is neither in tension nor in compression.

Figure 4.14 shows undeformed and deformed elements when bending occurs. The normal strain along line segment  $\Delta s$  is

$$\epsilon = \lim_{\Delta s \rightarrow 0} \frac{\Delta s' - \Delta s}{\Delta s}. \quad (4.39)$$

From Fig. 4.14, where  $r$  is the radius of curvature of the element's longitudinal axis,

$$\Delta x = \Delta s = r \Delta \theta,$$

$$\Delta s' = (r - y) \Delta \theta.$$

Substituting these equations into Eq. (4.39) gives

$$\epsilon = \lim_{\Delta s \rightarrow 0} \frac{(r - y) \Delta \theta - r \Delta \theta}{r \Delta \theta} = -\frac{y}{r}. \quad (4.40)$$

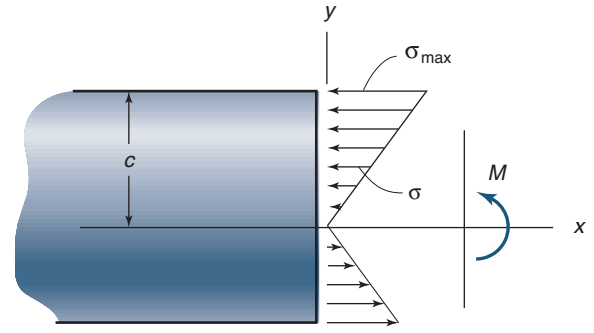


Figure 4.15: Profile view of bending stress variation.

The longitudinal normal strain will vary linearly with distance from the neutral axis. The maximum strain occurs at the outermost fiber, located at a distance,  $c$ , from the neutral axis. Therefore,

$$\frac{\epsilon}{\epsilon_{\max}} = -\frac{y/r}{c/r}$$

or

$$\epsilon = -\frac{y}{c} \epsilon_{\max}. \quad (4.41)$$

Similarly, a linear variation of normal stress over the cross-sectional area occurs, or

$$\sigma = -\frac{y}{c} \sigma_{\max}. \quad (4.42)$$

Figure 4.15 shows a profile view of the normal stress. For positive  $y$ , the normal stress is compressive and for negative  $y$ , the normal stress is tensile. The normal stress is zero at the neutral axis.

## 4.5.2 Bending Stress

From force equilibrium,

$$0 = \int_A dP = \int_A \sigma dA = \int_A -\frac{y}{c} \sigma_{\max} dA = -\frac{\sigma_{\max}}{c} \int_A y dA.$$

Because  $\sigma_{\max}$  is not equal to zero, this can only be assured if

$$\int_A y dA = 0. \quad (4.43)$$

Since the first moment of the member's cross-sectional area about the neutral axis must be zero, this requires that the neutral axis pass through the centroid. The moment may be expressed as

$$M = \int_A y dP = \int_A y \sigma dA = -\frac{\sigma_{\max}}{c} \int_A y^2 dA. \quad (4.44)$$

The area moment of inertia is

$$I = \int_A y^2 dA.$$

Substituting this relationship into Eq. (4.44) and solving for stress yields

$$\sigma_{\max} = -\frac{Mc}{I}. \quad (4.45)$$

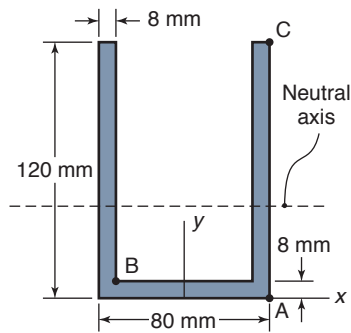


Figure 4.16: U-shaped cross section used in Example 4.10.

The stress at any intermediate distance  $y$  is

$$\sigma = -\frac{My}{I}. \quad (4.46)$$

Making use of Eqs. (3.22), (4.40), and (4.46) yields

$$\frac{1}{r} = \frac{M}{EI}. \quad (4.47)$$

From Eq. (4.47), when the bending moment is positive, the curvature is positive (i.e., concave in the  $y$ -direction as shown in Fig. 2.3).

### Example 4.10: Stress in Bending

**Given:** An aluminum alloy beam with the cross section shown in Fig. 4.16 experiences positive bending from an applied moment,  $M$ . The allowable stress is 150 MPa.

**Find:** (a) The maximum moment that can be applied to the beam. (b) The stresses at points A, B, and C when the maximum moment is applied.

**Solution:** (a) The cross-sectional area, if subscript 1 refers to a horizontal section and subscript 2 refers to a vertical section, is (see Fig. 4.16):

$$A = A_1 + 2A_2 = 8(80 - 16) + 2(120)(8) = 2432 \text{ mm}^2.$$

The centroid of the cross section is

$$\bar{y} = \frac{\bar{y}_1 A_1 + 2\bar{y}_2 A_2}{A} = \frac{4(64)(8) + 2(60)(8)(120)}{2432} = 48.21 \text{ mm}.$$

The distances from the neutral axis to the centroids of the horizontal and vertical bars are

$$d_{n1} = 48.21 - 4 = 44.21 \text{ mm},$$

$$d_{n2} = 60 - 48.21 = 11.79 \text{ mm}.$$

The area moment of inertia of the composite structure is

$$I = I_1 + A_1 d_{n1}^2 + 2(I_2 + A_2 d_{n2}^2)$$

or

$$I = \frac{64(8)^3}{12} + (64)(8)(44.2)^2 + 2 \left[ \frac{8(120)^3}{12} + 8(120)(11.79)^2 \right]$$

or  $I = 3.574 \times 10^6 \text{ mm}^4$ . The distances from the neutral axis to the points where the stress is to be evaluated are

$$d_{nA} = 48.21 \text{ mm},$$

$$d_{nB} = 48.21 - 8 = 40.21 \text{ mm},$$

$$d_{nC} = 120 - 48.21 = 71.79 \text{ mm}.$$

Point C is the farthest from the neutral axis and is thus the location where the stress is the largest. Furthermore, as discussed in Section 2.3, positive bending implies that the portion of the composite structure above the neutral axis is in compression while the portion below it is in tension. From Eq. (4.45), the maximum moment is

$$M_{\max} = \frac{\sigma_{\text{all}} I}{d_{nC}} = \frac{(150 \times 10^6) (3.574 \times 10^{-6})}{71.79 \times 10^{-3}} = 7468 \text{ Nm}.$$

(b) The stresses at the various points of interest are

$$\sigma_A = \frac{M_{\max} d_{nA}}{I} = \frac{(7468) (48.21 \times 10^{-3})}{3.574 \times 10^{-6}} = 100.7 \text{ MPa},$$

$$\sigma_B = \frac{M_{\max} d_{nB}}{I} = \frac{(7468) (40.21 \times 10^{-3})}{3.574 \times 10^{-6}} = 84.0 \text{ MPa},$$

$$\sigma_C = \sigma_{\text{all}} = -150 \text{ MPa}.$$

### 4.5.3 Curved Member

In a straight member, the normal stress and strain vary linearly with distance from the neutral axis, as shown in Eqs. (4.45) and (4.46). In a curved member, the stress and strain are not linearly related. Examples of curved members are hooks and chain links, which are not slender but have a high degree of curvature.

Figure 4.17 shows a curved member in bending. Positive bending causes surface  $dc$  to rotate through  $d\phi$  to  $d'c'$ . Note that  $y$  is negative from the neutral axis to the outer radius  $r_o$ , the region where the member is experiencing tension, and positive from the neutral axis to the inner radius  $r_i$ , the region where the member is experiencing compression. No bending occurs at the neutral axis; thus, the member is neither in compression nor in tension. The neutral axis occurs at a radius of  $r_n$ . From Fig. 4.17, note that the neutral radius  $r_n$  and the centroidal radius  $\bar{r}$  are not the same, although they are the same for a straight member. The difference between  $r_n$  and  $\bar{r}$  is the eccentricity,  $e$ . Also, the radius  $r$  locates an arbitrary area element  $dA$ , as shown in the cross-sectional view of Fig. 4.17b.

The strain for an arbitrary radius,  $r$ , can be expressed as

$$\epsilon = \frac{(r - r_n) d\phi}{r\phi}. \quad (4.48)$$

The strain is zero when  $r$  is the neutral radius,  $r_n$ , and is largest at the outer fiber, or  $r = r_o$ . The normal stress can be written as

$$\sigma = \epsilon E = \frac{E(r - r_n) d\phi}{r\phi}. \quad (4.49)$$

For  $r$  less than  $r_n$  the stress is compressive and for  $r$  greater than  $r_n$  the stress is tensile.



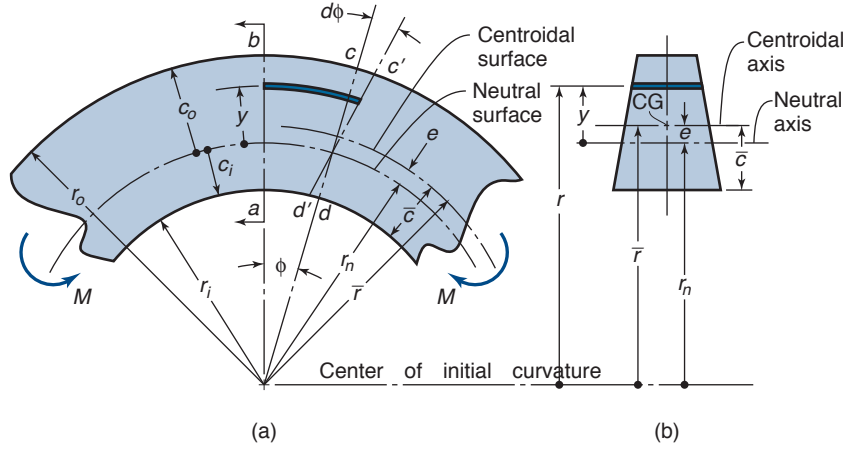


Figure 4.17: Curved member in bending. (a) Circumferential view; (b) cross-sectional view.

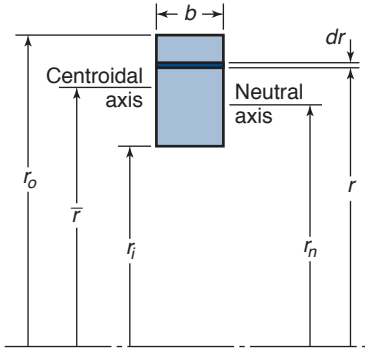


Figure 4.18: Rectangular cross section of curved member.

Solving for the strain and stress in Eqs. (4.48) and (4.49) requires the location of the neutral axis. This location is obtained by taking the sum of the normal stresses acting on the section and setting it to zero. Thus, making use of Eq. (4.49) gives

$$\int_A \sigma dA = \frac{E d\phi}{\phi} \int_A \frac{r - r_n}{r} dA = 0. \quad (4.50)$$

This equation reduces to

$$A - r_n \int_A \frac{dA}{r} = 0,$$

or

$$r_n = \frac{A}{\int_A \frac{dA}{r}}. \quad (4.51)$$

Equation (4.51) clearly indicates that the neutral radius is a function of the cross-sectional area.

### Rectangular Cross Sections

Figure 4.18 shows a rectangular cross section of a curved member with its centroidal and neutral axes. From Eq. (4.51), the neutral radius for a rectangular cross section is

$$r_n = \frac{b(r_o - r_i)}{\int_{r_i}^{r_o} \frac{b dr}{r}} = \frac{r_o - r_i}{\ln \left( \frac{r_o}{r_i} \right)}. \quad (4.52)$$

The centroidal radius is

$$\bar{r} = \frac{r_i + r_o}{2}. \quad (4.53)$$

The eccentricity is

$$e = \bar{r} - r_n = \frac{r_i + r_o}{2} - \frac{r_o - r_i}{\ln \left( \frac{r_o}{r_i} \right)}. \quad (4.54)$$

### Circular Cross Sections

The neutral radius for a circular cross section is

$$r_n = \frac{\bar{r} + \sqrt{\bar{r}^2 - c^2}}{2}, \quad (4.55)$$

where  $c$  is the radius of the cross section and  $\bar{r}$  is the location of the centroid. Having established the location of the neutral radius for two different cross sections of a curved member, consider again the stress in Eq. (4.49). The bending moment is the moment arm  $(r - r_n)$  multiplied by the force  $\sigma dA$  integrated over the cross-sectional area, or

$$M = \int (r - r_n)(\sigma dA).$$

Making use of Eq. (4.49) gives

$$\begin{aligned} M &= \frac{E d\phi}{\phi} \int \frac{(r - r_n)^2 dA}{r} \\ &= \frac{E d\phi}{\phi} \left( \int r dA - r_n A + r_n^2 \int \frac{dA}{r} \right). \end{aligned}$$

From Eq. (4.51), this equation reduces to

$$M = \frac{E d\phi}{\phi} \left( \int r dA - r_n A \right). \quad (4.56)$$

From the definition of a centroid,

$$\bar{r} = \frac{1}{A} \int r dA.$$

Equation (4.56) then becomes

$$M = E \frac{d\phi}{\phi} A e, \quad (4.57)$$

where

$$e = \bar{r} - r_n. \quad (4.58)$$

Substituting Eq. (4.49) into Eq. (4.57),

$$M = \frac{r \sigma A e}{r - r_n},$$

or

$$\sigma = \frac{M(r - r_n)}{A e r} = \frac{M y}{A e (r_n + y)}, \quad (4.59)$$

where

$$y = r - r_n. \quad (4.60)$$

The stress distribution is hyperbolic in shape. The maximum stress occurs at either the inner or outer surface:

$$\sigma_i = -\frac{M c_i}{A e r_i}, \quad (4.61)$$

$$\sigma_o = \frac{M c_o}{A e r_o}. \quad (4.62)$$

### Example 4.11: Stress in Curved Member

**Given:** A curved member with a rectangular cross section shown in Fig. 4.18 has the dimensions  $b = 25$  mm and  $h = r_o - r_i = 75$  mm, and is subjected to a bending moment of 2000 N-m. No other type of loading acts on the member. Positive bending occurs.

**Find:** The maximum stress for the following geometries:

- A straight member
- A member whose centroidal axis has a radius of  $\bar{r} = 375$  mm.
- A member whose centroidal axis has a radius of  $\bar{r} = 75$  mm.

**Solution:**

- For a straight member,

$$I = \frac{b h^3}{12} \quad \text{and} \quad c = \frac{h}{2}.$$

Therefore,

$$|\sigma| = \frac{M c}{I} = \frac{(2000)6}{(0.025)(0.075)^2} = 85.33 \text{ MPa}.$$

Therefore,

$$\begin{aligned} \sigma_i &= -85.33 \text{ MPa}, \\ \sigma_o &= 85.33 \text{ MPa}. \end{aligned}$$

- The outer and inner radii relative to the centroidal radius of 375 mm are

$$r_o = \bar{r} + \frac{h}{2} = 375 + \frac{75}{2} = 412.5 \text{ mm},$$

$$r_i = \bar{r} - \frac{h}{2} = 375 - \frac{75}{2} = 337.5 \text{ mm}.$$

From Eq. (4.52), the neutral radius is

$$r_n = \frac{r_o - r_i}{\ln\left(\frac{r_o}{r_i}\right)} = \frac{412.5 - 337.5}{\ln\left(\frac{412.5}{337.5}\right)} = 373.7 \text{ mm}.$$

Therefore,

$$e = \bar{r} - r_n = 375 - 373.7 = 1.3 \text{ mm}.$$

The distances from the neutral axis to the inner and outer fibers are

$$c_o = \frac{h}{2} + e = 37.5 + 1.3 = 38.8 \text{ mm},$$

$$c_i = \frac{h}{2} - e = 37.5 - 1.3 = 36.2 \text{ mm}.$$

The corresponding normal stresses are

$$\begin{aligned} \sigma_i &= -\frac{M c_i}{A e r_i} = -\frac{(2000)(0.0362)}{(0.075)(0.025)(0.0013)(0.3375)} \\ &= -88.0 \text{ MPa}, \\ \sigma_o &= \frac{M c_o}{A e r_o} = -\frac{(2000)(0.0388)}{(0.075)(0.025)(0.0013)(0.4125)} \\ &= 77.12 \text{ MPa}. \end{aligned}$$

Because the radius of curvature is large, there is little difference from the stresses found for the straight beam in part a.

- The outer and inner radii relative to the centroidal radius of 75 mm are

$$r_o = \bar{r} + \frac{h}{2} = 0.075 + \frac{0.075}{2} = 0.1125 \text{ mm},$$

$$r_i = \bar{r} - \frac{h}{2} = 0.075 - \frac{0.075}{2} = 0.0375 \text{ mm},$$

$$r_n = \frac{r_o - r_i}{\ln\left(\frac{r_o}{r_i}\right)} = \frac{0.1125 - 0.0375}{\ln\left(\frac{0.1125}{0.0375}\right)} = 0.06827 \text{ mm},$$

$$e = \bar{r} - r_n = 0.075 - 0.06827 = 0.00673 \text{ mm}.$$

Therefore,

$$c_o = \frac{h}{2} + e = 0.0375 + 0.00673 = 0.04423 \text{ mm},$$

$$c_i = \frac{h}{2} - e = 0.0375 - 0.00673 = 0.03077 \text{ mm},$$

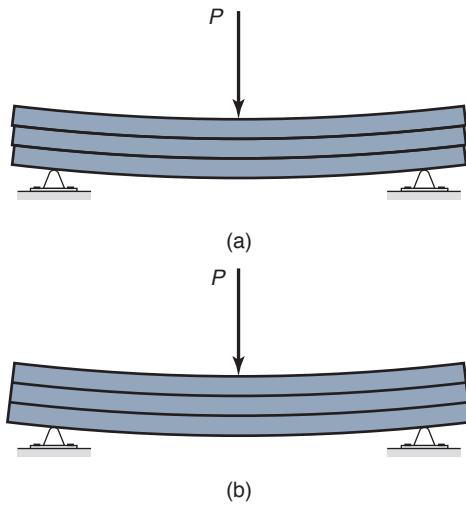


Figure 4.19: Development of transverse shear. (a) Boards not bonded together; (b) boards bonded together.

$$\begin{aligned}\sigma_i &= -\frac{Mc_i}{Aer_i} = -\frac{(2000)(0.03077)}{(0.075)(0.025)(0.00673)(0.0375)} \\ &= -130.0 \text{ MPa}, \\ \sigma_o &= -\frac{Mc_o}{Aer_o} = -\frac{(2000)(0.04423)}{(0.075)(0.025)(0.00673)(0.1125)} \\ &= 62.31 \text{ MPa}.\end{aligned}$$

Thus, the more curved the surface is, the greater the departure from the straight-beam results.

## 4.6 Transverse Shear Stress and Strain

In addition to the bending stresses considered in Section 4.5, moments can also cause shear stresses within the member. Figure 4.19 illustrates how transverse shear is developed. Figure 4.19a shows three boards that are not bonded together. The application of a force,  $P$ , will cause the boards to slide relative to one another and the stack will deflect as shown, with the ends no longer flush as they were when no load was applied. On the other hand, if the boards are bonded together, they will act as a single unit, as shown in Fig. 4.19b. In a solid beam the same shear stress is present. As a result of the internal shear stress distribution, shear strains will be developed and these will tend to distort the cross section in a rather complex manner. An undeformed bar, shown in Fig. 4.20a and made of a highly deformable material and marked with horizontal and vertical grid lines, tends to deform when a shear force is applied. The deformed pattern is shown in Fig. 4.20b. The squares near the top and bottom of the bar retain their original shapes. The strain on the center square of the bar will cause it to have the greatest deformation. The transverse shear stress causes the cross section to warp. Figure 4.20b shows that the deformation caused by transverse shear is much more complex than that caused by another type of loading (axial, torsion, or bending).

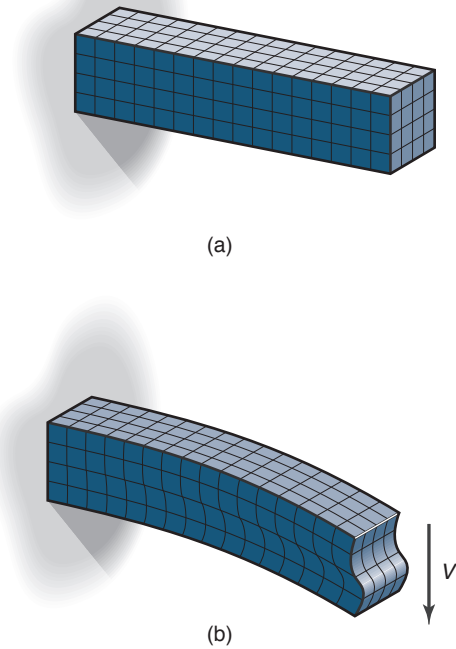


Figure 4.20: Cantilevered bar made of highly deformable material and marked with horizontal and vertical grid lines to show deformation due to transverse shear. (a) Undeformed; (b) deformed.

The transverse shear formulas also apply to Fig. 4.21. The shaded top segment of the element has been sectioned at  $y'$  from the neutral axis. This section has a width,  $w_t$ , at the section and has cross-sectional sides, each having an area  $A'$ . Because the resultant moments on each side of the element differ by  $dM$ , force equilibrium will only be satisfied from Fig. 4.21 if a longitudinal shear stress,  $\tau$ , acts over the bottom face of the segment. This longitudinal shear stress is also responsible for the results shown in Fig. 4.19a. The expression for the shear stress in the member at the point located a distance  $y'$  from the neutral axis is

$$\tau = \frac{VQ}{Iw_t}, \quad (4.63)$$

where

- $V$  = transverse shear force, N
- $I$  = moment of inertia of entire cross section computed about neutral axis,  $\text{m}^4$
- $w_t$  = width at point where  $\tau$  is determined, m
- $Q$  = first moment about neutral axis of shaded portion of Fig. 4.21 given by

$$Q = \int_{A'} y dA = \bar{y}' A', \quad (4.64)$$

and where  $A'$  is the cross-sectional area of the top portion shown in Fig. 4.21, and  $\bar{y}'$  is the distance to the centroid of  $A'$ , measured from the neutral axis. Applying the shear formula given in Eq. (4.63) for a rectangular cross section gives

$$\tau = \frac{6V}{bh^3} \left( \frac{h^2}{4} - y^2 \right), \quad (4.65)$$

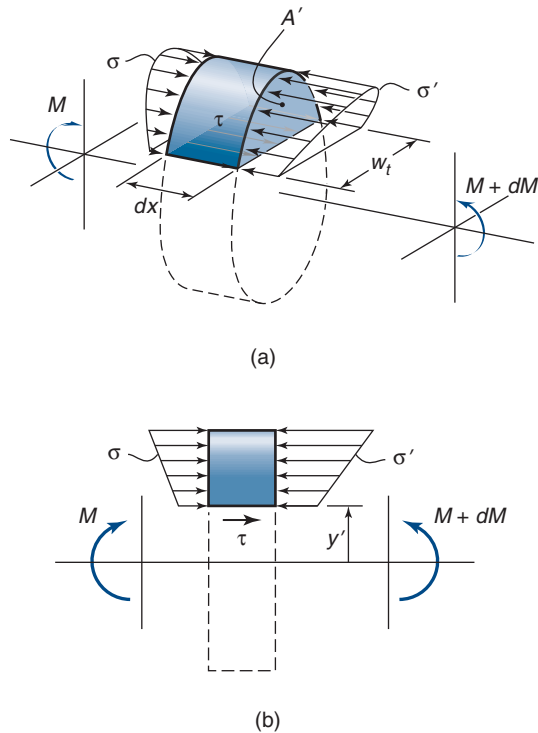


Figure 4.21: Three-dimensional and profile views of moments and stresses associated with shaded top segment of element that has been sectioned at  $y'$  about neutral axis. (a) Three-dimensional view; (b) profile view.

where  $b$  and  $h$  are the base and height of a rectangular section, respectively. From Eq. (4.65), the shear stress intensity for a rectangular cross section varies from zero at the top and bottom ( $y = \pm h/2$ ) to a maximum at the neutral axis ( $y = 0$ ). At other intermediate values it is parabolic in shape. For  $A = bh$  and  $y = 0$ , Eq. (4.65) becomes

$$\tau_{\max} = 1.5 \frac{V}{A}. \quad (4.66)$$

The maximum shear stress depends on the shape of the cross section, but this approach can be used for any arbitrary beam profile. Table 4.3 summarizes maximum values for common cross-sectional shapes. In all cases, shear stress is zero on extreme fibers, is maximum on the neutral axis, and has a parabolic distribution through the thickness.




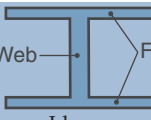
### Example 4.12: Stress Due to Transverse Shear

**Given:** A cantilever having a square cross section is loaded by a shear force perpendicular to the beam centerline at the free end. The sides of the square cross section are 50 mm, and the shear force is 10,000 N.

**Find:** Calculate the transverse shear stress at the beam centerline:

- If the shear force is parallel with two sides of the square cross section
- If the shear force is parallel with one of the diagonals of the square cross section

Table 4.3: Maximum shear stress for different beam cross sections.

Cross section	Maximum shear stress
 Rectangle	$\tau_{\max} = \frac{3V}{2A}$
 Circle	$\tau_{\max} = \frac{4V}{3A}$
 Round tube	$\tau_{\max} = \frac{2V}{A}$
 I-beam	$\tau_{\max} = \frac{V}{A_{\text{web}}}$

**Solution:** The area moment of inertia is

$$I = \frac{bh^3}{12} = \frac{(50)(50)^3}{12} = 520,800 \text{ mm}^4.$$

This moment is valid in all directions due to symmetry. Thus, the shear force and the area moment of inertia are the same for both parts of this example.

- The width of the point where  $\tau$  is calculated is 50 mm. The evaluation of  $Q$  is

$$Q = \int_A y dA = \int_0^{25} y(50) dy = \frac{50(25)^2}{2} = 15,625 \text{ mm}^3.$$

From Eq. (4.63) the bending shear stress is

$$\tau = \frac{VQ}{Iw_t} = \frac{(10,000)(15,625)}{(520,800)(50)} = 6.0 \text{ MPa}.$$

- The width at the point where  $\tau$  is applied is

$$w_t = \sqrt{2(50)^2} = 50\sqrt{2} = 70.71 \text{ mm}.$$

$Q$  is evaluated as

$$\begin{aligned} Q &= \int_0^{25\sqrt{2}} 2y(25\sqrt{2} - y) dy \\ &= \left[ 25\sqrt{2}y^2 - 2\left(\frac{y^3}{3}\right) \right]_{y=0}^{y=25\sqrt{2}} \\ &= 14,730 \text{ mm}^3. \end{aligned}$$

From Eq. (4.63) the bending shear stress is

$$\tau = \frac{VQ}{Iw_t} = \frac{(10,000)(14,730)}{(520,800)(70.71)} = 4.0 \text{ N/mm}^2 = 4.0 \text{ MPa}.$$

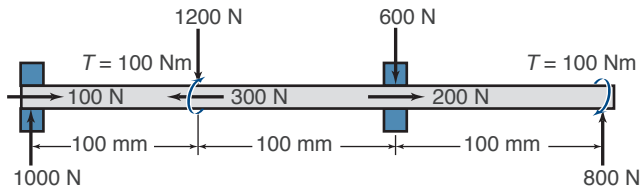


Figure 4.22: Shaft with loading considered in Example 4.13.

### Example 4.13: Critical Location in a Beam

**Given:** A shaft is loaded by the forces and torques shown in Fig. 4.22, which result from the actions of helical gears and the shaft's rolling element bearing supports. The shaft has a diameter of 25 mm.

**Find:** Determine the location in the shaft where the stresses are highest. What are the principal stresses at this location?

**Solution:** First of all, it should be noted that with a diameter of 25 mm, the following can be calculated:

$$A = \frac{\pi d^2}{4} = \frac{\pi(0.025)^2}{4} = 4.909 \times 10^{-4} \text{ m}^2,$$

$$I = \frac{\pi d^4}{64} = \frac{\pi(0.025)^4}{64} = 1.917 \times 10^{-8} \text{ m}^4,$$

$$J = \frac{\pi d^4}{32} = \frac{\pi(0.025)^4}{32} = 3.835 \times 10^{-8} \text{ m}^4.$$

The shear and moment diagrams are shown in Fig. 4.23. At first, it is not clear where the critical location is; the absolute shear force is highest between 0 and 100 mm, and the moment is highest at  $x = 100$  mm. However, the torque is highest between 100 and 300 mm, and the axial load is tensile between 100 and 200 mm but compressive between 0 and 100 mm.

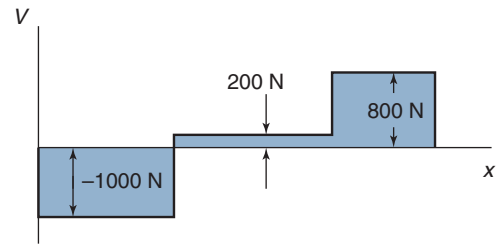
In practice, a designer must analyze *all* potential critical locations to determine the most critical. This example will analyze the location just to the right of the gear that acts at  $x = 100$  mm, where  $V = 200$  N,  $P = 300$  N,  $T = 100$  Nm, and  $M = 100$  Nm. These result in the stresses in Table 4.4.

Consider the cross section of the shaft shown in Fig. 4.24, with the stress element locations shown. At location A, the axial stress is tensile, but the bending stress is compressive; the resultant normal stress is  $\sigma_x = 0.611 - 65.11 = -64.60$  MPa. The shear stress distributions for torsion and shear are shown in Fig. 4.25; clearly at the top of the shaft, the shear stress due to the vertical shear force can be ignored, while the shear stress due to torsion is at its maximum value. Thus,  $\tau_{xz} = 32.59$  MPa.

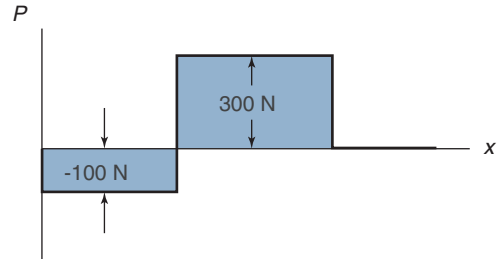
At location B, the bending stress is zero (see Fig. 4.25). Thus, the normal stress is due to axial force only, or  $\sigma_x = 0.611$  MPa. The shear stresses due to torsion and vertical shear are additive; thus,  $\tau_{xy} = 0.543 + 32.59 = 33.13$  MPa.

At location C, the normal stresses are both tensile; thus,  $\sigma_x = 0.611 + 65.21 = 65.82$  MPa. The shear stress is the same as at location A, but it is now negative, so that  $\tau_{xz} = -32.59$  MPa.

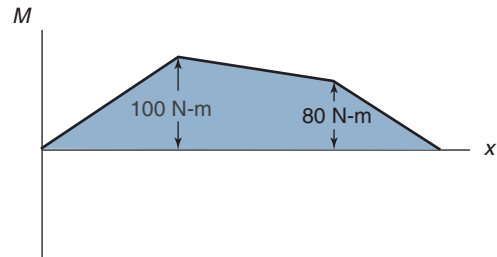
At location D, the bending stress is zero, so the normal stress is the same as at location B, or  $\sigma_x = 0.611$  MPa. The shear stress due to torsion is zero, but the shear stress due to the vertical shear force has its maximum value of 0.543 MPa.



(a)



(b)



(c)

Figure 4.23: (a) Shear force; (b) normal force and (c) bending moment diagrams for the shaft in Fig. 4.22.

From consideration of these stress elements, we conclude that the element at location C is critical; it has the largest normal and shear stresses. It has the stress state  $\sigma_x = 65.82$  MPa,  $\sigma_y = \sigma_z = 0$ ,  $\tau_{xz} = -32.59$  MPa, and  $\tau_{xy} = \tau_{yz} = 0$ . This is a two-dimensional stress state; therefore, one of the principal stresses is zero. The other two principal stresses can be obtained from Mohr's circle or from Eq. (2.16), using proper subscripts, as

$$\begin{aligned} \sigma &= \frac{\sigma_x + \sigma_z}{2} \pm \sqrt{\tau_{xz}^2 + \frac{(\sigma_x - \sigma_z)^2}{4}} \\ &= \frac{65.82}{2} \pm \sqrt{32.59^2 + \frac{65.82^2}{4}} \\ &= 32.91 \pm 73.45 \text{ MPa.} \end{aligned}$$

Therefore, the principal stresses are, in their proper order according to Eq. (2.18),  $\sigma_1 = 106.4$  MPa,  $\sigma_2 = 0$ , and  $\sigma_3 = -40.54$  MPa.



Table 4.4: Stresses obtained in Example 4.13.

Loading	Resultant maximum stress	Reference	Value
Axial	$\sigma_x = \frac{P}{A} = \frac{300}{4.909 \times 10^{-4}}$	Eq. (2.7)	0.611 MPa
Bending	$\sigma_x = \frac{Mc}{I} = \frac{(100)(0.0125)}{1.917 \times 10^{-8}}$	Eq. (4.45)	65.21 MPa
Vertical shear	$\tau_{xy} = \frac{4V}{3A} = \frac{4(200)}{3(4.909 \times 10^{-4})}$	Table 4.3	0.543 MPa
Torsion	$\tau = \frac{rT}{J} = \frac{(0.0125)(100)}{3.835 \times 10^{-8}}$	Eq. (4.32)	32.59 MPa

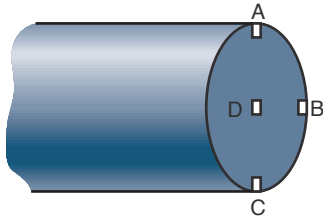
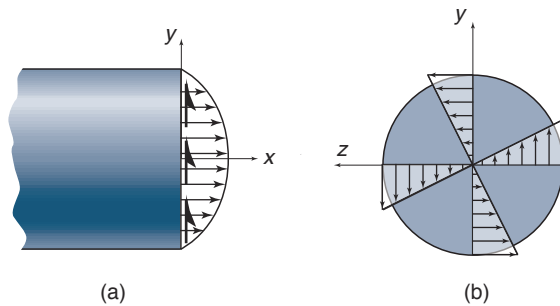
Figure 4.24: Cross section of shaft at  $x = 100$  mm, with identification of stress elements considered in Example 4.13.

Figure 4.25: Shear stress distributions. (a) Shear stress due to a vertical shear force; (b) shear stress due to torsion.

## Case Study: Design of a Shaft for a Coil Slitter

**Given:** Flat rolled sheets are produced in wide rolling mills, but many products are manufactured from strip stock. Figure 4.26a depicts a coil slitting line, where large sheets are cut into ribbons or strips. Figure 4.26b shows a shaft supporting the cutting blades. The rubber rollers support the sheet during cutting and prevent wrinkling. For such slitting lines the shafts that support the slitting knives are a highly stressed and critical component. Figure 4.26c is a free-body diagram of a shaft for a short slitting line where a single blade is placed in the center of the shaft and a motor drives the shaft through a pulley at the far right end.

**Find:** If the maximum shear stress is 40 MPa and the largest gage sheet causes a blade force of 2000 N, what shaft diameter is needed?

**Solution:** The reaction forces are found through statics to be  $R_A = 1720$  N and  $R_B = 2600$  N and are shown in Fig. 4.26c. Figure 4.27 shows the shear and bending moment diagrams. The maximum shear occurs just to the left of the pulley and equals 2880 N. The maximum bending moment is 430 Nm. In addition, there is a torque of 216 Nm between the pulley and the knife blade. Two locations must be analyzed: the location in the shaft where the moment is largest, and the location where the shear is largest.

- (a) Moment. The magnitude of the normal stress in the  $x$ -direction at the location of maximum moment is given by Eq. (4.45) as

$$\sigma_x = \frac{Mc}{I} = \frac{(430) \left( \frac{d}{2} \right)}{\frac{\pi d^4}{64}} = \frac{4380}{d^3}.$$

The shear stress due to the torque exerted on the pulley is, from Eq. (4.33),

$$\tau_{xy} = \frac{Tc}{J} = \frac{1100}{d^3}.$$

A Mohr's circle can be constructed as discussed in Design Procedure 2.5. The Mohr's circle for this case is shown in Fig. 4.28 and has a radius of  $2450 \text{ Nm}/d^3$ . Setting this equal to the maximum allowable shear stress of 40 MPa yields

$$\frac{2450}{d^3} = 40 \times 10^6.$$

Therefore,

$$d = 0.0394 \text{ m} = 39.4 \text{ mm}.$$

- (b) Shear. The maximum shear stress at the location of maximum shear is, from Table 4.1,

$$\tau_{\max} = \frac{4V}{3A} = \frac{4(2880)}{3 \left( \frac{\pi d^2}{4} \right)} = \frac{4890}{d^2}.$$

At one end of the shaft the torsion-induced shear stress is subtracted from this shear stress; at the other end, the effects are cumulative. Thus, the total shear is

$$\tau_{\text{tot}} = \frac{4890}{d^2} + \frac{1100}{d^3} = 40 \text{ MPa}.$$

Solving numerically gives  $d = 31.5$  mm.

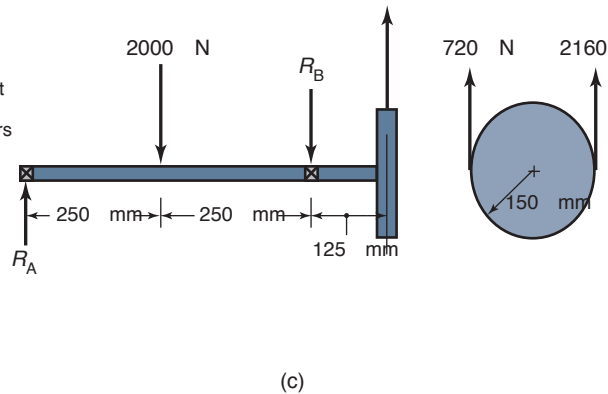
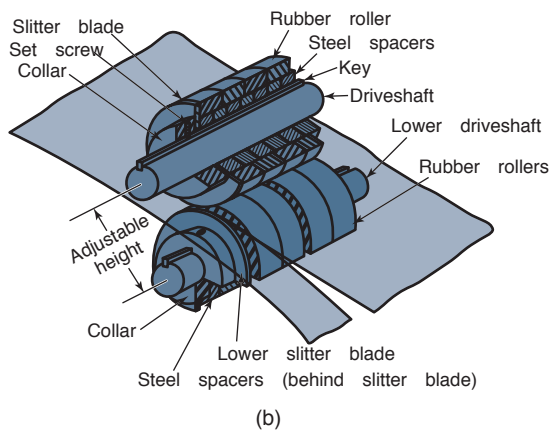
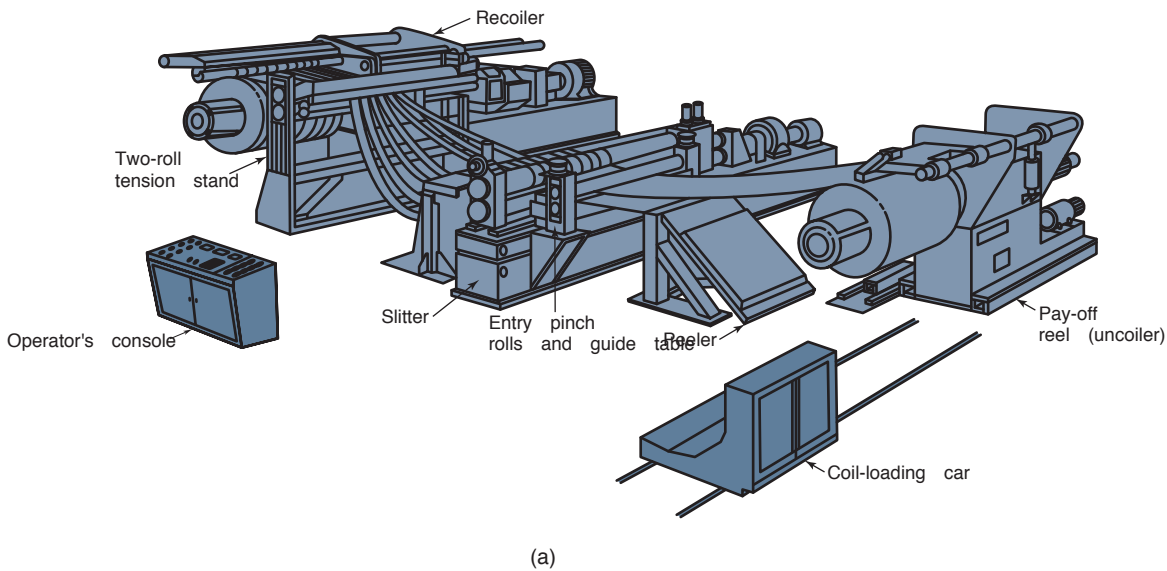


Figure 4.26: Design of shaft for coil slitting line. (a) Illustration of coil slitting line; (b) knife and shaft detail; (c) free-body diagram of simplified shaft for case study. Illustrations (a) and (b) are adapted from *Tool and Manufacturing Engineers Handbook, Fourth Edition, Volume 2 Forming*. Reprinted with permission of the Society of Manufacturing Engineers, ©1984.

(c) Discussion. As in most shaft applications the normal stresses due to bending determine the shaft diameter, so that a shaft with a diameter not less than  $39.4 \approx 40$  mm should be used. A number of points should be made regarding this analysis:

- When the normal stress due to bending was calculated, the shear stress due to shear was neglected, even though there was shear in the shaft at that location. However, the distribution of normal stress is such that it is extreme at the top and the bottom, where the shear stress is zero.
- When the maximum shear stress due to vertical shear was calculated, the effects of bending were ignored.
- The bending stress is zero at the neutral axis, the location of the maximum shear stress.
- There are two general shaft applications. Some shafts are extremely long, as in this problem, whereas others are made much shorter to obtain compact designs. A coil slitter can have shafting more than 10 m long, but more supporting bearings would be needed for stiffness. This shaft was used only as an illustrative example; in actuality, the supporting bearings would be placed much closer to the load application and more than two bearing packs would probably be appropriate.

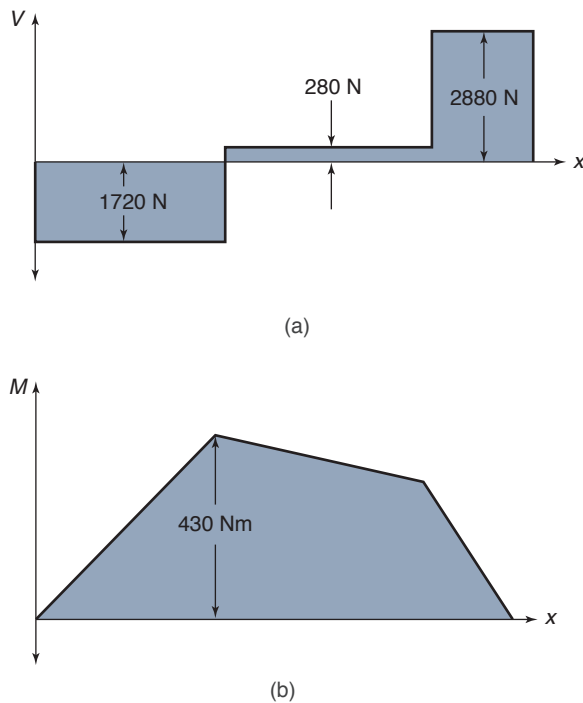


Figure 4.27: (a) Shear diagram and (b) moment diagram for idealized coil splitter shaft.

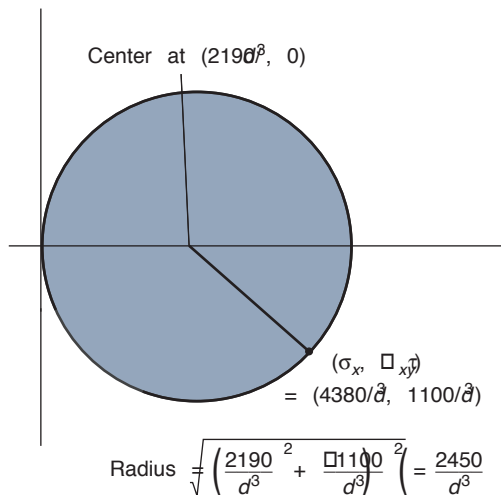


Figure 4.28: Mohr's circle at the location of maximum bending stress.

## 4.7 Summary

The first four chapters have provided the essentials needed to describe the stress and strain for the four types of loading (normal, torsional, bending, and transverse shear) that might occur. These stresses and strains will be used in designing machine elements later in the text. Each chapter attempted to build from the knowledge learned in previous chapters. It was assumed throughout the first four chapters that the member experiencing one of the four types of loading had a symmetric cross section and was made of a Hookian material. Chapter 4 started by defining centroid, moment of inertia, the parallel-axis theorem, radius of gyration, and section modulus. These concepts needed to be understood before stresses and strains resulting from normal, torsional, bending, or transverse shear could be explored. These definitions, which are used throughout the text, were followed by the stresses and strains found in the four types of loading. While evaluating the stress and strain due to normal loading, it was convenient to include the axial displacement and the spring rate. For torsional loading, the stresses and strains as well as the angular twist and angular spring rate were presented. Also, in discussing torsion, the relevant equations associated with power transfer were given. The stresses and strains associated with bending were explained, as well as the importance of the neutral axis. Both a straight and a curved member were analyzed. Section 4.6 defined the stresses associated with transverse shear. Deformations associated with bending and combined transverse loading were not covered in this chapter but are considered more fully in Chapter 5.

## Key Words

**area moment of inertia** also called *second moment of area*, a property of a cross section that relates bending stress, applied moment, and distance from the neutral axis,  $m^4$

**average normal stress** average normal load divided by cross-sectional area, Pa

**centroid of area** geometric center of an area, m

**mass moment of inertia** product of element's mass and square of element's distance from the axis,  $kg \cdot m^2$

**normal strain** elastic deformation divided by original length

**parallel-axis theorem** a theorem that allows calculation of the moment of inertia about any axis

**power** rate of doing work, or the product of force and velocity or torque and angular velocity, Nm/s

**radius of gyration** radius that when squared and multiplied by area gives area moment of inertia, m

**section modulus** moment of inertia divided by farthest distance from centroidal axis to outer fiber of solid,  $m^3$

**spring rate** normal load divided by elastic deformation, N/m

**torsion** loading resulting in twisting of shaft

## Summary of Equations

### Beam cross sections:

Centroid of area:  $\bar{x} = \frac{A_1\bar{x}_1 + A_2\bar{x}_2 + \dots}{A_1 + A_2 + \dots}$  and

$$\bar{y} = \frac{A_1\bar{y}_1 + A_2\bar{y}_2 + \dots}{A_1 + A_2 + \dots}$$

Moment of inertia:  $I_x = \int_A y^2 dA$  and  $I_y = \int_A x^2 dA$

Polar moment of inertia:  $J = I_x + I_y$

Parallel-axis theorem:  $I_{x'} = I_x + Ad_y^2$

Radius of gyration:  $r_g = \sqrt{\frac{I}{A}}$

Section modulus:  $Z_m = I/c$

Mass moment of inertia:  $I_{mx} = \int (y^2 + z^2) dm_a$ , etc.

**Normal stress:**  $\sigma = \frac{P}{A}$

**Normal strain:**  $\epsilon = \frac{\delta}{l} = \frac{\sigma}{E}$

**Shear stress in torsion:**  $\tau = \frac{Tr}{J}$

**Deflection in torsion:**  $\theta = \frac{Tl}{GJ}$

**Power:**  $h_p = Pu = Tw$

**Bending stress:**  $\sigma = -\frac{My}{I}$

**Radius of curvature in bending:**  $\frac{1}{r} = \frac{M}{EI}$

**Internal shear stress due to transverse shear:**  $\tau = \frac{VQ}{Iw_t}$

### Spring rate:

Tension member:  $k = \frac{AE}{l}$

Torsion:  $k = \frac{T}{\theta} = \frac{JG}{l}$

## Recommended Readings

- Beer, F.P., Johnson, E.R., DeWolf, J., and Mazurek, D. (2011) *Mechanics of Materials*, 6th ed., McGraw-Hill.
- Craig, R.R. (2011) *Mechanics of Materials*, 3rd ed., Wiley.
- Gere, J.M., and Goodno, B.J. (2012) *Mechanics of Materials*, 8th ed., CL Engineering.
- Hibbeler, R.C. (2010) *Mechanics of Materials*, 8th ed., Prentice-Hall.
- Popov, E.P. (1968) *Introduction to Mechanics of Solids*, Prentice-Hall.
- Popov, E.P. (1999) *Engineering Mechanics of Solids*, 2nd ed., Prentice-Hall.
- Riley, W.F., Sturges, L.D., and Morris, D.H. (2006) *Mechanics of Materials*, 6th ed., Wiley.
- Shames, I.H., and Pitarresi, J.M. (2000) *Introduction to Solid Mechanics*, 3rd ed., Prentice-Hall.
- Ugural, A.C. (2007) *Mechanics of Materials*, Wiley.

## Reference

Timoshenko and Goodier (1970) *Theory of Elasticity*, 3rd ed., McGraw-Hill.

## Questions

- 4.1 What is the centroid of an area?
- 4.2 What is the difference between the moment of inertia and the second moment of area?
- 4.3 Describe the importance of the parallel-axis theorem.

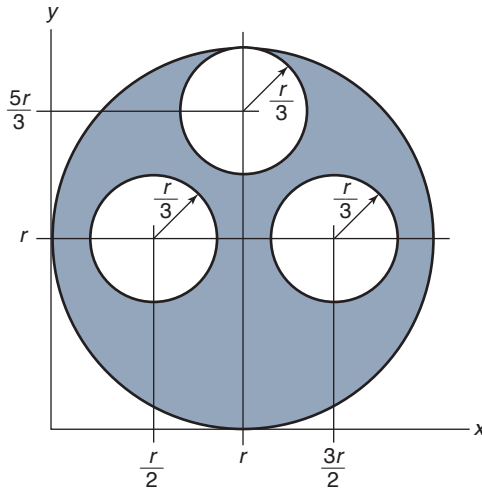
- 4.4 How is the radius of gyration used?
- 4.5 Explain the difference between a beam and a shaft.
- 4.6 What is the equation for normal stress for a bar loaded in uniaxial tension?
- 4.7 Does a torque acting on a shaft lead to shear or normal stresses?
- 4.8 In the equation  $\tau = \frac{VQ}{Iw_t}$ , what is  $Q$ ?
- 4.9 What is the equation for normal stress in a beam that is loaded by a bending moment?
- 4.10 What is the equation for vertical shear stress in a beam that is loaded in internal shear?
- 4.11 What is Saint-Venant's principle?
- 4.12 Explain how a shaft transmits power.
- 4.13 What is the section modulus of an area?
- 4.14 What is the difference between a moment and a torque, with respect to stresses they cause?
- 4.15 What is the polar moment of inertia?

## Qualitative Problems

- 4.16 Explain why an I-beam can support a higher bending moment than an H-Beam. That is, why is orientation important for an I-beam?
- 4.17 Why are tubes more efficient at supporting bending moments than cylinders? Is this also true for torsion?
- 4.18 Is it possible for the centroid of an area to be outside of the area? Explain.
- 4.19 List the functions of the web and flange in an I-beam.
- 4.20 It is desired to drill a hole through a beam with a rectangular cross-section, transverse to its axis. Where would you recommend that the hole be placed?
- 4.21 Does the stiffness of a balloon increase when it is inflated? Why or why not?
- 4.22 Explain why the tension test specimen shown in Fig. 3.1 uses a smaller test section than the cross section at the grips. Often, such a specimen has a parabolic profile with a minimum value at its center. Explain why.
- 4.23 Construct a Design Procedure for determining the critical location in a beam. *Hint:* Make extensive use of Example 4.13.
- 4.24 Explain why a beam is much stiffer in axial loading than in torsion or in bending.
- 4.25 Refer to Table 4.2 and explain the conditions under which you would consider a cylinder to be a rod.

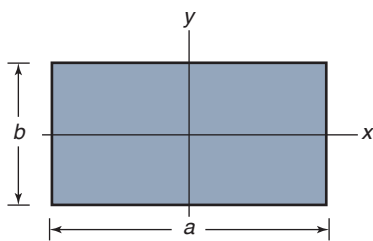
## Quantitative Problems

- 4.26** An area in the  $x$ - $y$  coordinate system, as shown in Sketch *a*, consists of a large circle having radius  $r$  out of which are cut three smaller circles having radii  $r/3$ . Find the  $x$ - and  $y$ -coordinates for the centroid. The radius  $r$  is 10 cm. *Ans.*  $\bar{x} = 10$  cm,  $\bar{y} = 8.889$  cm.



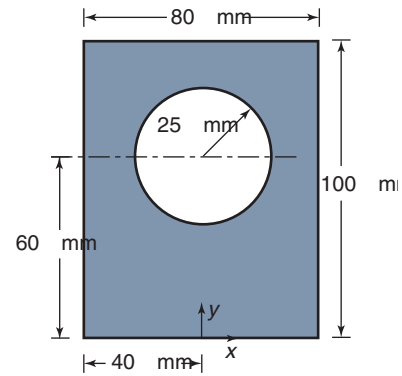
Sketch *a*, for Problems 4.26 and 4.27.

- 4.27** The circular surface in Sketch *a* has circular cutouts glued onto it below the top cutout such that the centroids of the three cutouts are at  $\bar{x} = r$  and  $\bar{y} = r/3$ . Find the  $x$ - and  $y$ -coordinates for the centroid ( $r = 10$  cm). *Ans.*  $\bar{x} = 10$  cm,  $\bar{y} = 7.037$  cm.
- 4.28** The rectangular area shown in Sketch *b* has side lengths of  $a$  in the  $x$ -direction and  $b$  in the  $y$ -direction. Find the moments of inertia  $I_x$  and  $I_y$  and the polar moment of inertia  $J$  for the rectangular surface. *Ans.*  $I_x = \frac{1}{12}ab^3$ .



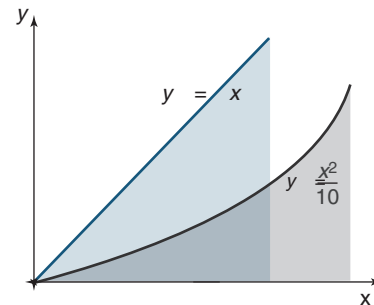
Sketch *b*, for Problem 4.28.

- 4.29** Derive the area moment of inertia for the hollow circular area shown in Table 4.1.
- 4.30** Derive the area moment of inertia for the elliptical quadrant shown in Table 4.1.
- 4.31** Derive the area moment of inertia for the triangular section shown in Table 4.1.
- 4.32** Derive the area moment of inertia for a rectangular section with a cutout as shown in Sketch *c*. *Ans.*  $I_y = 4.141 \times 10^{-6} \text{ m}^4$ ,  $I_x = 2.202 \times 10^{-5} \text{ m}^4$ .



Sketch *c*, for Problem 4.32.

- 4.33** Evaluate the moment of inertia of the shape bounded by the curves shown in Sketch *d*, up to a value of  $x = 3$ . *Ans.*  $I_x = 6.646 \text{ m}^4$ ,  $I_y = 15.39 \text{ m}^4$ ,  $J = 22.04 \text{ m}^4$ .



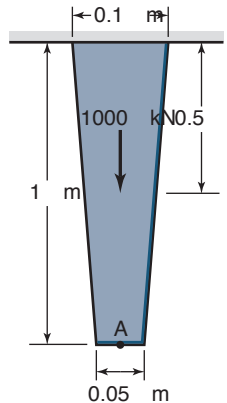
Sketch *d*, for Problem 4.33.

- 4.34** An elevator is hung by a steel rope. The rope has a cross-sectional area of  $250 \text{ mm}^2$  and a modulus of elasticity of 70 GPa. The upward acceleration when the elevator starts is  $4 \text{ m/s}^2$ . The rope is 100 m long and the elevator weighs 1000 kg. Determine the stress in the rope, the elongation of the rope due to the elevator's weight, and the extra elongation due to the acceleration. *Ans.*  $\sigma = 55.2 \text{ MPa}$ ,  $\delta_{wt} = 56.06 \text{ mm}$ ,  $\delta_{acc} = 22.86 \text{ mm}$ .
- 4.35** The 700-m-long cables in a suspension bridge are stressed to a 200-MPa tensile stress. The total force in each cable is 10 MN. Calculate the cross-sectional area, the total elongation of each cable, and the spring rate when the modulus of elasticity is 70 GPa. *Ans.*  $A = 0.05 \text{ m}^2$ ,  $\delta = 2 \text{ m}$ ,  $k = 5 \text{ MN/m}$ .
- 4.36** A 1.00-m-long steel piston in a hydraulic cylinder exerts a force of 40 kN. The piston is made of AISI 1080 steel and has a diameter of 50 mm. Calculate the stress in the piston, the elongation, and the spring rate. *Ans.*  $\sigma = -20.41 \text{ MPa}$ ,  $\delta = 9.859 \times 10^{-5} \text{ m}$ ,  $k = 405.7 \text{ MN/m}$ .
- 4.37** A steel pillar supporting a highway bridge is 14 m high and made of steel tubing having an outer diameter of 1.5 m and a wall thickness of 30 mm. The weight carried by the pillar is 12 MN. Calculate the deformation of the pillar, the spring rate, and the stress in the pillar. *Ans.*  $\sigma = -86.6 \text{ MPa}$ ,  $\delta = -5.86 \text{ mm}$ ,  $k = 2.048 \text{ GN/m}$ .
- 4.38** The foundation of a bronze statue is made of a 3-m-high conical tube of constant wall thickness (8 mm). The



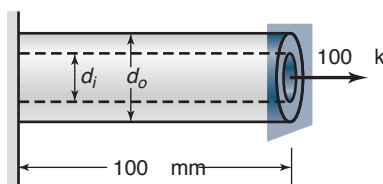
tube's outer diameter is 200 mm at the top (just under the statue) and 400 mm at the ground. The tube material is AISI 316 stainless steel. The statue weighs 16,000 N. Calculate the deformation of the tube, the spring rate, and the maximum and minimum compressive stresses in the tube. *Ans.*  $\delta = -35.48 \mu\text{m}$ ,  $k = 450.9 \text{ MN/m}$ ,  $\sigma_{\max} = -3.33 \text{ MPa}$ ,  $\sigma_{\min} = -1.63 \text{ MPa}$ .

- 4.39 Calculate the deflection at point A of the hanging cone shown in Sketch *e* if the cone is constructed of aluminum. *Ans.*  $\delta = 1.369 \text{ mm}$ .



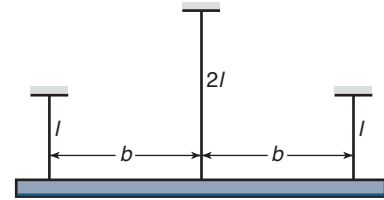
Sketch *e*, for Problem 4.39.

- 4.40 An electric motor transmits 100 kW to a gearbox through a 50-mm-diameter solid steel shaft that rotates at 1000 rpm. Find the torque transmitted through the shaft and the angular torsion of the 1-m-long shaft. *Ans.*  $T = 955 \text{ Nm}$ ,  $\theta = 1.12^\circ$ .
- 4.41 The torque-transmitting shaft in Problem 4.40 is too heavy for the application, so it is exchanged for a circular tube having a 50-mm outside diameter and a 40-mm inside diameter. Find the angular torsion of the tube-formed shaft, which is 1 m long, when 100 kW is transmitted at 1000 rpm. The shear modulus is  $80,000 \text{ N/mm}^2$ . Also find the maximum shear stress in the tube and the percentage of weight decrease from the solid shaft. *Ans.*  $\theta = 1.888^\circ$ , 64% weight savings.
- 4.42 A torque-transmitting, hollow steel shaft with a circular cross section has an outer diameter of 50 mm and an inner diameter of 40 mm. Find the maximum length possible for the shaft if the torsion should be below  $5^\circ$  at a torque of 2000 N-m. *Ans.*  $l = 1.258 \text{ m}$ .
- 4.43 An aluminum core having a diameter  $d_i$  of 30 mm is placed within a tubular steel shaft having a diameter  $d_o$  of 50 mm, as shown in Sketch *f*. A flange is welded to the end of the shaft, and a pulley force of 200 kN is applied. The shaft is 100 mm long. Find the deflection at the end of the shaft and the stresses induced in the aluminum and steel sections of the shaft. Assume that the moduli of elasticity are 207 GPa for steel and 70 GPa for aluminum. *Ans.*  $\delta = 0.6647 \text{ mm}$ ,  $\sigma_{\text{al}} = 46.5 \text{ MPa}$ ,  $\sigma_s = 132.9 \text{ MPa}$ .



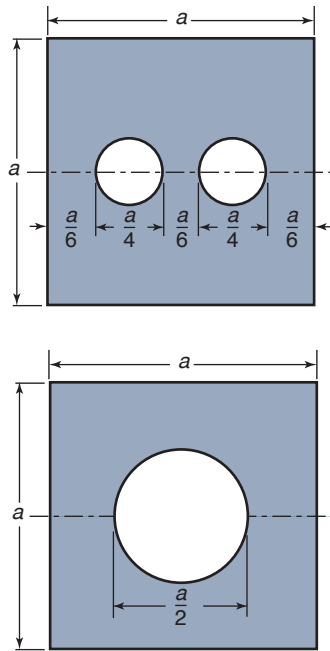
Sketch *f*, for Problem 4.43.

- 4.44 A bar of weight  $W$  is supported horizontally by three weightless rods as shown in Sketch *g*. Assume that the cross-sectional areas,  $A$ , the moduli of elasticity,  $E$ , and the yield stresses,  $S_y$ , are the same for the three rods. What is the maximum weight that can be supported? *Ans.*  $W = 2.5S_yA$ .

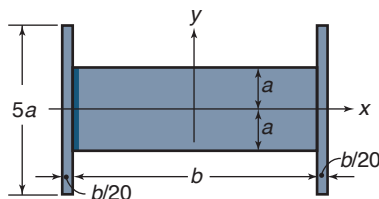


Sketch *g* for Problem 4.44.

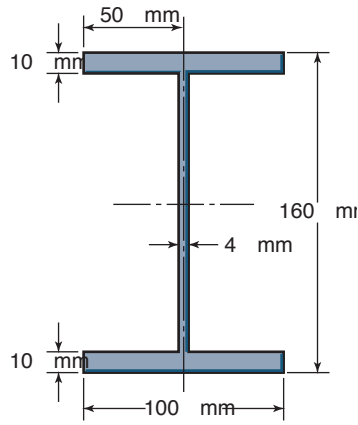
- 4.45 The bronze statue described in Problem 4.38 is asymmetrical, so that when a gale force wind blows against it, a twisting torque of 800 N-m is applied to the tube. Calculate how much the statue twists. The tube's wall thickness, 6 mm at the top and 12 mm at the ground, is assumed to be proportional to its diameter. *Ans.*  $\theta = 0.01569^\circ$ .
- 4.46 Determine the minimum diameter of a solid shaft used to transmit 500 kW of power from a 3000-rpm motor so that the shear stress does not exceed 50 MPa. *Ans.*  $d = 54.48 \text{ mm}$ .
- 4.47 A steel coupling is used to transmit a torque of 30,000 N-m. The coupling is connected to the shaft by a number of 10-mm-diameter bolts placed equidistant on a pitch circle of 0.4-m diameter. The inner diameter of the coupling is 0.1 m. The allowable shear stress on the bolts is 500 MPa. Find the minimum number of bolts needed. *Ans.* 6.
- 4.48 A shaft and a coupling are to transmit 50 kW of power at an angular speed of 1000 rpm. The coupling is connected to the shaft by 10 bolts, 20 mm in diameter, placed on a pitch circle of 200 mm. For an allowable stress on the bolts of 100 MPa, are the bolts able to transfer this power? *Ans.* Yes.
- 4.49 A beam transmitting a bending moment  $M$  of 5000 N-m has a square cross section with sides of 100 mm. The weight is decreased by making either one or two axial circular holes along the beam, as shown in Sketch *h*. Determine whether one or two holes gives the lowest weight for the beam at a given bending stress. Neglect the transverse shear stress. *Ans.* Two holes gives lower weight.

Sketch *h*, for Problem 4.49

- 4.50** A straight beam is loaded at the ends by moments  $M$ . The area moment of inertia for the beam is  $I = a^3b/12$ . Find the bending stress distribution in the beam when  $M = 1000$  N-m,  $a = 3$  cm, and  $b = 6$  cm. Also find the radius of curvature to which the beam is bent. The beam's modulus of elasticity is 207 GPa. *Ans.*  $\sigma = (7.407 \text{ GN/m}^3)y$ ,  $r = 27.95$  m.
- 4.51** The beam in Problem 4.50 is bent in a perpendicular direction so that  $I = \frac{1}{12}ab^3$ . Find the bending stress distribution and the radius of curvature to which the beam is bent. *Ans.*  $r = 111.8$  m.
- 4.52** A curved bar has a rectangular cross section with height  $h = r_o - r_i = 50$  mm and width  $b = 100$  mm. Its inner radius is 200 mm. Find the distance between the neutral axis and the centroid. *Ans.*  $e = 0.9290$  mm.
- 4.53** The curved bar in Problem 4.52 is loaded with a bending moment of 3000 N-m. Find the stress at the innermost and outermost radii. *Ans.*  $\sigma_i = -77.73$  MPa,  $\sigma_o = 6.699$  MPa.
- 4.54** Two beams with rectangular cross sections  $a \times b$  are placed on top of each other to form a beam having height  $2a$  and width  $b$ . Find the area moments of inertia  $I_x$  and  $I_y$  for the two beams:
- When they are welded together along the length.  
*Ans.*  $I_x = \frac{2}{3}ba^3$ ,  $I_y = \frac{1}{6}b^3a$ .
  - When they are not welded together.

Sketch *i*, for Problem 4.55

- 4.55** Two thin steel plates having width  $b/20$  and height  $5a$  are placed one at each side of the two beams in Problem 4.54, as shown in Sketch *i*. Find the moments of inertia around the  $x$ - and  $y$ -axes:
- When the plates are not welded together. *Ans.*  $I_x = 1.21ba^3$ ,  $I_y = 0.304ab^3$ .
  - When they are welded together as in Sketch *i*.
  - When they are welded together to form a closed tube  $5a \times 1.1b$ . *Ans.*  $I_x = 9.21ba^3$ .
- 4.56** A cantilevered beam with a rectangular cross section is loaded by a force perpendicular to the beam centerline at the free end. The cross section is 100 mm high and 25 mm wide. The vertical load at the beam end is 40,000 N. Calculate how long the beam should be to give tensile and compressive stresses 10 times higher than the maximum shear stress. Also, calculate these stresses. *Ans.*  $l = 250.0$  mm.
- 4.57** A cantilevered beam with a circular-tube cross section has an outer diameter of 100 mm and a wall thickness of 10 mm. The load perpendicular to the beam is 15 000 N, and the beam is 1.2 m long from the point of force to the wall where the beam is fastened. Calculate the maximum bending and shear stresses. *Ans.*  $\sigma_{\max} = 171.2$  MPa,  $\tau_{\max} = 7.958$  MPa.
- 4.58** A fishing rod is made of glass-fiber-reinforced plastic in the form of a tube having an outer diameter of 10 mm and a wall thickness of 1.5 mm. The glass fibers are parallel to the tube axis, so that the bending shear stress is carried by the plastic and the bending stresses are carried by the fibers. The fishing rod is 2 m long. Determine whether the rod fails from tensile stresses in the fibers or from shear overstressing in the plastic. The bending strength of the fiber-reinforced plastic is 800 MPa, and its shear strength is 3.2 MPa.
- 4.59** Two aluminum beams, like the one shown in Fig. 4.16, are welded together to form a closed cross section with dimensions of  $240 \times 80$  mm. The weld was badly done, so that the wall is only 2 mm thick instead of 8 mm. The allowable shear stress in the weld is 50 MPa, whereas the maximum allowable bending stress is 150 MPa. Find whether the 2-m-long beam fails first at the outermost fibers or at the welds.
- 4.60** Obtain the largest principal stresses at  $x = 200$  mm for the shaft considered in Example 4.13. *Ans.*  $\sigma_1 = 68.31$  MPa.
- 4.61** To decrease as much as possible the weight of beams subjected to bending, the center of gravity of the cross section is placed as far away from the beam center of gravity as possible. A beam supporting a floor has a cross section as shown in Sketch *j*. The bending moment acting on the beam is 3000 N-m and the shear force is 1000 N. Calculate the maximum bending stress and maximum shear stress. *Ans.*  $\sigma_{\max} = 19.7$  MPa,  $\tau_{\max} = 1.74$  MPa.

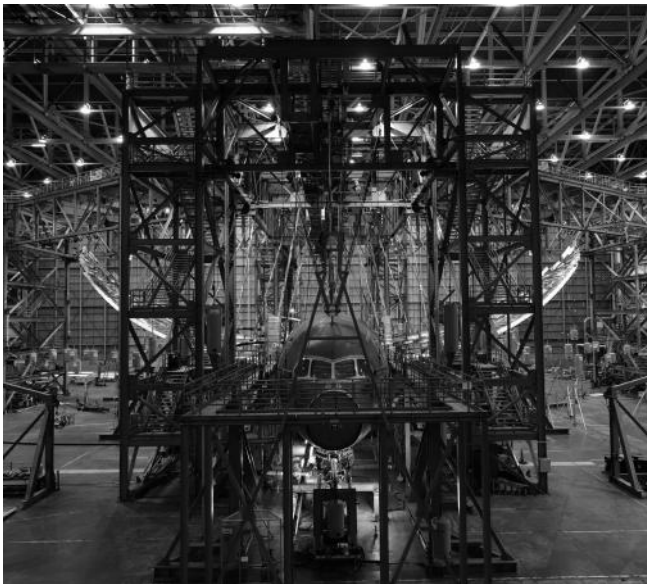
Sketch *j*, for Problem 4.61

## Design and Projects

- 4.62** Using a deck of playing cards and two small C-clamps, demonstrate the importance of internal shear in the ability of a beam to support bending moments.
- 4.63** Design a minimum weight cantilever with a rectangular cross-section that supports a load at its free end and does not exceed a specified stress anywhere in the beam. Consider (a) a constant-thickness and (b) a constant width cross-section.
- 4.64** Using a single sheet of foam board and glue, design and construct a beam that supports the largest possible load across a span.
- 4.65** For a beam with the cross-section shown in Sketch *i*, select a location for a strain gage rosette if it is to detect complicated loadings.
- 4.66** With very old trees, it can be seen that the inside is old and rotten, but an exterior ring remains vibrant and strong. Explain why this allows trees to live longer than if the central region lived longer than the outside.

# Chapter 5

## Deformation



Testing of 787 Dreamliner wings. Source: Courtesy of Boeing Corp.

*Let me tell you the secret that has led me to my goal. My strength lies in my tenacity.*

Louis Pasteur

Often, deflection is as important as stress in determining the acceptability of a design, and machine components are often sized in order to achieve acceptable deflections. This chapter presents a number of important approaches for calculating the deflection of beams and other structures. The topics discussed in Chapters 2 through 4 are built upon to demonstrate the methods used to calculate deflection of beams, using both direct integration of moment diagrams or using singularity functions. When complicated loadings exist on a body that encounters small strains (i.e., a linear elastic situation), the method of superposition is a powerful approach to calculate the deflection of the body by considering all loads in tractable combinations. Strain energy approaches, including Castigliano's Theorem, are then presented. These approaches are especially valuable for impact or energy loadings.

### Contents

- 5.1 Introduction 116
- 5.2 Moment-Curvature Relation 116
- 5.3 Singularity Functions 117
- 5.4 Method of Superposition 120
- 5.5 Strain Energy 120
- 5.6 Castigliano's Theorem 123
- 5.7 Summary 126

### Examples

- 5.1 Deflection Obtained by Direct Integration 117
- 5.2 Deflection of a Beam by Singularity Functions 118
- 5.3 Deflection of a Cantilever Using Singularity Functions 118
- 5.4 Deflection of Statically Indeterminate Beam Using Singularity Functions 119
- 5.5 Deflection of a Cantilever Through Superposition 120
- 5.6 Strain Energy in Shaft 122
- 5.7 Deflection of a Beam From Castigliano's Theorem 124
- 5.8 Deflection of a Cantilever Using Castigliano's Theorem 125
- 5.9 Castigliano's Theorem Applied to a Pinned Structure 125
- 5.10 Deflection of a Bent Beam from Castigliano's Theorem 126

### Design Procedures

- 5.1 Deflection by Singularity Functions 117
- 5.2 Procedure for Using Castigliano's Theorem 124

## Symbols

$A$	area, m <sup>2</sup>
$a$	length dimension, m
$b$	length dimension, m
$C_1, C_2$	constants
$c$	distance from neutral axis to outer fiber, m
$E$	modulus of elasticity, Pa
$G$	shear modulus of elasticity, Pa
$h$	height, m
$I$	area moment of inertia, m <sup>4</sup>
$J$	polar moment of inertia, m <sup>4</sup>
$l$	length, m
$M$	moment, N-m
$P$	force, N
$Q$	load applied at point of deformation, N
$q$	load intensity, N/m
$R$	reaction force, N
$T$	torque, N-m
$U$	strain energy, N-m
$V$	shear force, N
$v$	volume, m <sup>3</sup>
$w_o$	unit step load distribution, N/m
$x, y, z$	Cartesian coordinates, m
$\gamma$	shear strain
$\delta$	deformation (deflection), m
$\delta_{\max}$	maximum deformation (deflection), m
$\delta_P$	deflection at location of applied load, m
$\epsilon$	strain
$\theta$	slope
$\nu$	Poisson's ratio
$\sigma$	normal stress, Pa
$\tau$	shear stress, Pa

## Subscripts

$a, b$	solids $a$ and $b$
$H$	horizontal
$V$	vertical

## 5.1 Introduction

The focus of Chapters 2 through 4 has been on describing load, stress, and strain for various conditions that may occur in machine elements. Knowing the design stress and making sure it is less than the yield strength for ductile materials and less than the ultimate strength for brittle materials are important for a safe design. However, attention also needs to be paid to strain limitation and displacement, since a machine element can fail if a part deforms excessively. For example, in high-speed machinery with close tolerances, excessive deflections can cause interference between moving parts. Excessive deflection of a spindle on a milling machine would compromise the tolerances that could be achieved; many other situations exist where deflection is of great importance. This chapter attempts to quantify the deformation that may occur in a great variety of machine elements.

Chapter 4 described the deformation for normal stresses (Section 4.3) and defined the angle of twist for torsional stress (Section 4.4.1) as well as the spring rate and the angular spring rate for normal and torsional stresses. This chapter focuses on describing the deformation for distributed loading, as occurs in a beam. Some approaches described are the integral method, the singularity function, the method of superposition, and Castigliano's theorem.

## 5.2 Moment-Curvature Relation

Figure 4.14b shows a deformed element of a straight beam in pure bending. The **radius of curvature**,  $r$ , can be expressed in Cartesian coordinates as

$$\frac{1}{r} = \frac{\frac{d^2y}{dx^2}}{\left[1 + \left(\frac{dy}{dx}\right)^2\right]^{3/2}}. \quad (5.1)$$

However,  $dy/dx$  is much less than unity, so that

$$\frac{1}{r} = \frac{d^2y}{dx^2}. \quad (5.2)$$

Substituting Eq. (5.2) into Eq. (4.47) gives

$$\frac{d^2y}{dx^2} = \frac{M}{EI}. \quad (5.3)$$

This equation relates the transverse displacement to a bending moment. Even though an approximation to the curvature was used in reducing Eq. (5.1) to Eq. (5.2) that is valid only for small bending angles, this is a reasonable approximation for most beams. Equation (5.3) is the **moment-curvature relation** and is sometimes referred to as the *equation of the elastic line*.

It is convenient to summarize the load intensity, shear force, moment, slope, and deformation in the following group of ordered derivatives:

$$\frac{q}{EI} = \frac{d^4y}{dx^4} \quad (5.4)$$

$$-\frac{V}{EI} = \frac{d^3y}{dx^3} \quad (5.5)$$

$$\frac{M}{EI} = \frac{d^2y}{dx^2} \quad (5.3)$$

$$\theta = \frac{dy}{dx} \quad (5.6)$$

$$y = f(x) \quad (5.7)$$

If SI units are used in these equations, the appropriate units are newtons per meter for load intensity, newtons for shear force, newton-meters for moment, and meters for deformation. Slope is dimensionless, meaning that it is given in radians.

Integrating Eq. (5.3) gives the dimensionless slope at any point  $x$  as

$$EI \frac{dy}{dx} = EI\theta = -Mx + C_1. \quad (5.8)$$

Integrating Eq. (5.8) gives the deflection at any point  $x$  as

$$EIy(x) = -M \frac{x^2}{2} + C_1x + C_2. \quad (5.9)$$

Note that integrating the load intensity function will produce the negative of the shear force distribution, or

$$-V(x) = \int_0^x q(x) dx. \quad (5.10)$$

Furthermore, integrating the shear force gives the negative of the moment, or



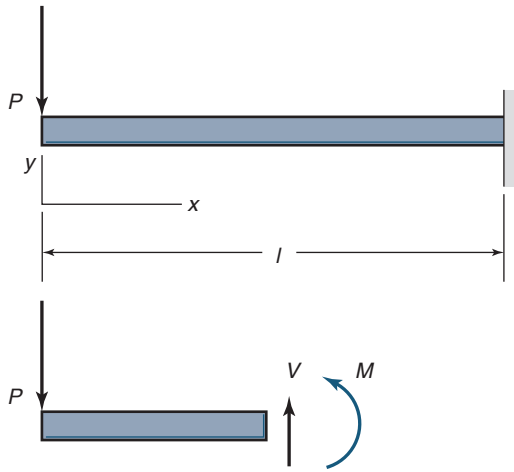


Figure 5.1: Cantilevered beam with concentrated force applied at free end.

$$M(x) = - \int_0^x V(x) dx. \quad (5.11)$$

Equations (5.8) to (5.11) are used in directly obtaining the deflection due to any type of loading.

### Example 5.1: Deflection Obtained by Direct Integration

**Given:** A perpendicular force,  $P$ , acts at the end of a cantilevered beam with length  $l$ , as shown in Fig. 5.1. Assume that the cross section is constant along the beam and that the material is the same throughout, thus implying that the area moment of inertia,  $I$ , and the modulus of elasticity,  $E$ , are constant.

**Find:** The slope and deformation at any  $x$ , and the location and value of the maximum slope.

**Solution:** The moment is  $M = -Px$ . From Eq. (5.3),

$$\frac{d^2y}{dx^2} = \frac{M}{EI} = -\frac{Px}{EI}.$$

Integrating once gives

$$\frac{dy}{dx} = -\frac{Px^2}{2EI} + C_1.$$

Integrating again gives

$$y = -\frac{Px^3}{6EI} + C_1x + C_2.$$

The boundary conditions are

1. At  $x = l$ ,  $y = 0$
2. At  $x = l$ ,  $dy/dx = 0$

From boundary condition 2,

$$C_1 = \frac{Pl^2}{2EI}.$$

Therefore,

$$y = -\frac{Px^3}{6EI} + \frac{Pl^2x}{2EI} + C_2.$$

Making use of boundary condition 1 gives

$$C_2 = \frac{Pl^3}{6EI} - \frac{Pl^3}{2EI} = -\frac{Pl^3}{3EI}.$$

Therefore,

$$y = \frac{P}{6EI} (-x^3 + 3l^2x - 2l^3),$$

and thus

$$\frac{dy}{dx} = \frac{P(l^2 - x^2)}{2EI}.$$

The maximum slope occurs at  $x = 0$  and is

$$\left(\frac{dy}{dx}\right)_{x=0} = \frac{Pl^2}{2EI}.$$

## 5.3 Singularity Functions

A **singularity function** permits expressing in one equation what would normally be expressed in several separate equations with boundary conditions. Singularity functions were introduced in Section 2.8.3, and their application to beam deflection is straightforward using Eqs. (5.4) through (5.7).

### Design Procedure 5.1: Deflection by Singularity Functions

1. Draw a free-body diagram showing the forces acting on the system.
2. Use force and moment equilibria to establish reaction forces acting on the system.
3. Obtain an expression for the load intensity function for all the loads acting on the system while making use of Table 2.2.
4. Integrate the negative load intensity function to give the shear force and then integrate the negative shear force to give the moment.
5. Make use of Eq. (5.9) to describe the deflection at any location.
6. Plot the following as a function of  $x$ :
  - (a) Shear
  - (b) Moment
  - (c) Slope
  - (d) Deflection

### Example 5.2: Deflection of a Beam by Singularity Functions

**Given:** A beam with a load applied between simply supported ends.

**Find:** The deflection for any  $x$  by using singularity functions.

**Solution:** Figure 5.2a shows a free-body diagram of the simply supported beam, while Fig. 5.2b has a section of the beam. From Table 2.2, for concentrated forces, the load intensity equation for the forces shown in Fig. 5.2b can be written as

$$q(x) = \frac{Pb}{l} \langle x \rangle^{-1} - P \langle x - a \rangle^{-1}. \quad (a)$$

Integrating twice gives the moment as

$$M(x) = \frac{Pb}{l} \langle x \rangle^1 - P \langle x - a \rangle^1. \quad (b)$$

Making use of Eq. (5.3) gives

$$EI \frac{d^2 y}{dx^2} = M(x) = \frac{Pb}{l} \langle x \rangle^1 - P \langle x - a \rangle^1. \quad (c)$$

Because  $EI$  is constant along the beam, integrating Eq. (c) gives

$$EI \frac{dy}{dx} = \frac{Pb}{2l} \langle x \rangle^2 - \frac{P}{2} \langle x - a \rangle^2 + C_1. \quad (d)$$

Integrating again gives

$$EI y = \frac{Pb}{6l} \langle x \rangle^3 - \frac{P}{6} \langle x - a \rangle^3 + C_1 x + C_2. \quad (e)$$

The boundary conditions are

1.  $y = 0$  at  $x = 0$ , which results in  $C_2 = 0$ .
2.  $y = 0$  at  $x = l$ , so that

$$C_1 = -\frac{Pbl}{6} + \frac{Pb^3}{6l} = \frac{Pb}{6l} (b^2 - l^2) = -\frac{Pb}{6l} (l^2 - b^2). \quad (f)$$

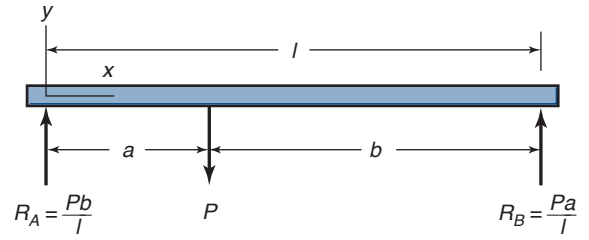
or

$$y(x) = -\frac{P}{6EI} \left[ \frac{xb}{l} (l^2 - x^2 - b^2) + \langle x - a \rangle^3 \right]. \quad (g)$$

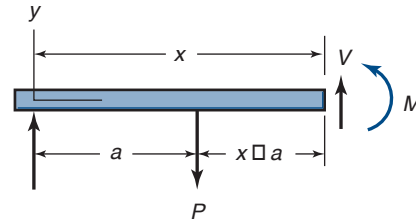
Note from Eq. (g) that when  $x \leq a$  the last term on the right side of the equal sign is zero, and when  $x > a$  the angular brackets become round brackets. (For more information about angular brackets see Section 2.8.3. Also note that from Fig. 5.2 that positive  $y$  is upward; in Eq. (g),  $y$  is negative, meaning deflection is downward. This can be intuitively confirmed by inspecting Fig. 5.2.)

### Example 5.3: Deflection of a Cantilever Using Singularity Functions

**Given:** A cantilevered beam has a unit step distribution over a part of the beam as shown in Fig. 5.3. The beam is clamped or built into the structure at A and free at C. The unit step distribution begins at the free end.



(a)



(b)

Figure 5.2: Free-body diagram of force anywhere between simply supported ends. (a) Complete beam; (b) portion of beam.

**Find:** Derive a general expression for the deflection at any  $x$  and at the free end by using singularity functions. Also, describe the deflection for two special cases: (a) When no unit step load is applied, and (b) When the unit step load is applied over the entire length.

**Solution:** The load intensity equation for the forces and moments shown in Fig. 5.3c can be expressed by using Table 2.2 as

$$q(x) = w_o b \langle x \rangle^{-1} - w_o b \left( a + \frac{b}{2} \right) \langle x \rangle^{-2} - w_o \langle x - a \rangle^0.$$

Integrating twice gives

$$M(x) = w_o b \langle x \rangle^1 - w_o b \left( a + \frac{b}{2} \right) \langle x \rangle^0 - \frac{w_o}{2} \langle x - a \rangle^2.$$

Making use of Eq. (5.3) gives

$$EI \frac{d^2 y}{dx^2} = w_o b \langle x \rangle^1 - w_o b \left( a + \frac{b}{2} \right) \langle x \rangle^0 - \frac{w_o}{2} \langle x - a \rangle^2.$$

Integrating once gives

$$EI \frac{dy}{dx} = \frac{w_o b}{2} \langle x \rangle^2 - w_o b \left( a + \frac{b}{2} \right) \langle x \rangle^1 - \frac{w_o}{6} \langle x - a \rangle^3 + C_1.$$

Integrating again gives

$$EI y(x) = \frac{w_o b}{6} \langle x \rangle^3 - \frac{w_o b}{2} \left( a + \frac{b}{2} \right) \langle x \rangle^2 - \frac{w_o}{24} \langle x - a \rangle^4 + C_1 x + C_2.$$

The boundary conditions are:

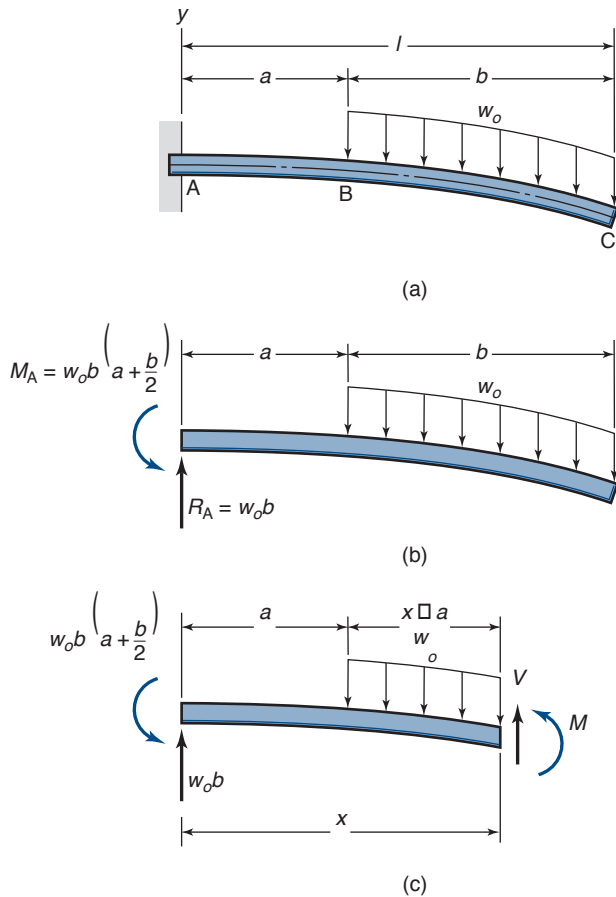


Figure 5.3: Cantilevered beam with unit step distribution over part of beam. (a) Loads and deflection acting on cantilevered beam; (b) free-body diagram of forces and moments acting on entire beam; (c) free-body diagram of forces and moments acting on portion of beam.

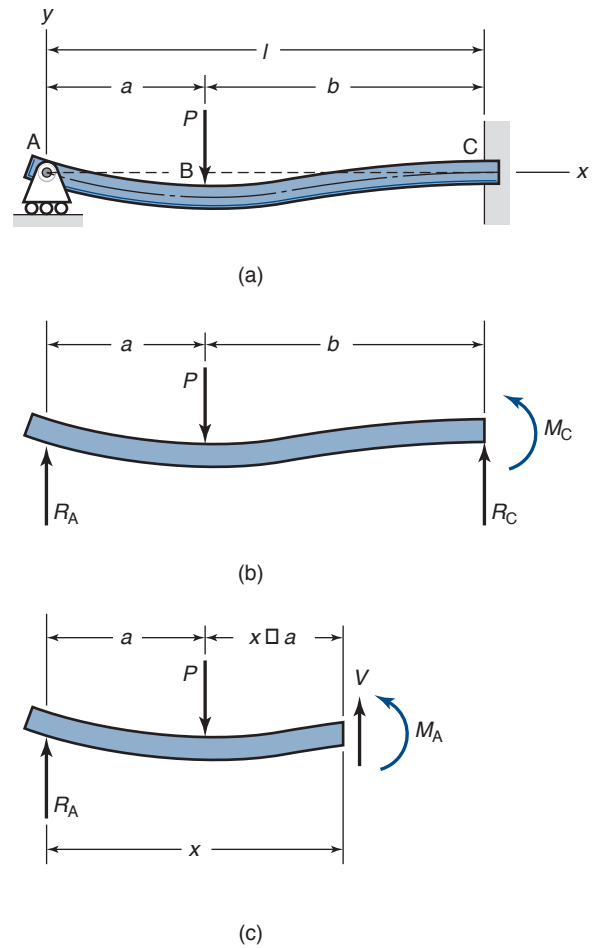


Figure 5.4: Pinned-fixed beam with concentrated force acting anywhere along beam. (a) Sketch of assembly; (b) free-body diagram of entire beam; (c) free-body diagram of part of beam.

1.  $\frac{dy}{dx} = 0$  at  $x = 0$ , or  $C_1 = 0$
2.  $y = 0$  at  $x = 0$ , or  $C_2 = 0$

Therefore,

$$y = \frac{w_o}{EI} \left[ \frac{bx^3}{6} - \frac{bx^2}{2} \left(a + \frac{b}{2}\right) - \frac{1}{24} \langle x - a \rangle^4 \right].$$

The deflection at the free end, or where  $x = a + b$ , is

$$\begin{aligned} y_l &= -\frac{w_o}{EI} \left[ \frac{b^4}{24} + \frac{b(a+b)^2}{2} \left(a + \frac{b}{2}\right) - \frac{b(a+b)^3}{6} \right] \\ &= -\frac{w_o b}{EI} \left[ \frac{a^3}{3} + \frac{3}{4} a^2 b + \frac{ab^2}{2} + \frac{b^3}{8} \right]. \end{aligned}$$

(a) For the special case of  $b = 0$ ,  $y_{\max} = 0$  (no deflection occurs).

(b) For the special case of  $a = 0$ ,

$$y_l = -\frac{w_o b^4}{8EI}.$$

In this situation the unit step extends completely across the length  $l$ .

### Example 5.4: Deflection of Statically Indeterminate Beam Using Singularity Functions

**Given:** A beam is fixed at one end and has its other end simply supported. A concentrated force acts at any point along the beam, as shown in Fig. 5.4.

**Find:** Determine a general expression for the deflection of the beam by using singularity functions.

**Solution:** Note from Fig. 5.4b that there are three unknowns,  $R_A$ ,  $R_C$ , and  $M_C$ . The force and moment equilibrium conditions produce only two equations. A solution is to take one of the reaction forces as an unknown and express the other two in terms of that unknown. Thus,

$$R_C = P - R_A, \quad (a)$$

$$M_C = -Pb + R_A l. \quad (b)$$

The load intensity equation for the forces shown in Fig. 5.4a can be expressed as

$$q(x) = R_A \langle x \rangle^{-1} - P \langle x - a \rangle^{-1}. \quad (c)$$

Integrating twice gives the moment as

$$M_B(x) = R_A \langle x \rangle^1 - P \langle x - a \rangle^1. \quad (d)$$

Making use of Eq. (5.3) gives

$$EI \frac{d^2 y}{dx^2} = M(x) = R_A x - P \langle x - a \rangle^1. \quad (e)$$

Integrating once gives

$$EI \frac{dy}{dx} = R_A \frac{x^2}{2} - \frac{P}{2} \langle x - a \rangle^2 + C_1. \quad (f)$$

Integrating again gives the deflection as

$$EI y = R_A \frac{x^3}{6} - \frac{P}{6} \langle x - a \rangle^3 + C_1 x + C_2. \quad (g)$$

The boundary conditions are:

1.  $y = 0$  at  $x = 0$ , which results in  $C_2 = 0$
2.  $\frac{dy}{dx} = 0$  at  $x = l$  gives

$$C_1 = -R_A \frac{l^2}{2} + \frac{P}{2} (l - a)^2. \quad (h)$$

Therefore,

$$EI y = R_A \frac{x^3}{6} - \frac{P}{6} \langle x - a \rangle^3 - \frac{R_A l^2 x}{2} + \frac{Px}{2} (l - a)^2. \quad (i)$$

3.  $y = 0$  at  $x = l$ :

$$R_A = \frac{Pb^2}{2l^3} (3l - b). \quad (j)$$

The general expression for the deformation is

$$y = \frac{P}{6EI} \left[ \frac{xb^2}{2l^3} (-3l^3 + 3lx^2 + 3bl^2 - bx^2) - \langle x - a \rangle^3 \right]. \quad (k)$$

Substituting Eq. (j) into Eq. (d) gives

$$M_B(x) = \frac{Pxb^2}{2l^3} (3l - b) - P \langle x - a \rangle^1. \quad (l)$$

Note that

$$M_B(x = 0) = 0, \quad (m)$$

$$M_B(x = a) = \frac{Pb^2 a}{2l^3} (3l - b), \quad (n)$$

$$M_B(x = l) = \frac{Pb^2 l}{2l^2} (3l - b) - Pb = -\frac{Pab}{2l^2} (2l - b). \quad (o)$$

From Eqs. (n) and (o), the moment is negative at  $x = a$  and positive at  $x = l$ , but is not clear whether the maximum magnitude exists at  $x = a$  or at  $x = l$ . When  $a = (\sqrt{2} - 1)l = 0.414l$ , the magnitude of the bending moment at B equals that at C. When  $a < 0.414l$ , the greater moment occurs at B; and when  $a > 0.414l$ , the greater moment occurs at C.

## 5.4 Method of Superposition

The **method of superposition** uses the principle that the deflection at any point in a body is equal to the sum of the deflections caused by each load acting separately. Thus, if a beam

is loaded by  $n$  separate forces, the deflection at a particular point is the sum of the  $n$  deflections, one for each force. This method depends on the linearity of the governing relations between the load and the deflection, and it involves reducing complex conditions of load and support into a combination of simple loading conditions for which solutions are available. The solution of the original problem then takes the form of a superposition of these solutions. The solution assumes that the deflection of the beam is linearly proportional to the applied load. Thus, for  $n$  different loads, Eq. (5.3) can be written as

$$\begin{aligned} EI \frac{d^2 y}{dx^2} &= EI \frac{d^2}{dx^2} (y_1 + y_2 + \cdots + y_n) \\ &= M_1 + M_2 + \cdots + M_n. \end{aligned} \quad (5.12)$$

Table 5.1 gives solutions for some simple beam deflection situations that may be combined to produce the deflection for a more complex situation. Additional cases are summarized in Appendix D.

### Example 5.5: Deflection of a Cantilever Through Superposition

**Given:** Figure 5.5 shows a cantilevered beam (i.e., fixed at one end and free at the other end). A moment is applied at the free end, and a concentrated force is applied at a distance,  $a$ , from the fixed end.

**Find:** Use the method of superposition to determine the deflection at the free end.

**Solution:** Figure 5.5b depicts the deflection with one end fixed and one end free for a concentrated force at any point within the length of the beam. Figure 5.5c shows a moment applied to the free end and the deformation. From Table 5.1 the individual deflections can be obtained directly as

$$y_{l,1} = -\frac{Pa^2}{6EI} (3l - a) \quad (a)$$

and

$$y_{l,2} = \frac{Ml^2}{2EI}. \quad (b)$$

The resultant deflection from the method of superposition is

$$y_l = y_{l,1} + y_{l,2} = \frac{-Pa^2(3l - a) + 3Ml^2}{6EI}. \quad (c)$$

The deflection at any point on the beam is

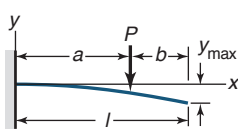
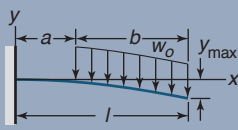
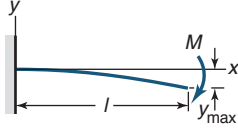
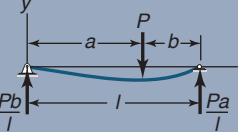
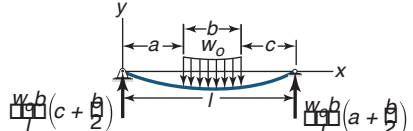
$$y = -\frac{P}{6EI} [\langle x - a \rangle^3 - x^3 + 3x^2 a] + \frac{Mx^2}{2EI}. \quad (d)$$

## 5.5 Strain Energy

Statically indeterminate beams and beams of varying material properties or cross sections cannot be successfully analyzed by using the methods discussed thus far. Also, when a loading is energy related (such as an object striking a beam with a given initial velocity), the exact forces are not readily apparent. For this reason *energy methods* are often very useful.

When loads are applied to a machine element, it will deform. In the process, the external work done by the loads will be converted into internal work (called **strain energy**), provided that no energy is lost in the form of heat. This strain

Table 5.1: Deflection for common cantilever and simply-supported beam conditions. See also Appendix D.

Type of loading	Deflection
	$y = -\frac{P}{6EI} \left( \langle x - a \rangle^3 - x^3 + 3x^2 a \right)$ <p>When <math>b = 0</math>, <math>y = -\frac{P}{6EI} (3lx^2 - x^3)</math></p> <p>and <math>y_{\max} = y(l) = -\frac{PL^3}{3EI}</math></p>
	$y = -\frac{w_o}{24EI} \left[ 4bx^3 - 12bx^2 \left( a + \frac{b}{2} \right) - \langle x - a \rangle^4 \right]$ <p>When <math>a = 0</math> and <math>b = l</math>, <math>y = \frac{w_o}{24EI} (6l^2 x^2 - 4lx^3 + x^4)</math></p> <p>and <math>y_{\max} = -\frac{w_o l^4}{8EI}</math></p>
	$y = -\frac{Mx^2}{2EI}, y_{\max} = -\frac{Ml^2}{2EI}$
	$y = \frac{P}{6EI} \left( \frac{b}{l} \langle x \rangle^3 - \langle x - a \rangle^3 + 3a^2 x - 2alx - \frac{a^3 x}{l} \right)$
	$y = \frac{w_o b}{24lEI} \left\{ 4 \left( c + \frac{b}{2} \right) x^3 - \frac{l}{b} \left( \langle x - a \rangle^4 - \langle x - a - b \rangle^4 \right) + x \left[ b^3 + 6bc^2 + 4b^2c + 4c^3 - 4l^2 \left( c + \frac{b}{2} \right) \right] \right\}$

energy is stored in the body. The unit of strain energy is newton-meters. Strain energy is always positive even if the stress is compressive because stress and strain are always in the same direction. The symbol  $U$  is used to designate strain energy.

### 5.5.1 Normal Stress

When a tension test specimen is subjected to an axial load, a volume element (shown in Fig. 5.6) is subjected to an axial force and the force develops a stress

$$dP = \sigma_z dA = \sigma_z dx dy \quad (5.13)$$

on the top and bottom faces of the element after it undergoes a vertical elongation of  $\epsilon_z dz$ .

Because the force,  $\Delta P$ , is increased uniformly from zero to its final magnitude  $dP$  when the displacement  $\epsilon_z dz$  is attained, the average force magnitude  $dP/2$  times the displacement  $\epsilon_z dz$  is the strain energy or

$$dU = \left( \frac{1}{2} dP \right) \epsilon_z dz.$$

Making use of Eq. (5.13) and the fact that  $dv = dx dy dz$  gives

$$dU = \frac{1}{2} \sigma_z \epsilon_z dv. \quad (5.14)$$

In general, if the member is subjected only to a uniaxial normal stress, the strain energy is

$$U = \int_v \frac{\sigma \epsilon}{2} dv. \quad (5.15)$$

Also, if the material acts in a linear-elastic manner, Hooke's law can be applied and Eq. (3.3) can be substituted into Eq. (5.15) giving

$$U = \int_v \frac{\sigma^2}{2E} dv. \quad (5.16)$$

For axial loading of a beam of length  $l$ , making use of Eq. (2.7) gives

$$U = \int_v \frac{P^2}{2EA^2} dv, \quad (5.17)$$

but  $dv = A dx$ , so that

$$U = \int_0^l \frac{P^2}{2AE} dx = \frac{P^2 l}{2AE}. \quad (5.18)$$

If the loading is from bending moments, making use of Eq. (4.46) gives

$$U = \int_v \frac{\sigma^2}{2E} dv = \int \frac{M^2 y^2}{2EI^2} dv.$$

Since  $dv = dA dx$ , where  $dA$  represents an element of the cross-sectional area. Also, recall that  $M^2/2EI^2$  is a function of  $x$  alone; then,

$$U = \int_0^l \frac{M^2}{2EI^2} \left( \int y^2 dA \right) dx.$$

Equation (5.7) then gives

$$U = \int_0^l \frac{M^2}{2EI} dx. \quad (5.19)$$



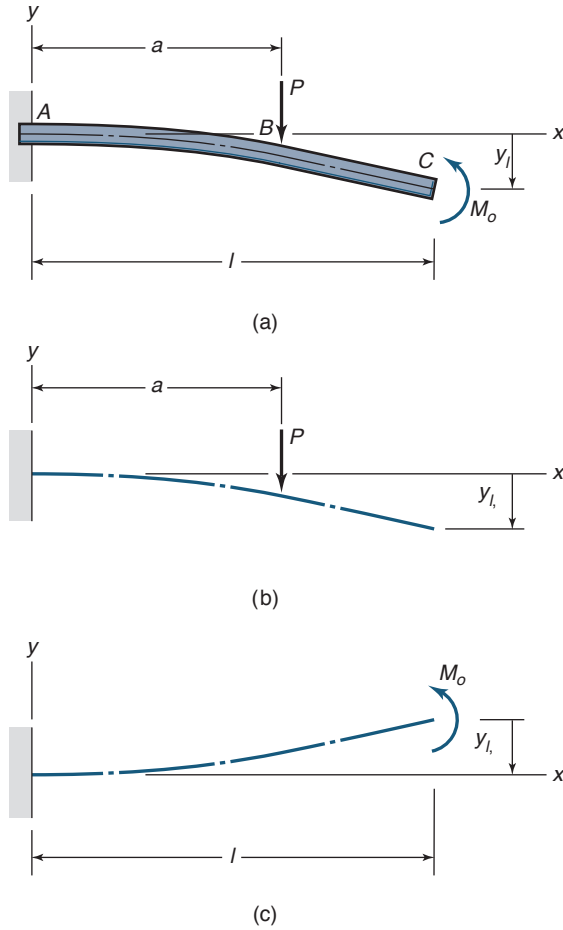


Figure 5.5: Beam fixed at one end and free at the other with moment applied to free end and concentrated force at any distance from free end. (a) Complete assembly; (b) free-body diagram showing effect of concentrated force; (c) free-body diagram showing effect of moment.

### 5.5.2 Shear Stress

Consider the volume element shown in Fig. 5.7. The shear stress causes the element to deform such that only the shear force  $dV = \tau dx dy$ , acting on the top of the element, is displaced  $\gamma dz$  relative to the bottom surface. Only the vertical surfaces rotate, and therefore the shear forces on these surfaces do not contribute to the strain energy. Thus, the strain energy stored in the element due to a shear stress,  $\tau$ , is

$$dU = \frac{1}{2} (\tau dx dy) \gamma dz,$$

or

$$dU = \frac{1}{2} \tau \gamma dv. \quad (5.20)$$

Integrating over the entire volume gives the strain energy stored in the member due to shear stress as

$$U = \int_v \frac{\tau \gamma}{2} dv. \quad (5.21)$$

Making use of Hooke's law for shear stress, expressed in Eq. (4.28), gives

$$U = \int_v \frac{\tau^2}{2G} dv. \quad (5.22)$$

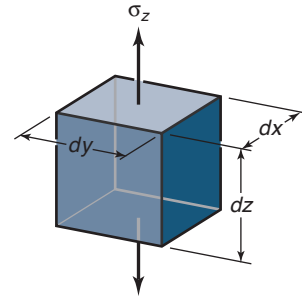


Figure 5.6: Element subjected to normal stress.

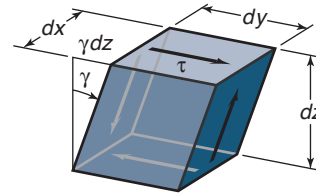


Figure 5.7: Element subjected to shear stress.

For strain energy in torsion of circular shafts, making use of Eqs. (4.27) to (4.33) gives

$$U = \int_v \frac{T^2 r^2}{2GJ^2} dv,$$

but  $dv = dA dx$ , and thus  $T^2/2GJ^2$  is a function of  $x$  only, so that

$$U = \int_0^l \frac{T^2}{2GJ^2} \left( \int r^2 dA \right) dx.$$

Making use of Eq. (4.30) gives

$$U = \int_0^l \frac{T^2}{2GJ} dx. \quad (5.23)$$

If the shaft has a uniform cross section,

$$U = \frac{T^2 l}{2GJ}. \quad (5.24)$$

Recall that Table 4.1 contains values of  $J$  for a number of different cross sections, but Eq. (5.24) can be used only for cross sections with circular symmetry.

### Example 5.6: Strain Energy in a Shaft

**Given:** A 1-m-long solid shaft with circular cross section has a diameter of 40 mm over 0.5 m of the length and 30 mm over the rest of the length. The shaft is subjected to a torque of 1100 N-m. The shaft material is AISI 1080 high-carbon steel.

**Find:** Calculate the strain energy in the shaft; also calculate the ratio of the strain energies stored in the thinner and thicker parts of the shaft.

**Solution:** From Eq. (5.23),

$$U = \int_0^l \frac{T^2}{2GJ} dx = \frac{T^2}{2G} \left( \frac{1}{J_1} \int_0^{0.5} dx + \frac{1}{J_2} \int_{0.5}^{1.0} dx \right).$$

From Table 3.1 for steel,  $E = 207$  GPa and  $\nu = 0.3$ . From Eq. (3.7), the shear modulus is

$$G = \frac{E}{2(1+\nu)} = \frac{(207 \times 10^9)}{2(1+0.3)} = 79.6 \text{ GPa}.$$

For a solid circular cross section,

$$J_1 = \frac{\pi r^4}{2} = \frac{\pi (0.02)^4}{2} = 25.13 \times 10^{-8} \text{ m}^4,$$

$$J_2 = \frac{\pi}{2} (0.015)^4 = 7.952 \times 10^{-8} \text{ m}^4.$$

The strain energy becomes

$$U = \frac{1100^2}{2(79.6 \times 10^9)} \left( \frac{10^8}{25.13} + \frac{10^8}{7.952} \right) \left( \frac{1}{2} \right) = 62.91 \text{ N-m}.$$

The ratio of the energy stored in the two parts can be expressed as

$$\frac{U_1}{U_2} = \frac{J_2}{J_1} = \frac{(7.952 \times 10^{-8})}{(25.13 \times 10^{-8})} = 0.3164.$$

### 5.5.3 Transverse Shear Stress

The strain energy due to shear stress can be obtained from Eq. (4.65). For a rectangular cross section with width  $b$  and height  $h$ ,

$$\tau = \frac{3V}{2A} \left( 1 - \frac{y^2}{c^2} \right) = \frac{3V}{2bh} \left( 1 - \frac{y^2}{c^2} \right). \quad (5.25)$$

Substituting this equation into Eq. (5.22) and integrating gives

$$U = \frac{1}{2G} \left( \frac{3V}{2bh} \right)^2 \int \left( 1 - \frac{y^2}{c^2} \right)^2 dv.$$

Setting  $dv = b dx dy$  results in

$$U = \frac{9V^2}{8Gbh^2} \int_{-c}^c \left( 1 - \frac{2y^2}{c^2} + \frac{y^4}{c^4} \right) dy \int_0^l dx.$$

Integrating yields

$$U = \frac{9V^2 l}{8Gbh^2} \left( y - \frac{2y^3}{3c^2} + \frac{y^5}{5c^4} \right)_{y=-c}^{y=c}.$$

Substituting the limits gives

$$U = \frac{6V^2 lc}{5Gbh^2}.$$

Recalling that  $c = h/2$ ,

$$U = \frac{3V^2 l}{5Gbh}. \quad (5.26)$$

This is the general strain energy due to transverse shear stress for a rectangular cross section. Table 5.1 summarizes the

strain energy for four types of loading. Recall that the transverse shear is valid only for a rectangular cross section. For torsion, Table 4.1 should be used for  $J$ , the polar area moment of inertia for a circular cross section. For bending,  $I$  corresponds to  $I_x$  in Table 4.1, since the beam axis is in the  $x$ -direction.

### 5.5.4 General State of Stress

The total strain energy due to a general state of stress can be expressed as

$$U = \int_v \left( \frac{\sigma_x \epsilon_x}{2} + \frac{\sigma_y \epsilon_y}{2} + \frac{\sigma_z \epsilon_z}{2} \right) dv + \int_v \left( \frac{\tau_{xy} \gamma_{xy}}{2} + \frac{\tau_{yz} \gamma_{yz}}{2} + \frac{\tau_{xz} \gamma_{xz}}{2} \right) dv. \quad (5.27)$$

Making use of Eq. (B.54) gives

$$U = \int_v \frac{1}{2E} (\sigma_x^2 + \sigma_y^2 + \sigma_z^2) dv - \int_v \frac{\nu}{E} (\sigma_x \sigma_y + \sigma_y \sigma_z + \sigma_z \sigma_x) + \int_v \frac{1}{G} (\tau_{xy}^2 + \tau_{yz}^2 + \tau_{xz}^2) dv. \quad (5.28)$$

If only the principal stresses  $\sigma_1$ ,  $\sigma_2$ , and  $\sigma_3$  act on the elements, Eq. (5.28) reduces to

$$U = \int_v \left[ \frac{1}{2E} (\sigma_1^2 + \sigma_2^2 + \sigma_3^2) - \frac{\nu}{E} (\sigma_1 \sigma_2 + \sigma_2 \sigma_3 + \sigma_3 \sigma_1) \right] dv. \quad (5.29)$$

## 5.6 Castigliano's Theorem

It is often necessary to calculate the elastic deformation due to distributed loads that are not as simple as those already presented. Castigliano's theorem can be applied to a wide range of deflection problems. Extensive use is made here of the strain energy material presented in Section 5.5.

**Castigliano's theorem** states that when a body is elastically deformed by a system of loads, the deflection at any point,  $p$ , in any direction,  $a$ , is equal to the partial derivative of the strain energy (with the system of loads acting) with respect to a load at  $p$  in the direction  $a$ , or

$$y_i = \frac{\partial U}{\partial Q_i}. \quad (5.30)$$

The load  $Q_i$  is applied to a particular point of deformation and therefore is not a function of  $x$ . Thus, it is permissible to take the derivative with respect to  $Q_i$  before integrating for the general expressions for the strain energy. Also, the load may be any of the loads presented in Section 2.3 and throughout the text: normal, shear, bending, and transverse shear. Table 5.2 shows the strain energy for the various types of loading.

The best way to understand how to apply Castigliano's theorem is to observe how it is used in a number of different examples. Examples 5.7 through 5.10 demonstrate various features of Castigliano's approach.

Table 5.2: Strain energy for four types of loading.

Loading type	Factors involved	Strain energy for special case where all three factors are constant with $x$	General expression for strain energy
Axial	$P, E, A$	$U = \frac{P^2 l}{2EA}$	$U = \int_0^l \frac{P^2}{2EA} dx$
Bending	$M, E, I$	$U = \frac{M^2 l}{2EI}$	$U = \int_0^l \frac{M^2}{2EI} dx$
Torsion	$T, G, J$	$U = \frac{T^2 l}{2GJ}$	$U = \int_0^l \frac{T^2}{2GJ} dx$
Transverse shear (rectangular section)	$V, G, A$	$U = \frac{3V^2 l}{5GA}$	$U = \int_0^l \frac{3V^2}{5GA} dx$

## Design Procedure 5.2: Procedure for Using Castigliano's Theorem

The following procedure is to be employed in using Castigliano's theorem:

1. Obtain an expression for the total strain energy, including:
  - (a) Loads ( $P, M, T, V$ ) acting on the element (use Table 5.2)
  - (b) A fictitious force  $Q$  acting at the location and in the direction of the desired deflection
2. Obtain deflection from  $y = \partial U / \partial Q$ .
3. If  $Q$  is fictitious, set  $Q = 0$  and solve the resulting equation.

## Example 5.7: Deflection of a Beam From Castigliano's Theorem

**Given:** The simply supported beam shown in Fig. 5.2 with the force  $P$  applied at  $x = l/2$ .

**Find:** Determine the deflection,  $\delta_P$ , at the location of the applied force by using Castigliano's theorem. Consider both bending and transverse shear.

**Solution:** Because of symmetry, the deflection at the point of an applied force can be obtained by doubling the solution from zero to  $l/2$ . The two types of loading being applied to the beam are:

(a) Bending

$$M = \frac{Px}{2} \quad \text{and} \quad \frac{dM}{dP} = \frac{x}{2}. \quad (a)$$

(b) Transverse shear

$$V = \frac{P}{2} \quad \text{and} \quad \frac{dV}{dP} = \frac{1}{2}. \quad (b)$$

By making use of Table 5.2 the total strain energy can be expressed as

$$U = 2 \int_0^{l/2} \frac{M^2}{2EI} dx + 2 \int_0^{l/2} \frac{3V^2}{5GA} dx. \quad (c)$$

Using Eqs. (a) and (b) this equation becomes

$$U = \int_0^{l/2} \frac{P^2 x^2}{4EI} dx + \int_0^{l/2} \frac{3P^2}{10GA} dx.$$

From Castigliano's theorem

$$-\delta_P = \frac{\partial U}{\partial P} = + \int_0^{l/2} \frac{Px^2}{2EI} dx + \int_0^{l/2} \frac{3P}{5GA} dx.$$

Because  $P, E, I, G$ , and  $A$  are not functions of  $x$ , this equation becomes

$$\delta_P = -\frac{Pl^3}{48EI} - \frac{3Pl}{10GA}. \quad (d)$$

The first term on the right side is due to bending and the second is due to transverse shear.

To better understand the bending and transverse shear contributions to the total deflection at the applied force, assume that the beam has a rectangular cross section. From Table 4.1 for a rectangular shape,  $I = bh^3/12$  and  $A = bh$ . Substituting these expressions into Eq. (d) gives

$$\delta_P = -\frac{Pl^3}{4Ebh^3} - \frac{3Pl}{10Gbh} \quad (e)$$

which can be rewritten as

$$\delta_P = -\frac{3Pl}{10Gbh} \left[ \left( \frac{5}{6} \right) \left( \frac{G}{E} \right) \left( \frac{l}{h} \right)^2 + 1 \right]. \quad (f)$$

For carbon steel  $G/E = 0.383$ . The length-to-height ratio,  $l/h$ , of a beam is typically at least 10. Assume that the smallest value is  $l/h = 10$ . After substituting the values for  $G/E$  and  $l/h$  into Eq. (f), the first term within the brackets is 32 times the second term. Thus, in most applications, the transverse shear term will be considerably smaller than the bending moment term (typically, less than 3%). This is an important finding that will be used often; for beams, deflections and energies can be assumed to be due to bending only.

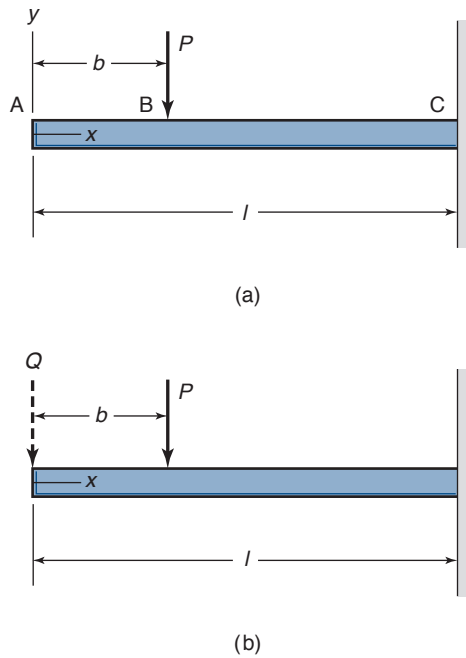


Figure 5.8: Cantilevered beam with concentrated force acting at a distance  $b$  from free end. (a) Coordinate system and significant points shown; (b) fictitious force,  $Q$ , shown along with concentrated force,  $P$ .

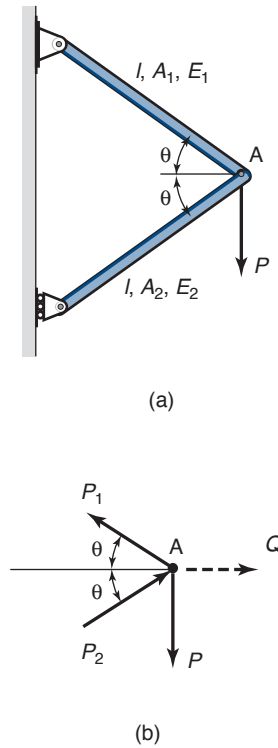


Figure 5.9: System arrangement. (a) Entire assembly; (b) free-body diagram of forces acting at point A.

### Example 5.8: Deflection Using Castigliano's Theorem

**Given:** A cantilevered beam has a concentrated force acting at a distance,  $b$ , from the free end, as shown in Fig. 5.8.

**Find:** Determine the deflection at the free end using Castigliano's theorem. Transverse shear can be neglected.

**Solution:** Note from Fig. 5.8 that, since no force is acting at the free end, a fictitious force is created. The moment at any  $x$  can be expressed as

$$M = -Qx - P \langle x - b \rangle.$$

The only force contributing to the total strain rate is the bending moment; from Table 5.2:

$$U = \frac{1}{2EI} \int_0^l [Q^2 x^2 + 2Q_x P \langle x - b \rangle + (P \langle x - b \rangle)^2] dx.$$

From Castigliano's theorem

$$\delta_A = \frac{\partial U}{\partial Q} = \frac{1}{2EI} \left[ \frac{2Ql^3}{3} + 2P \int_0^l x \langle x - b \rangle dx \right]. \quad (a)$$

Thus, setting  $Q = 0$  and integrating gives

$$\delta_A = \frac{P}{6EI} [l^2 (2l - 3b) + b^3]. \quad (b)$$

### Example 5.9: Castigliano's Theorem Applied to a Pinned Structure

**Given:** The assembly shown in Fig. 5.9a can be made of different materials and have different cross-sectional areas in its two equal parts, denoted by the subscripts 1 and 2.

**Find:** Calculate the horizontal displacement at the point of vertical force application by using Castigliano's theorem.

**Solution:** Note from the free-body diagram in Fig. 5.9b that, since no force is acting horizontally, a fictitious force  $Q$  has to be created. From force equilibrium of the vertical and horizontal forces

$$\sum P_v = 0 \rightarrow -P + P_1 \sin \theta + P_2 \sin \theta = 0,$$

$$\sum P_H = 0 \rightarrow Q - P_1 \cos \theta + P_2 \cos \theta = 0.$$

Solving for  $P_1$  and  $P_2$  gives

$$P_1 = \frac{1}{2} \left( \frac{P}{\sin \theta} + \frac{Q}{\cos \theta} \right) \quad \text{and} \quad \frac{\partial P_i}{\partial Q} = \frac{1}{2 \cos \theta}. \quad (a)$$

$$P_2 = \frac{1}{2} \left( \frac{P}{\sin \theta} - \frac{Q}{\cos \theta} \right) \quad \text{and} \quad \frac{\partial P_i}{\partial Q} = -\frac{1}{2 \cos \theta}. \quad (b)$$

From Table 5.2 the total strain energy for axial loading can be written as

$$U = \frac{P_1^2 l}{2A_1 E_1} + \frac{P_2^2 l}{2A_2 E_2}.$$

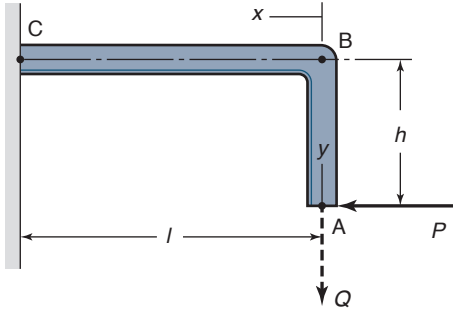


Figure 5.10: Cantilevered beam with 90° bend acted upon by horizontal force,  $P$ , at free end.

From Castigliano's theorem, the horizontal displacement at point A is

$$\delta_{A,H} = \frac{\partial U}{\partial Q} = \frac{1}{2} \left( \frac{2P_1 \frac{\partial P_1}{\partial Q}}{A_1 E_1} + \frac{2P_2 \frac{\partial P_2}{\partial Q}}{A_2 E_2} \right).$$

Substituting Eqs. (a) and (b) into the above equation gives

$$\delta_{A,H} = \frac{l}{4A_1 E_1} \left( \frac{P}{\sin \theta} + \frac{Q}{\cos \theta} \right) \frac{1}{\cos \theta} - \frac{l}{4A_2 E_2} \left( \frac{P}{\sin \theta} - \frac{Q}{\cos \theta} \right) \frac{1}{\cos \theta}.$$

Setting  $Q = 0$  gives

$$\delta_{A,H} = \frac{lP}{4 \sin \theta \cos \theta} \left( \frac{1}{A_1 E_1} - \frac{1}{A_2 E_2} \right). \quad (c)$$

Note that if the beam sections 1 and 2 have the same cross-sectional area and are made of the same material (i.e., the modulus of elasticity is the same), Eq. (c) gives  $\delta_{A,H} = 0$ , and thus there would not be any horizontal displacement.

### Example 5.10: Deflection of a Bent Beam from Castigliano's Theorem

**Given:** Figure 5.10 shows a cantilevered beam with a 90° bend acted on by a horizontal force  $P$  at the free end.

**Find:** Calculate the vertical deflection at the free end if transverse shear is neglected. Use Castigliano's theorem.

**Solution:** Note from Fig. 5.10 that, since no vertical force exists at the free end, a fictitious force was created. Thus, the four components used to define the total strain energy are:

- (a) Bending in AB, where  $M_{AB} = Py$
- (b) Bending in BC, where  $M_{BC} = Qx + Ph$
- (c) Axial load in AB of magnitude  $Q$
- (d) Axial load in BC of magnitude  $P$

From Table 5.2 the total strain energy can be written as

$$U = \int_0^h \frac{P^2 y^2}{2EI} dy + \int_0^l \frac{(Qx + Ph)^2}{2EI} dx + \int_0^h \frac{Q^2 dy}{2EA} + \int_0^l \frac{P^2 dx}{2EA}$$

Since the beam's material and cross sections are the same in sections AB and BC, from Castigliano's theorem

$$\delta_{A,V} = \int_0^l \frac{(Qx + Ph)x dx}{EI} + \int_0^h \frac{Q dy}{EA} = \frac{Ql^3}{3EI} + \frac{Phl^2}{2EI} + \frac{Qh}{EA}$$

Setting  $Q = 0$  gives

$$\delta_{A,V} = \frac{Phl^2}{2EI}.$$

## 5.7 Summary

The three main failure modes for machine elements are (a) from being overstressed, (b) from excessive elastic deformations, and (c) from the lack of a tribological film. This chapter described the deformations that machine elements, especially beams, may experience. Deformations due to distributed and concentrated loads were both considered. For a distributed load four major approaches to describing the deformations were presented: the moment-curvature relation, singularity functions, the method of superposition, and Castigliano's theorem. Each has its particular strengths and limitations. The type of load being applied (normal, bending, shear, or transverse shear) determines the approach. Castigliano's theorem is the most versatile of the four approaches considered, since it can be applied to a wide range of deflection problems.

## Key Words

**Castigliano's theorem** theorem that when a body is elastically deformed by a system of loads, deflection at any point in any direction is equal to the partial derivative of strain energy (for the system of loads) with respect to load in the direction of interest

**method of superposition** principle that deflection at any point in beam is equal to sum of deflections caused by each load acting separately

**moment-curvature relation** relationship between beam curvature and bending moment

**radius of curvature** distance from center to inside edge of beam in bending

**singularity function** function that permits expressing in one equation what would normally be expressed in several separate equations with boundary conditions

**strain energy** internal work that was converted from external work done by applying load



## Summary of Equations

Beam equations:

$$\text{Radius of curvature: } \frac{d^2 y}{dx^2} = \frac{M}{EI}$$

$$\text{Load intensity: } \frac{q}{EI} = \frac{d^4 y}{dx^4}$$

$$\text{Shear force: } -\frac{V}{EI} = \frac{d^3 y}{dx^3} = \int_0^x q(x) dx$$

$$\text{Moment: } \frac{M}{EI} = \frac{d^2 y}{dx^2} = -\int_0^x V(x) dx$$

$$\text{Slope: } \theta = \frac{dy}{dx}$$

Strain energy:

$$\text{Normal stress: } U = \frac{P^2 l}{2AE}$$

$$\text{Bending stress: } U = \int_0^l \frac{M^2}{2EI} dx$$

$$\text{Torque: } U = \frac{T^2 l}{2GJ}$$

$$\text{Transverse shear: } U = \frac{3V^2 l}{5Gbh} \text{ (rectangular cross section)}$$

$$\text{Castigliano's Theorem: } y_i = \frac{\partial U}{\partial Q_i}$$

## Recommended Readings

- Beer, F.P., Johnson, E.R., DeWolf, J., and Mazurek, D. (2011) *Mechanics of Materials*, 6th ed., McGraw-Hill.
- Budynas, R.G., and Nisbett, J.K. (2011), *Shigley's Mechanical Engineering Design*, 9th ed., McGraw-Hill.
- Craig, R.R. (2001) *Mechanics of Materials*, 2nd ed., Wiley.
- Hibbeler, R.C. (2010) *Mechanics of Materials*, 8th ed. Prentice-Hall.
- Juvinal, R.C., and Marshek, K.M. (2012) *Fundamentals of Machine Component Design*, 5th ed., Wiley.
- Norton, R.L. (2011) *Machine Design*, 4th ed., Prentice-Hall.
- Popov, E.P. (1999) *Engineering Mechanics of Solids*, 2nd ed., Prentice-Hall.
- Riley, W.F., Sturges, L.D., and Morris, D.H. (2006) *Mechanics of Materials*, 6th ed., Wiley.
- Ugural, A.C. (2007) *Mechanics of Materials*, Wiley.

## Questions

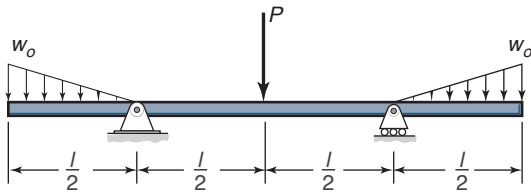
- 5.1 How are bending moment and deflection related in beams?
- 5.2 What is the moment-curvature relation?
- 5.3 How can one obtain deflection in a beam?
- 5.4 How does stress depend on the radius of curvature in a beam?
- 5.5 What are singularity functions?
- 5.6 What is the Method of Superposition?
- 5.7 What is the difference between strain and strain energy?
- 5.8 What is Castigliano's Theorem?
- 5.9 Why was a fictitious load used in Example 5.9?
- 5.10 What are the units of slope in Eq. (5.6)?

## Qualitative Problems

- 5.11 It was mentioned in the text that the radius of curvature in a beam is measured from the center of curvature to the inside surface of the beam. Can the radius of curvature ever equal zero? Explain.
- 5.12 Design Procedure 2.1 discussed singularity functions. Which of the rules are useful for the material presented in this chapter?
- 5.13 In general, what method for calculating beam deflection would you use for an impact loading?
- 5.14 Can the Method of Superposition be used for impact loads? Explain.
- 5.15 Could you use Castigliano's Theorem in Example 5.9 if the bars are replaced by cables? Why or why not?
- 5.16 List the strengths and weaknesses of singularity functions compared to direct integration in order to obtain beam deflection.
- 5.17 How can Castigliano's Theorem be used for statically indeterminate beams?
- 5.18 Define Castigliano's Theorem without the use of equations.
- 5.19 Can Castigliano's Theorem be used for viscoelastic materials? Explain.
- 5.20 Assume that the summary of the chapter is not present and write a suitable one- or two-page summary.

## Quantitative Problems

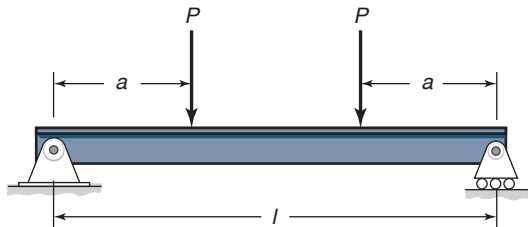
- 5.21 A beam is loaded by a concentrated bending moment  $M$  at the free end. Find the vertical and angular deformations along the beam by using the equation of the elastic line, Eq. (5.3). *Ans.*  $y = -\frac{Mx^2}{2EI}$ .
- 5.22 A simply supported beam of length  $l$  carries a force  $P$ . Find the ratio between the bending stresses in the beam when  $P$  is concentrated in the middle of the beam and evenly distributed along it. Use the moment-curvature relation given in Eq. (5.3). Also, calculate the ratio of the deformations at the middle of the beam. *Ans.*  $\frac{y_{\text{conc}}}{y_{\text{dist}}} = 1.6$ .
- 5.23 A simply supported beam with length  $l$  is centrally loaded with a force  $P$ . How large a moment needs to be applied at the ends of the beam
  - (a) To maintain the slope angle of zero at the supports? *Ans.*  $M_o = \frac{1}{8}Pl$ .
  - (b) To maintain the midpoint of the beam without deformation when the load is applied? Use the equation of the elastic line, Eq. (5.3). *Ans.*  $M_o = \frac{1}{6}Pl$ .



Sketch a, for Problem 5.24

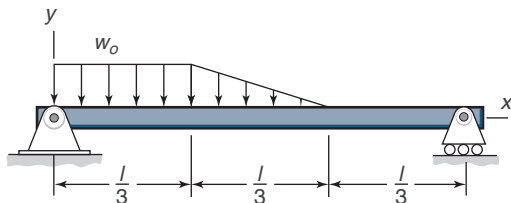
**5.24** Find the relation between  $P$  and  $w_o$  so that the slope of the deflected beam is zero at the supports for the loading conditions shown in Sketch a. Assume that  $E$  and  $A$  are constant. *Ans.*  $P = \frac{2}{3}w_o l$ .

**5.25** Given a simply supported beam with two concentrated forces acting on it as shown in Sketch b, determine the expression for the elastic deformation of the beam for any  $x$  by using singularity functions. Assume that  $E$  and  $I$  are constant. Also determine the location of maximum deflection and derive an expression for it.



Sketch b, for Problem 5.25

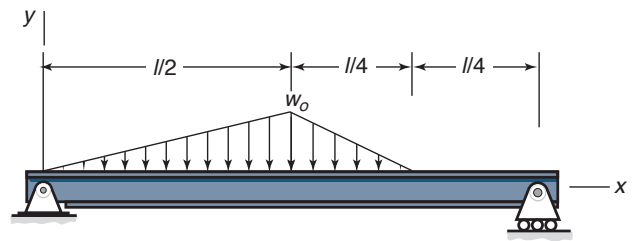
**5.26** For the loading condition described in Sketch c obtain the internal shear force  $V(x)$  and the internal moment  $M(x)$  by using singularity functions. Draw  $V(x)$ ,  $M(x)$ ,  $q(x)$ , and  $y(x)$  as a function of  $x$ . Assume that  $w_o = 9$  kN/m and  $l = 3$  m.



Sketch c, for Problem 5.26

**5.27** A simply supported beam is shown in Sketch d with  $w_o = 4$  kN/m and  $l = 12$  m.

- Draw the free-body diagram of the beam.
- Use singularity functions to determine shear force, bending moment, slope, and deflection.
- Construct diagrams of shear force, bending moment, slope, and deflection.

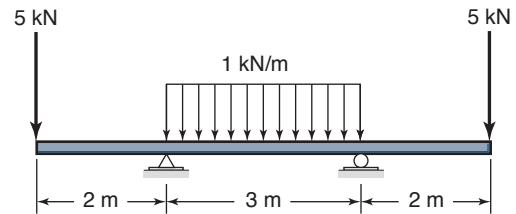


Sketch d, for Problem 5.27

**5.28** The simply supported beam in Problem 5.25 is altered so that instead of a concentrated force  $P$ , a concentrated moment  $M$  is applied at the same location. The moments are positive and act parallel with each other. Determine the deformation of the beam for any position  $x$  along it by using singularity functions. Assume that  $E$  and  $I$  are constant. Also, determine the location of the maximum deflection.

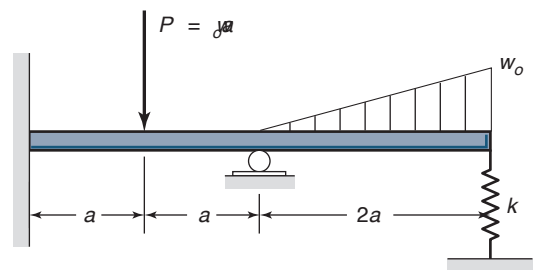
**5.29** The simply supported beam considered in Problem 5.28 has moments applied in opposite directions so that the moment at  $x = a$  is  $M_o$  and at  $x = l - a$  the moment is  $-M_o$ . Find the elastic deformation of the beam by using singularity functions. Also, determine the location and size of the maximum deflection.

**5.30** Given the loading condition shown in Sketch e, find the deflection at the center and ends of the beam. Assume that  $EI = 750$  kNm<sup>2</sup>. *Ans.*  $y_{\text{end}} = -0.05477$  m,  $y_{\text{mid}} = 0.01359$  m.



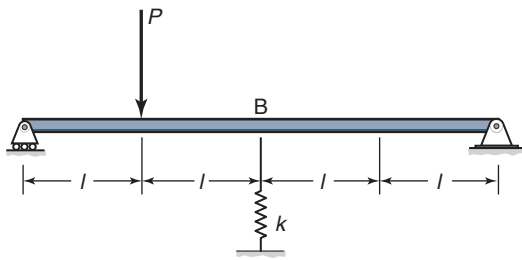
Sketch e, for Problem 5.30

**5.31** Given the loading condition shown in Sketch f obtain an expression for the deflection at any location on the beam. Assume that  $EI$  is constant.

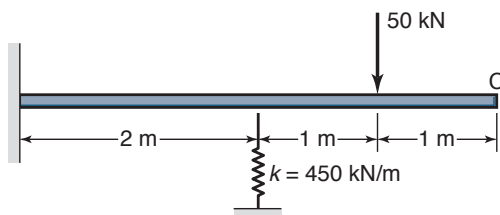


Sketch f, for Problem 5.31

**5.32** Given the loading condition and spring shown in Sketch g determine the stiffness of the spring so that the bending moment at point B is zero. Assume that  $EI$  is constant. *Ans.*  $k = \frac{2EI}{l^3}$ .

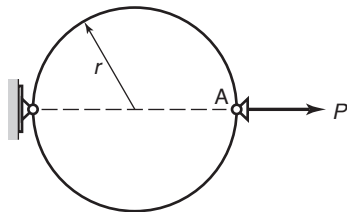
Sketch *g*, for Problem 5.32

- 5.33** When there is no load acting on the cantilevered beam shown in Sketch *h*, the spring has zero deflection. When there is a spring and a force of 20 kN is applied at point C, a deflection of 25 mm occurs at the spring. If a 50-kN load is applied at the location shown in Sketch *h*, what will be the deflection of the beam? Assume that the stiffness of the spring is 450 kN/m.

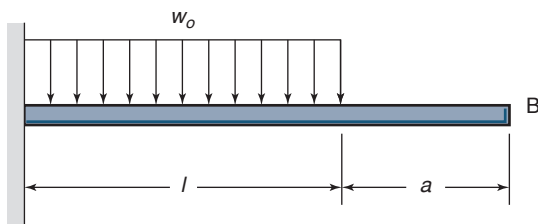
Sketch *h*, for Problem 5.33

- 5.34** Determine the deflection at point A and the maximum moment for the loading shown in Sketch *i*. Consider only bending effects and assume that  $EI$  is constant.

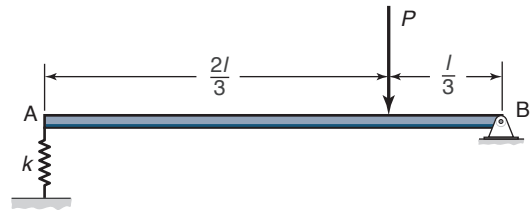
*Ans.*  $\delta_H = \frac{Pr^3\pi}{8EI}$ .

Sketch *i*, for Problem 5.34

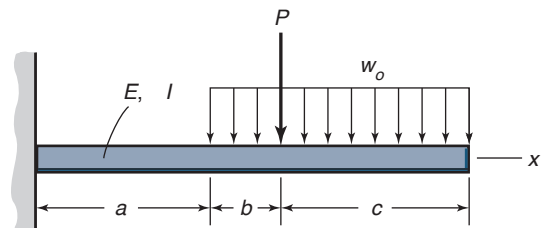
- 5.35** Determine the maximum deflection of the beam shown in Sketch *j*. *Ans.*  $y_{\max} = \frac{w_0 l^2}{24EI} (9l^2 + 20al + 12a^2)$ .

Sketch *j*, for Problem 5.35

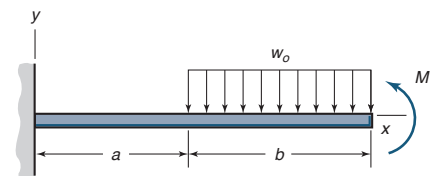
- 5.36** Determine the deflection at any point in the beam shown in Sketch *k* using singularity functions.

Sketch *k*, for Problem 5.36

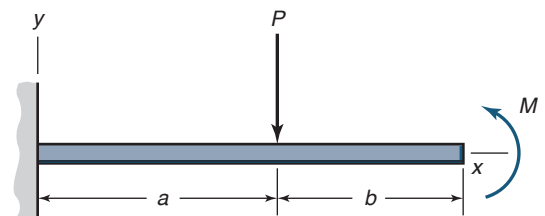
- 5.37** Determine the deformation of a cantilevered beam with loading shown in Sketch *l* as a function of  $x$ . Also determine the maximum bending stress in the beam and the maximum deflection. Assume that  $E = 207$  GPa,  $I = 2.50 \times 10^{-6} \text{ m}^4$ ,  $P = 1000$  N,  $w_0 = 3000$  N/m,  $a = 0.5$  m,  $b = 0.15$  m,  $c = 0.45$  m. The distance from the neutral axis to the outermost fiber of the beam is 0.040 m. *Ans.*  $y_{\max} = -0.5826$  mm,  $\sigma_{\max} = 33.44$  MPa.

Sketch *l*, for Problem 5.37

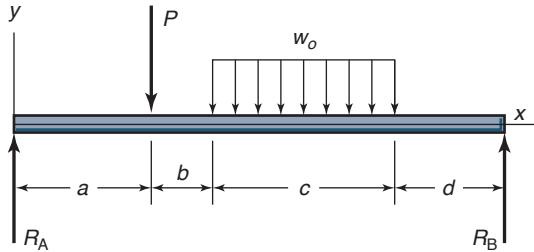
- 5.38** Given the loading shown in Sketch *m*, let  $a = 0.6$  m,  $b = 0.7$  m,  $M = 6500$  N-m, and  $w_0 = 20,000$  N/m. The beam has a square cross section with sides of 75 mm and the beam material has a modulus of elasticity of 207 GPa. Determine the beam deformation by using the method of superposition. Also, calculate the maximum bending stress and maximum beam deformation. *Ans.*  $y_{\max} = -3.988$  mm,  $\sigma_{\max} = 96.71$  MPa.

Sketch *m*, for Problem 5.38

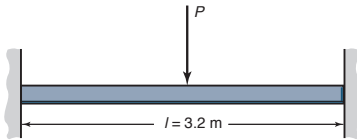
- 5.39** The cantilevered beam shown in Sketch *n* has both a concentrated force and a moment acting on it. Let  $a = 1$  m,  $b = 0.7$  m,  $P = 8700$  N, and  $M = 4000$  N-m. The beam cross section is rectangular with a height of 80 mm and a width of 35 mm. Also,  $E = 207$  GPa. Calculate the beam deformation by using the method of superposition. Find how large  $M$  has to be to give zero deformation at  $x = a$ . *Ans.*  $M = 5800$  Nm.

Sketch *n*, for Problem 5.39

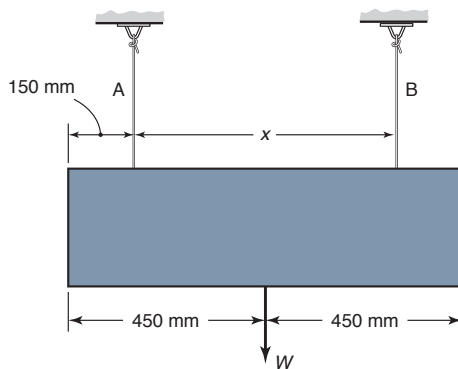
- 5.40** A simply supported beam has loads as shown in Sketch *o*. Calculate the beam deflection by using the method of superposition. Also, calculate the maximum bending stress and the deflection at mid-span. Assume that  $E = 207 \text{ GPa}$  and that the beam has a rectangular cross section with a height of 30 mm and a width of 100 mm. Also,  $P = 1200 \text{ N}$ ,  $w_o = 10,000 \text{ N/m}$ ,  $a = 0.2 \text{ m}$ ,  $b = 0.1 \text{ m}$ ,  $c = 0.4 \text{ m}$ , and  $d = 0.2 \text{ m}$ . *Ans.*  $\sigma_{\max} = 74.47 \text{ MPa}$ ,  $y_{\max} = -0.7277 \text{ mm}$ .

Sketch *o*, for Problem 5.40

- 5.41** The beam shown in Sketch *p* is fixed at both ends and center loaded with a force of 2300 N. The beam is 3.2 m long and has a square tubular cross section with an outside width of 130 mm and a wall thickness of 10 mm. The tube material is AISI 1080 high-carbon steel. Calculate the deformation along the beam by using the method of superposition. What is the deformation at mid-span? *Ans.*  $y(x = 1.6 \text{ m}) = 0.1593 \text{ mm}$ .

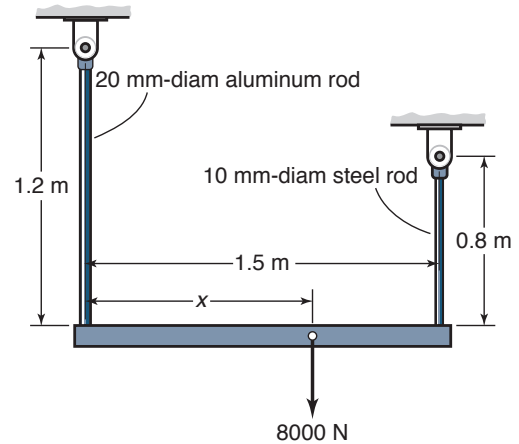
Sketch *p*, for Problem 5.41

- 5.42** Beam A shown in Sketch *q* is a 13-mm-diameter aluminum beam; beam B is an 8-mm-diameter steel beam. The lower member is of uniform cross section and is assumed to be rigid. Find the distance  $x$  if the lower member is to remain horizontal. Assume that the modulus of elasticity for steel is three times that for aluminum. *Ans.*  $x = 0.564 \text{ m}$ .

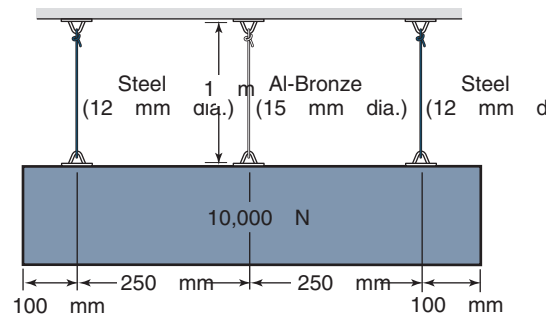
Sketch *q*, for Problem 5.42

- 5.43** An aluminum rod 20 mm in diameter and 1.2 m long and a nickel steel rod 10 mm in diameter and 0.8 m long are spaced 1.5 m apart and fastened to a horizontal beam

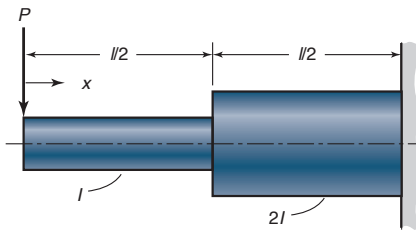
that carries an 8000-N load, as shown in sketch *r*. The beam is to remain horizontal after load is applied. Assume that the beam is weightless and absolutely rigid. Find the location  $x$  of the load and determine the stresses in each rod. *Ans.*  $x = 0.821 \text{ m}$ ,  $\sigma_A = 11.5 \text{ MPa}$ ,  $\sigma_B = 55.76 \text{ MPa}$ .

Sketch *r*, for Problem 5.43

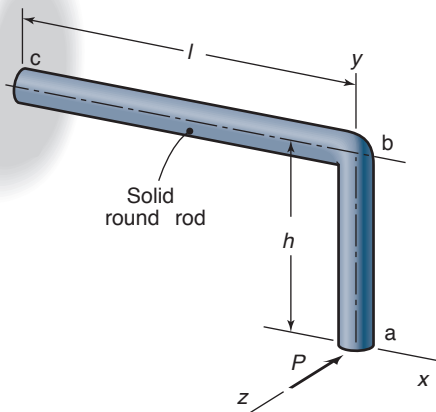
- 5.44** Find the force on each of the vertical wires shown in sketch *s*. The weight is assumed to be rigid and horizontal, implying that the three vertical bars are connected to the weight in a straight line. Also, assume that the support at the top of the bars is rigid. The bar materials and their circular cross-sectional area are given in the sketch. *Ans.*  $P_s = 3419 \text{ N}$ ,  $P_B = 3136 \text{ N}$ .

Sketch *s*, for Problem 5.44

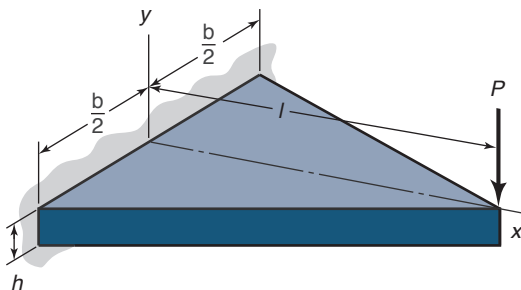
- 5.45** Two solid spheres, one made of aluminum alloy 2014 and the other made of AISI 1040 medium-carbon steel, are lowered to the bottom of the sea at a depth of 10,000 m. Both spheres have a diameter of 0.3 m. Calculate the elastic energy stored in the two spheres when they are at the bottom of the sea if the density of water is  $1000 \text{ kg/m}^3$  and the acceleration of gravity is  $9.807 \text{ m/s}^2$ . Also, calculate how large the steel sphere has to be to have the same elastic energy as the 0.3-m-diameter aluminum sphere. *Ans.*  $U_{al} = 960.6 \text{ Nm}$ ,  $U_s = 393.1 \text{ Nm}$ .
- 5.46** Use Castigliano's approach instead of singularity functions to determine the maximum deflection of the beam considered in Problem 5.25. Assume that transverse shear is negligible.
- 5.47** Using Castigliano's Theorem, find the maximum deflection of the two-diameter cantilevered beam shown in Sketch *t*. Neglect transverse shear. *Ans.*  $y = \frac{3Pl^3}{16EI}$ .

Sketch *t* for Problem 5.47

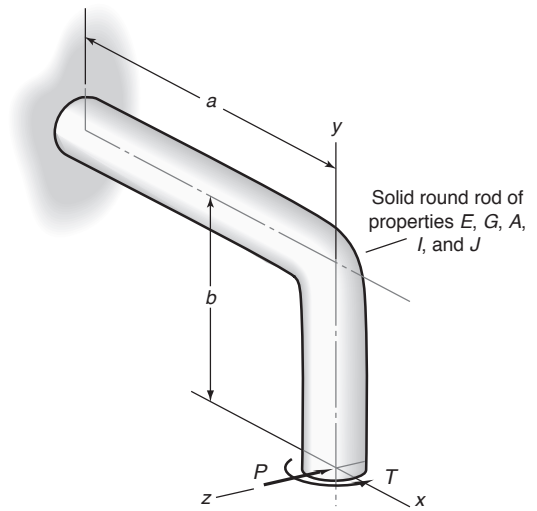
- 5.48** The right-angle-cantilevered bracket shown in Sketch *u* is loaded with force  $P$  in the  $z$ -direction. Derive an expression for the deflection of the free end in the  $z$ -direction by using Castigliano's Theorem. Neglect transverse shear effects.

Sketch *u* for Problem 5.48

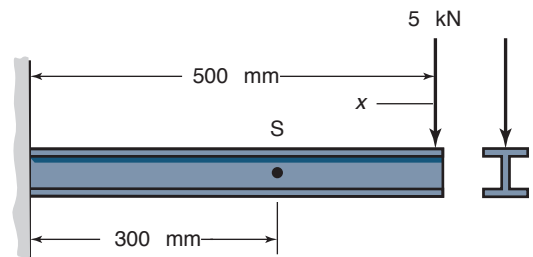
- 5.49** A triangular cantilevered plate is shown in Sketch *v*. Use Castigliano's Theorem to derive an expression for the deflection at the free end, assuming that transverse shear is neglected. *Ans.*  $\delta = \frac{6Pl^3}{Ebh^3}$ .

Sketch *v* for Problem 5.49

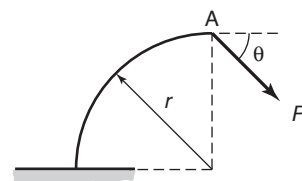
- 5.50** A right-angle-cantilevered bracket with concentrated load and torsional loading at the free end is shown in Sketch *w*. Using Castigliano's Theorem, find the deflection at the free end in the  $z$ -direction. Neglect transverse shear effects.

Sketch *w* for Problem 5.50

- 5.51** A cantilevered I-beam has a concentrated load applied to the free end as shown in Sketch *x*. What upward force at point S is needed to reduce the deflection at S to zero? Use Castigliano's Theorem. Transverse shear can be neglected. *Ans.*  $S_y = 10 \text{ kN}$ .

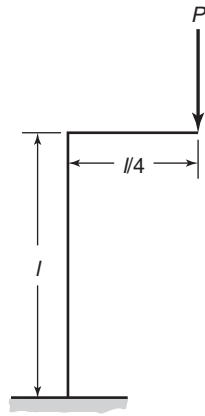
Sketch *x* for Problem 5.51

- 5.52** Using Castigliano's Theorem calculate the horizontal and vertical deflections at point A shown in Sketch *y*. Assume that  $E$  and  $A$  are constant.

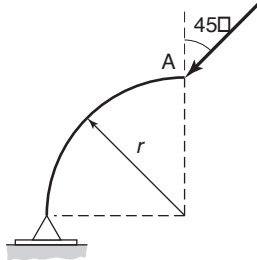
Sketch *y* for Problem 5.52

- 5.53** Calculate the deflection at the point of load application and in the load direction for a load applied as shown in Sketch *z*. Assume that  $E$  and  $I$  are constant.

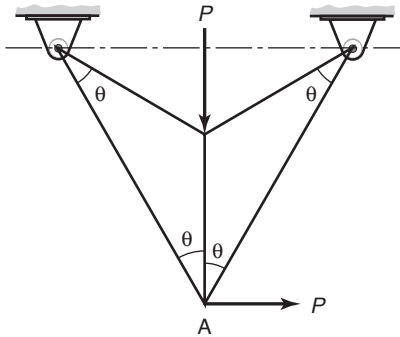


Sketch *z*, for Problem 5.53

- 5.54 Using Castigliano's Theorem determine the horizontal and vertical deflections at point A of Sketch *aa*. Assume that  $E$  and  $I$  are constant.

Sketch *aa* for Problem 5.54

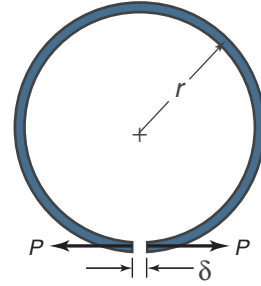
- 5.55 For the structure shown in Sketch *bb* find the force in each member and determine the deflection at point A. Assume that  $E$  and  $A$  are the same in each member.

Sketch *bb* for Problem 5.55

- 5.56 Obtain the maximum deflection of the beam given in Problem 2.59 as a function of the load  $P$ , span  $l$ , moment of inertia,  $I$ , and elastic modulus,  $E$ . *Ans.*  $y_{\max} = -0.2292Pl^3$ .

## Design and Projects

- 5.57 Construct a Design Procedure for the Method of Superposition.
- 5.58 Design an experiment to verify the energy stored in a beam is as given in Table 5.1.
- 5.59 Sketch *cc* shows a split ring used as a compression ring on an automotive piston (see also Fig. 12.31). To install the ring, it is necessary to open a gap  $\delta$  as shown. If  $EI$  of the cross section is constant, derive the required force  $P$  as a function of ring radius. *Ans.*  $P = \frac{\delta EI}{3\pi r^3}$ .

Sketch *cc*, for Problem 5.59

- 5.60 Consider the situation of a golf club striking a golf ball. Set up a system of equations to describe the deformation and motion of the golf ball.
- 5.61 Table 5.1 has an entry for the strain energy associated with transverse shear for a rectangular beam. Why is there no entry for circular cross-sections? Explain.
- 5.62 Assume you are the instructor of a course covering the subject matter in this chapter. Prepare two qualitative and two quantitative problems for the chapter and provide solutions.

## Chapter 6

# Failure Prediction for Static Loading



The liberty bell, a classic case of brittle fracture. Source: Shutterstock.

*The concept of failure is central to the design process, and it is by thinking in terms of obviating failure that successful designs are achieved.*

Henry Petroski, *Design Paradigms*

### Contents

- 6.1 Introduction 134
- 6.2 Stress Concentration 134
- 6.3 Fracture Mechanics 140
- 6.4 Modes of Crack Growth 141
- 6.5 Fracture Toughness 141
- 6.6 Failure Prediction for Uniaxial Stress State 143
- 6.7 Failure Prediction for Multiaxial Stress State 144
- 6.8 Summary 152

### Examples

- 6.1 Theoretical Stress Concentration Factor 135
- 6.2 Allowable Loads in the Presence of a Stress Concentration 136
- 6.3 Critical Crack Length 142
- 6.4 Allowable Crack Length 142
- 6.5 Uniaxial Failure of a Leaf Spring 143
- 6.6 Determination of von Mises Stress 145
- 6.7 Yielding of a Ductile Bar 146
- 6.8 Yield Criteria Applied to Design 146
- 6.9 Failure of a Brittle Bar 149
- 6.10 Selection of Yield and Failure Criteria 150

### Design Procedures

- 6.1 Fracture Mechanics Applied to Design 142
- 6.2 Selection of a Failure Criterion 150

### Case Study

- 6.1 Stress Concentrations for Complicated Geometries 150

Static failure involves excessive deformation or fracture under relatively constant loads, often complicated by the presence of geometric or material discontinuities called stress concentrations. Stress concentrations commonly occur when the cross section of a part changes over a short distance, so that the largest stress encountered is higher than the nominal stress. The chapter presents stress concentration factors for the common and important situations encountered in design. The chapter then investigates fracture mechanics, including the modes of crack displacement and the circumstances under which a crack can propagate across a part and cause its failure, including the importance of a material's fracture toughness. Uniaxial and multiaxial failure theories are then presented to provide criteria for failure (yielding, crumbling, or fracture) for different materials, and discusses the conditions when the different failure criterion are used.

## Symbols

$A$	area, $m^2$
$a$	half of crack length, $m$
$b$	plate width, $m$
$c$	distance from neutral axis to outer fiber, $m$
$D$	major diameter, $m$
$d$	diameter, $m$
$H$	major height, $m$
$h$	minor height, $m$
$I$	area moment of inertia, $m^4$
$J$	polar area moment of inertia, $m^4$
$K_c$	stress concentration factor
$K_{Ic}$	fracture toughness, $MPa\sqrt{m}$
$K_i$	stress intensity factor, $MPa\sqrt{m}$
$l$	length, $m$
$M$	bending moment, $N\cdot m$
$n_s$	safety factor
$P$	force, $N$
$q$	volume flow rate, $m^3/s$
$r$	radius, $m$
$S_{uc}$	ultimate stress in compression, $Pa$
$S_{ut}$	ultimate stress in tension, $Pa$
$S_y$	yield stress, $Pa$
$S_{yt}$	yield stress in tension, $Pa$
$T$	torque, $N\cdot m$
$u$	velocity, $m/s$
$Y$	geometry correction factor
$\sigma$	normal stress, $Pa$
$\sigma_e$	von Mises stress, $Pa$
$\sigma_1, \sigma_2, \sigma_3$	principal normal stresses, $Pa$
$\tau$	shear stress, $Pa$

## 6.1 Introduction

This chapter considers static loads, where the load is gradually applied and equilibrium is reached in a relatively short time. Under static loads, a machine element may often fail at sites of local stress concentration caused by geometrical or microstructural discontinuities. Calculation of stress concentration factors is examined in detail in Section 6.2, and the mechanics are explained through a flow analogy. Another failure mode that is often encountered is fracture, whereby cracks within a microstructure grow or propagate in an uncontrolled fashion, leading to failure. Fracture mechanics is a technique used to determine the stress level at which pre-existing cracks of known size will propagate, or the largest allowable crack for a given stress and material can be estimated. Geometric factors and a material property called fracture toughness are used in the theory. The chapter ends with failure criteria for both uniaxial and multiaxial stress states. The most common failure criteria in engineering practice are presented, and their applicability to different materials is discussed.

## 6.2 Stress Concentration

Stresses at or near a *discontinuity*, such as a hole in a plate, are higher than if the discontinuity did not exist. Figure 6.1 shows a rectangular bar with a hole under an axial load. The stress is largest near the hole; therefore, failure will first occur at the hole. The same can be deduced for any other discontinuity, such as a fillet (a narrowing in the width of a plate), a notch (a sharp groove or cut especially intended to initiate

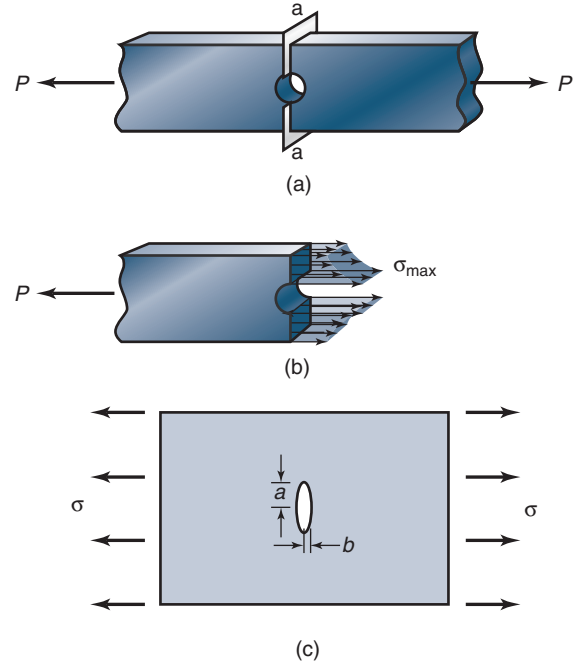


Figure 6.1: Rectangular plate with hole subjected to axial load. (a) Plate with cross-sectional plane. (b) Half of plate showing stress distribution. (c) Plate with elliptical hole subjected to axial load.

failure), an inclusion (such as a discontinuous fiber in a polymer matrix), or in the vicinity of applied loads.

A **stress raiser** is any discontinuity in a part that alters the stress distribution so that the elementary stress equations described in Ch. 4 no longer describe the stress in the part. The **stress concentration** is the region where stress raisers are present. The **stress concentration factor**,  $K_c$ , is the factor used to relate the actual maximum stress at the discontinuity to the average or nominal stress:

$$K_c = \frac{\sigma_{max}}{\sigma_{nom}}. \quad (6.1)$$

The stress concentration factor allows consideration of stress raisers without excessively complicating the mathematics. The value of  $K_c$  is usually determined by some experimental technique, such as photoelastic analysis of a plastic model of a part, or by analytical or numerical simulation of the stress field.

An understanding of stress concentrations can be obtained by considering the example of an elliptical hole in a plate loaded in tension, as depicted in Fig. 6.1c. The theoretical stress concentration at the edge of the hole is given by

$$K_c = 1 + 2 \left( \frac{a}{b} \right). \quad (6.2)$$

where  $a$  is the half-length of the ellipse transverse to the stress direction and  $b$  is the half-width in the direction of applied stress. Note that as  $b$  approaches zero, the ellipse becomes sharper, and the situation approaches that of a very sharp crack. If the crack is sharp and has a tip radius of  $\rho$ , the theoretical stress concentration factor is given by

$$K_c = 1 + 2 \left( \sqrt{\frac{a}{\rho}} \right). \quad (6.3)$$

For this case, the stress at the edge of the crack is very large (infinite in the limiting case of  $\rho = 0$ ). As either  $a$  approaches zero or  $b$  or  $\rho$  becomes very large, the effects of the stress concentration become smaller. Thus, the size and orientation of geometric discontinuities with respect to applied stress play a large role in determining the stress concentration. For more complicated situations, additional factors will play a role, as discussed in the following section.

It should also be noted that stress concentrations can arise from abrupt variations in material properties such as elastic modulus, thermal expansion coefficient, or thermal conductivity. The greater the change in properties in the area of interest, the higher the stress concentration. Thus, the design goal is to try to use constant geometries and use materials that have uniform properties. When this is not practical, the changes should be as gradual as possible.

### 6.2.1 Stress Concentration Factor Charts

As discussed above, the stress concentration factor is a function of the type and shape of the discontinuity (hole, fillet, or groove), and the type of loading being experienced. Consideration here will be limited to only two geometries, a flat plate and a round bar. Figures 6.2 to 6.4 display the stress concentration factor due to bending and axial load for a flat plate with a hole, fillet, or groove. These figures also give the expressions for nominal stresses. Many of these curves are developed from photoelastic studies. Note from Fig. 6.2a that a small hole in a plate loaded in tension ( $d/b \rightarrow 0$ ) leads to  $K_c = 3.0$ , which is consistent with Eq. (6.2). Figures 6.5 and 6.6 show the stress concentration factor for a round bar with a fillet and a groove, respectively. Figure 6.7 shows the stress concentration factor for a flat groove, such as is used as a seat for retaining rings (see Section 11.7). Figure 6.8 shows the effect of a radial hole in a shaft. These examples are by no means all the possible geometries, but are those most often encountered in practice; for other geometries, refer to Pilkey and Pilkey [2008] or Young and Budynas [2001].

From these figures, the following observations can be made about stress concentration factors:

1. The stress concentration factor,  $K_c$ , is independent of material properties.
2.  $K_c$  is significantly affected by part geometry. Note that as the radius of the discontinuity is decreased, the stress concentration is increased.
3.  $K_c$  is also affected by the type of discontinuity; the stress concentration factor is considerably lower for a fillet (Fig. 6.3) than for a hole (Fig. 6.2).

The stress concentration factors given in Figs. 6.2 to 6.8 were determined on the basis of static loading, with the additional assumption that the stress in the material does not exceed its proportional limit. In practice, this is usually approximated by the yield stress. If the material is brittle, the proportional limit is the rupture stress, so failure for this part will begin at the point of stress concentration when the proportional limit is reached. It is thus important to apply stress concentration factors when using brittle materials. On the other hand, if the material is ductile and subjected to a static load, designers often neglect stress concentration factors, since a stress that exceeds the proportional limit will not result in a crack. Instead, the ductile material will flow plastically and can strain harden. Furthermore, as a material yields near a stress concentration, deformation results in blunting of notches, so that the stress concentration is reduced. In applications where stiff designs and tight tolerances are essential,

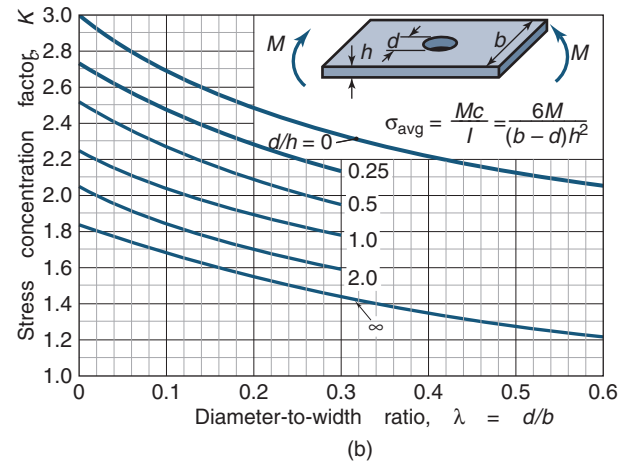
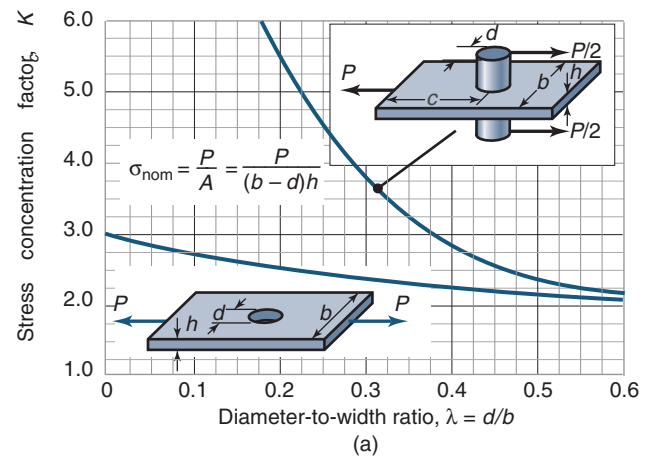


Figure 6.2: Stress concentration factors for rectangular plate with central hole. (a) Axial load and pin-loaded hole; (b) bending.

stress concentration should be considered regardless of material ductility.

### Example 6.1: Theoretical Stress Concentration Factor

**Given:** A flat plate made of a brittle material and a width of  $b = 20$  mm, a major height of  $H = 100$  mm, a minor height of  $h = 50$  mm, and a fillet radius of  $r = 10$  mm.

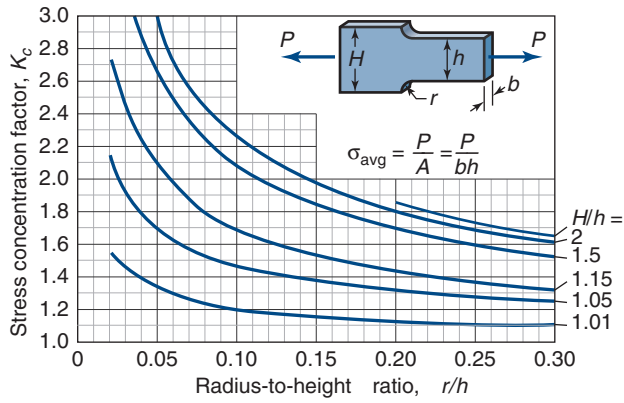
**Find:** The stress concentration factor and the maximum stress for the following conditions:

- (a) Axial loading with  $P = 10,000$  N
- (b) Pure bending with  $M = 100$  Nm
- (c) Axial loading of  $P = 10,000$  N, with fillet radius reduced to 5 mm.

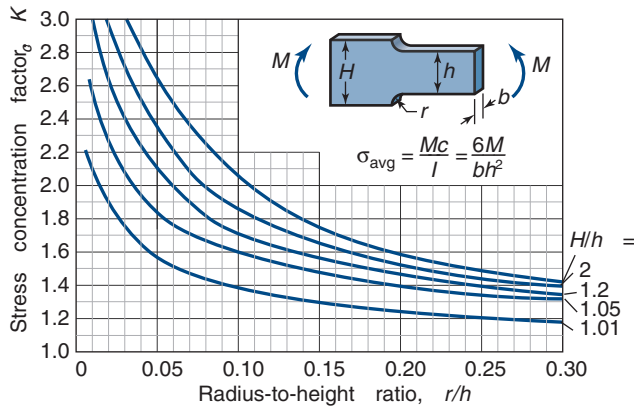
**Solution:**

- (a) Axial loading. Note from the geometry that

$$\frac{H}{h} = \frac{100}{50} = 2.0.$$

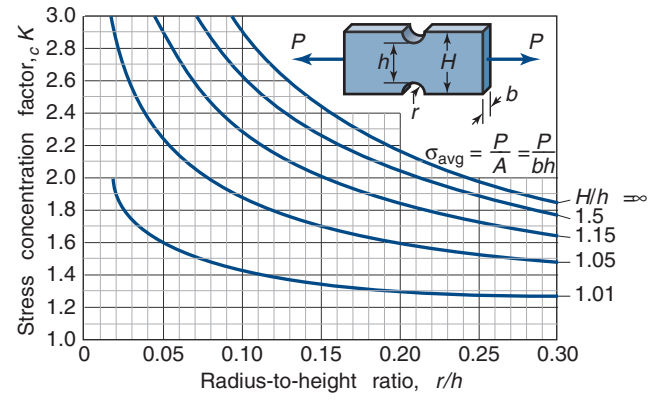


(a)

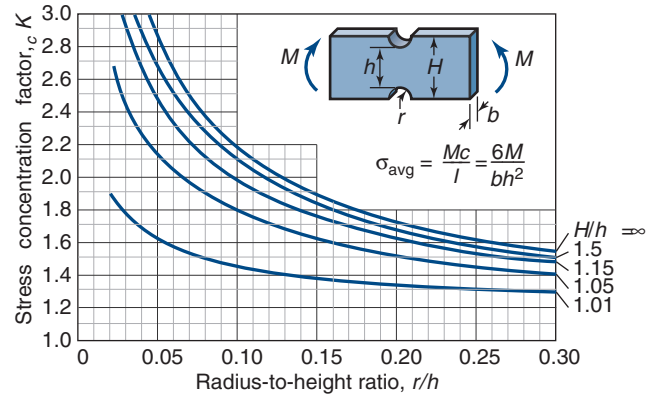


(b)

Figure 6.3: Stress concentration factors for rectangular plate with fillet. (a) Axial load; (b) bending.



(a)



(b)

Figure 6.4: Stress concentration factors for rectangular plate with groove. (a) Axial load; (b) bending.

$$\frac{H}{h} = \frac{100}{50} = 2.0.$$

Also,

$$\frac{r}{h} = \frac{10}{50} = 0.2.$$

From Fig. 6.3a,  $K_c = 1.8$ . From Eq. (6.1) and Fig. 6.3a, the maximum stress is

$$\sigma_{\max} = 1.8\sigma_{\text{avg}} = \frac{1.8(10,000)}{(0.02)(0.05)} = 18 \text{ MPa}.$$

(b) Pure bending. From Fig. 6.3b,  $K_c = 1.5$ . The maximum stress is

$$\sigma_{\max} = 1.5 \frac{6M}{bh^2} = \frac{9(100)}{(0.02)(0.05)^2} = 18 \text{ MPa}.$$

(c) Axial loading but with fillet radius changed to 5 mm. For this case

$$\frac{r}{h} = \frac{5}{50} = 0.1.$$

From Fig. 6.3a,  $K_c = 2.1$ . The maximum stress is

$$\sigma_{\max} = \frac{2.1P}{bh} = \frac{(2.1)(10,000)}{(0.02)(0.05)} = 21 \text{ MPa}.$$

Thus, reducing the fillet radius by one-half increases the maximum stress by around 17%.

## Example 6.2: Allowable Loads in the Presence of a Stress Concentration

**Given:** A 50-mm-wide, 5-mm-high rectangular plate has a 5-mm-diameter central hole. The allowable tensile stress is 700 MPa.

**Find:**

- The maximum tensile force that can be applied.
- The maximum bending moment that can be applied to reach the maximum stress.
- The maximum tensile force and the maximum bending moment if the hole is not present. Express the results as a ratio when compared to parts (a) and (b).

**Solution:**

(a) The diameter-to-width ratio is  $d/b = 5/50 = 0.1$ . The cross-sectional area with the hole is

$$A = (b-d)h = (50-5)5 = 225 \text{ mm}^2 = 0.225 \times 10^{-3} \text{ m}^2.$$

From Fig. 6.2a for  $d/b = 0.1$  the stress concentration factor  $K_c = 2.70$  for axial loading. The maximum force is

$$P_{\max} = \frac{(700 \times 10^6)(0.225 \times 10^{-3})}{2.70} = 58,330 \text{ N}.$$



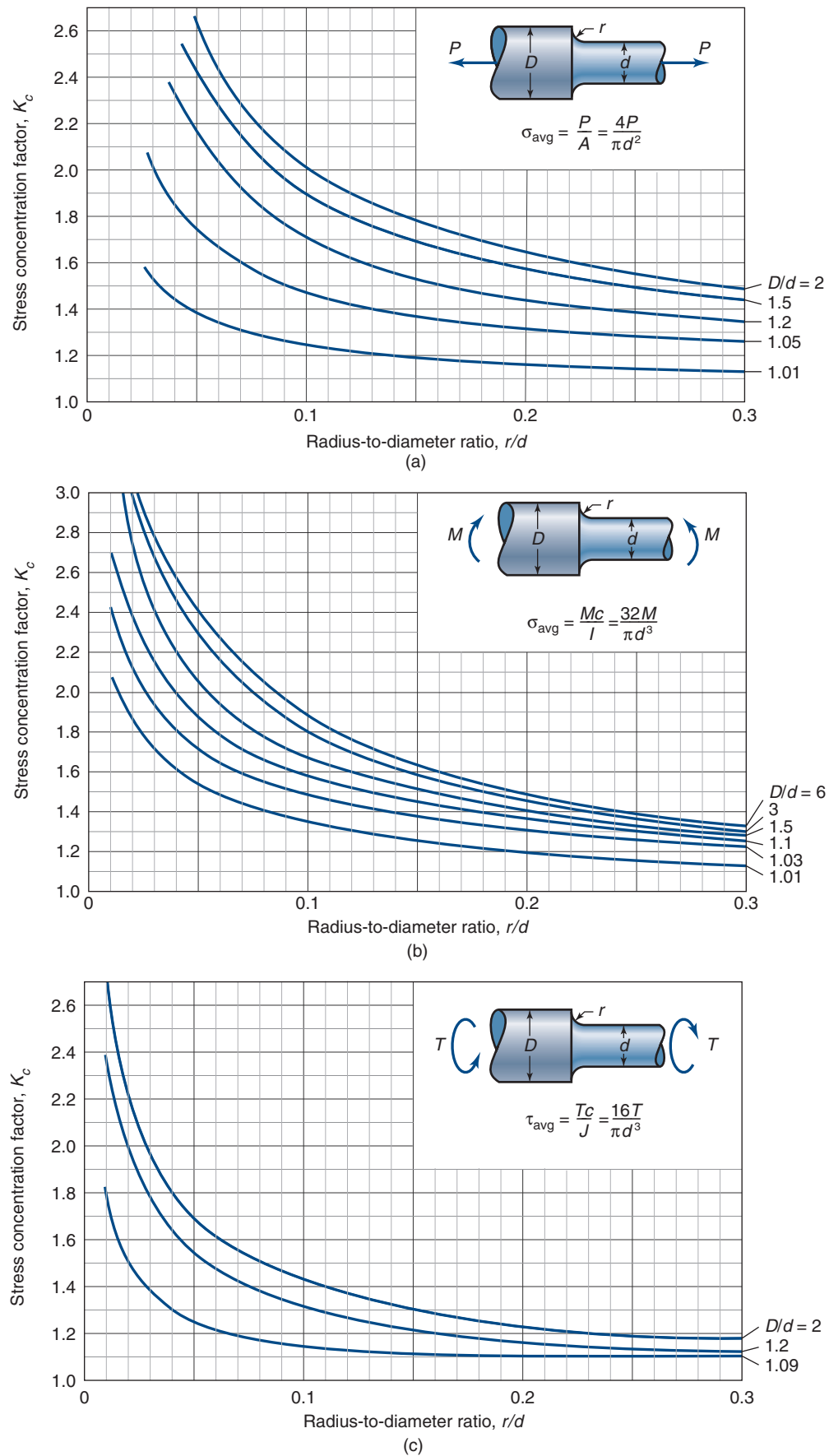


Figure 6.5: Stress concentration factors for round bar with fillet. (a) Axial load; (b) bending; (c) torsion.

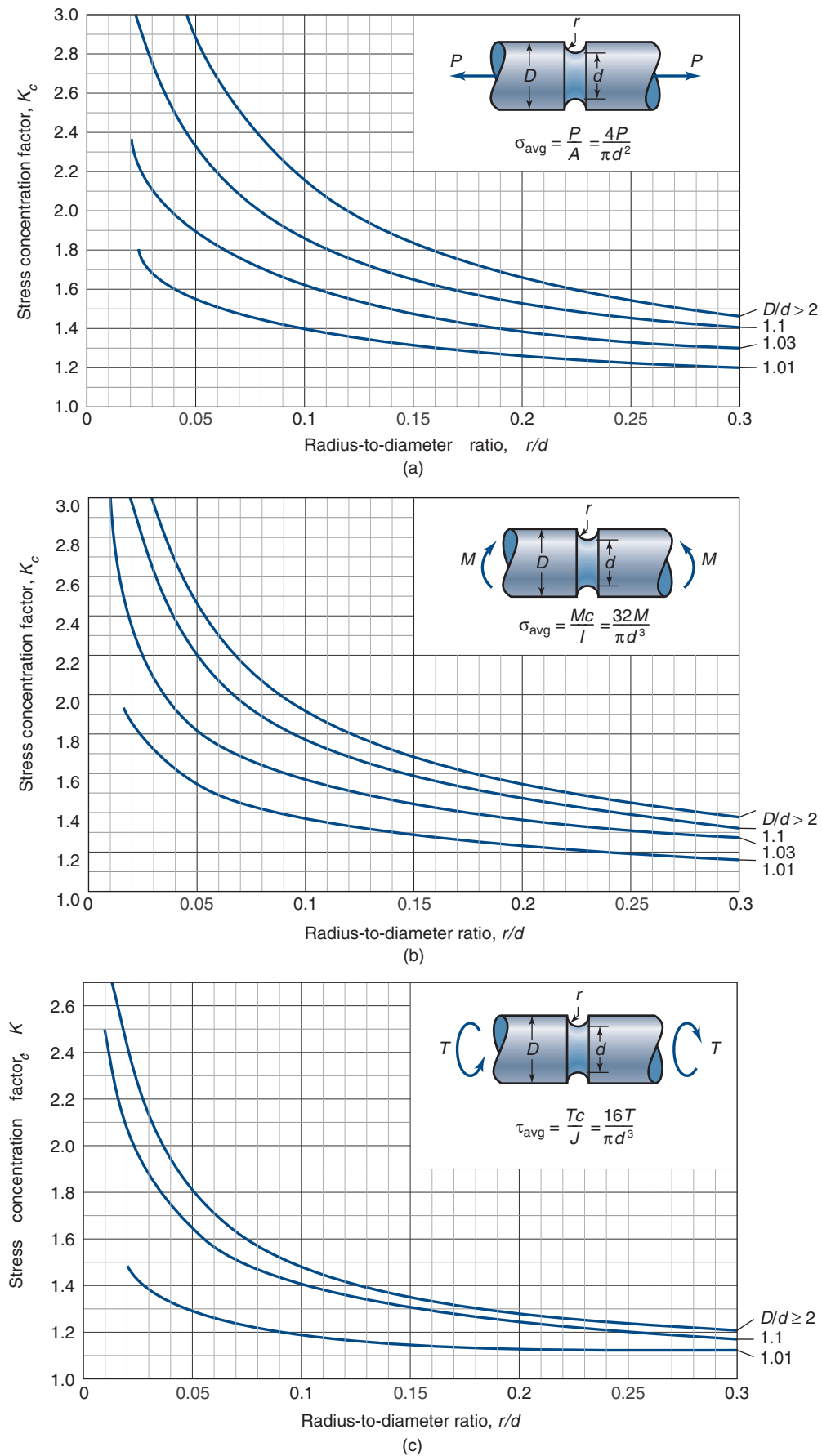
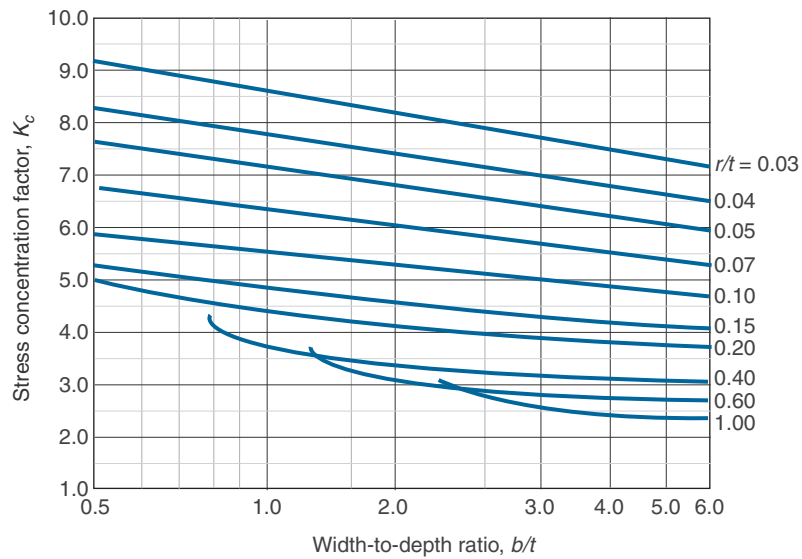
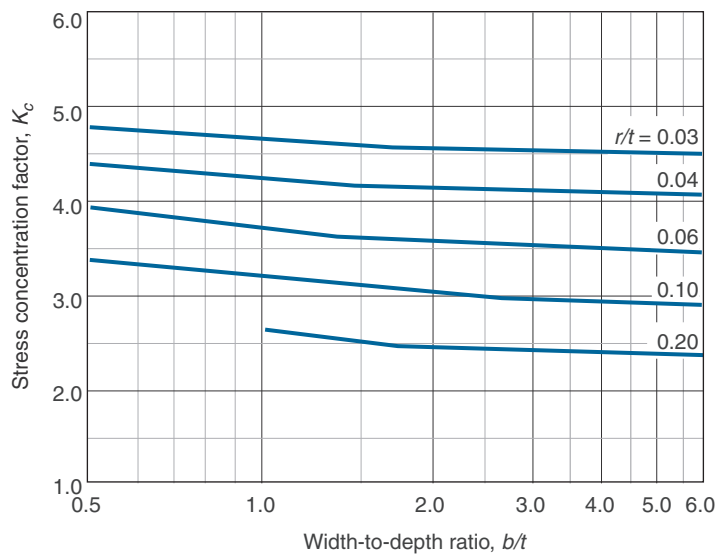
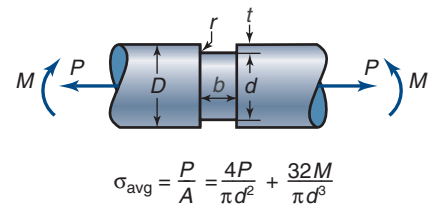


Figure 6.6: Stress concentration factors for round bar with groove. (a) Axial load; (b) bending; (c) torsion.



(a)



(b)

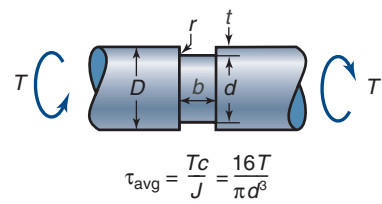


Figure 6.7: Stress concentration factors for round bar with a flat groove.

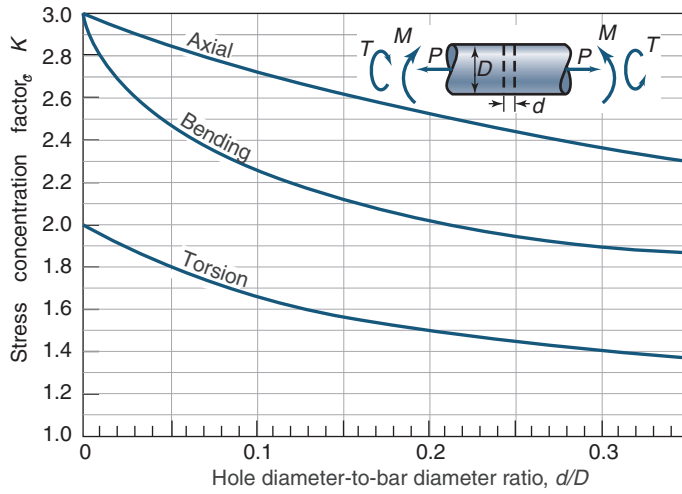


Figure 6.8: Stress concentration factors for round bar with hole.

**Nominal stresses:**

Axial load:

$$\sigma_{\text{avg}} = \frac{P}{A} = \frac{P}{(\pi D^2/4) - Dd}$$

Bending (plane shown is critical):

$$\sigma_{\text{nom}} = \frac{Mc}{I} = \frac{M}{(\pi D^3/32) - (dD^2/6)}$$

Torsion:

$$\tau_{\text{avg}} = \frac{Tc}{J} = \frac{T}{(\pi D^3/16) - (dD^2/6)}$$

- (b) From Fig. 6.2b for bending when  $d/b = 0.1$  and  $d/h = 5/5 = 1$ , the stress concentration factor is  $K_c = 2.04$ . The maximum bending moment is

$$\begin{aligned} M_{\text{max}} &= \frac{(b-d)h^2\sigma_{\text{all}}}{6K_c} \\ &= \frac{(0.225 \times 10^{-3})(5 \times 10^{-3})(700 \times 10^6)}{6(2.04)} \\ &= 64.34 \text{ Nm.} \end{aligned}$$

- (c) The cross-sectional area without the hole is

$$A = bh = (50)5 = 250 \text{ mm}^2 = 0.250 \times 10^{-3} \text{ m}^2.$$

Therefore,

$$P_{\text{max}} = \sigma_{\text{all}}A = (700 \times 10^6)(0.250 \times 10^{-3}) = 175 \text{ kN.}$$

The force ratio is  $175/58.33=3.00$ . For bending,

$$\begin{aligned} M_{\text{max}} &= \frac{\sigma_{\text{all}}bh^2}{6} = \frac{\sigma_{\text{all}}Ah}{6} \\ &= \frac{(700 \times 10^6)(0.25 \times 10^{-3})(5 \times 10^{-3})}{6} \\ &= 145.8 \text{ Nm.} \end{aligned}$$

The bending moment ratio is  $145.8/64.34 = 2.266$ .

potential in fluid mechanics and stress potential in solid mechanics are of the same form.

If the channel has constant dimensions throughout, the velocities are uniform and the streamlines are equally spaced. Similarly, for a bar of constant dimensions under axial load, the stresses are uniform and stress contours are equally spaced. At any point within the channel the flow must be constant, where the volume flow is

$$q = \int u \, dA. \quad (6.4)$$

From solid mechanics, the force must be constant at any location in the plate,

$$P = \int \sigma \, dA. \quad (6.5)$$

If the channel section changes sharply, the flow velocity increases near the shape change and, in order to maintain equal flow, the streamlines must narrow and crowd together. In a stressed member of the same cross section, the increase in stress is analogous to the increase in fluid velocity, or inversely to the change in the spacing of the streamlines. Figure 6.9a shows the stress distribution around the sharp corners of an axially loaded flat plate. The situation in Fig. 6.9a produces a stress concentration factor greater than 3. Recall from Eq. (6.1) that this implies that the maximum stress is more than three times greater than the average stress. However, this stress concentration factor can be reduced, typically from 3 down to around 1.5, by rounding the corners as shown in Fig. 6.9b. A still further reduction in stress concentration factor can be achieved by introducing small grooves or holes, as shown in Fig. 6.9c and d, respectively. In Fig. 6.9b to d, the design helps to reduce the rigidity of the material at the corners, so that the stress and strain are more evenly spread throughout the flat plate. The improvements in these designs can be gleaned from the flow analogy.

## 6.2.2 Flow Analogy

Good practice drives the designer to reduce or eliminate stress concentrations as much as is practical. Recommending methods of reducing the stress concentration requires better understanding of what occurs at the discontinuity to increase the stress. One way of achieving this understanding is to observe similarity between the velocity of fluid flow in a channel and the stress distribution of an axially loaded plate when the channel dimensions are comparable to the size of the plate. The analogy is accurate, since the equations of flow

## 6.3 Introduction to Fracture Mechanics

The science of flaw development and crack extension as a function of applied load is called **fracture mechanics**. A **crack**

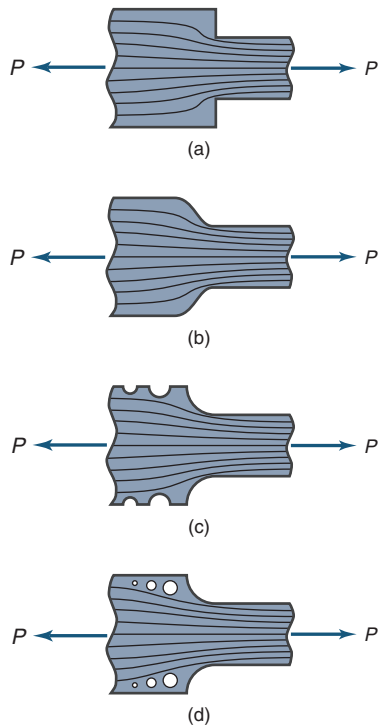


Figure 6.9: Axially loaded flat plate with fillet showing stress contours: (a) square corners, (b) rounded corners, (c) small grooves, and (d) small holes.

is an initially small (perhaps microscopic) flaw that exists under normal conditions on the surface and within the body of the material. No materials or manufacturing processes yield defect-free structures, hence such imperfections are always present. Under an applied stress, the crack can grow, resulting in a small extension; if the stress is high enough, the crack will grow rapidly and cause material failure by propagating across an entire cross section.

Lower stress is required to propagate a crack than to start one. Many consumer product packages are designed with a perforation or edge notch to allow a person to manually open the package; this is a demonstration of crack propagation. Clearly, without a perforation, such packaging would be much more difficult to open. Fracture can occur at stress levels well below the yield stress of a solid material. Fracture mechanics is a highly developed field, and is used extensively for fatigue (Ch. 7) or fatigue wear (Ch. 8). This chapter examines the critical crack length that will make a part fail under static loads. **Fracture control** consists of maintaining nominal stresses and existing cracks below a critical level for the material being used.

## 6.4 Modes of Crack Growth

There are three fundamental **modes of crack propagation**, as shown in Fig. 6.10:

1. *Mode I – opening*. The opening (or tensile) mode, shown in Fig. 6.10a, is the most often encountered mode of crack propagation. The crack faces separate symmetrically with respect to the crack plane.
2. *Mode II – sliding*. The sliding (or in-plane shearing) mode occurs when the crack faces slide relative to each

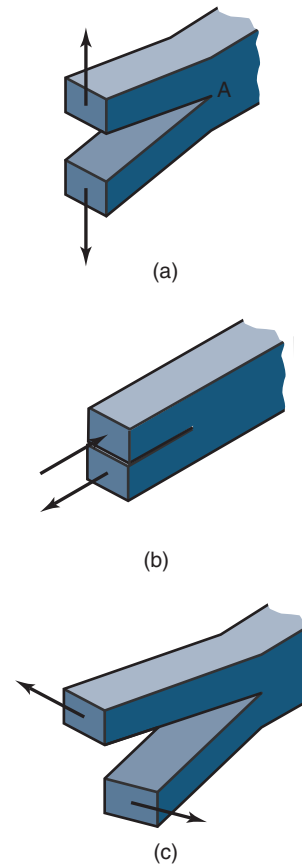


Figure 6.10: Three modes of crack displacement. (a) Mode I, opening; (b) Mode II, sliding; (c) Mode III, tearing.

other symmetrically with respect to the normal to the crack plane but asymmetrically with respect to the crack plane, as shown in Fig. 6.10b.

3. *Mode III – tearing*. The tearing (or antiplane) mode occurs when the crack faces slide asymmetrically with respect to both the crack plane and its normal, as illustrated in Fig. 6.10c.

The crack propagation modes are known by their Roman numeral designations given above (e.g., Mode I). Although Mode I is the easiest to visualize as a crack-propagating mechanism, applying the discussion of stress raisers in Section 6.2 to geometries such as Fig. 6.10 suggests that crack propagation will occur when stresses are higher at the crack tip than elsewhere in the solid.

## 6.5 Fracture Toughness

In this text, considerations of fracture toughness are restricted to Mode I crack propagation since this is the most commonly encountered failure. An important concept is that of **stress intensity factor**,  $K_i$ , which specifies the stress intensity at the crack tip (see point A in Fig. 6.10a). The SI unit of  $K_i$  is megapascals times meters<sup>1/2</sup> (MPa√m). The equation for stress intensity factor is

$$K_i = Y\sigma\sqrt{\pi a}, \quad (6.6)$$

where

$Y$  = dimensionless correction factor that accounts for



geometry of the part containing a crack  
 $\sigma$  = nominal stress, MPa  
 $a$  = one-half of crack length, m

The values of  $Y$  for common cases are summarized in Appendix C. Some assumptions imposed in deriving Eq. (6.6) are that the load is applied far from the crack and that the crack length,  $2a$ , is small relative to the width.

**Fracture toughness** is the critical value of stress intensity at which crack extension occurs, and is a material property. Fracture toughness is used as a design criterion in fracture prevention for brittle materials, just as yield strength is used as a design criterion to avoid plastic deformation in ductile materials. At fracture, the stress intensity factor, given by Eq. (6.6), will equal the fracture toughness. Table 6.1 shows room-temperature yield stress and fracture toughness data for selected engineering materials. Fracture toughness is denoted as  $K_{Ic}$  to indicate that it corresponds to Mode I and that it is a critical stress intensity factor.  $K_{Ic}$  depends on many factors, with the most important being temperature, strain rate, and microstructure. The magnitude of  $K_{Ic}$  diminishes with increasing strain rate and decreasing temperature. Furthermore, enhancing yield strength by a material treating process, such as strain hardening, produces a corresponding decrease in  $K_{Ic}$ .

## Design Procedure 6.1: Fracture Mechanics Applied to Design

The use of fracture mechanics in design generally involves the following steps for geometries that lend themselves to simple analysis. For more complicated geometries, fracture modes or loadings, a numerical analysis, and/or experimental design verification are usually required.

1. Given a candidate material, obtain its fracture toughness. See Table 6.1 for selected materials, or else find the value in the technical literature or from experiments.
2. The dimensionless correction factor for the part geometry,  $Y$ , can be obtained from Appendix C for common design situations.  $Y$  is tabulated for additional geometries by Pilkey and Pilkey [2008] and Young and Budynas [2001].
3. Equation (6.6) allows calculation of allowable stress as a function of semi-crack length,  $a$ ; similarly, the largest allowable crack (with length  $2a$ ) can be determined from the required stress.
4. If design criteria cannot be met, the following alternatives can be pursued:
  - (a) Increasing the part thickness will reduce the nominal stress,  $\sigma_{nom}$ .
  - (b) A different material with a higher fracture toughness can be selected.
  - (c) Local reinforcement of critical areas can be pursued, such as locally increasing thickness.
  - (d) The manufacturing process can have a significant impact on the initial flaw size. The class of operations (casting versus forging, compression molding versus extrusion, etc.), quality control procedures, and quality of incoming material are all important factors. See, for example, Kalpakjian and Schmid [2014] for further information.

## Example 6.3: Critical Crack Length

**Given:** The following two materials:

- (a) AISI 4340 steel, tempered at 260°C
- (b) Aluminum alloy 7075-T651

Assume that the applied stress of the material is 0.8 times the yield stress and that the dimensionless correction factor,  $Y$ , is unity.

**Find:** The critical crack length at room temperature.

**Solution:**

- (a) From Table 6.1 for AISI 4340,  $S_y = 1640$  MPa and  $K_{Ic} = 50$  MPa $\sqrt{\text{m}}$ . Therefore,

$$\sigma = 0.8S_y = 1310 \text{ MPa.}$$

From Eq. (6.6),

$$a = \frac{1}{\pi} \left( \frac{K_{Ic}}{Y\sigma} \right)^2 = \frac{1}{\pi} \left[ \frac{(50.0)}{(1)(1310)} \right]^2 = 0.000464 \text{ m.}$$

Since this is one-half the critical crack length, the critical crack length for AISI 4340 steel is 0.928 mm.

- (b) From Table 6.1 for aluminum alloy 7075-T651,  $S_y = 505$  MPa and  $K_{Ic} = 29$  MPa $\sqrt{\text{m}}$ . Therefore,

$$\sigma = 0.8S_y = 404 \text{ MPa.}$$

From Eq. (6.6)

$$a = \frac{1}{\pi} \left( \frac{K_{Ic}}{Y\sigma} \right)^2 = \frac{1}{\pi} \left[ \frac{29}{(1)(404)} \right]^2 = 0.00164 \text{ m,}$$

or a critical crack length of 3.28 mm. Note that the stronger material (the steel) has a smaller critical crack length.

## Example 6.4: Allowable Crack Length

**Given:** A container used for compressed air is made of aluminum alloy 2024-T351. The required safety factor against yielding is 1.6, and the largest crack allowed through the thickness of the material is 6 mm. Assume  $Y = 1$ .

**Find:**

- (a) The stress intensity factor and the safety factor guarding against brittle fracture
- (b) Whether a higher safety factor will be achieved if the material is changed to a stronger aluminum alloy 7075-T651. Use the same crack dimensions, as this relates to an inspection capability.

**Solution:**

- (a) From Table 6.1 for aluminum alloy 2024-T351,  $S_y = 325$  MPa and  $K_{Ic} = 36$  MPa $\sqrt{\text{m}}$ . The nominal stress is

$$\sigma_{nom} = \frac{S_y}{n_s} = \frac{325}{1.6} = 203.1 \text{ MPa.}$$

The crack half-length is  $a = 3$  mm = 0.003 m. The stress intensity factor from Eq. (6.6) is

Table 6.1: Yield stress and fracture toughness data for selected engineering materials at room temperature.

Material	Yield strength, $S_y$ MPa	Fracture toughness, $K_{Ic}$ MPa $\sqrt{\text{m}}$
<b>Metals</b>		
Aluminum alloys		
2014-T4	450	29
2024-T3	390	34
2024-T351	325	36
7075-T651	505	29
7079-T651	470	33
Steels		
A340 tempered at 260° C	1640	50.0
A340 tempered at 425° C	1420	87.4
D6AC, tempered at 540° C	1495	102
A538	1722	111
Titanium alloys		
Ti-6Al-4V	820	106
Ti-13V-11Cr-3Al	1130	27
Ti-6Al-6V-2S	1080	37
Ti-6Al-2Sn-4Zr-6Mo	1180	26
<b>Ceramics</b>		
Aluminum oxide	—	3.0-5.3
Silicon nitride	—	4-8
Silicon carbide	—	2-5
Soda-lime glass	—	0.7-0.8
Concrete	—	0.2-1.4
<b>Polymers</b>		
Polymethyl methacrylate	20-50	1-3
Polystyrene	30-80	1-2
Polycarbonate	60-70	2.5-3
Polyvinyl chloride	40-50	2-3

$$\begin{aligned}
 K_i &= Y \sigma_{\text{nom}} \sqrt{\pi a} \\
 &= (1) (203.1 \times 10^6) \sqrt{\pi (0.003)} \\
 &= 19.72 \text{ MPa}\sqrt{\text{m}}.
 \end{aligned}$$

The safety factor for brittle fracture is then

$$n_{s,f} = \frac{K_{Ic}}{K_i} = \frac{36}{19.72} = 1.826.$$

- (b) From Table 6.1 for the stronger aluminum alloy 7075-T651,  $S_y = 505 \text{ MPa}$  and  $K_{Ic} = 29 \text{ MPa}\sqrt{\text{m}}$ . The safety factor guarding against yielding is

$$n_{s,y} = 1.6 \left( \frac{505}{325} \right) = 2.49.$$

Thus, the increased strength of 7075-T651 results in a higher safety factor guarding against yielding. The safety factor guarding against crack propagation is then

$$\frac{K_{Ic}}{K_i} = \frac{29}{19.72} = 1.47.$$

Note that the stronger material will fail more easily from crack propagation. These examples demonstrate that material strength can be counterintuitive with respect to failure, and that consideration of fracture toughness is important for fault tolerant design (see Section 7.12).

## 6.6 Failure Prediction for Uniaxial Stress State

Experimental data exist for uniaxial stress states and are widely available. Failure is predicted if the design stress,  $\sigma_d$ , is greater than the known allowable stress,  $\sigma_{\text{all}}$ . The safety factor from Eq. (1.1) in the uniaxial stress state can be expressed as

$$n_s = \frac{\sigma_{\text{all}}}{\sigma_d}. \quad (6.7)$$

Of course, the larger  $n_s$  is, the safer is the design, and values of  $n_s < 1$  mean that a redesign is necessary.

### Example 6.5: Uniaxial Failure of a Leaf Spring

**Given:** The leaf springs of a truck's rear wheels are loaded in pure bending (see Section 17.6). The 8-ton axle load is taken up by the two springs, giving a bending moment of 9800 N-m in each spring at the load application point. The steel used for the spring is AISI 4340, tempered at 260°C. The dimensions of the leaf spring are such that the width is 10 times the thickness. Assume a safety factor of 5.

**Find:** The cross section of the leaf spring.

**Solution:** From Table 6.1 for AISI 4340 steel tempered at 260°C,  $S_y = 1640 \text{ MPa}$ . The design stress from Eq. (6.7) is

$$\sigma_d = \frac{\sigma_{\text{all}}}{n_s} = \frac{1640}{5} = 328 \text{ MPa}. \quad (a)$$

From Table 4.1 for a rectangular section,

$$I = \frac{bh^3}{12} \quad \text{and} \quad c = h/2. \quad (b)$$

It is given that  $b = 10h$ . Substituting Eq. (b) into Eq. (4.45) gives the magnitude of the bending design stress as

$$\sigma_d = \frac{Mc}{I} = \frac{9800(h/2)}{(10h)h^3/12} = \frac{5880}{h^3}. \quad (c)$$

Making use of Eq. (a) gives

$$328 \times 10^6 = \frac{5880}{h^3},$$

or

$$h^3 = \frac{5880}{328 \times 10^6} = 17.93 \times 10^{-6} \text{ m}^3,$$

so that

$$h = 0.026 \text{ m} = 26 \text{ mm}.$$

The cross section of the leaf spring is thus  $26 \times 260 \text{ mm}$ .

## 6.7 Failure Prediction for Multiaxial Stress State

A multiaxial stress state can be biaxial or triaxial. In practice, it is difficult to devise experiments to cover every possible combination of critical stresses because tests are expensive and a large number is required to obtain results with good confidence. Therefore, a theory is needed that compares the normal and shear stresses  $\sigma_x, \sigma_y, \sigma_z, \tau_{xy}, \tau_{yz},$  and  $\tau_{xz}$  with the uniaxial stress, for which experimental data are relatively easy to obtain. Several failure prediction theories are presented for a multiaxial stress state while under static loading.

### 6.7.1 Ductile Materials

As discussed in Section 3.2, most metals and thermoplastic polymers are considered to be *ductile*. There are exceptions, however: metal castings are not as ductile as wrought or cold-worked parts and can thus behave in a brittle manner. Ductile materials typically have the same tensile strength as compressive strength and are not as susceptible to stress raisers as are brittle materials. For the purposes of this text, a ductile material is considered to have failed when it yields. Although in some applications a small amount of plastic deformation may be acceptable, this is rarely the case in machinery elements. Two theories of yield criteria are presented next: the maximum-shear-stress theory and the distortion-energy theory.

#### Maximum-Shear-Stress Theory

The **maximum-shear-stress theory** (MSST) was first proposed by Coulomb [1773] but was independently developed by Tresca [1868] and is therefore often called the **Tresca yield criterion**. Tresca noted that plastically deforming platinum exhibited bright shear bands under small strains, indicating that metals deformed under shear in all circumstances and that the shear was highly localized on well-defined planes. His observations led to the MSST, which states that a part subjected to any combination of loads will fail (by yielding or fracturing) whenever the maximum shear stress exceeds a critical value. The critical value can be determined from standard uniaxial tension tests. Experimental evidence verifies

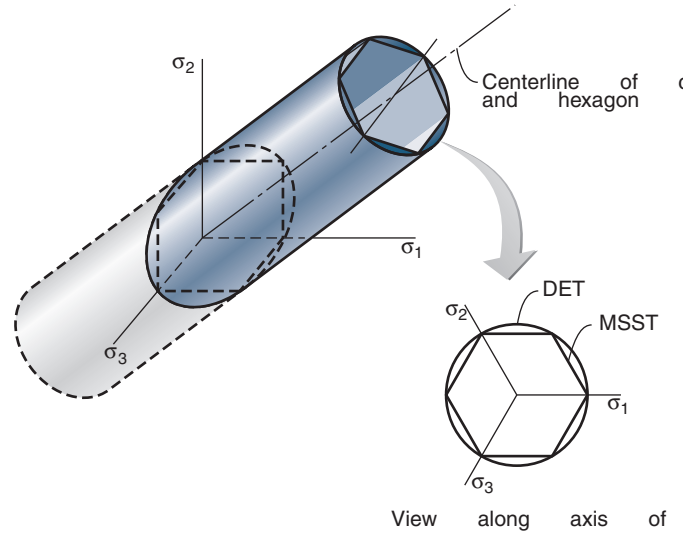


Figure 6.11: Three-dimensional yield locus for MSST and DET.

that the MSST is a good theory for predicting yielding of ductile materials, and it is a common approach in design. If the nomenclature  $\sigma_1 \geq \sigma_2 \geq \sigma_3$  is used for the principal stresses in accordance with Eq. (2.18), the maximum shear stress theory predicts yielding when

$$\sigma_1 - \sigma_3 = \frac{S_y}{n_s}, \quad (6.8)$$

where  $S_y$  is the yield strength of the material and  $n_s$  is the safety factor.

For a three-dimensional stress state, the maximum-shear-stress theory provides an envelope describing the stress combinations that cause yielding, as illustrated in Fig. 6.11. The curve, defined by a yield criterion, is known as a *yield locus*. Any stress state in the interior of the yield locus results in elastic deformation. Points outside the yield locus are not possible because such stress states would cause yielding in the solid before these stresses could be attained. Stress states outside the yield locus cannot be supported by the material. If a situation arises that would increase the material strength (such as strain rate effects or work hardening), the yield locus expands, so that fracture may not necessarily be the result.

It is helpful to present the yield criterion in a plane stress circumstance, for which there will be two principal stresses in the plane as well as a principal stress equal to zero perpendicular to the plane. Figure 6.12 graphically depicts failure prediction in the plane stress state by the maximum-shear-stress theory. The principal stresses used in the figure are labeled as  $\sigma_1$  and  $\sigma_2$ , but the ordering of normal stresses ( $\sigma_1 \geq \sigma_2 \geq \sigma_3$ ) is not being enforced. Remember that the principal stress outside the page is zero. In the first quadrant, where  $\sigma_1$  and  $\sigma_2$  are by definition positive, this means that the value of  $\sigma_3$  in Eq. (6.8) would be zero and that yielding would occur whenever  $\sigma_1$  or  $\sigma_2$  reached the uniaxial yield strength,  $S_y$ . In the second quadrant, where  $\sigma_1$  is negative and  $\sigma_2$  is positive, Eq. (6.8) would result in a line as shown in Fig. 6.12. The third and fourth quadrants of the curve follow the same reasoning in their development.

#### Distortion-Energy Theory

The **distortion-energy theory** (DET), also known as the **von Mises criterion**, postulates that failure is caused by the elas-

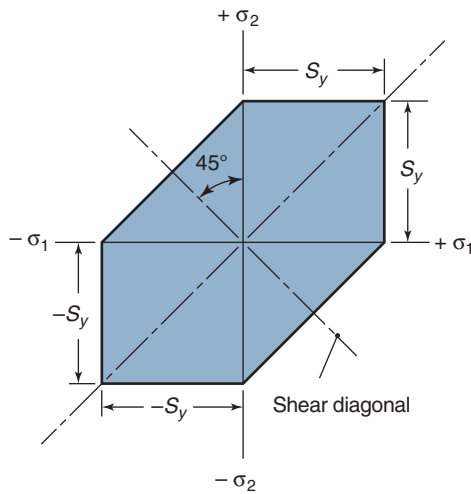


Figure 6.12: Graphical representation of maximum-shear-stress theory (MSST) for biaxial stress state ( $\sigma_z = 0$ ).

tic energy associated with shear deformation in the material. This theory is valid for ductile materials and predicts yielding under combined loading and works well (although the differences between the DET and the MSST are small).

The DET can be derived mathematically in a number of ways, but one of the more straightforward is based on the hypothesis that yielding occurs when the root mean shear stress exceeds a critical value. Mathematically, this can be expressed as

$$[(\sigma_1 - \sigma_2)^2 + (\sigma_2 - \sigma_3)^2 + (\sigma_3 - \sigma_1)^2]^{1/2} = \text{Constant}. \quad (6.9)$$

Since in uniaxial yielding,  $\sigma_1 = S_y$  and  $\sigma_2 = \sigma_3 = 0$ , the constant in Eq. (6.9) is evaluated as  $\sqrt{2}S_y$ . Eq. (6.9) then becomes

$$\frac{1}{\sqrt{2}} [(\sigma_1 - \sigma_2)^2 + (\sigma_2 - \sigma_3)^2 + (\sigma_3 - \sigma_1)^2]^{1/2} = S_y. \quad (6.10)$$

Incorporating the safety factor, Eq. (6.10) becomes

$$\sigma_e = \frac{1}{\sqrt{2}} [(\sigma_1 - \sigma_2)^2 + (\sigma_2 - \sigma_3)^2 + (\sigma_3 - \sigma_1)^2]^{1/2} = \frac{S_y}{n_s}, \quad (6.11)$$

where  $\sigma_e$  is the **von Mises stress**. For a biaxial stress state, assuming  $\sigma_3 = 0$ , the von Mises stress is given by

$$\sigma_e = (\sigma_1^2 + \sigma_2^2 - \sigma_1\sigma_2)^{1/2} = (\sigma_x^2 + \sigma_y^2 - \sigma_x\sigma_y + 3\tau_{xy}^2)^{1/2}. \quad (6.12)$$

The DET yield locus is shown in Fig. 6.11 for a three-dimensional stress state and in Fig. 6.13 for plane stress loading (biaxial stress state). Compared to the MSST, the DET has the advantage that the yield criterion is continuous in its first derivative, an important consideration for applications in plasticity.

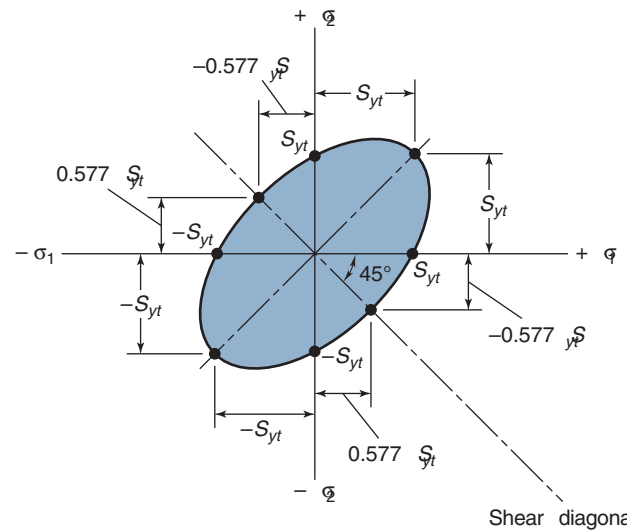


Figure 6.13: Graphical representation of distortion-energy theory (DET) for biaxial stress state ( $\sigma_z = 0$ ).

### Example 6.6: Determination of von Mises Stress

**Given:** In the rear-wheel suspension of the Volkswagen Beetle, the spring motion was provided by a torsion bar fastened to an arm on which the wheel was mounted, as depicted in Fig. 6.14. The torque in the torsion bar was created by a 2500-N force acting on the wheel from the ground through a 300-mm lever arm. Because of space limitations, the bearing holding the torsion bar was situated 100 mm from the wheel shaft. The diameter of the torsion bar was 28 mm.

**Find:** The stresses in the torsion bar at the bearing by using the distortion-energy theory.

**Solution:** The stresses acting on the torsion bar are a shear stress from torsion and a perpendicular tensile/compressive stress from bending, resulting in a plane stress loading (see Example 4.13). Using Eq. (4.33) gives the shear stress from torsion as

$$\tau = \frac{Tc}{J} = \frac{2500(0.3)(0.014)32}{\pi(0.028)^4} \text{ Pa} = 174.0 \text{ MPa}.$$

Using Eq. (4.45) gives the tensile stress from bending as

$$\sigma = \frac{Mc}{I} = \frac{2500(0.1)(0.014)64}{\pi(0.028)^4} \text{ Pa} = 116.0 \text{ MPa}.$$

From Eq. (2.16), the principal normal stresses then are

$$\begin{aligned} \sigma_{1,2} &= \frac{\sigma_x + \sigma_y}{2} \pm \sqrt{\tau_{xy}^2 + \left(\frac{\sigma_x - \sigma_y}{2}\right)^2} \\ &= \frac{116.0}{2} \pm \sqrt{(174.0)^2 + \left(\frac{116.0}{2}\right)^2}, \end{aligned}$$

or  $\sigma_1 = 241.4 \text{ MPa}$  and  $\sigma_2 = -125.4 \text{ MPa}$ . From Eq. (6.12), the von Mises stress is

$$\begin{aligned} \sigma_e &= (\sigma_1^2 + \sigma_2^2 - \sigma_1\sigma_2)^{0.5} \\ &= [(241.4)^2 + (-125.4)^2 - 241.4(-125.4)]^{0.5} \\ &= 322.9 \text{ MPa}. \end{aligned}$$

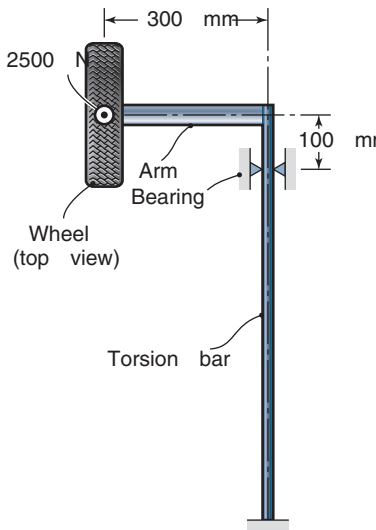


Figure 6.14: Rear wheel suspension used in Example 6.6.

### Example 6.7: Yielding of a Ductile Bar

**Given:** A round, cantilevered bar made of a ductile material is subjected to a torque applied to the free end.

**Find:** Determine when yielding will occur by using (a) the MSST and (b) the DET.

**Solution:** Figure 6.15 shows the cantilevered bar, the stresses acting on an element, and a Mohr's circle representation of the stress state. Since the goal is to determine stresses at yielding, the safety factor will be taken as  $n_s = 1$ . The principal stresses are  $\sigma_1 = \tau_1$  and  $\sigma_3 = -\tau_1$ .

(a) Using Eq. (6.8) the MSST predicts failure if

$$|\sigma_1 - \sigma_3| = 2\tau_{\max} = \frac{S_y}{n_s},$$

or

$$\tau_{\max} = 0.5S_y. \quad (a)$$

(b) Using Eq. (6.11) yields

$$\begin{aligned} \sigma_e &= [\sigma_1^2 - \sigma_1\sigma_2 + \sigma_2^2]^{1/2} \\ &= [\tau_1^2 - \tau_1(-\tau_1) + (-\tau_1)^2]^{1/2} = \sqrt{3}\tau_1 \\ &= \sqrt{3}\tau_{\max} = \frac{S_y}{n_s}, \end{aligned}$$

or

$$\tau_{\max} = \frac{1}{\sqrt{3}}S_y = 0.577S_y. \quad (b)$$

Equations (a) and (b) show that the MSST and the DET are in fairly good agreement. This circumstance, that is, a loading of pure shear, results in the greatest difference between the MSST and the DET, suggesting that both theories will give close to the same results.

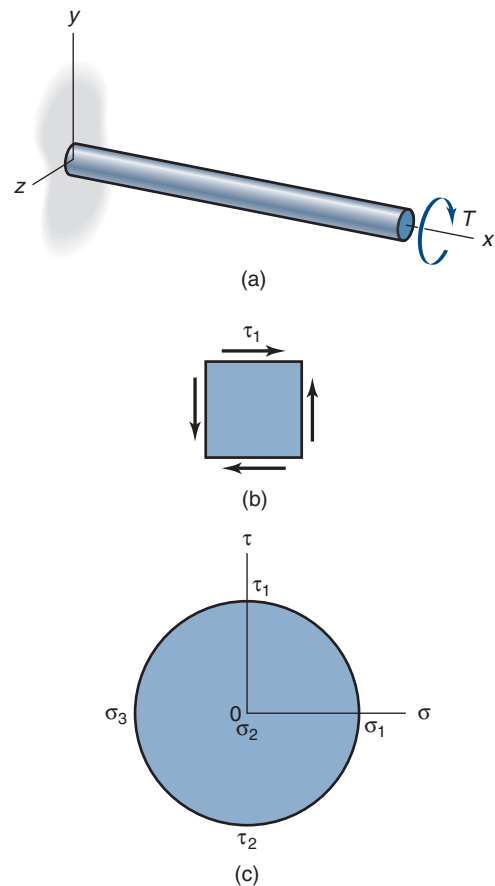


Figure 6.15: Cantilevered, round bar with torsion applied to free end (used in Example 6.7). (a) Bar with coordinates and load; (b) stresses acting on an element; (c) Mohr's circle representation of stresses.

### Example 6.8: Yield Criteria Applied to Design

**Given:** A round, cantilevered bar, similar to that considered in Example 6.7, is subjected not only to torsion but also to a transverse load at the free end, as shown in Fig. 6.16a. The bar is made of a ductile material having a yield stress of 350 MPa. The transverse force is 2000 N and the torque is 100 Nm applied to the free end. The bar is 150 mm long and a safety factor of 2 is assumed. Transverse shear can be neglected.

**Find:** Determine the minimum diameter to prevent yielding by using both (a) the MSST and (b) the DET.

**Solution:** Figure 6.16b shows the stress element on the top of the bar at the wall. Note that, in this example,  $\sigma_z = 0$ , so that the element encounters plane or biaxial stress. The critical section occurs at the wall. By using Eqs. (4.45) and (4.33) the normal and shear stresses can be written as

$$\sigma_x = \frac{Mc}{I} = \frac{Pl(d/2)}{\pi d^4/64} = \frac{32Pl}{\pi d^3},$$

$$\tau_{xy} = \frac{Tc}{J} = \frac{T(d/2)}{\pi d^4/32} = \frac{16T}{\pi d^3}.$$



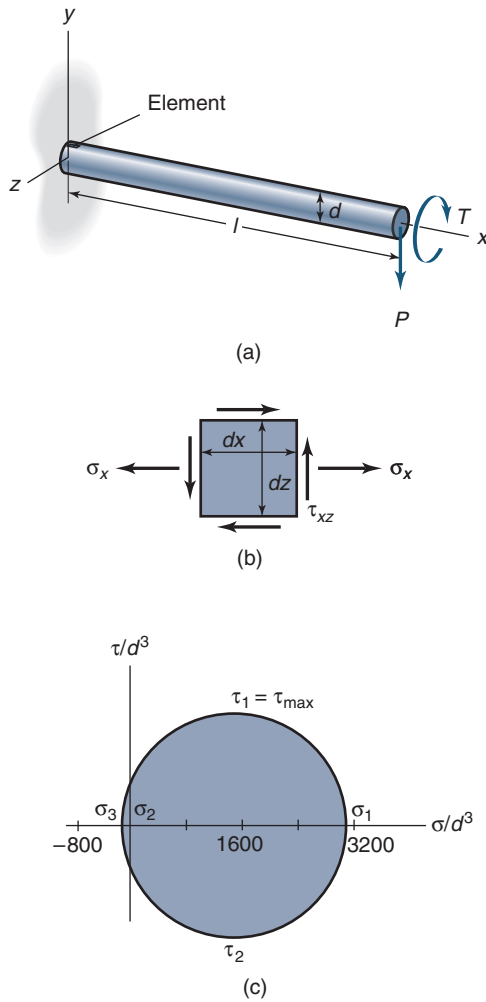


Figure 6.16: Cantilevered, round bar with torsion and transverse force applied to free end (used in Example 6.8). (a) Bar with coordinates and loads; (b) stresses acting on element at top of bar and at wall; (c) Mohr's circle representation of stresses.

From Eq. (2.16), the principal normal stresses in biaxial stress can be written as

$$\begin{aligned}\sigma_{1,2} &= \frac{\sigma_x}{2} \pm \sqrt{\left(\frac{\sigma_x}{2}\right)^2 + \tau_{xz}^2} \\ &= \frac{16Pl}{\pi d^3} \pm \sqrt{\left(\frac{16Pl}{\pi d^3}\right)^2 + \left(\frac{16T}{\pi d^3}\right)^2}.\end{aligned}$$

Therefore,

$$\sigma_{1,2} = \frac{16}{\pi d^3} \left( Pl \pm \sqrt{(Pl)^2 + T^2} \right).$$

Substituting for  $P$  and  $l$  results in

$$\sigma_{1,2} = \frac{16}{\pi d^3} \left[ (2000)(0.150) \pm \sqrt{(2000)^2(0.150)^2 + (100)^2} \right].$$

Therefore,

$$\sigma_1 = \frac{3140}{d^3} \quad \text{and} \quad \sigma_2 = -\frac{82.6}{d^3}.$$

Note that the stresses are in the wrong order; to ensure  $\sigma_1 \geq \sigma_2 \geq \sigma_3$ , they are rearranged so that  $\sigma_1 = 3140/d^3$ ,  $\sigma_2 = 0$ , and  $\sigma_3 = -82.6/d^3$ .

From Eq. (2.19), the maximum and principal shear stresses can be written as

$$\tau_{1,2} = \pm \sqrt{\tau_{xy}^2 + \frac{(\sigma_x - \sigma_z)^2}{4}},$$

or

$$\begin{aligned}\tau_{\max} &= \tau_1 = \frac{16}{\pi d^3} \sqrt{(Pl)^2 + T^2} \\ &= \frac{16}{\pi d^3} \sqrt{(2000)^2(0.150)^2 + (100)^2}.\end{aligned}$$

Therefore,

$$\tau_{\max} = \tau_1 = \frac{1610}{d^3}.$$

(a) Using Eq. (6.8), the MSST predicts that failure will be avoided if

$$|\sigma_1 - \sigma_3| = 2\tau_1 = 2\tau_{\max} < \frac{S_y}{n_s}.$$

Therefore,

$$\left| \frac{3140}{d^3} + \frac{82.6}{d^3} \right| < \frac{350 \times 10^6}{2},$$

or  $d = 0.0210 \text{ m} = 21.0 \text{ mm}$ .

(b) This is a plane stress state, since one of the principal stresses is zero. Therefore, Eq. (6.12) yields

$$\begin{aligned}\sigma_e &= \left[ \left( \frac{3140}{d^3} \right)^2 + \left( \frac{3140}{d^3} \right) \left( \frac{82.6}{d^3} \right) + \left( \frac{82.6}{d^3} \right)^2 \right]^{1/2} \\ &= \frac{3180}{d^3}.\end{aligned}$$

Thus, using Eq. (6.11) the DET predicts that failure occurs when

$$\begin{aligned}\sigma_e &= \frac{S_y}{n_s}, \\ \frac{26,950}{d^3} &= \frac{50,000}{2}.\end{aligned}$$

Hence  $d = 20.9 \text{ mm}$ . Note that both theories give approximately the same solution.

## 6.7.2 Brittle Materials

As discussed in Chapter 3, brittle materials do not yield, but instead they fracture. Thus, a failure criterion applied to brittle materials addresses the circumstances under which the material will literally break. One important consideration with brittle materials is that their strengths in compression are usually much greater than their strengths in tension. Consequently, the failure criterion will show a difference in tensile and compressive behavior. Three failure criteria are presented next: the maximum-normal-stress theory, the internal friction theory, and the modified Mohr theory.

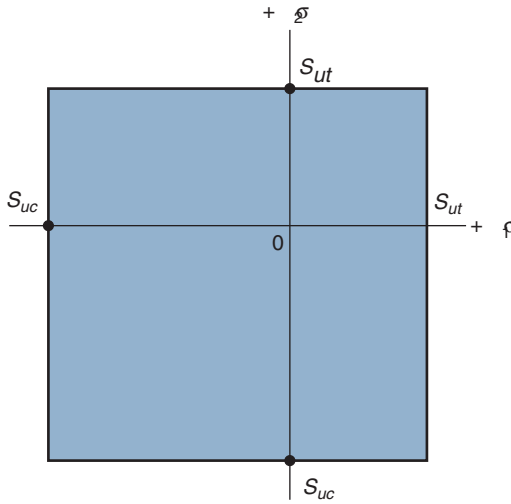


Figure 6.17: Graphical representation of maximum-normal-stress theory (MNST) for a biaxial stress state ( $\sigma_z = 0$ ).

### Maximum Normal Stress Theory

The **maximum-normal-stress theory** (MNST) states that a part subjected to any combination of loads will fail when the greatest positive principal stress exceeds the material's tensile strength or when the greatest negative principal stress exceeds the compressive strength. This theory matches experiments best for fibrous brittle materials and some glasses, but other failure criteria give better general predictions and the MNST is not usually recommended. It is presented here as an alternative for some special materials and because it is simple mathematically. Failure will occur, using the MNST theory, if

$$\sigma_1 \geq \frac{S_{ut}}{n_s}, \quad (6.13)$$

or

$$\sigma_3 \leq -\frac{S_{uc}}{n_s}, \quad (6.14)$$

where

$\sigma_1 \geq \sigma_2 \geq \sigma_3$  = principal normal stresses, Pa  
 $S_{ut}$  = uniaxial ultimate strength in tension, Pa  
 $S_{uc}$  = uniaxial ultimate strength in compression, Pa  
 $n_s$  = safety factor

Note that failure is predicted to occur when either Eq. (6.13) or (6.14) is satisfied.

Figure 6.17 graphically presents failure prediction for brittle materials in the biaxial stress state by the MNST. The  $\sigma_1 - \sigma_2$  plot for biaxial stresses (i.e.,  $\sigma_3 = 0$ ) shows that the MNST predicts failure for all combinations of  $\sigma_1$  and  $\sigma_2$  falling on the boundary of the shaded area in Fig. 6.17; any stress state within the shaded area represents an elastic stress state.

### Internal Friction Theory

The MNST is most useful for brittle or fibrous materials and some glasses, and is not generally applicable to other materials. Most brittle materials, such as ceramics and cast metals widely used in machine components, have behavior that departs from the MNST, and a different fracture theory is needed. Furthermore, the maximum shear stress theory is difficult to apply to brittle materials, since their strength in compression is so much higher than the tensile strength. In

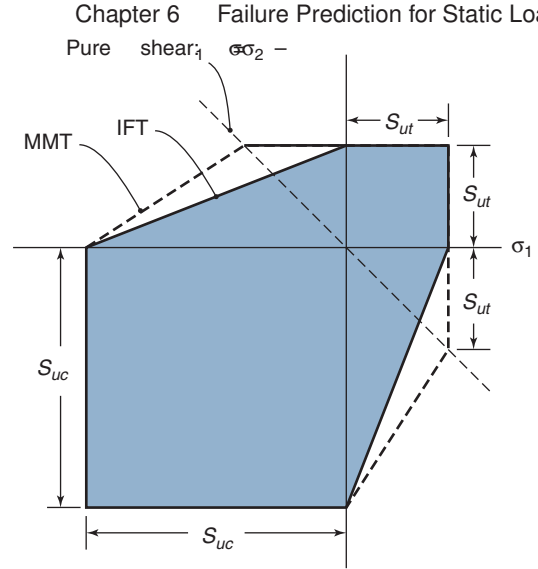


Figure 6.18: Internal friction theory and modified Mohr theory for failure prediction of brittle materials.

addition, some materials, such as certain magnesium alloys, are ductile but are stronger in tension than in compression. A logical extension to the MSST is to separate compressive and tensile strengths. In mathematical terms,

If  $\sigma_1 > 0$  and  $\sigma_3 < 0$ ,

$$\frac{\sigma_1}{S_{ut}} - \frac{\sigma_3}{S_{uc}} = \frac{1}{n_s}. \quad (6.15)$$

If  $\sigma_3 > 0$ ,

$$\sigma_1 = \frac{S_{ut}}{n_s}; \quad (6.16)$$

and if  $\sigma_1 < 0$ ,

$$\sigma_3 = -\frac{S_{uc}}{n_s}, \quad (6.17)$$

where

$\sigma_1 \geq \sigma_2 \geq \sigma_3$  = principal stresses, Pa  
 $S_{ut}$  = fracture strength in tension, Pa  
 $S_{uc}$  = fracture strength in compression, Pa  
 $n_s$  = safety factor

Although this would appear to be an arbitrary extension of the MSST, Eqs. (6.15) to (6.17) can be derived analytically if internal friction is considered. For this reason, this fracture criterion is known as the **internal friction theory** (IFT) and is also known as the **Coulomb-Mohr theory**. The IFT has the advantage of being more accurate than either the MNST or MSST for materials that have a pronounced difference in tensile and compressive strengths. Figure 6.18 depicts the IFT for a two-dimensional stress state ( $\sigma_3 = 0$ ).

### Modified Mohr Theory

The IFT has an analytical basis, but the **modified Mohr theory** arose through efforts at fitting test data. The modified Mohr theory (MMT) best predicts brittle material behavior, especially in the fourth quadrant in Fig. 6.17. The MMT can be expressed as follows:

If  $\sigma_1 > 0$  and  $\sigma_3 < -S_{ut}$ ,

$$\sigma_1 - \frac{S_{ut}\sigma_3}{S_{uc} - S_{ut}} = \frac{S_{uc}S_{ut}}{n_s S_{uc} - S_{ut}}. \quad (6.18)$$

If  $\sigma_3 > -S_{ut}$ ,

$$\sigma_1 = \frac{S_{ut}}{n_s}. \quad (6.19)$$

If  $\sigma_1 < 0$ ,

$$\sigma_3 = \frac{S_{uc}}{n_s}. \quad (6.20)$$

Figure 6.18 depicts the MMT, along with the IFT, to demonstrate that there is only a slight difference between the two criteria.

### Example 6.9: Failure of a Brittle Bar

**Given:** Repeat Example 6.7 but with the cantilever constructed from a brittle material.

**Find:** Determine when fracture will occur by using (a) the MNST, (b) the IFT, and (c) the MMT. Assume that the compressive strength of the material is twice its tensile strength.

**Solution:** Just as in Example 6.7, the stress state is  $\sigma_1 = \tau_1$ ,  $\sigma_2 = 0$ , and  $\sigma_3 = -\tau_1$ .

(a) Using Eq. (6.13) the MNST predicts failure if

$$\sigma_1 > \frac{S_{ut}}{n_s} \quad \text{or} \quad \tau_1 = \tau_{\max} \geq \frac{S_{ut}}{n_s}. \quad (a)$$

Tensile fracture stress was used in Eq. (a) because the material will fail in tension before it fails in compression.

(b) Recall that, when using the IFT,  $\sigma_1$  is positive and  $\sigma_3$  is negative. Thus, Eq. (6.14) yields

$$\frac{\sigma_1}{S_{ut}} - \frac{\sigma_3}{S_{uc}} = \frac{1}{n_s},$$

or

$$\frac{\tau_1}{S_{ut}} - \frac{(-\tau_1)}{2S_{ut}} = \frac{1}{n_s}.$$

Solving for  $\tau_1$ ,

$$\tau_1 = \frac{2}{3} \frac{S_{ut}}{n_s}. \quad (b)$$

(c) An examination of Figures 6.17 and 6.18 shows that for pure shear there is no difference between the MMT and the MNST.

### 6.7.3 Selecting Failure Criteria

Selecting a failure criterion to use in design is somewhat of an art. Figure 6.19 shows some test data on biaxial failures or yielding for several materials. The DET fits ductile materials slightly better than does the MSST, but most of the data fall between the two curves. Although the DET fits the data well for ductile solids, the MSST is often applied. The MSST is mathematically simple and conservative, meaning that for a given circumstance the MSST will predict yielding at lower loads than does the DET. Thus, because there is an added safety factor in using the MSST, it is often used in design. On the other hand, many commercial stress analyses and finite element codes use a von Mises stress to graphically present results, and thus there is a natural tendency to use a DET in such circumstances.

Ductile materials are produced with high repeatability in terms of strength, so designers can use either failure criterion with good confidence. Brittle materials are somewhat more

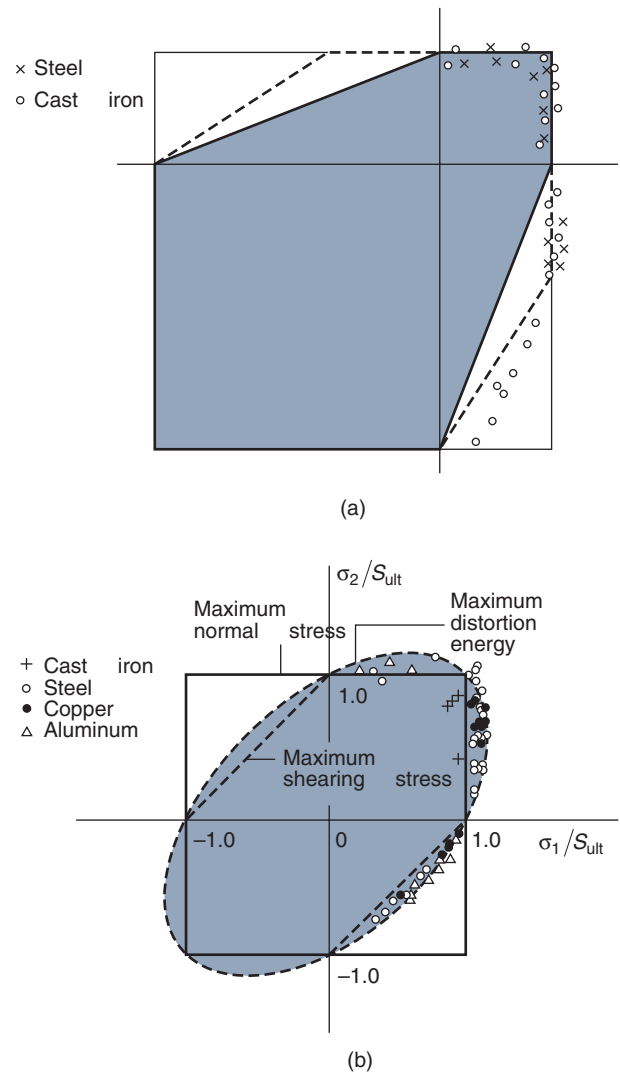


Figure 6.19: Experimental verification of yield and fracture criteria for several materials. (a) Brittle fracture. (b) Ductile yielding. Source: Data from Dowling [1993] and Murphy [1964].

difficult to analyze because their material properties generally vary much more than those of ductile materials. Owing to the statistical nature of brittle material properties, experimental strength verification is usually preferred over theoretical predictions for most applications.

When a ductile material is tested, as in tension, measured yield stresses deviate little among specimens, especially if the specimens have been obtained from the same batch in its production. Thus, relatively few experiments are needed to specify the strength of a ductile material with good certainty. For most brittle materials, however, many more tests must be performed to accurately assess the strength distribution. Test specimens do not fail at the same stress, even if they were manufactured in the same batch with the same processes. It is difficult to give a strength value for a brittle material with any great certainty.

A student of engineering design often wonders why the IFT theory is presented at all if the MMT better fits brittle material data, as is suggested by Fig. 6.19. Given the variation in strengths between brittle test specimens, the difference in the three failure criteria presented here is insignificant. To

the question, “Which theory is better or best?” no absolute answer can be given, and a designer or organization should use the one with which it has the most experience and history.

The IFT and the MSST are identical for most metals because the yield strengths of metals in compression and tension are approximately equal. Thus, applying the IFT theory at all times would ensure a conservative solution. Designers are often reluctant to follow this procedure, since the IFT is the most complex criterion from a mathematical standpoint.

The failure criteria given in this chapter are difficult to apply to composite materials and polymers. The behavior of polymers is complex, and can include viscoplastic behavior, where a yield point is difficult to define. Composite materials require more complex failure theories to account for fiber length and orientation with respect to load; the interested reader is referred to Daniels and Ishai [2005], Reddy [1996], and Kaw [1997].

For the purposes of this text, ductile materials can be analyzed using the DET or the MSST. Brittle materials should be analyzed by using the MNST, the IFT, or the MMT. A wide variety of additional failure and yield criteria is given in the technical literature. However, those presented in this chapter are by far the most commonly applied, and a suitable yield criterion can usually be chosen from those presented.

Design Procedure 6.2 summarizes some of the main concerns and gives general suggestions on selection of a failure criterion.

### Design Procedure 6.2: Selection of a Failure Criterion

Given a material, where the tensile and compressive yield, ultimate and/or fracture stresses are known, the following steps can be used to help select a failure criterion:

1. For a ductile metal, where the strength is the same in tension and compression, use either the MSST or DET. These criteria are fairly close, with the largest difference of 15% occurring for pure shear in a plane stress loading. The MSST is more conservative; that is, it predicts yielding at a lower stress level than DET.
2. If a ductile metal has a different strength in compression than in tension, such as with certain magnesium alloys, the IFT or MMT are reasonable options.
3. Brittle materials are difficult to analyze using failure criteria, and confidence in strength values is difficult to obtain. However, the IFT leads to good results without the mathematical complication of the MMT.
4. For circumstances where improved performance is required, MMT may be justified over the IFT.

Regardless of these suggestions, failure criteria are often specified for the designer by their customer, employer, or supplier. Sometimes, more elaborate yield criterion are used, such as those that incorporate viscoelastic behavior or creep. This design procedure is generally applicable, but deviations in industrial practice are not uncommon.

Table 6.2: Safety factors from using different criteria for three different materials used in Example 6.10.

Part	Criterion	Equation used	Safety factor
a)	MSST	(6.7)	1.5
	DET	(6.10)	1.73
b)	MSST	(6.7)	1.28
	DET	(6.10)	1.33
c)	IFT	(6.14)	1.61
	MMT	(6.17)	1.69

### Example 6.10: Selection of Yield and Failure Criteria

**Given:** The following materials and loadings (remaining stresses are zero):

- (a) Pure aluminum:  $S_y = 30$  MPa,  $\sigma_x = 10$  MPa,  $\sigma_y = -10$  MPa,  $\tau_{xy} = 0$
- (b) 0.2% carbon steel:  $S_y = 295$  MPa,  $\sigma_x = -0$  MPa,  $\sigma_y = -200$  MPa,  $\tau_{xy} = 75$  MPa
- (c) Gray cast iron:  $S_{ut} = 125$  MPa,  $S_{uc} = 450$  MPa,  $\sigma_x = -100$  MPa,  $\sigma_y = 50$  MPa,  $\tau_{xy} = 0$

**Find:** The safety factors for these circumstances.

**Solution:** The results are summarized in Table 6.2. Note that the yield criteria selected for aluminum and steel are the MSST and the DET, since these are recognized as ductile metals. The loading for the aluminum corresponds to pure shear (see Section 2.14), and this loading will have the largest difference between the MSST and DET as can be seen from the resulting safety factors. The loading for the steel is not pure shear, and the yield criteria are in good agreement.

Cast iron is not a ductile material, so that neither the MSST or the DET should be applied. Design Procedure 6.2 notes that the IFT yields good results without the mathematical complexity of the MMT. As can be seen from Table 6.2, the difference in safety factors that result from the IFT and MMT is fairly small, so that either could be used.

### Case Study: Stress Concentration Factors for Complicated Geometries

The stress concentration factors presented in Section 6.2.1 and in Appendix C are applicable to most design circumstances, but it is not unusual to encounter different and often more complex geometries. Departure from the circumstances given in Figs. 6.2 through 6.8 can involve the use of non-linear materials, varying thickness, more complex geometries, closely spaced stress concentrations, or combined loadings. This case study presents the common methods of determining stress concentration factors for more complex situations.

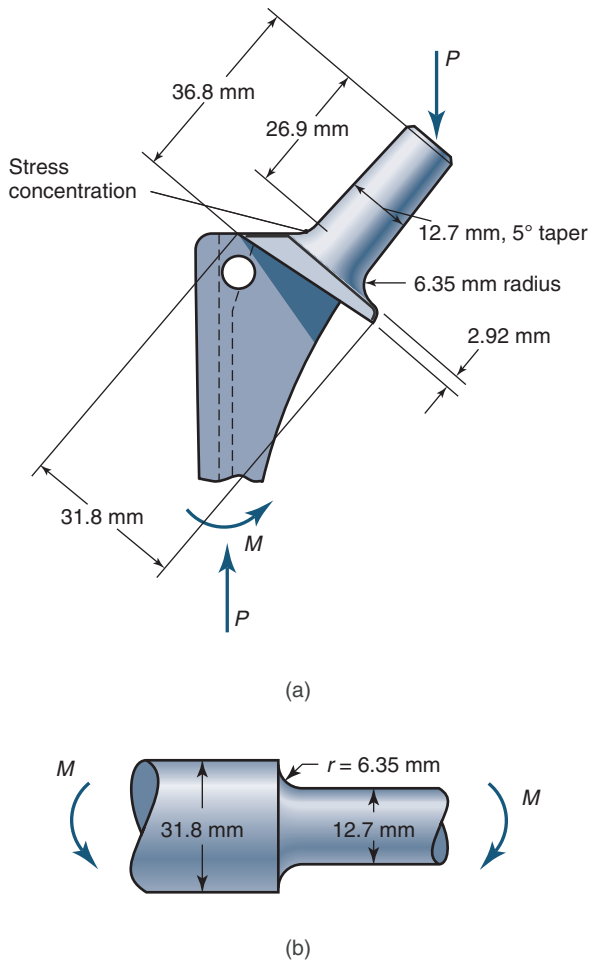


Figure 6.20: (a) Schematic illustration of a portion of a total hip replacement with selected dimensions; (b) idealized geometry used to estimate the stress concentration factor at the fillet.

### Stress Concentration Charts

The charts presented in Section 6.2.1 are a small subset of those that have been developed to date. Performing an Internet search or review of standard handbooks of stress concentration factors may result in a chart that best matches a particular design condition. This is often the quickest and best approach to determining a stress concentration factor.

Often, a circumstance that is close to the design problem can be found, but not one that matches it exactly. For example, Fig. 6.20a shows a section of a total hip replacement, with a fillet from the transition of a tapered section and the portion of the stem that is inserted into a femur. The loading encountered is combined compression and bending, and the cross section transitions from circular at the base of the taper to rounded trapezoidal at the stem. An estimate of the stress concentration associated with this geometry can be obtained using the approximated geometry in Fig. 6.20 and Fig. 6.5c, even though the geometry is not exactly the same.

Such estimates are often very useful; they can confirm that designs have high or low safety factors and may justify additional investigations or verify that they are unnecessary. During preliminary design work, this approach can be used to verify that design approaches have merit while avoiding the cost and delay of more elaborate investigations.

Regardless, designs for critical applications (such as the total hip replacement in Fig. 6.20) will require further analysis and verification before they are finalized.

### Finite Element Analysis

Finite element analysis (FEA) is a numerical approach that has become very widely used with the proliferation of powerful computers and dedicated software. A detailed treatment of this powerful approach is not within the scope of this book, but the interested reader is directed to the texts by Fish and Belytschko [2007] or Hughes [2000]. This Case Study provides a short outline of the approach.

FEA requires *discretization* of a geometry into a mesh of *elements*; the elements are commonly triangles, quadrilaterals, bar segments, bricks, etc., defined by their *nodes*. It is not uncommon for meshes to consist of thousands of elements and nodes. After discretization, constraints are applied to some nodes and loads are applied to others.

Several FEA programs exist, but the general numerical solution approach is always based on matrix methods. A compliance matrix is assembled for the entire mesh from the compliances of the individual elements; this matrix is then inverted and the displacements of element nodes are determined for the system. Application of Hooke's Law [see Eq. (B.55)] yields the stresses in each element from the displacements at each node.

Depending on the element type, stresses are evaluated at one or more locations within the element. For a simple quadrilateral element, for example, the stress may be evaluated only at its center. For this reason, it must be recognized that highly localized stress concentrations will require small elements near the stress raiser to accurately capture its value. However, the elements cannot be so small that the accuracy of the computer processor limits the analysis. Furthermore, widespread use of small elements results in long computation times.

Experienced analysts will locate many small elements near suspected stress raisers and will place larger elements elsewhere in order to achieve reasonable computation times while capturing close estimates of stress concentrations. Depending on the complexity of the part, it may be necessary to refine meshes to make certain that results are accurate and confirm simulations. If designs are modified, new meshes have to be constructed and the software run to obtain a new result. Thus, finite element analysis should be recognized as a powerful tool, but not without its costs and limitations.

Figure 6.21 depicts a typical mesh for determining the stress associated with a hole in a plate under tension. The figure shows a wireframe representation in order to highlight the elements and their distributions; commonly, the von Mises stresses are plotted as contours. Regardless, one can see the larger elements located away from the stress concentration. The maximum element size is a user-defined parameter in the automatic meshing routines.

### Photoelasticity

Certain transparent materials display *birefringence*, wherein a ray of light encounters two refractive indices within the material, and is broken into two rays. Some materials display birefringence only under applied stress; for these materials, the magnitude of the stress determines the extent of birefringence at any point. When a polarized light is passed through the material, the two refractive indices manifest themselves in a phase difference that produces a fringe pattern in a polariscope (Fig. 6.22). Analysis of the refringence pattern allows direct measurement of stresses everywhere in the part geometry.



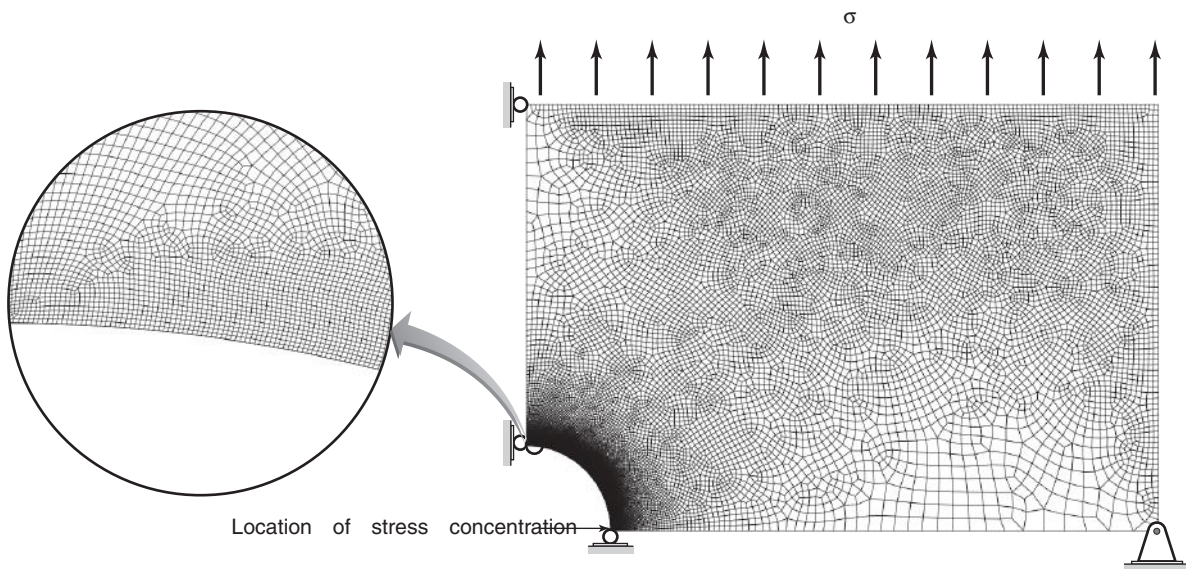


Figure 6.21: Example of a finite element mesh to capture the value of a stress concentration corresponding to Fig. 6.2. Only one-fourth of the problem has been discretized to take advantage of symmetry. Note the large number of elements located near the stress raiser. Boundary conditions and applied loads have been added for image clarity.

Photoelasticity can be applied to three-dimensional stress states and specimens, but the approach is complicated and, as a result, the approach is usually limited to plane stress. In fact, Figs. 6.3 and 6.4 were obtained from photoelastic methods and later confirmed by analytical solutions.

Photoelasticity has become less common since the proliferation of FEA, but it is still used for experimental verification. The cost and time involved in preparing physical specimens can be quite high, and skilled technicians are required to obtain good results. Further details on photoelastic stress analysis can be found in Doyle [2004].

#### Experimental Confirmation

Critical applications or complex geometries are usually confirmed by mechanical testing to ensure that intended loads can be safely supported. Such tests can be performed at a number of levels. For example, experiments can be conducted on components, systems or assemblies, or entire products to make sure that they support required loads and are robust designs. Further, testing may involve idealized loading, actual field trials, or any level of complexity in between. Rarely is the stress concentration directly measured, but instead failure loads as a whole are determined.

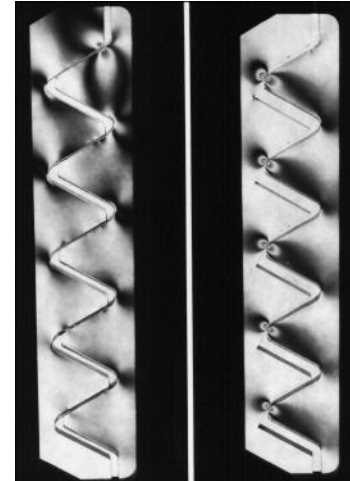


Figure 6.22: Photoelastic comparison of threaded fastener profiles comparing load distribution. The left image shows a conventional profile where load per tooth varies widely, and the right shows a Spiralock<sup>®</sup> profile with more uniform stresses on each tooth. *Source:* Courtesy of Stanley Engineered Fastening - Spiralock.

## 6.8 Summary

Of the approaches that can be used to determine stress concentration factors, the use of stress concentration charts from the technical literature (of which Figs. 6.2 through 6.8 are examples) represents the most cost-effective method. Especially in the age of the Internet, it is also usually the fastest approach as well. The finite element method has become an extremely widespread approach as well, but it has drawbacks of longer lead time and therefore higher cost. Experimental confirmation of designs is also relatively expensive and time consuming, but may be necessary to obtain confidence in the safety and suitability of designs.

## Key Words

**Coulomb-Mohr theory** a failure theory for materials with different strengths in tension and compression; identical to the internal friction theory

**crack** small flaw, always present, that can compromise material strength

**distortion-energy theory** postulate that failure is caused by elastic energy associated with deformation; identical to von Mises criterion

**fracture control** maintenance of nominal stress and crack size below critical level

**fracture toughness** critical value of stress intensity at which crack extension occurs

**internal friction theory** failure criterion accounting for difference between compressive and tensile strengths of brittle materials; identical to Coulomb-Mohr theory

**maximum-normal-stress theory** theory that yielding will occur whenever the greatest positive principal stress exceeds the tensile yield strength or whenever the greatest negative principal stress exceeds the compressive yield strength

**maximum-shear-stress theory** theory that yielding will occur when the largest shear stress exceeds a critical value; identical to the Tresca criterion

**modes of crack propagation** principal mechanisms for cracks to enlarge: Mode I, opening through tension; Mode II, sliding or in-plane shearing; Mode III, tearing

**modified Mohr theory** failure postulate similar to Coulomb-Mohr theory, except that curve is altered in quadrants II and IV of plane stress plot of principal stresses

**stress concentration** region where stress raiser is present

**stress concentration factor** factor used to relate actual maximum stress at discontinuity to nominal stress

**stress intensity factor** stress intensity at crack tip

**stress raiser** discontinuity that alters stress distribution so as to increase maximum stress

**Tresca yield criterion** theory that yielding will occur when the largest shear stress exceeds a critical value; identical to maximum-shear-stress theory

**von Mises criterion** postulate that failure is caused by elastic energy associated with deformation; identical to distortion-energy theory

**von Mises stress** effective stress based on von Mises criterion

## Summary of Equations

**Stress concentration factor:**

$$\text{Definition: } K_c = \frac{\text{Actual maximum stress}}{\text{Average stress}}$$

$$\text{Elliptical hole in plate loaded in tension: } K_c = 1 + 2 \left( \frac{a}{b} \right)$$

**Fracture Toughness:**  $K_{Ic} = Y \sigma_{\text{nom}} \sqrt{\pi a}$

**Failure Prediction for Uniaxial Stress State:**  $n_s = \frac{\sigma_{\text{all}}}{\sigma_d}$

## Failure Prediction for Multiaxial Stress State:

Maximum shear stress theory (MSST, or Tresca):

$$n_s = \frac{S_y}{\sigma_1 - \sigma_3}$$

von Mises stress:

$$\sigma_e = \frac{1}{\sqrt{2}} [(\sigma_1 - \sigma_2)^2 + (\sigma_3 - \sigma_1)^2 + (\sigma_3 - \sigma_2)^2]^{1/2}$$

Distortion energy theory (DET, or von Mises):  $n_s = \frac{S_y}{\sigma_e}$

Maximum normal stress theory (MNST):

$$n_s = \frac{S_{ut}}{\sigma_1} \text{ or } n_s = \frac{S_{uc}}{\sigma_3}, \text{ whichever is lower.}$$

Internal Friction Theory (IFT, or Coulomb-Mohr):

$$\text{If } \sigma_1 > 0 \text{ and } \sigma_3 < 0, \frac{\sigma_1}{S_{ut}} - \frac{\sigma_3}{S_{uc}} = \frac{1}{n_s}$$

$$\text{If } \sigma_3 > 0, n_s = \frac{S_{ut}}{\sigma_1}$$

$$\text{If } \sigma_1 < 0, n_s = \frac{S_{uc}}{\sigma_3}$$

Modified Mohr Theory (MMT):

$$\text{If } \sigma_1 > 0 \text{ and } \sigma_3 < -S_{ut}, \frac{\sigma_1}{S_{uc} - S_{ut}} = \frac{S_{uc} S_{ut}}{n_s S_{uc} - S_{ut}}$$

$$\text{If } \sigma_3 > -S_{ut}, n_s = \frac{S_{ut}}{\sigma_1}$$

$$\text{If } \sigma_1 < 0, \sigma_3 = \frac{S_{uc}}{n_s}$$

## Recommended Readings

- Anderson, T.L. (2005), *Fracture Mechanics — Fundamentals and Applications*, 3rd ed., CRC Press.
- Budynas, R.G., and Nisbett, J.K. (2011), *Shigley's Mechanical Engineering Design*, 9th ed., McGraw-Hill.
- Hill, R. (1950) *The Mathematical Theory of Plasticity*, Oxford.
- Dowling, N.E. (1993) *Mechanical Behavior of Materials*, Pearson.
- Juvinall, R.C., and Marshek, K.M. (2012) *Fundamentals of Machine Component Design*, 5th ed., Wiley.
- Mott, R. L. (2014) *Machine Elements in Mechanical Design*, 4th ed., Pearson.
- Norton, R.L. (2011) *Machine Design*, 4th ed., Pearson Education.
- Sun, C.T., and Jin, Z.-H. (2012) *Fracture Mechanics*, Elsevier.

## References

- ASM International (1989) *Guide to Selecting Engineering Materials*, American Society for Metals.
- Bowman, K.J. (2004) *Mechanical Behavior of Materials*, Wiley.
- Coulomb, C.A. (1773) *Sur une Application des Regles de maximis et minimis a quelques problemes de statique relatifs a l'architecture*.
- Daniels, I.M., and Ishai, O. (2005) *Engineering Mechanics of Composite Materials* 2nd ed., Oxford.
- Dowling, N.E. (1993) *Mechanical Behavior of Materials*, Pearson.
- Doyle, J.F. (2004) *Experimental Stress Analysis: Completing the Solution of Partially Specified Problems*, Wiley.
- Fish, J., and Belytschko, T. (2007) *A First Course in Finite Elements*, Wiley.
- Hughes, T.J.R. (2000) *The Finite Element Method*, Dover.
- Kalpajian, S., and Schmid, S.R. (2014) *Manufacturing Engineering and Technology*, 7th ed., Pearson.
- Kaw, A.K. (1997) *Mechanics of Composite Materials*, CRC Press.

- Murphy, G. (1964) *Advanced Mechanics of Materials*, McGraw-Hill.
- Pilkey, W.D., and Pilkey, D.F. (2008) *Peterson's Stress Concentration Factors*, 3rd ed., Wiley.
- Reddy, J.N. (1996) *Mechanics of Laminated Composite Plates*, CRC Press.
- Tresca, H. (1868) "Mem. prenetes par divers savants," vol. 59, p. 754, *Comptes Rendus Acad. Sci.*
- Young, W.C., and Budynas, R. (2001) *Roark's Formulas for Stress and Strain*, 7th ed., McGraw-Hill.

## Questions

- 6.1 What is a stress concentration?
- 6.2 What is a stress concentration factor?
- 6.3 Define the term "crack" as relates to material fracture.
- 6.4 List the modes of crack growth.
- 6.5 What is fracture toughness?
- 6.6 Is a material with a high fracture toughness a ductile material? Explain.
- 6.7 What is the maximum shear stress theory?
- 6.8 Do the distortion energy criterion and maximum shear stress criterion give very different results? Explain.
- 6.9 Without the use of equations, define the von Mises stress.
- 6.10 What is a yield locus?
- 6.11 What is the MNST and the IFT?
- 6.12 For what materials is the IFT most useful?

## Qualitative Problems

- 6.13 A round bar has a fillet with  $r/d = 0.15$  and  $D/d = 1.5$ . The bar transmits both bending moment and torque. A new construction is considered to make the shaft stiffer and stronger by making it equally thick on each side of the fillet or groove. Determine whether that is a good idea.
- 6.14 Are stress concentrations more severe for tension, bending, or torsion for a bar with a groove?
- 6.15 A diamond cutting tool is used to make a shallow but sharp groove in a glass plate. The glass is struck with a hard rubber mallet to produce a well-defined cut at the location of the groove. Referring to the discussions in this chapter, explain the phenomena that are important in this application.
- 6.16 Explain why the approach used to cut glass will not work for a ductile aluminum.
- 6.17 A plate of titanium is diffusion bonded to a plate of aluminum. There are no holes, grooves, fillets, or notches in either member, and the two plates are then exposed to uniform tension. Sketch the stress distribution through the thickness of the plates. Is there a stress concentration? Explain.
- 6.18 Give three examples of each mode of crack growth described in Section 6.4.

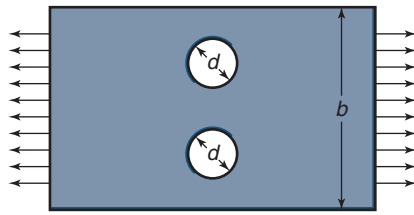
- 6.19 List and briefly explain the variables that can influence the fracture toughness of a material.
- 6.20 Some magnesium alloys have a lower strength in compression than in tension. What failure criterion would you use for such a material? Produce an equivalent sketch as Fig. 6.11 for this failure criterion.
- 6.21 If a material strain hardens, what effect does plastic deformation have on the yield locus?
- 6.22 Figs. 6.2 through 6.8 do not show stress concentrations for compressive loadings. Why not?
- 6.23 Review Fig. 6.4 and plot the stress concentration factor as a function of  $r/h$  for the case where the grooves are semicircular.
- 6.24 Figure 7.3 shows an R.R. Moore test specimen for fatigue tests. Explain why this specimen has its shape, and estimate the stress concentration factor.

## Quantitative Problems

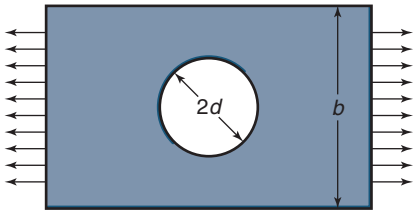
- 6.25 Complete the following table:

Shape	Loading	Geometry (mm)	$r$ (mm)	$K_c$
Plate w/ hole	Tension	$b=50, d=5$	—	
Plate w/ hole	Bending	$b=50, d=5$	—	
Plate w/ fillet	Tension	$H=100, h=50$		2.0
Bar w/ fillet	Tension	$D=50, d=25$		2.0
Bar w/ groove	Torsion	$D=10, d=9.09$	0.9	

- 6.26 Given that the stress concentration factor is 3.81 for a machine element made of steel with a modulus of elasticity of 207 GPa, find the stress concentration factor for an identical machine element made of aluminum instead of steel. The modulus of elasticity for aluminum is 69 GPa.
- 6.27 A flat part with constant thickness  $b$  is loaded in tension as shown in Fig. 6.3a. The height changes from 50 to 87 mm with a radius  $r = 4.0$  mm. Find how much lower a load can be transmitted through the bar if the height increases from 50 to 100 mm and the radius increases from 4.0 to 10 mm. *Ans.* 10% higher load.
- 6.28 A flat steel plate axially loaded as shown in Sketch *a* has two holes for electric cables. The holes are situated beside each other and each has a diameter  $d$ . To make it possible to draw more cables, the two holes are replaced with one hole having twice the diameter  $2d$ , as shown in Sketch *b*. Assume that the ratio of diameter to width is  $d/b = 0.2$  for the two-hole plate. Which plate will fail first?



(a)



(b)

Sketches a and b, for Problem 6.28

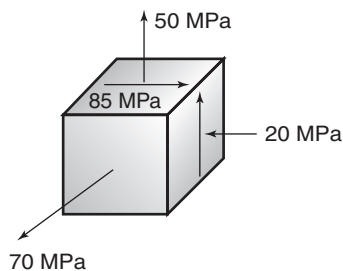
**6.29** A 5-mm thick, 100-mm wide AISI 1020 steel rectangular plate has a central elliptical hole 8 mm in length transverse to the applied stress and 2 mm in diameter along the stress. Determine the applied load that causes yielding at the edge of the hole. *Ans.* 92.43 kN.

**6.30** A 250-mm wide plate loaded in tension contains a 50 mm long, 10 mm wide slot. Estimate the stress concentration by:

- Approximating the slot as an ellipse that is inscribed within the slot.
- Obtaining the stress concentration at the edge of the slot by taking a section through the slot and approximating the geometry as a rectangular plate with a groove.

**6.31** A machine has three circular shafts, each with fillets giving stress concentrations. The ratio of fillet radius to shaft diameter is 0.1 for all three shafts. One of the shafts transmits a tensile force, one transmits a bending torque, and one transmits torsion. Because they are stressed exactly to the stress limit ( $n_s = 1$ ), a design change is proposed doubling the notch radii to get a safety factor greater than 1. How large will the safety factors be for the three shafts if the diameter ratio is 2 ( $D/d = 2$ )? *Ans.*  $n_{s,tension} = 1.21$ ,  $n_{s,bending} = 1.19$ ,  $n_{s,torsion} = 1.17$ .

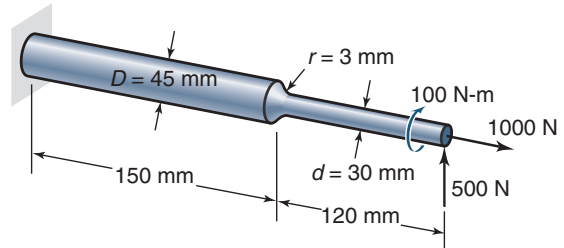
**6.32** A material with a yield strength of  $S_y = 350$  MPa is subjected to the stress state shown in Sketch c. What is the factor of safety based on the maximum shear stress and distortion energy theories? *Ans.* For MSST,  $n_s = 11.67$ .



Sketch c, for Problems 6.32 and 6.33

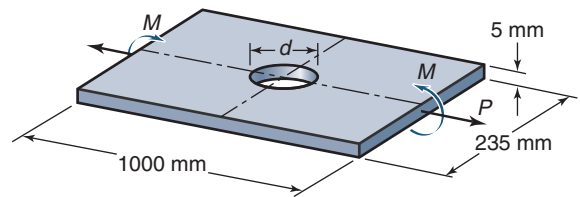
**6.33** A material subjected to the stresses shown in Sketch c is known to be yielding. What stress would cause yielding in uniaxial tension? *Ans.* For MSST,  $S_y = 30$  MPa.

**6.34** The shaft shown in Sketch d is subjected to tensile, torsional, and bending loads. Determine the principal stresses at the location of stress concentration. *Ans.*  $\sigma_1 = 53.0$  MPa,  $\sigma_2 = 0$ ,  $\sigma_3 = -12.27$  MPa.



Sketch d, for Problem 6.34

**6.35** A steel plate with dimensions shown in Sketch e is subjected to 150-kN tensile force and 300-N-m bending moment. The plate is made of AISI 1080 steel, quenched and tempered at 800°C. A hole is to be punched in the center of the plate. What is the maximum diameter of the hole for a safety factor of 1.5? *Ans.*  $d = 170$  mm.



Sketch e, for Problem 6.35

**6.36** A Plexiglas plate with dimensions 1 m  $\times$  1 m  $\times$  1 cm is loaded by a nominal tensile stress of 55 MPa in one direction. The plate contains a small crack perpendicular to the load direction. At this stress level a safety factor of 2 against crack propagation is obtained. Find how much larger the crack can get before it grows catastrophically. *Ans.*  $a_2 = 4a_1$ .

**6.37** A pressurized container is made of AISI 4340 steel. The wall thickness is such that the tensile stress in the material is 1000 MPa. The dimensionless geometry correction factor  $Y = 1$  for the given geometry. Find how big the largest crack can be without failure if the steel is tempered

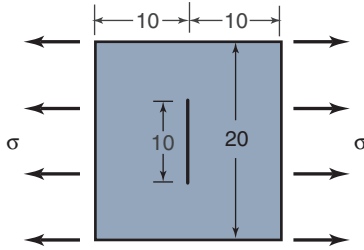
- At 260°C. *Ans.* 1.592 mm.
- At 425°C. *Ans.* 4.863 mm.

**6.38** Two tensile test rods are made of AISI 4340 steel tempered at 260°C and aluminum alloy 2024-T351. The dimensionless geometry correction factor  $Y = 1$ . Find how high a stress each rod can sustain if there is a crack of 1-mm half-length in each of them. *Ans.* AISI 4340:  $\sigma = 892$  MPa.

**6.39** A plate made of titanium alloy Ti-6Al-4V has the dimensionless correction factor  $Y = 1$ . How large can the largest crack in the material be if it still should be possible to plastically deform the plate in tension? *Ans.* 1.488 mm.



- 6.40** Consider the 2014-T4 aluminum plate shown in Sketch *f*. What is the largest tensile stress this plate can withstand? What is the largest center crack that can exist while ensuring that the material will still yield? *Ans.*  $\sigma = 115.7 \text{ MPa}$ ,  $l_c = 2.644 \text{ mm}$ .



Sketch *f*, for Problem 6.40. All dimensions are in millimeters.

- 6.41** For a plate with length 50 mm, width 25 mm, and thickness 5 mm, what is the ratio of allowable stress for a center-cracked specimen compared to an edge-cracked specimen? Assume the crack is 10 mm long for both cases. *Ans.*  $\sigma_{\text{edge}}/\sigma_{\text{center}} = 0.607$ .
- 6.42** A cylindrical pressure vessel constructed from 4340 steel tempered at  $260^\circ\text{C}$  has an outer diameter of 250 mm, a wall thickness of 2.5 mm, and an internal pressure of 4 MPa. What crack can be tolerated in the axial direction before fracture occurs? *Ans.*  $l_c = 39.8 \text{ mm}$ .
- 6.43** A 100-mm wide, 200-mm long plate made of titanium alloy Ti-6Al-4V has a single edge crack. How large can the crack be if it still should be possible to plastically deform the plate in tension? What if the plate is very long? *Ans.*  $l_c = 8.79 \text{ mm}$ .
- 6.44** A polymethylmethacrylate ( $K_{Ic} = 3 \text{ MPa}\sqrt{\text{m}}$ ) model of a gear has a 1-mm half-length crack formed in its fillet curve (where the tensile stress is maximum). The model is loaded until the crack starts to propagate. Assume that  $Y = 1.5$ . How much higher a load can a gear made of AISI 4340 steel tempered to  $425^\circ\text{C}$  carry with the same crack and the same geometry? *Ans.*  $\sigma_{\text{steel}}/\sigma_{\text{plexiglass}} = 29.13$ .
- 6.45** A pressure vessel made of aluminum alloy 2024-T351 is manufactured for a safety factor of 3.0 guarding against yielding. The material contains cracks through the wall thickness with a crack half-length less than 3 mm.  $Y = 1$ . Find the safety factor when considering crack propagation. *Ans.*  $n_s = 3.17$ .
- 6.46** The clamping screws holding the top lid of a nuclear reactor are made of AISI 4340 steel tempered at  $260^\circ\text{C}$ . They are stressed to a maximum level of 1250 MPa during a pressurization test before starting the reactor. Find the safety factor guarding against yielding and the safety factor guarding against crack propagation if the initial cracks in the material have  $Y = 1$  and  $a = 1 \text{ mm}$ . Also, find the safety factor if the same material is used, but tempered at  $425^\circ\text{C}$ . *Ans.* AISI 4340 tempered at  $260^\circ\text{C}$ :  $n_s = 0.714$ .
- 6.47** A glass tube used in a pressure vessel is made of aluminum oxide (sapphire) to make it possible to apply 30-MPa pressure and still have a safety factor of 2 guarding against fracture. For a soda-lime glass of the same geometry only 7.5-MPa pressure can be allowed if a safety

factor of 2 is to be maintained. Find the size of the cracks the glass tube can tolerate at 7.5 MPa pressure and a safety factor of 2.  $Y = 1$  for both tubes. *Ans.* Sapphire:  $l_c < 75.2 \mu\text{m}$ , glass:  $l_c < 65.6 \mu\text{m}$ .

- 6.48** A stress optic model used for demonstrating the stress concentrations at the ends of a crack is made of polymethylmethacrylate. An artificially made crack 50 mm long is perpendicular to the loading direction.  $Y = 1$ . Calculate the highest tensile stress that can be applied to the model without propagating the crack. *Ans.*  $\sigma_{\text{nom}} = 3.57 \text{ MPa}$ .
- 6.49** A passengerless airplane requires wings that are lightweight and resistant to fracture with cracks up to 2 mm in length. The dimensionless geometry correction factor  $Y$  is usually 1.5 for a safety factor of 2.
- (a) What is the appropriate alloy for this application? *Ans.* Either Aluminum 2020-T351 or Alloy steel 4340 tempered at  $425^\circ\text{C}$ .
- (b) If  $Y$  is increased to 4.5, what kind of alloy from Table 6.1 should be used? *Ans.* Al 2020-T351.
- 6.50** The anchoring of the cables carrying a suspension bridge are made of cylindrical AISI 1080 steel bars, quenched and tempered at  $800^\circ\text{C}$ , and are 200 mm in diameter. The force transmitted from the cable to the steel bar is 3.5 MN. Calculate the safety factor against yielding. *Ans.*  $n_s = 3.41$ .
- 6.51** The arm of a crane has two steel plates connected with a rivet that transfers the force in pure shear. The rivet is made of annealed AISI 1040 steel and has a circular cross section with a diameter of 25 mm. The load on the rivet is 15 kN. Calculate the safety factor according to the von Mises criterion. *Ans.*  $n_s = 5.67$ .
- 6.52** An aluminum alloy yields at a stress of 50 MPa in uniaxial tension. If this material is subjected to the stresses  $\sigma_1 = 25 \text{ MPa}$ ,  $\sigma_2 = 15 \text{ MPa}$ , and  $\sigma_3 = -26 \text{ MPa}$ , will it yield? Explain.
- 6.53** A material with a yield stress of 70 MPa is subjected to principal (normal) stresses of  $\sigma_1 = \sigma$ ,  $\sigma_2 = 0$ , and  $\sigma_3 = -\sigma/2$ . What is the value of  $\sigma$  when the metal yields according to the von Mises criterion? What if  $\sigma_2 = \sigma/3$ ? *Ans.*  $\sigma = 52.91 \text{ MPa}$ .
- 6.54** Assume that a material with a uniaxial yield strength  $S_y$  yields under a stress state of principal stresses  $\sigma_1$ ,  $\sigma_2$ , and  $\sigma_3$ , where  $\sigma_1 \geq \sigma_2 \geq \sigma_3$ . Show that the superposition of a hydrostatic stress  $p$  on this system (such as placing the specimen in a chamber pressurized with a liquid) does not affect yielding. In other words, the material will still yield according to yield criteria.
- 6.55** A machine element is loaded so that the principal normal stresses at the critical location for a biaxial stress state are  $\sigma_1 = 100 \text{ MPa}$  and  $\sigma_2 = -50 \text{ MPa}$ . The material is ductile with a yield strength of 300 MPa. Find the safety factor according to
- (a) The maximum-shear-stress theory (MSST) *Ans.*  $n_s = 2.00$ .
- (b) The distortion-energy theory (DET) *Ans.*  $n_s = 2.27$ .



**6.56** A bolt is tightened, subjecting its shank to a tensile stress of 80 MPa and a torsional shear stress of 50 MPa at a critical point. All of the other stresses are zero. Find the safety factor at the critical point by the DET and the MSST. The material is high-carbon steel (AISI 1080, quenched and tempered at 800°C). Will the bolt fail because of the static loading? *Ans.*  $n_{s,DET} = 3.22$ ,  $n_{s,MSST} = 2.97$ .

**6.57** A torque is applied to a piece of chalk used in a classroom until the chalk cracks. Using the maximum-normal-stress theory (MNST) and assuming the tensile strength of the chalk to be small relative to its compressive strength, determine the angle of the cross section at which the chalk cracks. *Ans.*  $45^\circ$ .

**6.58** A cantilevered bar 500 mm long with square cross section has 25-mm sides. Three perpendicular forces are applied to its free end, a 1000 N force is applied in the  $x$ -direction, a 100 N force is applied in the  $y$  direction, and an equivalent force of 100 N is applied in the  $z$ -direction. Calculate the equivalent stress at the clamped end of the bar by using the DET when the sides of the square cross section are parallel with the  $y$ - and  $z$ -directions. *Ans.*  $\sigma_e = 40$  MPa.

**6.59** A shaft transmitting torque from a gearbox to the rear axle of a truck is unbalanced, so that a centrifugal load of 500 N acts at the middle of the 3-m-long shaft. The annealed AISI 1040 tubular steel shaft has an outer diameter of 70 mm and an inner diameter of 58 mm. Simultaneously, the shaft transmits a torque of 3000 N-m. Use the DET to determine the safety factor guarding against yielding. *Ans.*  $n_s = 2.39$ .

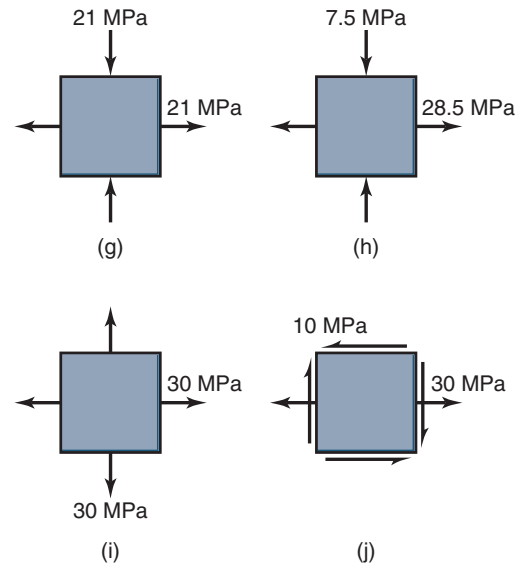
**6.60** The right-angle-cantilevered bracket used in Problem 5.30, Sketch  $w$ , has a concentrated force of 1000 N and a torque of 300 N-m. Calculate the safety factor. Use the DET and neglect transverse shear. Assume that the bracket is made of annealed AISI 1040 steel and use the following values:  $a = 0.5$  m,  $b = 0.3$  m,  $d = 0.035$  m,  $E = 205$  GPa, and  $\nu = 0.3$ . *Ans.*  $n_s = 1.76$ .

**6.61** A 100-mm-diameter shaft is subjected to a 10-kN-m steady bending moment, an 8-kN-m steady torque, and a 120-kN axial force. The yield strength of the shaft material is 600 MPa. Use the MSST and the DET to determine the safety factors for the various types of loading. *Ans.*  $n_s = 4.21$ .

**6.62** Use the MSST and the DET to determine the safety factor for 2024-T4 aluminum alloy for each of the following stress states:

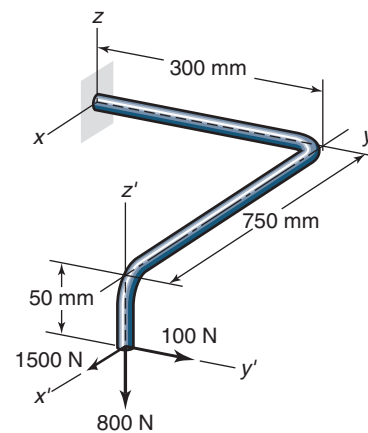
- $\sigma_x = 10$  MPa,  $\sigma_y = -60$  MPa. *Ans.*  $n_{s,MSST} = 4.64$ .
- $\sigma_x = \sigma_y = \tau_{xy} = -30$  MPa. *Ans.*  $n_{s,DET} = 5.42$ .
- $\sigma_x = -\sigma_y = 36$  MPa, and  $\tau_{xy} = 65$  MPa. *Ans.*  $n_{s,MSST} = 1.67$ .
- $\sigma_x = 2\sigma_y = -112$  MPa, and  $\tau_{xy} = 33$  MPa. *Ans.*  $n_{s,DET} = 2.31$ .

**6.63** Four different stress elements, each made of the same material, are loaded as shown in Sketches  $g$ ,  $h$ ,  $i$ , and  $j$ . Use the MSST and the DET to determine which element is the most critical. *Ans.* Sketch  $j$  is most critical.



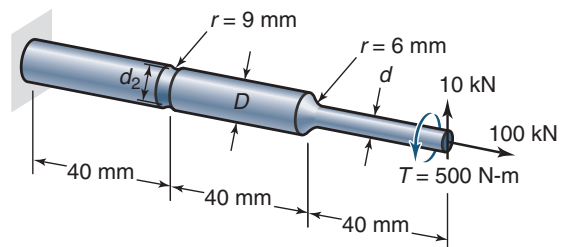
Sketches  $g$ ,  $h$ ,  $i$ , and  $j$ , for Problem 6.63

**6.64** The rod shown in Sketch  $k$  is made of annealed AISI 1040 steel and has two  $90^\circ$  bends. Use the MSST and the DET to determine the minimum rod diameter for a safety factor of 2 at the most critical section. *Ans.*  $d = 35$  mm.



Sketch  $k$ , for Problem 6.64

**6.65** The shaft shown in Sketch  $l$  is made of AISI 1020 steel, quenched and tempered at 870°C. Determine the most critical section by using the MSST and the DET. Dimensions of the various diameters shown in Sketch  $j$  are  $d = 30$  mm,  $D = 45$  mm, and  $d_2 = 40$  mm.



Sketch  $l$ , for Problem 6.65

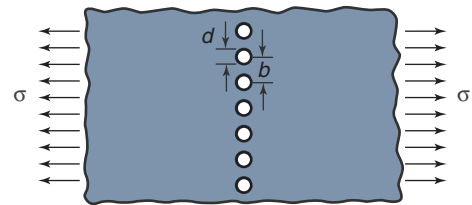
## Design and Projects

- 6.66** Design a test apparatus and procedure that will produce the data depicted in Fig. 6.19.
- 6.67** A plate of titanium is diffusion bonded to a plate of aluminum. The plates are then loaded in tension. Is there a stress raiser present? A hole is then drilled through the plates, and they are loaded by uniform tension. Sketch the stress distribution through the thickness of the plates at the critical location.
- 6.68** Perform an Internet search and summarize the important characteristics of Izod and Charpy tests. What properties do these tests measure?
- 6.69** A steel plate 100 mm in width is to be loaded in tension. If you need to locate a hole with a 25 mm diameter somewhere in the plate, would you place it in the center, at the edge, or an intermediate location? Explain.
- 6.70** Using a pair of shears, carefully cut the top of a beverage can in half and prepare a drawing of the cross section. What failure mode is used to open the can? Explain.
- 6.71** Derive the allowable pressure in a pressure vessel as a function of its dimensions and material yield strength for the von Mises and Tresca yield criterion. Consider both a spherical and cylindrical pressure vessel.
- 6.72** Take a long cylindrical balloon and, with a thin felt-tip pen, mark a small square on it. What will be the shape of this square after you blow up the balloon, (1) a larger square, (2) a rectangle with its long axis in the circumferential directions, (3) a rectangle with its long axis in the longitudinal direction, or (4) an ellipse? Perform this experiment and, based on your observations, explain the results, using appropriate equations. Assume that the material the balloon is made up of is perfectly elastic and isotropic and that this situation represents a thin-walled closed-end cylinder under internal pressure.
- 6.73** It has been proposed to modify the von Mises yield criterion as

$$(\sigma_1 - \sigma_2)^a + (\sigma_2 - \sigma_3)^a + (\sigma_3 - \sigma_1)^a = \text{Constant}$$

where  $a$  is an even integer larger than 2. Plot this yield criterion for  $a = 4$  and  $a = 12$ , along with the Tresca and von Mises criterion, in plane stress. For what types of materials is such a modified yield criterion useful? Explain.

- 6.74** During plastic deformation, metals act as incompressible solids. Derive the effective Poisson's ratio for plastically deforming metals.
- 6.75** It is common practice to use a radius on an inner shoulder, and a chamfer at an external corner. (a) Using appropriate sketches and/or equations, explain why this is the case, and why a chamfered inner shoulder is not practical. (b) If a  $45^\circ$  chamfer is produced, it is common to specify a leg,  $c$ , of a chamfer to be  $c = 0.1\sqrt{d}$ , where  $d$  is the shaft diameter in millimeters. Replot Fig. 6.5 as a function of diameter using this rule.
- 6.76** It was mentioned in Section 6.7.2 that some magnesium alloys are well-suited for the internal friction theory because their strength in compression is lower than their strength in tension. Review the technical literature, and write a one-page summary explaining why the behavior of these magnesium alloys is unique.
- 6.77** Review the technical literature and find the analytical solutions for the case of Fig. 6.3b.
- 6.78** Sketch  $m$  shows an axial plate with a row of circular holes. Qualitatively sketch the stress concentration factor you expect to see as a function of  $d/b$ . Then review the technical literature and obtain the stress concentration factor for this situation. A rule of thumb for metals is that rivets should have a spacing not less than three times the diameter. What stress concentration factor results from the associated hole spacing?



Sketch  $m$ , for Problem 6.78.

- 6.79** For the materials in Table 6.1, calculate the largest allowable center crack that can exist in a long tension member while still yielding. Assume the member has a width of (a) 25 mm, and (b) 1 mm. Include the geometry correction factor,  $Y$ , in your analysis.

## Chapter 7

# Fatigue and Impact



Aloha Airlines Flight 243, a Boeing 737-200, taken April 28, 1988. The midflight fuselage failure was attributed to corrosion-assisted fatigue. Source: AP Photos.

*All machine and structural designs are problems in fatigue because the forces of Nature are always at work and each object must respond in some fashion.*

Carl Osgood, *Fatigue Design*

This chapter introduces the essential concepts of fatigue and impact. Fatigue is a process wherein a material accumulates damage due to a cyclic load; this damage compromises strength and can lead to brittle fracture, even for ductile materials. In fatigue, flaws initially present in the material grow until one dominates; this crack then propagates through the part with every stress cycle. The chapter begins with an analysis of Mode I fracture with uniaxial stresses, and presents S-N diagrams and associated theories for uniaxial fully alternating stresses. Some materials have an endurance limit; if the stresses remain below the endurance limit, then a fatigue failure is not likely. Many factors that affect the endurance limit are discussed, including stress concentrations, surface finish, temperatures, residual stresses, part size, and desired reliability. For materials without an endurance limit, fault tolerant design approaches are needed to avoid fatigue failures. The chapter also describes failure when there is a significant mean stress, as well as when the stress state is more complicated. Fracture mechanics approaches to fatigue are also introduced. The chapter ends with a discussion of impact stresses that result from dynamic loadings.

### Contents

- 7.1 Introduction 160
- 7.2 Fatigue 160
- 7.3 Cyclic Stresses 162
- 7.4 Strain Life Theory of Fatigue 162
- 7.5 Fatigue Strength 163
- 7.6 Fatigue Regimes 168
- 7.7 Stress Concentration Effects 169
- 7.8 The Modified Endurance Limit 171
- 7.9 Cumulative Damage 175
- 7.10 Influence of Nonzero Mean Stress 176
- 7.11 Influence of Multi-Axial Stress States 180
- 7.12 Fracture Mechanics Approach to Fatigue 182
- 7.13 Linear Impact Stresses and Deformations 183
- 7.14 Summary 186

### Examples

- 7.1 Cyclic Stresses 162
- 7.2 Determination of the Endurance Limit using the Staircase Approach 167
- 7.3 High Cycle, Finite Life Fatigue 169
- 7.4 Fatigue Stress Concentration Factors 170
- 7.5 Endurance Limits and Modification Factors 174
- 7.6 Endurance Limits and Modification Factors for Square Cross Section 175
- 7.7 Cumulative Damage 176
- 7.8 Effect of Nonzero Mean Stress 177
- 7.9 Safety Factor Using the Modified Goodman Criterion 178
- 7.10 Fault Tolerant Design 182
- 7.11 Impact Stresses 184

### Design Procedures

- 7.1 Methods to Maximize Design Life 161
- 7.2 Staircase Approach 167
- 7.3 Estimation of Endurance Limit 174

### Case Study

- 7.1 Fault Tolerant Design in Aircraft 185

## Symbols

$A$	area, $m^2$
$a$	fatigue strength exponent
$b$	width, m
$b_s$	slope
$C$	constant used in Eq. (7.47)
$C_1, C_2$	integration constants
$\bar{C}$	intercept
$c$	distance from neutral axis to outer fiber of solid, m
$d$	diameter, m
$E$	modulus of elasticity, Pa
$e, f$	factors used in Eq. (7.19)
$g$	gravitational acceleration, $9.807 \text{ m/s}^2$
$H$	height including two notch radii, m
$h$	height without two notch radii, m
$I$	area moment of inertia, $m^4$
$I_m$	impact factor
$K$	stress intensity factor, $\text{MPa}\sqrt{m}$
$K_c$	stress concentration factor
$K_f$	fatigue stress concentration factor
$k$	spring rate, N/m
$\Delta K$	stress intensity range, $\text{MPa}\sqrt{m}$
$k_f$	surface finish factor
$k_m$	miscellaneous factor
$k_r$	reliability factor
$k_s$	size factor
$k_t$	temperature factor
$l_c$	crack length, m
$M$	bending moment, N-m
$m$	constant used in Eq. (7.47)
$N$	fatigue life in cycles
$N'$	number of cycles to failure at a specific stress
$N'_t$	total number of cycles to failure
$n'$	number of cycles at a specific stress when $n' < N'$
$n_s$	safety factor
$P$	force, N
$q_n$	notch sensitivity factor
$R$	stress ratio, $\sigma_{\min}/\sigma_{\max}$
$R_a$	arithmetic average roughness, m
$r$	notch radius, m
$S_e$	modified endurance limit, Pa
$S'_e$	endurance limit, Pa
$S_f$	modified fatigue strength, Pa
$S'_f$	fatigue strength, Pa
$S'_i$	strength at $10^3$ cycles for ductile material, Pa
$S'_l$	fatigue strength where high-cycle fatigue begins, Pa
$S_u$	ultimate strength, Pa
$S_y$	yield strength, Pa
$u$	sliding velocity, m/s
$W$	weight, N
$Y$	plate size correction factor
$\alpha$	fatigue ductility exponent
$\alpha_i$	cyclic ratio $n'_i/N'_i$
$\delta$	deflection, m
$\delta_{st}$	static deflection, m
$\epsilon'_f$	fatigue ductility coefficient
$\phi$	phase angle between bending and torsion, rad
$\Delta\epsilon$	total strain
$\sigma$	stress, Pa
$\sigma'_f$	stress at fracture, Pa
$\sigma_r$	stress range, Pa
$\tau$	shear stress, Pa

## Subscripts

$a$	alternating
$f$	final
$i$	integer
$m$	mean
ref	reference

## 7.1 Introduction

This chapter focuses on understanding and predicting component failure under cyclic and impact loading, conditions that occur in most machine elements. Fluctuating loads induce fluctuating stresses that often result in failure due to cumulative damage. To better understand failures due to fluctuating stresses, consider the back and forth bending of a paper clip. Bending results in compressive and tensile stresses on opposite sides of the paper clip, and these stresses reverse with the bending direction. Thus, the stress at any point around the paper clip will vary as a function of time. Repeated bending of the paper clip will eventually exhaust the material, resulting in failure.

Stresses and deflections in impact loading are in general much greater than those found in static loading; thus, dynamic loading effects are important. A material's physical properties are a function of loading speed. Higher loading rates usually result in increased yield and ultimate strengths. Some examples in which impact loading have to be considered are bumpers and guideways, as well as components of crushing machinery, hammer and hammermills, tampers and the like.

## 7.2 Fatigue

In the 19th century, the First Industrial Revolution was in full swing. Coal was mined, converted into coke, and used to smelt iron from ore. The iron was used to manufacture bridges, railroads, and trains that brought more coal to the cities, allowing more coke to be produced, etc., in a spiral of ever-increasing production. But then bridges, the monuments to engineering accomplishment, began failing. Even worse, they would fail in extremely confusing ways. A 50-ton locomotive could pass over a bridge without incident; a farmer driving a horse-drawn wagon full of hay would subsequently cause the bridge to collapse. Fear gripped the populace, as people believed death awaited on the bridges (Fig. 7.1).

Today, we no longer fear our "aging infrastructure," certainly not to the extent of the late 19th century. The road construction and improvements that delay traffic from time to time make collapses of civil engineering works, such as bridges, truly rare. But **fatigue** failures, as we now know them to be, are not at all rare in machine elements. Fatigue (and *fatigue wear*, Section 8.9.3) is the single largest cause of failure in metals, estimated to be 90% of all metallic failures. Fatigue failures, especially in structures, are catastrophic and insidious, occurring suddenly and often without warning. For that reason, engineers must apply fatigue considerations in design.

Fatigue has both microscopic and macroscopic aspects. That is, although a rolling-element bearing failing by surface spalling and a shaft breaking in two are quite different events, both the bearing and the shaft have failed due to fatigue. The failure stresses were considerably lower than the yield strengths of the materials. The rolling-element bearing suffered surface fatigue failure; the shaft, structural fatigue





Figure 7.1: “On the Bridge,” an illustration from *Punch* magazine in 1891 warning the populace that death was waiting for them on the next bridge. Note the cracks in the iron bridge.

failure. Thus, fatigue failure occurs at relatively low stress levels to a component or structure subjected to fluctuating or cyclic stresses.

Some of the basic concepts associated with fatigue are the following:

1. Fatigue is a complex phenomenon and no universal theories to describe the behavior of materials subjected to cyclic loadings exist; instead, there is a large number of theories, each tailored to particular materials.
2. Fatigue failures act in brittle fashion even in ductile metals; little if any gross plastic deformation is associated with fatigue.
3. Most of the engineering design experience in fatigue is based on an experimental understanding of carbon steel behavior. Much effort has been directed toward extending these semi-empirical rules to other ferrous and non-ferrous metals, as well as ceramics, polymers, and composite materials.
4. Fatigue involves the accumulation of damage within a material. Damage usually consists of cracks that grow by a small distance with each stress cycle.
5. Experiments have shown that fatigue cracks generally begin at a surface and propagate through the bulk. Therefore, much attention is paid to the quality of surfaces in fatigue-susceptible machine elements. However, if large subsurface flaws or stress raisers exist in the substrate, fatigue cracks can initiate below the surface.
6. Flaws grow uniformly and simultaneously at several sites until one flaw becomes dominant and grows more rapidly than the others. At this point, the flaw is considered a crack.
7. Fatigue testing is imperative to confirm safe mechanical design.

The last of these points cannot be overemphasized. This book concentrates on theoretical approaches that can guide a designer, but there is much uncertainty in fatigue failures.

Guidelines will be presented that are often difficult to directly apply to specific materials, manufacturing processes, or components. Application of these methodologies without experimental verification of designs is acceptable for students, preliminary design or design analysis, but rarely for commercial products. It is also common to use large safety factors whenever possible for components subjected to fatigue.

The total life of a component or structure is the time it takes a crack to initiate plus the time it needs to propagate through the cross-section. Design life can be maximized as summarized in Design Procedure 7.1.

### Design Procedure 7.1: Methods to Maximize Design Life

1. *Minimizing initial flaws, especially surface flaws.* Great care is taken to produce fatigue-resistant surfaces through processes such as grinding or polishing that produce exceptionally smooth surfaces. These surfaces are then carefully protected before a product is placed into service.
2. *Maximizing crack initiation time.* Compressive surface residual stresses are imparted (or at least tensile residual stresses are relieved) through manufacturing processes such as shot peening or burnishing, or by a number of surface treatments.
3. *Maximizing crack propagation time.* Substrate properties, especially those that retard crack growth, are also important. For example, in some materials fatigue cracks will propagate more quickly along grain boundaries than through grains. In this case, using a material that has elongated grains transverse to the direction of fatigue crack growth can extend fatigue life (e.g., by using cold-worked components instead of castings).
4. *Maximizing the critical crack length.* Fracture toughness (Section 6.5) is an essential material property, and materials with higher fracture toughnesses are generally better suited for fatigue applications.

Given a finite number of resources, which one of the approaches in Design Procedure 7.1 should the designer emphasize? Ever-smoother surfaces can be manufactured at ever-increasing costs but at ever-decreasing payoff as the surface valleys become smaller. Maximizing initiation time allows parts to function longer with little or no loss in performance. Maximizing propagation time can allow cracks to be detected before they become catastrophic, the approach previously called the “doctrine of manifest danger” (Section 1.4.1). Maximizing the critical crack length can lead to long life with a greater likelihood of recognizing an imminent failure. All of these approaches have merit and are pursued from time to time. The proper emphasis, just as with the safety factor, is product and material specific and is best decided through experience.

The designer’s job is to select a material and a processing route that will lead to successful products. However, fatigue is an extremely complex subject. This chapter introduces approaches to design for cyclic loading. In practice, extreme caution should be used in applying any of these approaches without generous safety factors and/or experimental confirmation.



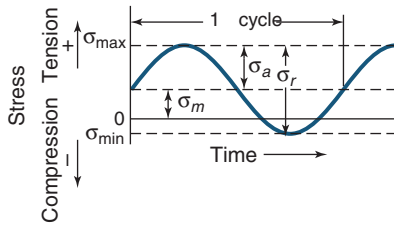


Figure 7.2: Variation in nonzero cyclic mean stress.

### 7.3 Cyclic Stresses

A **cyclic stress** is time dependent, but the variation is such that the stress sequence repeats itself. The stresses may be axial (tensile or compressive), flexural (bending), or torsional (twisting). Figure 7.2 shows an idealized cyclic variation of a stress that varies with time. Also shown are several parameters used to characterize fluctuating cyclic stress. A stress cycle ( $N = 1$ ) constitutes a single application and removal of a load and then another application and removal of the load in the opposite direction. Thus,  $N = 1/2$  means that the load is applied once and then released. The stress amplitude alternates about a **mean stress**,  $\sigma_m$ , defined as

$$\sigma_m = \frac{\sigma_{\max} + \sigma_{\min}}{2}. \quad (7.1)$$

The **stress range**,  $\sigma_r$ , is the difference between  $\sigma_{\max}$  and  $\sigma_{\min}$ , namely,

$$\sigma_r = \sigma_{\max} - \sigma_{\min}. \quad (7.2)$$

The **stress amplitude**,  $\sigma_a$ , is one-half of the stress range, or

$$\sigma_a = \frac{\sigma_r}{2} = \frac{\sigma_{\max} - \sigma_{\min}}{2}. \quad (7.3)$$

The **stress ratio**,  $R$ , is the ratio of minimum and maximum stress, or

$$R = \frac{\sigma_{\min}}{\sigma_{\max}}. \quad (7.4)$$

Four frequently encountered patterns of constant-amplitude cyclic stress are:

1. **Completely reversed** ( $\sigma_m = 0$ ,  $R = -1$ )
2. **Nonzero mean** (as shown in Fig. 7.2)
3. **Released tension** ( $\sigma_{\min} = 0$ ,  $R = 0$ ,  $\sigma_m = \sigma_{\max}/2$ )
4. **Released compression** ( $\sigma_{\max} = 0$ ,  $R = \infty$ ,  $\sigma_m = \sigma_{\min}/2$ )

#### Example 7.1: Cyclic Stresses

**Given:** Breakaway bolts are used to fasten street light poles and fire hydrants to their foundations; these bolts are intended to withstand normal loads such as from the wind, but when struck by a vehicle, their limited ductility causes them to fail. The pole or hydrant is then allowed to move and this reduces the severity of an automobile impact. Consider the case where a bolt is tightened so that it is in tension, but a wind loading applies a compressive stress, so that the repeating stress is  $\sigma = \pm 100$  MPa.

**Find:** The mean stress, the range of stress, the stress amplitude, and the stress ratio for the breakaway bolt.

**Solution:** Equations (7.1) through (7.4) are needed to solve this problem. The mean stress is

$$\sigma_m = \frac{\sigma_{\max} + \sigma_{\min}}{2} = \frac{100 - 100}{2} = 0.$$

The range of stress is

$$\sigma_r = \sigma_{\max} - \sigma_{\min} = 100 - (-100) = 200 \text{ MPa}.$$

The alternating stress is

$$\sigma_a = \frac{\sigma_r}{2} = \frac{200}{2} = 100 \text{ MPa}.$$

The stress ratio is

$$R = \frac{\sigma_{\min}}{\sigma_{\max}} = \frac{-100}{100} = -1.$$

### 7.4 Strain Life Theory of Fatigue

As discussed in Section 7.2, fatigue is a damage accumulation process that manifests itself through crack propagation, but no crack propagation is possible without plastic deformation at the crack tip. Although the volume stressed highly enough for plastic deformation can be extremely small, if the stress fields remain elastic, no crack propagation is possible. However, recall from Section 6.2 that the stress concentration associated with a sharp crack is very large, and even low stresses will therefore result in plastic deformation at the crack tip. Further, the use of bulk material properties, such as yield strength or ultimate strength, presents difficulties because cyclic loadings can change these values near a crack tip. They may increase or decrease depending on the material and its manufacturing history. Thus, the material strength at the location where cracks are propagating can differ from the bulk material strength listed in handbooks or obtained from tension tests.

Given these difficulties, several approaches have been suggested for dealing with the strain encountered at a crack tip and predicting fatigue failure. One of the better known is the **Manson-Coffin relationship**, which gives the total strain amplitude as the sum of the elastic and plastic strain amplitudes and relates this to life:

$$\frac{\Delta\epsilon}{2} = \frac{\sigma'_f}{E} (2N')^a + \epsilon'_f (2N')^\alpha, \quad (7.5)$$

where

$\Delta\epsilon$  = total strain, including both plastic and elastic components

$\sigma'_f$  = stress at fracture in one stress cycle, Pa

$E$  = elastic modulus of material, Pa

$N'$  = number of cycles that will occur before failure

$\epsilon'_f$  = fatigue ductility coefficient (true strain corresponding to fracture in one stress cycle)

$a$  = fatigue strength exponent

$\alpha$  = fatigue ductility exponent

Table 7.1 gives some typical values of the material properties  $a$  and  $\alpha$ .

The Manson-Coffin relationship is difficult to use in practice because the total strain,  $\Delta\epsilon$ , is difficult to determine. Stress concentration factors, such as those presented in Chapter 6, are readily available in the technical literature, but strain concentration factors in the plastic range are nowhere to be

Table 7.1: Cyclic properties of some metals. *Source:* After Shigley and Mitchell [1983] and Suresh [1998].

Material	Condition <sup>a</sup>	Yield strength $S_y$ MPa	Fracture strength $\sigma_f$ MPa	Fatigue ductility coefficient, $\epsilon'_f$	Fatigue strength exponent, $a$	Fatigue ductility exponent, $\alpha$
<b>Steel</b>						
1015	Normalized	228	827	0.95	-0.110	-0.64
4340	Tempered	1172	1655	0.73	-0.076	-0.62
1045	Q&T <sub>a</sub> 27° C	—	2140	—	-0.065	-1.00
1045	Q&T 150° C	1720	2720	0.07	-0.055	-0.60
1045	Q&T 260° C	1275	2275	0.25	-0.080	-0.68
1045	Q&T 315° C	965	1790	0.35	-0.070	-0.69
4142	Q&T 27° C	2070	2585	—	-0.075	-1.00
4142	Q&T 200° C	1720	2650	0.07	-0.076	-0.76
4142	Q&T 315° C	1340	2170	0.09	-0.081	-0.66
4142	Q&T 370° C	1070	2000	0.40	-0.080	-0.73
4142	Q&T 450° C	900	1550	0.45	-0.080	-0.75
<b>Aluminum</b>						
1100	Annealed	97	193	1.80	-0.106	-0.69
2014	T6	462	848	0.42	-0.106	-0.65
2024	T351	379	1103	0.22	-0.124	-0.59
5456	H311	234	724	0.46	-0.110	-0.67
7075	T6	469	1317	0.19	-0.126	-0.52
<b>Titanium</b>						
Ti-6Al-4V	Solution treated+aged	1185	2030	0.841	-0.104	-0.69
<b>Nickel</b>						
Inconel X	Annealed	700	2255	1.16	-0.117	-0.75

<sup>a</sup> Q&T: Quenched and tempered.

found. The advantage of the Manson-Coffin equation is that it gives insight into important properties in fatigue strength determination. It shows the importance of strength as well as ductility, and it leads to the conclusion that as long as there is a cyclic plastic strain, no matter how small, there will eventually be failure.

## 7.5 Fatigue Strength

### 7.5.1 Rotating-Beam Experiments

Fatigue is inherently probabilistic; that is, there is a great range of performance within samples prepared from the same materials. In previous problems and case studies, a valuable approach called the worst-case scenario was described. To apply this approach to fatigue, a designer would select surface finishes, notch sizes, initial flaw size, etc. that minimize the fatigue strength of the candidate specimen. However, this process would result in fatigue specimens with zero strength, a situation that does nothing to aid designers. Thus, data on fatigue often reflect the best-case scenario, and do not reflect actual environments. The designer is strongly cautioned that great care must be taken in applying fatigue design theories based on best case scenarios to critical applications.

Because fatigue is a damage accumulation phenomenon, initial flaws have a large effect on performance. No manufacturing process produces defect-free parts; indeed, it is not uncommon to encounter thousands, even millions, of flaws per cubic millimeter. The flaws are distributed in size, shape, location and orientation, they are often close enough to violate Saint-Venant's principal (see Section 4.3), so that the associated stress concentrations interfere with and compound each other. Analytical approaches that derive fatigue strengths from first principles are thus very difficult, and most knowledge on material fatigue is experiment-based.

Experimental approaches to fatigue use either exemplars or idealized, standard specimens. The former are more reliable and best for critical applications. The latter are often

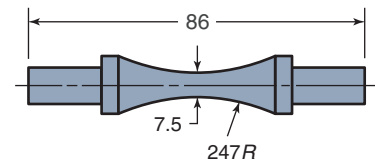


Figure 7.3: R.R. Moore machine fatigue test specimen. Dimensions in millimeters.

used when a direct simulation of the loading environment is cost prohibitive.

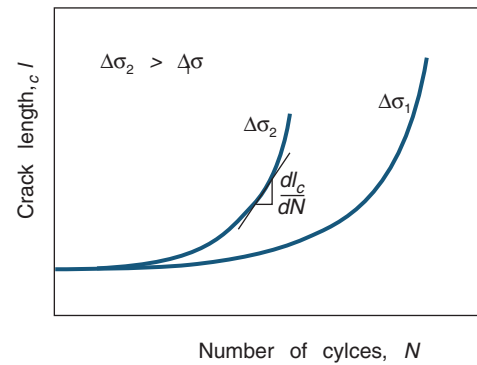
To establish the fatigue strength of an exemplar, a series of tests is performed. The test apparatus duplicates as nearly as possible the stress conditions (stress level, time frequency, stress pattern, etc.) in practice. The exemplar duplicates as nearly as possible any manufacturing and treatment processes. Such experiments give the most direct indication of a component's survivability in the actual loading environment.

To test idealized, standard specimens, a rotating-beam fatigue testing machine is often used, such as the Moore rotating-beam machine. The specimen is subjected to pure bending, and no transverse shear is imposed. The specimen has specific dimensions (Fig. 7.3) and a highly polished surface, with a final polishing in the axial direction to avoid circumferential scratches. If the specimen breaks into two equal pieces, the test is indicative of the material's fatigue strength. If the pieces are unequal, a material or surface flaw has skewed the results. The test specimen is subjected to completely reversed ( $\sigma_m = 0$ ) stress cycling at a relatively large maximum stress amplitude, usually two-thirds of the static ultimate strength, and the cycles to failure are counted. Thus, for each specimen at a specific stress level, the test is conducted until failure occurs. The procedure is repeated on other identical specimens, progressively decreasing the maximum stress amplitude.

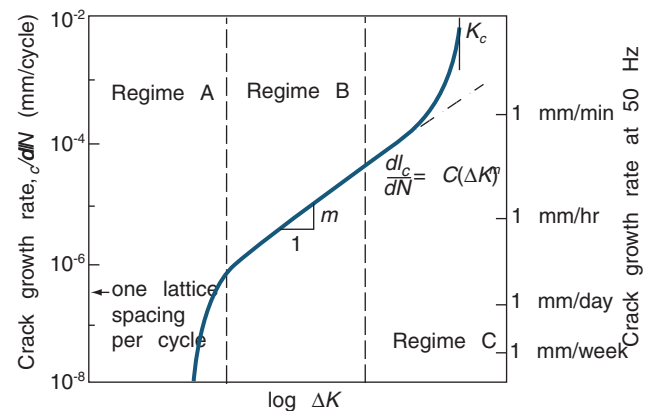
### 7.5.2 Regimes of Fatigue Crack Growth

Figure 7.4a shows the size of a fatigue crack as a function of number of cycles for two stress ratios. Figure 7.4b illustrates the rate of crack growth, and more clearly shows three different regimes of crack growth:

1. *Regime A* is a period of very slow crack growth. Note that the crack growth rate can be even smaller than an atomic spacing of the material per cycle. Regime A should be recognized as a period of non-continuum failure processes. The fracture surfaces are faceted or serrated in this regime, indicating crack growth is primarily due to shear deformations within a grain. The growth rate is so small that crack lengths may be negligible over the life of the component if this regime is dominant. Regime A is strongly affected by material microstructure, environmental effects, and stress ratio,  $R$ .
2. *Regime B* is a period of moderate crack growth rate, often referred to as the **Paris regime**. In this regime, the rate of crack growth is influenced by several factors, involving material microstructure, mechanical load variables, and the environment. Thus, it is not surprising that crack propagation rates cannot be determined for a given material or alloy from first principles, and testing is required to quantify the growth rate.
3. *Regime C* is a period of high-growth rate, where the maximum stress intensity factor for the fatigue cycle approaches the fracture toughness of the material. Material microstructural effects and loadings have a large influence on crack growth, and additional static modes such as cleavage and intergranular separation can occur.



(a)



(b)

### 7.5.3 Microstructure of Fatigue Failures

As discussed above, even the most ductile materials can exhibit brittle behavior in fatigue, and will fracture with little or no plastic deformation. The reasons for this are not at all obvious, but an investigation of fatigue fracture microstructure can help explain this behavior.

A typical fatigue fracture surface is shown in Fig. 7.5, and has the following features:

1. Near the origin of the fatigue crack (Point B in Fig. 7.5), the surface is *burnished*, or very smooth. In the early stages of fatigue, the crack grows slowly and elastic deformations result in microscopic sliding between the two surfaces, resulting in a rubbing of the surfaces and associated mechanical polishing.
2. Near the final fracture location (Point A in Fig. 7.5), *striations* or *beachmarks* are clearly visible to the naked eye. During the last few cycles of a fatigue failure, the crack growth is very rapid, and these striations are indicative of fast growth and growth-arrest processes.
3. Microscopic striations can exist between these two extremes as shown in Fig. 7.5, and are produced by the slower growth of fatigue cracks at this location in the part.
4. The final fracture surface often looks rough and is indicative of brittle fracture, but it can also appear ductile depending on the material.

The actual pattern of striations depends on the particular geometry, material, and loading (Fig. 7.6), and can require experience to evaluate a failure cause.

Figure 7.4: Illustration of fatigue crack growth. (a) Size of a fatigue crack for two different stress ratios as a function of the number of cycles; (b) rate of crack growth, illustrating three regimes.

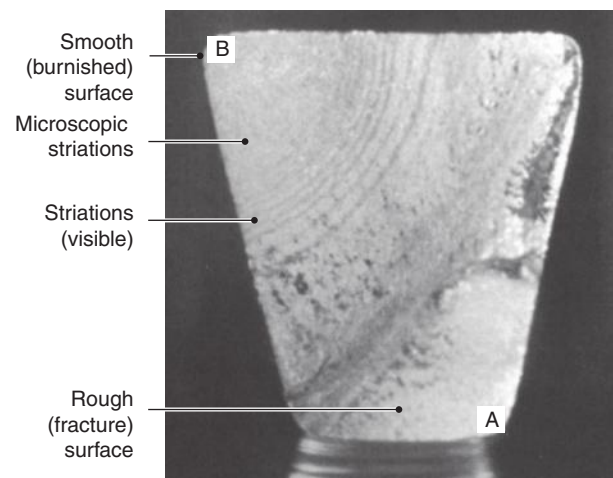


Figure 7.5: Cross section of a fatigued section, showing fatigue striations or beachmarks originating from a fatigue crack at B. Source: Rimmnac, C., et al., in *ASTM STP 918, Case Histories Involving Fatigue and Fracture*, copyright 1986, ASTM International. Reprinted with permission.

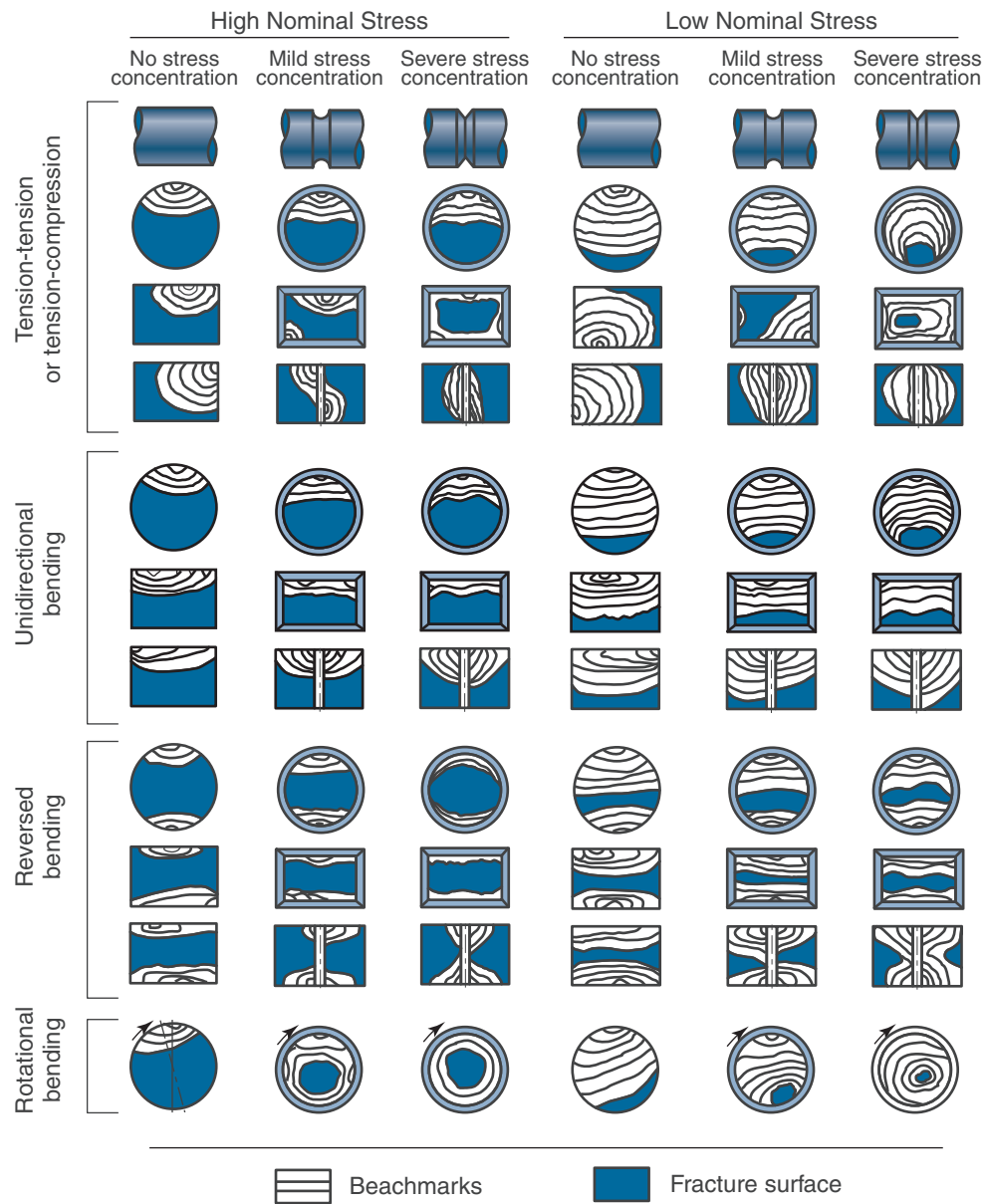


Figure 7.6: Typical fatigue-fracture surfaces of smooth and notched cross-sections under different loading conditions and stress levels. *Source:* Adapted from *Metals Handbook*, American Society for Metals [1975].

### 7.5.4 S-N Diagrams

Data from reversed bending experiments are plotted as the fatigue strength versus the logarithm of the total number of cycles to failure,  $N'_t$ , for each specimen. These plots are called **S-N diagrams** or **Wöhler diagrams** after August Wöhler, a German engineer who published his fatigue research in 1870. They are a standard method of presenting fatigue data and are useful and informative. Two general patterns for two classes of material, those with and those without endurance limits, emerge when plotting the fatigue strength versus the logarithm of the number of cycles to failure. Figure 7.7 shows typical results for several materials. Figure 7.7a presents test data for wrought steel. Note the large amount of scatter in the data, even with the great care used to prepare test specimens. Thus, material properties extracted from curves such as those in Fig. 7.7 are all somewhat suspect, and have significant variation between test specimens. Figure 7.7a also shows a common result. For some materials with **endurance limits**, such as ferrous and titanium alloys, a change in slope occurs at low stress levels, called a “knee” in the curve. This implies that an endurance limit  $S'_e$  is reached, below which failure will not occur (although this is strictly not true — see Section 7.6.3). This endurance limit  $S'_e$  represents the largest fluctuating stress that will *not* cause failure for an infinite number of cycles. For many steels the endurance limit ranges between 35 and 60% of the ultimate strength.

Most nonferrous alloys (e.g., aluminum, copper, and magnesium) *do not* have a significant endurance limit. Their fatigue strength continues to decrease with increasing cycles. Thus, fatigue will occur regardless of the stress amplitude. The fatigue strength for these materials is taken as the stress level at which failure will occur for some specified number of cycles (e.g.,  $10^6$  or  $10^7$  cycles).

Determining the endurance limit experimentally is lengthy and expensive. The Manson-Coffin relationship given by Eq. (7.5) demonstrates that the fatigue life will depend on the material's fracture strength during a single load cycle, suggesting a possible relationship between static material strength and strength in fatigue. Such a relationship has been noted by several researchers (see Fig. 7.8). The stress endurance limits of steel for three types of loading can be approximated as

$$\begin{aligned} \text{bending : } S'_e &= 0.5S_u \\ \text{axial : } S'_e &= 0.45S_u \\ \text{torsion : } S'_e &= 0.29S_u \end{aligned} \quad (7.6)$$

Equation (7.6) can be used to approximate the endurance limits for other ferrous alloys but it must be recognized that the limits can vary significantly from experimentally determined endurance limits. As depicted by the dashed line in Fig. 7.8, the maximum value of the endurance limit for ferrous alloys is taken as 690 MPa, regardless of the predictions from Eq. (7.6). Even if the ultimate strength and the type of loading are known for other ferrous metals, their endurance limits can be only be approximated from Eq. (7.6).

Other materials, for which there is much less experience, are nevertheless finding increasing uses in fatigue applications. Table 7.2 gives the approximate strengths in fatigue for various material classes. Figure 7.7c gives some stress-life curves for common polymers. Because polymers have a much greater variation in properties than metals, Fig. 7.7c should be viewed as illustrative of fatigue properties and not used for quantitative data.

Given a new material, or when experimental verification of an endurance limit is needed, it is often not required to develop the entire S-N diagram. The designer may only wish to

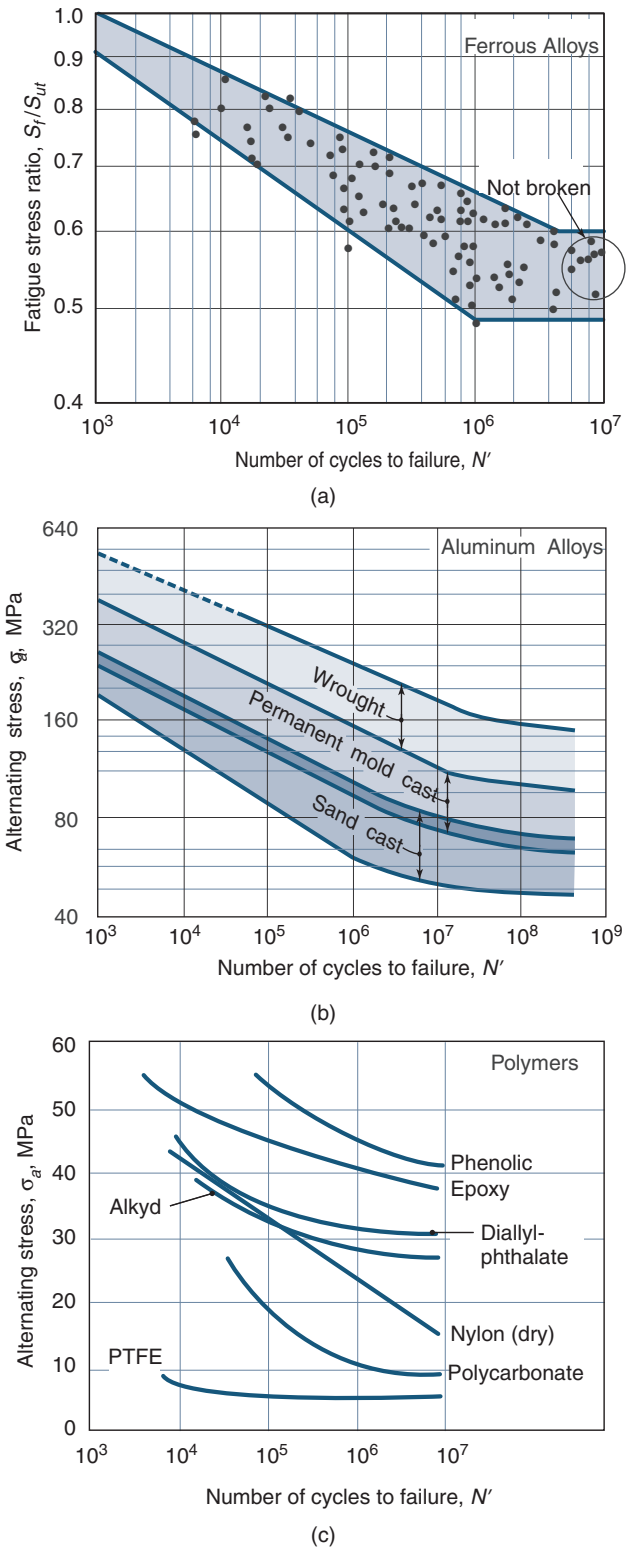


Figure 7.7: Fatigue strength as a function of number of loading cycles. (a) Ferrous alloys, showing clear endurance limit; (b) aluminum alloys, with less pronounced knee and no endurance limit; (c) selected properties of assorted polymer classes. Source: (a) Adapted from Lipson and Juvinall [1963], (b) Adapted from Juvinall and Marshek [1991], (c) Adapted from Norton [1996].



## Fatigue Strength

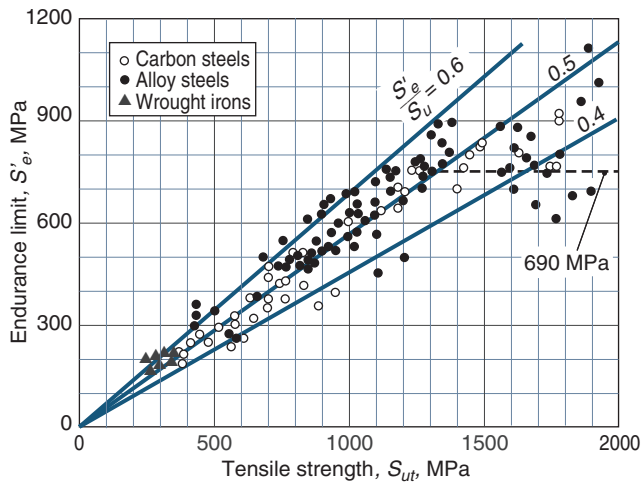


Figure 7.8: Endurance limit as a function of ultimate strength for wrought steels. Source: Adapted from Shigley and Mitchell [1983].

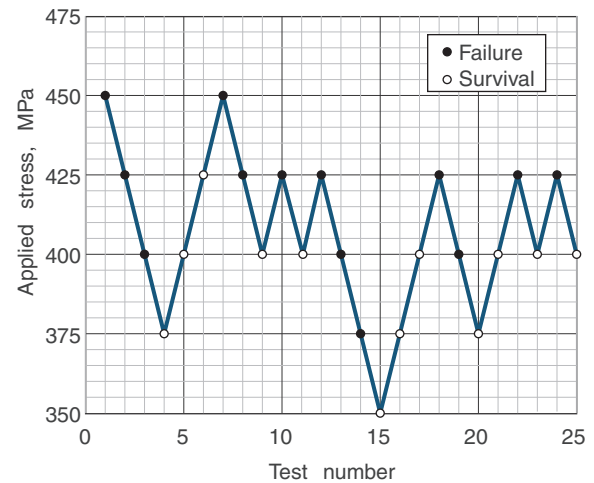


Figure 7.9: Typical results from fatigue tests using the staircase approach, and used in Example 7.2.

experimentally obtain the endurance limit, or the endurance limit at a desired number of stress cycles, using a minimum number of specimens in order to control costs and time required for evaluation. A valuable approach in this case is the **staircase** approach, also known as the *up-and-down* method as outlined in Design Procedure 7.2.

### Design Procedure 7.2: Staircase Approach

The staircase approach is useful for determining the endurance limit of a material when the complete S-N curve is not needed. This approach involves the following steps:

1. A designer must first estimate the endurance limit for the material of interest, either with a strength-based approach such as in Eq. (7.6), or through preliminary testing.
2. A test interval,  $d$ , is then selected, typically around 10% of the estimated endurance limit.
3. An initial test is performed at a stress level equal to the expected endurance limit.
4. If the specimen breaks, it is recorded as such and the next experiment will be performed at a stress level reduced by the stress interval.
5. At the desired duration (commonly  $10^6$  or  $10^7$  cycles), the test is stopped. If the specimen survives, it is recorded as such and the next experiment will be performed at a stress level increased by the stress interval.
6. A plot of typical results is shown in Fig. 7.9.
7. The mean endurance limit can be obtained from the following steps:
  - (a) Count the number of failures and survivals in the test results. Proceed with the analysis using the less common test result.

- (b) The number of events (failures or survivals) is assigned to  $n_i$  for each stress level  $\sigma_i$ . In this approach, the lowest stress level is denoted as  $\sigma_o$ , the next highest as  $\sigma_1$ , etc.

- (c) Obtain the quantity  $A_n$  from

$$A_n = \sum i n_i.$$

- (d) The endurance limit is then estimated from

$$S'_e = \sigma_o + d \left( \frac{A_n}{\sum n_i} \pm \frac{1}{2} \right),$$

where the plus sign is used if the more common experimental result is survival, and the minus sign is used if the more common event is failure.

8. It is recommended that at least 15 experiments be performed, although more can be helpful for more accurate quantification of the endurance limit.

The staircase approach can provide information about the mean endurance limit, and it also can allow characterization of the nature of the strength distribution. Further details about the potential benefits of this approach are contained in Lee, et al. [2005]. This approach is useful for evaluating endurance limit modification factors as well (see Section 7.8).

### Example 7.2: Determination of the Endurance Limit using the Staircase Approach

**Given:** The results of a series of 25 fatigue tests shown in Fig. 7.9. The expected endurance limit was  $\sigma_1 = 450$  MPa, with an interval of  $d = 25$  MPa.

**Find:** Determine the endurance limit,  $S_e$ , of the material.

Table 7.2: Approximate endurance limit for various materials.

Material	Number of cycles	Relation
Magnesium alloys	$10^8$	$S'_e = 0.35 S_u$
Copper alloys	$10^8$	$0.25S_u < S'_e < 0.5 S_u$
Nickel alloys	$10^8$	$0.35S_u < S'_e < 0.5 S_u$
Titanium	$10^7$	$0.45S_u < S'_e < 0.65 S_u$
Aluminum alloys	$5 \times 10^8$	$S'_e = 0.40 S_u$ ( $S_u < 330$ MPa) $S'_e = 130$ MPa ( $S_u \geq 330$ MPa)

**Solution:** This solution will follow the approach in Design Procedure 7.2, where the first six steps have been completed. From Step 7a, and Fig. 7.9, it can be seen that there are 13 failures and 12 survivals. Therefore, survival is the least common event, and will be used in this analysis. According to Step 7b, the following data are recorded:

$i$	$\sigma_i$ (MPa)	$n_i$
0	350	1
1	375	3
2	400	7
3	425	1
4	450	0

According to Step 7c,  $A_n$  is calculated from

$$A_n = \sum in_i = 0(1) + (1)(3) + 2(7) + (3)(1) = 20.$$

Therefore, according to Step 7d, the endurance limit is given by (noting that the more common result is failure):

$$\begin{aligned} S'_e &= \sigma_o + d \left( \frac{A_n}{\sum n_i} - \frac{1}{2} \right) \\ &= 350 + (25) \left( \frac{20}{12} - \frac{1}{2} \right) \\ &= 379 \text{ MPa.} \end{aligned}$$

## 7.6 Fatigue Regimes

The S-N diagram (Fig. 7.7a) shows different types of behavior as the number of cycles to failure increases. Two basic regimes are **low-cycle fatigue** (generally below 1000 stress cycles) and **high-cycle fatigue** (more than around 1000 but less than one million stress cycles). The slope of the line is much lower in low-cycle fatigue than in high-cycle fatigue.

Another differentiation can be made between **finite life** and **infinite life**. Figure 7.7a shows an endurance limit for ferrous alloys, below which any repeating stress will lead to infinite life in the component. Although a distinction between the finite-life and infinite-life portions of the curve is not always clear, for steels it occurs between  $10^6$  and  $10^7$  cycles. Thus, the finite-life classification is considered to hold for any loading below this range.

### 7.6.1 Low-Cycle Fatigue

Low-cycle fatigue is any loading that causes failure below 1000 cycles. This type of loading is common. A number of devices, such as latches on automotive glove compartments, studs on truck wheels, and setscrews fixing gear locations on

shafts, cycle fewer than 1000 times during their service lives. Surviving 1000 cycles means that these devices will last as long as intended.

For components in the low-cycle range, designers either ignore fatigue effects entirely or they reduce the allowable stress level. Ignoring fatigue seems to be a poor approach. However, the low-cycle portion of the curve in Fig. 7.7a has a small slope (i.e., the strength at 1000 cycles has not been reduced a great deal). Further, the  $y$ -intercept for the curve is the ultimate strength, not the yield strength. Since static design often uses the yield strength and not the ultimate strength in defining allowable stresses, static approaches are acceptable for designing low-cycle components. In fact, the safety factor compensates for the uncertainty in material strength due to cyclic loading.

Taking low-cycle effects into account allows modifying the material strength based on experimental data. The fatigue strength for steel at which high-cycle fatigue begins can be approximated as

$$\begin{aligned} \text{bending: } S'_l &= 0.9 S_u \\ \text{axial: } S'_l &= 0.75 S_u \\ \text{torsion: } S'_l &= 0.72 S_u \end{aligned} \quad (7.7)$$

### 7.6.2 High-Cycle, Finite-Life Fatigue

In many applications the number of stress cycles placed on a component during its service life is between  $10^3$  and  $10^7$ . Examples include car door hinges, aircraft body panels, and aluminum softball bats. Because the strength drops rapidly in this range (Fig. 7.7), strength needs to be expressed as a function of loading cycles. The fatigue strength at any location between  $S'_l$  and  $S'_e$  can generally be expressed as

$$\log S'_f = b_s \log N'_t + \bar{C}, \quad (7.8)$$

where  $b_s$  is the slope and  $\bar{C}$  the intercept of the finite-life portion of the S-N diagram. At the end points ( $S = S'_l$  for  $N = 1000$  and  $S = S'_e$  for  $N = 10^6$ ), Eq. (7.8) becomes

$$\log S'_l = b_s \log(10^3) + \bar{C} = 3b_s + \bar{C}, \quad (7.9)$$

$$\log S'_e = b_s \log(10^6) + \bar{C} = 6b_s + \bar{C}. \quad (7.10)$$

Subtracting Eq. (7.10) from Eq. (7.9) gives

$$b_s = -\frac{1}{3} \log \left( \frac{S'_l}{S'_e} \right). \quad (7.11)$$

Substituting Eq. (7.11) into Eq. (7.10) gives

$$\bar{C} = 2 \log \left( \frac{S'_l}{S'_e} \right) + \log S'_e = \log \left[ \frac{(S'_l)^2}{S'_e} \right]. \quad (7.12)$$

Thus, by using Eqs. (7.6) and (7.7), the slope  $b_s$  and the intercept  $\bar{C}$  can be determined for a specific type of loading. Knowing the slope and the intercept from Eq. (7.8) yields the fatigue strength as

$$S'_f = 10^{\bar{C}} (N'_t)^{b_s} \quad \text{for} \quad 10^3 \leq N'_t \leq 10^6. \quad (7.13)$$

If the fatigue strength is given and the number of cycles until failure is desired,

$$N'_t = \left( S'_f 10^{-\bar{C}} \right)^{1/b_s} \quad \text{for} \quad 10^3 \leq N'_t \leq 10^6. \quad (7.14)$$

Thus, by using Eqs. (7.6), (7.7), (7.11), and (7.12), the fatigue strength can be obtained from Eq. (7.13) or the number of cycles to failure can be determined from Eq. (7.14).

### Example 7.3: High Cycle, Finite Life Fatigue

**Given:** The pressure vessel lids of nuclear power plants are bolted down to seal the high pressure exerted by the water vapor (in a boiler reactor) or the pressurized water (in a pressurized water reactor). The ultimate strength of the bolt material is 1080 MPa. In the current design, the bolts are so heavily stressed that they are replaced after the reactors are opened 25 times.

**Find:** Determine the required stress for a life of 10,000 cycles.

**Solution:** Equations (7.6) and (7.7) for axial loading give  $S'_e = 0.45S_u$  and  $S'_l = 0.75S_u$ . Note that  $S'_l$  is for 1000 cycles and  $S'_e$  is for a life of  $10^6$  cycles. Equation (7.11) gives the slope as

$$b_s = -\frac{1}{3} \log \left( \frac{S'_l}{S'_e} \right) = -\frac{1}{3} \log \left( \frac{0.75S_u}{0.45S_u} \right) = -0.07395.$$

From Eq. (7.12), the intercept is

$$\bar{C} = \log \left[ \frac{(S'_l)^2}{S'_e} \right] = \log \left[ \frac{(0.75)^2(1080)^2}{(0.45)(1080)} \right] = 3.130.$$

Knowing the slope and intercept, Eq. (7.13) gives the fatigue strength as

$$S'_f = 10^{\bar{C}} (N'_t)^{b_s} = 10^{3.13} (10,000)^{-0.07395} = 682.7 \text{ MPa}.$$

Thus, the stress has to be decreased to 682.7 MPa to achieve a life of 10,000 cycles.

### 7.6.3 High-Cycle, Infinite-Life Fatigue

A number of applications call for infinite life, defined for steels as the number of cycles above which an endurance limit can be defined, usually taken as  $10^6$  cycles. If a material does not have an endurance limit, it cannot be designed for infinite life. Thus, aluminum alloys, for example, will always be designed for finite life (using the approach given in Section 7.6.2) or a fracture mechanics approach will be used (Section 7.12).

It should be recognized that the Manson-Coffin relationship given by Eq. (7.5) suggests that failure will always occur so long as the material encounters strain. Experimental investigations have confirmed this; there is apparently no cyclic stress level that materials can withstand without eventually failing by fatigue. However, the following should be noted:

- With materials such as the carbon steels in Fig. 7.7a, the knee in the curve is pronounced, so that the S-N diagram becomes almost horizontal at around a million stress cycles.
- Note that the  $x$ -axis of Fig. 7.7a is on a log scale. Thus, stresses below the endurance limit will cause failure, but only after a very large number of cycles. Often referred to as **gigacycle fatigue** because of the numbers of cycles that are typically involved, this regime has unique behavior. For example, instead of cracks propagating from

a surface or stress concentration, gigacycle fatigue failures often initiate at sub-surface material flaws.

- If a part will survive many millions, billions, or even trillions of cycles, this is essentially infinite life. That is, for most components this would translate into a useful life that far exceeds the intended life of the machine itself, so the part would never fail. Another rationale is that machine failures will undoubtedly occur in other components first, and that the machine will certainly be discarded before gigacycle fatigue becomes an issue.

For ferrous and titanium alloys, however, an infinite-life design approach based on an endurance limit can be followed. Basically, the designer determines an endurance limit and uses this strength as the allowable stress. Then, sizing and selection of components can proceed just as in static design. This approach, which is fairly complex, is described in the next sections.

## 7.7 Stress Concentration Effects

The Manson-Coffin equation [Eq. (7.5)] showed that the life of a component has a direct correlation with the strain to which it is subjected. Because locations of stress concentration are also locations of strain concentration, these locations can be seen as prime candidates for the promotion of fatigue crack initiation and growth. However, the stress concentration factor developed in Chapter 6 cannot be directly applied to fatigue applications since many materials will relieve stresses near a crack tip through plastic flow. That is, because some materials flow plastically near crack tips, fracture is avoided and the crack's growth is retarded.

For *static* loading, the stress concentration factor,  $K_c$ , is used, and for fatigue loading the fatigue stress concentration factor,  $K_f$ , is used, where

$$K_f = \frac{\text{Endurance limit for notch-free specimen}}{\text{Endurance limit for notched specimen}}. \quad (7.15)$$

A notch or stress concentration may be a hole, fillet, or groove, or a location of abrupt change in material properties. Recall from Section 6.2 that the theoretical stress concentration factor is a function of geometry. The fatigue stress concentration factor is not only a function of geometry but also a function of the material and type of loading. The consideration of the material is often dealt with by using a **notch sensitivity factor**,  $q_n$ , defined as

$$q_n = \frac{K_f - 1}{K_c - 1}, \quad (7.16)$$

or

$$K_f = 1 + (K_c - 1) q_n. \quad (7.17)$$

Note from Eq. (7.16) that the range of  $q_n$  is between zero (when  $K_f = 1$ ) and unity (when  $K_f = K_c$ ). From Eq. (7.17), observe that obtaining the fatigue stress concentration factor requires knowing the material's notch sensitivity and the type of loading.

Figure 7.10 is a plot of notch sensitivity versus notch radius for some commonly used materials and for various types of loading. For all the materials considered, the notch sensitivity approaches zero as the notch becomes very sharp (that is, as  $r$  approaches zero). Also, the harder and stronger steels tend to be more notch sensitive (have a large value of  $q_n$ ). This is not too surprising, since notch sensitivity is a measure of material ductility and the hardest steels have limited

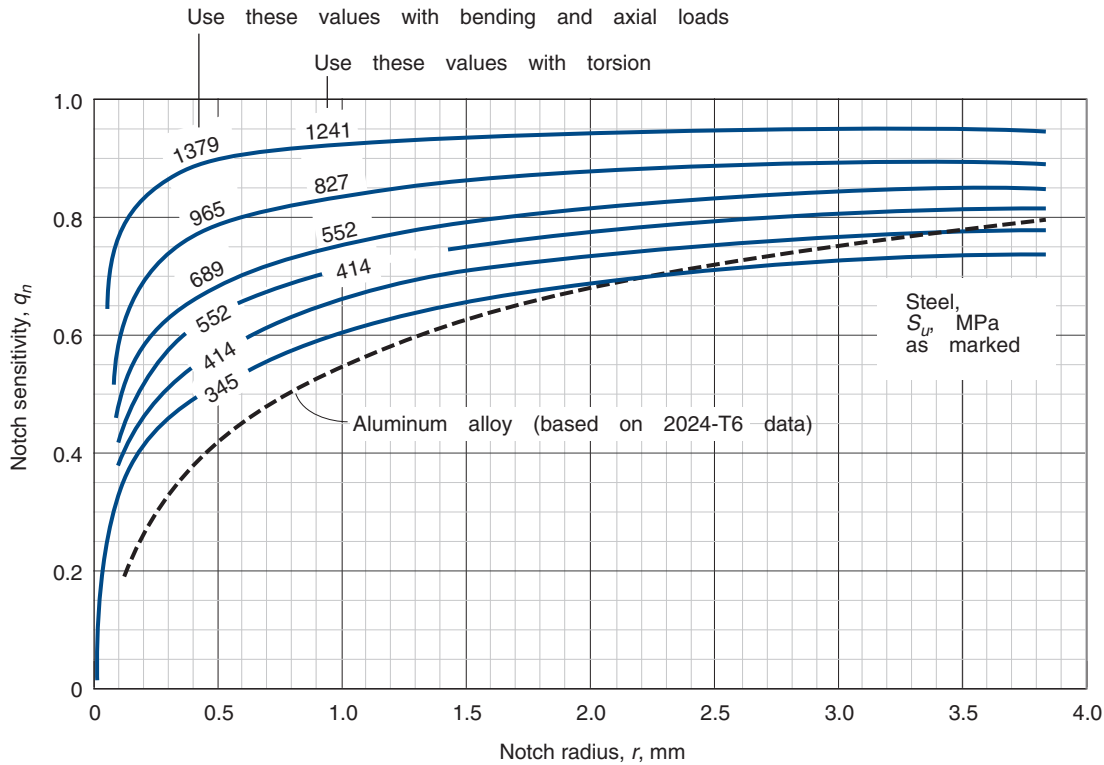


Figure 7.10: Notch sensitivity as a function of notch radius for several materials and types of loading. *Source:* Adapted from Sines and Waisman [1959].

ductility. Figure 7.10 also shows that a given steel is slightly more notch sensitive for torsional loading than for bending and axial loading.

To apply the effects of stress concentrations in fatigue, designers can either reduce the endurance limit or increase the applied stress by  $K_f$ . Sometimes designs are based on the ultimate tensile strength, and not the yield strength. In such a case, significant plastic deformation may occur near the stress concentration and reduce its magnitude. It may be reasonable to ignore stress concentrations or to incorporate them within a safety factor. Some design applications are not adversely affected by plastic flow, or else use highly elastic materials that deform sufficiently to relieve stress concentrations. All of these approaches can lead to successful designs. In general, the design constraints will provide guidance on the use of stress concentration factors. In this text, stress concentration factors are used to increase applied stresses, not to reduce allowable strength.

### Example 7.4: Fatigue Stress Concentration Factors

**Given:** The drive shaft for a Formula-1 racing car has a diameter of 30 mm and a half-circular notch with a 1-mm radius. The shaft was dimensioned for a coefficient of friction between the tires and the ground of 1.5 for equal shear and bending stresses. By mounting spoilers and a wing on the car, the load on the tires can be doubled at high speed without increasing the car's mass. Assume from the distortion-energy theory that the equivalent stress is  $\sigma_e = \sqrt{\sigma^2 + 3\tau^2}$ .

**Find:** Determine the fatigue stress concentration factors for bending and torsion of the drive shaft if the shaft material has an ultimate tensile strength of 965 MPa. Also, determine if increased acceleration or increased curve handling will give the higher risk of drive shaft failure.

**Solution:** From Fig. 7.10, for a notch radius of 1 mm and ultimate strength of 965 MPa, the notch sensitivity is 0.82 for bending and 0.85 for torsion. From Fig. 6.6b when  $r/d = 1/28 = 0.0357$  and  $D/d = 30/28 = 1.0714$ , the stress concentration factor is 2.2 for bending, and from Fig. 6.6c the stress concentration factor is 1.8 for torsion. From Eq. (7.17), the fatigue stress concentration factor due to bending is

$$K_f = 1 + (K_c - 1)q_n = 1 + (2.2 - 1)(0.82) = 1.98.$$

The fatigue stress concentration factor due to torsion is

$$K_f = 1 + (1.8 - 1)(0.85) = 1.68.$$

Let  $\sigma_{e1}$  be the equivalent stress for increased curve handling and  $\sigma_{e2}$  be the equivalent stress for increased acceleration. Doubling the load and using the distortion-energy theory results in

$$\frac{\sigma_{e1}}{\sigma_{e2}} = \frac{\sqrt{(2\sigma)^2 + 3\tau^2}}{\sqrt{\sigma^2 + 3(2\tau)^2}} = \frac{2\sqrt{1 + 0.75(\tau/\sigma)^2}}{\sqrt{1 + 12(\tau/\sigma)^2}}.$$

Recall that the shaft was dimensioned such that the shear and bending stresses are equal ( $\tau = \sigma$ ). Thus,



$$\frac{\sigma_{e1}}{\sigma_{e2}} = \frac{2\sqrt{1+0.75}}{\sqrt{1+12}} = 0.7338$$

so that

$$\sigma_{e2} = \frac{\sigma_{e1}}{0.7338} = 1.363\sigma_{e1}.$$

Therefore, increased acceleration gives a higher risk of drive shaft failure compared to increased curve handling.

## 7.8 The Modified Endurance Limit

As discussed in Section 7.5.1, fatigue experiments use the best possible circumstances for estimating fatigue performance. However, this situation cannot be guaranteed for design applications, so the component's endurance limit must be modified or reduced from the best-case scenario. This is done in practice by using endurance limit modification factors that take important factors into account. The endurance limit modification factors covered in this text are for completely reversed loading ( $\sigma_m = 0$ ). The **modified endurance limit** can be expressed as

$$S_e = k_f k_s k_r k_t k_m S'_e, \quad (7.18)$$

where

$S'_e$  = endurance limit from experimental apparatus under idealized conditions, Pa

$k_f$  = surface finish factor

$k_s$  = size factor

$k_r$  = reliability factor

$k_t$  = temperature factor

$k_m$  = miscellaneous factor

Note that the type of loading has already been incorporated into  $S'_e$  as presented in Eq. (7.6). As discussed in Section 7.7, the effects of stress concentrations are not included, since these factors are used to increase stress but not to reduce allowable strength.

Equation (7.18) should not be taken as an accurate prediction of endurance limit for complicated situations, but merely a reasonable *approximation* of what should be expected in practice. As will be seen, universally applicable correction factors do not exist, and those that are presented are experimentally based for controlled materials, loadings, and other parameters. This further confirms the observation stated above that experimental confirmation or the use of large safety factors are unavoidable in fatigue design.

### 7.8.1 Surface Finish Factor

The specimen shown in Fig. 7.3 has a highly polished surface finish with final polishing in the axial direction to smooth any circumferential scratches. Most machine elements do not have such a high-quality finish. The modification factor to incorporate the surface finish effect depends on the process used to generate the surface and on the material. Given a manufacturing process, Fig. 7.11a estimates the surface finish factor when the ultimate strength in tension is known, or else the coefficients from Table 7.3 can be used with the equation

$$k_f = eS_{ut}^f, \quad (7.19)$$

where

$k_f$  = surface finish factor

$S_{ut}$  = ultimate tensile strength of material, MPa

$e$  and  $f$  = coefficients defined in Table 7.3

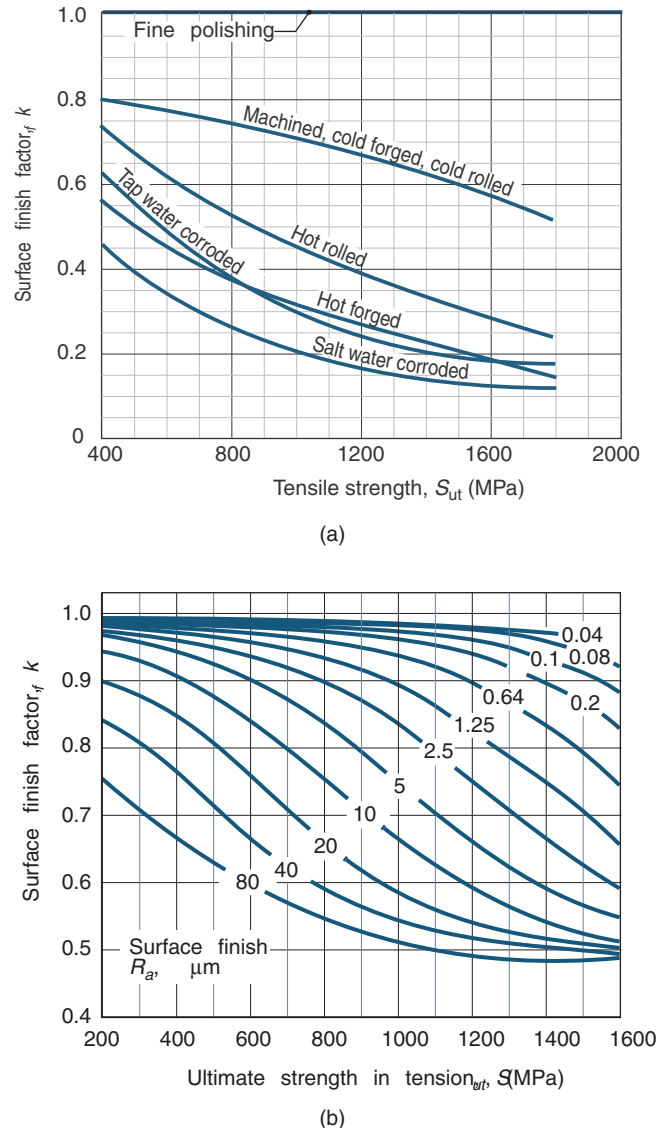


Figure 7.11: Surface finish factors for steel. (a) As a function of ultimate strength in tension for different manufacturing processes; (b) as a function of ultimate strength and surface roughness as measured with a stylus profilometer. Source: (a) Adapted from Juvinall and Marshek [1991] and data from the American Iron and Steel Institute; (b) adapted from Johnson [1967].



Table 7.3: Surface finish factor. *Source: Shigley and Mitchell [1983].*

Manufacturing process	Factor $e$	Exponent $f$
Grinding	1.58	-0.085
Machining or cold drawing	4.51	-0.265
Hot rolling	57.7	-0.718
As forged	272.0	-0.995

Note that Eq. (7.19) and Fig. 7.11a can give different results, especially for hot-working processes. This can be understood, recognizing the different sources for the expressions and data, and also because of the wide range of properties that can occur in these processes.

If the process used to obtain the surface finish is not known but the quality of the surface is known from the measured or prescribed arithmetic average surface roughness  $R_a$ , the surface finish factor can be obtained from Fig. 7.11b. Note also from the discussion of surface roughness that these values of  $k_f$  are approximate; surfaces are not fully characterized by their roughness, and deep and sharp circumferential scratches are the most detrimental to fatigue life, which may not be captured in the  $R_a$  roughness value.

These approaches are all approximate and are used only for well-controlled manufacturing processes. It is misleading to apply Table 7.3 for other circumstances or operations. For example, plasma spray operations tend to provide an extremely rough surface, but the fatigue properties are mainly determined by the surface layer beneath the plasma-sprayed coating. Further, the data in Table 7.3 are undoubtedly too stringent. With modern numerically controlled machine tools and improvements in tooling materials, superior finishes are routinely produced that will give slightly better performance from a fatigue standpoint.

## 7.8.2 Size Factor

The high-cycle fatigue apparatus used to obtain the endurance limit  $S'_e$  was for a specific diameter, namely, 7.62 mm, and often uses extruded or drawn steel bar stock. For metals, such extrusions have pronounced grain elongation in the direction transverse to fatigue crack growth. Also, the degree of cold work is high and the likelihood of large flaws is low. Similar effects are seen for ceramics and castings but for different reasons (smaller shrinkage pores, etc.). However, it must be noted that the size, shape, and number of flaws in a given cross section are strongly dependent on the manufacturing process.

Many researchers have suggested size factor expressions, but a simple approach suggested by Shigley and Mitchell [1983] is as follows for round bars. For bending or torsion the size factor is

$$k_s = \begin{cases} 1 & d \leq 8 \text{ mm} \\ 1.248d^{-0.112} & 8 \text{ mm} < d \leq 250 \text{ mm} \end{cases} \quad (7.20)$$

For axial loading  $k_s = 1$ .

For components that are not circular in cross-section the size factor is difficult to determine. However, an approach suggested by Kuguel [1969] is often referenced. This approach requires obtaining the cross-sectional area that is loaded above 95% of the maximum stress, denoted as  $A_{95}$ . (This is admittedly difficult to obtain for complicated cross sections.) Equating this to the portion of a circular cross sec-

Table 7.4: Reliability factors for six probabilities of survival.

Probability of survival, percent	Reliability factor, $k_r$
50	1.00
90	0.90
95	0.87
99	0.82
99.9	0.75
99.99	0.70

tion that is loaded above 95% of its maximum stress yields

$$d = \sqrt{\frac{A_{95}}{0.0766}}. \quad (7.21)$$

Equation (7.21) does not differentiate according to processing history, and this is a major shortcoming of the approach. For example, consider a steel bar that has been extruded to a diameter of 50 mm, and is then machined to produce a square cross section with a side length of 25 mm. Machining is a material removal process; it does nothing to improve the substrate microstructure. Any size effect present should be based on the 50 mm initial diameter, not the machined dimension or shape, since this reflects the material state with respect to initial flaws, grain sizes and shapes, etc.

## 7.8.3 Reliability Factor

Table 7.4 shows the reliability factor for various percentages of survival probability. This table is based on the endurance limit having a standard deviation of 8%, generally the upper limit for steels. The reliability factor for such a case can be expressed as

$$k_r = 0.512 \left[ \ln \left( \frac{1}{R} \right) \right]^{0.11} + 0.508, \quad (7.22)$$

where  $R$  is the probability of survival. The reliability factor as obtained from Table 7.4 or Eq. (7.22) can be considered only as a guide because the distribution is generally not well characterized for high values of reliability. It can also be assumed that Table 7.4 can be applied to materials other than steel, but care must be taken if the standard deviation is greater than 8%.

## 7.8.4 Temperature Factor

Many high-cycle fatigue applications take place under extremely high temperatures, such as in aircraft engines, where the material is much weaker than at room temperature. Conversely, in some applications, such as automobile axles in cold climates, the metal is generally less ductile than at room temperature.

In either case, the Manson-Coffin relationship given by Eq. (7.5) would suggest that a major factor affecting fatigue life is the strength in one loading cycle,  $\sigma'_f$ . It is therefore reasonable to follow one of two approaches. The designer can either (a) modify the ultimate strength of the material based on its properties at the temperature of interest before determining a material endurance limit in Eq. (7.18), or (b) use a temperature factor:

$$k_t = \frac{S_{ut}}{S_{ut, \text{ref}}} \quad (7.23)$$

where  $S_{ut}$  is the ultimate tensile strength of the material at the desired temperature and  $S_{ut, \text{ref}}$  is the ultimate tensile strength at a reference (usually room) temperature. Of

course, when fatigue experiments have been conducted at operating temperatures, the resulting endurance limit inherently accounts for the temperature, and  $k_t$  can be ignored.

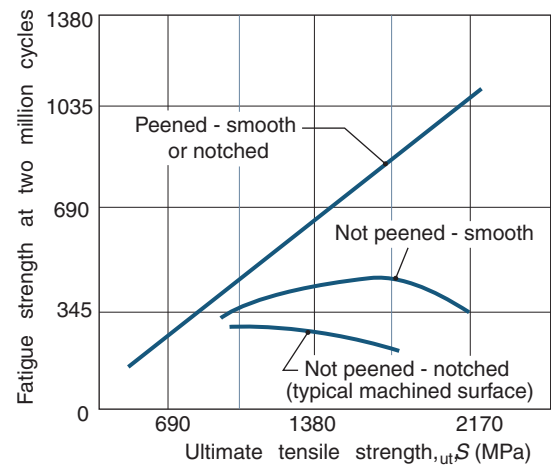
### 7.8.5 Miscellaneous Effects

Several other phenomena can affect a component's fatigue properties. Whereas the preceding sections have outlined methods for numerically approximating some effects, other considerations defy quantification. Among these are the following:

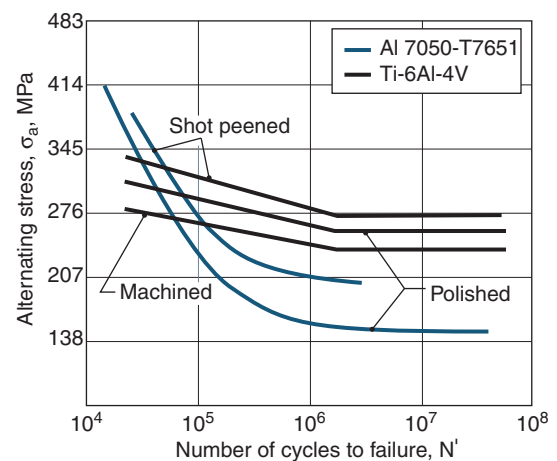
1. **Manufacturing history.** Manufacturing processes play a major role in determining the fatigue characteristics of engineering materials. This role is partially manifested in the size factor discussed in Section 7.8.2, but there are other effects as well. Because fatigue crack growth is often more rapid along grain boundaries than through grains, any manufacturing process affecting grain size and orientation can affect fatigue. Because some forming operations, such as rolling, extrusion, and drawing, lead to elongated grains, the material's fatigue strength will vary in different directions (anisotropy). With extrusion and drawing this effect is usually beneficial, since the preferred direction of crack propagation becomes the axial direction and crack propagation through the thickness is made more difficult by grain orientation and elongation in metals. Annealing a metal component relieves residual stresses, causes grains to become equiaxed, and may cause increased grain growth rates. Relieving tensile residual stresses at a surface is generally beneficial, but equiaxed or larger grains can be detrimental from a fatigue standpoint.
2. **Residual stresses** can result from manufacturing processes. A **residual stress** is caused by elastic recovery after nonuniform plastic deformation through a component's thickness. Compressive residual stress on a surface retards crack growth; tensile residual stress can encourage crack growth.

Compressive residual stresses can be imparted through shot or laser peening and roller burnishing and may be obtained in forging, extrusion, or rolling. **Shot peening** is a cold working process in which the surface of a part is impacted with small spherical media called shot. Each impact leads to plastic deformation at the workpiece surface, leading to compressive residual stress after elastic recovery. The layer under compressive residual stress is usually less than 1 mm thick, and the material bulk properties are unaffected. Crack development and propagation are severely retarded by compressive residual stresses; for this reason, shot peening is a common surface treatment for fatigue-susceptible parts such as gears, springs, shafts (especially at stress concentrations), connecting rods, etc.

The beneficial effect of shot peening on fatigue life can be seen in Fig. 7.12. Similar behavior can be found for other materials. This is an important tool for fatigue design because it represents one of the only strategies that *increases* the fatigue strength of materials, and this increase can be very large. For example, consider an aircraft landing gear, produced from steel with a 2068 MPa strength. Figure 7.12a shows that shot peening can increase the fatigue strength by a factor of 3 over a polished surface. Similar benefits are possible with other materials, but as seen in the figure, the more typical fatigue strength improvement is 15 to 30%.



(a)



(b)

Figure 7.12: The use of shot peening to improve fatigue properties. (a) Fatigue strength at  $2 \times 10^6$  cycles for high-strength steel as a function of ultimate strength; (b) typical S-N curves for non-ferrous metals. Source: Courtesy of J. Champaigne, Electronics, Inc.

3. **Coatings** can significantly affect fatigue. Some operations, such as carburizing, lead to a high carbon content in steel surface layers (and thus a high fracture strength) and impart a compressive residual stress on the surface. Electroplated surfaces can be porous and promote crack growth, reducing fatigue strengths by as much as 50%. Zinc plating is the main exception where the fatigue strength is not seriously affected. Anodized oxide coatings are also usually porous, reducing fatigue strength. Coatings applied at high temperatures, such as in chemical vapor deposition processes or hot dipping, may induce tensile residual stresses at the surface.
4. **Corrosion.** It is not surprising that materials operating in corrosive environments have lower fatigue strengths. The main adverse reactants in corroding metals are hydrogen and oxygen. Hydrogen diffuses into a material near a crack tip, aided by large tensile stresses at the tip, embrittling the material and aiding crack propagation. Oxygen causes coatings to form that are brittle or

porous, aiding crack initiation and growth. High temperatures in corrosive environments speed diffusion-based processes.

### Design Procedure 7.3: Estimation of Endurance Limit

This procedure is mainly intended for carbon steels, assuming that an endurance limit can be defined. Each of the correction factors are approximate, thus, the endurance limit estimation should be used with generous safety factors or as a basis for experimental design verification, especially if extended to non-ferrous materials. The preferred approach for determining endurance limit is to conduct a series of experiments. Since experiments can be conducted with the loading (bending, tension, shear, etc.) and manufacturing process, part size, etc. that closely match the application, this is the best way to minimize errors.

If an experimental investigation is impractical, the endurance limit can be estimated through the following procedure:

1. The endurance limit for a specimen ( $S'_e$ ) can be estimated for a type of loading from Eq. (7.6). This requires knowledge of the material's ultimate strength, which can be obtained from experiments or from tables of mechanical properties; some steel properties are summarized in Appendix A.
2. Note from Fig. 7.8 that the predicted value should not be assigned a value greater than 690 MPa.
3. The modified endurance limit ( $S_e$ ) is then obtained from Eq. (7.18), where:
  - (a) The surface finish factor,  $k_f$ , is obtained from Eq. (7.19) using coefficients from Table 7.3, or else  $k_f$  can be estimated from Fig. 7.11.
  - (b) The size factor,  $k_s$ , can be estimated from Eq. (7.20) for bending or torsion, with  $k_s=1$  for tension. If the part is not round, then an equivalent diameter can be obtained from Eq. (7.21). These equations have high uncertainty, but they do allow size effects to be considered without overly complicating the mathematics.
  - (c) The reliability factor,  $k_r$ , can be obtained from Table 7.4.
  - (d) The effects of temperature,  $k_t$ , are best obtained experimentally, but Eq. (7.23) gives a reasonable estimate for this factor.

It should be noted that additional factors can impact the fatigue strength, as discussed in Section 7.8.5.

### Example 7.5: Endurance Limits and Modification Factors

**Given:** Figure 7.13 shows a portion of a round shaft with a flat groove used to seat a retaining ring (see Section 11.7). In order to support the applied loads, a non-standard retaining ring is used so that the depth and width are larger than normal. AISI 1020 steel (quenched and tempered at 870°C) is used for the shaft, which is machined to its final dimensions.

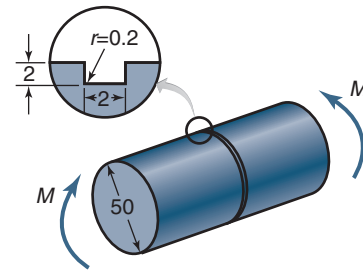


Figure 7.13: Round shaft with a retaining ring groove considered in Example 7.5. All dimensions are in millimeters.

**Find:** Estimate the modified endurance limit for the shaft and the allowable bending moment using a safety factor of 5.0. Use a reliability of 99% and no thermal or miscellaneous effects.

**Solution:** The modified endurance limit will be determined using the approach in Design Procedure 7.3, and will preserve its numbering scheme.

1. For this AISI 1020 steel, the ultimate strength is obtained from Table A.2 as 395 MPa. Equation (7.6) then gives the endurance limit for a test specimen constructed from this material as

$$S'_e = 0.5S_u = 0.5(395) = 197.5 \text{ MPa.}$$

Note that the endurance limit was determined for bending, consistent with the loading shown in Fig. 7.13.

2. Equation (7.18) will be used to estimate the modified endurance limit, but first the required correction factors will be obtained.

- (a) The surface finish factor is obtained from Eq. (7.19) using values of  $e = 4.51$  and  $f = -0.265$  from Table 7.3:

$$k_f = eS_{ut}^f = (4.51)(395)^{-0.265} = 0.92.$$

By comparison, Fig. 7.11a suggests a value of  $k_f = 0.85$ . These values are fairly close, and either could be used for the remainder of the problem. The value of  $k_f = 0.92$  will be arbitrarily selected for further derivations.

- (b) The size factor is obtained from Eq. (7.20) as

$$k_s = 1.248d^{-0.112} = 1.248(50)^{-0.112} = 0.80.$$

Note that 50 mm was used as the diameter in this calculation instead of the 46-mm groove dimension. If the groove dimension were used, it would have only minor effect in this case ( $k_s = 0.81$ ), but the reason for using the shaft diameter was because machining the groove does not have an effect on flaw elimination in the shaft material.

Regardless, it should be recognized that  $k_s$  is a rough estimate of size effect.

- (c) The reliability factor is obtained from Table 7.4 as  $k_r = 0.82$ .
- (d) Per the problem statement, the values of  $k_t$  and  $k_m$  are set equal to unity. Therefore, from Eq. (7.18),

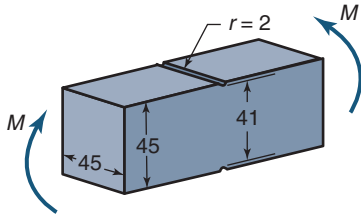


Figure 7.14: Drawn square profile with machined groove considered in Example 7.6. All dimensions are in millimeters.

$$\begin{aligned} S_e &= k_f k_s k_r k_t k_m S'_e \\ &= (0.92)(0.80)(0.82)(1)(1)(197.5) \\ &= 119 \text{ MPa.} \end{aligned}$$

To determine the allowable bending moment, it is necessary to determine the fatigue stress concentration factor,  $K_f$ . The approach is the same as in Example 7.4, where Fig. 6.7a yields  $K_c = 5.5$  (using  $r/t = 0.10$  and  $b/t = 1.0$ ). From Fig. 7.10 for  $S_{ut} = 395$  MPa and  $r = 0.2$  mm,  $q_n \approx 0.45$ . Therefore, from Eq. (7.17),

$$K_f = 1 + (K_c - 1)q_n = 1 + (5.5 - 1)(0.45) = 3.025 \approx 3.0.$$

The nominal stress at the groove root is given in Fig. 6.7a. Therefore,

$$K_f \sigma_{\text{avg}} = K_f \left( \frac{32M}{\pi d^3} \right) = \frac{S_e}{n_s}.$$

Solving for  $M$ ,

$$\begin{aligned} M &= \frac{\pi S_e d^3}{32 K_f n_s} \\ &= \frac{\pi (119 \times 10^6) (0.046)^3}{(32)(3.0)(5.0)} \\ &= 75.8 \text{ Nm.} \end{aligned}$$

### Example 7.6: Endurance Limits and Modification Factors for Square Cross Section

**Given:** Instead of the retaining ring for the shaft considered in Example 7.5, an integrated snap fastener (see Section 16.8) is being considered on a drawn square profile with machined groove as shown in Fig. 7.14. Note that the cross sectional areas of the shaft are very close to that in Example 7.5. As in Example 7.5, use AISI 1020 steel with a reliability of 99%, and no thermal or miscellaneous effects.

**Find:** Estimate the modified endurance limit for the shaft and the allowable bending moment using a safety factor of 5.0.

**Solution:** The procedure for calculating modified endurance limits is very similar to Example 7.5. The only correction factor that is different in this case is the size factor. Since the cross section is not circular, Eq. (7.21) will be used to obtain the diameter so that Eq. (7.20) can be applied.

As was discussed in Example 7.5, the size factor will be determined for the drawn cross section without the notch. Note that for bending, the maximum stress is at the outer dimension, or

$$\sigma = \frac{Mc}{I} = \frac{M}{I} \frac{0.045}{2} = 0.0245 \frac{M}{I}.$$

The location where the stress is 95% of the maximum is:

$$0.95 \left( \frac{M}{I} \right) \left( \frac{0.045}{2} \right) = \frac{My}{I},$$

so that  $y = 0.0214$  m. The area where the stress exceeds 95% of the maximum is (noting that there are tensile and compressive areas that contribute):

$$A_{95} = 2(0.045)(0.0225 - 0.0214) = 9.9 \times 10^{-5} \text{ m}^2.$$

From Eq. (7.21),

$$d = \sqrt{\frac{A_{95}}{0.0766}} = \sqrt{\frac{9.9 \times 10^{-5}}{0.0766}} = 0.0359 \text{ m.}$$

Therefore, Eq. (7.20) yields

$$k_s = 1.248(35.9)^{-0.112} = 0.836.$$

Note that this size effect does not differ much from the results of Example 7.5, nor should it. The manufacturing processes are very similar, so the flaws, grain structure, etc, should all be close. As stated above, the cross sections are very close as well. Therefore, the modified endurance limit is, from Eq. (7.18),

$$\begin{aligned} S_e &= k_f k_s k_r k_t k_m S'_e \\ &= (0.92)(0.836)(0.82)(1)(1)(197.5) \\ &= 124 \text{ MPa.} \end{aligned}$$

For this case, Fig. 6.4b yields  $K_c \approx 2.3$  ( $H/h = 1.1$ ,  $r/h = 0.048$ ). From Fig. 7.10,  $q_n \approx 0.65$ . Therefore,  $K_f = 1.845$ . Using the revised geometry,

$$K_f \sigma_{\text{avg}} = K_f \left( \frac{6M}{h^3} \right) = \frac{S_e}{n_s}.$$

Solving for  $M$ ,

$$M = \frac{S_e h^3}{6 K_f n_s} = \frac{(124 \times 10^6) (0.041)^3}{6(1.845)(5)} = 231 \text{ Nm.}$$

This geometry can support a larger moment, and this is attributable to the lower stress concentration.

## 7.9 Cumulative Damage

In constructing the S-N curve in Fig. 7.7, it was assumed that the cyclic variation was completely reversed ( $\sigma_m = 0$ ). Furthermore, for any stress level between the strengths  $S'_t$  and  $S'_e$ , say  $S'_1$ , the maximum stress level in the completely reversed variation was kept constant until failure occurred at  $N'_1$  cycles. Operating at stress amplitude  $S'_1$  for a number of cycles  $n'_1 < N'_1$  produced a smaller damage fraction. Because cyclic variations are often not constant in practice, engineers must deal with several different levels of completely reversed stress cycles. Operating over stress levels between  $S'_t$  and  $S'_e$ , say  $S'_i$ , at a number of cycles  $n'_i < N'_i$  results in the damage



fraction  $n'_i/N'_i$ . When the damage fraction due to different levels of stress exceeds unity, failure is predicted. Thus, failure is predicted if

$$\frac{n'_1}{N'_1} + \frac{n'_2}{N'_2} + \cdots + \frac{n'_i}{N'_i} \geq 1. \quad (7.24)$$

This formulation is frequently called the **linear damage rule** (sometimes called *Miner's rule*), since it states that the damage at any stress level is directly proportional to the number of cycles (assuming that each cycle at a given stress level does the same amount of damage). The rule also assumes that the stress sequence does not matter and that the rate of damage accumulation at a particular stress level is independent of the stress history. This is not strictly true, as it is well-known that more severe loadings cause disproportionate damage, especially if they occur early in the part's life. Despite these shortcomings, the linear damage rule remains popular, largely because it is so simple.

If  $N'_t$  is the total number of cycles to failure when there are different cyclic patterns (all of which are completely reversed), the ratio of the number of cycles at a specific stress level to the total number of cycles to failure is

$$\alpha_i = \frac{n'_i}{N'_t} \quad \text{or} \quad n'_i = \alpha_i N'_t. \quad (7.25)$$

Substituting Eq. (7.25) into Eq. (7.24), it is predicted that failure will occur if

$$\sum \frac{\alpha_i}{N'_i} \geq \frac{1}{N'_t}. \quad (7.26)$$

### Example 7.7: Cumulative Damage

**Given:** Consider a steel with an ultimate strength of 440 MPa, so that  $S'_l = 330$  MPa and  $S'_e = 200$  MPa. A complicated loading cycle is applied, so that the stress is 175 MPa for 20% of the time, 220 MPa for 30%, 250 MPa for 40%, and 275 MPa for 10%.

**Find:** The number of cycles until cumulative failure.

**Solution:** First of all, note from Eqs. (7.11) and (7.12) that

$$b_s = -\frac{1}{3} \log \left( \frac{S'_l}{S'_e} \right) = -\frac{1}{3} \log \left( \frac{330}{200} \right) = -0.0725,$$

$$\bar{C} = \log \left[ \left( \frac{S'_l}{S'_e} \right)^2 \right] = \log \left( \frac{330^2}{200^2} \right) = 2.736.$$

Note that  $S'_l = 175$  MPa is less than  $S'_e$ , so that  $N'_1 = \infty$ , implying that at this stress level failure will not occur. From Eq. (7.14) for the other three fatigue strength levels,

$$\begin{aligned} N'_2 &= \left( S'_f 10^{-\bar{C}} \right)^{1/b_s} \\ &= [(220)(10)^{-2.736}]^{-1/0.0725} \\ &= 2.683 \times 10^5 \text{ cycles,} \\ N'_3 &= [(250)(10)^{-2.736}]^{-1/0.0725} = 4.601 \times 10^4 \text{ cycles,} \\ N'_4 &= [(275)(10)^{-2.736}]^{-1/0.0725} = 1.236 \times 10^4 \text{ cycles.} \end{aligned}$$

Making use of Eq. (7.26) gives

$$\begin{aligned} \frac{\alpha_1}{N'_1} + \frac{\alpha_2}{N'_2} + \frac{\alpha_3}{N'_3} + \frac{\alpha_4}{N'_4} &= \frac{1}{N'_t}; \\ \frac{0.2}{\infty} + \frac{0.3}{2.683 \times 10^5} + \frac{0.4}{4.601 \times 10^4} + \frac{0.1}{1.236 \times 10^4} &= \frac{1}{N'_t}. \end{aligned}$$

This is solved as  $N'_t = 55,860$  cycles.

## 7.10 Influence of Nonzero Mean Stress

Other than in classifying cyclic behavior, completely reversed ( $\sigma_m = 0$ ) stress cycles have been assumed. Many machine elements involve fluctuating stresses about a nonzero mean. The experimental apparatus used to generate the results shown in Fig. 7.7 cannot apply mean and alternating stresses, so other test approaches are needed (such as tension-compression or combined stresses). If a material has been extensively characterized, the effect of a nonzero mean stress can be incorporated through a **Haigh diagram**, also called a *constant life diagram* as shown in Fig. 7.15. Because such data are not generally available, the influence of nonzero mean stress must be estimated by using one of several empirical relationships that determine failure at a given life when alternating and mean stresses are both nonzero.

### 7.10.1 Ductile Materials

Figure 7.16 shows how four empirical relationships estimate the influence of nonzero mean stress on fatigue life for ductile materials loaded in tension. The ordinate has both the yield strength,  $S_{yt}$ , and endurance limit,  $S_e$ , indicated, and the abscissa shows both the yield and ultimate strengths. The yield line shown is for reference purposes, as it indicates failure during the first loading cycle. Commonly used criteria for fatigue failure with a non-zero mean stress are shown in the figure.

The effects of stress concentrations on ductile materials (see Section 7.7) require further explanation. If there is a stress concentration and the yield stress is exceeded, then the deformed geometry is difficult to obtain. Recall from Eq. (3.21) that stress is proportional to strain for linearly elastic materials. However, during plastic deformation, stresses are related to strain increment. If the yield stress is exceeded, it is possible that plastic strains are negligible, but it is also possible that they are so large as to effectively eliminate the stress concentration effect. The amount of plastic strain that occurs depends on the nature of a part's supports, its ductility and strain hardening capability, and applied loads.

However, consider the situation where the mean stress is small; in Fig. 7.16 this would suggest that the endurance limit should not be exceeded, consistent with the approach in Section 7.8. Since the endurance limit is much smaller than the yield strength, it is reasonable to apply stress concentration effects to the alternating stress. Applying stress concentration effects to the mean stress has little impact because it was assumed these stresses are small. On the other hand, if the mean stress is large, then plastic deformation will relieve stress concentrations, and applying the fatigue stress concentration factor based on the original geometry to the alternating stress results in a conservative approach. Therefore, a common modeling simplification is to apply stress concentrations to alternating stresses but not mean stresses, and this is the approach followed in this text.

#### Gerber Line

The **Gerber line** is sometimes called the *Gerber parabolic relationship* because the equation is

$$\frac{K_f n_s \sigma_a}{S_e} + \left( \frac{n_s \sigma_m}{S_{ut}} \right)^2 = 1. \quad (7.27)$$

where



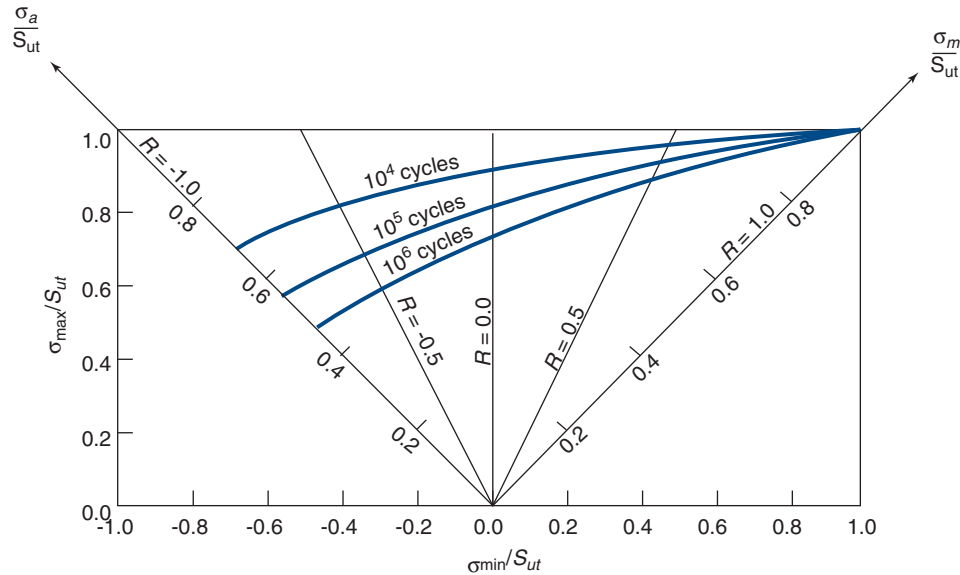


Figure 7.15: A typical Haigh diagram showing constant life curves for different combinations of mean and alternating stresses.

$S_e$  = modified endurance limit, Pa  
 $S_{ut}$  = ultimate strength in tension, Pa  
 $n_s$  = safety factor  
 $\sigma_a$  = alternating stress, Pa  
 $\sigma_m$  = mean stress, Pa  
 $K_f$  = fatigue stress concentration factor

This line passes through the central portion of the experimental failure points and hence should be the best predictor of failure, but the parabolic nature of the equation complicates mathematics.

#### Goodman Line

The **Goodman line** proposes connecting the modified endurance limit on the alternating stress axis with the ultimate strength in tension on the mean stress axis in Fig. 7.16 by a straight line, or

$$\frac{K_f \sigma_a}{S_e} + \frac{\sigma_m}{S_{ut}} = \frac{1}{n_s}. \quad (7.28)$$

Note the linearization of Eq. (7.28) relative to Eq. (7.27). Equation (7.28) fits experimental data reasonably well and is simpler to use than Eq. (7.27). The starting and ending points for the Goodman and Gerber lines are the same in Fig. 7.16, but between these points the Goodman line is linear and the Gerber line is parabolic.

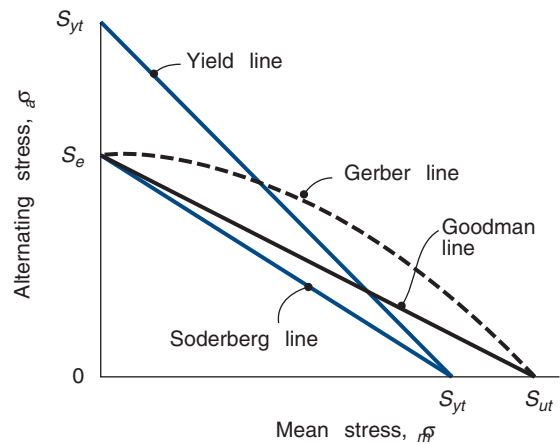


Figure 7.16: Influence of nonzero mean stress on fatigue life for tensile loading as estimated by four empirical relationships.

### Example 7.8: Effect of Nonzero Mean Stress

**Given:** A straight, circular rotating beam with a 30-mm diameter and a 1-m length has an axial load of 30,000 N applied at the end and a stationary radial load of 400 N. The beam is cold-drawn and the material is AISI 1040 steel. Assume that  $k_s = k_r = k_t = k_m = 1$ .

**Find:** The safety factor for infinite life by using the Goodman line.

**Solution:** From Table A.1 for AISI 1040 steel,  $S_u = 520$  MPa. From Fig. 7.11a for the cold-drawn process and  $S_u = 520$  MPa, the surface finish factor is 0.78. From Eq. (7.18), the modified endurance limit while making use of Eq. (7.6) is

$$\begin{aligned}
 S_e &= k_f k_s k_r k_t k_m S'_e \\
 &= (0.78)(1)(1)(1)(1)(0.45)(520) \\
 &= 182.5 \text{ MPa.}
 \end{aligned}$$

The bending stress from Eq. (4.45) gives the alternating stress that the beam experiences as

$$\sigma_a = \frac{Mc}{I} = \frac{(64)(400)(1)(0.03/2)}{\pi(0.03)^4} = 150.9 \text{ MPa.}$$

The mean stress due to the axial load is

$$\sigma_m = \frac{P_a}{A} = \frac{(30,000)(4)}{\pi(0.03)^2} = 42.44 \text{ MPa.}$$

For an unnotched beam  $K_f = 1$ . From Eq. (7.28),

$$\frac{K_f \sigma_a}{S_e} + \frac{\sigma_m}{520} = \frac{1}{n_s}.$$

Therefore,

$$\frac{(1)(150.9)}{182.5} + \frac{42.44}{520} = \frac{1}{n_s};$$

$$n_s = \frac{1}{0.9084} = 1.101.$$

Using the Goodman line, the safety factor for infinite life is 1.101.

### Soderberg Line

The **Soderberg line** is conservative and is given as

$$\frac{K_f \sigma_a}{S_e} + \frac{\sigma_m}{S_{yt}} = \frac{1}{n_s}. \quad (7.29)$$

Note from Fig. 7.16 and Eqs. (7.28) and (7.29) that the ultimate strength in the Goodman relationship has been replaced with the yield strength in the Soderberg relationship.

### Yield Line

To complete the possibilities, the **yield line** is given. It is used to define yielding on the first cycle, or

$$\frac{\sigma_a}{S_{yt}} + \frac{\sigma_m}{S_{yt}} = \frac{1}{n_s}. \quad (7.30)$$

This completes the description of the theories presented in Fig. 7.16.

### Modified Goodman Diagram

The Goodman relationship given in Eq. (7.28) is modified by combining fatigue failure with failure by yield. The complete **modified Goodman diagram** is shown in Fig. 7.17.<sup>1</sup> Thus, all points inside a modified Goodman diagram ABCDEFGH correspond to fluctuating stresses that should cause neither fatigue failure nor yielding. The word “complete” is used to indicate that the diagram is valid for both tension and compression. The word “modified” designates that the Goodman line shown in Fig. 7.16 has been modified in Fig. 7.17; that is, in Fig. 7.16 the Goodman line extends from the endurance limit on the alternating stress ordinate to the ultimate strength on the mean stress abscissa. In the modified Goodman diagram in Fig. 7.17, the Goodman line is modified such that for stresses larger than the yield strength the yield line BC is used. Thus, the modified Goodman diagram combines fatigue criteria as represented by the Goodman line and yield criteria as represented by the yield line. Note in Fig. 7.17 that lines AB, DE, EF, and HA are Goodman lines and that lines BC, CD, FG, and GH are yield lines. The static load is represented by line CG. Table 7.5 gives the equations and range of applicability for the construction of the Goodman and yield lines of the complete modified Goodman diagram. Note that when the ultimate and yield strengths are known for a specific material, as well as the corresponding endurance limit for a particular part made of that material, the modified Goodman diagram can be constructed.

<sup>1</sup>Equation (7.28) is referred to in the technical literature as either the *Goodman* or the *modified Goodman* relationship, since it was the combined contribution of multiple researchers. Figure 7.17 is often referred to as the *modified Goodman diagram*, as is done in this text, but is called an *enhanced modified Goodman diagram* in some sources.

Table 7.5: Equations and range of applicability for construction of complete modified Goodman diagram.

Line	Equation	Range
AB	$\sigma_{\max} = \frac{S_e}{K_f} + \sigma_m \left(1 - \frac{S_e}{S_u K_f}\right)$	$0 \leq \sigma_m \leq \frac{S_y - S_e/K_f}{1 - \frac{S_e}{K_f S_u}}$
BC	$\sigma_{\max} = S_y$	$\frac{S_y - \frac{S_e}{K_f}}{1 - \frac{S_e}{K_f S_u}} \leq \sigma_m \leq S_y$
CD	$\sigma_{\min} = 2 \sigma_m - S_y$	$\frac{S_y - \frac{S_e}{K_f}}{1 - \frac{S_e}{K_f S_u}} \leq \sigma_m \leq S_y$
DE	$\sigma_{\min} = \left(1 + \frac{S_e}{K_f S_u}\right) \sigma_m - \frac{S_e}{K_f}$	$0 \leq \sigma_m \leq \frac{S_y - \frac{S_e}{K_f}}{1 - \frac{S_e}{K_f S_u}}$
EF	$\sigma_{\min} = \sigma_m - \frac{S_e}{K_f}$	$\frac{S_e}{K_f} - S_y \leq \sigma_m \leq 0$
FG	$\sigma_{\min} = -S_y$	$-S_y \leq \sigma_m \leq \frac{S_e}{K_f} - S_y$
GH	$\sigma_{\max} = 2 \sigma_m + S_y$	$-S_y \leq \sigma_m \leq \frac{S_e}{K_f} - S_y$
HA	$\sigma_{\max} = \sigma_m + \frac{S_e}{K_f}$	$\frac{S_e}{K_f} - S_y \leq \sigma_m \leq 0$

As an example of the way the modified Goodman diagram aids in visualizing the various combinations of fluctuating stress, consider the mean stress indicated by point L in Fig. 7.17. The Goodman criterion indicates that this stress can fluctuate between points M and N. This fluctuation is sketched on the right of the figure.

Also shown in Fig. 7.17 are the four regions of mean stress on the abscissa. Table 7.6 gives the failure equation for each of these regions as well as the validity limits for each equation. Table 7.6 is an extremely valuable guide when applying the modified Goodman diagram.

### Example 7.9: Safety Factor Using the Modified Goodman Criterion

**Given:** For the beam given in Example 7.5 the bending moment varies between 50 and 200 Nm.

**Find:** Using the modified Goodman relationship, determine the safety factor guarding against fatigue failure.

**Solution:** From Example 7.5,  $S_{ut} = 395$  MPa and  $S_y = 295$  MPa. Also, it was determined in Example 7.5 that  $S_e = 119$  MPa and  $K_f = 3.0$ . The nominal stresses at the groove ( $d = 0.046$  m) are given by

$$\sigma_{\min} = \frac{32M_{\min}}{\pi d^3} = \frac{32(50)}{\pi(0.046)^3} = 5.232 \text{ MPa},$$

$$\sigma_{\max} = \frac{32M_{\max}}{\pi d^3} = \frac{32(200)}{\pi(0.046)^3} = 20.93 \text{ MPa}.$$

Therefore, from Eqs. (7.1) and (7.3),

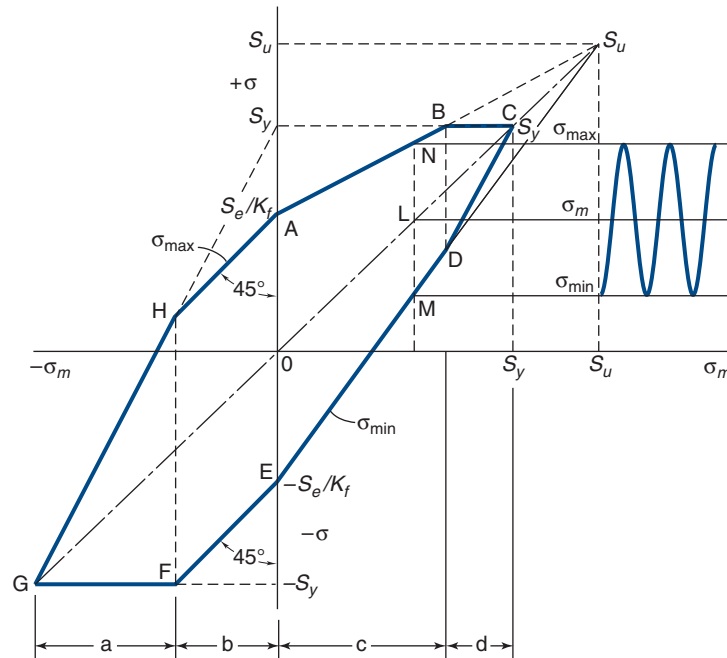


Figure 7.17: Complete modified Goodman diagram, plotting stress as ordinate and mean stress as abscissa.

Table 7.6: Failure equations and validity limits of equations for four regions of complete modified Goodman relationship.

Region in Fig. 7.16	Failure equation	Validity limits of equation
a	$\sigma_{\max} - 2\sigma_m = S_y/n_s$	$-S_y \leq \sigma_m \leq \frac{S_e}{K_f} - S_y$
b	$\sigma_{\max} - \sigma_m = \frac{S_e}{n_s K_f}$	$\frac{S_e}{K_f} - S_y \leq \sigma_m \leq 0$
c	$\sigma_{\max} + \sigma_m \left( \frac{S_e}{K_f S_u} - 1 \right) = \frac{S_e}{n_s K_f}$	$0 \leq \sigma_m \leq \frac{S_y - \frac{S_e}{K_f}}{1 - \frac{S_e}{K_f S_u}}$
d	$\sigma_{\max} = \frac{S_y}{n_s}$	$\frac{S_y - \frac{S_e}{K_f}}{1 - \frac{S_e}{K_f S_u}} \leq \sigma_m \leq S_y$

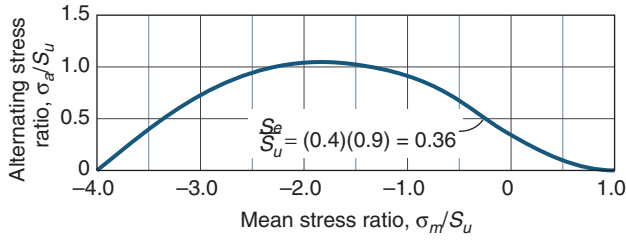


Figure 7.18: Alternating stress ratio as a function of mean stress ratio for axially loaded cast iron.

$$\sigma_a = \frac{\sigma_{\max} - \sigma_{\min}}{2} = \frac{20.93 - 5.232}{2} = 7.849 \text{ MPa},$$

$$\sigma_m = \frac{\sigma_{\max} + \sigma_{\min}}{2} = \frac{20.93 + 5.232}{2} = 13.08 \text{ MPa}.$$

In applying the modified Goodman approach, Table 7.6 is very valuable. Note the requirement for Region a to be valid, then note that

$$\frac{S_e}{K_f} - S_y = \frac{119}{3.0} - 295 = -255 \text{ MPa}.$$

However, since  $\sigma_m = 20.93$  MPa, this cannot be true and therefore Region a is not valid. Similarly, Region b cannot be valid since  $\sigma_m > 0$ . Note that

$$\frac{S_y - \frac{S_e}{K_f}}{1 - \frac{S_e}{K_f S_u}} = \frac{295 - \frac{119}{3.0}}{1 - \frac{119}{(3.0)(395)}} = 284 \text{ MPa}.$$

Since  $\sigma_m < 284$  MPa, Region c is valid and the failure equation from Table 7.6 is

$$\sigma_{\max} + \sigma_m \left( \frac{S_e}{K_f S_{ut}} - 1 \right) = \frac{S_e}{n_s} K_f;$$

$$20.93 + 13.08 \left( \frac{119}{(3.0)(395)} - 1 \right) = \frac{119}{(3.0)n_s}.$$

This is solved as  $n_s = 4.22$ .

## 7.10.2 Brittle Materials

Until recently, the use of brittle materials in a fatigue environment has been limited to gray cast iron in compression. Now, however, carbon fibers and ceramics have had significant use in fatigue environments. Figure 7.18 shows the alternating stress ratio as a function of the mean stress ratio for axially loaded cast iron. The figure is skewed since the compressive strength is typically several times greater than the tensile strength.

In Fig. 7.18, the dimensionalization of the alternating and mean stresses is with respect to the ultimate strength rather than to the yield strength as done for ductile materials. Also, the compressive mean stress permits large increases in alternating stress.

For brittle materials a stress raiser increases the likelihood of failure under either steady or alternating stresses, and it is customary to apply a stress concentration factor to both. Thus, designers apply the fatigue stress concentration factor  $K_f$  to the alternating component of stress for ductile materials but apply the stress concentration factor  $K_c$  to both

the alternating and mean components of stress for brittle materials.

For a single normal stress in brittle materials, the equation for the safety factor with a steady stress  $\sigma_m$  and with the ultimate tensile strength  $S_{ut}$  as the basis of failure is

$$n_s = \frac{S_{ut}}{K_c \sigma_m}. \quad (7.31)$$

With an alternating stress,  $\sigma_a$ , and a modified endurance limit,  $S_e$ :

$$n_s = \frac{S_e}{K_c \sigma_a}. \quad (7.32)$$

For a single shear stress on a brittle component and with a steady shear stress,  $\tau_m$ , the safety factor is

$$n_s = \frac{S_{ut}}{K_{cs} \tau_m \left[ 1 + \frac{S_{ut}}{S_{uc}} \right]}. \quad (7.33)$$

With an alternating shear stress,  $\tau_a$ , and a modified endurance limit,  $S_e$ :

$$n_s = \frac{S_e}{K_{cs} \tau_a \left[ 1 + \frac{S_{ut}}{S_{uc}} \right]}. \quad (7.34)$$

## 7.11 Influence of Multi-Axial Stress States

The previous sections have considered fatigue failures for uniaxial stress states. Most machine element applications encounter more complicated loading conditions. Two special cases are important. The first situation is where the applied stresses are in phase, a situation referred to as **simple multi-axial stress**. For example, a cylindrical pressure vessel that is periodically pressurized will have a hoop and axial stress that are both directly related to the pressure, so that they are subjected to their maximum and minimum values at the same time. On the other hand, a shaft with two gears mounted on it will see a periodic variation in normal forces and torques applied by the gears; these may be caused by forcing functions in the driven machinery. Clearly, the normal forces and torques do not have to be in phase in this circumstance; this situation is called **complex multiaxial stress**.

Caution should be given that the current theoretical approaches for multi-axial stress states are even less developed than uniaxial fatigue approaches, so that experimental confirmation of designs is even more imperative.

### 7.11.1 Simple Multiaxial Stress

#### Fully Reversing Stresses

For *fully reversing, simple multiaxial stresses*, the mean stress is zero for all applied normal and shear stresses. For such a circumstance, experimental evidence suggests that a combination of an equivalent von Mises effective stress, defined from the alternating principal stress components, can be used in conjunction with uniaxial fatigue failure criteria. That is, an effective stress can be defined from

$$\sigma'_e = \sqrt{\sigma_{a,1}^2 + \sigma_{a,2}^2 + \sigma_{a,3}^2 - \sigma_{a,1}\sigma_{a,2} - \sigma_{a,2}\sigma_{a,3} - \sigma_{a,1}\sigma_{a,3}}. \quad (7.35)$$

If the stress state is two-dimensional (with  $\sigma_{a,3} = 0$ ), this equation can be written as

$$\sigma'_e = \sqrt{\sigma_{a,1}^2 + \sigma_{a,2}^2 - \sigma_{a,1}\sigma_{a,2}}. \quad (7.36)$$

The safety factor can then be calculated from

$$n_s = \frac{S_f}{\sigma'_e} \quad \text{or} \quad n_s = \frac{S_e}{\sigma'_e}. \quad (7.37)$$

$S_f$  is used for finite life applications and is the fatigue strength at the desired life.  $S_e$  is used for infinite life applications. Recall that all fatigue strength reduction factors are incorporated in  $S_f$  and  $S_e$ . Stress concentration effects should be applied in Eqs. (7.35) and (7.36).

### Simple Multiaxial Stresses with Non-zero Mean

A number of studies have addressed the situation where the applied stresses are in phase, but the mean stress is non-zero. Two of the more common theories are referred to as the **Sines method** and the **von Mises method**. These theories use the common approach of defining an effective alternating and mean stress, and then inserting these effective stresses in the Modified Goodman failure criterion given in Table 7.5.

The approach of Sines and Waisman [1959] uses the following equivalent stresses:

$$\begin{aligned} \sigma'_a &= \frac{1}{\sqrt{2}} \{ (\sigma_{a,x} - \sigma_{a,y})^2 + (\sigma_{a,y} - \sigma_{a,z})^2 \\ &\quad + (\sigma_{a,z} - \sigma_{a,x})^2 + 6(\tau_{a,xy}^2 + \tau_{a,yz}^2 + \tau_{a,zx}^2) \}^{1/2}, \end{aligned} \quad (7.38)$$

$$\sigma'_m = \sigma_{m,x} + \sigma_{m,y} + \sigma_{m,z}. \quad (7.39)$$

For a two-dimensional stress state ( $\sigma_z = \tau_{xz} = \tau_{yz} = 0$ ), these equations can be simplified to

$$\sigma'_a = \sqrt{\sigma_{a,x}^2 + \sigma_{a,y}^2 - \sigma_{a,x}\sigma_{a,y} + 3\tau_{a,xy}^2}, \quad (7.40)$$

$$\sigma'_m = \sigma_{m,x} + \sigma_{m,y}. \quad (7.41)$$

Note that the mean component of shear stress does not appear in these equations. This is acceptable for some circumstances, but is non-conservative for situations where a stress concentration such as a notch or fillet is present. For this reason, another approach using the von Mises effective stresses defines the effective alternating and mean stresses as

$$\begin{aligned} \sigma'_a &= \frac{1}{\sqrt{2}} [(\sigma_{a,x} - \sigma_{a,y})^2 + (\sigma_{a,y} - \sigma_{a,z})^2 \\ &\quad + (\sigma_{a,z} - \sigma_{a,x})^2 + 6(\tau_{a,xy}^2 + \tau_{a,yz}^2 + \tau_{a,zx}^2)]^{1/2}, \end{aligned} \quad (7.42)$$

$$\begin{aligned} \sigma'_m &= \frac{1}{\sqrt{2}} [(\sigma_{m,x} - \sigma_{m,y})^2 + (\sigma_{m,y} - \sigma_{m,z})^2 \\ &\quad + (\sigma_{m,z} - \sigma_{m,x})^2 + 6(\tau_{m,xy}^2 + \tau_{m,yz}^2 + \tau_{m,zx}^2)]^{1/2}, \end{aligned} \quad (7.43)$$

or, for a two dimensional stress state with  $\sigma_{a,z} = \sigma_{m,z} = \tau_{a,xz} = \tau_{a,yz} = \tau_{m,xz} = \tau_{m,yz} = 0$ ,

$$\sigma'_a = \sqrt{\sigma_{a,x}^2 + \sigma_{a,y}^2 - \sigma_{a,x}\sigma_{a,y} + 3\tau_{a,xy}^2}, \quad (7.44)$$

$$\sigma'_m = \sqrt{\sigma_{m,x}^2 + \sigma_{m,y}^2 - \sigma_{m,x}\sigma_{m,y} + 3\tau_{m,xy}^2}. \quad (7.45)$$

One of the difficulties in applying these theories is that conflicts may arise in determining stress concentration factors and fatigue strengths depending on the loading condition selected. Recall from Eq. (7.7) that  $S'_f$  will vary depending on whether the loading is bending, axial, or torsional. If the loading is a combination of these loadings, it is not clear how to calculate  $S'_f$ . Similarly, stress concentration factors can be defined based on the loading; thus, it is not obvious which value to use in Table 7.5. Recognizing that an experimental verification of a design is imperative for critical applications, it is reasonable to follow any of the following approximations:

1. Perform a worst-case scenario, using the smallest resulting strengths and largest stress concentrations that result from the loading.
2. Since Mode I failure is usually most critical, calculate strengths and stress concentrations based on axial loads when they are present. If normal stresses are present due to bending moments, calculate material strengths and stress concentration effects based on bending.
3. An experienced engineer can evaluate the applied stresses to determine which is the most likely failure mode. That is, if the torsional stresses are dominant, it is reasonable to calculate strengths and concentration factors based on torsion. However, this is a very subjective approach that all but guarantees experimental confirmation of the design will be required.

### 7.11.2 Complex Multiaxial Stresses

For complex multiaxial stress states, where the normal and shear stress maxima and minima do not occur at the same time, failure theories are not well developed. True asynchronous situations cannot be analyzed with existing failure theories, and an experimental program may be required. A designer's goal in such circumstances is to obtain estimates of machine element dimensions for use in the experimental program. The following approaches have been applied for complex multiaxial stress states:

1. It has been shown that the fatigue strength of some metals is not less than their strengths in a simple multiaxial stress state. Thus, it may be reasonable to approximate the stresses as synchronous, and to analyze the situation as a simple multiaxial stress state using Eqs. (7.38) through (7.39) or (7.42) through (7.43).
2. For situations where the loading consists of bending and torsion (such as is commonly encountered in shafts), an approach in the American Society of Mechanical Engineers Boiler Code can be used. This approach defines an effective stress given by:

$$\sigma_s = \frac{\sigma}{\sqrt{2}} \left[ 1 + 3 \left( \frac{\tau}{\sigma} \right)^2 + \sqrt{1 + \frac{6\tau}{\sigma} \cos 2\phi + 9 \left( \frac{\tau}{\sigma} \right)^4} \right]^{\frac{1}{2}}, \quad (7.46)$$

where

$\sigma$  = bending stress amplitude including stress concentration effects

$\tau$  = torsional stress amplitude including stress concentration effects

$\phi$  = phase angle between bending and torsion



Equation (7.46) can be used to obtain both mean and alternating components of stress. It can be shown by comparing Eqs. (7.46) and (7.42) through (7.43) that the von Mises approach is conservative for any phase difference or stress ratio. However, this is true only for high cycle fatigue, and can be non-conservative for finite life applications. Since shafts are usually designed for infinite life, this is rarely a concern.

3. Behavior for a given loading and material combination may be well-quantified within an organization, or can be found in the technical literature.

## 7.12 Fracture Mechanics Approach to Fatigue

With the increasing interest in materials without clear endurance limits, special attention must be paid to damage accumulation and replacing fatigued components before catastrophic failure can occur. Indeed, this is a main design challenge in the aircraft industry, where aluminum alloys, although they have no endurance limit, are used because of their high strength-to-weight ratios. Routine nondestructive evaluation to determine the size of flaws in stress-bearing members is conducted to identify and remove suspect components. This approach is called **fault-tolerant design** since it recognizes the presence of defects and allows the use of a material as long as the defects remain smaller than a critical size.

Recall the situation depicted in Fig. 7.4b, where Regime B is active. If the slope  $m$  is reasonably small, a part can have a long service life before the crack size becomes critical, and this is indeed a common circumstance. Paris et al. [1961] hypothesized that crack growth in such a cyclic loading should follow the rule

$$\frac{dl_c}{dN} = C (\Delta K)^m, \quad (7.47)$$

where  $dl_c/dN$  is the change in crack length per load cycle ( $l_c$  is the crack length and  $N$  is the number of stress cycles),  $C$  and  $m$  are empirical constants, and  $\Delta K$  is the stress intensity range defined as

$$\Delta K = K_{\max} - K_{\min}, \quad (7.48)$$

where  $K_{\max}$  and  $K_{\min}$  are the maximum and minimum stress intensity factors, respectively, around a crack during a loading cycle. For a center-cracked plate with crack length  $l_c = 2a$ , recall from Eq. (6.6) that

$$K_{\max} = Y \sigma_{\max} \sqrt{\pi a}, \quad (7.49)$$

where  $\sigma_{\max}$  is the maximum far-field stress and  $Y$  is a correction factor to account for finite plate sizes. Table 7.7 summarizes conservative values of  $C$  and  $m$  for steels, while Fig. 7.19 gives fatigue crack propagation data for a variety of materials. Appendix C gives values of  $Y$ . Equation (7.47) is known as the **Paris power law** and is the most widely used equation in fracture mechanics approaches to fatigue problems. Suresh [1998] has derived the life of a component based on the Paris power law as

$$N = \frac{2}{(m-2)CY^m(\Delta\sigma)^m\pi^{m/2}} \times \left\{ \frac{1}{(l_{co})^{(m-2)/2}} - \frac{1}{(l_{cf})^{(m-2)/2}} \right\}, \quad (7.50)$$

Table 7.7: Paris law constants for various metals. Data represents worst-case (fastest) crack growth rates reported for the material.

Material	$C$ , $\frac{\text{mm/cycle}}{(\text{MPa} \sqrt{\text{m}})^m}$	$m$
<b>Steel</b>		
Ferritic-pearlitic	$6.89 \times 10^{-9}$	3.0
Martensitic	$1.36 \times 10^{-7}$	2.25
Austenitic	$5.61 \times 10^{-9}$	3.25
<b>Aluminum</b>		
6061-T6	$5.88 \times 10^{-8}$	3.17
2024-T3	$1.6 \times 10^{-11}$	3.59

unless  $m = 2$ , when the fatigue life is

$$N = \frac{1}{CY^2(\Delta\sigma)^2\pi} \ln \frac{l_{cf}}{l_{co}}, \quad (7.51)$$

where

- $N$  = fatigue life in cycles
- $C$  and  $m$  = material constants
- $Y$  = correction factor to account for finite plate sizes
- $\Delta\sigma$  = range of far-field stresses to which component is subjected
- $l_{co}$  = initial crack size
- $l_{cf}$  = critical crack size based on fracture mechanics

### Example 7.10: Fault Tolerant Design

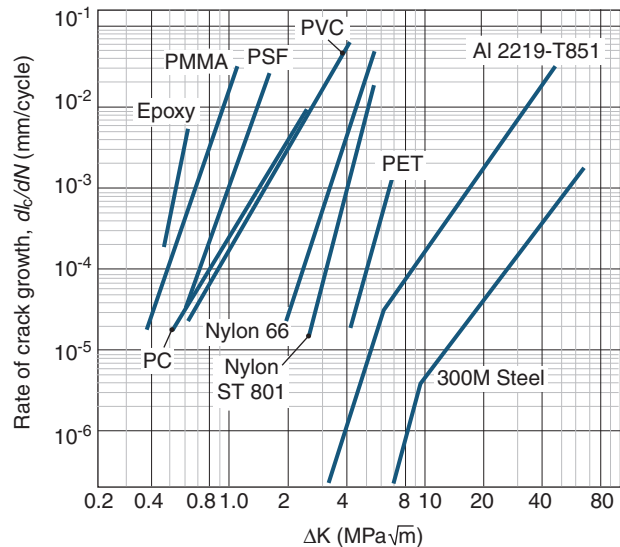
**Given:** An aluminum alloy aircraft component in the form of a 100-mm-wide plate is subjected to a 100-MPa stress during pressurization of the aircraft cabin. Superimposed on this stress is a fluctuation arising from vibration, with an amplitude of 10 MPa and a frequency of 45 Hz. Nondestructive crack detection techniques do not detect any flaws, but the smallest detectable flaw is 0.2 mm.

**Find:** Determine the minimum expected life of the component. If upon reinspection a centered 1.1-mm-long crack is found, what is the expected life from the time of inspection? Use a fracture toughness of  $29 \text{ MPa}\sqrt{\text{m}}$  and a fracture stress of 260 MPa and assume  $m = 2.5$  and  $C = 6.9 \times 10^{-12} \text{ m/cycle}$  for  $\Delta\sigma$  in MPa.

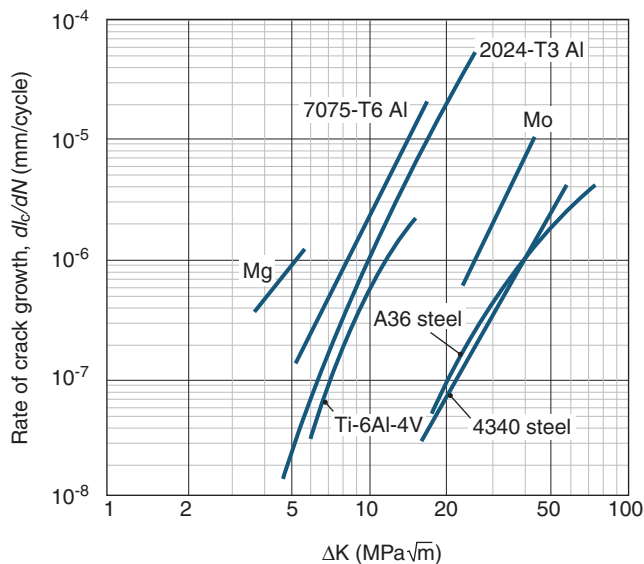
**Solution:** The critical crack length  $l_{cf}$  is given by Eq. (6.5) and is found to be 1.60 mm. A worst-case scenario would occur if the largest undetectable flaw resulting in the largest value of  $Y$  were located in the geometry. This flaw occurs for the double-edge-cracked tension specimen, where  $Y$  equals 2.0. Therefore, the life is found from Eq. (7.50) as

$$N = \frac{2}{(m-2)CY^m(\Delta\sigma)^m\pi^{m/2}} \times \left\{ \frac{1}{(l_{co})^{(m-2)/2}} - \frac{1}{(l_{cf})^{(m-2)/2}} \right\} = 324 \text{ hr.}$$

If  $l_{co} = 1.1 \text{ mm}$ , the life until fracture is approximately 47 hr.



(a)



(b)

Figure 7.19: Fatigue crack growth data for a variety of materials. (a) Selected polymers in comparison to aluminum and steel; (b) selected metal alloys. *Source:* Adapted from Bowman [2004].

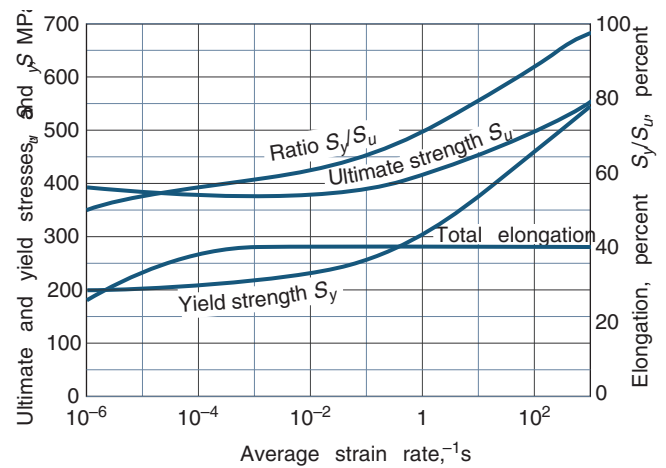


Figure 7.20: Mechanical properties of mild steel at room temperature as function of average strain rate.

## 7.13 Linear Impact Stresses and Deformations

This chapter thus far has focused on cyclic load variation; this section focuses on **impact loading**. Throughout most of this text a load is applied to a body gradually such that when the load reaches a maximum it remains constant or static. For the material covered thus far in this chapter, the loading is **dynamic** (i.e., it varies with time). When loads are rapidly applied to a body as in impact loading, the stress levels and deformations induced are often much larger than those in static or cyclic loading.

The properties of the material are a function of the loading speed; the more rapid the loading, the higher both the yield and ultimate strengths of the material. Figure 7.20 shows the variation of the mechanical properties with loading speed for a typical mild steel. For average strain rates from  $10^{-1}$  to  $10^3 \text{ s}^{-1}$  the yield strength increases significantly.

If no energy is lost during impact, the conservation of energy can be applied. Consider a simple block falling a distance  $h$  and striking a spring compressed a distance  $\delta_{\max}$  before momentarily coming to rest. If the mass of the spring is neglected and it is assumed that the spring responds elastically, conservation of energy requires that the kinetic energy be completely transformed into elastic strain energy:

$$W(h + \delta_{\max}) = \frac{1}{2}(k\delta_{\max})\delta_{\max}, \quad (7.52)$$

where  $k$  is the spring constant in N/m and  $W$  is the weight of the block. Equation (7.52) can be expressed as a quadratic equation:

$$\delta_{\max}^2 - \frac{2W}{k}\delta_{\max} - 2\left(\frac{W}{k}\right)h = 0. \quad (7.53)$$

Solving for  $\delta_{\max}$

$$\delta_{\max} = \frac{W}{k} + \sqrt{\left(\frac{W}{k}\right)^2 + 2\left(\frac{W}{k}\right)h}. \quad (7.54)$$

If the weight is applied statically (or gradually) to the spring, the static displacement is

$$\delta_{st} = \frac{W}{k}. \quad (7.55)$$

Substituting Eq. (7.55) into Eq. (7.54) gives

$$\delta_{\max} = \delta_{st} + \sqrt{(\delta_{st})^2 + 2\delta_{st}h},$$

or

$$\delta_{\max} = \delta_{st} \left( 1 + \sqrt{1 + \frac{2h}{\delta_{st}}} \right). \quad (7.56)$$

From the maximum displacement in Eq. (7.56) the maximum force is

$$P_{\max} = k\delta_{\max}. \quad (7.57)$$

Recall that in dropping the block from some distance,  $h$ , the maximum force  $P_{\max}$  on impact is essentially instantaneous. The block will continue to oscillate until the motion dampens and the block assumes the static position. This analysis assumes that when the block first makes contact with the spring, the block does not rebound, that is, it does not separate from the spring. Making use of the spring constant  $k$  in Eqs. (7.55) and (7.57) relates the static and dynamic effects.

The impact factor can be expressed as

$$I_m = \frac{\delta_{\max}}{\delta_{st}} = \frac{P_{\max}}{W} = 1 + \sqrt{1 + \frac{2h}{\delta_{st}}}. \quad (7.58)$$

Note that once the impact factor is known, the impact load, stresses, and deflections can be calculated. The impact stress is

$$\sigma = \frac{P_{\max}}{A}, \quad (7.59)$$

where  $A$  is the area of the spring surface,  $\text{m}^2$ . If, instead of the block dropping vertically, it slides with a velocity,  $u$ , on a surface that provides little frictional resistance (so that it can be neglected) and the block impacts the spring, the block's kinetic energy is transformed into stored energy in the spring, or

$$\frac{1}{2} \left( \frac{W}{g} \right) u^2 = \frac{1}{2} k \delta_{\max}^2, \quad (7.60)$$

where  $g$  is gravitational acceleration ( $9.807 \text{ m/s}^2$ ). Note that the right side of Eq. (7.52) is identical to the right side of Eq. (7.60). Solving for  $\delta_{\max}$  in Eq. (7.60) gives

$$\delta_{\max} = \sqrt{\frac{Wu^2}{gk}}. \quad (7.61)$$

By using Eq. (7.55), Eq. (7.61) becomes

$$\delta_{\max} = \sqrt{\frac{\delta_{st}u^2}{g}}. \quad (7.62)$$

In both situations the moving body (the block) is assumed to be rigid, and the stationary body (the spring) is assumed to be deformable. The material is assumed to behave in a linear-elastic manner. Thus, whether a block falls a distance  $h$  and impacts on a spring, or a block moves at a velocity  $u$  and strikes a spring, the formulation for the deformation, the impact force, or the impact stress can be determined.

### Example 7.11: Impact Stresses

**Given:** A diver jumps up 0.6 m on the free end of a diving board before diving into the water. Figure 7.21 shows a sketch of the diver and the dimensions of the diving board. The supported end of the diving board is fixed. The modulus of elasticity is 69 GPa and the yield strength is 220 MPa. The weight of the diver is 900 N.

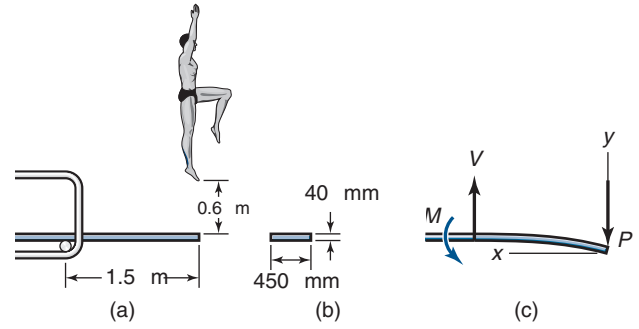


Figure 7.21: Diver impacting diving board, used in Example 7.11. (a) Side view; (b) front view; (c) side view showing forces and coordinates.

**Find:** The safety factor for impact loading based on yielding.

**Solution:** Equations (7.54) and (7.55) should be used to determine the maximum deflection at impact at the end of the diving board. The spring rate is not given and will need to be determined. The forces acting are shown in Fig. 7.21c. From Eq. (5.3),

$$\frac{d^2y}{dx^2} = \frac{M}{EI} = -\frac{Px}{EI}.$$

Integrating this equation gives

$$EI \frac{dy}{dx} = -\frac{Px^2}{2} + C_1,$$

where  $C_1$  is an integration constant. Integrating again gives

$$EIy = -\frac{Px^3}{6} + C_1x + C_2,$$

where  $C_2$  is another integration constant. The boundary conditions are

1.  $x = l, y' = 0$ , leading to  $C_1 = \frac{Pl^2}{2}$
2.  $x = l, y = 0$ , resulting in  $C_2 = -\frac{Pl^3}{3}$

The deflection at the end of the board ( $x = 0$  in Fig. 7.21c) is of interest. Therefore,

$$EIy = -\frac{Px^3}{6} + \frac{Pl^2x}{2} - \frac{Pl^3}{3},$$

or

$$\frac{6EIy}{P} = -x^3 + 3l^2x - 2l^3,$$

so that

$$\delta = -\frac{Pl^3}{3EI}.$$

The spring constant is

$$k = -\frac{P}{\delta} = \frac{3EI}{l^3},$$

where  $I$  is the area moment of inertia given by

$$I = \frac{bh^3}{12} = \frac{(0.45)(0.04)^3}{12} = 2.40 \times 10^{-6} \text{ m}^4,$$

$l$  is the length (given as 1.5 m) and  $E$  is the modulus of elasticity (69 GPa). Therefore,

$$k = \frac{3(69 \times 10^9)(2.40 \times 10^{-6})}{(1.5)^3} = 147.2 \text{ kN/m}.$$

From Eq. (7.55),

$$\delta_{st} = \frac{W}{k} = \frac{900 \text{ N}}{147.2 \text{ kN/m}} = 0.00611 \text{ m}.$$

From Eq. (7.58), the impact factor is

$$\begin{aligned} I_m &= \frac{\delta_{\max}}{\delta_{st}} \\ &= 1 + \sqrt{1 + \frac{2h}{\delta_{st}}} \\ &= 1 + \sqrt{1 + \frac{2(0.6)}{0.006144}} \\ &= 14.01. \end{aligned}$$

Therefore,

$$\delta_{\max} = I_m \delta_{st} = (14.01)(0.006144) = 0.08566 \text{ m}.$$

From Eq. (7.57),

$$P_{\max} = k \delta_{\max} = (147.2 \times 10^3)(0.08566) = 12.61 \text{ kN}.$$

The maximum bending stress from Eq. (4.45) is

$$\sigma_{\max} = \frac{Mc}{I} = \frac{(12,610)(1.5)(0.020)}{2.40 \times 10^{-6}} = 157.6 \text{ MPa}.$$

The yield stress is given as 220 MPa. The safety factor for yielding is

$$n_s = \frac{S_y}{\sigma_{\max}} = \frac{(220 \times 10^6)}{157.6 \times 10^6} = 1.396.$$

Thus,  $n_s > 1$  and thus failure should not occur; however, because the safety factor is just above 1, the margin of safety is a minimum.

## Case Study 7.1: Fault Tolerant Design in Aircraft

Aircraft are a particularly important application of fatigue design theory, especially fault tolerant design. Since the weight of an aircraft needs to be minimized to control fuel consumption, materials with high strength-to-weight ratios (see Section 3.7.2) are required. Historically, this has necessitated the widespread use of aluminum and titanium alloys, and also composite materials. Unfortunately, these materials often do not display clear endurance limits. A designer can then opt to incorporate very large safety factors, but this would have adverse effects on fuel economy and would make commercial aviation impractical.

### Maintenance Intervals

The alternative that is followed in the aviation industry is to pursue periodic inspection and maintenance. These maintenance tasks address a wide variety of concerns, including evaluation of brakes, replacement of lubricants and working



(a)



(b)

Figure 7.22: (a) Exterior view of Boeing 747-400 during a D check; (b) inspection of landing gear component for structural integrity. *Source:* Courtesy of Lufthansa Technik.

fluids, inspection of bearings, etc. This case study emphasizes the structural components of aircraft and the methodologies used to prevent fatigue failure during use.

The four classes of maintenance on an aircraft are, along with their approximate interval:

- **A check.** An A check is performed approximately every 500 flight hours. This check is generally performed overnight at an airport gate, and includes visual inspection for obvious damage, corrosion, and deterioration.
- **B check.** B checks are not generally used with modern aircraft, but in the past consisted of similar tasks as the A check with marginally more detailed procedures. A B check is also generally performed overnight at an airport gate.



- **C check.** C checks are generally performed every 12 months of operation or based on flight hours. C checks are high-level tests that are performed in an airplane hangar and use extensive tooling and equipment, and generally take a few days. As related to the aircraft structure, the C check involves a thorough inspection of the structure, and can include non-destructive approaches such as ultrasonic or eddy current inspection. Examination for corrosion or cracks, especially at locations of stress concentration, is carefully performed.
- **D check.** A D Check is a very comprehensive check for an aircraft, and has been characterized as completely disassembling the aircraft and replacing worn or damaged components so that the aircraft is brought to an as-new condition. This characterization is an exaggeration, but a D check does involve extensive evaluation of structural components.

A D check occurs roughly every five years and can cost over \$2 million. Figure 7.22a shows a general view of a D check, while Figure 7.22b shows details of non-destructive evaluation of a landing gear structural component during a D check.

Note that the intervals given are only approximate, as each aircraft has a maintenance cycle as defined by the manufacturer and approved by governing bodies such as the Federal Aviation Administration or European Aviation Safety Agency. Modern inspection intervals are determined by damage growth intervals such as predicted by Eq. (7.50), whereas in the past these were based on service experience. There is no limit to the service life of a damage-tolerant aircraft if necessary inspections and corrective actions are carried out.

### Design Considerations

Aircraft designers have a very sophisticated understanding of aircraft loads during normal operation and for reasonably foreseeable conditions (wind gusts, hard landings, fuselage pressurization, etc.) that can occur during flight. Computational tools are used in the design stage, and parts are sized so that the largest loads can be safely supported.

It should be noted that many components have complex geometries and loadings, and the loadings can change direction during different maneuvers. Therefore, it has been recognized that multiple site damage is a concern with aircraft structures.

In designing a structural component, fault or damage tolerance can be fundamentally incorporated by selecting proper materials that have a low crack growth rate for the stress intensities encountered in service (see Section 7.12). A given material also defines the maximum damage that can be sustained under extreme loads (see Section 6.5), that is, the allowable crack length (or contributions from multiple cracks) that still allow the plane to fly safely under foreseeable conditions. Stress analysis results in a stress intensity factor that allows prediction of crack growth rates in materials (see Fig. 7.19). Often, initial cracks are smaller than the detection threshold of measurement systems, so designs use the detection threshold as the assumed initial flaw size in these conditions. Therefore, inspection intervals can be defined to ensure that damage is detected before a catastrophic failure occurs. Further, inspection procedures and devices can be developed to capture failure modes of particular concern.

Design for disassembly is not usually a criterion considered by designers, but it certainly is essential for C and D checks on aircraft. Even so, many components are exceedingly difficult to access or test. Recognizing this, larger safety factors or more fatigue resistant materials are used for components that are especially difficult to inspect and re-pair/replace, even though this may have a cost penalty.

### Summary

There is considerable pressure on aircraft manufacturers to extend the interval between service checks. The sophistication with respect to fatigue design has advanced considerably in the past two decades, so that maintenance hours per airplane associated with fatigue and corrosion issues have decreased by an order of magnitude. It has often been noted that flying in commercial aircraft is the safest form of travel, and this is attributable to the widespread use of fault tolerant design.

## 7.14 Summary

Failures in components or structures are often caused by fluctuating stresses. If the stress variation sequence repeats itself, it is called cyclic. The various cyclic patterns were described. The fatigue strength versus the logarithm of the number of cycles to failure was presented for materials with and without an endurance limit. Ferrous materials tend to have endurance limits, and nonferrous materials tend not to have endurance limits. The endurance limit for ferrous materials is a function of the type of loading the component is subjected to. Also, *low-cycle* fatigue failure has been classified as occurring at less than  $10^3$  cycles, and *high-cycle* fatigue failure as occurring above  $10^3$  cycles.

The endurance limit has been experimentally determined for a specimen of specific size with a mirror-like surface finish. The specimen was precisely prepared and tested under controlled conditions. In practice, conditions differ significantly from those in a test situation. To more accurately characterize the conditions that prevail in practice, the modified endurance limit is used. The surface finish and size factors are used along with a fatigue stress concentration factor.

Various approaches for estimating when failure will occur under nonzero mean cyclic stresses were also considered. The Soderberg, Gerber, Goodman, and modified Goodman theories were presented. These theories allow the variation of mean and alternating stresses. The construction of a complete modified Goodman diagram was shown, and fatigue and yield criteria were used. Failure equations were given for specific regions of the modified Goodman diagram.

Most of the results presented were for ductile materials, but the behavior of brittle materials was briefly described. The major difference between brittle and ductile materials is that the compressive and tensile strengths are nearly identical for ductile materials whereas for brittle materials the compressive strength is several times greater than the tensile strength.

Impact loading has to be considered when loads are rapidly applied. The stress levels and deformations induced are much larger than with static or cyclic loading. The more rapid the loading, the higher the yield and ultimate strengths of a material. By equating the kinetic and elastic strain energies, two types of impact loading were considered: a block falling from a given height onto a spring, and a block sliding downward into a spring. An impact factor, maximum and static deformations, and maximum and static loads were also obtained.



## Key Words

**cyclic stress** stress sequence that repeats over time

**dynamic** adjective indicating variation with time

**endurance limit** stress level below which infinite life can be realized

**fatigue** failure, at relatively low stress levels, of structures that are subject to fluctuating and cyclic stresses

**finite life** life until failure due to fatigue

**Gerber line** parabolic relationship taking mean and alternating stresses into account

**Goodman line** theory connecting modified endurance limit and ultimate strength on plot of alternating stress versus mean stress

**high-cycle fatigue** fatigue failure that occurs above  $10^3$  cycles but below  $10^6$  cycles

**impact loading** load rapidly applied to body

**infinite life** stress levels that do not cause fatigue failure

**low-cycle fatigue** fatigue failure that occurs below  $10^3$  cycles

**Manson-Coffin relationship** theoretical approach to fatigue based on strain

**mean stress** average of minimum and maximum stresses in cycle

**Miner's rule** same as linear damage rule

**modified endurance limit** corrections for endurance limit based on surface finish, material, specimen size, loading type, temperature, etc.

**modified Goodman diagram** diagram that defines all stress states not resulting in fatigue failure or yielding

**notch sensitivity** material property that reflects ability of ductile materials to be less susceptible to stress raisers in fatigue

**Paris power law** postulate that crack growth in cyclic loading follows power law

**residual stress** internal stress usually caused by manufacturing process

**Soderberg line** theory connecting modified endurance limit and yield strength on plot of alternating stress versus mean stress

**S-N diagram** plot of stress level versus number of cycles before failure

**staircase** an approach used to determine the endurance limit of a material by varying the applied stress on a modest number of samples.

**stress amplitude** one-half of stress range

**stress range** difference between maximum and minimum stresses in cycle

**stress ratio** ratio of minimum and maximum stresses

**Wöhler diagram** same as S-N diagram

**yield line** failure criterion that postulates yielding on first cycle of cyclic loading with nonzero mean

## Summary of Equations

### Cyclic Stresses:

$$\text{Mean stress: } \sigma_m = \frac{\sigma_{\max} + \sigma_{\min}}{2}$$

$$\text{Stress range: } \sigma_r = \sigma_{\max} - \sigma_{\min}$$

$$\text{Stress amplitude: } \sigma_a = \frac{\sigma_r}{2} = \frac{\sigma_{\max} - \sigma_{\min}}{2}$$

### Finite Life Fatigue:

Manson-Coffin Relationship:

$$\frac{\Delta \epsilon}{2} = \frac{\sigma'_f}{E} (2N')^a + \epsilon'_f (2N')^\alpha$$

Strength as a function of loading cycles:

$$\log S'_f = b_s \log N'_t + \bar{C},$$

$$b_s = -\frac{1}{3} \log \left( \frac{S'_t}{S'_e} \right), \bar{C} = \log \left[ \frac{(S'_t)^2}{S'_e} \right]$$

High cycle fatigue limits:

Lower limit ( $N \approx 10^3$ ): for bending,  $S'_l = 0.9S_u$ ;

for axial loads,  $S'_l = 0.75S_u$ ;

for torsion,  $S'_l = 0.72S_u$ .

Upper limit ( $N \approx 10^6$  or  $10^7$ ):  $S'_e = 0.5S_u$ ;

for axial loads,  $S'_e = 0.45S_u$ ;

for torsion,  $S'_e = 0.29S_u$ .

Life as a function of stress:  $N'_t = (S'_f 10^{-\bar{C}})^{1/b_s}$

**Fatigue Stress Concentrations:**  $K_f = 1 + (K_c - 1)q_n$

**Modified Endurance Limit:**  $S_e = k_f k_s k_r k_m S'_e$

Surface finish factor:  $k_f = eS_{ut}^f$

Size factor:

$$k_s = \begin{cases} 1 & d \leq 8 \text{ mm} \\ 1.189d^{-0.112} & 8 \text{ mm} < d \leq 250 \text{ mm} \end{cases}$$

Temperature factor:  $k_t = \frac{S_{ut}}{S_{ut, \text{ref}}}$

### Cumulative Damage:

Miner's rule:  $\frac{n'_1}{N'_1} + \frac{n'_2}{N'_2} + \dots + \frac{n'_i}{N'_i} \geq 1$

### Effect of Nonzero Mean Stress:

Gerber parabola:  $\frac{K_f n_s \sigma_a}{S_e} + \left( \frac{n_s \sigma_m}{S_{ut}} \right)^2 = 1$

Goodman line:  $\frac{K_f \sigma_a}{S_e} + \frac{\sigma_m}{S_{ut}} = \frac{1}{n_s}$

Soderberg line:  $\frac{K_f \sigma_a}{S_e} + \frac{\sigma_m}{S_{yt}} = \frac{1}{n_s}$

Yield line:  $\frac{\sigma_a}{S_{yt}} + \frac{\sigma_m}{S_{yt}} = \frac{1}{n_s}$

### Multiaxial Stresses:

Simple, fully reversing:  $n_s = \frac{S_e}{\sigma'_e}$

where

$$(\sigma'_e)^2 = \sigma_{a,1}^2 + \sigma_{a,2}^2 + \sigma_{a,3}^2 - \sigma_{a,1}\sigma_{a,2} - \sigma_{a,2}\sigma_{a,3} - \sigma_{a,1}\sigma_{a,3}$$

Simple, nonzero mean:

Sines method:

$$2(\sigma'_a)^2 = (\sigma_{a,x} - \sigma_{a,y})^2 + (\sigma_{a,y} - \sigma_{a,z})^2 + (\sigma_{a,z} - \sigma_{a,x})^2 + 6(\tau_{a,xy}^2 + \tau_{a,yz}^2 + \tau_{a,zx}^2)$$

$\sigma'_m = \sigma_{m,x} + \sigma_{m,y} + \sigma_{m,z}$   
von Mises method:

$$2(\sigma'_a)^2 = (\sigma_{a,x} - \sigma_{a,y})^2 + (\sigma_{a,y} - \sigma_{a,z})^2 + (\sigma_{a,z} - \sigma_{a,x})^2 + 6(\tau_{a,xy}^2 + \tau_{a,yz}^2 + \tau_{a,zx}^2)$$

$$2(\sigma'_m)^2 = (\sigma_{m,x} - \sigma_{m,y})^2 + (\sigma_{m,y} - \sigma_{m,z})^2 + (\sigma_{m,z} - \sigma_{m,x})^2 + 6(\tau_{m,xy}^2 + \tau_{m,yz}^2 + \tau_{m,zx}^2)$$

Complex multiaxial stresses:

$$\sigma_s = \frac{\sigma}{\sqrt{2}} \left[ 1 + 3 \left( \frac{\tau}{\sigma} \right)^2 + \sqrt{1 + 6 \frac{\tau}{\sigma} \cos 2\phi + 9 \left( \frac{\tau}{\sigma} \right)^4} \right]^{1/2}$$

### Fracture Mechanics Approach

Paris equation:  $\frac{dl_c}{dN} = C(\Delta K)^m$

Predicted life:

$$N = \frac{2}{(m-2)CY^m(\Delta\sigma)^m\pi^{m/2}} \times \left\{ \frac{1}{(l_{c0})^{(m-2)/2}} - \frac{1}{(l_{cf})^{(m-2)/2}} \right\}$$

if  $m = 2$ ,  $N = \frac{1}{CY^2(\Delta\sigma)^2\pi} \ln \frac{l_{cf}}{l_{c0}}$

### Impact

Maximum deformation:  $\delta_{\max} = \delta_{st} \left( 1 + \sqrt{1 + \frac{2h}{\delta_{st}}} \right)$

Impact factor:  $I_m = 1 + \sqrt{1 + \frac{2h}{\delta_{st}}}$

## Recommended Readings

- Anderson, T.L. (2004) *Fracture Mechanics: Fundamentals and Applications*, 3rd ed., CRC Press.
- Bannantine, J.A., Comer, J.J., and Handrock, J.L. (1989) *Fundamentals of Metal Fatigue Analysis*, Prentice-Hall.
- Bathias, C., and Paris, P.C. (2005) *Gigacycle Fatigue in Mechanical Practice*. Wiley.
- Bathias, C., and Pineau, A. (2010) *Fatigue of Materials and Structures*. Wiley.
- Budynas, R.G., and Nesbitt, J.K. (2011), *Shigley's Mechanical Engineering Design*, 9th ed., McGraw-Hill.
- Juvinall, R.C. (1967) *Engineering Considerations of Stress, Strain, and Strengths*, McGraw-Hill, New York.
- Madayag, A.F. (1969) *Metal Fatigue: Theory and Design*, Wiley, New York.
- Freiman, S., and Mecholsky Jr., J.J. (2012) *The Fracture of Brittle Materials: Testing and Analysis*. Wiley.
- Lee, Y.-L., Pan, J., Hathaway, R., and Barkey, M. (2005) *Fatigue Testing and Analysis*. Elsevier.
- Manson, S.S., and Halford, G.R. (2006) *Fatigue and Durability of Structural Materials*. American Society for Metals.
- Newman, J.C., and Plascik, R.S., eds. (2000) *Fatigue Crack Growth Thresholds, Endurance Limites, and Design*, STP 1372, American Society for Testing and Materials.
- Nicholas, T. (2006) *High Cycle Fatigue – A Mechanics of Materials Perspective*. Elsevier.
- Norton, R.L. (2011) *Machine Design*, 4th ed., Prentice Hall.
- Rice, R.C., ed., (1988) *Fatigue Design Handbook*, Society of Automotive Engineers, Warrendale, PA.

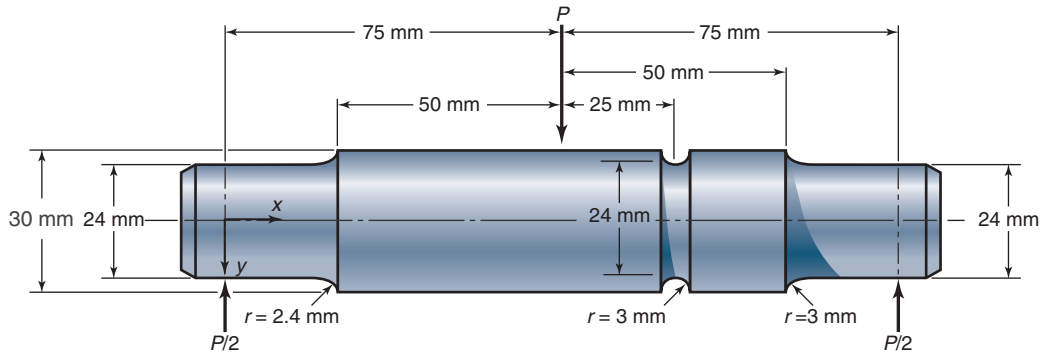
- Schijve, J. (2009) *Fatigue of Structures and Materials*, Springer.
- Stephens, R.I., Fatemi, A., Stephens, R.R., Fuchs, H.O., and Fatemi, A. (2000) *Metal Fatigue in Engineering*, 2nd ed., Wiley.
- Suresh, S. (1998) *Fatigue of Materials*, 2nd ed., Cambridge University Press.
- Zahavi, E., and Torbilo, V. (1996) *Fatigue Design*, CRC Press.

## References

- Bowman, K. (2004) *Mechanical Behavior of Materials*, Wiley.
- Johnson, R.C. (1967) *Predicting Part Failures Part I "Machine Design"*, vol. 45, p. 108.
- Juvinall, R.C., and Marshek, K.M. (1991) *Fundamentals of Machine Component Design*, Wiley.
- Kuguel, R. (1969), "A Relation Between Theoretical Stress Concentration Factor and Fatigue Notch Factor Deduced from the Concept of Highly Stressed Volume.", *Proceedings ASTM*, v. 61, pp. 732-748.
- Lipson, C., and Juvinall, R.C. (1963) *Handbook of Stress and Strength*, Macmillan.
- Metals Handbook*, American Society for Metals, 1975.
- Norton, R.L. (1996) *Machine Design*, Prentice-Hall.
- Paris, P.C., Gomez, M.P., and Anderson, W.P. (1961) *A Rational Analytic Theory of Fatigue*, *Trend Engineering*, University of Washington, v. 13, no. 1, pp. 9-14.
- Shigley, J.E., and Mitchell, L.D. (1983) *Mechanical Engineering Design*, 4th ed. McGraw-Hill.
- Sines G., and Waisman, J.L. (1959) *Metal Fatigue*, McGraw-Hill.
- Suresh, S. (1998) *Fatigue of Materials*, 2nd ed. Cambridge University Press.

## Questions

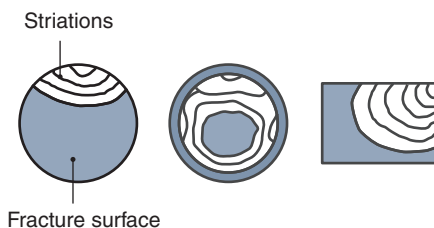
- 7.1 Define *fatigue* and *fatigue wear*. Explain how they are related.
- 7.2 Sketch a completely reversing and a released tension stress cycle.
- 7.3 How does residual stress affect fatigue?
- 7.4 What is a cyclic stress?
- 7.5 What is the difference between a flaw and a crack?
- 7.6 Define stress range, stress amplitude, and stress ratio.
- 7.7 What is the difference between fatigue strength and endurance limit?
- 7.8 What is the Paris regime of crack growth?
- 7.9 Are there always striations on a fatigue fracture surface?
- 7.10 What is an S-N diagram? Sketch a typical S-N diagram for steel and one for aluminum.
- 7.11 What is the notch sensitivity of a material?
- 7.12 Why does the modified endurance limit depend on the manufacturing process used to produce a part?
- 7.13 Explain the reasons that there is a size factor required to determine the modified endurance limit.
- 7.14 Why does shot peening improve fatigue strength?

Sketch *b*, for Problem 7.35

- 7.15** What are the similarities between the Goodman line and the Gerber parabola?
- 7.16** What is Miner's rule?
- 7.17** List the theories that incorporate the influence of mean stress on fatigue failure.
- 7.18** What is fault tolerant design?
- 7.19** What is the Paris law?
- 7.20** Define impact. Why are impact stresses larger than static stresses?

## Qualitative Problems

- 7.21** Review the Manson-Coffin relationship and identify all of the important variables, explaining how each impacts fatigue crack growth.
- 7.22** List the factors that influence the endurance limit of a carbon steel. Rank them in order of importance.
- 7.23** In Fig. 7.4, Regime A shows crack growth rates slower than a lattice spacing per cycle. Explain how this is possible.
- 7.24** Identify the point where fatigue started and the direction of crack growth for the cross-sections shown in Sketch *a*.

Sketch *a*, for Problem 7.24

- 7.25** Is there an endurance limit for aluminum or copper alloys? Explain.
- 7.26** According to the Manson-Coffin equation, stresses that induce deformation will eventually result in fatigue failure. Does this mean that there cannot be an endurance limit? Explain.

- 7.27** Demonstrate that Example 7.3 produces the same results regardless of units.
- 7.28** List factors that affect surface finish that are not included in Eq. (7.19).
- 7.29** List factors that can be incorporated into the miscellaneous effects modification factor on endurance limit.
- 7.30** Without using equations, explain the advantages of using the modified Goodman approach.
- 7.31** Give three examples each of parts that (a) encounter fewer than 1000 cycles; (b) encounter more than 1000 but less than 1 million cycles, and (c) encounter more than 1 million cycles.

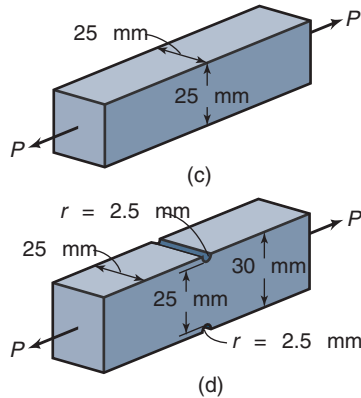
## Quantitative Problems

- 7.32** Using the information in Fig. 7.19, estimate the constants  $C$  and  $m$  from Eq. (7.47) and construct a table of these values for different materials.
- 7.33** A tuning fork is hit with a pencil and starts to vibrate with a frequency of 440 Hz. The maximum bending stress in the tuning fork is 2 MPa at the end positions. Calculate the mean stress, the range of stress, the stress amplitude, and the stress ratio. Also, calculate how much stress the tuning fork can sustain without being plastically deformed if it is made of AISI 1080 steel, quenched and tempered at 800°C. *Ans.*  $\sigma_m = 0$ ,  $\sigma_r = 4$  MPa,  $R = -1$ .
- 7.34** The jack for a Volvo consists of a mechanism in which the lift screw extends horizontally through two corners of the mechanism while the other two corners apply a force between the ground and the car to be lifted. Strain gage measurements show that the maximum compressive stress in the jack is 150 MPa when the car is jacked up so high that both wheels on one side of the car are in the air and the load on the jack is 8000 N. How many times can the jack be used for a small truck that weighs 6 tons and loads the jack to 15,000 N before it fails from fatigue? The jack material is AISI 1080 steel, quenched and tempered at 800°C. *Ans.* 807,800 cycles.
- 7.35** The shaft shown in Sketch *b* rotates at high speed while the imposed loads remain static. The shaft is machined from ground, high-carbon steel (AISI 1080, quenched

and tempered at 800°C). If the loading is sufficiently large to produce a fatigue failure after 1 million cycles, where would the failure most likely occur? Show all necessary computations and reasoning.

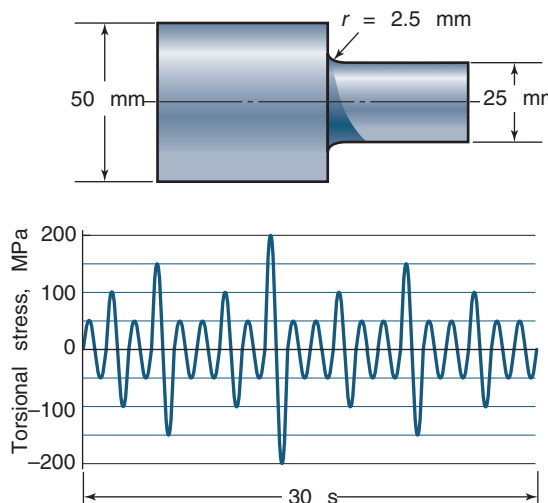
**7.36** For each of the annealed AISI 1040 steel bars shown in Sketches *c* and *d* determine

- The static tensile load causing fracture. *Ans.*  $P = 325 \text{ kN}$ .
- The alternating (completely reversing) axial load  $\pm P$  that would be just on the verge of producing eventual fatigue failure. *Ans.*  $P_{\text{notched}} = 62.5 \text{ kN}$ .



Sketches *c* and *d*, for Problem 7.36

**7.37** A stepped shaft, as shown in Sketch *e*, was machined from high-carbon steel (AISI 1080, quenched and tempered at 800°C). The loading is one of completely reversed torsion. During a typical 30 s of operation under overload conditions the nominal stress in the 25-mm diameter section was calculated to be as shown. Estimate the life of the shaft when it is operating continually under these conditions. *Ans.* 19.8 hours.



Sketch *e*, for Problem 7.37

**7.38** A flood-protection dam gate is supposed to operate only once per week for 100 years, but after 30 years of use it needs to be operated twice per day (each time the high tide comes in). Find how much lower the bending stress

must be from then on to still give a total life of 100 years. The material being fatigued is medium-carbon steel (annealed AISI 1040). *Ans.* 20% lower stress.

**7.39** A hydraulic cylinder has a piston diameter  $D = 100 \text{ mm}$  and a piston rod diameter  $d = 33 \text{ mm}$ . The hydraulic pressure alternately applied to each side of the piston is  $p = 35 \text{ MPa}$ . This pressure induces in the rod a compressive force of  $\pi p D^2/4$  or a tensile force of  $\pi p (D^2 - d^2)/4$ , depending on which side of the piston the pressure is applied. The piston rod material is martensitic stainless steel (AISI 410). Find the endurance life of the piston rod. *Ans.* 11,370 cycles.

**7.40** A 20-mm-diameter shaft transmits a variable torque of  $600 \pm 300 \text{ N}\cdot\text{m}$ . The frequency of the torque variation is  $0.1 \text{ s}^{-1}$ . The shaft is made of high-carbon steel (AISI 1080, quenched and tempered at 800°C). Find the endurance life of the shaft. *Ans.* 789,200 cycles, or 2192 hr.

**7.41** For the shaft in Problem 7.40 determine how large the shaft diameter has to be for infinite life. *Ans.*  $d = 22.5 \text{ mm}$ .

**7.42** A notched bar has the diameter  $D = 25 \text{ mm}$ , notch radius  $r = 0.5 \text{ mm}$ , and the bottom diameter of the notch is 24 mm. It experiences rotational bending fatigue. Determine which of the steels AISI 1020, 1040, 1080, or 316 will give the highest allowable bending moment for infinite life. Calculate that moment.

**7.43** A straight, circular rotating beam has a diameter of 30 mm and a length of 1 m. At the end of the beam a stationary load of 600 N is applied perpendicularly to the beam, giving a bending deformation. Find which surface machining method can be used to give infinite life to the rotating beam if it is made of

- AISI 1020 steel, quenched and tempered at 870°C.
- AISI 1080 steel, quenched and tempered at 800°C.

Note that  $k_s = k_r = k_m = 1$ .

**7.44** The pedals on a bicycle are screwed into the crank with opposite threads, one left-hand thread and one right-hand thread, to ensure that the pedals do not accidentally unscrew. Just outside the thread is a 0.75-mm-radius fillet connecting the 12.5-mm-diameter threaded part with an 11-mm-diameter central shaft in the pedal. Make a careful sketch of the geometry. The shaft is made of AISI 4340 alloy steel tempered at a low temperature to give an ultimate stress of 2 GPa. Find the fatigue stress concentration factor for the fillet, and calculate the maximum allowable pedal force for infinite life if the force from the foot is applied 70 mm from the fillet. *Ans.* 1090 N.

**7.45** During the development of a new submarine a 1-to-20 model was used. The model was tested to find if there was any risk of fatigue failure in the full-size submarine. To be on the safe side, the stresses in the model were kept 25% higher than the stresses in the full-size submarine. Is it possible to conclude that the full-size submarine will be safe if the model was safe at a 25% higher stress level?

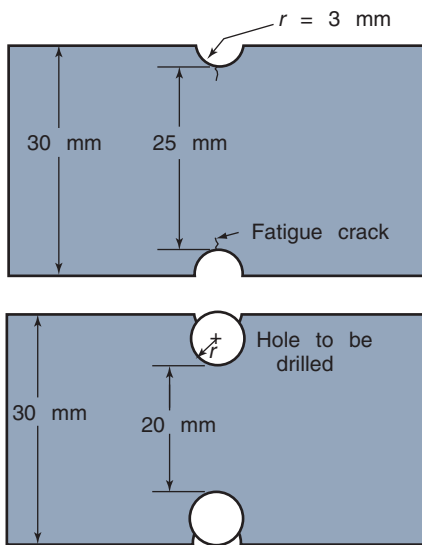
**7.46** During the development of a new car it was found that the power from the motor was too high for the gearbox. When maximum torque was transmitted through



the gearbox, 50% of the gearboxes failed within the required lifetime of 800 hr. How much stronger should the gearbox be made to ensure that only one gearbox out of 1000 would fail within 800 hr? *Ans.* 33% stronger.

- 7.47 A tension member in service has been inspected and a fatigue crack has been discovered as shown in sketch *f*. A proposed solution is to drill a hole at the tip of the crack, the intent being to reduce the stress concentration at the crack tip. The material is 30-mm-thick annealed AISI 1040 medium carbon steel, and was produced through forging. If the load is a completely reversing 15 kN and the original design is as shown,

- What was the original factor of safety? *Ans.*  $n_s = 2.9$ .
- What is the smallest drilled hole which restores the safety factor to that of the original design? (Use the nearest 5 mm increment that is satisfactory.) Use a reliability of 90%. *Ans.* 5 mm



Sketch *f*, for Problem 7.47

- 7.48 Truck gearboxes are dimensioned for infinite life at maximum torque regarding contact stresses and bending stresses for all gear steps. Car gearboxes are dimensioned for finite life according to typical running conditions. Maximum torque for the first gear can typically be maintained only 3 to 6 s for each acceleration before the maximum speed is reached. If a driver accelerates at full power 20 times per day for 20 years on the first gear, the required life is only 60 to 120 hr. The normal load spectrum gives a life of 200,000 km for 99% of the gearboxes. A driver uses the car twice a year to move his 10-ton boat 50 km (the distance between his home and the harbor) during the 10-year life of the car. Calculate how much of the 200,000-km nominal life of the gearbox is consumed by the boat moving if the life is inversely proportional to the load raised to the 3.2 power. Assume that during the move the gearbox load is four times higher than normal. *Ans.* 42.25% of the gearbox life.

- 7.49 The hand brakes of a bicycle are often the same type for the front and rear wheels. The high center of gravity (compared with the distance between the wheels) will

increase the contact force between the front wheel and the ground and will decrease the contact force between the rear wheel and the ground when the brakes are applied. If equal force is applied to each of the two brakes, the rear wheel will start sliding while the front wheel is still rolling. The manufacturer of the brake wires did not know about this difference between the front and rear wheels, so the wires were dimensioned as if the wheels had equal contact force and thus needed equal force in the two brake wires. The wires were originally dimensioned to withstand 20 years' use with brake applications at a force necessary to lock the two (equally loaded) wheels. How long will the life of the wires be if the friction between the front wheel and the ground is just enough to lift the rear wheel from the ground? Assume the endurance life is proportional to the stress raised to the  $-10$  power.

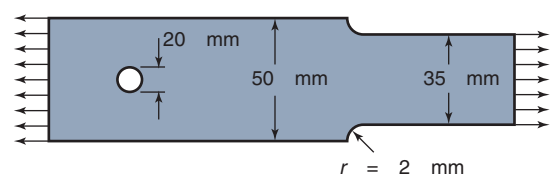
- 7.50 Ball bearings often run at varying loads and speeds. Bearing life is inversely proportional to the contact stress raised to the  $10/3$  power for a number of bearing types. For ball bearings the contact stresses are approximately proportional to the third root of the load. A ball bearing in a gearbox is dimensioned to have a life of 1752 million revolutions, half of which are at half the maximum motor torque, one-quarter at full motor torque, and one-quarter at 75% of full motor torque. Calculate the bearing life if the motor torque is kept constant at the maximum level. *Ans.* 681 million revolutions.

- 7.51 A round cold-drawn steel bar with a solid cross-section is subjected to a cyclic force that ranges from a maximum of 10 kN in tension to a minimum of 5 kN in compression. The ultimate strength of the steel is 600 MPa and the yield strength is 400 MPa. The critical safety factor is 2. Determine the following:

- The modified endurance limit as a function of diameter. *Ans.*  $S_e = (279 \text{ MPa})d^{-0.112}$ .
- The cross-sectional area that will produce fatigue failure and the corresponding diameter. *Ans.*  $d = 10 \text{ mm}$ .
- The region (a, b, c, or d) in Fig. 7.15, assuming modified Goodman criteria, and why.

- 7.52 Both bars used in Problem 7.36 and shown in sketches *c* and *d* are made from cold-drawn, medium-carbon steel (annealed AISI 1040). Determine the safety factor for each bar. The load varies from 10 to 40 kN. Use the modified Goodman relationship.

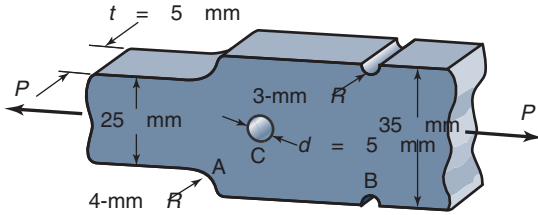
- 7.53 The 10-mm-thick component in sketch *g* is designed with a fillet and a hole. The load varies from 50 to 10 kN. The following strengths are given:  $S_u = 390 \text{ MPa}$  and  $S_y = 282 \text{ MPa}$ . Using the modified Goodman failure theory, determine the safety factor for the hole as well as for the fillet. At which location will failure first occur? Will the component fail? Explain. *Ans.*  $n_{s, \text{fillet}} = 1.16$ .



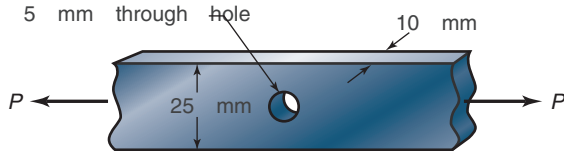
Sketch *g*, for Problem 7.53



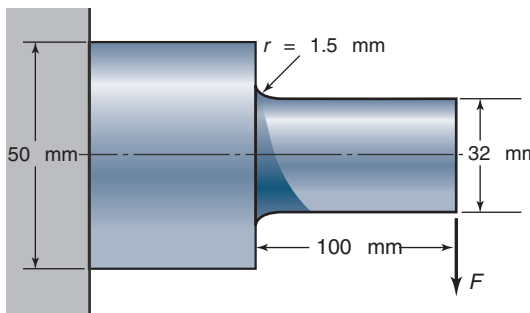
- 7.54** The flat bar shown in Sketch *h* is made of cold-drawn, high-carbon steel (AISI 1080, quenched and tempered at 800°C). The cyclic, non-zero, mean axial load varies from a minimum of 2 kN to a maximum of 10 kN. Using the Goodman failure theory, determine the safety factors for the hole, the fillet, and the groove. Also, indicate where the flat bar will first fail. *Ans.*  $n_{s,\text{hole}} = 2.97$ ,  $n_{s,\text{fillet}} = 3.25$ .

Sketch *h*, for Problem 7.54

- 7.55** A straight, circular rotating beam with a diameter of 50 mm and a length of 1 m has an axial load of 3000 N applied at the end and a stationary radial load of 400 N. The beam is cold-drawn and the material is titanium. Note that  $k_s = k_r = k_m = 1$ . Find the safety factor  $n_s$  for infinite life by using the Goodman line. *Ans.*  $n_s = 5.269$ .
- 7.56** The annealed AISI 1040 steel bar shown in sketch *i* is subjected to a tensile load fluctuating between 4500 and 12,000 N. Estimate the factor of safety using the Goodman criterion. *Ans.*  $n_s = 3.5$ .

Sketch *i*, for Problem 7.56

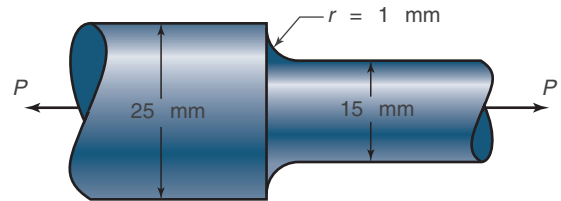
- 7.57** The cantilever shown in sketch *j* carries a downward load  $F$  that varies from 2000 to 4000 N.
- Compute the resulting safety factor for static and fatigue failure if the bar is made from annealed AISI 1040 steel. *Ans.*  $n_{s,\text{static}} = 2.82$ .
  - If the notch sensitivity is assumed to remain constant, what fillet radius is needed for a fatigue failure safety factor of 3.0? *Ans.*  $r = 6.4$  mm.

Sketch *j*, for Problem 7.57

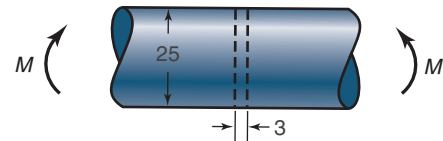
- 7.58** The 10-mm thick component in Problem 7.53 is constructed from AISI 1020 steel (quenched and tempered at 870°C), but is used at elevated temperature so that its yield strength is 70% of its room temperature value, and its ultimate strength is 60% of its room temperature value.

- If the desired reliability is 90%, what completely reversing load can be supported without failure? *Ans.*  $P_{\text{max}} = 33.6$  kN.
- If the load varies from 5000 to 10,000 N, what is the safety factor guarding against fatigue failure? Use the Goodman failure criterion. *Ans.*  $n_s = 4.9$ .

- 7.59** The stepped rod shown in sketch *k* is subjected to a tensile force that varies between 15,000 and 30,000 N. The rod has a machined surface finish everywhere except the shoulder area, where a grinding operation has been performed to improve the fatigue resistance of the rod. Using a 99% probability of survival, determine the safety factor for infinite life if the rod is made of AISI 1080 steel, quenched and tempered at 800°C. Use the Goodman line. Does the part fail at the fillet? Explain.

Sketch *k*, for Problem 7.59

- 7.60** A section of a 25-mm-diameter shaft shown in Sketch *l* is drawn from AISI 1080 (quenched and tempered at 800°C) carbon steel, and has a 3-mm-diameter through-hole drilled (machined) into it. During service, the shaft encounters a bending moment that varies from -15 to 45 Nm. For a reliability of 99.5%, determine the safety factor using the Goodman line. *Ans.*  $n_s = 3.432$ .

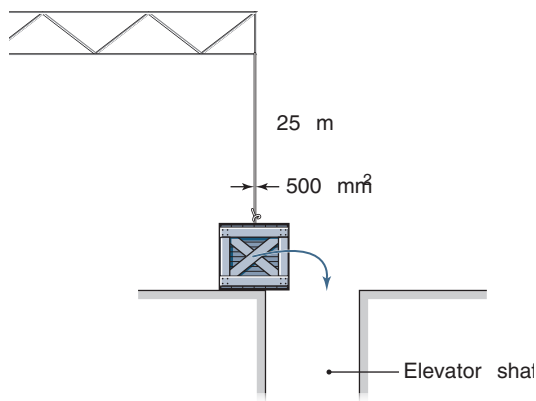
Sketch *l*, for Problem 7.60

- 7.61** A 5000 kg elevator is supported by a stranded steel cable having a  $2.0 \times 10^{-3}$ -m<sup>2</sup> cross-section and an effective modulus of elasticity of 82.7 GPa. As the elevator is descending at a constant velocity of 2 m/s, an accident causes the cable, 20 m above the elevator, to suddenly stop. Determine the static elongation of the cable, the impact factor, the maximum elongation, and the maximum tensile stress developed in the cable. *Ans.*  $\sigma_{\text{max}} = 227$  MPa.

- 7.62** A person is planning a bungee jump from a 40-m-high bridge. Under the bridge is a river with crocodiles, so the person does not want to be submerged into the water. The rubber rope fastened to the ankles has a spring constant of 3600 N divided by the length of the rope. The distance from the ankles to the top of the head is 1.75 m, and the person weighs 80 kg. Calculate how long the rope should be. *Ans.* 21.29 m.

**7.63** A toy with a bouncing 50-mm-diameter steel ball has a compression spring with a spring constant of 100,000 N/m. The ball falls from a 3-m height down onto the spring (which can be assumed to be weightless) and bounces away and lands in a hole. Calculate the maximum force on the spring and the maximum deflection during the impact. The steel ball density is 7840 kg/m<sup>3</sup>. *Ans.* 1743 N.

**7.64** At a building site a 1-ton container hangs from a crane wire and is then placed on the floor so that the wire becomes unloaded. The container is pushed to the elevator shaft where it is to be lowered as shown in Sketch *m*. By mistake there is a 1-m slack in the wire from the crane when the container falls into the elevator shaft. Calculate the maximum force in the wire if it has a cross-sectional steel surface of 500 mm<sup>2</sup> and an effective modulus of elasticity of 70 GPa and is 25 m long from the crane to the container. *Ans.* 175.8 kN.



Sketch *m*, for Problem 7.64

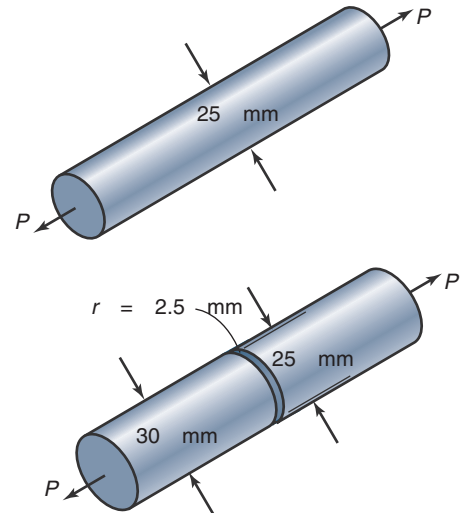
**7.65** Modern kitchen drawers have small rubber springs mounted onto the sides of the inside of the front plate to take up the force and stop the drawer when it is being closed. The spring constant for each of the two rubber springs is 400 kN/m. The drawer is full of cutlery, which weighs 5 kg, and is closed with a speed of 0.5 m/s. Calculate the maximum force in each rubber spring if the drawer itself weighs 1 kg and

- The cutlery is in a container that is fixed to the drawer so that it moves with the drawer. *Ans.*  $P = 548$  N.
- The cutlery is in a plastic container that can slide 80 mm with a coefficient of friction of 0.25 inside the drawer. *Ans.*  $P = 229.7$  N.

**7.66** Car doors are easy to slam shut but difficult to press shut by hand force. The door lock has two latches, the first easily engaged and the second requiring the rubber seal around the door to be quite compressed before it can engage. The rubber seal has a spring constant of 50,000 N/m at the locked position for the door, and the mass moment of inertia for the door around its hinges is 2.5 kg-m<sup>2</sup>. The distance between the lock and the hinges is 1 m. Calculate the force needed to press the car door shut at the lock if a speed of 0.8 m/s at the lock slams it shut. *Ans.* 282.8 N.

**7.67** Sketch *n* shows two bar designs. In the left sketch, the bar is cold drawn and has no stress concentrations. In

the sketch on the right, a groove has been machined into the bar, with the groove root diameter being the same as the outer diameter as the bar on the left. The bar is produced from low-carbon steel (AISI 1020, quenched and tempered at 870°C). Find the completely reversing force,  $P$ , that can be supported based on the endurance limit. *Ans.*  $P = 48.21$  kN.



Sketch *n*, for Problem 7.67

**7.68** Repeat Problem 7.67 assuming that the bar is loaded by a completely reversing bending moment,  $M$ . *Ans.*  $M = 20.9$  Nm.

**7.69** For the two bars given in Problem 7.67, determine the safety factor guarding against fatigue failure if the load varies between 4 and 20 kN. *Ans.* Using Goodman,  $n_s = 4.39$ .

**7.70** A center-cracked plate made of 2024-T3 aluminum has a width of 100 mm, a thickness of 4 mm, and an initial crack length of  $l = 3$  mm. If the applied tensile load varies between 30 and 50 kN, estimate the number of cycles that causes the crack to grow large enough to cause the part to fracture. *Ans.*  $N = 119,500$  cycles.

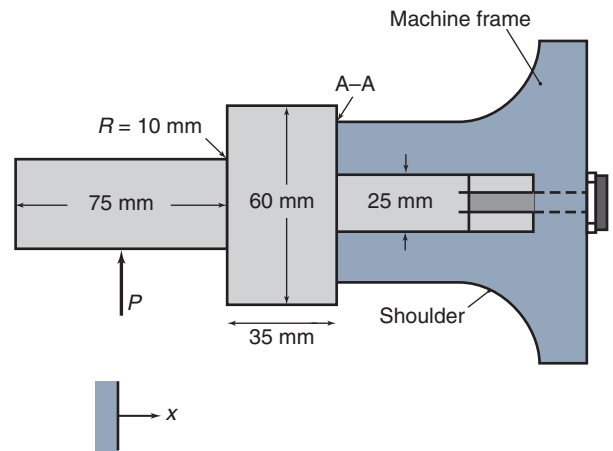
**7.71** A fatigue failure of Ti-6Al-4V titanium alloy shows microscopic striations that have an average spacing of  $0.5 \times 10^{-7}$  mm. Determine the average stress intensity factor that would produce such striations. The failed part was a center-cracked tension member, with a thickness of 15 mm and a width of 100 mm and a load of 90 kN applied in released tension. Determine the crack length at fracture. *Ans.*  $l_c = 16$  mm.

## Synthesis and Design

**7.72** It was noted in the chapter that a fatigue crack has a large stress concentration associated with it because of its sharpness. One innovative approach to improving fatigue strength in polymers involves distributing encapsulated uncured polymer within a material; when a fatigue crack encounters and breaks open such as a capsule, the liquid coats the fatigue crack and blunts it. List the parameters that you expect will affect the performance of such a material. Give a short justification for each item in your list.

- 7.73** Design a test method for determining the rate of fatigue crack growth in a test specimen.
- 7.74** It is estimated that an average person takes two million steps per year. Conduct a literature search and examine how bone responds to flaw generation and crack growth associated with fatigue.
- 7.75** Conduct a literature and Internet search and write a one-page paper on the circumstances associated with the Aloha Airlines flight from 1988 depicted in the chapter's opening photograph. Include a failure description and the technical reasons for the failure.
- 7.76** In rotating beam fatigue tests, specimens are loaded in four-point bending. Would the measured endurance limit be higher or lower if the test was conducted in three-point bending? What about tension? Explain your answer using appropriate sketches and equations from Ch. 4.
- 7.77** Perform an Internet search to obtain an illustration and description of the *Mannesmann* process for manufacturing tubes. Explain how fatigue plays a role in the Mannesmann process.
- 7.78** Design a test method to estimate the endurance limit of a material for different mean stresses (see Fig. 7.13).
- 7.79** It is well-known that fatigue testing of polymers must take place at low speeds so that there are no thermal effects in the material near the crack tip. Explain the reasons why heat is generated in fatigue testing. List the physical and mechanical properties that will influence the maximum allowable test speed and explain why you think they are important.
- 7.80** An engineer working for a manufacturer of mechanical power presses is assisting in the development of a new size of machine. When starting to design a new brake stud, the engineer finds the information in sketch *o* from an existing computer-assisted drawing (CAD) of a machine with the closest capacity to the new project. The brake stud supports the brake on the cam shaft of the mechanical power press. The brake actuates with

every cycle of the press, stopping the ram at the top-dead-center position so that an operator can remove a workpiece from the dies and insert another workpiece for the next cycle. If the stud fails, the press could continue to coast downward and could result in a serious injury.

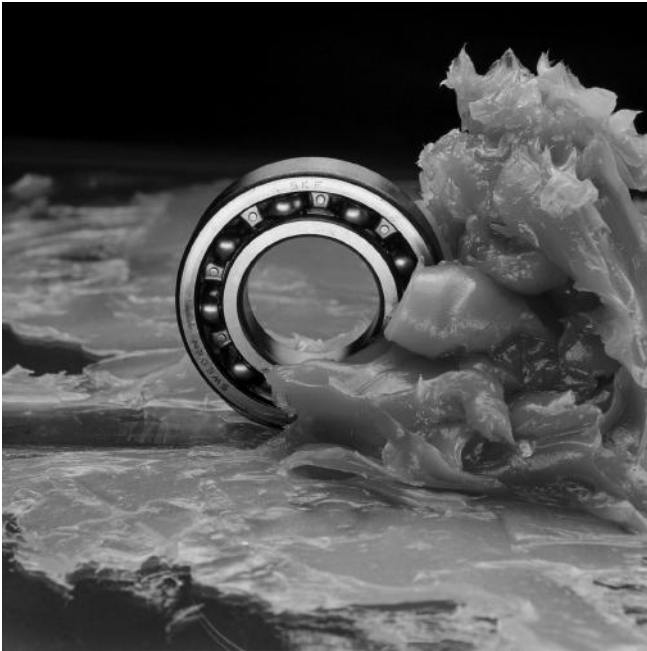


Sketch *o* for Problem 7.80.

Focusing on section A-A the engineer recognizes that no fillet radius had been specified for the brake stud for machines sold previously. Conversations with machinists who routinely worked on the part led to the conclusion that the common practice was to undercut the fillet to make sure assembly was complete; the fillet radius in effect was the radius of the machine tool insert, a value as low as 3 mm. The immediate concern is whether a product recall is in order, since a brake stud failure could result in a machine operator's hands being in a die while the machine fails to stop after a cycle. Analyze the system and determine whether or not the machine is safe as manufactured. The carbon steel used for the stud has a minimum ultimate strength of 500 MPa, and no yield strength was prescribed in the drawing.

## Chapter 8

# Lubrication, Friction, and Wear



Greases are a necessary lubricant for many applications, including rolling element bearings, for the reduction of friction and wear. *Source:* Courtesy of SKF USA, Inc.

*...among all those who have written on the subject of moving forces, probably not a single one has given sufficient attention to the effect of friction in machines..."*

Guillaume Amontons

This chapter introduces the essential tribological concepts of surfaces, lubrication, friction and wear, each of which plays a critical role in the performance and reliability of machine elements. Surfaces are investigated in detail, including common definitions to quantify roughness and a general discussion of their physical nature. Conformal contacts such as in journal bearings, and non-conformal contacts such as gears and rolling-element bearings are differentiated. The field of Hertzian contact for non-conformal surfaces is presented. Lubrication theory is developed in terms of the film parameter and the regimes of lubrication, including boundary, partial, and hydrodynamic lubrication. Boundary lubrication typically occurs at low speeds, with inviscid lubricants, and/or high loads, and is always a concern during startup. In boundary lubrication, load is transferred between the asperities of surfaces in contact. At the other extreme, hydrodynamic lubrication involves transfer of load across a pressurized lubricant film that completely separates the surfaces. Surfaces that transfer load through a combination of direct asperity contact and pressurized lubricants involve partial lubrication. Elastohydrodynamic lubrication is a condition that is common in machine elements and is therefore also included. Basically, elastohydrodynamic lubrication involves circumstances where the surfaces are separated by a fluid film and where elastic deformation of the surfaces are large compared to the film thickness. Friction and wear theory are also summarized, including the important Archard wear law used to predict the life of machine elements subjected to adhesive or abrasive wear.

### Contents

- 8.1 Introduction 196
- 8.2 Surface Parameters 196
- 8.3 Conformal and Nonconformal Surfaces 197
- 8.4 Hertzian Contact 198
- 8.5 Bearing Materials 203
- 8.6 Lubricant Rheology 205
- 8.7 Regimes of Lubrication 211
- 8.8 Friction 214
- 8.9 Wear 216
- 8.10 Summary 220

### Examples

- 8.1 Hertzian Contact I - Ball in Ring 200
- 8.2 Hertzian Contact II - Ball in Groove 202
- 8.3 Hertzian Contact III - Rectangular Contact 203
- 8.4 Units of Viscosity 206
- 8.5 Kinematic Viscosity 207
- 8.6 Piezoviscous Effects 207
- 8.7 Viscosity-Temperature Effects 211
- 8.8 Film Parameter 211
- 8.9 Application of the Archard Wear Law 217

### Design Procedure

- 8.1 Wear Avoidance Hierarchy 218

### Case Study

- 8.1 Wear in Orthopedic Implants 218



## Symbols

$A$	area, $m^2$
$A_o$	sum of projected areas in sliding, $m^2$
$A_r$	sum of real areas in contact, $m^2$
$b^*$	contact semiwidth, m
$C_1, C_2$	constants used in Eq. (8.26)
$D_x$	diameter of contact ellipse along $x$ -axis, m
$D_y$	diameter of contact ellipse along $y$ -axis, m
$E$	modulus of elasticity, Pa
$E'$	effective elastic modulus, Pa
$\mathcal{E}$	complete elliptic integral of second kind
$F$	friction force, N
$\mathcal{F}$	complete elliptic integral of first kind
$H$	hardness of softer material, Pa
$h$	film thickness, m
$h_{\min}$	minimum film thickness, m
$k_e$	ellipticity parameter, $D_y/D_x$
$k_1$	adhesive wear constant
$k_2$	abrasive wear constant
$L$	sliding distance, m
$N$	number of measurements of $z_i$
$p$	pressure, Pa
$p_H$	Hertzian contact pressure, Pa
$p_{\max}$	maximum pressure, Pa
$R$	radius, m; curvature sum, m
$R_a$	arithmetic average surface roughness, m
$R_q$	root-mean-square surface roughness, m
$r$	radius, m
$S_y$	yield stress in tension, Pa
$s$	shear strain rate, $s^{-1}$
$u$	velocity, m/s
$u_b$	velocity of upper surface, m/s
$v$	wear volume, $m^3$
$W$	normal load, N
$W'$	dimensionless load for rectangular contact
$w'$	load per unit width, N/m
$w_a$	squeeze velocity, m/s
$x, y, z$	Cartesian coordinate system, m
$z$	coordinate in direction of film, m
$z_i$	height from reference line, m
$\alpha_r$	radius ratio, $R_y/R_x$
$\delta_{\max}$	maximum deformation, m
$\eta$	absolute viscosity, Pa·s
$\eta_k$	kinematic viscosity, $m^2/s$
$\eta_o$	absolute viscosity at $p = 0$ and at constant temperature, Pa·s
$\theta$	cone angle, rad
$\Lambda$	dimensionless film parameter
$\mu$	coefficient of sliding friction
$\nu$	Poisson's ratio
$\xi$	pressure-viscosity coefficient, $m^2/N$
$\rho$	density, $kg/m^3$
$\tau$	shear stress, Pa

## Subscripts

$a$	solid $a$
$b$	solid $b$

## 8.1 Introduction

**Tribology** is generally defined as the study of lubrication, friction, and wear, and it plays a significant role in machine element life and performance. The importance of tribology should not be underestimated — the famous Jost Report [1966] attributed tribology-related failures and design

shortcomings to be in excess of 10% of gross domestic product in developed countries. For machine elements to be designed properly, not only must the design stress be less than the allowable stress and the deformation not exceed some maximum value, but also tribological considerations must be properly addressed. The interaction of surfaces in relative motion should not be regarded as a special subject; like the strength of materials, tribology is basic to most machine elements.

This chapter presents the lubrication, friction, and wear considerations that are important in the successful design of machine elements. Sections 8.2 and 8.3 introduce the concepts of surface roughness and conformity, which are essential design considerations for most machine elements. The situation of Hertzian contact, involving concentrated stresses in nonconformal applications such as bearings, gears, and cams, is analyzed in Section 8.4. Bearing materials are summarized in Section 8.5. Lubrication is essential for the long life of rolling element bearings, journal bearings, gears of all kinds, and many other applications in machine design and manufacturing. Section 8.6 describes the properties of lubricants, while Section 8.7 introduces the important concept of lubrication regimes that has a dominant effect on component life and performance. Friction is discussed in Section 8.8 and wear in Section 8.9; both can have a large impact on the robustness, life, and performance of machine elements such as brakes and clutches, wire ropes, chains, rubber belts, threaded fasteners, etc.

This chapter is intended to provide tribological background in order to better understand machine element design. Of course, this chapter is highly abstracted, and the interested reader can find much more information in the Recommended Readings.

## 8.2 Surface Parameters

Designing machine elements is ultimately a problem of two surfaces that are either in direct contact or separated by a thin fluid film. In either case, the surface roughness and texture are important in ensuring long component life. Consider a surface profile as depicted in Fig. 8.1, which has been measured with a *stylus profilometer*. There are numerous other surface measuring instruments available, some of which will measure areas and not just traces across a surface, but Fig. 8.1 displays some typical features that are important to keep in mind. Note that the magnification in the vertical direction is 1000 and that in the horizontal is 20, so that the ratio of vertical to horizontal magnification is 50:1. Directional differences in magnification are often not appreciated, leading to a false impression of the nature of surfaces. Real engineering surfaces are much smoother than profilometer traces would suggest, mainly due to this magnification difference.

The surface profile in Fig. 8.1 shows the surface height variation relative to a mean reference line. By definition, the areas above and below the mean line are equal. **Surface roughness** can then be defined as a measure of surface de-

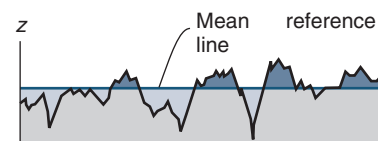


Figure 8.1: Surface profile showing surface height variation relative to mean reference line.



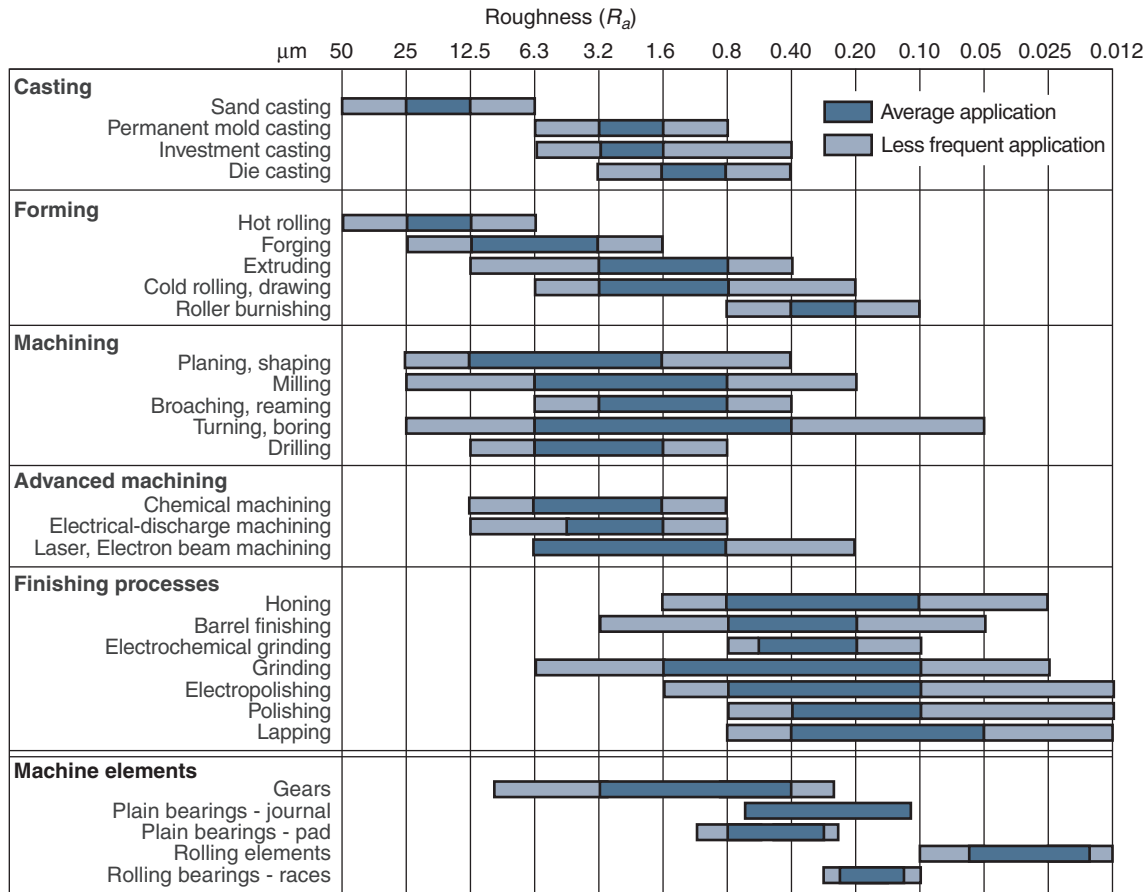


Figure 8.2: Typical arithmetic average surface roughness ( $R_a$ ) for various manufacturing processes and machine components. Source: Adapted from Kalpakjian and Schmid [2010] and Hamrock et al. [2004].

parture from the mean line. Two different surface roughness parameters are in common use:

1. **Centerline average** or **arithmetic average** surface roughness, denoted by  $R_a$ ,

$$R_a = \frac{1}{N} \sum_{i=1}^N |z_i|, \quad (8.1)$$

where  $z_i$  is the vertical distance from the reference line and  $N$  is the number of height measurements taken.

2. **Root-mean-square** (rms) surface roughness, denoted by  $R_q$ ,

$$R_q = \left( \frac{1}{N} \sum_{i=1}^N z_i^2 \right)^{\frac{1}{2}}. \quad (8.2)$$

$R_q$  emphasizes surface peaks and valleys more than  $R_a$  and is sometimes preferred for that reason. If a Gaussian height distribution is assumed,  $R_q$  has the additional advantage of being the standard deviation of the profile. For a simple sinusoidal distribution, the ratio of  $R_q$  to  $R_a$  is

$$\frac{R_q}{R_a} = \frac{\pi}{2\sqrt{2}} = 1.11. \quad (8.3)$$

Figure 8.2 gives typical values of the arithmetic average for various processes and components considered in Chap-

ters 9 through 19. Note from this figure that as higher precision processes are applied, the  $R_a$  values decrease significantly. The finest process shown is lapping, which produces an  $R_a$  between 0.012 and 0.8  $\mu\text{m}$ . A general trend which must be recognized is that the processes that produce smooth surfaces are slower and more expensive than those that produce rougher surfaces. Thus, the specification of a surface roughness for a particular application will have significant cost implications.

### 8.3 Conformal and Nonconformal Surfaces

**Conformal surfaces** fit snugly into each other so that the load is carried over a relatively large area. For example, the lubrication area of a journal bearing would be  $2\pi$  times the radius times the length. The load-carrying surface area remains essentially constant even if the load is increased. Journal bearings (Fig. 8.3) and slider bearings (see Fig. 12.9) have conformal surfaces. In journal bearings, the radial clearance between the journal and the sleeve is typically one-thousandth of the journal diameter; in slider bearings, the inclination of the bearing surface to the runner is typically one part in a thousand.

Many machine elements have surfaces that do not conform to each other. The full burden of the load must then be

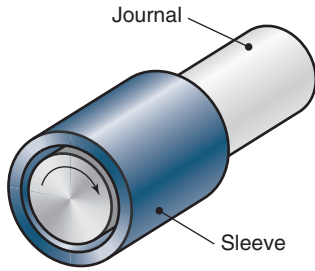


Figure 8.3: Conformal surfaces.

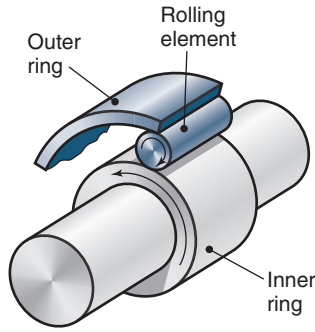


Figure 8.4: Nonconformal surfaces.

carried by a small area. The contact area of a nonconformal conjunction is typically three orders of magnitude smaller than that of a conformal conjunction. In general, the area between **nonconformal surfaces** enlarges considerably with increasing load, but it is still smaller than the contact area between conformal surfaces. Some examples of nonconformal surfaces are mating gear teeth, cams and followers, and rolling-element bearings (Fig. 8.4).

## 8.4 Hertzian Contact

The text up to this point has mainly been focused on distributed loading. This section describes not only the deformation due to concentrated loading but also the associated surface and subsurface stresses. The focus is mostly on elliptical contacts, but rectangular contact situations are also presented. The theory presented in this section is based on the work of Hertz [1881], and is therefore referred to as **Hertzian contact**.

### 8.4.1 Elliptical Contacts

The undeformed geometry of nonconformal contacting solids can be represented in general terms by two ellipsoids, as shown in Fig. 8.5. Two solids with different radii of curvature in a pair of principal planes ( $x$  and  $y$ ) passing through the conjunction make contact at a single point under the condition of zero applied load. Such a condition is called **point** or **elliptical contact** because of the shape of the contact patch. It is assumed throughout this book that convex surfaces like those in Fig. 8.5 exhibit positive curvature; concave surfaces exhibit negative curvature. Figure 8.6 shows elements and bearing races and their curvature conventions. The importance of the sign of the radius of curvature will be shown to be extremely important, and allows extension of Hertzian contact equations to a wide variety of machine elements.

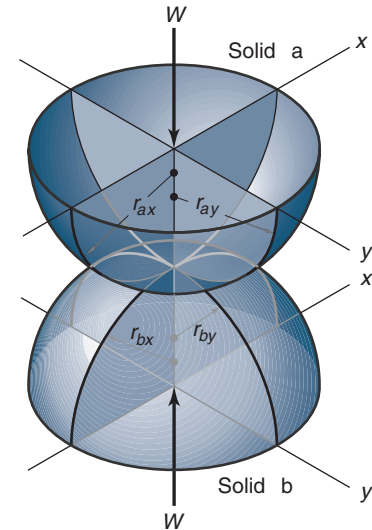


Figure 8.5: Geometry of contacting elastic solids.

Note that if coordinates  $x$  and  $y$  are chosen such that

$$\frac{1}{r_{ax}} + \frac{1}{r_{bx}} \geq \frac{1}{r_{ay}} + \frac{1}{r_{by}}, \quad (8.4)$$

coordinate  $x$  then determines the direction of the *minor axis* of the contact area when a load is applied, and  $y$ , the direction of the *major axis*. Since the coordinate system at this point is arbitrary, the direction of the rolling or entraining motion is always considered to be along the  $x$ -axis. Depending on the machine element geometry, the minor axis can be in either the rolling or transverse direction.

#### Curvature Sum

The curvature sum, which is important in analyzing contact stresses and deformation, is

$$\frac{1}{R} = \frac{1}{R_x} + \frac{1}{R_y}, \quad (8.5)$$

where

$$\frac{1}{R_x} = \frac{1}{r_{ax}} + \frac{1}{r_{bx}}, \quad (8.6)$$

$$\frac{1}{R_y} = \frac{1}{r_{ay}} + \frac{1}{r_{by}}. \quad (8.7)$$

Equations (8.5) to (8.7) effectively redefine the problem of two ellipsoidal solids in contact in terms of an equivalent solid of radii  $R_x$  and  $R_y$  in contact with a plane.

The **radius ratio**,  $\alpha_r$ , is

$$\alpha_r = \frac{R_y}{R_x}. \quad (8.8)$$

Thus, if Eq. (8.4) is satisfied,  $\alpha_r > 1$ ; and if it is not satisfied,  $\alpha_r < 1$ .

Machine elements with nonconformal surfaces generally have a range of radius ratios from 0.03 to 100. For example, for a traction drive involving a disk rolling on a plane,  $\alpha_r$  is typically 0.03; for a ball-on-plane contact,  $\alpha_r = 1.0$ , and for a contact so wide it approaches line contact,  $\alpha_r$  can be 100 or more, such as in a cylindrical roller bearing against a bearing race (see Figs. 8.6 and 13.1b). Some further examples of machine elements with radius ratios less than one

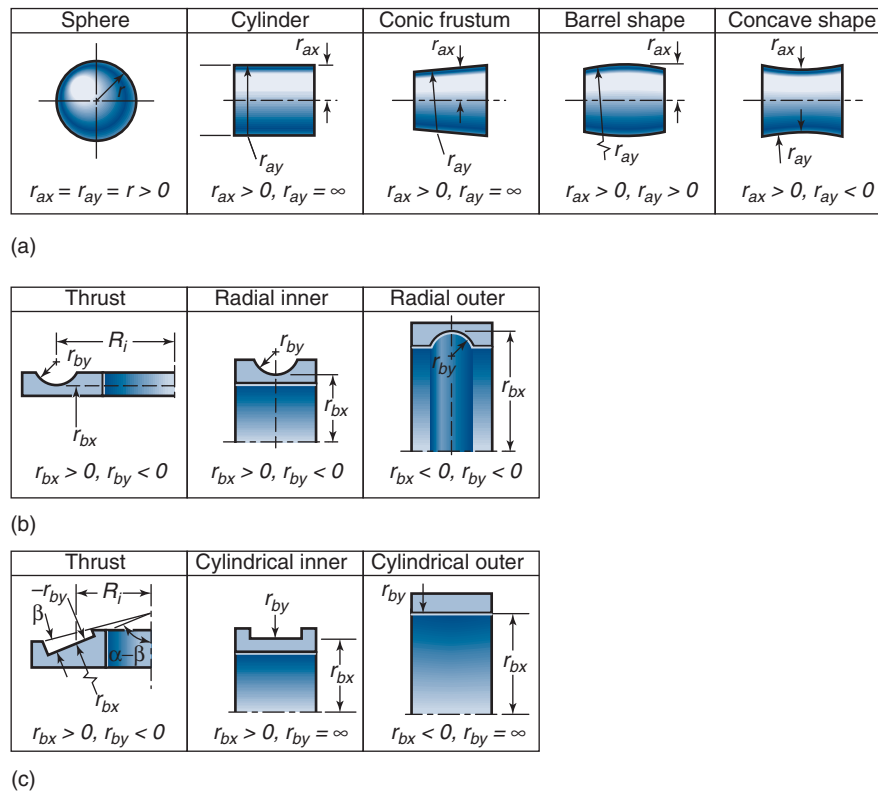


Figure 8.6: Sign designations for radii of curvature. (a) Rolling elements; (b) ball bearing races; (c) rolling bearing races.

are some (Novikov) gear contacts, locomotive wheel-rail contacts, and roller-flange contacts in a radially loaded roller bearing. Some further examples of machine elements with radius ratios greater than 1 are rolling-element bearings and most gears. These components are considered in more detail later in the text, but the general information on contact geometry of nonconformal surfaces is an important consideration.

### Ellipticity Parameter

The **ellipticity parameter**,  $k_e$ , is defined as the ratio of elliptical contact diameter in the  $y$ -direction (transverse direction) to the elliptical contact diameter in the  $x$ -direction (direction of entraining motion), or

$$k_e = \frac{D_y}{D_x}. \quad (8.9)$$

If  $\alpha_r \geq 1$ , the contact ellipse will be oriented with its major diameter transverse to the direction of motion, and consequently  $k_e \geq 1$ ; otherwise, the major diameter would lie along the direction of motion with both  $\alpha_r < 1$  and  $k_e < 1$ . To avoid confusion, the commonly used solutions to the surface deformation and stresses are presented only for  $\alpha_r > 1$ .

Note that the ellipticity parameter is a function only of the solids' radii of curvature, but not of load. This is because as the load increases, the semiaxes in the  $x$ - and  $y$ -directions of the contact ellipse increase proportionately to each other so that the ellipticity parameter remains constant.

### Contact Pressure

When an elastic solid is subjected to a load, stresses are produced that increase as the load is increased. These stresses are

associated with deformations, which are defined by strains. Unique relationships exist between stresses and their corresponding strains, as shown in Appendix B. For elastic solids, the stresses are linearly related to the strains, with the proportionality constant adopting different values for different materials, as discussed in Section 3.6. The modulus of elasticity,  $E$ , and Poisson's ratio,  $\nu$ , are two important parameters that are used in this chapter to describe contacting solids.

When two elastic nonconformal solids are brought together under a load, a contact area develops whose shape and size depend on the applied load, the elastic properties of the materials, and the curvature of the surfaces. When the two solids shown in Fig. 8.5 have a normal load applied to them, the contact area is elliptical. As stated above, such contacts are therefore referred to as **elliptical** or **point contacts**, although the former is preferred in this text. For the special case where  $r_{ax} = r_{ay}$  and  $r_{bx} = r_{by}$  the resulting contact is a circle rather than an ellipse, and is sometimes called **circular contact**. When  $r_{ay}$  and  $r_{by}$  are both infinite, the initial line contact develops into a rectangle when load is applied, so such circumstances are referred to as **line** or **rectangular contacts**.

Hertz [1881] considered the stresses and deformations in two perfectly smooth, ellipsoidal, contacting solids much like those shown in Fig. 8.5. His experiments involved investigations or highly polished glass lenses bearing against an optical flat, and his application of classical elasticity theory to this problem has formed the basis of stress calculations for machine elements such as ball and roller bearings, gears, and cams and followers. Hertz made the following assumptions:

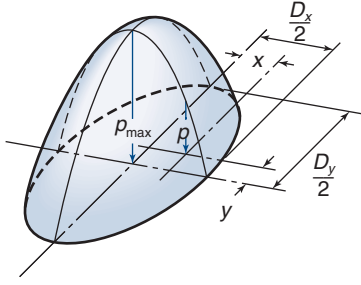


Figure 8.7: Pressure distribution in ellipsoidal contact.

1. The materials are homogeneous and the yield stress is not exceeded anywhere in the contacting bodies. The materials will therefore be approximated as linear elastic solids.
2. No tangential forces are induced between the solids, that is, the contact is frictionless.
3. The solids are continuous, without cracks or discontinuities in their surfaces.
4. Contact is limited to a small portion of the surface such that the dimensions of the contact region are small compared to the radii of the ellipsoids.
5. The solids are at rest and in equilibrium.

Making use of these assumptions, Hertz applied the following expression for the pressure distribution within an ellipsoidal contact (shown in Fig. 8.7):

$$p_H = p_{\max} \left[ 1 - \left( \frac{2x}{D_x} \right)^2 - \left( \frac{2y}{D_y} \right)^2 \right]^{\frac{1}{2}}, \quad (8.10)$$

where  $D_x$  and  $D_y$  are the diameters of contact ellipse in the  $x$ - and  $y$ -directions, respectively. The maximum pressure is

$$p_{\max} = \frac{6W}{\pi D_x D_y}, \quad (8.11)$$

where  $W$  is the normal applied load. Equation (8.10) determines the distribution of pressure or compressive stress on the common interface, which is clearly a maximum at the contact center and decreases to zero at the periphery.

### Simplified Solutions

The classical Hertzian solution requires the calculation of the ellipticity parameter,  $k_e$ , as well as the complete elliptic integrals of the first and second kinds,  $\mathcal{F}$  and  $\mathcal{E}$ . This calculation involves finding a solution to a transcendental equation relating  $k_e$ ,  $\mathcal{F}$ , and  $\mathcal{E}$  to the geometry of the contacting solids and is usually accomplished by some iterative numerical procedure. Hamrock and Brewe [1983] conducted a numerical analysis and curve-fit the data to obtain the simplified equations shown in Table 8.1. From this table, the ellipticity parameter for the complete radius ratio range found in machine elements can be expressed as

$$k_e = \alpha_r^{2/\pi}. \quad (8.12)$$

Figure 8.8 shows the ellipticity parameter and the elliptic integrals of the first and second kinds ( $\mathcal{F}$  and  $\mathcal{E}$ , respectively)

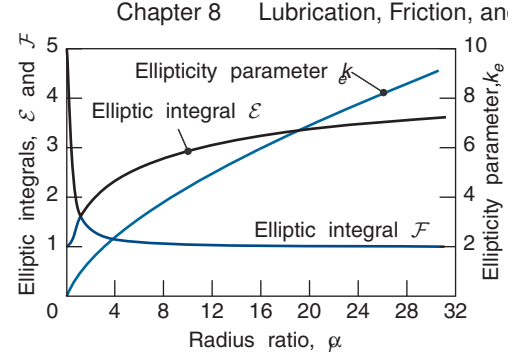


Figure 8.8: Variation of ellipticity parameter and elliptic integrals of first and second kinds as function of radius ratio.

for a radius ratio range usually encountered in machine elements. Note from Fig. 8.8 that  $\mathcal{F} = \mathcal{E} = \pi/2$  when  $\alpha_r = 1$ . Also, both  $\mathcal{F}$  and  $\mathcal{E}$  have discontinuous derivatives at  $\alpha_r = 1$ , thus the need for two columns in Table 8.1.

When the ellipticity parameter,  $k_e$ , the normal applied load,  $W$ , Poisson's ratio,  $\nu$ , and the modulus of elasticity,  $E$ , of the contacting solids are known, the major and minor axes of the contact ellipse ( $D_y$  and  $D_x$ ) and the maximum deformation at the contact center can be written as

$$D_y = 2 \left( \frac{6k_e^2 \mathcal{E} W R}{\pi E'} \right)^{\frac{1}{3}}, \quad (8.13)$$

$$D_x = 2 \left( \frac{6\mathcal{E} W R}{\pi k_e E'} \right)^{\frac{1}{3}}, \quad (8.14)$$

$$\delta_{\max} = \mathcal{F} \left[ \frac{9}{2\mathcal{E} R} \left( \frac{W}{\pi k_e E'} \right)^2 \right]^{\frac{1}{3}}, \quad (8.15)$$

where

$$E' = \frac{2}{\frac{(1 - \nu_a^2)}{E_a} + \frac{(1 - \nu_b^2)}{E_b}}. \quad (8.16)$$

Note from these equations that  $D_y$  and  $D_x$  are proportional to  $W^{1/3}$ , and  $\delta_{\max}$  is proportional to  $W^{2/3}$ .

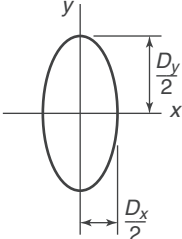
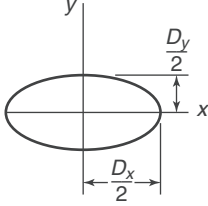
### Example 8.1: Hertzian Contact I – Ball in Ring

**Given:** A solid sphere of 20 mm radius ( $r_{ax} = r_{ay} = 20$  mm) rolls on the inside of a cylindrical outer race (see Fig. 8.6) with a 100-mm internal radius ( $r_{bx} = -100$  mm) and a large width in the axial direction. The sphere is made of silicon nitride and the outer race is made of stainless steel. The normal applied load is 1000 N.

**Find:**

- (a) Curvature sum,  $R$
- (b) Ellipticity parameter,  $k_e$
- (c) Elliptic integrals of the first and second kinds,  $\mathcal{F}$  and  $\mathcal{E}$
- (d) Effective modulus of elasticity,  $E'$
- (e) Dimensions of elliptical contact,  $D_x$  and  $D_y$

Table 8.1: Simplified elliptical contact equations.

Property	Radius ratio range	
	$1 \leq \alpha_r \leq 100$	$0.01 \leq \alpha_r \leq 1.0$
Geometry		
Ellipticity ratio	$k_e = \alpha_r^{2/\pi}$	$k_e = \alpha_r^{2/\pi}$
Elliptic integrals	$\mathcal{F} = \frac{\pi}{2} + \left(\frac{\pi}{2} - 1\right) \ln \alpha_r$	$\mathcal{F} = \frac{\pi}{2} - \left(\frac{\pi}{2} - 1\right) \ln \alpha_r$
	$\mathcal{E} = 1 + \frac{\pi - 2}{2\alpha_r}$	$\mathcal{E} = 1 + \left(\frac{\pi}{2} - 1\right) \alpha_r$

(f) Maximum Hertzian pressure or stress on surface,  $p_{\max}$

(g) Maximum deformation,  $\delta_{\max}$

**Solution:**

(a) Note that  $r_{bx}$  is negative, so from Eqs. (8.5) to (8.7),

$$\frac{1}{R_x} = \frac{1}{r_{ax}} + \frac{1}{r_{bx}} = \frac{1}{0.02} - \frac{1}{0.10} = 40 \text{ m}^{-1};$$

$$\frac{1}{R_y} = \frac{1}{r_{ay}} + \frac{1}{r_{by}} = \frac{1}{0.02} + \frac{1}{\infty} = 50 \text{ m}^{-1};$$

$$\frac{1}{R} = \frac{1}{R_x} + \frac{1}{R_y} = 40 + 50 = 90 \text{ m}^{-1}.$$

Therefore,  $R_x = 0.025 \text{ m}$ ,  $R_y = 0.02 \text{ m}$ , and the curvature sum  $R = 0.0111 \text{ m}$ .

(b)  $\alpha_r$  is obtained from Eq. (8.8) as

$$\alpha_r = R_y/R_x = 0.020/0.025 = 0.80.$$

Therefore, the ellipticity parameter is given by Eq. (8.12) as

$$k_e = \alpha_r^{2/\pi} = (0.80)^{2/\pi} = 0.8676.$$

(c) From Table 8.1, the elliptic integrals of the first and second kinds are (note that  $0.01 \leq \alpha_r \leq 1$ ):

$$\mathcal{F} = \frac{\pi}{2} - \left(\frac{\pi}{2} - 1\right) \ln(0.8) = 1.69,$$

$$\mathcal{E} = 1 + \left(\frac{\pi}{2} - 1\right) (0.8) = 1.457.$$

(d) From Table 3.1,  $E_a = 314 \text{ GPa}$ ,  $E_b = 193 \text{ GPa}$ ,  $\nu_a = 0.26$ , and  $\nu_b = 0.30$ . The effective modulus of elasticity is obtained from Eq. (8.16) as

$$\begin{aligned} E' &= \frac{2}{\frac{(1-\nu_a^2)}{E_a} + \frac{(1-\nu_b^2)}{E_b}} \\ &= \frac{2}{\frac{(1-0.26^2)}{314 \times 10^9} + \frac{(1-0.32^2)}{193 \times 10^9}} \\ &= 262.5 \text{ GPa}. \end{aligned}$$

(e) The dimensions of the elliptical contact, from Eqs. (8.13) and (8.14), are

$$\begin{aligned} D_y &= 2 \left( \frac{6k_e^2 \mathcal{E} W R}{\pi E'} \right)^{\frac{1}{3}} \\ &= 2 \left[ \frac{6(0.8676)^2 (1.457) (1000) (0.0111)}{\pi (262.5 \times 10^9)} \right]^{\frac{1}{3}} \\ &= 0.8915 \times 10^{-3} \text{ m}. \end{aligned}$$

$$\begin{aligned} D_x &= 2 \left( \frac{6 \mathcal{E} W R}{\pi k_e E'} \right)^{\frac{1}{3}} \\ &= 2 \left[ \frac{6(1.457) (1000) (0.0111)}{\pi (0.8676) (262.5 \times 10^9)} \right]^{\frac{1}{3}} \\ &= 1.024 \times 10^{-3} \text{ m}. \end{aligned}$$

(f) The maximum pressure, from Eq. (8.11), is

$$\begin{aligned} p_{\max} &= \frac{6W}{\pi D_x D_y} \\ &= \frac{6(1000)}{\pi (0.8915 \times 10^{-3}) (1.024 \times 10^{-3})} \\ &= 2.092 \text{ GPa}. \end{aligned}$$

(g) The maximum deformation at the center of the conjunction is calculated from Eq. (8.15), noting first that



$$\frac{W}{\pi k_e E'} = \frac{1000}{\pi(0.8676)(262.5 \times 10^9)} = 1.398 \times 10^{-9},$$

so that

$$\delta_{\max} = (1.6981) \left[ \frac{4.5 (1.398 \times 10^{-9})^2}{(1.457)(0.0111)} \right]^{\frac{1}{3}},$$

which is solved as  $\delta_{\max} = 13.90 \mu\text{m}$ .

## Example 8.2: Hertzian Contact II – Ball in Groove

**Given:** The balls in a deep-groove ball bearing have a 17-mm diameter. The groove in the inner race has an 8.84-mm radius; the radius from the center of the race to the bottom of the groove is 27.5 mm. A 20,000 N is applied. The ball and race are both made of steel.

**Find:**

- (a) The dimensions of the contact ellipse, and
- (b) The maximum deformation.

**Solution:**

- (a) Note from Fig. 8.6, and using an  $a$  subscript for the ball and a  $b$  for the groove, that  $r_{ax} = r_{ay} = 8.5 \text{ mm}$ ,  $r_{bx} = 27.5 \text{ mm}$ , and  $r_{by} = -8.84 \text{ mm}$ . From Eqs. (8.6) and (8.7) the curvature sums in the  $x$ - and  $y$ -directions are

$$\frac{1}{R_x} = \frac{1}{r_{ax}} + \frac{1}{r_{bx}} = \frac{1}{8.5 \times 10^{-3}} + \frac{1}{27.5 \times 10^{-3}},$$

or  $R_x = 0.00649 \text{ m} = 6.49 \text{ mm}$ . Similarly,

$$\frac{1}{R_y} = \frac{1}{r_{ay}} + \frac{1}{r_{by}} = \frac{1}{8.5 \times 10^{-3}} - \frac{1}{8.84 \times 10^{-3}},$$

which yields  $R_y = 0.221 \text{ m}$ . From Eqs. (8.5),

$$\frac{1}{R} = \frac{1}{R_x} + \frac{1}{R_y} = 158.5 \text{ m}^{-1},$$

or  $R = 0.00631 \text{ m} = 6.31 \text{ mm}$ . Using Eq. (8.8) gives the radius ratio as

$$\alpha_r = \frac{R_y}{R_x} = \frac{0.221}{0.00649} = 34.0.$$

From Table 8.1, the ellipticity parameter and the elliptic integrals of the first and second kinds are (note that  $1 \leq \alpha_r \leq 100$ ):

$$k_e = \alpha_r^{2/\pi} = 34.0^{2/\pi} = 9.446,$$

$$\mathcal{F} = \frac{\pi}{2} + \left( \frac{\pi}{2} - 1 \right) \ln \alpha_r = \frac{\pi}{2} + \left( \frac{\pi}{2} - 1 \right) \ln 34.0,$$

or  $\mathcal{F} = 3.584$ .

$$\mathcal{E} = 1 + \frac{\pi - 2}{2\alpha_r} = 1 + \frac{\pi - 2}{2(34.0)} = 1.017.$$

The effective modulus of elasticity is

$$E' = \frac{E}{1 - \nu^2} = \frac{207 \times 10^9}{1 - 0.3^2} = 227.5 \text{ GPa}.$$

From Eqs. (8.13) and (8.9), the dimensions of the contact ellipse are

$$\begin{aligned} D_y &= 2 \left( \frac{6k_e^2 \mathcal{E} W R}{\pi E'} \right)^{\frac{1}{3}} \\ &= 2 \left[ \frac{6(9.446)^2 (1.017) (20,000) (0.00631)}{\pi (227.5 \times 10^9)} \right]^{\frac{1}{3}} \\ &= 9.162 \text{ mm}, \\ D_x &= \frac{D_y}{k_e} = \frac{9.162}{9.446} = 0.9699 \text{ mm}. \end{aligned}$$

- (b) The maximum deformation at the center of contact is calculated from Eq. (8.15), but note first that

$$\frac{W}{\pi k_e E'} = \frac{20,000}{\pi(9.446) ((227.5 \times 10^9))} = 2.962 \times 10^{-9},$$

so that

$$\begin{aligned} \delta_{\max} &= \mathcal{F} \left[ \frac{9}{2\mathcal{E}R} \left( \frac{W}{\pi k_e E'} \right)^2 \right]^{\frac{1}{3}} \\ &= 3.584 \left[ \frac{9 (2.962 \times 10^{-9})^2}{2(1.017)(0.00631)} \right]^{\frac{1}{3}} \\ &= 65.68 \mu\text{m}. \end{aligned}$$

## 8.4.2 Rectangular Contacts

For rectangular conjunctions, the contact patch has infinite width. This type of contact is exemplified by a cylinder loaded against a plane, a flat-bottomed groove, or another parallel cylinder, or by a roller loaded against an inner or outer cylindrical race. In these situations, the contact semi-width is given by

$$b^* = R_x \left( \frac{8W'}{\pi} \right)^{\frac{1}{2}}, \quad (8.17)$$

where the dimensionless load is

$$W' = \frac{w'}{E' R_x}, \quad (8.18)$$

and  $w'$  is the load per unit length along the contact. The maximum deformation for a rectangular conjunction is

$$\delta_{\max} = \frac{2W' R_x}{\pi} \left[ \ln \left( \frac{2\pi}{W'} \right) - 1 \right]. \quad (8.19)$$

The maximum Hertzian contact pressure in a rectangular conjunction can be written as

$$p_{\max} = E' \left( \frac{W'}{2\pi} \right)^{\frac{1}{2}}. \quad (8.20)$$

### Example 8.3: Hertzian Contact III - Rectangular Contact

**Given:** A solid cylinder of 20 mm radius ( $r_{ax} = 20$  mm and  $r_{ay} = \infty$ ) rolls around the inside of an outer race with a 100-mm internal radius ( $r_{bx} = -100$  mm) and a large width in the axial ( $y$ ) direction ( $r_{by} = \infty$ ). The cylinder is made of silicon nitride and the outer race is made of stainless steel. The normal applied load per unit length is 1000 N/m.

**Find:**

- Curvature sum  $R$
- Semiwidth of contact  $b^*$
- Maximum Hertzian contact pressure  $p_{\max}$
- Maximum deformation  $\delta_{\max}$

Also, compare the results with those of Example 8.2.

**Solution:**

- From Example 8.1,  $E' = 262.5$  GPa. The curvature sum is

$$\frac{1}{R_x} = \frac{1}{r_{ax}} + \frac{1}{r_{bx}} = \frac{1}{0.02} - \frac{1}{0.10} = 40 \text{ m}^{-1},$$

so that  $R_x = 0.025$  m. The dimensionless load is obtained from Eq. (8.18) as:

$$\begin{aligned} W' &= \frac{w'}{E'R_x} \\ &= \frac{1000}{(2.625 \times 10^{11})(2.5 \times 10^{-2})} \\ &= 1.524 \times 10^{-7}. \end{aligned}$$

- From Eq. (8.17), the semiwidth of the contact is

$$\begin{aligned} b^* &= R_x \left( \frac{8W'}{\pi} \right)^{\frac{1}{2}} \\ &= (0.025) \left[ \frac{8(1.524 \times 10^{-7})}{\pi} \right]^{\frac{1}{2}} \\ &= 15.57 \mu\text{m}. \end{aligned}$$

- The maximum contact pressure is given by Eq. (8.20):

$$\begin{aligned} p_{\max} &= E' \left( \frac{W'}{2\pi} \right)^{\frac{1}{2}} \\ &= (2.625 \times 10^{11}) \left[ \frac{(1.524 \times 10^{-7})}{2\pi} \right]^{\frac{1}{2}} \\ &= 40.88 \text{ MPa}. \end{aligned}$$

- The maximum deformation at the center of the contact is, from Eq. (8.19),

$$\begin{aligned} \delta_{\max} &= \frac{2W'R}{\pi} \left[ \ln \left( \frac{2\pi}{W'} \right) - 1 \right] \\ &= \frac{2(1.524 \times 10^{-7})(2.5 \times 10^{-2})}{\pi} \\ &\quad \times \left[ \ln \left( \frac{2\pi}{1.524 \times 10^{-7}} \right) - 1 \right], \end{aligned}$$

$$\text{or } \delta_{\max} = 0.0401 \mu\text{m}.$$

## 8.5 Bearing Materials

Materials for conformal surfaces will be discussed here, since these materials apply to hydrodynamic bearings (Chapter 12) as well as more general cases such as guideways or unlubricated sleeves. Materials for rolling-element bearings and gears will be expanded upon in Chapters 13 and 14, respectively. Bearing materials for conformal surfaces fall into two major categories:

- Metallics:** babbitts, bronzes, aluminum alloys, porous metals, and metal overlays such as silver, babbitts, and indium.
- Nonmetallics:** plastics, rubber, carbon-graphite, wood, ceramics, cemented carbides, metal oxides (e.g., aluminum oxide), and glass.

### 8.5.1 Metals

#### Tin- and Lead-Base Alloys

**Babbitts**, also known as **white metals**, are either tin or lead-base alloys having excellent embeddability and conformability characteristics. The babbitts are among the most widely used materials for lubricated bearings.

Tin- and lead-base babbitts have relatively low load-carrying capacity. This capacity is increased by metallurgically bonding these alloys to stronger backing materials such as steel, cast iron, or bronze. Fatigue strength is increased by decreasing the thickness of the babbitt lining. The optimum thickness of the bearing layer varies with the application, but is generally between 0.02 and 0.12 mm.

Table 8.2 shows the composition and physical properties of some of the most common tin- and lead-base alloys. Note the significant effect of temperature in decreasing the strength of these alloys. The effect of various percentages of alloying elements on the mechanical and physical properties of tin- and lead-base alloys can also be significant. Increasing the copper or the antimony generally increases the hardness and the tensile strength and decreases the ductility.

#### Copper-Lead Alloys and Bronzes

Copper-lead alloys are commonly used as lining materials on steel-backed bearings. These alloys have high fatigue resistance and can operate at higher temperatures, but they have poor antiseizure properties. They are also used in automotive and aircraft internal combustion engines and in diesel engines. Their high lead content provides a good bearing surface but makes them susceptible to corrosion. Their corrosion resistance and antiseizure properties are improved when they are used as trimetal bearings with a lead-tin or lead-indium overlay electrodeposited onto the copper-lead surface.

Table 8.2: Physical and mechanical properties of selected white metal bearing alloys. *Source:* From Hamrock et al. [2004].

Alloy number	Nominal composition (%)					Specific gravity	Yield strength, MPa		Compressive strength, MPa		Brinell hardness	
	Sn	Sb	Pb	Cu	As		20° C	100° C	20° C	100° C	20° C	100° C
1	91.0	4.5	—	4.5	—	7.34	30.3	18.3	88.6	47.9	17.0	8.0
2	89.0	7.5	—	3.5	—	7.39	42.0	20.6	102.7	60.0	24.5	12.0
3	84.0	8.0	—	8.0	—	7.46	45.4	21.7	121.3	68.3	27.0	14.5
7	10.0	15.0	74.55	—	0.45	9.73	24.5	11.0	107.9	42.4	22.5	10.5
8	5.	15.0	79.55	—	0.45	10.04	23.4	12.1	107.6	42.4	20.0	9.5

Table 8.3: Mechanical properties of selected bronze and copper alloy bearing materials *Source:* Abstracted from Hamrock, et al. [2004].

Material	Designation	Brinell hardness	Tensile strength, MPa	Maximum temperature, °C	Allowable stress, MPa
Copper lead	SAE 480	25	55.2	177	13.8
High-lead tin bronze	AMS 4840	48	172.5	204	20.7
Semiplastic bronze	SAE 67	55	207	232	20.7
Leaded red bronze	SAE 40	60	242	232	24.2
Bronze	SAE 660	60	242	232	27.6
Phosphor bronze	SAE 64	63	242	232	27.6
Gunmetal	SAE 62	65	310	260	27.6
Navy G	SAE 620	68	276	260	27.6
Leaded gunmetal	SAE 63	70	276	260	27.6
Aluminum bronze	ASTM B148-52-9c	195	621	260	31.1

Several bronze alloys, including lead, tin, and aluminum bronzes, are used extensively as bearing materials. Some are described in Table 8.3. Because of their good structural properties, they can be used without a steel backing. Lead bronzes, which contain up to 25% lead, provide higher load-carrying capacity and fatigue resistance and a higher temperature capability than the babbitt alloys. Tin contents up to about 10% are used to improve mechanical properties. Lead bronze bearings are used in pumps, diesel engines, railroad cars, home appliances, and many other applications.

Tin bronzes, which contain 9 to 20% tin and small quantities of lead (usually < 1%), are harder than lead bronzes and are therefore used in heavier-duty applications.

## 8.5.2 Nonmetallics

### Polymers

Although nonmetallic materials such as rubber and graphite have found increasing application, polymeric and plastic materials have had a very large impact in tribological machine elements. The limits of applying nonmetallic materials are shown in Table 8.4. The specific limits shown in this table are load-carrying capacity, maximum temperature, maximum speed, and  $pu$  limit, where  $p$  is the pressure in Pa and  $u$  is the surface speed in m/s.

Of the thermoplastic materials, **nylon** has been recognized as a valuable bearing material, as has the remarkable low-friction polymer polytetrafluoroethylene (PTFE), or **teflon**. The great merit of these materials is that they can operate well without lubricants, although their mechanical properties generally limit their application to lightly loaded conditions and often to low speeds and conforming surfaces.

Nylon has good abrasion resistance, a low wear rate, and good embeddability. Like most plastics, it has good anti-seizure properties and softens or chars rather than seizing. Cold flow (creep) under load is one of its main disadvantages. This effect can be minimized by supporting thin nylon liners in metal sleeves. Nylon bearings are used in house-

hold applications such as kitchen mixers and blenders and for other lightly loaded applications. Nylon is not affected by petroleum oils and greases, food acids, milk, etc., and thus can be used in applications where these fluids are encountered.

Teflon is resistant to chemical attack by many solvents and chemicals and can be used up to 260°C. Like nylon, it has a tendency to creep. Teflon in its unmodified form also has the disadvantages of low stiffness, a high thermal expansion coefficient, low thermal conductivity, and poor wear resistance. These poor properties are greatly improved by adding fibers such as glass, ceramics, metal powders, metal oxides, graphite, or molybdenum disulfide.

**Phenolics** are another important class of plastic bearing material. These are in the form of laminates, made by infiltrating sheets of either paper or fabric with phenolic resin, stacking the sheets, and curing with heat and pressure to bond them together. Other filling materials, such as graphite and molybdenum disulfide, are added in powdered form to improve lubrication qualities and strength.

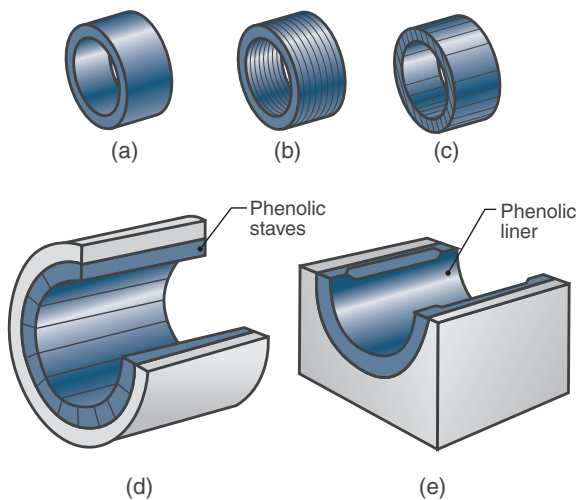
Laminated phenolics operate well with steel or bronze journals when lubricated with oil, water, or other liquids. They have good resistance to seizure. One main disadvantage of these materials is their low thermal conductivity (about 1/150 that of steel), which prevents them from dissipating frictional heat readily and can result in their failure by charring.

### Graphite

In addition to its excellent self-lubricating properties, **graphite** has several advantages over conventional materials and lubricants. It can withstand temperatures of approximately 370°C in an oxidizing atmosphere such as air and can be used in inert atmospheres ranging from cryogenic temperatures to 700°C. Graphite is highly resistant to chemical attack and can be used with low-viscosity lubricants, including water, gasoline, or air. A  $pv$  value of 15,000 is typically used for graphite when lubricated. In general, low speeds and light loads should be used in nonlubricated applications.

Table 8.4: Limits of application of nonmetallic bearing materials. *Source:* Abstracted from Hamrock, et al. [2004].

Material	Allowable stress, MPa	Maximum temperature, °C	Maximum speed, m/s	$pu$ limit, N/m-s
Carbon graphite	4.1	399	12.7	$525 \times 10^3$
Phenolics	41.4	93	12.7	$525 \times 10^3$
Nylon	6.9	93	5.1	$105 \times 10^3$
PTFE (Teflon)	3.4	260	.51	$35 \times 10^3$
Reinforced PTFE	17.2	260	5.1	$350 \times 10^3$
PTFE fabric	414.0	260	.25	$875 \times 10^3$
Polycarbonate (Lexan)	6.9	104	5.1	$105 \times 10^3$
Acetal resin (Delrin)	6.9	82	5.1	$105 \times 10^3$
Rubber	0.34	66	7.6	$525 \times 10^3$
Wood	13.8	66	10.2	$525 \times 10^3$

Figure 8.9: Phenolic laminate bearings. (a) Tubular bearing; (b) circumferentially laminated bearing; (c) axially laminated bearing; (d) stave bearing; (e) molded bearing. *Source:* Hamrock et al. [2004].

Graphite is commonly used for pump shaft bearings, impeller wear rings in centrifugal pumps, and journal and thrust bearings in covered motor pumps and for many other applications. Because of its low thermal expansion coefficient, graphite liners are often shrink-fit into steel sleeves (see Section 10.6). The steel backing provides mechanical support, improves heat transfer, and helps to maintain shaft clearance.

### 8.5.3 Bearing Configurations

Figure 8.9 shows the various configurations of phenolic laminates used in bearings. Tubular bearings (Fig. 8.9a) are used where complete bushings are required. Bearings in which the load is taken by the edges of the laminations (Fig. 8.9b and c) are used in light-duty service. Stave bearings (Fig. 8.9d) are used mainly for stern-tube and rudder-stock bearings on ships and for guide bearings on vertical turbines. Molded bearings (Fig. 8.9e) are used for roll-neck bearings in steel mills or for ball-mill bearings.

Other materials may be applied to bearing surfaces in several ways, as shown in Fig. 8.10:

- **Solid bearing** (Fig. 8.10a). Bearings are machined directly from a single material (cast iron, aluminum alloys, bronzes, porous metals, etc.).
- **Lined bearing** (Fig. 8.10b). Bearing material is bonded

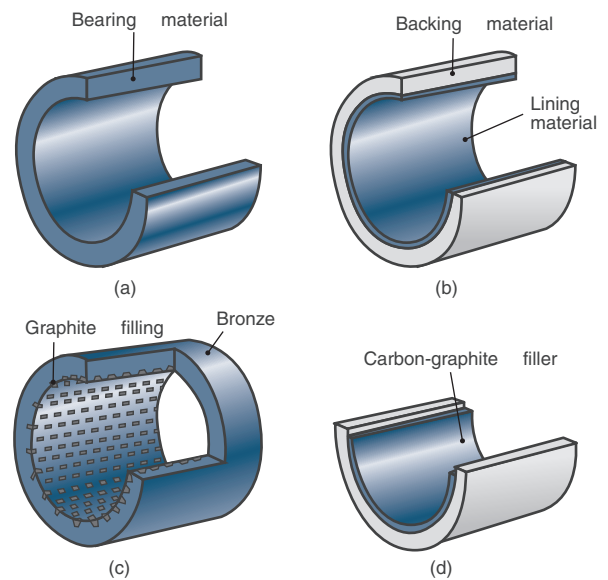


Figure 8.10: Different forms of bearing surfaces. (a) Solid bearing; (b) lined bearing; (c) filled bearing; (d) shrink-fit bearing.

to a stronger backing material. The thickness of the bearing lining may range from 0.25 mm to as much as 13 mm. Most modern bonding techniques are metallurgical, although chemical and mechanical methods are also used. The lining material may be cast, sprayed, electrodeposited, or chemically applied.

- **Filled bearing** (Fig. 8.10c). A stronger bearing material is impregnated with a bearing material that has better lubricating properties (e.g., graphite impregnated into a bronze backing).
- **Shrink-fit liner bearing** (Fig. 8.10d). Carbon-graphite or plastic liners are shrunk into a metal backing sleeve or held by retaining devices such as setscrews.

## 8.6 Lubricant Rheology

A **lubricant** is any substance that reduces friction and wear and provides smooth running and a satisfactory life, and **rheology** is the study of the flow and deformation of matter. Most lubricants are liquids (such as mineral oils, synthetic

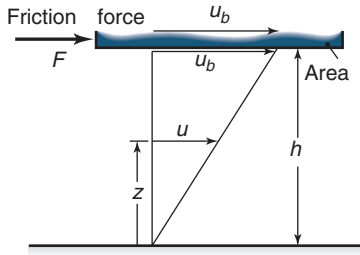


Figure 8.11: Slider bearing illustrating absolute viscosity.

esters, silicone fluids, and water), but they may also be solids (such as graphite or molybdenum disulfide) for use in dry bearings, greases for use in rolling-element bearings, or gases (such as air) for use in gas bearings. The physical and chemical interactions between the lubricant and the lubricating surfaces must be understood in order to provide the machine elements with satisfactory life.

When interposed between solid surfaces, a lubricant facilitates relative sliding or rolling, and controls friction and wear. Separation of the surfaces is, however, not the only function of a lubricant. Liquid lubricants have desirable secondary properties and characteristics:

1. They can be drawn in between moving parts by hydrodynamic action.
2. They have relatively high heat capacity to cool the contacting parts.
3. They are easily blended with chemical additives to give a variety of properties, such as corrosion resistance, detergency, or surface-active layers.
4. They can remove wear particles.
5. They are thermal insulators.
6. They damp vibrations and reduce impact loads.

Liquid lubricants can be divided into those of petroleum origin, known as mineral oils, and those of animal or vegetable origin, known as fatty oils; synthetic oils are often grouped with the latter. For a lubricant to be effective, it must be viscous enough to maintain a lubricant film under operating conditions and to remove heat from machine elements. On the other hand, the lubricant should be as inviscid as possible to minimize power requirements at startup (especially cold starts) and to avoid power loss due to viscous drag. The most important lubricant property, the viscosity, is considered in the following subsections.

### 8.6.1 Absolute Viscosity

**Absolute or dynamic viscosity** can be defined in terms of the simple model shown in Fig. 8.11, which depicts two parallel flat plates separated by a constant distance,  $h$ , with the upper plate moving with velocity  $u_b$  and the lower plate stationary. To move the upper plate of area  $A$  at a constant velocity across the surface of the oil and cause adjacent layers to flow past each other, a tangential force must be applied. Since the oil will “wet” and cling to the two surfaces, the bottommost layer will not move at all, the topmost layer will move with a velocity equal to the velocity of the upper plate, and the layers between the plates will move with velocities directly proportional to their distances,  $z$ , from the stationary plate.

This type of orderly movement in parallel layers is known as streamline, laminar, or viscous flow.

The shear stress on the oil causing relative movement of the layers is equal to  $F/A$ . The shear strain rate,  $s$ , of a particular layer is defined as the ratio of its velocity to its perpendicular distance from the stationary surface,  $z$ , and is constant for each layer:

$$s = \frac{u}{z} = \frac{u_b}{h}. \quad (8.21)$$

The shear strain rate has the unit of reciprocal seconds.

Newton correctly deduced that the force required to maintain a constant velocity,  $u_b$ , of the upper surface is proportional to the area and the shear strain rate or

$$F = \frac{\eta A u_b}{h}, \quad (8.22)$$

where  $\eta$  is the absolute viscosity. By rearranging Eq. (8.22), the absolute viscosity can be expressed as

$$\eta = \frac{F/A}{u_b/h} = \frac{\text{Shear stress}}{\text{Shear strain rate}}. \quad (8.23)$$

It follows from Eq. (8.23) that the unit of viscosity must be the unit of shear stress divided by the unit of shear strain rate. The units of viscosity for three different systems in general use are:

1. SI units: newton-second per square meter ( $\text{N}\cdot\text{s}/\text{m}^2$ ) or, since a newton per square meter is also called a pascal, pascal-second ( $\text{Pa}\cdot\text{s}$ ).
2. cgs units: dyne-second per square centimeter, or *centipoise*, where  $1 \text{ cP} = 10^{-2} \text{ P}$ .
3. English units: pound force-second per square inch ( $\text{lb}\cdot\text{s}/\text{in}^2$ ), called a *reyn* in honor of Osborne Reynolds

Conversion of absolute viscosity from one system to another can be facilitated by Table 8.5. To convert from a unit in the column on the left side of the table to a unit at the top of the table, multiply by the corresponding value given in the table.

### Example 8.4: Units of Viscosity

**Given:** An absolute viscosity of  $0.04 \text{ N}\cdot\text{s}/\text{m}^2$ .

**Find:** The absolute viscosity in reyn, centipoise, and poise.

**Solution:** Using Table 8.5 gives

$$\eta = 0.04 \text{ N}\cdot\text{s}/\text{m}^2 = (0.04) \text{ Pa}\cdot\text{s} = 5.8 \times 10^{-6} \text{ lb}\cdot\text{s}/\text{in}^2$$

Note also that

$$\eta = 0.04 \text{ N}\cdot\text{s}/\text{m}^2 = 0.04 \text{ Pa}\cdot\text{s} = 5.8 \times 10^{-6} \text{ reyn}$$

and

$$\eta = 0.04 \text{ N}\cdot\text{s}/\text{m}^2 = 0.004 \times 10^3 \text{ cP} = 40 \text{ cP} = 0.4 \text{ P}.$$

### 8.6.2 Kinematic Viscosity

In many situations it is convenient to use **kinematic viscosity** rather than absolute viscosity. The kinematic viscosity,  $\eta_k$ , is:

$$\eta_k = \frac{\text{Absolute viscosity}}{\text{Density}} = \frac{\eta}{\rho}. \quad (8.24)$$

The ratio given in Eq. (8.24) is literally kinematic; all terms involving force or mass have canceled out. The units of kinematic viscosity are



Table 8.5: Absolute viscosity conversion factors.

To convert from	To			
	cP	kgf-s/m <sup>2</sup>	N-s/m <sup>2</sup>	lb-s/in. <sup>2</sup>
	Multiply by			
cP	1	$1.02 \times 10^{-4}$	$10^{-3}$	$1.45 \times 10^{-7}$
kgf-s/m <sup>2</sup>	$9.807 \times 10^3$	1	9.807	$1.422 \times 10^6$
N-s/m <sup>2</sup>	$10^3$	$1.02 \times 10^4$	1	$1.45 \times 10^6$
reyn, or lb-s/in. <sup>2</sup>	$6.90 \times 10^6$	$7.03 \times 10^6$	$6.9 \times 10^6$	1

1. SI units: square meters per second (m<sup>2</sup>/s)
2. cgs units: square centimeters per second (cm<sup>2</sup>/s), called a *stoke*
3. English units: square inches per second (in<sup>2</sup>/s)

### Example 8.5: Kinematic Viscosity

**Given:** Both mercury and water have an absolute viscosity of 1.5 cP at 5°C, but mercury has 13.6 times higher density than water. Assume density changes associated with temperature increases are small.

**Find:** The kinematic viscosities of mercury and water at 5°C and at 90°C.

**Solution:** Figure 8.12 gives the absolute viscosities of various fluids as a function of temperature. At 90°C the absolute viscosity of water is 0.32 cP, and for mercury it is 1.2 cP. The kinematic viscosity of mercury at 5°C is

$$\eta_k = \frac{\eta}{\rho} = \frac{1.5 \times 10^{-3}}{13,600} = 0.110 \times 10^{-6} \text{ m}^2/\text{s},$$

and at 90°C it is

$$\eta_k = \frac{\eta}{\rho} = \frac{1.2 \times 10^{-3}}{13,600} = 0.0882 \times 10^{-6} \text{ m}^2/\text{s}.$$

The kinematic viscosity of water at 5°C is

$$\eta_k = \frac{\eta}{\rho} = \frac{1.5 \times 10^{-3}}{1000} = 1.50 \times 10^{-6} \text{ m}^2/\text{s},$$

and at 90°C it is

$$\eta_k = \frac{\eta}{\rho} = \frac{0.32 \times 10^{-3}}{1000} = 0.32 \times 10^{-6} \text{ m}^2/\text{s}.$$

Although mercury has the same absolute viscosity as water at 5°C and 3.75 times higher absolute viscosity at 90°C, the kinematic viscosities for mercury are much lower than those for water because of mercury's high density.

### 8.6.3 Viscosity-Pressure Effects

In highly loaded contacts such as ball bearings, gears, and cams, the pressure is high enough to increase the lubricant viscosity significantly. The increase of a lubricant's viscosity with pressure is known as a **viscosity-pressure effect** or **piezoviscous effect**, and is especially pronounced in mineral oils and other fluids with a large molecular chain length. The Barus equation relates the viscosity and pressure for isothermal conditions as

$$\eta = \eta_o \exp(\xi p), \quad (8.25)$$

where  $p$  is the pressure,  $\eta_o$  is the absolute viscosity at ambient pressure ( $p = 0$ ) and at a constant temperature, and  $\xi$  is the **pressure-viscosity coefficient** of the lubricant.

Table 8.6 lists the kinematic viscosities in square meters per second and the absolute viscosities in centipoise of various fluids at zero pressure and different temperatures. These values of the absolute viscosity correspond to  $\eta_o$  in Eq. (8.25) for the particular fluid and temperature used. The pressure-viscosity coefficients,  $\xi$ , for these fluids, expressed in square meters per newton, are given in Table 8.7. The values correspond to  $\xi$  in Eq. (8.25).

### Example 8.6: Piezoviscous Effects

**Given:** A synthetic paraffin and a fluorinated polyether are used at a temperature of 99°C.

**Find:**

- (a) The pressure at which the two oils have the same absolute viscosity
- (b) The pressure at which the paraffin is 100 times less viscous than the fluorinated polyether

**Solution:**

- (a) From Table 8.6, the viscosity of the synthetic paraffin at 99°C is 0.0347 Ns/m<sup>2</sup>, and the fluorinated polyether has a viscosity of 0.0202 Ns/m<sup>2</sup>. From Table 8.7, the pressure-viscosity coefficient at 99°C for the paraffin is  $1.51 \times 10^{-8} \text{ m}^2/\text{N}$  and for the polyether it is  $3.24 \times 10^{-8} \text{ m}^2/\text{N}$ . Using Eq. (8.25) and equating the viscosity gives

$$0.0347e^{1.51 \times 10^{-8} p} = 0.0202e^{3.24 \times 10^{-8} p}$$

$$1.72e^{1.51 \times 10^{-8} p} = e^{3.24 \times 10^{-8} p}$$

$$1.72 = \frac{e^{3.24 \times 10^{-8} p}}{e^{1.51 \times 10^{-8} p}} = e^{1.73 \times 10^{-8} p}.$$

Therefore,

$$p = \frac{\ln 1.72}{1.73 \times 10^{-8}} = 31.3 \text{ MPa}.$$

- (b) Using Eq. (8.25) while letting the paraffin be 100 times less viscous than the polyether gives

$$1.72(100)e^{1.51 \times 10^{-8} p} = e^{3.24 \times 10^{-8} p},$$

$$172 = e^{1.73 \times 10^{-8} p}.$$

Therefore,  $p = 2.97 \times 10^{-8} \text{ Pa} = 0.297 \text{ GPa}$ . This may seem to be a very high pressure, but it is not an unusual pressure for non-conformal contacts such as rolling element bearings or gears.

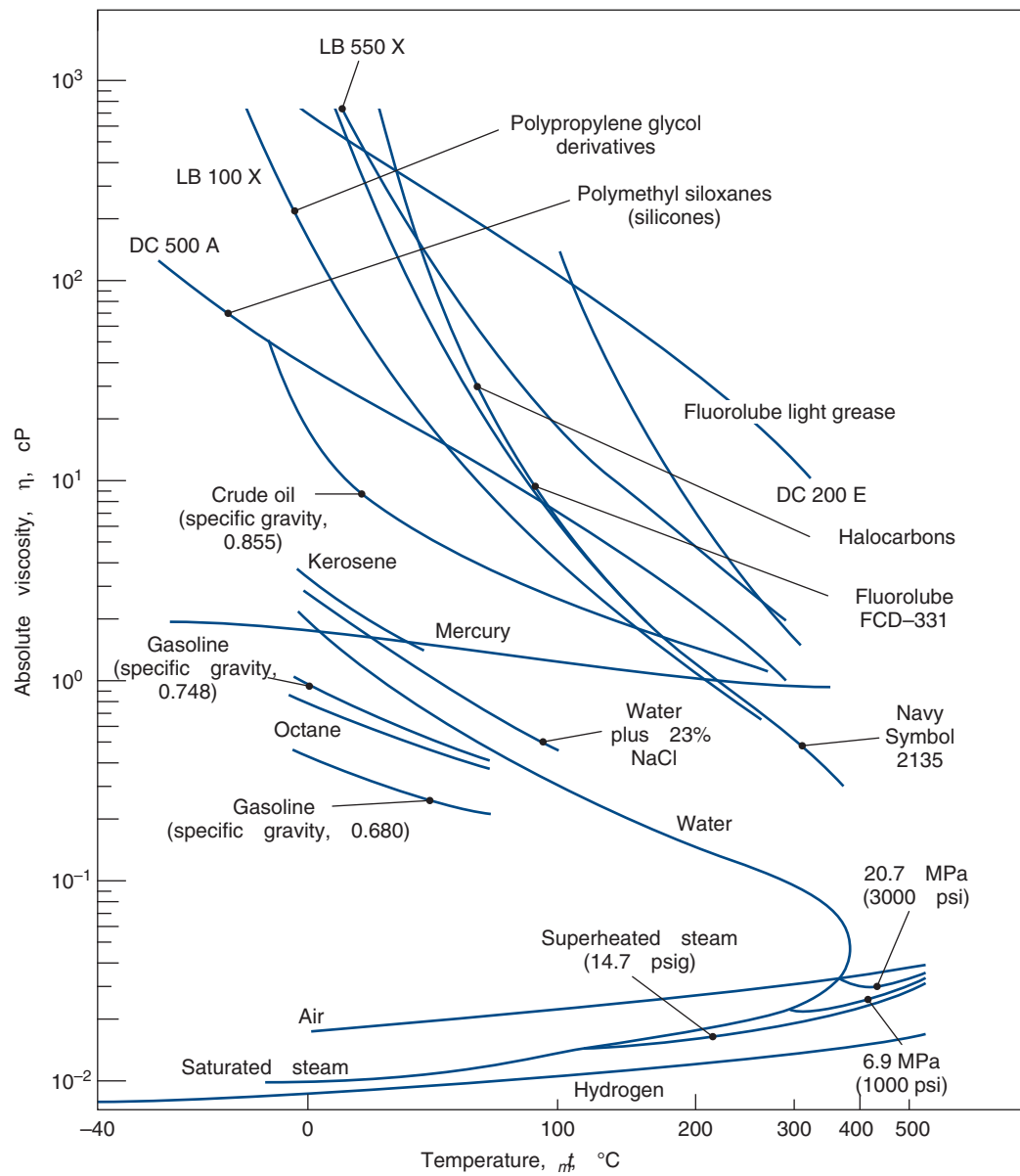


Figure 8.12: Absolute viscosities of a number of fluids for a wide range of temperatures.

Table 8.6: Absolute and kinematic viscosities of various fluids at atmospheric pressure and different temperatures.

Fluid	Absolute viscosity at $p = 0$ , $\eta_o$ , N-s/m <sup>2</sup>			Kinematic viscosity at $p = 0$ $\eta_k$ , m <sup>2</sup> /s		
	Temperature, °C			Temperature, °C		
	38	99	149	38	99	149
Advanced ester	0.0253	0.00475	0.00206	$2.58 \times 10^{-5}$	$0.51 \times 10^{-5}$	$0.23 \times 10^{-5}$
Formulated advanced ester	0.0276	0.00496	0.00215	$2.82 \times 10^{-5}$	$0.53 \times 10^{-5}$	$0.24 \times 10^{-5}$
Polyalkyl aromatic	0.0255	0.00408	0.00180	$3.0 \times 10^{-5}$	$0.50 \times 10^{-5}$	$0.23 \times 10^{-5}$
Synthetic paraffinic oil	0.375	0.0347	0.0101	$44.7 \times 10^{-5}$	$4.04 \times 10^{-5}$	$1.3 \times 10^{-5}$
Synthetic paraffinic oil plus antiwear additive	0.375	0.0347	0.0101	$44.7 \times 10^{-5}$	$4.04 \times 10^{-5}$	$1.3 \times 10^{-5}$
C-ether	0.0295	0.00467	0.00220	$2.5 \times 10^{-5}$	$0.41 \times 10^{-5}$	$0.20 \times 10^{-5}$
Superrefined naphthenic mineral oil	0.0681	0.00686	0.00274	$7.8 \times 10^{-5}$	$0.82 \times 10^{-5}$	$0.33 \times 10^{-5}$
Synthetic hydrocarbon (traction fluid)	0.0343	0.00353	0.00162	$3.72 \times 10^{-5}$	$0.40 \times 10^{-5}$	$0.19 \times 10^{-5}$
Fluorinated polyether	0.181	0.0202	0.00668	$9.66 \times 10^{-5}$	$1.15 \times 10^{-5}$	$0.4 \times 10^{-5}$

Table 8.7: Pressure-viscosity coefficients of various fluids at different temperatures.

Fluid	Temperature, °C		
	38	99	149
	Pressure-viscosity coefficient, $\xi$ , m <sup>2</sup> /N		
Advanced ester	$1.28 \times 10^{-8}$	$0.987 \times 10^{-8}$	$0.851 \times 10^{-8}$
Formulated advanced ester	$1.37 \times 10^{-8}$	$1.00 \times 10^{-8}$	$0.874 \times 10^{-8}$
Polyalkyl aromatic	$1.58 \times 10^{-8}$	$1.25 \times 10^{-8}$	$1.01 \times 10^{-8}$
Synthetic paraffinic oil	$1.99 \times 10^{-8}$	$1.51 \times 10^{-8}$	$1.29 \times 10^{-8}$
Synthetic paraffinic oil plus antiwear additive	$1.96 \times 10^{-8}$	$1.55 \times 10^{-8}$	$1.25 \times 10^{-8}$
C-ether	$1.80 \times 10^{-8}$	$0.980 \times 10^{-8}$	$0.795 \times 10^{-8}$
Superrefined naphthenic mineral oil	$2.51 \times 10^{-8}$	$1.54 \times 10^{-8}$	$1.27 \times 10^{-8}$
Synthetic hydrocarbon (traction fluid)	$3.12 \times 10^{-8}$	$1.71 \times 10^{-8}$	$0.939 \times 10^{-8}$
Fluorinated polyether	$4.17 \times 10^{-8}$	$3.24 \times 10^{-8}$	$3.02 \times 10^{-8}$

### 8.6.4 Viscosity-Temperature Effects

The viscosity of mineral and synthetic oils decreases with increasing temperature; therefore, the temperature at which a viscosity measurement is taken must be reported. Figure 8.13 shows how absolute viscosity varies with temperature. Figure 8.12 presents the absolute viscosity of several fluids for a wide temperature range. The interesting point of this figure is how drastically the slope and level of viscosity change for different fluids. The viscosity varies by five orders of magnitude, with the slope being highly negative for fluids and positive for gases.

Figure 8.13 gives the viscosity of Society of Automotive Engineers (SAE) oils as a function of temperature. The SAE standards allow for a range of values, and specify a kinematic viscosity, which results in the approximate absolute viscosity curves shown in Fig. 8.13. Real lubricants have viscosities that are functions of strain rate, which serves as another reminder that Fig. 8.13 does not provide exact values. Further, SAE specifies viscosity only at one temperature for the lubricants in Fig. 8.13a, namely 100°C (212°F). Multigrade oils, shown in Fig. 8.13b, have a low temperature viscosity requirement defined at -18°C (0°F), which they must meet in addition to the high temperature viscosity requirement. This demanding set of requirements can be met through the use of viscosity index modifiers. Such complicated formulations require specific characterization of viscosity as functions of temperature and strain rate. However, the data in Fig. 8.13 and Table 8.8 are sufficient for most design and analysis tasks.

The viscosities of SAE oils can also be approximated for

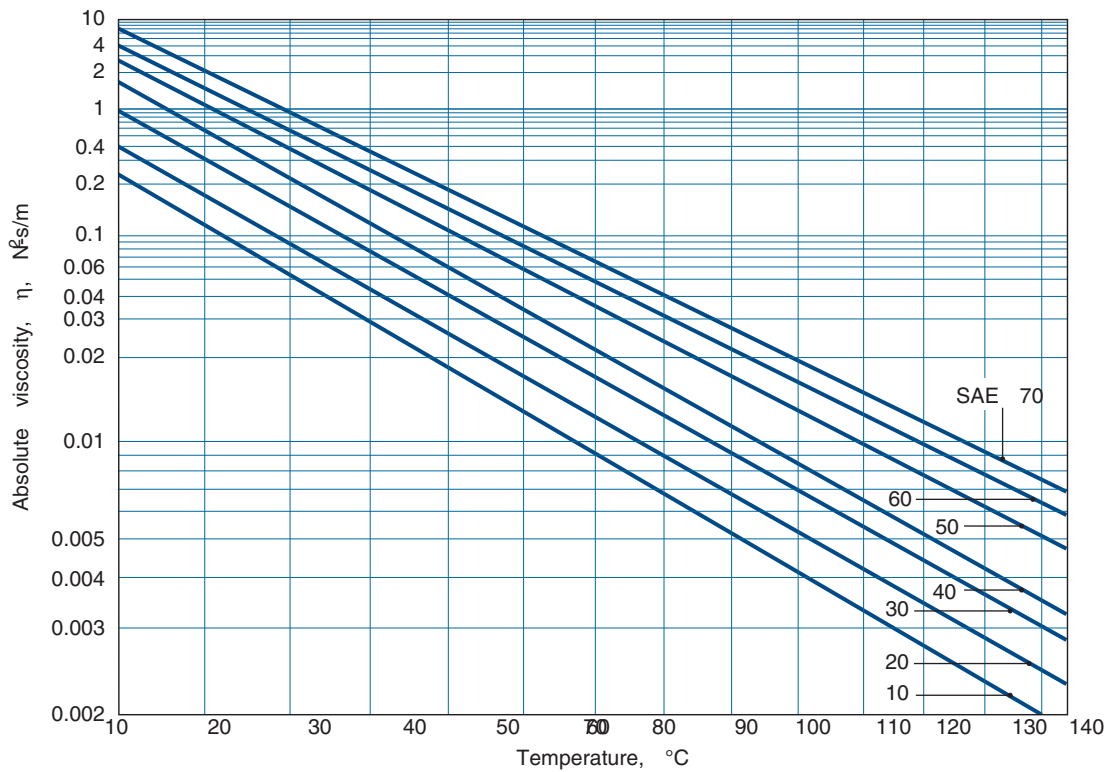
Table 8.8: Curve fit data for SAE single grade oils for use in Eq. (8.26). Source: From Seirig and Dandage [1982].

SAE Grade	Constant $C_1$		Constant $C_2$
	reyn	N-s/m <sup>2</sup>	
10	$1.58 \times 10^{-8}$	$1.09 \times 10^{-4}$	1157.5
20	$1.36 \times 10^{-8}$	$9.38 \times 10^{-5}$	1271.6
30	$1.41 \times 10^{-8}$	$9.73 \times 10^{-5}$	1360.0
40	$1.21 \times 10^{-8}$	$8.35 \times 10^{-5}$	1474.4
50	$1.70 \times 10^{-8}$	$1.17 \times 10^{-4}$	1509.6
60	$1.87 \times 10^{-8}$	$1.29 \times 10^{-4}$	1564.0

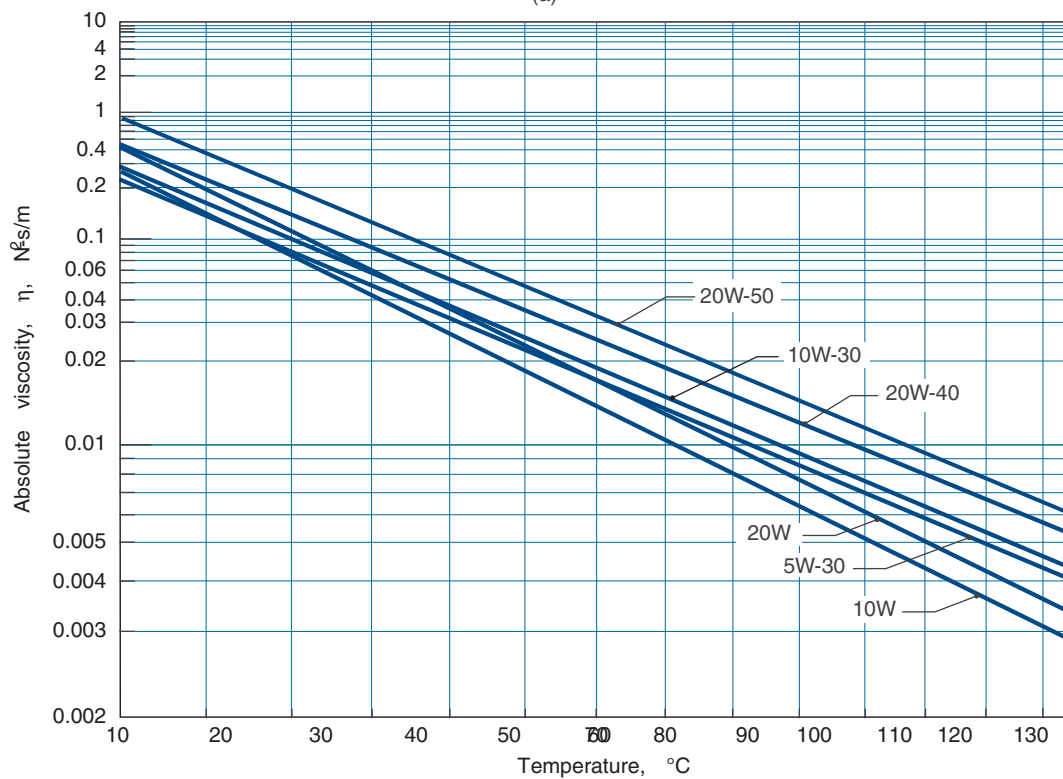
the temperatures in Fig. 8.13 using the curve fit

$$\eta = \begin{cases} C_1 \exp\left(\frac{C_2}{t_F + 95}\right) & \text{English units} \\ C_1 \exp\left(\frac{C_2}{1.8t_C + 127}\right) & \text{S.I. units} \end{cases} \quad (8.26)$$

where  $C_1$  and  $C_2$  are constants given in Table 8.8 and  $t_F$  and  $t_C$  are the lubricant temperature in °F or °C, respectively. Note that Eq. (8.26) can give slightly different results than Fig. 8.13, since the strain rates at evaluation are slightly different.



(a)



(b)

Figure 8.13: Absolute viscosities of SAE lubricating oils at atmospheric pressure. (a) Single grade oils; (b) multigrade oils.

### Example 8.7: Viscosity-Temperature Effects

**Given:** An SAE 10 oil is used in a car motor where the working temperature is 110°C.

**Find:** How many times more viscous would the oil be at startup when the temperature is 10°C?

**Solution:** Figure 8.13 gives the viscosity as 0.0033 N-s/m<sup>2</sup> at 110°C and 0.22 N-s/m<sup>2</sup> at 10°. The viscosity ratio is 0.22/0.0033 = 66.67. Alternatively, Eq. (8.26) can be used to obtain the viscosity at 10°C as 0.990 N-s/m<sup>2</sup> and 0.003839 at 110°, resulting in a viscosity ratio of 258. The viscosity at low temperatures is suspect using Eq. (8.26); however, this clearly demonstrates that the startup viscosity is much lower than the viscosity during operation.

## 8.7 Regimes of Lubrication

Some machine elements such as hydrodynamic bearings (Ch. 12) require lubricants to function; others such as rolling-element bearings (Ch. 13) and gears (Ch. 14-15) would have compromised life and performance in the absence of effective lubrication. Lubrication engineering is a topic worthy of detailed study; this section presents a general overview, emphasizing fundamental topics that have a direct impact on machine elements. The discussion begins with the introduction of the film parameter, and its use to define the regime of lubrication. Each regime is then summarized, using surface roughness (Section 8.2) and lubricant rheology (Section 8.6) to explain performance.

### 8.7.1 Film Parameter

When machine elements such as rolling-element bearings, gears, hydrodynamic journal and thrust bearings, and seals (all of which are considered later in this text) are adequately designed and lubricated, the surfaces are completely separated by a lubricant film. Endurance testing of ball bearings, for example, has demonstrated that when the lubricant film is thick enough to separate the contacting bodies, bearing fatigue life is greatly extended (see Section 13.9.5 and Fig. 13.24). Conversely, when the film is not thick enough to provide full separation between the asperities in the contact zone, bearing life is adversely affected by the high shear stresses resulting from direct metal-to-metal contact.

An important parameter that indicates the effectiveness of lubrication is the **film parameter**, given by

$$\Lambda = \frac{h_{\min}}{\left(R_{qa}^2 + R_{qb}^2\right)^{\frac{1}{2}}}, \quad (8.27)$$

where  $h_{\min}$  is the minimum film thickness, and  $R_{qa}$  and  $R_{qb}$  are the rms surface roughnesses of the two surfaces. The film parameter is used to define the four important lubrication regimes. The range for these four regimes is

1. *Boundary lubrication*,  $\Lambda < 1$
2. *Partial lubrication*,  $1 \leq \Lambda < 3$
3. *Hydrodynamic lubrication*,  $3 \leq \Lambda$
4. *Elastohydrodynamic lubrication*,  $3 \leq \Lambda < 10$

These values are only approximate, but give useful insight into the importance of lubrication.

**Running-in** is a process that affects the film parameter. Reviewing Fig. 8.14, it can be seen that surfaces contact at asperity peaks. If microscale wear takes place at these asperity peaks, and material is removed, then the remaining surface is smoother as a result. This process allows wear to occur so that the mating surfaces can adjust to each other to provide for smooth running; this type of wear can be viewed as beneficial. The film parameter will increase with running-in, since the composite surface roughness will decrease. Running-in also has a significant effect on the shape of the asperities that is not captured by the composite surface roughness. With running-in the tips of the asperities in contact become flattened and are less aggressive, also leading to less wear.

### Example 8.8: Film Parameter

**Given:** Gears for an excavator are manufactured by sand casting. The as-cast surface is measured to have a root-mean-square roughness of  $R_a = 18 \mu\text{m}$ . This high surface roughness makes the gear wear rapidly. The film thickness for the grease-lubricated gears is calculated to be  $h_{\min} = 1.6 \mu\text{m}$ .

**Find:** To what surface finish should the sand-cast gears be machined to give a film parameter of 1? What manufacturing process would you select for this application?

**Solution:** Using Eq. (8.27) while assuming that the roughnesses are equal on the two surfaces gives

$$\Lambda = \frac{h_{\min}}{\left(R_{qa}^2 + R_{qb}^2\right)^{1/2}} = \frac{h_{\min}}{R_q \sqrt{2}}.$$

Solving for  $R_q$ ,

$$R_q = \frac{h_{\min}}{\Lambda \sqrt{2}} = \frac{1.6}{1 \sqrt{2}} = 1.131 \mu\text{m}.$$

Recall from Eq. (8.3) that  $R_q/R_a$  is around 1.11 for a sinusoidal distribution, and this will be assumed here to obtain an estimate of required centerline average roughness. Therefore, the surface finish needs to be around  $R_a = 1.131/1.11 = 1.02 \mu\text{m}$ . Figure 8.2 shows that for a surface roughness of  $1 \mu\text{m}$ , grinding is the fastest and cheapest method of achieving these surface finishes (honing does not apply to gear geometries). Smoother surfaces can be manufactured by electropolishing, polishing, and lapping, but these processes are considerably more expensive.

### 8.7.2 Boundary Lubrication

In **boundary lubrication**, the solids are not separated by the lubricant, thus, fluid film effects are negligible and there is significant asperity contact. The nature of surface contact is governed by the physical and chemical properties of thin surface films of molecular proportions. The properties of the bulk lubricant are of minor importance, and the coefficient of friction is essentially independent of fluid viscosity. The frictional characteristics are determined by the properties of the solids and the lubricant film at the common interfaces. The surface films vary in thickness from 1 to 10 nm, depending on the lubricant's molecular size.

Figure 8.14 illustrates the film conditions existing in fluid film and boundary lubrication. The surface slopes and film thicknesses in this figure are greatly distorted for purposes of illustration. To scale, real engineering surfaces would appear



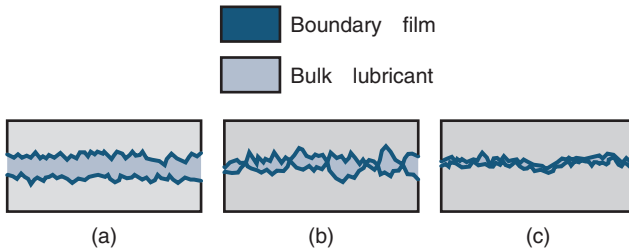


Figure 8.14: Regimes of lubrication. (a) Fluid film lubrication – surfaces completely separated by bulk lubricant film. This regime is sometimes further classified as thick or thin film lubrication. (b) Partial lubrication – both bulk lubricant and boundary film play a role. (c) Boundary lubrication – performance depends essentially on a boundary film.

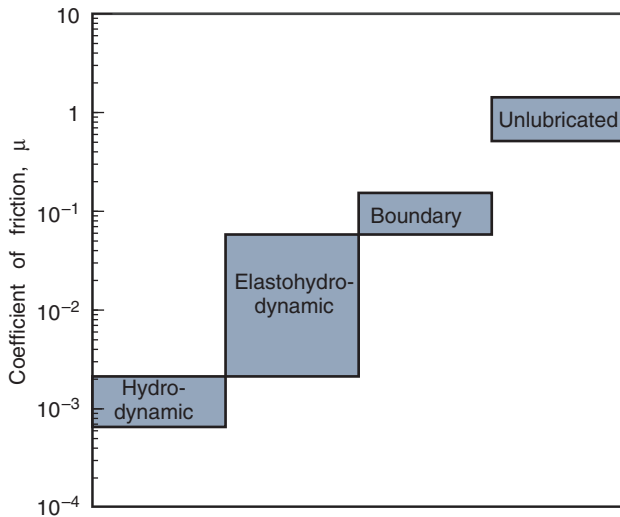


Figure 8.15: Bar diagram showing coefficient of friction for various lubrication conditions. *Source:* Hamrock et al. [2004].

as gently rolling hills with almost imperceptible topography rather than sharp peaks. The surface asperities are not in contact for fluid film lubrication but are in contact for boundary lubrication.

Figure 8.15 shows the behavior of the coefficient of friction in the different lubrication regimes. In boundary lubrication, although the friction is much higher than in the hydrodynamic regime, it is still much lower than for unlubricated surfaces. The mean coefficient of friction increases a total of three orders of magnitude in transitioning from the hydrodynamic to the boundary regime.

Figure 8.16 shows the wear rate in the various lubrication regimes as determined by the operating load. In the hydrodynamic and elastohydrodynamic regimes, there is little or no wear because there is no asperity contact. In the boundary lubrication regime, the degree of asperity interaction and the wear rate increase as the load increases. The transition from boundary lubrication to an unlubricated condition is marked by a drastic change in wear rate. As the relative load is increased in the unlubricated regime, the wear rate increases until scoring or seizure occurs and the machine element can no longer operate successfully. Most machine elements cannot operate long with unlubricated surfaces. Figures 8.15 and 8.16 show that the friction and wear of unlubricated ma-

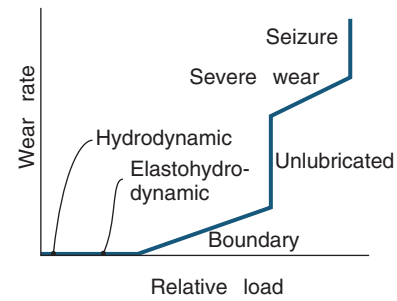


Figure 8.16: Wear rate for various lubrication regimes.

chine element surfaces can be greatly decreased by providing boundary lubrication. Effective boundary lubrication is achieved by lubricant chemistry, usually by including alcohols or fatty acids to the lubricant that attach to and protect metal surfaces, or by providing compounds that develop protective coatings. Boundary lubricants are tailored for particular materials, so that a formulation for steel sliding against steel cannot always be used for bronze sliding against steel. Indeed, additives in such a lubricant may be benign with respect to steel but corrosive to bronze, and would therefore shorten life.

Boundary lubrication is used for machine elements with heavy loads and low running speeds, where it is difficult to achieve fluid film lubrication. In addition, all machine elements encounter boundary lubrication at startup. Mechanisms such as door hinges operate under boundary lubrication conditions; other boundary lubrication applications are those where low cost is of primary importance, such as in rubbing sleeve bearings.

### 8.7.3 Partial Lubrication

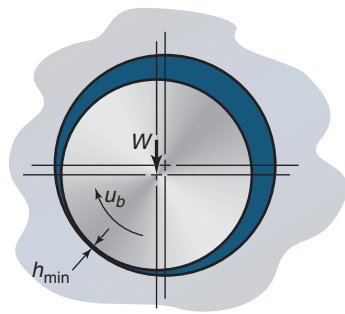
If the pressures in lubricated machine elements are too high or the running speeds are too low, the lubricant film will be penetrated. Some contact will then take place between the asperities, and **partial lubrication** (sometimes called **mixed lubrication**) will occur. The behavior of the conjunction in a partial lubrication regime is governed by a combination of boundary and fluid film effects. Interaction takes place between one or more molecular layers of boundary lubricating films, and, at the same time, a partial fluid film lubrication action develops between the solids. The average film thickness in a partially lubricated conjunction is typically between 0.001 and 1  $\mu\text{m}$ .

Since some load is transferred between contacting asperities, it is essential that a lubricant for partial lubrication incorporate chemical additives just as if it were to be used for a boundary lubrication circumstance. Thus, the concerns mentioned above regarding formulation apply for partial lubrication as well.

It is important to recognize that the transition from boundary to partial lubrication does not take place instantaneously as the severity of loading is increased, but rather a decreasing proportion of the load is carried by pressures within the fluid that fills the space between the opposing solids. As the load increases, a larger part of the load is supported by the contact pressure between the asperities of the solids.

### 8.7.4 Hydrodynamic Lubrication

**Hydrodynamic lubrication (HL)** generally occurs with conformal surfaces lubricated by a viscous fluid. A positive



Conformal surfaces

$p_{\max} \sim 5 \text{ MPa}$

$h_{\min} = f(W, u_b, \eta_0, R_x, R_y) > 1 \mu\text{m}$

No elastic effect

Figure 8.17: Characteristics of hydrodynamic lubrication.

pressure develops in a hydrodynamically lubricated journal or thrust bearing because the bearing surfaces converge and their relative motion and the viscosity of the fluid develop a lubricant film that separates the surfaces. The existence of this positive pressure implies that a normal applied load may be supported. The magnitude of the pressure developed (usually less than 5 MPa) is not generally high enough to cause significant elastic deformation of the surfaces.

The minimum film thickness in a hydrodynamically lubricated bearing is a function of normal applied load,  $W$ , velocity,  $u_b$ , lubricant absolute viscosity,  $\eta_0$ , and geometry ( $R_x$  and  $R_y$ ). Figure 8.17 summarizes some of these characteristics of hydrodynamic lubrication. The minimum film thickness,  $h_{\min}$ , as a function of entraining speed,  $u_b$ , and applied load,  $W$ , for sliding motion is given as

$$(h_{\min})_{\text{HL}} \propto \left(\frac{u_b}{W}\right)^{\frac{1}{2}} \quad (8.28)$$

In practice, the minimum film thickness normally exceeds  $1 \mu\text{m}$ .

In hydrodynamic lubrication, the films are generally thick, so that opposing solid surfaces are prevented from coming into contact. This condition is often called the ideal form of lubrication because it provides low friction and very low wear. Lubrication of the solid surfaces is governed by the bulk physical properties of the lubricant, notably the viscosity; the frictional characteristics arise purely from the shearing of the viscous lubricant.

For a normal load to be supported by a bearing, positive pressure profiles must be developed over the bearing length. Figure 8.18 illustrates three ways of developing positive pressure in hydrodynamically lubricated bearings. For positive pressure to be developed in a **slider bearing** (Fig. 8.18a and Section 12.3) the lubricant film thickness must be decreasing in the sliding direction. In a **squeeze film bearing** (Fig. 8.18b and Section 12.5) the bearing surfaces approach each other with velocity,  $w_a$ , providing a valuable cushioning effect; positive pressures will be generated only when the film thickness is diminishing. In an **externally pressurized bearing**, sometimes called a *hydrostatic bearing* (Fig. 8.18c and Section 12.6), the pressure inside the bearing supports the load. The load-carrying capacity is independent of bearing motion and lubricant viscosity. A main advantage of these bearings is the absence of wear at startup as there is with a slider bearing.

## 8.7.5 Elastohydrodynamic Lubrication

**Elastohydrodynamic lubrication (EHL)** is a form of hydrodynamic lubrication where elastic deformation of the surfaces becomes significant. Often, EHL is called a “condition”, and not a “regime” of lubrication, although it is included here because of its importance to machine elements. Historically, EHL may be viewed as one of the major developments in machine design theory of the 20th century. An increased understanding of EHL has led to dramatic performance improvements in machinery of all types. The important features in a hydrodynamically lubricated slider bearing, namely converging film thickness, sliding motion, and a viscous fluid between the surfaces, are also important for EHL. EHL is normally associated with nonconformal surfaces and fluid film lubrication. There are two distinct forms: hard and soft EHL.

**Hard EHL** relates to materials of high elastic modulus, such as metals and ceramics. In this form of lubrication, elastic deformation and pressure-viscosity effects are both important. Figure 8.19 gives the characteristics of hard elastohydrodynamically lubricated conjunctions. The maximum pressure is typically between 0.5 and 4 GPa; the minimum film thickness normally exceeds  $0.1 \mu\text{m}$ . These conditions are dramatically different from those found in a hydrodynamically lubricated conjunction summarized in Fig. 8.17. At loads normally experienced in nonconformal machine elements, the elastic deformations are two orders of magnitude larger than the minimum film thickness. Furthermore, the lubricant viscosity can vary by as much as 20 orders of magnitude within the lubricated conjunction. The minimum film thickness is a function of the same parameters as for hydrodynamic lubrication (Fig. 8.17) but with the additions of the effective elastic modulus,  $E'$ , and the pressure-viscosity coefficient,  $\xi$ , of the lubricant. Engineering applications where hard EHL is important include gears (Ch. 14 and 15) and rolling-element bearings (Ch. 13).

**Soft EHL** relates to materials of low elastic modulus, such as rubber and polymers. Figure 8.20 summarizes the characteristics of soft EHL. In soft EHL, the elastic distortions are large, even with light loads. The maximum pressure for soft EHL is 0.5 to 4 MPa (typically 1 MPa), in contrast to 0.5 to 4 GPa (typically 1 GPa) for hard EHL. This low pressure has a negligible effect on the viscosity variation throughout the conjunction. The minimum film thickness is a function of the same parameters as in hydrodynamic lubrication with the addition of the effective elastic modulus. The minimum film thickness for soft EHL is typically  $1 \mu\text{m}$ . Engineering applications where EHL is important for low-elastic-modulus materials include seals, natural human joints, and a number of lubricated machine elements that use rubber as a material. The common features of hard and soft EHL are that the local elastic deformation of the solids provides coherent fluid

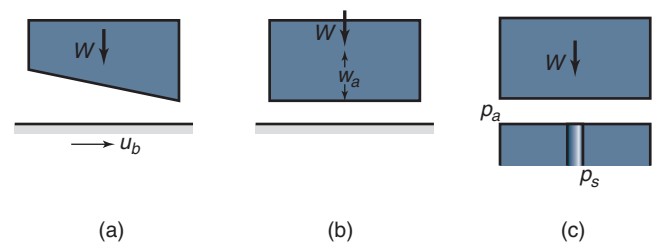
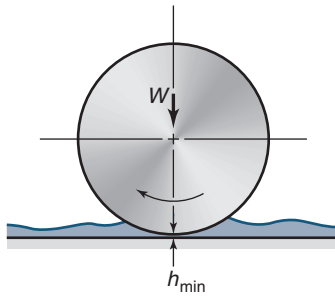


Figure 8.18: Mechanisms of pressure development for hydrodynamic lubrication. (a) Slider bearing; (b) squeeze film bearing; (c) externally pressurized bearing. Source: Hamrock et al. [2004].

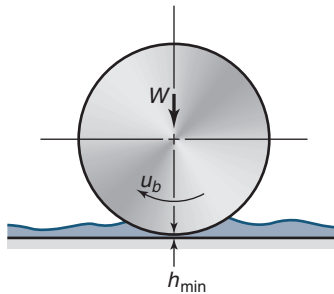
Table 8.9: Typical coefficients of friction for combinations of unlubricated metals in air.

Material	Coefficient of friction, $\mu$
<b>Self-mated metals in air</b>	
Gold	2.5
Silver	0.8-1
Tin	1
Aluminum	0.8-1.2
Copper	0.7-1.4
Indium	2
Magnesium	0.5
Lead	1.5
Cadmium	0.5
Chromium	0.4
<b>Pure metals and alloys sliding on steel (0.13% carbon) in air</b>	
Silver	0.5
Aluminum	0.5
Cadmium	0.4
Copper	0.8
Chromium	0.5
Indium	2
Lead	1.2
Copper - 20% lead	0.2
Whitemetal (tin based)	0.8
Whitemetal (lead based)	0.5
$\alpha$ -brass (copper - 30% zinc)	0.5
Leaded $\alpha/\beta$ brass (copper - 40% zinc)	0.2
Gray cast iron	0.4
Mid steel (0.13% carbon)	0.8



Nonconformal surfaces  
High-elastic-modulus material.  
(e.g., steel)  
 $\rho_{\max} \sim 0.5$  to 4 GPa  
 $h_{\min} = (W, \mu, R, R', E') > 0.1 \mu$   
Elastic & viscous effects both im

Figure 8.19: Characteristics of hard EHL.



Nonconformal surfaces (e.g., rubber)  
 $\rho_{\max} \sim 0.5$  to 4 MPa  
 $h_{\min} = (W, \mu, R, R', E') \sim 1 \mu$   
Elastic effects predominate

Figure 8.20: Characteristics of soft EHL.

films and that asperity interaction is largely prevented. Lack of asperity interaction implies that the frictional resistance to motion is due only to lubricant shearing and is therefore relatively low.

## 8.8 Friction

**Friction** is the force resisting relative movement between surfaces in contact. The two main classes of friction are sliding and rolling, as shown in Fig. 8.21. Whereas sliding surfaces are conformal, rolling friction involves nonconformal surfaces. However, most rolling contacts do experience some sliding.

In both rolling and sliding contacts, a tangential force,  $F$ , in the direction of motion is needed to move the upper body over the stationary lower body. The ratio between the tangential force and the normal applied load,  $W$ , is known as the **coefficient of friction**,  $\mu$ :

$$\mu = \frac{F}{W}. \quad (8.29)$$

Rolling and sliding friction varies from 0.001 in lightly loaded rolling-element bearings to greater than 10 for clean metals sliding against themselves in vacuum. For most common materials sliding in air, the value of  $\mu$  lies in a narrow

range from approximately 0.1 to 2.0. Table 8.9 gives typical coefficients of sliding friction for unlubricated metals in air; note that the range is 0.2 to 2.5, one order of magnitude.

### 8.8.1 Low Friction

In a number of situations low friction is desirable; for example,

1. Turbines and generators in electric or hydroelectric power stations, which use oil-lubricated hydrodynamic bearings
2. Gyroscopes, spinning at very high speeds, which use gas-lubricated hydrodynamic bearings

Friction can be reduced by using special low-friction materials, by lubricating the surface if it is not already being done, or by using clever designs that convert sliding motion into rolling. Reducing the wear and heat produced by friction are important factors in extending machine element life.

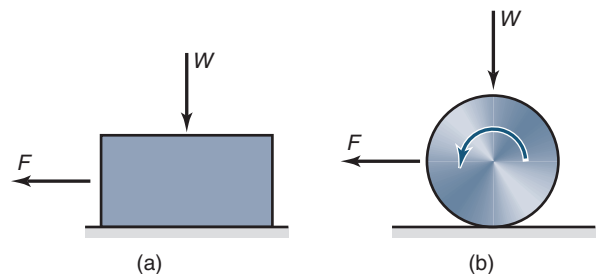


Figure 8.21: Friction force in (a) sliding and (b) rolling.

## 8.8.2 High Friction

In some situations, high friction is desirable, for example:

1. Brakes
2. Interaction between a shoe and a walking surface
3. Interaction between tire and road
4. Interaction between a nail and the wood into which it is hammered
5. Grip between a nut and a bolt

It must be emphasized that in these applications the friction must be high but controlled.

## 8.8.3 Laws of Dry Friction

The three **laws of friction** may be stated as follows:

1. The friction force is proportional to the normal load, as given by Eq. (8.29).
2. The friction force is not dependent on the apparent area of the contacting solids; that is, it is independent of the size of the solid bodies.
3. The friction force is independent of the sliding velocity.

These laws are applicable for most sliding conditions in the absence of a lubricant. The first two laws are normally called **Amonton's law**; he rediscovered them in 1699, with Leonardo da Vinci usually given the credit for discovering them some 200 years earlier.

The first two laws are found today to be generally satisfied for metals but are violated when polymers are the solid materials in contact. The third law of friction is less well founded than the first two laws. The friction force needed to begin sliding is usually greater than that necessary to maintain it. However, once sliding is established, the coefficient of friction is often nearly independent of sliding velocity.

A phenomenon important to machine element design is **stick-slip**. When stick-slip occurs, the friction force fluctuates between two extreme values. All stick-slip processes are caused by the fact that the friction force does not remain constant as a function of some other variable, such as distance, time, or velocity.

## 8.8.4 Sliding Friction of Metals

### Adhesive Friction

Bowden and Tabor [1973] recognized that surfaces in contact touch only at points of asperity interaction, and that very high stresses induced in such small areas would lead to local plastic deformation. The penetration of an asperity into the opposing surface can be likened to a miniature hardness test, and the mean normal stress over the real areas of asperity contact can be represented by the hardness,  $H$ , of the softer material. Likewise, if  $\tau$  represents the shear stress of the asperity junctions, the normal applied load is  $W$ , and the friction force is  $F$ , then the coefficient of friction  $\mu$  can be expressed as

$$\mu = \frac{F}{W} = \frac{A_r \tau}{A_r H} = \frac{\tau}{H}. \quad (8.30)$$

This expression is an important step in understanding friction, although it is incomplete because it neglects the more complex nature of asperity interactions and deformations

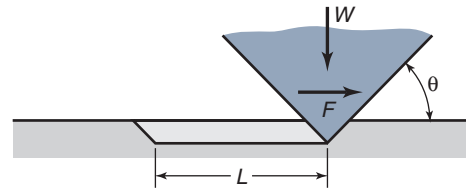


Figure 8.22: Conical asperity having mean angle  $\theta$  plowing through a softer material. Also simulates abrasive wear.

and accounts only for the adhesive element of friction. These limitations are apparent when it is recognized that for metals  $\tau \approx 0.5S_y$  and  $H \approx 3S_y$ , where  $S_y$  is the yield strength. Thus, from Eq. (8.30), all clean metals should have a coefficient of friction of  $1/6$ , which is not representative of experimental findings.

### Abrasive Friction

Another approach to friction is that a force would be required to move hard asperities through or over another surface and that the resulting microcutting motion represents a friction process. If the sum of the projected areas of the indenting asperities perpendicular to the sliding direction is  $A_o$ , and if the mean stress resisting plastic deformation of the softer material that is being cut is equal to the hardness, then the friction force,  $F$ , can be expressed as

$$F = A_o H. \quad (8.31)$$

The normal applied load,  $W$ , carried by a number of asperities can be expressed as

$$W = AH,$$

where  $A$  is the contact area. The coefficient of friction then becomes

$$\mu = \frac{F}{W} = \frac{A_o}{A}. \quad (8.32)$$

Figure 8.22 shows a conical asperity having a mean angle  $\theta$ . The coefficient of friction for this geometry is

$$\mu = \frac{A_o}{A} = \frac{2}{\pi} \tan \theta. \quad (8.33)$$

Note that only the front end of the conical asperity shown in Fig. 8.22 is in contact with the opposing surface.

### Combined Adhesion and Abrasion

If both molecular (adhesive) and deformation (plowing) mechanisms occur, the coefficient of friction is a function of both, or

$$\mu = \frac{\tau}{H} + \frac{2}{\pi} \tan \theta. \quad (8.34)$$

Experiments have demonstrated that the adhesion term [first term on the right side of Eq. (8.34)] plays a major role in determining the friction between metals. The abrasive term is dominant when there is a significant hardness mismatch between the materials in contact. In any case, both adhesive and abrasive contributions to friction are always present, and their isolation is difficult, so that a single friction coefficient is usually reported for a material pair.



### 8.8.5 Sliding Friction of Polymers

The coefficient of friction is usually lower for machine elements made of polymers, such as polyethylene, acrylics, polystyrene, and nylon, than for those made of metals. For clean copper on steel, the coefficient of friction is 1.0, but for most plastics it is typically 0.3 or so. Coefficients of friction in sliding contact, as measured experimentally, vary from as low as 0.02 to 100 or even higher. This is not surprising, in view of the many variables involved in friction.

One major difference between the frictional behavior of polymers and metals is the effect of load and geometry. Geometry refers to the shape of the surfaces, whether they are flat or curved and, if they are curved, how sharp the curvature is. With metals, the area of *true* contact is determined only by the load and the yield pressure and not by the shape of the surfaces. Polymers deform viscoelastically, implying that deformation depends on the normal applied load,  $W$ , the geometry, and the time of loading. For a fixed time of loading and fixed geometry, for example, a sphere on a flat surface, the area of true contact is not proportional to the load as it is with metals, but is proportional to  $W^n$ , where  $n$  is less than 1 and usually near  $3/4$ . Therefore,

$$F \propto W^{3/4} \quad \text{for polymers} \quad (8.35)$$

$$F \propto W \quad \text{for metals} \quad (8.36)$$

and the difference in friction behavior is quite significant.

### 8.8.6 Sliding Friction of Rubber

Rubber is an extreme example of an elastic material that can achieve large deformations. Regardless of the amount that rubber becomes distorted, it will return to its original shape when the deforming force is removed, as long as the rubber is not torn or cut. Not surprisingly, the friction of rubber often deviates significantly from the laws of friction developed for metals. The friction depends on the load and the geometry of the contacting surfaces.

For rubber, the relationship between friction force and the normal applied load is

$$F \propto W^{2/3}. \quad (8.37)$$

Rubber is truly an elastic solid and this relationship is valid over a wide load range.

## 8.9 Wear

**Wear** has long been recognized as very important and is usually considered detrimental in machine elements. In a more general sense, practically everything wears out, yet the fundamental actions that govern the process remain elusive. In fact, it remains true that today's engineer is better equipped to design a machine element to withstand known loads than to predict a given life of the machine element.

Wear is the progressive loss of material from the operating surface of a body occurring as a result of loading and relative motion at the surface. Wear can be classified by the physical nature of the underlying process, such as abrasion, adhesion, and fatigue. These three main types of wear are considered in this section. Other types of wear, such as erosion, fretting, and corrosion, are beyond the scope of this text.

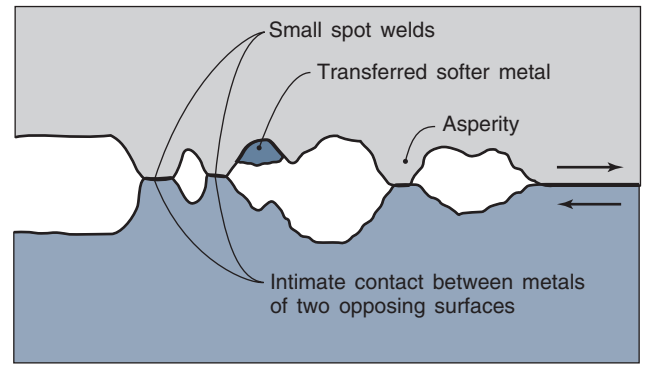


Figure 8.23: Adhesive wear model.

### 8.9.1 Adhesive Wear

Figure 8.23 shows the mechanism of **adhesive wear**, where material is transferred from one surface to the other by solid-phase welding. Adhesive wear is the most common type of wear and the least preventable. Observe from Fig. 8.23 that, as the moving asperities pass each other, the microscopic weld breaks and, unless the fracture occurs on the original interface, material is removed from one surface or the other. Usually, the surface having the lower strength loses material.

The volume of material removed by wear,  $v$ , is directly proportional to the sliding distance,  $L$ , and the normal applied load,  $W$ , and is inversely proportional to the hardness,  $H$ , of the softer of the two materials, or

$$v \propto \frac{WL}{H}. \quad (8.38)$$

After a dimensionless adhesive wear coefficient,  $k_1$ , is introduced, Eq. (8.38) becomes

$$v = k_1 \frac{WL}{3H}. \quad (8.39)$$

Equation (8.39) is known as the **Archard wear law**. The dimensionless adhesive wear coefficient,  $k_1$ , can be interpreted as a measure of the probability that any interaction between asperities of the two surfaces in contact will produce a wear particle due to any of the wear mechanisms. Thus, if  $k_1$  is 1, every junction involving surface contact will produce a wear fragment; if  $k_1 = 0.1$ , one-tenth of the contacts between surfaces will produce a wear fragment. Studies have shown that, for unlubricated surfaces, the lowest value of  $k_1$  is obtained for polyethylene sliding on steel. For this situation  $k_1 = 1 \times 10^{-7}$ , which can be interpreted as 1 in 10 million contacts will produce a wear fragment.

Table 8.10 shows some typical values of  $k_1$  for several materials in contact. As presented in Eq. (8.39), the wear volume is a function not only of  $k_1$  but also of the hardness of the softer of the two materials in contact. For example, although the *wear coefficient* for polyethylene on steel is one-tenth that for tungsten carbide sliding on itself, the *wear volume* is 10 times larger because tungsten carbide wears 10 times less than the polymer. Therefore, the volume of the wear fragments is considerably smaller because tungsten is several orders of magnitude harder than polyethylene.

Table 8.10 also gives the coefficient of friction. The wear constant varies by eight orders of magnitude for the various rubbing materials, but the coefficient of friction varies by only one order of magnitude. To understand why the wear constant varies so much more than the friction coefficient, consider the case of steel sliding against steel. At low loads and



Table 8.10: Coefficients of rubbing friction and adhesive wear constant for nine rubbing materials.

Rubbing materials	Coefficient of friction, $\mu$	Adhesive wear coefficient, $k_1$
Gold on gold	2.5	0.1-1
Copper on copper	1.2	0.01-0.1
Mild steel on mild steel	0.6	$10^{-2}$
Brass on hard steel	0.3	$10^{-3}$
Lead on steel	0.2	$2 \times 10^{-5}$
Polytetrafluoroethylene (teflon) on steel	0.2	$2 \times 10^{-5}$
Stainless steel on hard steel	0.5	$2 \times 10^{-5}$
Tungsten carbide on tungsten carbide	0.35	$10^{-6}$
Polyethylene on steel	0.5	$5 \times 10^{-8}$

speeds, wear is low, and contact occurs at oxide-covered asperities. The oxides prevent gross adhesion, and the wear particles are generally observed to be small black particles of iron oxide. At high loads and speeds, the oxide is penetrated or broken, and asperity contact is between the substrate materials. The microwelds at asperity surfaces are much stronger in this case, and this is reflected in the wear particles, which are typically larger and consist of metal flakes. As discussed above, it is very important that wear tests duplicate a machine element's working environment as much as is practical to obtain valuable data.

### Example 8.9: Application of the Archard Wear Law

**Given:** A journal bearing in a dam gate moves slowly and operates under a high load. The entire bearing is made of AISI 1040 steel. To increase the bearing life, a material change is considered for one of the surfaces.

**Find:** Which of the following materials will give the longest life: brass, lead, polytetrafluoroethylene (PTFE), or polyethylene? The hardness for brass is 225 MPa, for lead it is 30 MPa, for PTFE it is 50 MPa, and for polyethylene it is 70 MPa.

**Solution:** From Eq. (8.39) the wear volume is

$$v = k_1 \frac{WL}{3H}.$$

The wear volume is a minimum when  $H/k_1$  is a maximum. Making use of Table 8.10 to obtain the wear coefficient for the materials being considered gives

Brass:

$$\frac{H}{k_1} = \frac{225 \times 10^6}{10^{-3}} = 225 \text{ GPa.}$$

Lead:

$$\frac{H}{k_1} = \frac{30 \times 10^6}{(2 \times 10^{-5})} = 1500 \text{ GPa.}$$

PTFE:

$$\frac{H}{k_1} = \frac{50 \times 10^6}{(2 \times 10^{-5})} = 2500 \text{ GPa.}$$

Polyethylene:

$$\frac{H}{k_1} = \frac{70 \times 10^6}{5 \times 10^{-8}} = 1,400,000 \text{ GPa.}$$

Thus, polyethylene will give much longer life than any of the other materials.

### 8.9.2 Abrasive Wear

**Abrasive wear** arises when two interacting surfaces are in direct physical contact and one is significantly harder than the other. Under a normal load the asperities of the harder surface penetrate into the softer surface, producing plastic deformation. Figure 8.22 shows a simple abrasive wear model where a hard conical asperity with slope  $\theta$  under a normal load,  $W$ , plows through the softer surface, removing material and producing a groove. The amount of material lost by abrasive wear is

$$v \approx \frac{2k_1}{\pi} \frac{\tan \theta}{H} WL = \frac{k_1 k_2 WL}{H}, \quad (8.40)$$

where  $k_1$  is an adhesive wear coefficient, given in Table 8.10, and  $k_2$  is an abrasive wear coefficient, given by

$$k_2 = \frac{2 \tan \theta}{\pi}. \quad (8.41)$$

For most asperities  $\theta$  is small, typically between  $5^\circ$  and  $10^\circ$ .

A similarity of form is evident between Eqs. (8.39) and (8.40), and it is clear that the general **laws of wear** can be stated as follows:

1. Wear increases with sliding distance.
2. Wear increases with normal applied load.
3. Wear decreases as the hardness of the sliding surface increases.

These laws, along with Eqs. (8.39) and (8.40), reveal the role of the principal variables in abrasive wear, but there are sufficient exceptions to the predicted behavior to justify a measure of caution in their use. Furthermore, wear rates, or the life of rubbing components, cannot be determined without some knowledge of the wear coefficients, which are experimentally determined.

Adhesive and abrasive wear are always present, and are difficult to isolate. For that reason, Eq. (8.40) is simplified to Eq. (8.39) and is used to quantify the combined contributions of both wear modes. Obviously, wear tests need to reproduce the application's conditions as much as is practical to obtain reasonable wear rates. The data presented in the tables in this chapter are good estimates of friction and wear coefficients encountered by machine elements, but critical designs need experimental verification.

## Design Procedure 8.1: Wear Avoidance Hierarchy

Wear is a phenomenon that commonly arises in machine elements. It should be noted that wear is not always detrimental - a running-in period, for example, consists of controlled wear that can make surfaces smoother and more conformal, and transfer loads more efficiently. Regardless, when one encounters excessive wear, the following is a reasonable hierarchy of modifications to investigate, ordered roughly in terms of decreasing cost effectiveness.

1. If a lubricant is not being used, use a lubricant if possible.
2. Follow the wear laws; that is, reduce load, decrease the sliding distance, or increase the hardness of the softer surface.
3. Substitute materials that have less propensity for adhesive wear. Consider the use of hard, chemically inert coatings that can reduce wear.
4. If wear is unavoidable, design the system so that wear does not occur on expensive and difficult-to-replace components. Instead, use pads, spacers, or other elements that wear preferentially and can be replaced at lower cost, such as brake pads bearing against a rotor (see Section 18.3).
5. If a lubricant is being used:
  - (a) Increase the film thickness by using a lubricant with a higher viscosity and/or viscosity pressure coefficient when possible.
  - (b) Make the surfaces smoother so that the film parameter is increased and more load is carried by the lubricant than asperities.
  - (c) If the application encounters boundary lubrication, make certain the lubricant contains effective chemical additives, but that their concentration is not so high as to cause corrosion.
  - (d) Make certain that excessive temperatures are not encountered; use chillers or heat exchangers to maintain lubricant temperature at reasonable levels.

### 8.9.3 Fatigue Wear

For nonconformal contacts in such machine elements as rolling-element bearings, gears, friction drives, cams, and tappets, a prevalent form of failure is **fatigue wear**. Fatigue wear will form the basis of mathematical models that describe the useful life of rolling element bearings (see Section 13.9) and gears (see Section 14.12), and will be discussed in greater detail later. In this section, a brief introduction to fatigue wear mechanisms is given.

In **fatigue wear**, the removal of material results from a complicated process driven by a cyclic load. Figure 8.24 illustrates the stresses developed on and below the surface that deform and weaken the metal. Cyclic loading causes defects

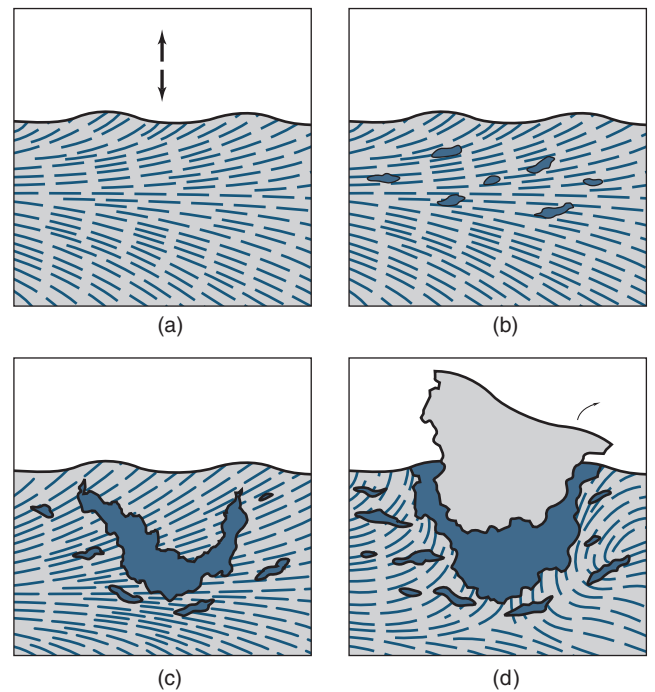


Figure 8.24: Fatigue wear simulation. (a) Machine element surface is subjected to cyclic loading; (b) defects and cracks develop near the surface; (c) the cracks grow and coalesce, eventually extending to the surface until (d) a wear particle is produced, leaving a fatigue spall in the material.

or cracks to develop below the surface. Eventually, the defects coalesce near the surface. Material at the surface then *spalls*, or is broken away, degrading the component's surface and releasing work-hardened particles that can accelerate abrasive wear. Fatigue wear occurs in nonconformal machine elements, even in well-lubricated situations.

A group of apparently identical nonconformal machine elements subjected to identical loads, speeds, lubrication, and environmental conditions may exhibit wide variation in failure times. For this reason the fatigue wear process must be treated statistically. Thus, the fatigue life of a bearing is normally defined in terms of its statistical ability to survive a certain period of time or by the allowable wear before the component ceases to function adequately. The only requirement for fatigue failure is that the surface material should be loaded. The other wear mechanisms require not only loading but also physical contact between the surfaces. If the surfaces are separated by a lubricant film, adhesive and abrasive wear are virtually eliminated, but fatigue wear can still occur.

## Case Study 8.1: Wear in Orthopedic Implants

Total joint arthroplasty has been an extremely successful procedure over the past five decades, and has seen continued technological advances and performance improvements. Examples of very successful implant designs are the total hip replacement (THR) and total knee replacement (TKR) depicted in Fig. 8.25. A wide variety of materials and designs have been used, and designs have evolved and have been discarded as new approaches have come to the fore.

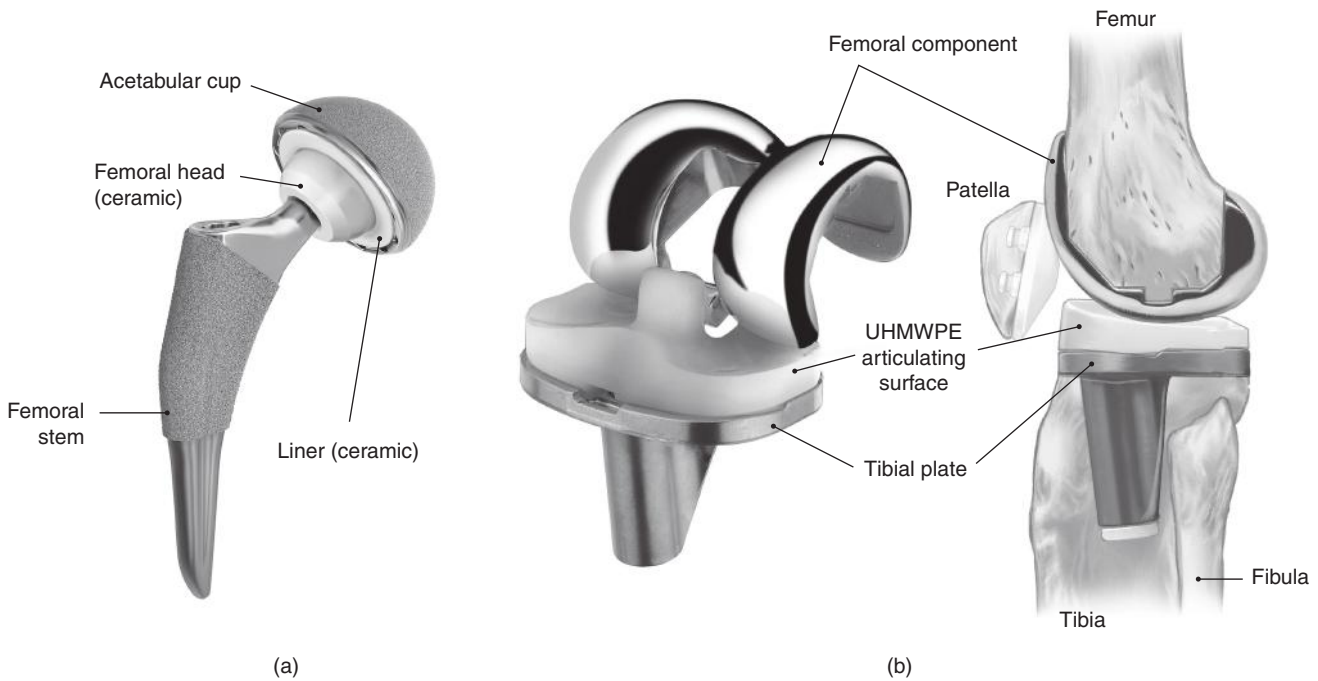


Figure 8.25: Examples of common orthopedic implants. (a) Total hip replacement, using a metal-on-metal interface. Source: Courtesy of DePuy Synthes Joint Reconstruction; (b) Total knee replacement using a metal-on-polymer interface. Source: Courtesy of Zimmer, Inc.

Selection of materials for orthopedic articulating surfaces is a difficult undertaking. In addition to the need for long life without the need of service, and the absence of effective lubrication, it is essential that the materials be biocompatible.

A number of material combinations satisfy these requirements and are used in artificial joints, with the most common involving metal (usually a cobalt-chrome alloy) on polyethylene, or metal-on-metal. For total hip replacements, ceramic-on-ceramic designs are also available, which are thought to develop significantly higher film parameters (see Section 8.7) because the polished ceramic has a much lower roughness than metal or polymer components.

It should be noted that designs have improved dramatically in the 21st century, and joint replacements that used to last an average of around seven years now routinely record average lives of twenty years or more. Material improvements continue, so that future designs will certainly outperform current technologies.

### Conventional Polymers

A large number of polymers were investigated for use in total joint replacements starting in the 1960s, with ultra-high molecular weight polyethylene (UHMWPE) proving to be most successful. This material became preferred because of its low wear rates (see Table 8.10). Not only does this have a direct impact on the life of the polymer components, but also patient comfort, since wear particles can cause inflammation, pain, and *osteolysis*, or a loss of bone. Conventional UHMWPE performed well, but researchers identified a number of concerns, including:

- The manufacture and sterilization of UHMWPE led to the formation of free radicals (unbonded ends of polymer chains). Such free radicals led to oxidation, embrittlement, and higher wear rates.

- Loads from common activities such as walking or climbing stairs causes an unsteady load on the implants. The high-load stance phase of walking occurs in one direction of sliding, and the low-load swing stage occurs over an arc of motion.

It was found that the stance phase of walking led to orientation of UHMWPE crystals in the surface and near-surface, so that the crystals aligned with the sliding direction. Sliding from the swing phase is oblique to this orientation, and the wear associated with the low load swing phase was surprisingly high.

### Crosslinked Polyethylene

In the 1990s, it was found that the developments of cross-links in the polyethylene molecule can arrest crystal orientation and therefore significantly reduce the detrimental wear associated with the swing stage of walking. Technologies to develop large numbers of cross-links in UHMWPE were developed, resulting in dramatic increases in implant lives.

Cross-linked UHMWPE could not be introduced into orthopedic implants until approved by regulatory agencies such as the Food and Drug Administration in the United States. Approval of new materials can be a lengthy, involved, and expensive process, but for cross-linked UHMWPE the process required demonstration of benefits through wear testing in joint simulators. Joint simulators are elaborate devices that closely match biomechanical forces and sliding velocities. However, evaluation of a material requires between six and nine months of continuous testing. Since there were a number of manufacturing process variables that could affect the performance of cross-linked UHMWPE, accelerated wear tests were conducted using a pin-on-flat configuration.

These tests served to screen materials so that only the most favorable were tested in the expensive and time-consuming joint simulators. Wear coefficients measured in these experiments are used to estimate the life of implants from the Archard equation (see Section 8.9).

### Avoidance of Oxidation

As mentioned above, free radicals produced during sterilization of the UHMWPE led to oxidation and associated embrittlement of the polymer. Once this failure mode was identified, it became necessary to modify implant storage procedures; by packaging and storing the implants in a vacuum, oxygen could not bond at the free radical sites and the UHMWPE did not encounter embrittlement. Note that inside the body, there are no free oxygen molecules in the implant environment, so that embrittlement after placement in the body is not a concern. Recent efforts have focused upon blending or infiltrating UHMWPE with antioxidants, notably vitamin E, to prevent oxidation at free radicals.

### Summary

Material advances continue at a rapid pace, and implant designs that exploit new materials continue to be developed. For example, the low wear rates associated with new materials allow implant designers to produce smaller implants that are easier to place in the body. Further, larger radii can be pursued for total joint replacements so that the Hertz contact stresses are lower, dislocation of the implant is less likely, and larger lubricant films can be entrained. Such designs require high wear resistance in the interface materials because the sliding distance is larger. For example, in normal walking, the swing angle of the legs is fixed, so that the sliding distance encountered by a total hip replacement is directly proportional to the head radius. Larger heads result in proportionately larger sliding distances, as shown by Eq. (8.39). However, a decrease in the wear coefficient can still result in longer implant lives. Exciting designs are continually being introduced, but all require tribological sophistication.

## 8.10 Summary

In this chapter, conformal and nonconformal surfaces were defined. Conformal surfaces fit snugly into each other with a high degree of geometric conformity so that the load is carried over a relatively large area, and the area remains essentially constant as the load is increased. Nonconformal surfaces do not geometrically conform to each other and have small load-carrying areas that enlarge with increasing load but are still small relative to those of conformal surfaces.

A lubricant's physical and chemical actions within a lubricated conjunction were described for the four lubrication regimes: hydrodynamic, elastohydrodynamic, partial, and boundary. Hydrodynamic lubrication is characterized by conformal surfaces, where the lubricating film is thick enough to prevent the opposing solids from coming into contact. Three modes of pressure development within hydrodynamic lubrication were presented: slider, squeeze, and external pressurization.

Elastohydrodynamic lubrication (EHL) is characterized by nonconformal surfaces, without asperity contact of the solid surfaces. Two modes of EHL exist: hard and soft. Hard EHL typically occurs with metals, and soft EHL with elastomeric materials. The pressures developed in hard EHL are

high (typically between 0.5 and 4 GPa), so that elastic deformation of the solid surfaces becomes important, as do the pressure-viscosity effects of the lubricant.

In boundary lubrication, considerable asperity contact occurs, and the lubrication mechanism is governed by the physical and chemical properties of thin surface films that are of molecular size (from 1 to 10 nm). Partial or mixed lubrication is governed by a mixture of boundary and fluid film effects. Most of the scientific unknowns lie in this lubrication regime.

Features of rolling and sliding friction were presented, as well as the laws of friction. The coefficient of friction was defined as the ratio of the friction force to the normal applied load. Sliding friction of metals, polymers, plastics, and rubber was also discussed.

The useful life of engineering machine components is limited by breakage, obsolescence, and *wear*. Wear is the progressive loss of substance from the operating surface of a body occurring as a result of loading and relative motion at the surface. The most common forms of wear were discussed:

1. In adhesive wear, material transfers from one surface to another due to solid-phase welding.
2. In abrasive wear, material is displaced by hard particles.
3. In fatigue wear, material is removed by cyclic stress variations even though the surfaces may not be in contact.

## Key Words

**abrasive wear** wear caused by physical damage from penetration of a hard surface into a softer one

**absolute viscosity** shear stress divided by shear strain rate, having SI units of Pascal-second

**adhesive wear** wear caused by solid-state weld junctions of two surfaces

**boundary lubrication** lubrication condition where considerable asperity interaction occurs between solids and lubrication mechanism is governed by properties of thin surface films that are of molecular proportion

**centerline average roughness** a measure of roughness, denoted by  $R_a$ , defined by the mean distance of a surface from its mean line

**conformal surfaces** surfaces that fit snugly into each other with high degree of conformity as in journal bearings

**elastohydrodynamic lubrication** a lubrication condition where nonconformal surfaces are completely separated by lubricant film and no asperities are in contact

**ellipticity parameter** diameter of contact ellipse in  $y$ -direction divided by diameter of contact ellipse in  $x$ -direction

**fatigue wear** wear caused by propagation of subsurface damage to surface due to cyclic loading

**film parameter** minimum film thickness divided by composite surface roughness

**fluid film lubrication** lubrication condition where lubricated surfaces are completely separated by a lubricant film and no asperities are in contact



## Recommended Readings

**friction** force resisting relative movement between surfaces in contact

**hydrodynamic lubrication** fluid film lubrication of conformal surfaces as in journal bearings

**kinematic viscosity** absolute viscosity divided by density, with SI units of meter squared per second

**laws of friction** These can be summarized as:

1. Friction force is proportional to normal load.
2. Friction force is not dependent on apparent area of contact solids; that is, it is independent of size of solid bodies.
3. Friction force is independent of sliding velocity.

**laws of wear** These can be summarized as:

1. Wear increases with sliding distance.
2. Wear increases with normal applied load.
3. Wear decreases as hardness of sliding surface increases.

**lubricant** any substance that reduces friction and wear and provides smooth running and satisfactory life for machine elements

**mixed lubrication** same as partial lubrication

**nonconformal surfaces** surfaces that do not conform to each other very well as in rolling-element bearings

**partial lubrication** lubrication condition where the load between two surfaces in contact is transmitted partially through lubricant film and partially through asperity contact

**root-mean-square roughness** a measure of roughness, denoted by  $R_q$ , defined by the standard deviation of a surface from its mean line

**running-in** process through which beneficial wear causes surfaces to adjust to each other and improve performance

**tribology** study of lubrication, friction, and wear of moving or stationary parts

**wear** progressive loss of substance from operating surface of body occurring as a result of loading and relative motion of surface

## Summary of Equations

**Surface Roughness:**

$$R_a = \frac{1}{N} \sum_{i=1}^N |z_i|$$

$$R_q = \left( \frac{1}{N} \sum_{i=1}^N z_i^2 \right)^{\frac{1}{2}}$$

**Hertzian Contact:**

General:

$$\text{Effective elastic modulus: } E' = \frac{2}{\frac{(1 - \nu_a^2)}{E_a} + \frac{(1 - \nu_b^2)}{E_b}}$$

Elliptical contact:

$$\text{Curvature sum: } \frac{1}{R} = \frac{1}{R_x} + \frac{1}{R_y}$$

$$\text{Radius ratio: } \alpha_r = \frac{R_y}{R_x}$$

$$\text{Ellipticity parameter: } k_e = \frac{D_y}{D_x} = \alpha_r^{2/\pi}$$

$$\text{Maximum contact pressure: } p_{\max} = \frac{6W}{\pi D_x D_y}$$

$$\text{Contact dimensions: } D_y = 2 \left( \frac{6k_e^2 \mathcal{E} W R}{\pi E'} \right)^{\frac{1}{3}},$$

$$D_x = 2 \left( \frac{6 \mathcal{E} W R}{\pi k_e E'} \right)^{\frac{1}{3}}$$

Maximum elastic deformation:

$$\delta_{\max} = \mathcal{F} \left[ \frac{9}{2 \mathcal{E} R} \left( \frac{W}{\pi k_e E'} \right)^2 \right]^{\frac{1}{3}}$$

Rectangular contact:

$$\text{Dimensionless load: } W' = \frac{w'}{E' R_x}$$

$$\text{Contact semiwidth: } b^* = R_x \left( \frac{8W'}{\pi} \right)^{\frac{1}{2}}$$

$$\text{Maximum contact pressure: } p_{\max} = E' \left( \frac{W'}{2\pi} \right)^{\frac{1}{2}}$$

Maximum elastic deformation:

$$\delta_{\max} = \frac{2W' R_x}{\pi} \left[ \ln \left( \frac{2\pi}{W'} \right) - 1 \right]$$

**Lubricant Rheology:**

$$\text{Viscosity: } \eta = \frac{F/A}{u_b/h} = \frac{\text{Shear stress}}{\text{Shear strain rate}}$$

$$\text{Barus Law: } \eta = \eta_o \exp(\xi p)$$

$$\text{Viscosity of SAE oils: } \eta = C_1 \exp \left( \frac{C_2}{1.8t_c + 127} \right)$$

$$\text{Film Parameter: } \Lambda = \frac{h_{\min}}{\left( R_{qa}^2 + R_{qb}^2 \right)^{\frac{1}{2}}}$$

$$\text{Coefficient of Friction: } \mu = \frac{F}{W}$$

$$\text{Archard wear law: } v = k_1 \frac{WL}{3H}$$

## Recommended Readings

- Bhushan, B. (2002) *Introduction to Tribology*. John Wiley & Sons.
- Bhushan, B., ed. (2001) *Modern Tribology Handbook*. CRC Press.
- Dowson, D. (1998) *History of Tribology*, 2nd ed., Professional Engineering Publishing.
- Hamrock, B.J., Schmid, S.R., and Jacobson, B.O. (2004) *Fundamentals of Fluid Film Lubrication*, 2nd ed., Marcel-Dekker.
- Johnson, K.L. (1985) *Contact Mechanics*, Cambridge University Press.
- Ludema, K. (1996) *Friction, Wear, Lubrication: A Textbook in Tribology*, CRC Press.
- Szeri, A.Z. (2011) *Fluid Film Lubrication*, 2nd ed, Cambridge University Press.
- Stolarski, T.A. (2000) *Tribology in Machine Design*. Butterworth Heineman.
- Williams, J. (2005) *Engineering Tribology*. Cambridge University Press.

## References

- Bowden, F.P., and Tabor, D. (1973) *Friction—An Introduction to Tribology*, Anchor Press.
- Hamrock, B.J., and Brewe, D.E. (1983) "Simplified Solution



- for Stresses and Deformations," *J. Lub. Technol.*, Vol. 105, No. 2, pp. 171–177.
- Hamrock, B.J., Schmid, S.R., and Jacobson, B.O. (2004) *Fundamentals of Fluid Film Lubrication*, 2nd ed., Marcel-Dekker.
- Hertz, H. (1881) "The Contact of Elastic Solids," *J. Reine Angew. Math.*, vol. 92, pp. 156–171.
- Jost, H.P., *Committee on Tribology Report*, Ministry of Technology, 1966.
- Kalpakjian, S., and Schmid, S.R. (2010) *Manufacturing Engineering and Technology*, 6th ed., Pearson.
- Seirig, A.S., and Dandage, S. (1982) "Empirical Design Procedure for the Thermodynamic Behavior of Journal Bearings," *J. Lubr. Tech.*, v. 104, pp. 135–148.

## Questions

- 8.1 What is tribology?
- 8.2 Describe the difference between conformal and nonconformal surfaces.
- 8.3 What is an elliptical contact?
- 8.4 What is the difference between rectangular contact and line contact?
- 8.5 Under what conditions is the ellipticity ratio less than one?
- 8.6 What are the Hertz Approximations?
- 8.7 List the regimes of lubrication.
- 8.8 What is a babbitt?
- 8.9 What is elastohydrodynamic lubrication? How is it different from hydrodynamic lubrication?
- 8.10 List the differences between hard and soft EHL.
- 8.11 In boundary lubrication, what is the value of the film parameter?
- 8.12 What are the two measures of surface roughness?
- 8.13 Explain why running-in is useful.
- 8.14 What is the coefficient of friction?
- 8.15 What are the laws of friction?
- 8.16 What is adhesive wear?
- 8.17 What is the wear coefficient?
- 8.18 How does spalling occur?
- 8.19 What polymers are useful for sleeve bearings?
- 8.20 Define the term "wear."

## Qualitative Problems

- 8.21 Give five examples of Hertzian contact.
- 8.22 Give five examples of elastohydrodynamic lubrication.
- 8.23 Without using equations, define *viscosity*.
- 8.24 Give three examples where (a) friction and (b) wear are useful. Explain your answers.

- 8.25 List the similarities and differences between abrasive and adhesive wear.
- 8.26 Explain why wear tests can have large variations in results.
- 8.27 Can the film thickness ever become negative? Explain your answer.
- 8.28 Estimate the wear rate for a pencil on paper.
- 8.29 When you write on paper with a ball point pen, a thick ink film is deposited on the paper regardless of the force used in writing. Explain why.
- 8.30 Determine which of the following contact geometries is conformal and which is nonconformal:
  - (a) Meshing gear teeth
  - (b) Ball and inner race of a ball bearing
  - (c) Journal bearing
  - (d) Railway wheel and rail contact
  - (e) Car making contact with the road
  - (f) Egg and egg cup
  - (g) Human knee
- 8.31 Describe three applications for each of the four lubrication regimes: hydrodynamic lubrication, elastohydrodynamic lubrication, boundary lubrication, and partial lubrication.
- 8.32 Plot the friction coefficient versus the adhesive wear coefficient using the data in Table 8.10. Comment on the results.
- 8.33 Show that the contact patch between two equal cylinders pressed together with their axes at right angles is approximately circular.
- 8.34 List the requirements of a lubricant.
- 8.35 It is observed that the coefficient of friction between a pad and a guideway is 0.35. To reduce friction and wet the surfaces, kerosene (a very low viscosity fluid) is applied to the interface. Instead of reducing the friction, it is now measured to be 0.38. Provide an explanation for these measurements.

## Quantitative Problems

- 8.36 A single ball rolling in a groove has a 10-mm diameter and a 10-N normal force acting on it. The ball and the groove have a 207 GPa modulus of elasticity and a Poisson's ratio of 0.3. Assuming a 6.08-mm-radius groove in a semi-infinite steel block, determine the following:
  - (a) Contact zone dimensions. *Ans.*  $D_y = 0.3056 \text{ mm}$ ,  $D_x = 0.1016 \text{ mm}$ .
  - (b) Maximum elastic deformation. *Ans.*  $\delta_{\max} = 0.7045 \mu\text{m}$ .
  - (c) Maximum pressure. *Ans.* 0.6163 GPa.

**8.37** A solid cylinder rolls with a load against the inside of an outer cylindrical race. The solid cylinder radius is 20 mm and the race internal radius is 150 mm. The race and the roller have the same axial length. What is the radius of a geometrically equivalent cylinder near a plane? The cylinder is made of silicon nitride ( $E = 314$  GPa,  $\nu = 0.26$ ) and the race is made of stainless steel ( $E = 193$  GPa,  $\nu = 0.30$ ). If the normal applied load per unit width is 10,000 N/m, determine

- (a) Contact semiwidth *Ans.*  $b^* = 46.48 \mu\text{m}$ .
- (b) Maximum surface stress *Ans.*  $p_{\max} = 137.0$  MPa.
- (c) Maximum elastic deflection *Ans.*  $\delta_{\max} = 0.3321 \mu\text{m}$ .

Also, indicate what these values would be if the silicon nitride cylinder were replaced with a stainless steel cylinder.

**8.38** A 100-mm diameter shaft has a 20-mm diameter ball rolling around the outside. Find the maximum contact stress, the maximum deflection, and the contact dimensions if the ball load is 500 N. The ball is made of silicon nitride ( $E = 314$  GPa,  $\nu = 0.26$ ), and the shaft is made of steel ( $E = 206$  GPa,  $\nu = 0.30$ ). Also, determine these values if both ball and shaft are made of steel. *Ans.* For SiN on steel,  $D_y = 6.1911 \times 10^{-4}$  m,  $D_x = 5.513 \times 10^{-4}$  m,  $p_{\max} = 2.798$  GPa.

**8.39** The ball-outer-race contact of a ball bearing has a 17-mm ball diameter, an 8.84-mm outer-race groove radius, and a 44.52-mm radius from the bearing axis to the bottom of the groove. The load on the most highly loaded ball is 10,000 N. Calculate the dimensions of the contact ellipse and the maximum deformation at the center of the contact. The race and the ball are made of steel. *Ans.*  $D_y = 6.935$  mm,  $D_x = 0.9973$  mm.

**8.40** A hydrodynamic journal bearing is loaded with a normal load  $W$  and is rotating with a surface velocity  $u_b$ . Find how much higher rotational speed the bearing needs to maintain the same minimum film thickness if the load  $W$  is doubled.

**8.41** A hydrodynamic slider bearing lubricated with a mineral oil runs at 4000 rpm. Find how much thinner the oil film will be if the load is increased by a factor of 3. How much must the speed be increased to compensate for the higher load while keeping the oil film thickness constant?

**8.42** A hydrodynamic bearing operates with a film parameter of 6. Calculate how much lower the speed has to be to decrease the film parameter to 3.

**8.43** A machined steel surface has roughness peaks and valleys. The roughness wavelength is such that 400 peaks and 400 valleys are found during one roughness measurement. Find how much the arithmetic average surface roughness  $R_a = 0.2 \mu\text{m}$  will change if one of the surface roughness peaks and one of the valleys increases from 0.25 to 2.5  $\mu\text{m}$ . *Ans.*  $0.2056 \mu\text{m}$ .

**8.44** A surface with a triangular sawtooth roughness pattern has a peak-to-valley height of 4  $\mu\text{m}$ . Find the  $R_a$  and  $R_q$  values. *Ans.*  $R_a = 1.00 \mu\text{m}$ .

**8.45** A precision ball bearing has a race root-mean-square surface roughness of 0.07  $\mu\text{m}$  and a ball root-mean-square surface roughness of 0.02  $\mu\text{m}$ . Changing the

roughness of the components may give a higher  $\Lambda$  value. Determine which components to smooth if it costs equally as much to halve the roughness of the race as it costs to halve the roughness of the balls. Note that  $h_{\min} = 0.2 \mu\text{m}$ .

**8.46** The minimum film thickness in a particular application is 10  $\mu\text{m}$ . Assume that two surface roughnesses of the two ground surfaces being lubricated are identical. What lubrication regime would you expect the application to be operating in? Also, what is the maximum surface roughness allowed to achieve hydrodynamic lubrication? What manufacturing operation would you recommend to achieve this roughness?

**8.47** Two equally rough surfaces with rms surface roughness  $R_q$  are lubricated and loaded together. The oil film thickness is such that  $\Lambda = 3$ . Find the film parameter if one of the surfaces is polished so that  $R_q \rightarrow 0$  (i.e., the surface becomes absolutely smooth). *Ans.*  $\Lambda = 2.83$ .

**8.48** Two lubricated surfaces have rms surface roughnesses  $R_q$  of 0.23 and 0.04  $\mu\text{m}$ , respectively. By using a new honing machine either surface can be made twice as smooth. For good lubrication, which surface roughness is it most important to decrease?

**8.49** The absolute viscosity of a fluid at atmospheric conditions is  $5.00 \times 10^{-3}$  kgf-s/m<sup>2</sup>. Give this absolute viscosity in

- (a) Reyn. *Ans.*  $7.110 \mu\text{reyn}$ .
- (b) Poise. *Ans.*  $0.4904$  P.
- (c) Pound force-seconds per square inch.
- (d) Newton-seconds per square meter.

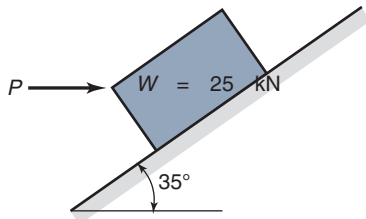
**8.50** Given a fluid with an absolute viscosity  $\eta$  between two 1-m<sup>2</sup> surfaces spaced 1 mm apart, find how fast the surfaces will move relative to each other if a 10-N force is applied in the direction of the surfaces when  $\eta$  is

- (a) 0.001 N-s/m<sup>2</sup> (water). *Ans.*  $u_b = 10$  m/s.
- (b) 0.100 N-s/m<sup>2</sup> (a thin oil at room temperature).
- (c) 10.0 N-s/m<sup>2</sup> (syrup; cold oil). *Ans.*  $u_b = 1$  mm/s.
- (d)  $10^8$  N-s/m<sup>2</sup> (asphalt).

**8.51** A polymer box stands on a slope. The box weighs 10 kg and the slope angle is 25°. To pull the box down the slope, a force  $F = 5$  N is required. The friction force is proportional to the load raised to 0.75. Find the additional weight needed in the box to make it slide down the slope. *Ans.* 5.60 kg.

**8.52** A moose suddenly jumps out onto a dry asphalt road 80 m in front of a car running at 108 km/hr. The maximum coefficient of friction between the rubber tires and the road is 1.0 when they just start to slide and 0.8 when the locked wheels slide along the road. It takes 1 s for the driver to apply the brakes after the moose jumps onto the road. Find whether the car can stop in time before it hits the moose

- (a) With locked wheels sliding along the road.
- (b) With an automatic braking system (ABS) that keeps the sliding speed so low that maximum friction is maintained.



Sketch a, for Problem 8.53

**8.53** Given a block on an incline as shown in sketch a, find the force  $P$  required

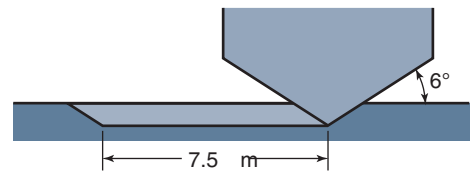
- (a) To prevent motion downward *Ans.* 9.59 kN.
- (b) To cause motion upward *Ans.* 29 kN.

The coefficient of friction is 0.25. Draw a free-body diagram for both situations showing the forces involved.

**8.54** Three equal blocks of plastic are carrying the weight of a steel slider. At first each block carries one-third of the weight, but the central block is made of polytetrafluoroethylene (PTFE) and the two outer blocks are made of polyethylene, so they have different adhesive wear constants (PTFE,  $k_1 = 2 \times 10^{-5}$ ; polyethylene,  $k_1 = 2 \times 10^{-8}$ ). Determine how the load redistributes between the blocks if the hardnesses of the plastics are assumed to be the same.

**8.55** Given the plastic blocks in Problem 8.54 and sharing the load so that the wear is equal on each block, find the coefficient of friction.

**8.56** A 50-kg copper piece is placed on a flat copper surface as shown in Sketch b. Assuming that copper has a hardness of 275 MPa, calculate the shear stress, the abrasive wear volume, and the adhesive wear volume. *Ans.*  $\tau = 312$  MPa,  $k_2 = 0.0669$ .



Sketch b, for Problem 8.56

## Design and Projects

**8.57** Design a test method for evaluating fatigue wear of rolling element bearings.

**8.58** Perform a literature search to determine if there is any relationship between friction and wear.

**8.59** Construct a Design Procedure that outlines the steps you would follow in order to (a) increase and (b) decrease friction when desired.

**8.60** Case Study 8.1 described tribological issues in total joint replacements. A new development involves *resurfacing implants*. Consult with the technical literature and manufacturer's documentation and list the advantages of resurfacing, and write a short paper on the associated tribology concerns.

**8.61** A bushing is to be selected for an application where the radial load is 350 N, the speed is 200 rpm, the mating surface is stainless steel, and a life of 3000 hours is needed. The shaft diameter is 25 mm. Select a material, and then specify the thickness and width of the bushing. Assume the maximum temperature encountered in operation is 60°C.

**8.62** Consider Eq. (8.10), and explain why the pressure distribution in an elastic solid cannot be described by

$$p_H = p_{\max} \left[ 1 - \left( \frac{2x}{D_x} \right)^3 - \left( \frac{2y}{D_y} \right)^3 \right]^{\frac{1}{2}}$$



# Part I I □ Machine Elements

## Outline

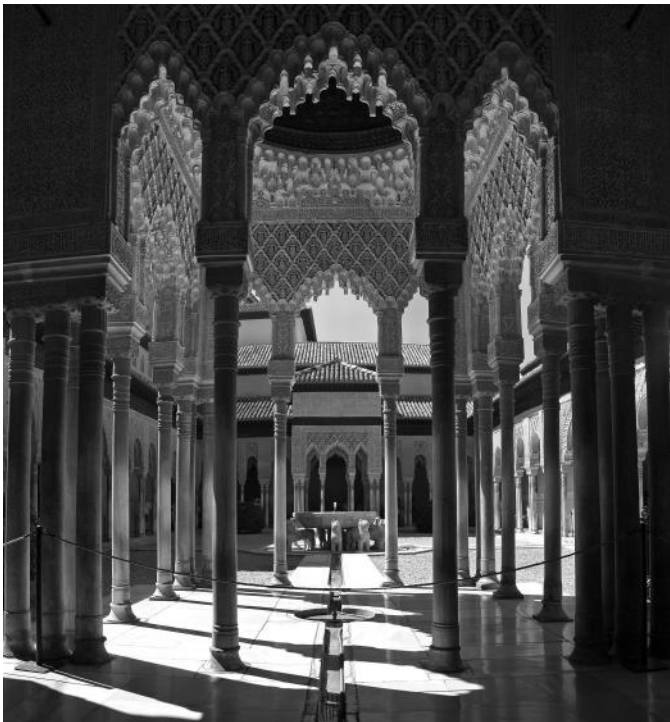
Chapter 9	Columns
Chapter 10	Stresses and Deformations in Cylinders
Chapter 11	Shafting and Associated Parts
Chapter 12	Hydrodynamic and Hydrostatic Bearings
Chapter 13	Rolling-Element Bearings
Chapter 14	General Gear Theory; Spur Gears
Chapter 15	Helical, Bevel, and Worm Gears
Chapter 16	Fasteners, Connections, and Power Screws
Chapter 17	Springs
Chapter 18	Brakes and Clutches
Chapter 19	Flexible Machine Elements

This page intentionally left blank



# Chapter 9

## Columns



Columns from the Alhambra in Granada, Spain. Source: Shutterstock.

*And as imagination bodies forth the forms of things unknown,  
The poet's pen turns them to shapes  
And gives to airy nothingness a local habitation and a name.*  
William Shakespeare, *A Midsummer Night's Dream*

### Contents

- 9.1 Introduction 228
- 9.2 Equilibrium Regimes 228
- 9.3 Concentrically Loaded Columns 229
- 9.4 End Conditions 231
- 9.5 Euler's Buckling Criterion 232
- 9.6 Johnson's Buckling Criterion 232
- 9.7 AISC Criteria 234
- 9.8 Eccentrically Loaded Columns 234
- 9.9 Summary 238

### Examples

- 9.1 Equilibrium Regimes 229
- 9.2 Material Effect on Buckling Load 231
- 9.3 Cross Section Effect on Buckling Load 233
- 9.4 Euler and Johnson Buckling 233
- 9.5 Eccentric Loading 236

### Case Study

- 9.1 Design Considerations for Lattice-Boom Cranes 237

### Design Procedure

- 9.1 Selecting a Buckling Equation 232

Compression members are widely used in machinery of all types. A column is a slender compression member that deforms laterally, or buckles, before stresses reach the yield strength of the material. In buckling, loads below a critical value can be supported, but once the critical load is exceeded, large deformations result. This chapter begins with a discussion of equilibrium regimes, in order to introduce nomenclature and concepts relevant to buckling. The classic derivation of Euler is then applied to elastically deforming columns, and so-called Euler buckling is described. For less slender columns, Johnson's buckling criterion is better suited to predict buckling loads. The American Institute of Steel Construction requirements and design methodology for compression members are then described and demonstrated. Finally, eccentric columns are investigated, where the applied load does not act through the column's centroid.

**Machine elements in this chapter:** Columns of all types; connecting rods, supports.

**Typical applications:** Lattice frameworks such as booms; machine frames; support structures; jacks and other actuators.

**Competing machine elements:** Compression springs (Chapter 17); in a general sense, beams (Chapters 4 and 5), power screws (Chapter 16).

## Symbols

$A$	cross sectional area, $m^2$
$C_c$	slenderness ratio
$C_1, C_2$	integration constants
$c$	distance from neutral axis to outer fiber of column, m
$d$	diameter, m
$E$	modulus of elasticity, Pa
$E_t$	tangent modulus, Pa
$e$	eccentricity, m
$g$	gravitational acceleration, $9.807 \text{ m/s}^2$
$h$	height, m
$I$	area moment of inertia, $m^4$
$l$	length, m
$l_e$	effective length of column, m
$M$	moment, N-m
$M'$	statically equivalent moment, N-m
$m_a$	mass, kg
$n$	an integer
$n_\sigma$	stress reduction factor in AISC criteria
$P$	force, N
$r_g$	radius of gyration, m
$S_y$	yield strength, Pa
$t$	time, s
$x$	length dimension of column, m
$y$	transverse dimension or deflection of column, m
$\theta$	position angle, deg
$\rho$	density, $kg/m^3$
$\sigma$	normal stress, Pa
$\sigma_{all}$	allowable normal stress, Pa

## Subscripts

cr	critical
$E$	Euler
$i$	inner
$J$	Johnson
$o$	outer
T	tangency point

## 9.1 Introduction

The basic understanding of loads, stresses, and deformations obtained in the preceding chapters is related here to columns. A **column** is straight and long (relative to its cross section) and is subjected to compressive, axial loads. The reason for a special consideration of columns is that failures due to yielding, determined from Eq. (4.22), and due to deformation, determined from Eq. (4.23), are not correct in predicting failures of long columns. Because of their slender shape, columns tend to deform laterally upon loading; and if the deflection becomes larger than their respective critical values, they fail catastrophically. This situation is known as **buckling**, which can be defined as a sudden large deformation of a structure due to a slight increase of the applied load, under which the structure had exhibited little, if any, deformation before this increase.

This chapter first describes the meaning of elastic stability and end conditions. It then establishes the various failure criteria for concentrically loaded columns and describes the nature of the instability that can occur, thus predicting when buckling will take place. It also establishes the failure criteria for eccentrically loaded columns, so that proper design of concentric and eccentric columns is ensured.

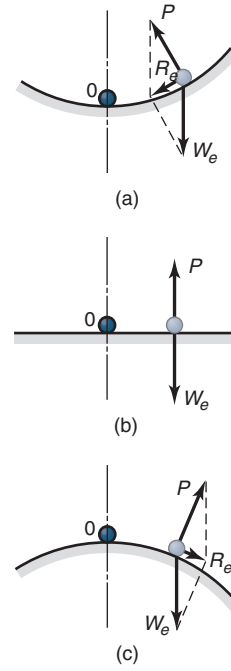


Figure 9.1: Depiction of equilibrium regimes. (a) Stable; (b) neutral; (c) unstable.

## 9.2 Equilibrium Regimes

To understand why columns buckle, it is first necessary to understand the equilibrium regimes. An important question is: When an equilibrium position is disturbed slightly, does the component tend to return to the equilibrium position or does it tend to depart even farther? To visualize what is happening, consider Fig. 9.1, which shows the three equilibrium regimes: stable, neutral, and unstable.

### 9.2.1 Stable Equilibrium

Figure 9.1a illustrates stable equilibrium. Assume that the surfaces are frictionless and that the sphere has a light weight. The forces on the sphere (gravity and normal surface reaction) are in balance whenever the surface is horizontal. The balanced position is indicated by a zero in the figure. Figure 9.1a shows the sphere displaced slightly from its equilibrium position. The forces on it no longer balance, but the resultant imbalance is a restoring force (i.e., gravity is accelerating the sphere back toward the equilibrium position). Such a situation is called *stable equilibrium*.

### 9.2.2 Neutral Equilibrium

Figure 9.1b considers the sphere in neutral equilibrium. After the sphere has been slightly displaced from the equilibrium position, it is still in equilibrium at the displaced position, and there is neither a tendency to return to the previous position nor to move to some other position. Equilibrium is always satisfied. Because the surface is flat, the sphere does not move after being placed in another position; this is *neutral equilibrium*.

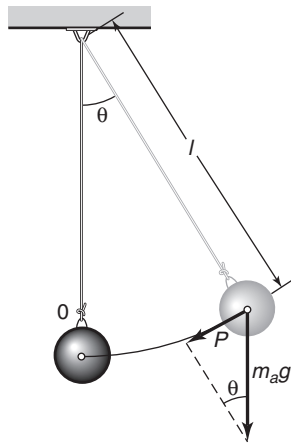


Figure 9.2: Pendulum used in Example 9.1.

### 9.2.3 Unstable Equilibrium

Figure 9.1c shows the case of unstable equilibrium, which is the opposite situation from that presented in Fig. 9.1a. When the sphere is displaced from its equilibrium position (either to the right or the left), the resultant imbalance is a disturbing force (i.e., it accelerates the sphere away from its equilibrium position). Such a situation is called *unstable equilibrium*. Gravity and convex surfaces cause the sphere to move farther from the balanced position.

Generalizing from this example, unstable equilibrium occurs if, for small displacements or *perturbations* from the equilibrium position, the disturbing forces tend to accelerate the part away from the equilibrium position. Columns in compression display unstable equilibrium and are unreliable and hazardous when overloaded; a small displacement can cause a catastrophic change in the configuration of a column. Thus, as the load on a column increases, a critical load is reached where unstable equilibrium occurs and the column will not return to its straight configuration. The load cannot be increased beyond this value unless the column is laterally restrained. Thus, for long, slender columns, a critical buckling load occurs. This critical buckling load (when divided by the cross sectional area) gives a critical buckling stress. For columns, this critical buckling stress is much lower than the yield strength of the material. Thus, columns will generally fail from buckling long before they fail from yielding.

The shape as well as the load establishes when buckling will occur. A column may be viewed as a straight bar with a large slenderness ratio,  $l/r$ , (typically 100) subjected to axial compression. Buckling occurs in such a column when it is loaded to a critical load and marked changes in deformation occur that do not result from the material yielding.

#### Example 9.1: Equilibrium Regimes

**Given:** A simple pendulum (Fig. 9.2) in which a ball is hung by a thin wire and is acted on by gravitational acceleration.

**Find:** Is the system's equilibrium neutral, stable, or unstable?

**Solution:** The force restoring the ball to the center position ( $\theta = 0$ ) is

$$P = m_a g \sin \theta. \quad (a)$$

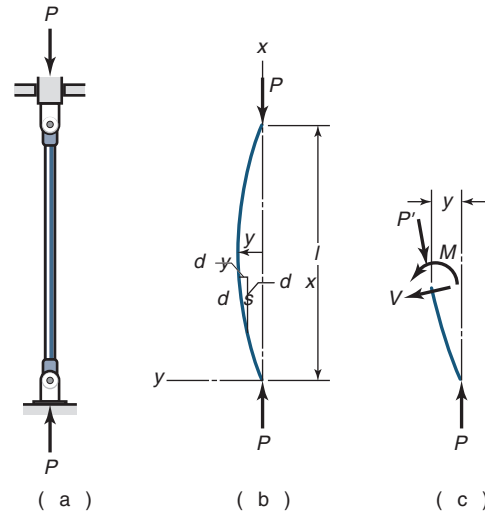


Figure 9.3: Column with pinned ends. (a) Assembly; (b) deformation shape; (c) load acting.

From simple harmonic motion

$$P = -m_a l \frac{d^2 \theta}{dt^2}. \quad (b)$$

Combining Eqs. (a) and (b) gives

$$\frac{d^2 \theta}{dt^2} = -\frac{g}{l} \sin \theta. \quad (c)$$

For any angle  $\theta$ , the angular acceleration  $d^2 \theta / dt^2$  has the opposite sign from  $\theta$  for  $-\pi \leq \theta \leq \pi$ . Thus, the ball will always return to the center position ( $\theta = 0$ ), implying that stable equilibrium prevails.

## 9.3 Concentrically Loaded Columns

### 9.3.1 Linear-Elastic Materials

Figure 9.3a shows a concentrically loaded column with pinned ends; thus, the ends are kept in position but are free to rotate. Assume that the column is initially straight and that the load is concentric; that is, it acts through the centroid as depicted in Fig. 9.3b. Figure 9.3c shows a free-body diagram of the loads acting on the column.

Equation (5.3) relates the moment and deflection as

$$M = EI \frac{d^2 y}{dx^2}. \quad (5.3)$$

Equilibrium of the section cut from the bar requires that  $M = -Py$ . Substituting this into Eq. (5.3) gives

$$\frac{d^2 y}{dx^2} + \frac{P}{EI} y = 0. \quad (9.1)$$

This is a homogeneous, second-order, linear differential equation with constant coefficients. The general solution of this

equation is

$$y = C_1 \sin \left( x \sqrt{\frac{P}{EI}} \right) + C_2 \cos \left( x \sqrt{\frac{P}{EI}} \right), \quad (9.2)$$

where  $C_1$  and  $C_2$  are integration constants. The boundary conditions are

1.  $y = 0$  at  $x = 0$ , resulting in  $C_2 = 0$
2.  $y = 0$  at  $x = l$ , so that

$$C_1 \sin \left( l \sqrt{\frac{P}{EI}} \right) = 0. \quad (9.3)$$

However,  $C_1$  cannot be equal to zero; otherwise, a trivial solution of  $y = 0$  results and the column will always remain straight, which is contrary to experience. The other possibility of satisfying Eq. (9.3) is for

$$\sin \left( l \sqrt{\frac{P}{EI}} \right) = 0, \quad (9.4)$$

which is satisfied when

$$l \sqrt{\frac{P}{EI}} = n\pi, \quad (9.5)$$

or, solving for  $P$ ,

$$P = \frac{n^2 \pi^2 EI}{l^2}, \quad (9.6)$$

where  $n$  is an integer (1, 2, ...). The smallest value of  $P$  is obtained for  $n = 1$ . Thus, the critical load,  $P_{cr}$ , for a column with pinned ends is

$$P_{cr} = \frac{\pi^2 EI}{l^2}. \quad (9.7)$$

This load is sometimes called the **Euler load**, named after the Swiss mathematician Leonhard Euler, who originally solved this problem in 1757.

An interesting aspect of Eq. (9.7) is that the critical load is independent of the material's strength, rather, it depends only on the column's dimensions (expressed in  $I$  and  $l$ ) and the material's modulus of elasticity,  $E$ . For this reason, as far as elastic buckling is concerned, long columns made, for example, of high-strength steel offer no advantage over those made of lower strength steel, since both steels have approximately the same modulus of elasticity.

Another interesting aspect of Eq. (9.7) is that the critical load capacity of a column will increase as the moment of inertia of the cross sectional area increases. Thus, columns are designed so that most of their cross sectional area is located as far as possible from the section's principal centroidal axes. This implies that a hollow tube is preferred over a solid section.

It is also important to realize that a column will buckle about the principal axis of the cross section having the least moment of inertia (the weakest axis). For example, a column having a rectangular cross section, such as a meter stick, as shown in Fig. 9.4, will buckle about the  $x$ -axis and not the  $y$ -axis.

Substituting Eq. (9.5) and  $C_2 = 0$  into Eq. (9.2) gives the buckling shape as

$$y = C_1 \sin \left( \frac{\pi x}{l} \right). \quad (9.8)$$

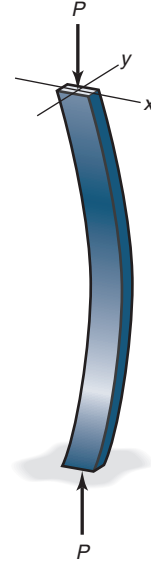


Figure 9.4: Buckling of rectangular section.

When  $x = l/2$ ,  $y = y_{\max}$  and  $C_1 = y_{\max}$ . Therefore,

$$y = y_{\max} \sin \left( \frac{\pi x}{l} \right). \quad (9.9)$$

Thus, the buckling shape varies sinusoidally, with zero at the ends and a maximum at half-length.

Engineers are often interested in defining the critical stress of a column. The radius of gyration,  $r_g$ , given in Eq. (4.14), is substituted into Eq. (9.7) giving the critical stress for the Euler equation as

$$(\sigma_{cr})_E = \frac{P_{cr}}{A} = \frac{\pi^2 E}{(l/r_g)^2}. \quad (9.10)$$

Also, the critical stress,  $\sigma_{cr}$ , is an average stress in the column just before the column buckles. This stress results in elastic strains and is therefore less than or equal to the material's yield strength.

### 9.3.2 Tangent Modulus

The preceding section determined the stress at which a column will buckle for a linear elastic material. As presented in Chapter 3, this is the case for most materials below the proportional limit. Above the proportional limit and up to the yield point the material may still be elastic, but it will not behave linearly. The effect is that the elastic modulus at the buckling stress in Eq. (9.10) may be significantly lower than one would expect from published values of elastic modulus. Equation (9.10) is often modified as

$$\sigma_{cr} = \frac{\pi^2 E_t}{(l/r_g)^2}, \quad (9.11)$$

where  $E_t$  is the **tangent modulus**, defined as the elastic modulus at the stress level in the column.

Equation (9.11) is called the **tangent modulus** or the **Engesser equation**. It is extremely difficult to apply in design, since the tangent modulus is rarely well quantified. However, it is mentioned here because of the importance of the tangent-modulus effect.

Table 9.1: Effective length for common column end conditions.

End condition description	Both ends pinned	One end pinned, one end fixed	Both ends fixed	One end fixed, one end free
---------------------------	------------------	-------------------------------	-----------------	-----------------------------

Illustration of end condition

Theoretical effective column length	$l_e = l$	$l_e = 0.7l$	$l_e = 0.5l$	$l_e = 2l$
Approximated end conditions <sup>a</sup>	$l_e = l$	$l_e = 0.8l$	$l_e = 0.65l$	$l_e = 2.1l$

<sup>a</sup> American Institute of Steel Construction, *Manual of Steel Construction*, 14th ed., [2011].

## 9.4 End Conditions

The Euler equation was developed above for columns with pinned ends, but other end constraints are possible. Table 9.1 shows four common end conditions. The Euler equation can be used for these circumstances by recognizing that end conditions change the effective length of the column. The critical load and stress given in Eqs. (9.7) and (9.10), respectively, are modified by replacing  $l$  with the effective length  $l_e$  for the corresponding end condition. Substituting  $l_e$  for  $l$  in Eqs. (9.7) and (9.10) gives

$$(P_{cr})_E = \frac{\pi^2 EI}{l_e^2}, \quad (9.12)$$

$$(\sigma_{cr})_E = \frac{(P_{cr})_E}{A} = \frac{\pi^2 E}{(l_e/r_g)^2}. \quad (9.13)$$

These equations for the critical load and stress for the Euler criterion (see Section 9.5) are valid for any end condition. Often, end conditions are not easily classified. Table 9.1 also provides recommendations from the American Institute of Steel Construction (AISC) where "ideal conditions are approximated."

### Example 9.2: Material Effect on Buckling Load

**Given:** A column has a square tubular cross section. The wall thickness is 10 mm and the column length is 12 m. The column is axially loaded in compression and has pinned ends. The mass of the tubular column must not exceed 200 kg.

**Find:** Determine which metal in Table 3.1 gives the highest buckling load; also, calculate the critical load.

**Solution:** The area of a square tubular cross section with outside dimension  $h$  is

$$A = h^2 - (h - 0.02)^2. \quad (a)$$

The mass of the column is

$$m_a = \rho A l = \rho l [h^2 - (h - 0.02)^2]. \quad (b)$$

The area moment of inertia for a square tube is

$$I = \frac{h^4 - (h - 0.02)^4}{12} = \frac{m_a [h^2 + (h - 0.02)^2]}{12\rho l}. \quad (c)$$

Substituting Eq. (c) into Eq. (9.7) gives the critical load as

$$P_{cr} = \frac{\pi^2 E m_a}{12\rho l^3} [h^2 + (h - 0.02)^2]. \quad (d)$$



Thus, the largest buckling load would result from the largest value of  $E/\rho$ . From Table 3.1, observe that magnesium would give the largest  $E/\rho$ , with  $E = 45$  GPa and  $\rho = 1740$  kg/m<sup>3</sup>. In Eq. (b), given that  $m_a = 200$  kg,  $l = 12$  m, and  $\rho = 1740$  kg/m<sup>3</sup>,

$$\frac{m_a}{\rho l} = 0.04(h - 0.01);$$

$$\frac{200}{(1740)(12)(0.04)} + 0.01 = h,$$

or  $h = 0.249$  m = 249 mm. From Eq. (d) the critical load is

$$P_{cr} = \frac{\pi^2 (45 \times 10^9) (200)}{12(1740) (12)^3} [(0.249)^2 + (0.229)^2]$$

$$= 2.82 \times 10^5$$

$$= 282 \text{ kN}.$$

## 9.5 Slenderness Ratio

As discussed above, the Euler equation holds for linear elastic materials, but this is not accurate near the yield point. The American Institute of Steel Construction [2011] assumes that the proportional limit of a material exists at one-half the yield strength, or that the allowable stress for elastic buckling is

$$\sigma_{all} = 0.5S_y, \quad (9.14)$$

where  $S_y$  is the yield strength as given in Appendix A for a variety of materials. Substituting Eq. (9.14) into Eq. (9.13) gives the **critical slenderness ratio**,  $C_c$ , from Euler's formula as

$$C_c = \left( \frac{l_e}{r_g} \right)_E = \sqrt{\frac{2E\pi^2}{S_y}}. \quad (9.15)$$

$C_c$  is called the critical slenderness ratio since it defines the applicability limit of Euler buckling. Below  $C_c$ , the tangent modulus effect will result in lower buckling stresses than predicted by the Euler equation, and a different buckling criterion must be used.

## 9.6 Johnson's Buckling Criterion

Figure 9.5 shows curves for normal stress as a function of slenderness ratio. Note the abrupt change in the Euler curve as it approaches the yield strength (see point A in Fig. 9.5), indicating a transition from buckling to compressive yielding or fracture. Because of the tangent modulus effect, the transition is not this abrupt, and the failure criterion needs to be modified at this location. Perhaps the most widely used modification is the **Johnson equation**:

$$(\sigma_{cr})_J = \frac{(P_{cr})_J}{A} = S_y - \frac{S_y^2}{4\pi^2 E} \left( \frac{l_e}{r_g} \right)^2. \quad (9.16)$$

Figure 9.5 shows the tangency point T, where the Euler and Johnson equations give the same prediction for buckling stress. This tangency point distinguishes between intermediate columns (Johnson range) and long columns (Euler range). To determine the value of  $(l_e/r_g)_T$ , Eqs. (9.13) and (9.16) are equated to yield

$$\frac{\pi^2 E}{(l_e/r_g)_T^2} = S_y - \frac{S_y^2}{4\pi^2 E} \left( \frac{l_e}{r_g} \right)_T^2;$$

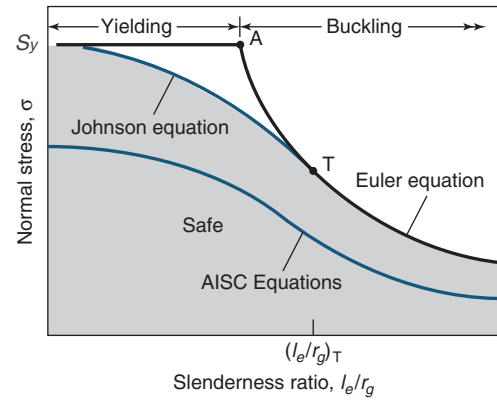


Figure 9.5: Normal stress as function of slenderness ratio obtained by Euler, Johnson, and AISC equations, as well as yield strength.

$$\left( \frac{l_e}{r_g} \right)_T^4 - \frac{4\pi^2 E}{S_y} \left( \frac{l_e}{r_g} \right)_T^2 + \frac{4\pi^4 E^2}{S_y^2} = 0. \quad (9.17)$$

Solving for  $(l_e/r_g)_T$  gives

$$\left( \frac{l_e}{r_g} \right)_T = \sqrt{\frac{2\pi^2 E}{S_y}} = \sqrt{\frac{\pi^2 EA}{P_{cr}}}. \quad (9.18)$$

## Design Procedure 9.1: Selecting a Buckling Equation

Often, one needs to design a column to support a given load, and constraints such as material, column length, etc., may be specified. It is often not clear beforehand whether a column will buckle according to the Euler or Johnson equations. The following procedure is useful in these cases:

1. Assume that the column buckles according to Eq. (9.7), or that it encounters Euler buckling. Use this equation to determine the column's geometry.
2. Calculate the critical slenderness ratio from Eq. (9.15) and (9.18), namely
$$C_c = \sqrt{2E\pi^2/S_y} = \sqrt{\pi^2 EA/P_{cr}}.$$
3. Calculate the slenderness ratio of the column from  $C = l_e/r_g$ , where  $r_g$  is given by Eq. (4.14) as  $r_g = \sqrt{I/A}$ .
4. If  $C \geq C_c$ , then the column is indeed described by the Euler equation and the cross section calculated in step 1 is applicable.
5. If  $C < C_c$ , the Johnson equation [Eq. (9.16)] must be used to determine the column geometry.

Note that an equally useful design rule can be derived where the Johnson equation is assumed to be correct, and the Euler equation is used otherwise.

### Example 9.3: Cross Section Effect on Buckling Load

**Given:** A column with one end fixed and the other free is to be made of aluminum alloy 2014. The column's cross sectional area is  $600 \text{ mm}^2$ , and its length is 2.5 m.

**Find:** The critical column buckling load for the following shapes:

- A solid round bar
- A cylindrical tube with a 50-mm outer diameter
- A square tube with a 50-mm outer dimension
- A square bar

**Solution:** From Table A.5 for aluminum alloy 2014,  $E = 72 \text{ GPa}$  and  $S_y = 97 \text{ MPa}$  (the O condition – annealed – is assumed). From Table 9.1 for one end fixed and one end free, the theoretical effective column length is  $l_e = 2l = 5 \text{ m}$ . Note that the approximated end conditions could be used to obtain a conservative result, but it will be assumed that the end conditions are well characterized, so that the theoretical effective lengths can be used. Consider the solid round bar. The cross sectional area is

$$A = \frac{\pi d^2}{4}$$

or

$$d = \sqrt{\frac{4A}{\pi}} = \sqrt{\frac{4(600)}{\pi}} = 27.64 \text{ mm}.$$

The area moment of inertia for this circular section is

$$I = \frac{\pi d^4}{64} = \frac{\pi (27.64)^4}{64} = 28,650 \text{ mm}^4.$$

The radius of gyration is

$$r_g = \sqrt{\frac{I}{A}} = \sqrt{\frac{28,650}{600}} = 6.910 \text{ mm}.$$

Therefore, the slenderness ratio is

$$\frac{l_e}{r_g} = \frac{5000}{6.91} = 723.6.$$

From Eq. (9.18),

$$\left(\frac{l_e}{r_g}\right)_T = \sqrt{\frac{2\pi^2 E}{S_y}} = \sqrt{\frac{2\pi^2 (72 \times 10^9)}{97 \times 10^6}} = 121.$$

Since  $l_e/r_g > (l_e/r_g)_T$ , the Euler formula applies and Eq. (9.12) gives the critical load at the onset of buckling as

$$P_{cr} = \frac{\pi^2 EI}{l_e^2} = \frac{\pi^2 (72 \times 10^9) (28,650 \times 10^{-12})}{(5.00)^2} = 814 \text{ N}.$$

At this point, the remaining geometries are analyzed in the same fashion. It can be shown that all of the cross sections given result in large slenderness ratios, so that Euler buckling is applicable, and the buckling load is estimated from Eq. (9.7). The summary of cross section dimensions and buckling loads are presented in Table 9.2 and Fig. 9.6.

Table 9.2: Summary of results for Example 9.3.

Description	$r_g$ (mm)	$I$ (mm <sup>4</sup> )	$C_c$	$P_{cr}$ (N)
Solid round bar	6.91	28,650	723.6	814
Cylindrical tube	16.27	$1.588 \times 10^5$	307	4514
Square tube	19.15	$2.20 \times 10^5$	261	6250
Solid square bar	7.071	$3.00 \times 10^4$	707	853

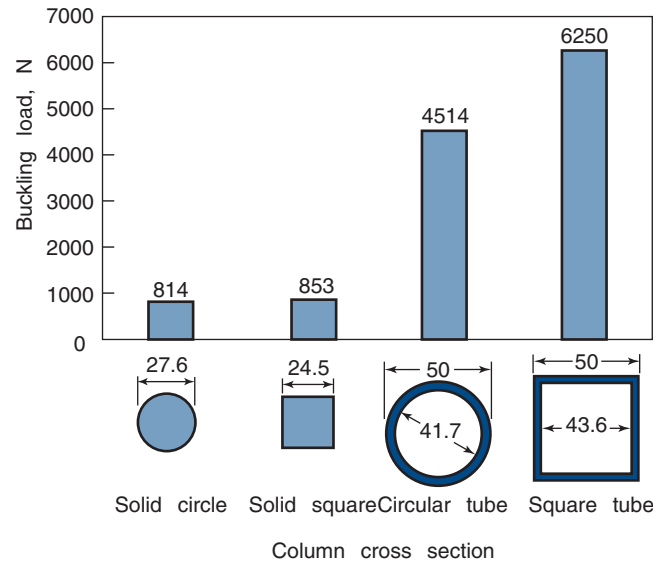


Figure 9.6: cross sectional areas, drawn to scale, from the results of Example 9.3, as well as critical buckling load for each cross sectional area.

### Example 9.4: Euler and Johnson Buckling

**Given:** A column with one end fixed and the other end pinned is made of a low-carbon steel with  $S_y = 295 \text{ MPa}$ . The column's cross section is rectangular with  $h = 15 \text{ mm}$  and  $b = 40 \text{ mm}$ .

**Find:** The buckling load for the following three lengths:

- 0.15 m
- 0.75 m
- 1.20 m

**Solution:** From Table 3.1 for low-carbon steel,  $E = 207 \text{ GPa}$ . The cross sectional area is

$$A = bh = (0.040)(0.015) = 0.00060 \text{ m}^2.$$

For a rectangular cross section, the area moment of inertia is

$$I = \frac{bh^3}{12} = \frac{(0.040)(0.015)^3}{12} = 1.125 \times 10^{-8} \text{ m}^4.$$

The radius of gyration is

$$r_g = \sqrt{\frac{I}{A}} = \sqrt{\frac{1.125 \times 10^{-8}}{0.00060}} = 0.00433 \text{ m} = 4.33 \text{ mm}.$$

- (a) From Table 9.1, for one end pinned and the other end fixed and  $l = 0.15 \text{ m}$ ,

$$l_e = 0.7l = 0.7(0.15) = 0.105 \text{ m}.$$

Therefore,

$$\frac{l_e}{r_g} = \frac{0.105}{0.00433} = 24.2.$$

From Eq. (9.18),

$$\left(\frac{l_e}{r_g}\right)_T = \sqrt{\frac{2\pi^2 E}{S_y}} = \sqrt{\frac{2\pi^2 (207 \times 10^9)}{295 \times 10^6}} = 117.7.$$

Since  $l_e/r_g < (l_e/r_g)_T$ , Eq. (9.16) (the Johnson equation) should be used. Note first that

$$\begin{aligned} \frac{1}{E} \left( \frac{S_y l_e}{2\pi r_g} \right) &= \frac{1}{207 \times 10^9} \left( \frac{(295 \times 10^6) (24.2)}{2\pi} \right) \\ &= 6.237 \times 10^6. \end{aligned}$$

Therefore,

$$\begin{aligned} P_{cr} &= A \left[ S_y - \frac{1}{E} \left( \frac{S_y l_e}{2\pi r_g} \right)^2 \right] \\ &= 0.00060 [(295 \times 10^6) - 6.237 \times 10^6] \\ &= 173 \text{ kN}. \end{aligned}$$

- (b) From Table 9.1, for one end pinned and one end fixed and  $l = 0.75 \text{ m}$ ,

$$l_e = 0.70l = 0.7(0.75) = 0.525 \text{ m};$$

$$\frac{l_e}{r_g} = \frac{0.525}{0.00433} = 121.$$

Since  $l_e/r_g > (l_e/r_g)_T$ , the Euler equation should be used. From Eq. (9.12),

$$\begin{aligned} P_{cr} &= \frac{\pi^2 EI}{l_e^2} \\ &= \frac{\pi^2 (207 \times 10^9) (1.125 \times 10^{-8})}{(0.525)^2} \end{aligned}$$

or  $P_{cr} = 83.4 \text{ kN}$ . Note that the slenderness ratio of this column is close to the critical slenderness ratio. Therefore, it is not surprising that the result from the Johnson equation is also 83.4 kN.

- (c) The Euler equation is definitely valid for  $l = 1.2 \text{ m}$ , so that

$$l_e = 0.7(1.2) = 0.840 \text{ m}.$$

The critical load is

$$\begin{aligned} P_{cr} &= \frac{\pi^2 EI}{l_e^2} \\ &= \frac{\pi^2 (207 \times 10^9) (1.125 \times 10^{-8})}{(0.840)^2} \\ &= 32.6 \text{ kN}. \end{aligned}$$

## 9.7 AISC Criteria

The American Institute of Steel Construction [2011] has produced design guidelines for elastic stability conditions. Although the guidelines are intended for steel, the wide use of steel in compression members makes the guidelines especially useful.

As shown by Eq. (9.11), the elastic modulus based on the linear-elastic portion of a stress-strain curve may lead to erroneous results. However, tangent-modulus data are not readily available in the technical literature and are difficult to obtain experimentally. The Johnson equation is needed for such circumstances. However, long columns are more difficult to design because they are extremely susceptible to defects in straightness or to eccentricity in loading. Therefore, a weighted reduction in the allowable stress is prescribed. The **AISC equations** correct for reductions in elastic modulus as the column stress exceeds the proportional limit of the material and use a sliding safety factor. For elastic buckling, the allowable stress is

$$\sigma_{all} = \frac{12\pi^2 E}{23 (l_e/r_g)^2}, \quad (9.19)$$

and for inelastic buckling,

$$\sigma_{all} = \frac{\left\{ 1 - \left[ \frac{(l_e/r_g)^2}{2C_c^2} \right] \right\} S_y}{n_\sigma}, \quad (9.20)$$

where  $C_c$  is the slenderness ratio for Euler buckling defined by Eq. (9.15) and  $n_\sigma$  is the reduction in allowable stress given by

$$n_\sigma = \frac{5}{3} + \frac{3(l_e/r_g)}{8C_c} - \frac{(l_e/r_g)^3}{8C_c^3}. \quad (9.21)$$

Note that  $n_\sigma$  is not a safety factor but a mandatory reduction in a material's allowable stress. Figure 9.5 compares the AISC as well as the Euler and Johnson equations. The American Association of State Highway and Transportation Officials (AASHTO) uses equations identical to Eqs. (9.19) and (9.20) but requires a constant stress reduction  $n_\sigma = 2.12$  for both elastic and inelastic buckling.

The AISC Criteria are not intended to predict the buckling load of a given column, but instead provide a design framework for steel columns. Better predictions of buckling load are obtained from the Euler or Johnson equations [Eqs. (9.12) and (9.16)], depending on the slenderness ratio as discussed in Design Procedure 9.1.

## 9.8 Eccentrically Loaded Columns

The applied load is not always applied through the centroid; the distance between the load and column axes is called the **eccentricity** and is designated by  $e$ . While loads can be eccentric, the load is usually parallel with the column axis, and this situation will be analyzed in this section. Just as for concentrically loaded columns (Section 9.3) the analysis of eccentricity is restricted at first to columns with pinned ends. Figure 9.7a shows a pinned column subjected to a compressive force acting at a distance  $e$  from the centerline of the undeformed column. This loading is statically equivalent to the axial load and bending moment  $M' = -Pe$  shown in Fig. 9.7b. As when considering concentrically loaded columns, small deflections and linear-elastic material behavior are assumed.

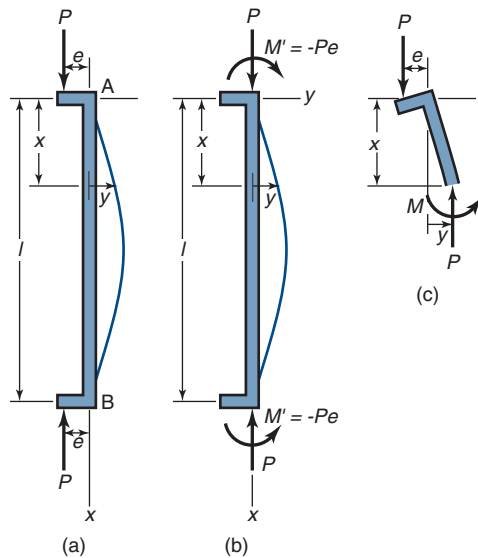


Figure 9.7: Eccentrically loaded column. (a) Eccentricity; (b) statically equivalent bending moment; (c) free-body diagram through arbitrary section.

From a free-body diagram of an arbitrary section shown in Fig. 9.7c, the internal moment in the column is

$$M = -P(e + y). \quad (9.22)$$

The differential equation for the deflection curve is obtained from Eqs. (5.3) and (9.22), or

$$\frac{d^2 y}{dx^2} + \frac{Py}{EI} = -\frac{Pe}{EI} = \text{Constant}. \quad (9.23)$$

Note that if the eccentricity is zero, Eqs. (9.23) and (9.1) are identical. The general solution to Eq. (9.23) is

$$y = C_1 \sin \left( x \sqrt{\frac{P}{EI}} \right) + C_2 \cos \left( x \sqrt{\frac{P}{EI}} \right) - e. \quad (9.24)$$

The boundary conditions are

1. at  $x = 0, y = 0$ , so that  $C_2 = e$ .
2. at  $x = l/2, dy/dx = 0$ .

Taking the derivative of Eq. (9.24) gives

$$\frac{dy}{dx} = C_1 \sqrt{\frac{P}{EI}} \cos \left( x \sqrt{\frac{P}{EI}} \right) - e \sqrt{\frac{P}{EI}} \sin \left( x \sqrt{\frac{P}{EI}} \right). \quad (9.25)$$

Using Eq. (9.25) and the second boundary condition gives

$$C_1 = e \tan \left( \frac{l}{2} \sqrt{\frac{P}{EI}} \right). \quad (9.26)$$

Substituting  $C_2 = e$  and Eq. (9.26) into Eq. (9.24) gives

$$y = e \left[ \tan \left( \frac{l}{2} \sqrt{\frac{P}{EI}} \right) \sin \left( x \sqrt{\frac{P}{EI}} \right) + \cos \left( x \sqrt{\frac{P}{EI}} \right) - 1 \right].$$

The maximum deflection occurs at  $x = l/2$ , so that

$$\begin{aligned} y_{\max} &= e \left[ \frac{\sin^2 \left( \frac{l}{2} \sqrt{\frac{P}{EI}} \right)}{\cos \left( \frac{l}{2} \sqrt{\frac{P}{EI}} \right)} + \cos \left( \frac{l}{2} \sqrt{\frac{P}{EI}} \right) - 1 \right] \\ &= e \left[ \sec \left( \frac{l}{2} \sqrt{\frac{P}{EI}} \right) - 1 \right]. \end{aligned} \quad (9.27)$$

The maximum stress on the column is caused by the axial load and the moment. The maximum moment occurs at the column's midheight and has a magnitude of

$$\begin{aligned} M_{\max} &= |P(e + y_{\max})|; \\ M_{\max} &= Pe \sec \left( \frac{l}{2} \sqrt{\frac{P}{EI}} \right). \end{aligned} \quad (9.28)$$

The maximum stress in the column is compressive and is

$$\sigma_{\max} = \frac{P}{A} + \frac{M_{\max} c}{I}.$$

Making use of Eq. (9.28) gives

$$\sigma_{\max} = \frac{P}{A} + \frac{Pec}{I} \sec \left( \frac{l}{2} \sqrt{\frac{P}{EI}} \right). \quad (9.29)$$

Since the radius of gyration is  $r_g^2 = I/A$ , Eq. (9.29) becomes

$$\sigma_{\max} = \frac{P}{A} \left[ 1 + \frac{ec}{r_g^2} \sec \left( \frac{l}{2r_g} \sqrt{\frac{P}{EA}} \right) \right], \quad (9.30)$$

where

- $P$  = critical load where buckling will occur in eccentrically loaded column, N
- $A$  = cross sectional area of column,  $\text{m}^2$
- $e$  = eccentricity of load measured from neutral axis of column's cross sectional area to load's line of action, m
- $c$  = distance from neutral axis to outer fiber of column, m
- $r_g$  = radius of gyration, m
- $l$  = length before load is applied, m
- $E$  = elastic modulus of column material, Pa

For end conditions other than pinned, the length is replaced with the effective length (using Table 9.1), and Eqs. (9.28) and (9.30) become

$$y_{\max} = e \left[ \sec \left( \frac{l_e}{2} \sqrt{\frac{P}{EI}} \right) - 1 \right], \quad (9.31)$$

$$\sigma_{\max} = \frac{P}{A} \left[ 1 + \frac{ec}{r_g^2} \sec \left( \frac{l_e}{2r_g} \sqrt{\frac{P}{EA}} \right) \right]. \quad (9.32)$$

Equation (9.31) is known as the **secant equation** and the parameter  $ec/r_g^2$  is called the **eccentricity ratio**. Note from Eq. (9.32) that it is not convenient to calculate the load explicitly.

Figure 9.8 shows the effect of slenderness ratio on normal stress for an eccentrically loaded column. These results are for structural grade steel where the modulus of elasticity is 207 GPa and the yield strength is 250 MPa. Note that

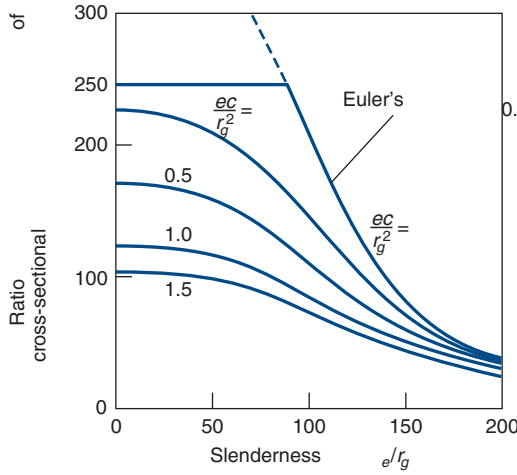


Figure 9.8: Stress variation with slenderness ratio for five eccentricity ratios, for structural steel with  $E = 207$  GPa and  $S_y = 250$  MPa.

as  $e$  approaches 0,  $\sigma$  approaches  $P/A$ , where  $P$  is the critical column load as established by the Euler formula [Eq. (9.12)].

The curves in Fig. 9.8 indicate that differences in eccentricity ratio have a significant effect on column stress when the slenderness ratio is small. On the other hand, columns with large slenderness ratios tend to fail at the Euler (or critical) load, regardless of the eccentricity ratio.

If  $\sigma_{\max} = \sigma_{\text{all}} = S_y/2$ , Eq. (9.32) becomes

$$P = \frac{S_y A/2}{1 + \frac{ec}{r_g^2} \sec\left(\frac{l_e}{2r_g} \sqrt{\frac{P}{EA}}\right)} = f(P). \quad (9.33)$$

Determining the load that results in buckling for eccentric columns cannot be done in closed form, and numerical or iterative methods are needed. For example, an initial guess for  $P$  is the value obtained from the concentric loading condition or

$$P = P_{\text{cr}}. \quad (9.34)$$

Using Eq. (9.34) in Eq. (9.33) gives a new value of  $P$ . This iterative process is continued until a desired accuracy is achieved.

### Example 9.5: Eccentric Loading

**Given:** A 1-m-long hollow 2014 aluminum alloy tube ( $S_y = 97$  MPa) with a 75-mm outside diameter, a 0.5-mm wall thickness, and with both ends pinned.

**Find:** The critical buckling load for

- Concentric loading
- Eccentric loading, with an eccentricity of 4 mm.

**Solution:**

- The inside diameter of the column is

$$d_i = d_o - 2t_h = 75 - 2(0.5) = 74 \text{ mm} = 0.074 \text{ m}.$$

The cross sectional area is

$$A = \frac{\pi}{4} (d_o^2 - d_i^2) = \frac{\pi}{4} [(0.075)^2 - (0.074)^2]$$

or  $A = 1.170 \times 10^{-4} \text{ m}^2$ . The area moment of inertia is

$$I = \frac{\pi}{64} (d_o^4 - d_i^4) = \frac{\pi}{64} [(0.075)^4 - (0.074)^4]$$

or  $I = 8.12 \times 10^{-8} \text{ m}^4$ . The radius of gyration is

$$r_g = \sqrt{\frac{I}{A}} = \sqrt{\frac{8.12 \times 10^{-8}}{1.17 \times 10^{-4}}} = 0.0263 \text{ m}$$

From Table 9.1 for a column with both ends pinned the effective length is equal to the actual length ( $l = l_e$ ). From Table 3.1 for 2014 aluminum alloy,  $E = 70$  GPa. From Eq. (9.18),

$$\left(\frac{l_e}{r_g}\right)_T = \sqrt{\frac{2\pi^2 E}{S_y}} = \sqrt{\frac{2\pi^2 (70 \times 10^9)}{97 \times 10^6}} = 119,$$

and

$$\frac{l_e}{r_g} = \frac{1}{0.0263} = 38.0.$$

Since  $l_e/r_g < (l_e/r_g)_T$ , the Johnson formula [Eq. (9.16)] should be used:

$$\begin{aligned} P_{\text{cr}} &= AS_y \left[ 1 - \frac{S_y}{4\pi^2 E} \left(\frac{l_e}{r_g}\right)^2 \right] \\ &= (0.28) (97 \times 10^6) \\ &\quad \times \left[ 1 - \frac{(97 \times 10^6) (38.0)^2}{4\pi^2 (70 \times 10^9)} \right], \end{aligned}$$

or  $P_{\text{cr}} = 10.8 \text{ kN}$ .

- The distance from the neutral axis to the outer fiber is  $c = d_o/2 = 0.0375 \text{ m}$ . The eccentricity ratio is

$$\frac{ce}{r_g^2} = \frac{(0.0375)(0.0040)}{(0.0263)^2} = 0.217;$$

$$P = P_{\text{cr}} = 10,800 \text{ N}$$

From Eq. (9.33), and noting that  $S_y A/2 = 5670 \text{ N}$ ,

$$P_1 = \frac{5670}{1 + 0.217 \sec \left[ \frac{38.0}{2} \sqrt{\frac{10,800}{(70 \times 10^9) (1.17 \times 10^{-4})}} \right]},$$

or  $P_1 = 4658 \text{ N}$ . A second iteration leads to

$$P_1 = \frac{5670}{1 + 0.217 \sec \left[ \frac{38.0}{2} \sqrt{\frac{4658}{(70 \times 10^9) (1.17 \times 10^{-4})}} \right]},$$

or  $P_2 = 4657 \text{ N}$ . Further iterations do not result in more accurate solutions. The critical load for the eccentric loading is 4657 N and that for the concentric loading is 10,800 N.



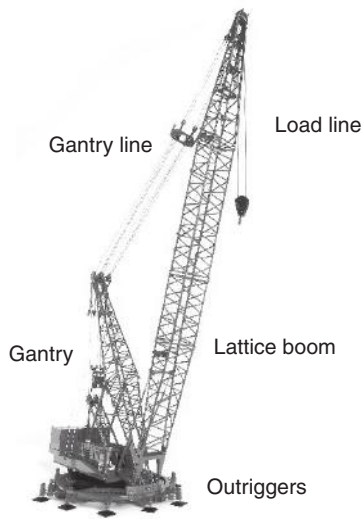


Figure 9.9: Schematic illustration of a Manitowoc 4100W RINGER crane, showing the lattice boom, outriggers, and load and gantry lines. *Source:* Courtesy of Manitowoc Co., Inc.

### Case Study 9.1: Design Considerations for Lattice-Boom Cranes

Lattice-boom cranes are extremely common for material handling, especially in the shipping and construction industries. A schematic of a lattice-boom crane is shown in Fig. 9.9. As opposed to telescoping boom cranes, hydraulic powered cranes, or gantry type cranes, lattice-boom cranes are intended for applications where loads are very high and long boom lengths are essential. Some of the design considerations for lattice-boom cranes are:

1. The booms are constructed from segments, such as the one shown in Fig. 9.10. The segment consists of a rectangular box defined at the corners by large channels, or cords with smaller cross-bracing spaced as shown. Boom segments are usually welded fabrications (see Section 16.6) and are joined together using prestressed threaded fasteners or pins (Sections 16.4 and 16.5). A typical boom segment is 3 to 12 meters long, so a crane with a long boom requires multiple segments to be assembled. It is not feasible to produce booms of long length directly, since manufacture and transport of the booms would be overly burdensome.
2. The load is supported by the *load line*, and the *gantry lines* set the angle of the boom. Note that the boom is constructed in a horizontal position and then needs to be raised by the gantry. The weight of the boom causes a bending stress to be applied to the boom when it is lifted off the ground; this stress must be supported by the cords.
3. As can be shown from statics, the applied loads in the gantry and load lines result in pure compressive loading on the boom. Deviation from pure compressive loading occurs when the load line is not vertical, such as due to wind loadings. Crane manufacturers will specify environmental conditions (such as maximum wind speed) that should not be exceeded. However, if the load line deviates from the vertical, a horizontal force is applied to the tip of the boom, resulting in a bending moment that must be supported.

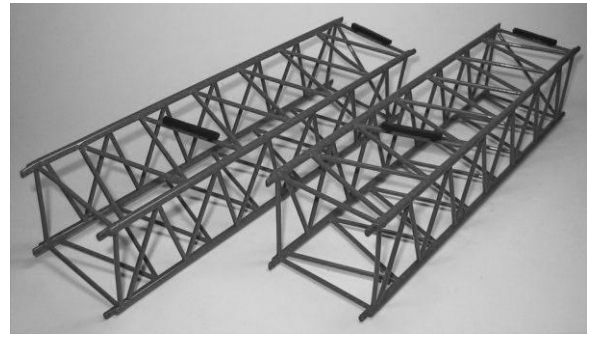


Figure 9.10: Illustration of a boom segment. A typical box boom consists of larger tubes or angle channels at the corners, supported by smaller braces or cords along the length. Boom segments are available in lengths ranging from 3-12 meters. *Source:* Courtesy of Manitowoc Co., Inc.

4. At low boom angles, boom buckling is not likely. This is because the large moment arm presented by the boom results in tipping of the crane should loads become excessive. Crane tipover is a serious concern, and a load chart provided by the manufacturer must be heeded to prevent such accidents. It should be noted that the crane's capacity depends on boom angle, length, and orientation with respect to the crane's axis. Special care must be taken to ensure that the crane's outriggers are properly deployed and that the ground beneath the outriggers will not collapse. (Shoring or repositioning of the crane are common corrective measures if ground strength is suspect.)
5. At high boom angles, the capacity of the crane is limited by the buckling strength of the boom. The lattice structure ensures that the cords will buckle in a high mode [see Eq. (9.6)], which can also be interpreted as a short effective length.

Buckling phenomena are well understood, and mathematical tools are available to confirm designs are adequate. Regardless, there are still occasional boom collapses, but almost always these involve misuse of cranes. Some examples are:

- In one accident, a crane boom collapsed during transport of a ship hull that was under construction. A large gantry crane normally used for this task was being repaired, so three lattice-boom cranes were used to move the hull. Clearly, the cranes cannot move while their outriggers are deployed, so the user would hook up the load lines, have the cranes raise the hull off the ground and then swing the booms to the side and lower the hull to the ground. After repositioning the cranes and resetting the outriggers, the procedure would be repeated. At some point, one of the lattice-booms buckled. A reconstruction of the accident showed that the loads that would cause boom buckling required a side load of around 20% of the vertical load — a situation that exceeded the side load that would be seen in a Class 1 hurricane!

- Another lattice-boom buckling failure involved a crane that was hooked up to an object that exceeded the crane's lift capability. That is, the load was so high that the hoist motor could not generate sufficient torque to raise the load. As a result, the crane operator attached the load to the load line at a high boom angle and applied a tension to the line until the hoist motor stalled, and then applied the hoist line brake. (The brake has a significantly higher capacity than the hoist motor.) It was only at this point that the operator lowered the outriggers. Since each outrigger can lift the entire crane and its maximum load, and the outriggers raise the crane a few inches above the ground, this had the effect of lifting the load. Not surprisingly, the boom buckled when the crane user rotated the crane superstructure.

Normally, lattice-booms are extremely reliable and of great utility. Extreme misuse is usually involved when such a boom buckles.

## 9.9 Summary

In an attempt to better understand column buckling, three equilibrium regimes were studied. Stable, neutral, and unstable equilibrium were explained by observing what happens to a sphere or cylinder on concave, flat, and convex surfaces. It was concluded that when columns are in unstable equilibrium, they can buckle. A small displacement can cause a catastrophic change in the configuration of the column. As the load on a column is increased, a critical load is reached where unstable equilibrium will occur and the column will not return to its straight configuration. Thus, for long, slender columns there is a critical buckling load. The column's critical buckling stress was also determined to be much less than the yield strength of the material. End conditions were found to affect the critical buckling load. The effective length was used to handle four types of end condition. The Euler and Johnson buckling criteria were developed for concentrically loaded columns. Eccentrically loaded columns were also studied and the secant formulas were derived.

## Key Words

- AISC equations** estimations of allowable stress for prevention of buckling in structures (corrections for capacity as column stress exceeds proportional limit)
- buckling** sudden large deformation of a structure due to slight increase of applied load
- column** straight and long (relative to cross sectional dimension) member subjected to compressive axial loads
- eccentricity ratio** measure of how far a load is applied from a cross section's centroid
- Essenger equation** an expression that incorporates the tangent modulus into buckling load calculations
- Euler load** a statement of the critical load of an elastic column
- Johnson equation** an equation used to determine the critical load for inelastic buckling

**secant equation** an expression that allows calculation of column deflection due to eccentric loading

**slenderness ratio** measure of column slenderness

**tangent modulus** elastic modulus at a given stress level

**tangent-modulus equation** same as Essenger equation

## Summary of Equations

**Euler buckling equation:**  $P_{cr} = \frac{n^2 \pi^2 EI}{l^2}$

**Critical stress in Euler buckling:**  $(\sigma_{cr})_E = \frac{P_{cr}}{A} = \frac{\pi^2 E}{(l/r_g)^2}$

**Inelastic buckling (Essenger equation):**  $\sigma_{cr} = \frac{\pi^2 E_t}{(l/r_g)^2}$

**Critical slenderness ratio:**  $C_c = \left(\frac{l_e}{r_g}\right)_E = \sqrt{\frac{2E\pi^2}{S_y}}$

**Johnson equation:**  $(\sigma_{cr})_J = \frac{(P_{cr})_J}{A} = S_y - \frac{S_y^2}{4\pi^2 E} \left(\frac{l_e}{r_g}\right)^2$

**AISC buckling equations:**

Elastic buckling:  $\sigma_{all} = \frac{12\pi^2 E}{23 (l_e/r_g)^2}$

Inelastic buckling:  $\sigma_{all} = \frac{\left\{1 - \left[\frac{(l_e/r_g)^2}{2C_c^2}\right]\right\} S_y}{n_\sigma}$

where  $n_\sigma = \frac{5}{3} + \frac{3(l_e/r_g)}{8C_c} - \frac{(l_e/r_g)^3}{8C_c^3}$

**Secant equation:**  $y_{max} = e \left[ \sec \left( \frac{l_e}{2} \sqrt{\frac{P}{EI}} \right) - 1 \right]$

## Recommended Readings

- Budynas, R.G., and Nisbett, J.K. (2011), *Shigley's Mechanical Engineering Design*, 9th ed., McGraw-Hill.
- Juvinall, R.C., and Marshek, K.M. (2012) *Fundamentals of Machine Component Design*, 5th ed., Wiley.
- Ketter, R.L., Lee, G.C., and Prawel, S.P. (1979) *Structural Analysis and Design*, McGraw-Hill.
- Manual of Steel Construction* (2011) 14th ed., American Institute of Steel Construction.
- Norton, R.L. (2011) *Machine Design*, 4th ed., Prentice Hall.
- Popov, E.P. (1999) *Engineering Mechanics of Solids*, 2nd ed., Prentice-Hall.
- Timoshenko, S.P., and Goodier, J.N. (1970) *Theory of Elasticity*, McGraw-Hill.
- Ugural, A.C., and Fenster, S.K. (2003) *Advanced Strength and Applied Elasticity*, 4th ed., Prentice-Hall.
- Willems, A. (2009) *Structural Analysis in Theory and Practice*, Elsevier.

## Reference

- American Institute of Steel Construction (AISC) (2011) *Manual of Steel Construction*, 14th ed.

## Questions

- 9.1 What is a column?
- 9.2 Define the terms neutral, stable, and unstable equilibrium.
- 9.3 What is the Euler equation?
- 9.4 Describe the tangent modulus using a stress strain curve that is typical for a carbon steel.
- 9.5 What is the slenderness ratio of a column?
- 9.6 Explain why the Euler equation does not contain the material's yield strength.
- 9.7 What is the Johnson equation?
- 9.8 What are the AISC criteria for buckling?
- 9.9 Define the eccentricity ratio.
- 9.10 What is the secant equation?

## Qualitative Problems

- 9.11 A person rides a bike on a flat level road. Is this a neutral, stable, or unstable equilibrium position? Explain.
- 9.12 A golf ball is placed
- On top of a small hill
  - On a horizontal flat plane
  - In a shallow groove
- Identify the type of equilibrium for each condition. Justify your answer.
- 9.13 List the assumptions necessary for Euler buckling to take place.
- 9.14 Review Table 9.1 and explain the reasons that the theoretical effective column length and approximated end conditions have the values listed.
- 9.15 Martensitic steels can be produced that have yield strengths as high as 1800 MPa, but they are difficult to form into structural shapes and are more expensive than other steels. List the advantages of using such materials in compression members.
- 9.16 Refer to Eq. (9.20) and determine if the reduction in allowable stress is larger or smaller for slender columns compared to more compact columns. Explain why you think this trend is justified.
- 9.17 Review Design Procedure 9.1. If the first step assumed the Johnson equation is appropriate, explain how the remainder of the Design Procedure would need to be modified.

## Quantitative Problems

- 9.18 A column has pinned ends and is axially loaded in compression. The length is 6 m and the weight is 2310 N, but the form of the cross section can be changed. The column is made of steel (annealed AISI 1040). Find the Euler buckling load for

- A solid circular section. *Ans.*  $P_{cr} = 113.0 \text{ kN}$ .
- A solid square section. *Ans.*  $P_{cr} = 118.2 \text{ kN}$ .
- A circular tube with outer diameter of 100 mm. *Ans.*  $P_{cr} = 241.8 \text{ kN}$ .
- A square tube with outside dimension of 100 mm. *Ans.*  $P_{cr} = 354.7 \text{ kN}$ .

- 9.19 A column with both ends pinned is 3 m long and has a tubular section with an outer diameter of 30 mm and wall thickness of 5 mm. Find which material given in Tables A.1 through A.4 produces the highest buckling load. Also, give the buckling loads for AISI 1080 steel (quenched and tempered at 800°C), aluminum alloy 2014, and molybdenum. *Ans.* For AISI 1080,  $P_{cr} = 7245 \text{ N}$ .
- 9.20 Determine the critical stresses for the four column cross sections considered in Problem 9.18 if the column length is 10 m and constructed from AISI 1080 steel, quenched and tempered at 800°C. *Ans.* For a solid square cross section,  $\sigma_{cr} = 8.511 \text{ MPa}$ .
- 9.21 A column is axially loaded in compression. The ends were specified to be fixed, but because of a manufacturing error they had
- One end fixed and the other pinned
  - Both ends pinned

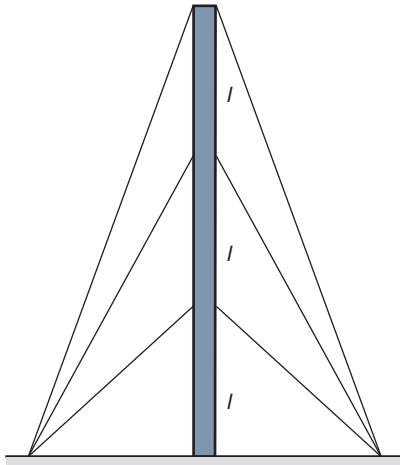
Find how much the critical elastic buckling load is decreased because of the errors. Also, calculate the buckling loads for the 4-m-long column made of annealed AISI 1040 steel having a solid, square cross section with 30-mm sides for the three end conditions. Assume the theoretical effective column length. *Ans.* For fixed-fixed,  $P_{cr} = 11.26 \text{ kN}$ .

- 9.22 An elastic column has one end pinned and the other end fixed in a bushing so that the values given in Table 9.1 do not apply. Instead, the effective length is  $l_e = 0.83l$ . The cross section of the column is a circular tube with an outer diameter of 80 mm and 3.0-mm wall thickness; the column is 10 m long. Calculate the elastic buckling load if the column is made of
- AISI 1080 steel. *Ans.* 15.97 kN.
  - Polycarbonate. *Ans.* 183 N.
- 9.23 An elastic AISI 1020 (quenched and tempered at 870°C) steel column has both ends pinned. It is 12.5 m long and has a square tubular cross section with an outside dimension of 160 mm and 4-mm wall thickness. Its compressive axial load is 100 kN.
- Determine the safety factors guarding against buckling and yielding. *Ans.*  $n_{s, \text{buckling}} = 1.325$ ,  $n_{s, \text{yielding}} = 7.36$ .
  - If the ends are changed to fixed and the material is changed to aluminum alloy 2014, calculate the safety factors guarding against buckling and yielding.

- 9.24 A beam has both ends mounted in stiff rubber bushings giving bending moments in the beam ends proportional to the angular displacements at the beam ends. Calculate the effective beam length if the angular spring constant at the ends is  $\partial M / \partial \theta = 10^5 \text{ N-m/radian}$  in all directions. The beam is 3 m long and has a solid circular cross section of AISI 1080 steel (quenched and tempered at 800°C) with a 24-mm diameter. *Ans.* 1.534 m.

**9.25** Two solid circular columns are made of different materials, steel and aluminum. The cross sectional areas are the same and the moduli of elasticity are 207 GPa for the steel and 72 GPa for the aluminum. Find the ratio of the critical buckling lengths for the columns, assuming that the same buckling load is applied to both columns. *Ans.*  $l_{es}/l_{ea} = 1.696$ .

**9.26** A television mast shown in Sketch *a* consists of a circular tube with an outer diameter  $d_o$  and a wall thickness  $t_h$ . Calculate how long the distance  $l$  between the anchoring points for the guy wires can be if the mast should deform plastically rather than buckle.



Sketch *a*, for Problem 9.26

**9.27** A 3-m-long column of square, solid cross section with both ends fixed must sustain a critical load of  $3 \times 10^5$  N. The material is steel with a modulus of elasticity of 207 GPa and a yield stress of 700 MPa. Determine the following:

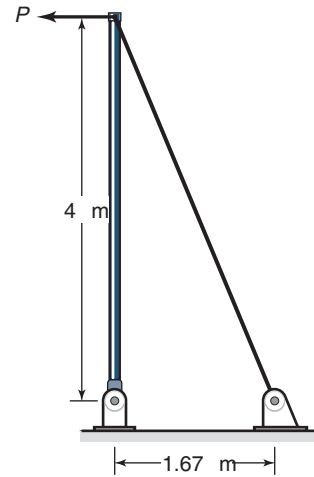
- What minimum dimensions of the cross section are permitted without having failure? Should the Euler or the Johnson equation be used? *Ans.*  $w = 0.045$  m.
- If the critical load is increased by two orders of magnitude to  $P_{cr} = 3 \times 10^7$  N, what minimum dimensions of the cross section are permitted without failure? Also, indicate whether the Euler or the Johnson equation should be used.

**9.28** A solid, round column with a length of 5 m and a diameter of 50 mm is fixed at one end and is free at the other end. The material's yield strength is 300 MPa and its modulus of elasticity is 207 GPa. Assuming concentric loading of the column, determine the following:

- The critical load. *Ans.*  $P_{cr} = 6.268$  kN.
- The critical load if the free end is also fixed (i.e., both ends are now fixed). *Ans.*  $P_{cr} = 534$  kN.

**9.29** A circular-cross-section bar with a diameter of 50 mm and a length of 1.25 m is axially loaded. The bar is made of medium-carbon steel. Both ends are pinned. Determine

- Whether the Johnson or the Euler formula should be used.
- The critical load. *Ans.* 382 kN.



Sketch *b*, for Problem 9.30

**9.30** A low-carbon-steel pipe (AISI 1020, quenched and tempered at 870°C), as shown in sketch *b*, has an outer diameter of 50 mm and a thickness of 5 mm. If the pipe is held in place by a guy wire, determine the largest horizontal force  $P$  that can be applied without causing the pipe to buckle. Assume that the ends of the pipe are pin connected. *Ans.* 9.154 kN.

**9.31** A 20-mm-diameter, medium-carbon steel (annealed AISI 1040) rod is loaded as a column with pinned ends. If the critical load is 100 kN, how long can the rod be and still carry the following percentages of the critical load: (a) 90%, (b) 50%, and (c) 2%? Also, indicate whether the Johnson or the Euler equation should be used. *Ans.* (a) 0.3256 m; (b) 0.5663 m; (c) 2.832 m.

**9.32** Most types of steel have similar moduli of elasticity but can have widely different yield strength properties depending on the alloy and the heat treatment. For a column having a solid, circular cross section with a diameter of 25 mm, the yield strengths for three steels are 300, 600, and 1000 MPa. Find for each steel the critical column length where buckling would be described by the Euler equation. *Ans.* For  $S_y = 300$  MPa,  $l_e = 0.7294$  m.

**9.33** For a fixed cross sectional area of a tubular steel column, find the geometry that would give the highest buckling load. The minimum column wall thickness is 5 mm.

**9.34** A rectangular cross section tube is axially loaded in compression. The tube's outside dimensions are 70 and 90 mm, it is 4 m long with both ends pinned; the wall thickness is 10 mm. Determine which of the steels in the table in Appendix A.2 should be used so that the Euler equation is applicable.

**9.35** The column considered in Problem 9.34 is made of annealed AISI 1020 steel, quenched and tempered at 870°C. Find the critical buckling load. *Ans.* 360 kN.

**9.36** A 2.5-m-long column with one end fixed and the other end free is made of aluminum alloy 2014-O and has a solid, round cross section. Determine the diameter of the column for the following loads

- $P = 800$  kN. *Ans.*  $d = 0.1547$  m.
- $P = 1500$  kN.



- 9.37** A 1-m-long column with a 60-mm × 100-mm rectangular cross section and made of aluminum alloy 2014-O is subjected to a compressive axial load. Determine the critical buckling load
- If both ends are fixed. *Ans.* 565 kN.
  - If one end is fixed and the other is free. *Ans.* 316 kN.
  - If the load is applied eccentrically at a distance of 10 mm for case b. *Ans.* 109.6 kN.
- 9.38** A column with pinned ends and solid rectangular cross section with dimensions of 35 mm × 60 mm is made of annealed AISI 1040 steel. The 4-m-long column is loaded with an eccentricity of 15 mm. Find the elastic deflection if a 100-N compressive load is applied; also, calculate how large a load can be applied without permanent deformation occurring. *Ans.*  $y_{\max} = 68 \mu\text{m}$ ,  $P = 21.94 \text{ kN}$ .
- 9.39** The column considered in Problem 9.38 is subjected to a varying load in the range of 0 to 24,000 N. Calculate and plot the deformation as a function of the axial load.

## Synthesis and Design

- 9.40** Obtain an aluminum beverage can and carefully cut the can in half and measure the wall thickness and can diameter. Calculate the critical buckling load for the can and indicate if this is greater than or less than your weight. Try to step onto another empty can. Does the can buckle? Explain why or why not. Assume the yield strength is 180 MPa and the elastic modulus is 69 GPa.
- 9.41** Using a compression test machine, compress bars of different lengths to provide experimental data for Table 9.1. It may be prudent to calculate required column lengths for a given cross section to make sure that elastic and inelastic buckling regimes are investigated.
- 9.42** Derive an expression for the weight of a column with a solid circular cross section as a function of material properties, length, and applied load assuming Euler buckling. What combination of material properties lead to the lightest weight column?
- 9.43** Obtain an expression for the height of a cylindrical column that will buckle under its own weight (assume Euler buckling). Compare the height that can be achieved for the materials on the inside front cover.
- 9.44** In *double modulus theory*, it is recognized that during buckling the tensile side of the column's cross section should use the tangent modulus of elasticity, whereas on the compressive side it may be better to use the original elastic modulus. Model the cross section of a material with two moduli,  $E_t$  and  $E$ , and show that the buckling load is
- $$P_{\text{cr}} = \frac{\pi^2 E_r I}{L^2}$$
- where  $E_r$  is the *reduced modulus* given by  $E_r = E_t \frac{I_1}{I} + E \frac{I_2}{I}$  and  $I_1$  and  $I_2$  are the fractions of the moment of inertia on the tensile and compressive sides of the column, respectively.
- 9.45** Conduct a literature search and obtain design rules for buckling of aluminum that are analogous to Eqs. (9.19) through (9.21).
- 9.46** A fishing pole uses eyelets to guide the fishing line. Obtain a fishing pole and demonstrate that the pole is stiffer if all of the eyelets are used compared to when only the one at the top of the pole is used. Explain why.
- 9.47** In Case Study 9.1, it was explained that lattice booms are intended to buckle in a high buckling mode. Make a careful sketch of the buckling mode for a lattice boom section both with and without side load.



This page intentionally left blank

## Chapter 10

# Stresses and Deformations in Cylinders



A common beverage can. Along with food containers, these are the most common pressure vessels. *Source:* Shutterstock.

*In all things, success depends on previous preparation. And without such preparation there is sure to be failure.*

*Confucius, Analects*

### Contents

- 10.1 Introduction 244
- 10.2 Tolerances and Fits 244
- 10.3 Pressurization Effects 245
- 10.4 Rotational Effects 250
- 10.5 Press Fits 252
- 10.6 Shrink Fits 254
- 10.7 Summary 256

### Examples

- 10.1 Interference and Class of Fit 245
- 10.2 Thin-Walled Cylinder 247
- 10.3 Internally Pressurized Thick-Walled Cylinder 249
- 10.4 Design of a Thick-Walled Cylinder 250
- 10.5 Press Fit 251
- 10.6 Rotating Cylinder 252
- 10.7 Interference Fit 253
- 10.8 Disassembly of Interference Fit 254
- 10.9 Shrink Fit 254
- 10.10 Thermal Stresses 255

### Design Procedure

- 10.1 Stress Analysis of Thick-Walled Cylinders 249

### Case Study

- 10.1 Design of a Shot Sleeve for a Die Casting Machine 255

This chapter investigates the stresses and deformations that occur in internally or externally pressurized cylinders. This basic geometry sees many practical applications, including pressure vessels such as gas storage cylinders, food and beverage cans and bottles, fuel tanks, hydraulic actuators and gun barrels; press and shrink fits; hydraulic and pneumatic tubing used for delivery of pressurized fluid; and pumps and motors. The chapter begins with a discussion of tolerances, allowances, and fits, which are essential for understanding the demanding design constraints that are needed for press and shrink fits. Classes of fit and recommended tolerances for different applications are summarized. The membrane stresses for thin-walled pressure vessels are stated, and the full linear elastic solution for thick-walled pressure vessels is derived and simplified for common special cases. This theory is then applied to press and shrink fits, two very common methods of assembly. The required assembly force for press fits and the allowable torque that can be achieved for both press and shrink fits are derived.

**Machine elements in this chapter:** Pressure vessels, press and shrink fits, hydraulic lines and pipelines.

**Typical applications:** Liquid and gas storage, assembly of parts onto shafts, actuators such as hydraulic cylinders, gun barrels.

**Competing machine elements:** Keyways, setscrews, splines and couplings (Chapter 11), power screws (Chapter 16), welding (Chapter 16).

## Symbols

$A$	cross-sectional area, $\text{m}^2$
$C_1, C_2$	integration constants
$c$	radial clearance, m
$d$	diameter, m
$E$	modulus of elasticity, Pa
$l$	length, m
$n_s$	safety factor
$P$	force, N
$P_b$	body force per volume, $\text{N}/\text{m}^3$
$p$	pressure, Pa
$r$	radius, m
$S_y$	yield strength, Pa
$T$	torque, N-m
$t_h$	thickness, m
$t_l$	tolerance, m
$\Delta t_m$	temperature change, $^{\circ}\text{C}$
$x, y, z$	Cartesian coordinates, m
$\alpha$	cone angle, deg
$\beta$	coefficient of linear thermal expansion, $(^{\circ}\text{C})^{-1}$
$\delta$	interference or displacement, m
$\epsilon$	strain
$\theta$	circumferential direction, rad
$\mu$	coefficient of friction
$\nu$	Poisson's ratio
$\rho$	density, $\text{kg}/\text{m}^3$
$\sigma$	normal stress, Pa
$\omega$	angular velocity, $\text{rad}/\text{s}$

## Subscripts

$a$	axial
$c$	circumferential
$e$	von Mises
$f$	fit
$h$	hub
$i$	inner or internal
$o$	outer or external
$r$	radial
$s$	shaft
$t$	tangential
$t_m$	temperature change
$\theta$	circumferential direction

## 10.1 Introduction

Just as the last chapter dealt with a specific loading and the unique stresses and strains acting on columns, this chapter deals with internally and/or externally pressurized cylinders. Many important engineering applications rely on this condition.

The material in this chapter is important for understanding machine elements presented later in the text. Section 10.2 discusses tolerances and fits, a concept that is essential for design of mating parts. Section 10.3 addresses thin- and thick-walled cylinders and the stresses that develop due to internal and external pressurization, and Section 10.4 includes rotational effects. Using the theoretical approaches developed, press and shrink fits are covered in Sections 10.5 and 10.6, so that the casual reader may wish to proceed directly to those sections.

Stresses and deformations of thin-walled, thick-walled, internally pressurized, externally pressurized, and rotating cylinders are considered, as well as press and shrink fits. The material developed in this chapter is important to shaft-

ing (Chapter 11) and to a number of machine elements, such as rolling-element bearings (Chapter 13) and hydrodynamic bearings (Chapter 12).

## 10.2 Tolerances and Fits

A number of definitions about tolerancing are important in design:

1. **Tolerance**,  $t_l$ , is the maximum variation in the size of a part. Two types of tolerance are:
  - (a) **Bilateral tolerance** — A part is permitted to vary both above and below the nominal size, such as  $25 \pm 0.030$ .
  - (b) **Unilateral tolerance** — A part is permitted to vary either above or below the nominal size, but not both, such as  $25^{+0.000}_{-0.030}$ .
2. **Nominal diameter**,  $d$ , is the approximate size; allowances and tolerances are applied with respect to the nominal dimension.
3. **Allowance**,  $a$ , is the difference between the nominal diameters of mating parts. Allowance is used when the mating parts have a measurable positive gap between them.
4. **Interference**,  $\delta$ , is the actual difference in the size of mating parts. Interference is used when the mating parts have an overlap, and can be considered the inverse of allowance.

Note that the tolerances of the shaft,  $t_{ls}$ , and the hub,  $t_{lh}$ , may be different.

Because it is impossible or impractical from a manufacturing perspective to make parts to an exact size, tolerances are used to control the variation between mating parts. Two examples illustrate the importance of tolerancing:

1. In hydrodynamic bearings (Chapter 12) a critical part of the design is the specification of the radial clearance between the journal and the bearing. The typical value is on the order of 0.02 mm. However, variations in the journal's outside diameter and the bearing's inside diameter cause larger or smaller clearances. Such variations must be accounted for in analyzing bearing performance. Too small a clearance could cause failure; too large a clearance would reduce the precision of the machine and adversely affect the lubrication. Thus, tolerancing and accuracy of the dimensions can have a significant effect on the performance of hydrodynamic bearings.
2. Rolling-element bearings (Chapter 13) are often designed to be installed on a shaft (Chapter 11) with an interference fit. The inside diameter of the bearing inner race is smaller than the outside diameter of the shaft where the bearing is to be seated. A significant force is required to press the bearing onto the shaft, thus imposing significant stresses on both the shaft and the bearing. Specification of the shaft diameter relative to the bearing bore size is important to ensure that failure due to overstressing the members does not occur. Proper tolerancing of the members will greatly contribute to successful design.

Table 10.1: Classes of fit.

Class	Type	Applications
1 (Loose)	Clearance	Where accuracy is not essential, such as in building and mining equipment
2 (Free)	Clearance	In rotating journals with speeds of 600 rpm or greater, such as in engines and some automotive parts
3 (Medium)	Clearance	In rotating journals with speeds under 600 rpm, such as in precision machine tools and precise automotive parts
4 (Snug)	Clearance	Where small clearance is permissible and where mating parts are not intended to move freely under load
5 (Wringing)	Interference	Where light tapping with a hammer is necessary to assemble the parts
6 (Tight)	Interference	In semipermanent assemblies suitable for drive or shrink fits on light sections
7 (Medium)	Interference	Where considerable pressure is required for assembly and for shrink fits of medium sections; suitable for press fits on generator and motor armatures and for automotive wheels
8 (Shrink)	Interference	Where considerable bonding between surfaces is required, such as locomotive wheels and heavy crankshaft disks of large engines

Table 10.1 describes the eight classes of fit, the type of fit, and their applications. Note that for classes 1 to 4 the members are interchangeable but for classes 5 to 8 the members are not interchangeable. Having established classes of fit, the next task will be to indicate the tolerance applicable for a specific class. Table 10.2 gives the tolerances for various classes of fit in millimeters. In this table, the nominal diameter is designated by  $d$ .

Having established the allowance, interference, and tolerance, the next step is to establish the maximum and minimum diameters of the hub and shaft. Table 10.3 gives these dimensions for the two types of fit (clearance and interference). Tables 10.2 and 10.3 thus establish the upper and lower limits of the shaft and hub diameters for the eight classes of fit.

### Example 10.1: Interference and Class of Fit

**Given:** A medium-force interference fit is applied to a shaft with a nominal diameter of 75 mm.

**Find:** Determine the interference, the hole and shaft tolerances, and the hub and shaft diameters.

**Solution:** From Table 10.1, the class of fit is 7. From Table 10.2 for a class 7 fit,

$$\delta = 0.0005d = 0.0005(75) = 0.0375 \text{ mm},$$

$$t_{lh} = t_{ls} = 0.0052d^{1/3} = 0.0052(75)^{1/3} = 0.0219 \text{ mm}.$$

From Table 10.3 for interference fit, the hub diameter is

$$d_{h,\max} = d + t_{lh} = 75 + 0.0219 = 75.0219 \text{ mm};$$

$$d_{h,\min} = d = 75 \text{ mm}.$$

and the shaft diameter is

$$\begin{aligned} d_{s,\max} &= d + \delta + t_{ls} \\ &= 75 + 0.0375 + 0.0219 \\ &= 75.059 \text{ mm}, \\ d_{s,\min} &= d + \delta \\ &= 75 + 0.0219 \\ &= 75.0219 \text{ mm}. \end{aligned}$$

## 10.3 Pressurization Effects

This section presents thin-walled and thick-walled cylinders with internal and external pressurization. The material in this section is used for a wide range of applications, some of which are

1. Pressure vessels loaded internally and/or externally
2. Storage tanks
3. Gun barrels
4. Hydraulic and pneumatic cylinders
5. Transmission pipelines
6. Machine elements, such as rolling-element bearing races or gears pressed onto shafts

A distinction must be made between **thin-walled cylinders** and **thick-walled cylinders**. In this book, when a cylinder's inner diameter,  $d_i$ , is 40 times larger than its thickness  $t_h$ , it will be considered as thin-walled. For smaller ratios of cylinder inner diameter to thickness, thick-wall analysis should be used. This criterion is somewhat arbitrary and depends on the desired accuracy in stress analysis, but is a good guideline. Mathematically expressing the above gives

$$\frac{d_i}{t_h} > 40 \quad \rightarrow \quad \text{thin-walled cylinders}, \quad (10.1)$$

$$\frac{d_i}{t_h} < 40 \quad \rightarrow \quad \text{thick-walled cylinders}. \quad (10.2)$$

### 10.3.1 Thin-Walled Cylinders

Figure 10.1a shows a thin-walled cylinder subjected to internal pressure,  $p_i$ . It is assumed that the stress distribution is uniform throughout the thickness. The radial stress is small relative to the circumferential stress because  $t_h/d_i \ll 1$ . Thus, a small element can be considered to be in plane stress with the principal stresses shown in Fig. 10.1b.

Figure 10.2, the front view of the cylinder shown in Fig. 10.1, shows the forces acting on a small element due to the internal pressure. This element also has a length  $dl$  in the thickness direction. Applying force equilibrium in the radial direction gives

$$p_i r_i d\theta dl = 2\sigma_{\theta,\text{avg}} \sin\left(\frac{d\theta}{2}\right) t_h dl.$$

Since  $d\theta/2$  is small,  $\sin(d\theta/2) \approx d\theta/2$  and thus

$$\sigma_{\theta,\text{avg}} = \frac{p_i r_i}{t_h}. \quad (10.3)$$

Table 10.2: Recommended tolerances in *millimeters* for classes of fit.

Class	Allowance, $a$	Interference, $\delta$	Hub tolerance, $t_{lh}$	Shaft tolerance, $t_{ls}$
1	$0.0073d^{2/3}$	—	$0.0216d^{1/3}$	$0.0216d^{1/3}$
2	$0.0041d^{2/3}$	—	$0.0112d^{1/3}$	$0.0112d^{1/3}$
3	$0.0026d^{2/3}$	—	$0.0069d^{1/3}$	$0.0069d^{1/3}$
4	0.000	—	$0.0052d^{1/3}$	$0.0035d^{1/3}$
5	—	0.000	$0.0052d^{1/3}$	$0.0035d^{1/3}$
6	—	$0.00025d$	$0.0052d^{1/3}$	$0.0052d^{1/3}$
7	—	$0.0005d$	$0.0052d^{1/3}$	$0.0052d^{1/3}$
8	—	$0.0010d$	$0.0052d^{1/3}$	$0.0052d^{1/3}$

Table 10.3: Maximum and minimum diameters of shaft and hub for two types of fit.

Type of fit	Hub diameter		Shaft diameter	
	Maximum $d_{h,max}$	Minimum $d_{h,min}$	Maximum $d_{s,max}$	Minimum $d_{s,min}$
Clearance	$d + t_{lh}$	$d$	$d - a$	$d - a - t_{ls}$
Interference	$d + t_{lh}$	$d$	$d + \delta + t_{ls}$	$d + \delta$

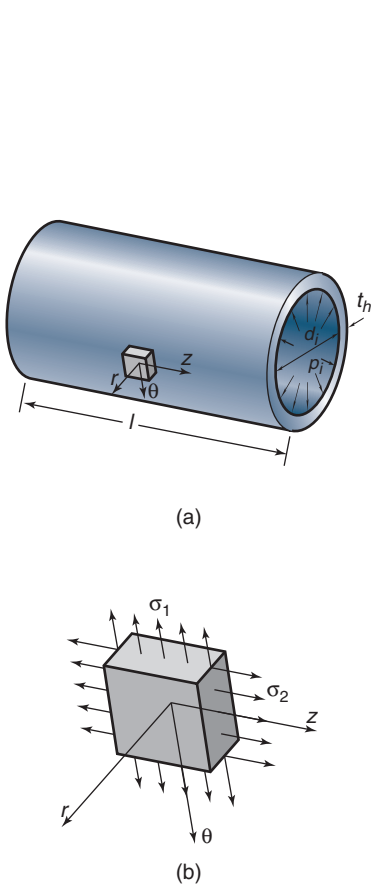


Figure 10.1: Internally pressurized thin-walled cylinder. (a) Stress element on cylinder; (b) stresses acting on element.

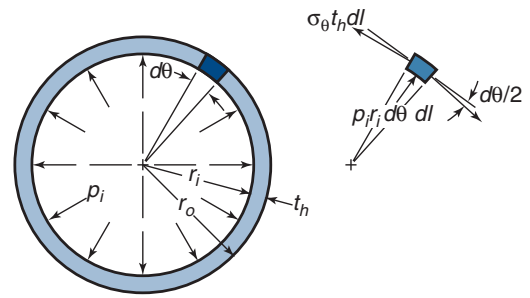


Figure 10.2: Front view of internally pressurized, thin-walled cylinder.

The  $\theta$  component of stress is called the tangential stress or **hoop stress**; the term originates from the manufacture of wooden barrels by shrinking a hot iron ring, or hoop, around closely fitting planks to achieve a seal. Note, for a thin-walled pressure vessel, that  $r_i \approx r$ , so that

$$\sigma_\theta = \frac{p_i r}{t_h}. \quad (10.4)$$

The area subjected to axial stress is

$$A = \pi(r_o^2 - r_i^2) = 2\pi r_{avg} t_h. \quad (10.5)$$

Thus, the average axial tensile stress is

$$\sigma_{z,avg} = \frac{p_i r_i^2}{r_o^2 - r_i^2} = \frac{p_i r_i^2}{2r_{avg} t_h}.$$

But since  $r_i \approx r$ ,

$$\sigma_z = \frac{p_i r}{2t_h}. \quad (10.6)$$

The stress in the radial direction is, from equilibrium,

$$\sigma_r = p. \quad (10.7)$$

However, the pressure is usually much smaller than  $\sigma_\theta$  or  $\sigma_z$ , so  $\sigma_r = 0$  is a reasonable approximation. Note that the circumferential (hoop) stress is twice the axial stress. In summary, the principal stresses for thin-walled cylinders are:



$$\sigma_1 = \sigma_\theta = \frac{p_i r}{t_h}, \quad (10.8)$$

$$\sigma_2 = \sigma_z = \frac{p_i r}{2t_h}, \quad (10.9)$$

$$\sigma_3 = \sigma_r = 0. \quad (10.10)$$

### Example 10.2: Thin-Walled Cylinder

**Given:** A 100-mm-inner-diameter cylinder made of a material with a yield strength of 400 MPa is subjected to an internal pressure of 2 MPa. Use a safety factor of 3 and assume that thin-wall analysis is adequate.

**Find:** Determine the wall thickness required to prevent yielding, based on

(a) Maximum-shear-stress theory (MSST)

(b) Distortion-energy theory (DET)

**Solution:** From Eqs. (10.8) through (10.10),

$$\sigma_1 = \sigma_\theta = \frac{p_i r}{t_h} = \frac{(2 \times 10^6)(0.050)}{t_h},$$

$$\sigma_2 = \sigma_z = \frac{p_i r}{2t_h} = \frac{(2 \times 10^6)(0.050)}{2t_h},$$

$$\sigma_3 = \sigma_r = 0.$$

Because  $\sigma_1 > \sigma_2 > \sigma_3$ , the principal stresses are ordered properly according to Eq. (2.18).

(a) From Eq. (6.8), yielding occurs according to the MSST when

$$\sigma_1 - \sigma_3 = \frac{S_y}{n_s}.$$

Substituting for  $\sigma_1$  and  $\sigma_3$  and solving for the thickness,

$$t_h = \frac{p_i r n_s}{S_y} = \frac{(2 \times 10^6)(0.050)(3)}{400 \times 10^6} = 0.75 \text{ mm}.$$

(b) Note in this case that  $\sigma_2 = \sigma_1/2$ . The von Mises stress for a biaxial stress state is obtained from Eq. (6.12) as:

$$\sigma_e = (\sigma_1^2 + \sigma_2^2 - \sigma_1 \sigma_2)^{1/2} = \left( \frac{3\sigma_1^2}{4} \right)^{1/2} = \sqrt{\frac{3}{4}} \sigma_1.$$

Substituting for  $\sigma_1$ ,

$$\sigma_e = (0.8660) \frac{(2 \times 10^6)(0.050)}{t_h} = \frac{(8.66 \times 10^4)}{t_h}.$$

From Eq. (6.11), yielding occurs when

$$\sigma_e = \frac{S_y}{n_s}.$$

Thus, yielding occurs when

$$t_h > \frac{(8.66 \times 10^4) n_s}{S_y} = \frac{(8.66 \times 10^4)(3)}{400 \times 10^6} = 0.650 \text{ mm}.$$

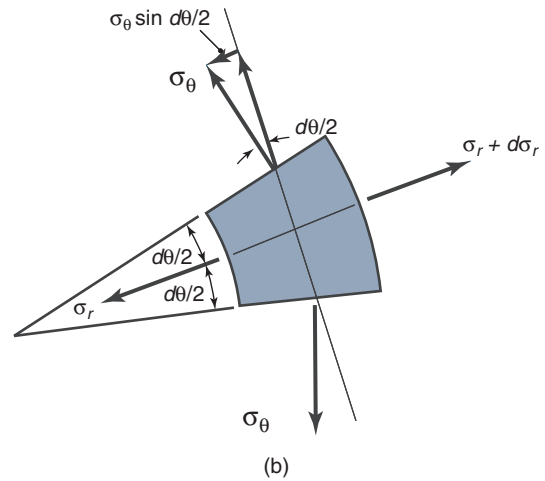
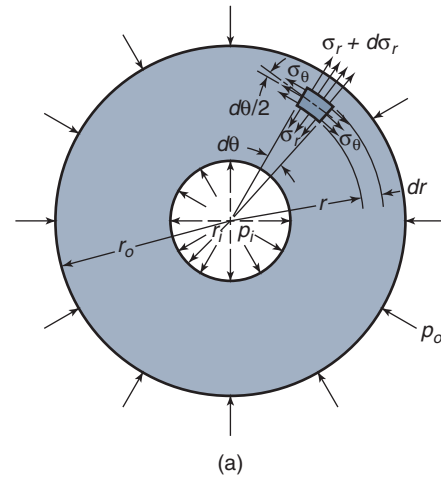


Figure 10.3: Complete front view of thick-walled cylinder internally and externally pressurized. (a) With stresses acting on cylinder; (b) detail of stresses acting on element.

### 10.3.2 Thick-Walled Cylinders

It was indicated in Section 10.3.1 that if the cylinder walls are thin, the circumferential or hoop stress,  $\sigma_\theta$ , can be assumed to be uniform throughout the wall thickness. This assumption cannot be made for thick-walled cylinders.

Figure 10.3a shows a radially loaded, thick-walled cylinder subjected to internal pressure,  $p_i$ , and external pressure,  $p_o$ . A stress element in the thick-walled cylinder is shown in Fig. 10.3b. Because the body and the loading are symmetrical about the axis, shear stresses in the circumferential and radial directions are not present, and only normal stresses  $\sigma_\theta$  and  $\sigma_r$  act on the stress element. The loading is two-dimensional; therefore, only plane stresses are involved. If an axial loading is superimposed [Eq. (10.6) developed in Section 10.3.1], the third principal stress is merely changed from zero to  $\sigma_z$ . Recall that Eq. (10.6) is valid regardless of cylinder thickness.

Figure 10.4 shows a cylindrical polar element before and after deformation. The radial and circumferential (hoop) displacements are given by  $\delta_r$  and  $\delta_\theta$ , respectively. The radial strain is given by:

$$\epsilon_r = \frac{\partial \delta_r}{\partial r} = \frac{\delta_r + \frac{\partial \delta_r}{\partial r} dr - \delta_r}{dr}. \quad (10.11)$$

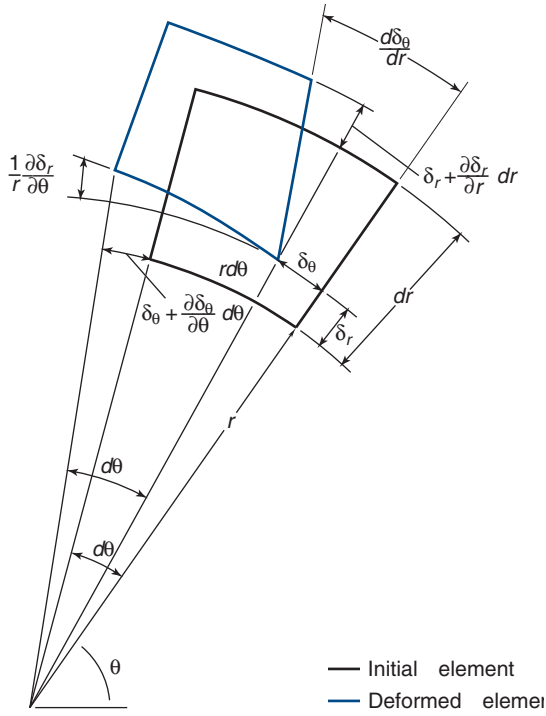


Figure 10.4: Cylindrical coordinate stress element before and after deformation.

The circumferential strain is associated with the displacement to the new radius  $r + \delta_r$ , or

$$\epsilon_\theta = \frac{(r + \delta_r)d\theta - r d\theta}{r d\theta} = \frac{\delta_r}{r}. \quad (10.12)$$

The circumferential variations shown in Fig. 10.4 will be ignored due to circular symmetry. Note that asymmetric cross sections, stress concentrations, or local yielding can cause such distortions, but these complications are assumed to be absent from the cylinder being analyzed. From Hooke's law, the stress-strain relationship for the biaxial stress state [see Eq. (B.58)], while making use of Eqs. (10.11) and (10.12), gives

$$\epsilon_r = \frac{\partial \delta_r}{\partial r} = \frac{1}{E}(\sigma_r - \nu \sigma_\theta), \quad (10.13)$$

$$\epsilon_\theta = \frac{\delta_r}{r} = \frac{1}{E}(\sigma_\theta - \nu \sigma_r). \quad (10.14)$$

The expressions for the radial and circumferential stresses are obtained from force equilibrium of the element. Figure 10.3b gives details of the stresses. Summing the forces in the radial direction gives

$$(\sigma_r + d\sigma_r)(r + dr) d\theta dz - \sigma_r r d\theta dz - 2\sigma_\theta \sin\left(\frac{d\theta}{2}\right) dr dz = 0. \quad (10.15)$$

For small  $d\theta$ ,  $\sin(d\theta/2) \approx d\theta/2$ , and Eq. (10.15) reduces to

$$\sigma_\theta = r \frac{d\sigma_r}{dr} + \sigma_r. \quad (10.16)$$

Equations (10.13), (10.14), and (10.16) are three equations with three unknowns  $\delta_r$ ,  $\sigma_r$ , and  $\sigma_\theta$ . Substituting

Eq. (10.16) into Eqs. (10.13) and (10.14) and then differentiating Eq. (10.14) with respect to  $r$  while equating Eqs. (10.13) and (10.14) gives

$$0 = 3 \frac{d\sigma_r}{dr} + r \frac{d^2 \sigma_r}{dr^2}. \quad (10.17)$$

Equation (10.17) can be rewritten as

$$0 = 2 \frac{d\sigma_r}{dr} + \frac{d}{dr} \left( r \frac{d\sigma_r}{dr} \right). \quad (10.18)$$

Integrating gives

$$0 = 2\sigma_r + r \frac{d\sigma_r}{dr} + C_1.$$

This equation can be rewritten as

$$0 = \frac{d}{dr} (r^2 \sigma_r) + C_1 r.$$

Integrating gives

$$\sigma_r = -\frac{C_1}{2} - \frac{C_2}{r^2}. \quad (10.19)$$

The boundary conditions for thick-walled cylinders pressurized both internally and externally are

1.  $\sigma_r = -p_i$  at  $r = r_i$
2.  $\sigma_r = -p_o$  at  $r = r_o$

Note the sign convention: a positive pressure results in a compressive (negative) stress; therefore, a negative sign appears in the boundary conditions. Applying the boundary conditions gives

$$\sigma_r = \frac{p_i r_i^2 - p_o r_o^2 + (p_o - p_i) \left( \frac{r_o r_i}{r} \right)^2}{r_o^2 - r_i^2}, \quad (10.20)$$

$$\frac{d\sigma_r}{dr} = -\frac{2(p_o - p_i)(r_o r_i)^2}{r^3(r_o^2 - r_i^2)}. \quad (10.21)$$

Substituting Eqs. (10.20) and (10.21) into Eq. (10.16) gives

$$\sigma_\theta = \frac{p_i r_i^2 - p_o r_o^2 + \left( \frac{r_i r_o}{r} \right)^2 (p_o - p_i)}{r_o^2 - r_i^2}. \quad (10.22)$$

Equations (10.20) and (10.22) are valuable for the general case of a thick-walled cylinder subjected to internal and external pressurization. Some special cases yield less complicated expressions that are useful for machinery applications.

### Internally Pressurized

If, as in many applications, the outer pressure,  $p_o$ , is zero, Eqs. (10.20) and (10.22) reduce to

$$\sigma_r = \frac{p_i r_i^2 \left( 1 - \frac{r_o^2}{r^2} \right)}{r_o^2 - r_i^2}, \quad (10.23)$$

$$\sigma_\theta = \frac{p_i r_i^2 \left( 1 + \frac{r_o^2}{r^2} \right)}{r_o^2 - r_i^2}. \quad (10.24)$$

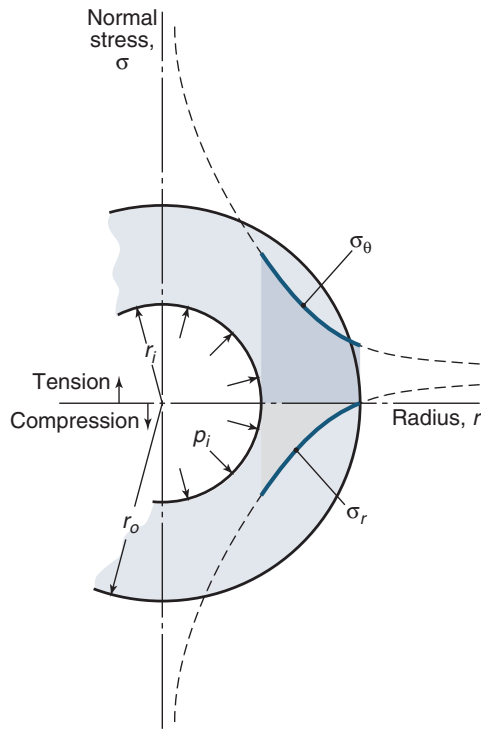


Figure 10.5: Internally pressurized, thick-walled cylinder showing circumferential (hoop) and radial stress for various radii.

Figure 10.5 shows the radial and circumferential (hoop) stresses in an internally pressurized cylinder. The circumferential stress is tensile and the radial stress is compressive. Further, the maximum stresses occur at  $r = r_i$  and are

$$\sigma_{r_{\max}} = -p_i, \quad (10.25)$$

$$\sigma_{\theta_{\max}} = p_i \left( \frac{r_o^2 + r_i^2}{r_o^2 - r_i^2} \right). \quad (10.26)$$

From Eq. (10.14), the circumferential strains for internal pressurization as evaluated at the location of maximum stress are

$$\epsilon_{\theta} = \frac{\delta_r}{r_i} = \frac{p_i}{E} \left( \frac{r_o^2 + r_i^2}{r_o^2 - r_i^2} + \nu \right), \quad (10.27)$$

where  $\nu$  is Poisson's ratio. The radial displacement is outward and is given by

$$\delta_r = \frac{p_i r_i}{E} \left( \frac{r_o^2 + r_i^2}{r_o^2 - r_i^2} + \nu \right). \quad (10.28)$$

### Example 10.3: Internally Pressurized Thick-Walled Cylinder

**Given:** A hydraulic cylinder can be pressurized to 100 MPa. The inner radius of the cylinder is 100 mm and the wall thickness is 35 mm.

**Find:** The tangential and axial stresses in the cylinder wall at the inner diameter for both thin- and thick-wall analysis.

**Solution:** From the thin-wall theory given in Eqs. (10.8) and (10.9), the following can be written:

$$\sigma_1 = \frac{p_i r}{t_h} = \frac{(100 \times 10^6)(0.1)}{0.035} = 285.7 \text{ MPa},$$

$$\sigma_2 = \frac{p_i r}{2t_h} = 142.9 \text{ MPa}.$$

From thick-wall theory with internal pressurization, Eq. (10.26) gives

$$\sigma_{\theta, \max} = p_i \left( \frac{r_o^2 + r_i^2}{r_o^2 - r_i^2} \right) = (100 \times 10^6) \left( \frac{0.135^2 + 0.10^2}{0.135^2 - 0.10^2} \right),$$

which is solved as  $\sigma_{\theta, \max} = 343.2 \text{ MPa}$ . Assuming the axial stress is uniform throughout the wall,

$$\sigma_z = \frac{\pi r_i^2 p_i}{\pi(r_o^2 - r_i^2)} = \frac{(0.10)^2 (100 \times 10^6)}{0.135^2 - 0.10^2} = 121.6 \text{ MPa}.$$

Note in this case there is a substantial difference between the thick- and thin-wall approaches.

### Externally Pressurized

If the internal pressure is zero and the cylinder is externally pressurized, Eqs. (10.20) and (10.22) reduce to

$$\sigma_r = \frac{p_o r_o^2}{r_o^2 - r_i^2} \left( \frac{r_i^2}{r^2} - 1 \right), \quad (10.29)$$

$$\sigma_{\theta} = -\frac{p_o r_o^2}{r_o^2 - r_i^2} \left( \frac{r_i^2}{r^2} + 1 \right). \quad (10.30)$$

Figure 10.6 shows the radial and circumferential stresses in an externally pressurized cylinder. Note that both stresses are compressive. Furthermore, the maximum circumferential stress occurs at  $r = r_i$  and the maximum radial stress occurs at  $r = r_o$ . These expressions are

$$\sigma_{r, \max} = -p_o, \quad (10.31)$$

$$\sigma_{\theta, \max} = -\frac{2r_o^2 p_o}{r_o^2 - r_i^2}. \quad (10.32)$$

## Design Procedure 10.1: Stress Analysis of Thick-Walled Cylinders

A common design problem is to determine the largest permissible external and/or internal pressure to which a cylinder can be subjected without failure. Axial stresses, if present, are negligibly small. The following design procedure is useful for such circumstances:

1. For internal pressurization, both the radial and circumferential stresses are largest at the inner radius. The von Mises stress for this plane stress case can be shown to be

$$\sigma_e = p_i \sqrt{\frac{3r_o^4 + r_i^4}{(r_o^2 - r_i^2)^2}},$$

so that the allowable internal pressure is, from Eq. (6.8),

$$p_i = \frac{S_y}{n_s} \frac{r_o^2 - r_i^2}{\sqrt{3r_o^4 + r_i^4}}.$$

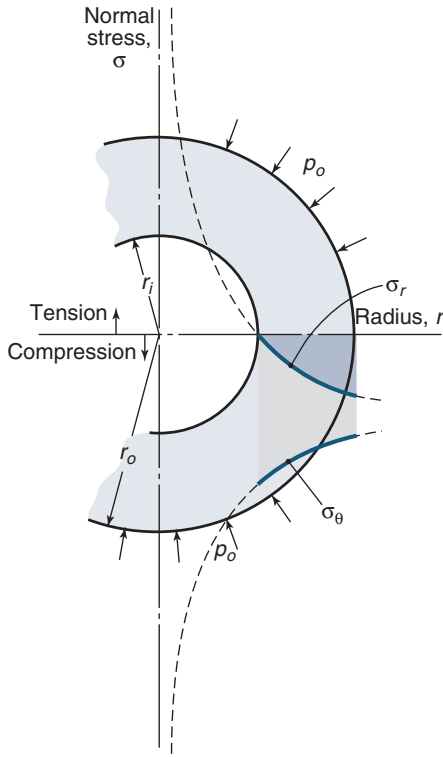


Figure 10.6: Externally pressurized, thick-walled cylinder showing circumferential (hoop) and radial stress for various radii.

2. For external pressurization, it can be shown that the larger von Mises stress occurs at the inner radius, with the stresses of  $\sigma_r = 0$  and  $\sigma_\theta$  given by Eq. (10.32). This yields an expression of allowable external pressure of:

$$p_o = \frac{S_y}{n_s} \frac{r_o^2 - r_i^2}{2r_o^2}.$$

3. For combined internal and external pressurization, Eqs. (10.20) and (10.22) need to be substituted into a failure criterion from Ch. 6, such as the DET given for plane stress in Eqs. (6.10) and (6.11).

### Example 10.4: Design of a Thick Walled Cylinder

**Given:** A thick-walled cylinder with 0.3-m internal diameter and 0.4-m external diameter has a maximum circumferential (hoop) stress of 250 MPa. The material has a Poisson's ratio of 0.3 and a modulus of elasticity of 207 GPa.

**Find:** Determine the following:

- For internal pressurization ( $p_o = 0$ ) the maximum pressure to which the cylinder may be subjected.
- For external pressurization ( $p_i = 0$ ) the maximum pressure to which the cylinder may be subjected.
- The radial displacement of a point on the inner surface for the situation presented in part a.

### Solution:

- (a) From Eq. (10.26) for internal pressurization,

$$p_i = \frac{\sigma_{\theta\max} (r_o^2 - r_i^2)}{r_o^2 + r_i^2} = \frac{(250 \times 10^6) (0.2^2 - 0.15^2)}{0.2^2 + 0.15^2},$$

which results in  $p_i = 70$  MPa.

- (b) From Eq. (10.32) for external pressurization,

$$p_o = -\frac{\sigma_{\theta\max} (r_o^2 - r_i^2)}{2r_o^2} = \frac{(250 \times 10^6) (0.2^2 - 0.15^2)}{2(0.2)^2},$$

which is solved as  $p_o = 54.69$  MPa.

- (c) The radial displacement for internally pressurized cylinders is obtained from Eq. (10.28) as

$$\begin{aligned} \delta_{r,\max} &= \frac{p_i r_i}{E} \left( \frac{r_o^2 + r_i^2}{r_o^2 - r_i^2} + \nu \right) \\ &= \frac{(70 \times 10^6) (0.15)}{(207 \times 10^9)} \left( \frac{0.2^2 + 0.15^2}{0.2^2 - 0.15^2} + 0.3 \right) \\ &= 1.96 \times 10^{-4} \text{ m} = 0.196 \text{ mm}. \end{aligned}$$

## 10.4 Rotational Effects

Rotating cylinders are encountered in a number of machine elements such as flywheels, gears, pulleys, and sprockets. This section considers rotation of the cylinder while assuming no pressurization ( $p_i = p_o = 0$ ).

If a body force is included when considering the stresses acting on the elements shown in Fig. 10.3, Eq. (10.16) becomes

$$\frac{\sigma_\theta - \sigma_r}{r} - \frac{d\sigma_r}{dr} - P_b = 0, \quad (10.33)$$

where  $P_b$  is the body force per volume. Here, the body force is the rotating inertia force that acts radially and is given by

$$P_b = r\omega^2 \rho, \quad (10.34)$$

where

$\omega$  = angular velocity, rad/s

$\rho$  = mass density, kg/m<sup>3</sup>

$r$  = radius of cylinder, m

Two special cases are considered: a cylinder with a central hole and a solid cylinder. The resulting equations are presented in this section since the derivation is similar to that presented in Section 10.3.

### 10.4.1 Cylinder with Central Hole

The circumferential (hoop) and radial stresses for a rotating cylinder with a central hole but neglecting pressurization are

$$\sigma_\theta = \frac{3 + \nu}{8} \rho \omega^2 \left[ r_i^2 + r_o^2 + \frac{r_i^2 r_o^2}{r^2} - \frac{1 + 3\nu}{3 + \nu} r^2 \right], \quad (10.35)$$

$$\sigma_r = \frac{3 + \nu}{8} \rho \omega^2 \left( r_i^2 + r_o^2 - \frac{r_i^2 r_o^2}{r^2} - r^2 \right). \quad (10.36)$$

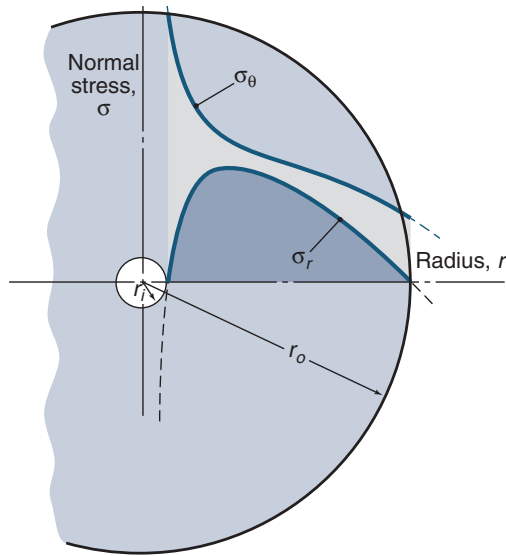


Figure 10.7: Stresses in rotating cylinder with central hole and no pressurization.

Figure 10.7 shows the variation of stress with radius. Note that both stresses are tensile. The radial stress is zero at the inner and outer radii, with a maximum occurring between  $r_i$  and  $r_o$ . The circumferential stress is a maximum at  $r = r_i$  and exceeds the radial stress for any value of radius. The maximum circumferential stress is

$$\sigma_{\theta, \max} = \frac{3 + \nu}{4} \rho \omega^2 \left[ r_o^2 + \frac{r_i^2(1 - \nu)}{3 + \nu} \right]. \quad (10.37)$$

The maximum radial stress can be obtained by differentiating Eq. (10.36) with respect to  $r$  and setting the result equal to zero. Thus,

$$\sigma_{r, \max} = \frac{3 + \nu}{8} \rho \omega^2 (r_i - r_o)^2. \quad (10.38)$$

The location of maximum stress is

$$r = \sqrt{r_i r_o}. \quad (10.39)$$

### Example 10.5: Rotating Press Fit

**Given:** Two concentric AISI 1040 steel tubes are press fit together at 110 MPa (see Section 10.5). The nominal sizes of the tubes are 100-mm outer diameter and 80-mm inner diameter and 80-mm outer diameter and 60-mm inner diameter, respectively.

**Find:** How fast does the combined tube have to rotate to decrease the press-fit pressure to zero?

**Solution:** By assuming linear elastic behavior, the press-fit pressure of 110 MPa has to be compensated for by an equally large radial stress at the fit radius. Equation (10.36) thus gives

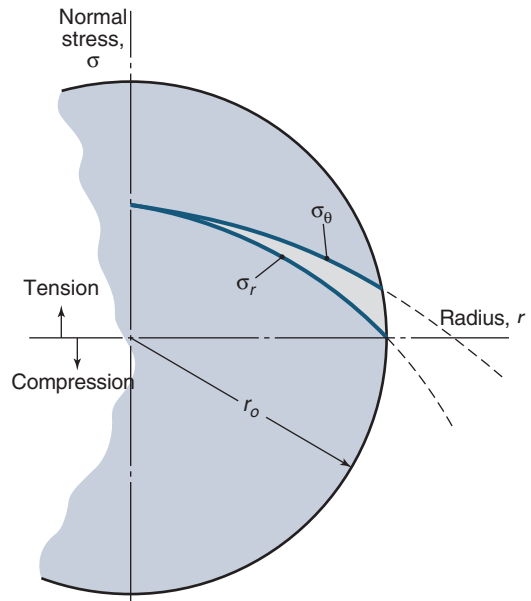


Figure 10.8: Stresses in rotating solid cylinder with no pressurization.

$$\begin{aligned} \sigma_r &= \frac{3 + \nu}{8} \rho \omega^2 \left( r_i^2 + r_o^2 - \frac{r_i^2 r_o^2}{r^2} - r^2 \right) \\ &= \frac{(3 + 0.3)}{8} (7850) \omega^2 \\ &\quad \times \left[ (0.03)^2 + (0.05)^2 - \frac{(0.03)^2 (0.05)^2}{(0.04)^2} - (0.04)^2 \right] \\ &= 110 \text{ MPa.} \end{aligned}$$

This results in

$$\omega = 9288 \text{ rad/s} = 88,700 \text{ rpm.}$$

Thus, at 88,700 rpm the press-fit pressure becomes zero. This very high rotational speed clearly shows that press fits of tubes do not loosen due to inertial effects in such machine elements. However, their torque transmission capability may be reduced at higher speeds.

### 10.4.2 Solid Cylinder

Setting  $r_i = 0$  in Eqs. (10.35) and (10.36) gives the circumferential and radial stresses when considering rotation of a solid cylinder but neglecting pressurization effects. The results are

$$\sigma_{\theta} = \frac{3 + \nu}{8} \rho \omega^2 \left[ r_o^2 - \frac{r^2(1 + 3\nu)}{3 + \nu} \right], \quad (10.40)$$

$$\sigma_r = \frac{3 + \nu}{8} \rho \omega^2 (r_o^2 - r^2). \quad (10.41)$$

Figure 10.8 shows the stress distribution for both stress components as a function of radius for a solid cylinder. Note that both stresses are tensile, with the maximum occurring at  $r = 0$  and both having the same value at that location. The maximum stress is

$$\sigma_{\theta, \max} = \sigma_{r, \max} = \frac{3 + \nu}{8} \rho (r_o \omega)^2. \quad (10.42)$$

Some interesting observations can be made in comparing Eqs. (10.37) and (10.38) with Eq. (10.42). As  $r_i$  becomes very



small, Eqs. (10.38) and (10.42) are in complete agreement. However, as  $r_i$  approaches 0, Eqs. (10.37) and (10.42) differ by a factor of two with respect to circumferential stress. This difference is due to the radial stress in the inner portion of the solid cylinder, which decreases the circumferential stress.

### Example 10.6: Rotating Cylinder

**Given:** A cylindrical flywheel is press fitted on a solid shaft. Both are made of AISI 1080 steel, so that  $\rho = 7850 \text{ kg/m}^3$ . The press-fit pressure is 185 MPa, the shaft diameter is 100 mm, and the outside diameter of the flywheel is 550 mm.

**Find:** The shaft speed when the press-fit pressure is eliminated by centrifugal effects.

**Solution:** When the radial stress due to centrifugal acceleration at the shaft surface is equal to the original press-fit pressure, the flywheel will start to separate from the shaft. From Table 3.1 and Eq. (10.41),

$$\begin{aligned}\sigma_r &= \frac{(3 + \nu)\rho\omega^2 (r_o^2 - r^2)}{8} \\ &= \frac{(3 + 0.3)(7850)\omega^2 (0.275^2 - 0.050^2)}{8} \\ &= 185 \times 10^6 \text{ Pa.}\end{aligned}$$

Solving for angular velocity,

$$\omega = 883.9 \text{ rad/s} = 8441 \text{ rpm.}$$

Thus, at 8441 rpm the press-fit pressure becomes zero. This speed is high, but not unreasonable for a flywheel mounted shaft; thus, press fits can fail in this manner for overspeeding shafts with flywheels, and their torque transmission can be compromised at even lower speeds.

## 10.5 Press Fits

In a **press fit**, the pressure,  $p_f$ , is caused by the radial interference between the shaft and the hub. This pressure increases the radius of the hole and decreases the radius of the shaft. Section 10.2 described shaft and hub dimensions in terms of tolerance, which results in specific fits. This section focuses on the stress and strain found in press fits and uses equations developed in Section 10.3.2 for thick-walled cylinders.

Figure 10.9 shows a side view of interference in a press fit; there is a radial displacement of the hub,  $\delta_{rh}$ , and a radial displacement of the shaft,  $\delta_{rs}$ . Figure 10.10 shows the front view of an interference fit. In Fig. 10.10a, the cylinders are assembled with an interference fit; in Fig. 10.10b, the hub and shaft are disassembled and the dimensions of each are clearly shown. This figure also shows that the interference pressure acts internally for the hub and externally for the shaft. The shaft is shown as a tube in order to present the most general case.

### 10.5.1 Hub

Using Eq. (10.14), the hub displacement is

$$\delta_{rh} = \frac{r_f}{E_h} (\sigma_\theta - \nu_h \sigma_r), \quad (10.43)$$

where  $E_h$  is the elastic modulus and  $\nu_h$  is the Poisson's ratio of the hub material, respectively. For internally pressurized,

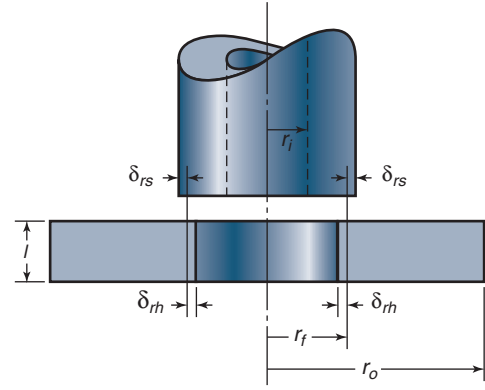


Figure 10.9: Side view showing interference in press fit of hollow shaft to hub.

thick-walled cylinders and from Eqs. (10.23) and (10.24), the radial and circumferential stresses for the hub while letting  $p_i = p_f$ ,  $r = r_f$ , and  $r_i = r_f$ , are

$$\sigma_r = \frac{p_f r_f^2 \left(1 - \frac{r_o^2}{r_f^2}\right)}{r_o^2 - r_f^2} = -p_f, \quad (10.44)$$

and

$$\sigma_\theta = \frac{p_f r_f^2 \left(1 + \frac{r_o^2}{r_f^2}\right)}{r_o^2 - r_f^2} = \frac{p_f (r_o^2 + r_f^2)}{r_o^2 - r_f^2}. \quad (10.45)$$

Substituting Eqs. (10.44) and (10.45) into Eq. (10.43) gives

$$\delta_{rh} = \frac{r_f p_f}{E_h} \left( \frac{r_o^2 + r_f^2}{r_o^2 - r_f^2} + \nu_h \right). \quad (10.46)$$

Since  $\delta_{rh}$  is positive, the radial displacement of the hub is outward.

### 10.5.2 Shaft

Using Eq. (10.14), the displacement of the shaft is

$$\delta_{rs} = \frac{r_f}{E_s} (\sigma_\theta - \nu_s \sigma_r), \quad (10.47)$$

where  $E_s$  is the elastic modulus and  $\nu_s$  is Poisson's ratio of shaft material, respectively. The circumferential and radial stresses for externally pressurized, thick-walled cylinders can be obtained from Eqs. (10.29) and (10.30) by letting  $p_o = p_f$ ,  $r_o = r_f$ , and  $r = r_f$ , yielding

$$\sigma_r = \frac{p_f r_f^2}{r_f^2 - r_i^2} \left( \frac{r_i^2}{r_f^2} - 1 \right) = -p_f \quad (10.48)$$

and

$$\sigma_\theta = -\frac{p_f r_f^2}{r_f^2 - r_i^2} \left( \frac{r_i^2}{r_f^2} + 1 \right) = -\frac{p_f (r_f^2 + r_i^2)}{r_f^2 - r_i^2}. \quad (10.49)$$

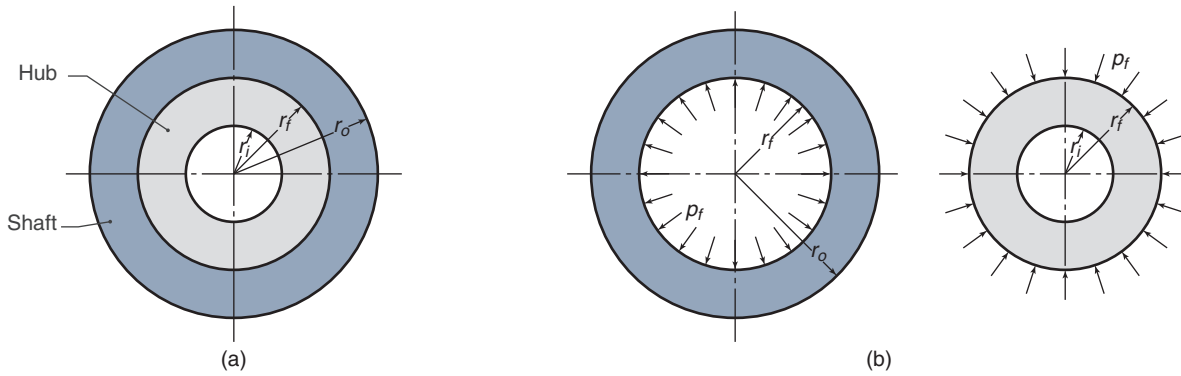


Figure 10.10: Front view showing (a) cylinder assembled with an interference fit and (b) hub and hollow shaft disassembled (also showing interference pressure).

Substituting Eqs. (10.48) and (10.49) into Eq. (10.47) gives

$$\delta_{rs} = -\frac{r_f p_f}{E_s} \left( \frac{r_f^2 + r_i^2}{r_f^2 - r_i^2} - \nu_s \right). \quad (10.50)$$

Because the first term in parentheses in Eq. (10.50) is greater than unity and the Poisson's ratio is less than or equal to 0.5,  $\delta_{rs}$  is negative; hence, shaft displacement is directed inward toward the center of the shaft.

### 10.5.3 Interference Fit

The total radial displacement in an interference fit is shown in Fig. 10.9. Recall that outward deflection (expansion of the inside diameter of the hub) is positive and inward deflection (reduction of the outside diameter of the shaft) is negative. Thus, the total radial interference is

$$\begin{aligned} \delta_r &= \delta_{rh} - \delta_{rs} \\ &= r_f p_f \left[ \frac{r_o^2 + r_f^2}{E_h (r_o^2 - r_f^2)} + \frac{\nu_h}{E_h} + \frac{r_f^2 + r_i^2}{E_s (r_f^2 - r_i^2)} - \frac{\nu_s}{E_s} \right]. \end{aligned} \quad (10.51)$$

If the shaft and the hub are made of the same material,  $E = E_s = E_h$  and  $\nu = \nu_s = \nu_h$ , so that Eq. (10.51) reduces to

$$\delta_r = \frac{2r_f^3 p_f (r_o^2 - r_i^2)}{E (r_o^2 - r_f^2) (r_f^2 - r_i^2)}. \quad (10.52)$$

Furthermore, if the shaft is solid rather than hollow,  $r_i = 0$  and Eq. (10.52) further reduces to

$$\delta_r = \frac{2r_f p_f r_o^2}{E (r_o^2 - r_f^2)}. \quad (10.53)$$

From these equations, it can be seen that if the radial displacement is known, the interference pressure can be readily obtained or vice-versa.

### 10.5.4 Force and Torque

The maximum force to assemble a press fit depends on the thickness and length of the outer member, the difference in

diameters of the mating shaft and hub, and the coefficient of friction,  $\mu$ . The maximum shear stress is

$$\tau_{\max} = p_f \mu = \frac{P_{\max}}{A} = \frac{P_{\max}}{2\pi r_f l}. \quad (10.54)$$

The torque that can be transmitted by the press fit is

$$T = P_{\max} r_f = 2\pi \mu r_f^2 l p_f. \quad (10.55)$$

It should be noted that the axial and circumferential stresses are related to the maximum stress by

$$\tau_a^2 + \tau_c^2 = \tau_{\max}^2,$$

where

$$\tau_a = \frac{P_a}{2\pi r_f l} = \text{axial stress}$$

$$\tau_c = \frac{P_c}{2\pi r_f l} = \text{circumferential stress}$$

Thus, the assembly and disassembly force given by Eq. (10.54) can be reduced by twisting or rotating the outer member while applying an axial force.

### Example 10.7: Interference Fit

**Given:** A 150-mm-diameter steel shaft is to have a press fit with a 300-mm-outside-diameter cast iron hub. The hub is 25 mm long and defines the contact length. The maximum circumferential stress is to be 30 MPa. The moduli of elasticity are 207 GPa for steel and 100 GPa for cast iron. The Poisson's ratio for both steel and cast iron is 0.3 and the coefficient of friction for the two materials is 0.12. That is,

$$r_f = 75 \text{ mm}, \quad r_i = 0,$$

$$r_o = 150 \text{ mm}, \quad E_s = 207 \text{ GPa},$$

$$E_h = 100 \text{ GPa}, \quad \nu_s = \nu_h = 0.3,$$

$$\mu = 0.12, \quad l = 25 \text{ mm}, \quad \sigma_{\theta, \max} = 30 \text{ MPa}.$$

**Find:**

- (a) The interference
- (b) The axial force required to press the hub on the shaft
- (c) The torque that this press fit can transmit

**Solution:**

- (a) From Eq. (10.45), the interference pressure is

$$\begin{aligned} p_f &= \frac{\sigma_{\theta, \max} (r_o^2 - r_f^2)}{r_o^2 + r_f^2} \\ &= \frac{(30 \times 10^6) (0.150^2 - 0.075^2)}{0.150^2 + 0.075^2} \\ &= 18 \text{ MPa.} \end{aligned}$$

From Eq. (10.51), the maximum permissible radial interference is

$$\delta_r = r_f p_f \left[ \frac{r_o^2 + r_f^2}{E_h (r_o^2 - r_f^2)} + \frac{\nu_h}{E_h} + \frac{r_f^2 + r_i^2}{E_s (r_f^2 - r_i^2)} - \frac{\nu_s}{E_s} \right],$$

which is solved as  $\delta_r = 31.1 \text{ } \mu\text{m}$ .

- (b) From Eq. (10.54), the force required for the press fit is

$$\begin{aligned} P_{\max} &= 2\pi\mu r_f l p_f \\ &= (2)(\pi)(0.12)(0.075)(0.025) (18 \times 10^6) \\ &= 25.4 \text{ kN.} \end{aligned}$$

- (c) From Eq. (10.55), the torque is

$$T = P_{\max} r_f = (25.4 \times 10^3) (0.075) = 1910 \text{ N-m.}$$

### Example 10.8: Disassembly of Interference Fit

**Given:** A wheel hub is press fit onto a 105-mm-diameter solid shaft. The coefficient of friction is 0.11 and the hub and shaft material is AISI 1080 steel. The hub's outer diameter is 160 mm and its width is 120 mm. The radial interference between the shaft and the hub is  $65 \text{ } \mu\text{m}$  (the shaft diameter is  $130 \text{ } \mu\text{m}$  larger than the inside diameter of the hub).

**Find:** The axial force necessary to dismount the hub.

**Solution:** Equation (10.53) gives the relationship between radial displacement and pressure as:

$$\delta_r = \frac{2r_f p_f r_o^2}{E (r_o^2 - r_f^2)},$$

or

$$(65 \times 10^{-6}) = \frac{(2)(0.0525)p_f(0.080)^2}{(207 \times 10^9) [(0.080)^2 - (0.0525)^2]}.$$

This is solved as  $p_f = 72.96 \text{ MPa}$ . The axial force necessary to dismount the hub is

$$P = \mu p_f A = (0.11) (72.96 \times 10^6) \pi (0.105)(0.120),$$

or  $P = 317.7 \text{ kN}$ .

## 10.6 Shrink Fits

In producing a **shrink fit**, it is common to heat the outer component (hub) in order to expand it beyond the interference, and then slip it over the inner component (shaft); cooling then contracts the outer component. The temperature change produces thermal strain, even in the absence of stress. Although thermal strain is not exactly linear with temperature change, for temperature changes of  $100^\circ$  or  $200^\circ\text{C}$ , a linear approximation is reasonable. According to this linear relationship, the temperature difference necessary for the outer component to obtain the required expansion over the undeformed solid shaft is

$$\Delta t_m = \frac{\delta_r}{\beta r_f}, \quad (10.56)$$

where  $\beta$  is the coefficient of thermal expansion (see Table 3.1 and Fig. 3.16). Equation (10.56) can be expressed in terms of radial strain as

$$\epsilon_r = \frac{\delta_r}{r_f} = \beta \Delta t_m. \quad (10.57)$$

The deformation is

$$\delta_r = \epsilon_r r_f = \beta \Delta t_m r_f. \quad (10.58)$$

These equations are valid not only for shrink fits of shaft and hub but also for a wide range of thermal problems.

The strain due to a temperature change may be added algebraically to a local strain by using the *principle of superposition* (see Section 5.4). Therefore, the normal strain due to normal load and temperature effects is

$$\epsilon = \epsilon_\sigma + \epsilon_{t_m}, \quad (10.59)$$

where  $\epsilon_\sigma$  is the strain due to normal stress and  $\epsilon_{t_m}$  is the strain due to temperature change. Thus, the general (triaxial stress state) stress-strain relationship given by Eq. (B.54) can incorporate thermal strain as follows:

$$\epsilon_x = \frac{1}{E} [\sigma_x - \nu (\sigma_y + \sigma_z)] + \beta \Delta t_m, \quad (10.60)$$

$$\epsilon_y = \frac{1}{E} [\sigma_y - \nu (\sigma_z + \sigma_x)] + \beta \Delta t_m, \quad (10.61)$$

$$\epsilon_z = \frac{1}{E} [\sigma_z - \nu (\sigma_x + \sigma_y)] + \beta \Delta t_m. \quad (10.62)$$

### Example 10.9: Shrink Fit

**Given:** A 250-mm-long steel tube, with a cross-sectional area of  $5 \times 10^{-4} \text{ m}^2$ , expands in length by 0.2 mm from a stress-free condition at  $25^\circ\text{C}$  when the tube is heated to  $250^\circ\text{C}$  and subjected to a compressive force from its supports.

**Find:** The load and stress acting on the steel tube.

**Solution:** From Table 3.1 for steel,  $\beta = 11 \times 10^{-6} \text{ } ^\circ\text{C}^{-1}$ , and from Eq. (10.57),

$$\epsilon = \beta \Delta t_m = (11 \times 10^{-6}) (225) = 2.475 \times 10^{-3}.$$

Therefore, from Eq. (2.31),

$$\Delta l = l \epsilon = (0.25) (2.47 \times 10^{-3}) = 0.619 \text{ mm.}$$

Because the measured expansion was only 0.20 mm, the constraint due to compressive normal loading must apply a force sufficient to deflect the tube axially by

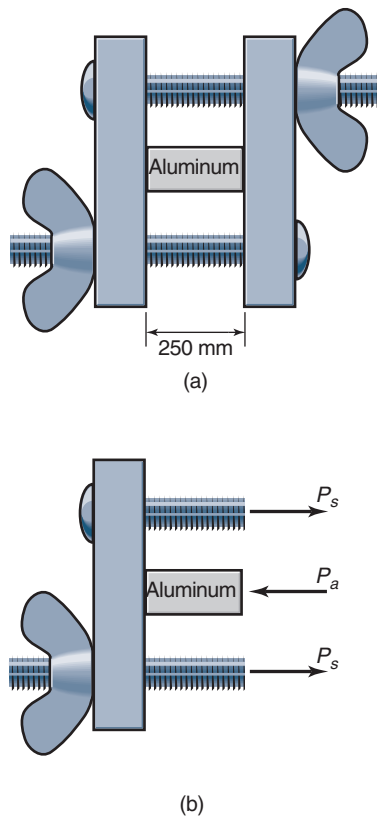


Figure 10.11: (a) Block placed between two rigid jaws of a clamp, and (b) associated forces.

$$\delta = 0.619 - 0.2 = 0.419 \text{ mm.}$$

From Table 3.1, the modulus of elasticity is 207 GPa. Therefore, from Eq. (4.26),

$$P = \frac{AE\delta}{l} = \frac{(5 \times 10^{-4})(207 \times 10^9)(0.419 \times 10^{-3})}{0.25},$$

or  $P = 173 \text{ kN}$ . This is the compressive, normal, axial load being exerted on the steel tube. The axial stress is

$$\sigma = -\frac{P}{A} = -\frac{173 \times 10^3}{5 \times 10^{-4}} = -347 \text{ MPa.}$$

### Example 10.10: Thermal Stresses

**Given:** A block of aluminum alloy is placed between two rigid jaws of a clamp, and the jaws are tightened to a snug state. The temperature of the entire assembly is raised by  $250^\circ\text{C}$  in an oven. The cross-sectional areas are  $65 \text{ mm}^2$  for the block and  $160 \text{ mm}^2$  for the stainless steel screws.

**Find:** The stresses induced in the screws and the block.

**Solution:** Figure 10.11 shows the block-and-screw assembly and the forces acting on these components. From force equilibrium,

$$P_a = 2P_s, \quad (a)$$

where subscript  $a$  refers to the aluminum block and subscript  $s$  refers to the stainless steel screws. Compatibility requires that the length changes of the block and the screws be the same, or

$$\delta_a = \delta_s. \quad (b)$$

Thermal expansion will induce an axial force as shown in Fig. 10.11b. The displacements of the block and screws are

$$\delta_a = \beta_a l \Delta t_m - \frac{P_a l}{E_a A_a}, \quad (c)$$

$$\delta_s = \beta_s l \Delta t_m + \frac{P_s l}{E_s A_s}. \quad (d)$$

Substituting Eqs. (a), (c), and (d) into Eq. (b) gives

$$P_s = \frac{\Delta t_m (\beta_a - \beta_s)}{\frac{1}{E_s A_s} + \frac{2}{E_a A_a}}. \quad (e)$$

From Table 3.1,  $E_a = 70 \text{ GPa}$ ,  $E_s = 193 \text{ GPa}$ ,  $\beta_a = 24 \times 10^{-6} (\text{°C})^{-1}$ , and  $\beta_s = 17 \times 10^{-6} (\text{°C})^{-1}$ . It is given that  $A_a = 65 \text{ mm}^2$  and  $A_s = 160 \text{ mm}^2$ ; substituting these values into Eq. (e) gives the force acting on each screw as

$$P_s = \frac{(250)(24 - 17)(10^{-6})}{\frac{1}{(193 \times 10^9)(160 \times 10^{-6})} + \frac{2}{(70 \times 10^9)(65 \times 10^{-6})}},$$

or  $P_s = 3708 \text{ N}$ . The force acting on the aluminum block is

$$P_a = 2P_s = 7416 \text{ N.}$$

The axial stresses of the block and screw are

$$\sigma_a = \frac{P_a}{A_a} = -\frac{7416}{(65 \times 10^{-6})} = -114.1 \text{ MPa,}$$

$$\sigma_s = \frac{P_s}{A_s} = \frac{3708}{(160 \times 10^{-6})} = 23.18 \text{ MPa.}$$

Note that the stress acting on the aluminum block is compressive, and that acting on the screws is tensile.

### Case Study: Design of a Shot Sleeve for a Die Casting Machine

Die casting is a common and important manufacturing process. A wide variety of products are produced through die casting, such as personal computer and camera frames, automotive structural components, fasteners, toy cars, and the like. In die casting, molten metal is placed in a shot sleeve and injected into a metal die outfitted with cooling lines to extract the heat and cause the cast metal to solidify quickly. A schematic illustration of a die casting machine is shown in Figure 10.12. In order for the process to be economically viable, a number of characteristics should be noted:

- The tooling is very expensive, and therefore a fairly large production run is required to justify the use of this process. Therefore, the cycle time (and cooling time) must be short in order to achieve required production runs.

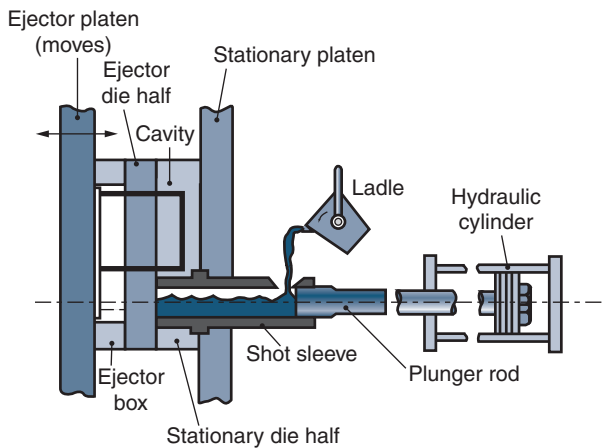


Figure 10.12: Schematic illustration of a die casting machine. Source: Kalpakjian and Schmid [2010].

- Recognizing that the cooling time should be very short, it is essential that the molten metal be injected into the die under high pressure and velocity to ensure that the mold is filled completely before local solidification results in a blocked channel, causing underfill. Injection pressures can be as high as 70 MPa, although 15 to 20 MPa is more typical.
- The molten metal is transferred to the die casting machine from a furnace and held temporarily in the *shot sleeve*. The shot sleeve must have sufficient volume to fill the die cavity.
- When the metal is injected into the cavity, a high pressure is generated in the shot sleeve through the compressive action of a hydraulic cylinder.
- The die obviously must have a higher melting temperature than the metal being cast; this usually limits the tooling to die steels, and the workpiece metal to non-ferrous alloys such as aluminum, magnesium, or copper alloys.

There are two basic kinds of die casting: the *hot chamber* process where the dies are maintained at a high temperature to aid in filling of the cavity, and the *cold chamber* process, where no provisions are provided to heat the die, and in fact the dies can be cooled through forced coolant flow. In the hot chamber process, the injection pressures can be as high as 35 MPa, while in the cold chamber process, pressures of 70 MPa are typical, but they can be as high as 150 MPa.

A thin-walled tube could be designed to contain such pressures (see Section 10.3.1), but the radius would be very small so that sufficient metal volume for reasonably sized parts would be unavailable. Instead, shot sleeves are designed as thick-walled cylindrical pressure vessels. A material typically used for this application is H13 steel, which has an ultimate strength of 768 MPa at room temperature and 650 MPa at casting temperatures for non-ferrous metals.

A machine may have a useful life of many decades, with a shot every few seconds. In designing such a shot sleeve, the fatigue strength of the H13 steel needs to be estimated using the procedures of Ch. 7.

The loading in this case consists of hoop and radial stresses only — significant axial stresses are not developed in the sleeve. On one end, the hydraulic cylinder applies a force that compresses the fluid and on the nozzle end the cylinder is mounted so that it does not see such loads.

Another major concern with shot sleeves is wear (Section 8.9), usually due to erosion of the sleeve material or abrasion of the plunger rod rubbing against the cylinder. For this reason, shot sleeves are often produced with a cylinder liner (see Design Procedure 8.1) that can be replaced periodically.

## 10.7 Summary

In this chapter, it was shown that fits must be specified to ensure the proper mating assembly of a shaft and a hub because it is impossible to manufacture these parts with exactly the desired dimensions. A system was devised to tolerate small dimensional variations of the mating shaft and hub without sacrificing their proper functioning.

Pressurization effects on cylinders were considered. Thin-wall and thick-wall analyses were described for both internal and external pressurization. These effects are important in a large number of applications, ranging from pressure vessels to gun barrels. A major assumption made in the thin-wall analysis was that the circumferential (hoop) stress is uniform throughout the wall thickness. This assumption is not valid for thick-wall analysis. Ranges of diameter to thickness were discussed for thin- and thick-wall analyses. For thick-wall situations, radial and circumferential variations with radius for both internal and external pressurization were shown. For internal pressurization, the maximum stress occurred at the inner radius for both radial and circumferential components, with the radial stress being compressive and the circumferential stress tensile. For external pressurization, the maximum radial stress occurred at the outer radius and the maximum circumferential stress occurred at the inner radius, with both stress components being compressive.

Rotational effects while assuming no pressurization of cylinders were also considered. Rotational effects are important in such machine elements as flywheels, gears, and pulleys. The rotating inertial force was considered in establishing the radial and circumferential stresses for both a cylinder with a central hole and a solid cylinder. The chapter ended with consideration of press and shrink fits of a shaft and a hub. The interference, axial force, and torque were developed for these situations.

## Key Words

**allowance** difference between nominal diameters of mating parts

**bilateral tolerance** variation above and below nominal size

**hoop stress** circumferential stress in pressure vessel

**interference** difference in size of mating parts

**nominal diameter** approximate size of element

**press fit** connections where interfacial pressure is due to interference between mating parts and assembly is accomplished by elastic deformation due to large forces



**shrink fit** connections where interfacial pressure is due to interference between mating parts and assembly is accomplished by heating outer component

**thick-walled cylinder** cylinder whose ratio of diameter to thickness is less than 40

**thin-walled cylinder** cylinder where radial stress is negligible, approximately true for diameter-to-thickness ratios greater than 40

**tolerance** maximum variation in part size

**unilateral tolerance** variation above or below nominal size, but not both

## Summary of Equations

### Thin-Walled Cylinders

$$\text{Hoop stress: } \sigma_{\theta, \text{avg}} = \frac{p_i r_i}{t_h}$$

$$\text{Longitudinal stress: } \sigma_z = \frac{p_i r}{2t_h}$$

### Thick-Walled Cylinders

General:

$$\text{Radial strain: } \epsilon_r = \frac{\partial \delta_r}{\partial r} = \frac{1}{E} (\sigma_r - \nu \sigma_{\theta})$$

$$\text{Circumferential strain: } \epsilon_{\theta} = \frac{\delta_r}{r} = \frac{1}{E} (\sigma_{\theta} - \nu \sigma_r)$$

$$\text{Radial stress: } \sigma_r = \frac{p_i r_i^2 - p_o r_o^2 + (p_o - p_i) \left( \frac{r_o r_i}{r} \right)^2}{r_o^2 - r_i^2}$$

$$\text{Circumferential stress: } \sigma_{\theta} = \frac{p_i r_i^2 - p_o r_o^2 - \left( \frac{r_i r_o}{r} \right)^2 (p_o - p_i)}{r_o^2 - r_i^2}$$

Internally Pressurized:

Maximum radial stress (at  $r = r_i$ ):  $\sigma_{r, \text{max}} = -p_i$

Maximum circumferential stress (at  $r = r_i$ ):

$$\sigma_{\theta, \text{max}} = p_i \left( \frac{r_o^2 + r_i^2}{r_o^2 - r_i^2} \right)$$

Circumferential strain (at  $r = r_i$ ):

$$\epsilon_{\theta} = \frac{\delta_r}{r_i} = \frac{p_i}{E} \left( \frac{r_o^2 + r_i^2}{r_o^2 - r_i^2} + \nu \right)$$

$$\text{Radial displacement: } \delta_r = \frac{p_i r_i}{E} \left( \frac{r_o^2 + r_i^2}{r_o^2 - r_i^2} + \nu \right)$$

Externally Pressurized:

Maximum radial stress (at  $r = r_o$ ):  $\sigma_{r, \text{max}} = -p_o$

Maximum circumferential stress (at  $r = r_i$ ):

$$\sigma_{\theta, \text{max}} = -\frac{2r_o^2 p_o}{r_o^2 - r_i^2}$$

Circumferential strain (at  $r = r_i$ ):

$$\epsilon_{\theta} = \frac{\delta_r}{r_i} = \frac{p_i}{E} \left( \frac{r_o^2 + r_i^2}{r_o^2 - r_i^2} + \nu \right)$$

$$\text{Radial displacement: } \delta_r = \frac{p_i r_i}{E} \left( \frac{r_o^2 + r_i^2}{r_o^2 - r_i^2} + \nu \right)$$

### Press Fits

Hub:

$$p_f r_f^2 \left( 1 - \frac{r_o^2}{r_f^2} \right)$$

$$\text{Radial stress: } \sigma_r = \frac{p_f r_f^2 \left( 1 - \frac{r_o^2}{r_f^2} \right)}{r_o^2 - r_f^2} = -p_f$$

Circumferential stress:

$$\sigma_{\theta} = \frac{p_f r_f^2 \left( 1 + \frac{r_o^2}{r_f^2} \right)}{r_o^2 - r_f^2} = \frac{p_f (r_o^2 + r_f^2)}{r_o^2 - r_f^2}$$

Radial displacement:

$$\delta_{rh} = \frac{r_f p_f}{E_h} \left( \frac{r_o^2 + r_f^2}{r_o^2 - r_f^2} + \nu_h \right)$$

Shaft:

$$\text{Radial stress: } \sigma_r = -p_f$$

$$\text{Circumferential stress: } \sigma_{\theta} = -\frac{p_f (r_f^2 + r_i^2)}{r_f^2 - r_i^2}$$

Radial displacement:

$$\delta_{rs} = -\frac{r_f p_f}{E_s} \left( \frac{r_f^2 + r_i^2}{r_f^2 - r_i^2} - \nu_s \right)$$

Interference:

General:

$$\delta_r = \delta_{rh} - \delta_{rs} = r_f p_f \left[ \frac{r_o^2 + r_f^2}{E_h (r_o^2 - r_f^2)} + \frac{\nu_h}{E_h} + \frac{r_f^2 + r_i^2}{E_s (r_f^2 - r_i^2)} - \frac{\nu_s}{E_s} \right]$$

For  $E_s = E_h = E$  and  $\nu_s = \nu_h = \nu$ :

$$\delta_r = \frac{2r_f^3 p_f (r_o^2 - r_i^2)}{E (r_o^2 - r_f^2) (r_f^2 - r_i^2)}$$

For  $E_s = E_h = E$  and  $\nu_s = \nu_h = \nu$  and  $r_i = 0$ :

$$\delta_r = \frac{2r_f p_f r_o^2}{E (r_o^2 - r_f^2)}$$

Assembly force:  $P_{\text{max}} = 2\pi \mu r_f l p_f$

Torque:  $T = P_{\text{max}} r_f = 2\pi \mu r_f^2 l p_f$

**Shrink Fits:**  $\delta_r = \beta \Delta t_m r_f$

## Recommended Readings

- Beer, F.P., Johnson, E.R., DeWolf, J., and Mazurek, D. (2011) *Mechanics of Materials*, 6th ed., McGraw-Hill.
- Budynas, R.G., and Nisbett, J.K. (2011), *Shigley's Mechanical Engineering Design*, 9th ed., McGraw-Hill.
- Chuse, R., and Carson, B.E. (1993) *Pressure Vessels*, 7th ed., McGraw-Hill.
- Craig, R.R. (2001) *Mechanics of Materials*, 2nd ed., Wiley.
- Harvey, J.F. (1991) *Theory and Design of Pressure Vessels*, 2nd ed., Van Nostrand Reinhold.
- Hibbeler, R.C. (2010) *Mechanics of Materials*, 8th ed, Prentice-Hall.
- Megyesy, E.F. (2008) *Pressure Vessel Handbook*, 14th ed., Pressure Vessel Handbook Publishing, Inc.
- Mott, R.L. (2014) *Machine Elements in Mechanical Design*, 5th ed., Pearson.
- Riley, W.F., Sturges, L.D., and Morris, D.H. (2006) *Mechanics of Materials*, 6th ed, Wiley.
- Timoshenko, S., and Goodier, J. (1970) *Theory of Elasticity*, McGraw-Hill.
- Ugural, A.C. and Fenster, S.K. (2011) *Advanced Mechanics of Materials and Applied Elasticity*, 5th ed, Prentice-Hall.

## Reference

- Kalpakjian, S., and Schmid, S.R. (2010) *Manufacturing Engineering and Technology*, 6th ed., Pearson.

## Questions

- 10.1 What is the difference between tolerance and allowance?
- 10.2 Define bilateral and unilateral tolerance.
- 10.3 What is the difference between interference and allowance?
- 10.4 When is a cylinder considered to have a thin wall versus a thick wall?
- 10.5 What are the names of the principal stresses in cylindrical coordinates?
- 10.6 What are the principal stresses for a thin-walled cylinder under internal pressurization?
- 10.7 What is a hoop stress? Why is it so called?
- 10.8 What effect does rotation have on the stresses associated with internal pressurization of a cylinder?
- 10.9 What is a press fit? A shrink fit?
- 10.10 Define “hub” and “shaft.”

## Qualitative Problems

- 10.11 Give five examples of thin-walled and thick-walled pressure vessels.
- 10.12 Give two examples of internally pressurized and externally pressurized cylinders.
- 10.13 Is the radial stress compressive when the pressurization is internal or external?
- 10.14 Why is the coefficient of thermal expansion important? Would you select a material with a high or low coefficient of thermal expansion for a hub? Explain.
- 10.15 Explain the different classes of fit.
- 10.16 Review Table 10.2 and explain the exponents on the diameter for calculation of recommended allowance and tolerance.
- 10.17 What would happen if the hub's yield strength is exceeded during assembly of a press fit? What interference fit would result in this case?
- 10.18 Can the yield strength be exceeded in a shrink fit? Why or why not?
- 10.19 Using the derivation in Section 10.5, write the expressions for the force and pressure encountered by a nail when it is hammered into wood. Explain why pilot holes are drilled into wood for larger nails or harder wood.
- 10.20 List the concerns you would have in designing shrink or press fits with composite materials while using the theory developed in Sections 10.5 and 10.6.

## Quantitative Problems

- 10.21 A journal bearing is to be manufactured with optimum geometry for minimum power loss for a given load and speed. The relative clearance  $c/r = 0.001$ ; the journal diameter is 100 mm. Find the accuracy to which the bearing parts have to be manufactured so that there is no more than  $\pm 5\%$  error in the relative clearance.
- 10.22 A press fit between a solid steel shaft and a steel housing is dimensioned to be of Class 7. By mistake the shaft is ground at  $22^\circ\text{C}$  higher temperature than originally anticipated, so that when the shaft cools, the diameter is slightly too small. The shaft material is AISI 1040 steel. What is the class of fit between the shaft and the housing because of this mistake? Also, if the grinding temperature were  $50^\circ\text{C}$  higher rather than  $22^\circ\text{C}$  higher, what is the class of fit? *Ans.* At  $22^\circ\text{C}$ , Class 6; at  $50^\circ\text{C}$ , Class 4.
- 10.23 A cylinder with a 0.30-m inner diameter and a 0.40-m outer diameter is internally pressurized to 100 MPa. Determine the maximum shear stress at the outer surface of the cylinder. *Ans.*  $\tau_{\max} = 128.5 \text{ MPa}$ .
- 10.24 A rubber balloon has the shape of a cylinder with spherical ends. At low pressure the cylindrical part is 300 mm long with a diameter of 20 mm. The rubber material has constant thickness and is linearly elastic. How long will the cylindrical part of the balloon be when it is inflated to a diameter of 100 mm? Assume that the rubber's modulus of elasticity is constant and that the Poisson's ratio is 0.5.
- 10.25 A thin-walled cylinder containing pressurized gas is fixed by its two ends between rigid walls. Obtain an expression for the wall reactions in terms of cylinder length  $l$ , thickness  $t_h$ , radius  $r$ , and internal pressure  $p_i$ . *Ans.*  $P = \pi p_i r^2 (1 - 2\nu)$ .
- 10.26 A pressurized cylinder has an internal pressure of 1 MPa, a thickness of 8 mm, a length of 4 m, and a diameter of 1.00 m. The cylinder is made of AISI 1080 steel. What are the hoop and axial strains upon pressurization? What is the volume increase of the cylinder due to the internal pressure? *Ans.*  $\epsilon_z = 60.39 \mu\text{m/m}$ ,  $\epsilon_\theta = 256.6 \mu\text{m/m}$ .
- 10.27 A 1-m-diameter cylindrical container with two hemispherical ends is used to transport gas. The internal pressure is 5 MPa and the safety factor is 2.5. Using the MSST determine the container thickness. Assume that the tangential strains of the cylinder and the sphere are equal, since they are welded joints. The material is such that  $E = 200 \text{ GPa}$ ,  $S_y = 430 \text{ MPa}$ , and  $\nu = 0.3$ . *Ans.* Wall:  $t_h = 14.53 \text{ mm}$ ; cap:  $t_h = 7.267 \text{ mm}$ .
- 10.28 A solid cylindrical shaft made of AISI 1020 steel (quenched and tempered at  $870^\circ\text{C}$ ) rotates at a speed that produces a safety factor of 2.5 against the stress causing yielding. To instrument the shaft, a small hole is drilled in its center for electric wires. At the same time the material is changed to AISI 1080 steel that has been quenched and tempered at  $800^\circ\text{C}$ . Find the safety factor against yielding of the new shaft. *Ans.*  $n_s = 1.59$ .
- 10.29 A flywheel is mounted on a tubular shaft. The shaft's inner diameter is 25 mm and its outer diameter is 50 mm. The flywheel is a cylindrical disk with an inner diameter of 50 mm, an outer diameter of 300 mm, and a thickness of 35 mm. Both the shaft and the flywheel are made of

AISI 1080 steel. The flywheel is used to store energy, so that the rotational acceleration is proportional to the angular speed  $\omega$ . The angular acceleration  $\partial\omega/\partial t$  is to be held to within  $\pm 0.2\omega$ . Calculate the shaft speed  $\omega$  at which the flywheel starts to slide on the shaft if the press-fit pressure at  $\omega = 0$  is 127 MPa and the coefficient of friction between the shaft and the flywheel is 0.13. *Ans.*  $N = 14,980$  rpm.

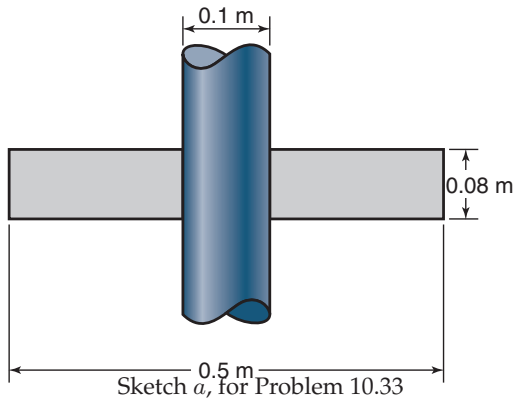
**10.30** Assume that the flywheel and the shaft given in Problem 10.29 are made of aluminum alloy 2014 instead of steel. Find the speed at which the flywheel will start to slide if the coefficient of friction is 0.14 and the press-fit pressure is 30 MPa. *Ans.*  $N = 12,210$  rpm.

**10.31** The flywheel and the shaft given in Problem 10.29 are axially loaded by a force of 60,000 N. Calculate the shaft speed at which the flywheel starts to slide on the shaft. *Ans.*  $N = 8606$  rpm.

**10.32** A 150-mm-diameter solid steel shaft is to have a press fit with a 300-mm-outer-diameter by 125-mm-long hub made of cast iron. The maximum allowable hoop stress is 35 MPa. The moduli of elasticity are 207 GPa for steel and 170 GPa for cast iron. Poisson's ratio for steel and cast iron is 0.3. The coefficient of friction for both steel and cast iron is 0.11. Determine the following:

- Total radial interference. *Ans.*  $\delta_r = 51.6 \mu\text{m}$ .
- Axial force required to press the hub on the shaft. *Ans.*  $F_{\max} = 272$  kN.
- Torque transmitted with this fit. *Ans.*  $T = 40.8$  kN-m.

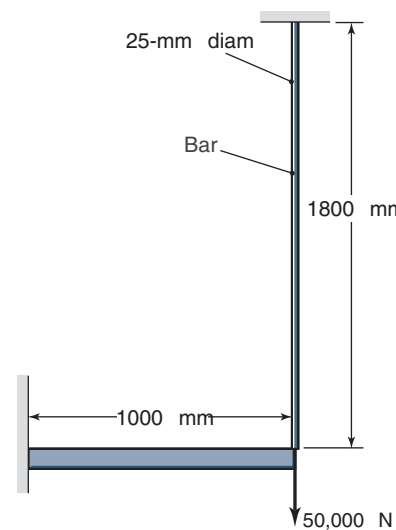
**10.33** A flat, 0.5-m-outer-diameter, 0.1-m-inner-diameter, 0.08-m-thick steel disk shown in Sketch *a* is shrink fit onto a shaft. If the assembly is to transmit a torque of 75 kN-m, determine the fit pressure and the total radial interference. The coefficient of friction is 0.25. *Ans.*  $p_f = 238.7$  MPa,  $\delta_r = 0.1201$  mm.



**10.34** A flat, 0.1-m-outer-diameter, 0.05-m-inner-diameter, 0.100-m-thick steel disk is shrink fit onto a shaft with a 0.02-m inner diameter. If the assembly is to transmit a torque of 12 kN-m, determine the fit pressure and the total radial interference. The coefficient of friction is 0.25. *Ans.*  $p_f = 122.2$  MPa,  $\delta_r = 44.9 \mu\text{m}$ .

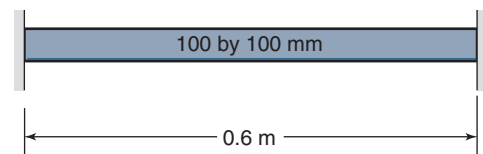
**10.35** A supported cantilevered beam is loaded as shown in Sketch *b*. If at the time of assembly the load was zero and the beam was horizontal, determine the stress in the round rod after the load is applied and the temperature is lowered by  $70^\circ\text{C}$ . The beam moment of inertia is

$I_{\text{beam}} = 9.8 \times 10^7 \text{ mm}^4$ . The beam and rod material are both high-carbon steel. *Ans.*  $\sigma = 132$  MPa.

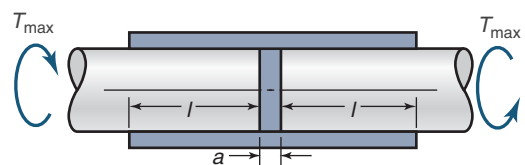


**10.36** A 0.25-m-long tube (with properties  $E = 200$  GPa and  $\beta = 11 \times 10^{-6}/^\circ\text{C}$ ) having a cross-sectional area of  $0.0002 \text{ m}^2$  is installed with fixed ends so that it is stress-free at  $25^\circ\text{C}$ . In operation the tube is heated throughout to a uniform  $250^\circ\text{C}$ . Measurements indicate that the fixed ends separate by 0.2 mm. What loads are exerted on the ends of the tube, and what are the resultant stresses? *Ans.*  $\sigma = -335$  MPa.

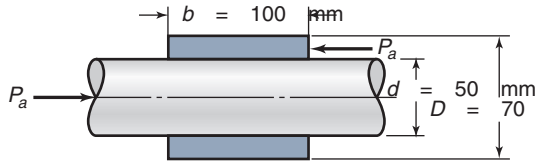
**10.37** A solid square bar is constrained between two fixed supports as shown in sketch *c*. The square bar has a cross-section of 100 by 100 mm and is 0.6 m long. The bar just fits between fixed supports at the initial temperature of  $25^\circ\text{C}$ . If the temperature is raised to  $100^\circ\text{C}$ , determine the average thermal stress developed in the bar. Assume that  $E = 200 \text{ GPa}$  and  $\beta = 11 \times 10^{-6}/^\circ\text{C}$ . *Ans.*  $\sigma = -165$  MPa.



**10.38** Two stiff shafts are connected by a thin-walled elastic tube to a press-fit connection as shown in Sketch *d*. The contact pressure between the shafts and the tube is  $p$ . The coefficient of friction is  $\mu$ . Calculate the maximum torque  $T_{\max}$  that can be transmitted through the press fit. Describe and calculate what happens if the torque decreases from  $T_{\max}$  to  $\theta T_{\max}$  where  $0 < \theta < 1$ .



- 10.39** A 50-mm-diameter steel shaft and a 25-mm-long cylindrical bushing of the same material with an outer diameter of 80 mm have been incorrectly shrink fit together and have to be dismantled. What axial force is needed for this operation if the diametral interference is  $50\text{ }\mu\text{m}$  and the coefficient of friction is 0.2? *Ans.*  $P_{\max} = 49.5\text{ kN}$ .
- 10.40** A bushing press fit on a shaft shown in Sketch *e* is going to be dismantled. What axial force  $P_a$  is needed to dismount the bushing if, at the same time, the bushing transmits a torque  $T = 500\text{ N}\cdot\text{m}$ ? The diametral interference is  $\delta = 30\text{ }\mu\text{m}$ , the coefficient of friction is  $\mu = 0.3$ , and the modulus of elasticity is  $E = 210\text{ GPa}$ . *Ans.*  $P_a = 144.0\text{ kN}$ .

Sketch *e*, for Problem 10.40

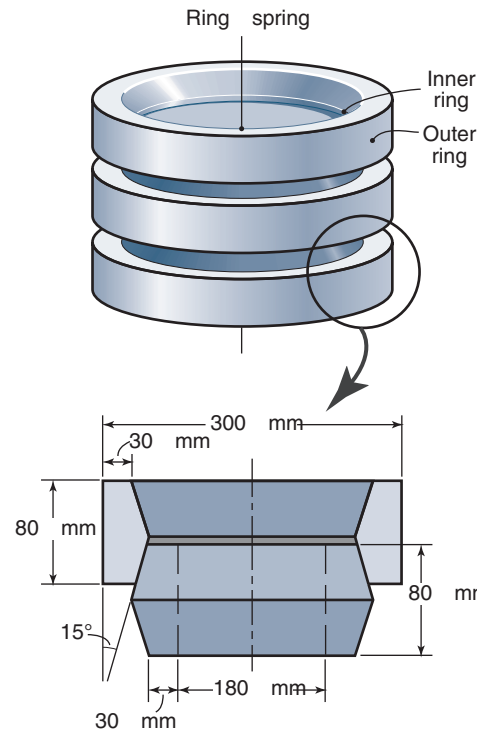
- 10.41** To help in dismantling the wheel in Example 10.8, both an axial force and a torque are applied at the shaft-flywheel junction. How large a torque is needed to decrease the axial force to 40 kN when the wheel is dismantled? *Ans.*  $T = 16.5\text{ kNm}$ .
- 10.42** Two AISI 1040 steel cylinders are press fit on each other. The inner diameter is 200 mm, the common diameter is 300 mm, and the outer diameter is 400 mm. The radial interference of the two cylinders is 0.1 mm.
- Draw the radial and tangential stress distributions due to the press fit.
  - If the internal pressure is 207 MPa and the external pressure is 50 MPa, determine the radial and tangential stress distributions due only to these pressures.
  - Superimpose the stress distributions from (a) and (b) to obtain the total radial and tangential stress distribution.

- 10.43** A thick-walled cylinder is placed freely inside another thick-walled cylinder. What pressure is induced on the surfaces between the two cylinders by internally pressurizing the inner cylinder? *Hint:* Equate the radial displacement of the outer wall of the inner cylinder with that of the inner wall of the outer cylinder.
- 10.44** A 0.5-m-outer-diameter, 0.1-m-inner-diameter, 0.1-m-thick flat disk is shrink fit onto a solid shaft. Both the shaft and the disk are made of high-carbon steel. The assembly transmits 20 MW at 2000 rpm. Calculate the minimum temperature to which the disk must be heated for this shrink fit. The coefficient of friction is 0.25. *Ans.*  $\Delta t_m = 222.5^\circ\text{C}$ .

- 10.45** Two shafts are connected by a shrink-fit bushing with an outer diameter of 120 mm. The diameter of each shaft is 80 mm and each shaft is 2 m long. Before the shrink-fit bushing was mounted, the diametral interference was  $\delta = 80\text{ }\mu\text{m}$ . The bushing and the shaft are made of steel with a modulus of elasticity  $E = 210\text{ GPa}$ . Find the allowable temperature increase without slip in the press fit if a power of 200 kW is transmitted and the far ends

of the shafts cannot move axially. The coefficient of thermal expansion is  $11.5 \times 10^{-6}/^\circ\text{C}$ , and the coefficient of friction is 0.1. The axial length of the bushing press fit on each shaft is 80 mm. The rotational speed is 1500 rpm. *Ans.*  $\Delta t_m = 63.29^\circ\text{C}$ .

- 10.46** A 15-mm-thick, 100-mm-wide ring is shrunk onto a 100-mm-diameter shaft. The diametral interference is  $75\text{ }\mu\text{m}$ . Find the surface pressure in the shrink fit and the maximum torque that can be transmitted if the coefficient of friction  $\mu = 0.10$ . The modulus of elasticity  $E = 210\text{ GPa}$ . *Ans.*  $p_f = 32.15\text{ MPa}$ ,  $T = 5050\text{ Nm}$ .

Sketch *f*, for Problem 10.47

- 10.47** A railway car buffer has a spring consisting of 11 outer rings and 11 inner rings where one of each ring type is a half-ring at the end of the spring. On one occasion a railway car with a total mass of 10,000 kg rolls until it hits a rigid stop. The force stopping the car is equal in the outer and the inner rings. The speed of the car just before the stop is 18 km/hr. Find the compression of the outer and inner rings and the stresses in the rings if the coefficient of friction  $\mu = 0.25$  and the modulus of elasticity  $E = 210\text{ GPa}$ . The ring dimensions are shown in Sketch *f*. When a spring of this type is compressed, the spring rate  $k$  (i.e., force divided by deformation) is

$$k = \frac{P}{\delta} = \frac{\pi E \tan \alpha \tan(\alpha + \gamma)}{n \left( \frac{r_o}{A_o} + \frac{r_i}{A_i} \right)}$$

where

$\alpha$  = cone angle for spring  
 $\gamma$  = friction angle  
 $\tan \gamma = \mu$  = coefficient of friction  
 $r_o, r_i$  = radii to surface center of gravity  
 $A_o, A_i$  = cross-sectional areas of rings

- 10.48** A railway car weighing 20 tons has in each end two buffers of the type described in Problem 10.47. The data are  $A_y = A_i = 200 \text{ mm}^2$ ,  $r_y = 70 \text{ mm}$ ,  $r_i = 60 \text{ mm}$ ,  $n = 20$ ,  $\alpha = 14^\circ$ ,  $\gamma = 7^\circ$ , and  $E = 206 \text{ GPa}$ . The car hits a rigid stop with a speed of 1 m/s. Find the maximum force in each buffer and the energy absorbed. At what speed will the car bounce back?
- 10.49** For the situation in Example 10.4, find the maximum pressures if the yield stress is 250 MPa, not the allowable circumferential stress. *Ans.*  $p_i = 60.0 \text{ MPa}$ ,  $\delta_{r,\max} = 0.168 \text{ mm}$ .

## Synthesis and Design

- 10.50** Show that the principal stresses for a thin-walled, spherical pressure vessel are given by  $\sigma_1 = \sigma_2 = \frac{pr}{2t}$ .
- 10.51** Derive the expressions in Design Procedure 10.1.
- 10.52** Vitrified grinding wheels use a brittle but strong ceramic bond between abrasive particles. Serious accidents have been known to occur when a grinding wheel is damaged but still used, or when it is oversped. Considering the material in Section 10.4 and an appropriate failure theory from Chapter 6, develop an expression to predict grinding wheel failure.
- 10.53** Design an experiment to measure the interference pressure in press fits and shrink fits.
- 10.54** Consider the situation where a hub is assembled onto a shaft using an interference fit. If an adhesive is also inserted inside the hub-shaft combination, will this increase the assembly force? Explain your answer.



This page intentionally left blank

# Chapter 11

## Shafting and Associated Parts



A selection of overhead valve camshafts for automotive engines. Source: Courtesy of AVL Schrick.

*When a man has a vision, he cannot get the power from the vision until he has performed it on the Earth for the people to see.*

Black Elk, Oglala Sioux visionary

### Contents

- 11.1 Introduction 264
- 11.2 Design of Shafts for Static Loading 264
- 11.3 Fatigue Design of Shafts 267
- 11.4 Additional Shaft Design Considerations 271
- 11.5 Critical Speed of Rotating Shafts 272
- 11.6 Keys, Roll Pins, Splines and Set Screws 275
- 11.7 Retaining Rings and Pins 278
- 11.8 Flywheels 279
- 11.9 Couplings 285
- 11.10 Summary 288

### Examples

- 11.1 Static Design of a Shaft 266
- 11.2 Fatigue Design of a Shaft 269
- 11.3 Fatigue Design of a Shaft Under Combined Loading 269
- 11.4 Critical Shaft Speed 274
- 11.5 Key Design 276
- 11.6 Flywheel Design 282
- 11.7 Flywheel Stresses 283

### Design Procedures

- 11.1 Shafts 271
- 11.2 Keys 275
- 11.3 Flywheels 282

This chapter focuses on shafts and related machine elements. Shafts are an essential component of most machines, and are mainly used for power transmission. Shafts are designed to transmit torque and support bending moments and axial loads; they also must be designed so that they do not deflect excessively. This includes dynamic instability as well as static and fatigue loadings. Shafts utilize a number of machine elements to provide functionality. For example, when a torque needs to be transmitted between a shaft and a machine element, that element can be mounted onto the shaft with a key or spline. If a machine element needs to be located at a certain location on a shaft axis, such as against a shoulder, then a retaining ring, set screw, or pin is often used. This chapter also discusses flywheels, which are used to store energy and provide smooth, jerk-free motion. Finally, a wide assortment of coupling types are described. Couplings are used to connect two shafts, and different coupling designs are able to accommodate misalignment and damping of vibration.

**Machine elements described in this chapter:** Shafts, keys, splines, set screws, retaining rings, flywheels, couplings.

**Typical applications:** *Shafts:* widespread use to transmit power to a point of operation, automotive crankshafts, cam shafts. *Keys, splines, and set screws:* used to transmit torque to another machine element's hub, such as for gears, pulleys, wire rope drums, mixer agitators, and flywheels. *Retaining rings:* used to fix the axial location of a component, such as rolling element bearing races, pulleys, wheels, bearing sleeves, and gears. *Flywheels:* automotive engines, crushing machinery, milling machinery, and machine tools. *Couplings:* used to connect two shafts, most commonly between the power source or motor shaft and the drive shaft.

**Competing machine elements:** *Shafts:* gear drives (Chapters 14 and 15), belt and wire rope drives (Chapter 19). *Keys, splines, set screws, retaining rings:* weldments, threaded retainers and adhesive joints (Chapter 16), press and shrink fits (Chapter 10). *Flywheels:* fluid couplings, large gears. *Couplings:* clutches (Chapter 18) and gear drives (Chapters 14 and 15).

## Symbols

$A$	area, m <sup>2</sup>
$\bar{A}$	constant defined in Eq. (11.26)
$\bar{B}$	constant defined in Eq. (11.27)
$C_1$	integration constant
$C_f$	coefficient of fluctuation, Eq. (11.80)
$C_t$	ring correction factor
$c$	distance from neutral axis to outer fiber, m
$d$	diameter, m
$d_m$	mean spline diameter, m
$d_s$	set screw diameter, m
$E$	modulus of elasticity, Pa
$g$	gravitational acceleration, 9.807 m/s <sup>2</sup>
$h$	height, m
$I$	area moment of inertia, m <sup>4</sup>
$I_m$	mass moment of inertia, kg-m <sup>2</sup>
$J$	polar area moment of inertia, m <sup>4</sup>
$K_c$	stress concentration factor
$K_e$	kinetic energy, N-m
$K_f$	fatigue stress concentration factor
$k$	spring rate, N/m
$k_f$	surface finish factor
$k_r$	reliability factor
$k_s$	size factor
$l$	length, m
$l_s$	spline length, m
$M$	moment, N-m
$M_f$	performance index, J/kg
$m_a$	mass, kg
$n$	number of teeth
$n_s$	safety factor
$P$	normal force, N
$P_t$	retaining force, N
$p$	pressure, Pa
$p_f$	interference pressure, Pa
$q_n$	notch sensitivity factor
$r$	radius, m
$S_e$	modified endurance limit, Pa
$S_e'$	endurance limit, Pa
$S_{se}$	shear modified endurance limit, Pa
$S_{sy}$	shear yield strength, Pa
$S_u$	ultimate strength, Pa
$S_{ut}$	ultimate tensile strength, Pa
$S_y$	yield strength, Pa
$T$	torque, N-m
$T_l$	load torque, N-m
$T_m$	mean torque, N-m
$t$	time, s
$t_h$	thickness, m
$U$	potential energy, N-m
$u$	velocity, m/s
$W$	load, N
$w$	width, m
$x, y, z$	Cartesian coordinates, m
$\delta$	deflection, m
$\theta$	cylindrical polar coordinate, deg
$\theta_{\omega_{\max}}$	location within a cycle where speed is maximum, deg
$\theta_{\omega_{\min}}$	location within a cycle where speed is minimum, deg
$\nu$	Poisson's ratio
$\rho$	density, kg/m <sup>3</sup>
$\sigma$	normal stress, Pa
$\sigma_e$	critical stress using distortion-energy theory, Pa
$\sigma_\phi$	normal stress acting on oblique plane, Pa
$\tau$	shear stress, Pa

$\tau_\phi$	shear stress acting on oblique plane, Pa
$\phi$	oblique angle, deg
$\omega$	angular speed, rad/s
$\omega_\phi$	fluctuation speed, rad/s

## Subscripts

$a$	alternating
$c$	compression
$i$	inner
$m$	mean
$o$	outer
$r$	radial
$s$	shear
$\theta$	circumferential
$\omega$	speed
1,2,3	principal axes

## 11.1 Introduction

This chapter begins by discussing the design of shafts, making extensive use of the material from Sections 2.8 through 2.12 and Ch. 4 to develop stresses. The failure theories presented in Section 6.7 are used for static failure prediction in Section 11.2; the material in Ch. 7 is used to develop design rules for fatigue of shafts in Section 11.3. Here, combinations of loading are presented, whereas previously each type of loading was considered independently. It is important that this material be understood before proceeding with this chapter. The critical speed of rotating shafts is discussed in Section 11.5. The dynamics and the first critical speed are important, since the rotating shaft becomes dynamically unstable and large vibrations are likely to develop.

Keys, pins, and splines are used to attach devices to a shaft, and are discussed in Section 11.6. These devices use friction or mechanical interference to transmit a torque. Axial position of parts on a shaft can be done with retaining rings, cotter pins, or a number of similar devices. The design of flywheels and couplings are considered in Sections 11.8 and 11.9. Flywheels are valuable energy storage devices that also provide smooth operation. Couplings are used when two shafts need to be connected and are available in a wide variety of forms, the most common of which are presented.

## 11.2 Design of Shafts for Static Loading

A **shaft** is a rotating or stationary member usually having a circular cross-section much smaller in diameter than in length, and used for power transmission. Machine elements such as gears, pulleys, cams, flywheels, cranks, sprockets, and rolling-element bearings are mounted on shafts, and as such require a well-designed shaft as a prerequisite to their proper function. The loading on the shaft can include combinations of bending (almost always fluctuating); torsion (may or may not be fluctuating); shock; or axial, normal, or transverse forces. All of these types of loading were considered in Chapter 4. Some of the main considerations in designing a shaft are strength, using yield or fatigue (or both) as a criterion; deflection; or the dynamics established by the critical speeds. In general, the shaft diameter will be the variable used to satisfy the design, although in many practical applications the shaft may not have a constant diameter.

Shaft design must consider both static and fatigue failure possibilities. While at first it may appear that considering fatigue only would result in conservative designs, this is not always the case. For example, it is common that a rotating shaft sees predominantly uniform stresses, but on rare occasions encounters a much more significant stress cycle. Cumulative damage as discussed in Section 7.9 can be considered, with Miner's rule as stated in Eq. (7.24) applied to design the shaft. However, the high loading may be a rare event, such as is caused by a machine malfunction or improper operation. Thus, it may occur only extremely rarely, if at all, so that its contribution to fatigue crack growth may be minor.

Even with an overload or malfunction, there is usually some limit to the stresses that are applied to the shaft. For example, the loads can be controlled by using keys or pins (Section 11.6) or slip clutches (Section 18.10). In such circumstances, it is important to make sure that the shaft does not fail statically, especially since the shaft is usually the most difficult component to service or replace. Not surprisingly, shafts are often designed with very large safety factors.

A number of different loading conditions are considered here. Typically, the designer must establish either the minimum shaft diameter to successfully support applied loads or the safety factor for a specific design. This can be done using the approaches in Chapters 2 and 4, but the problem is so common that simplified solutions for each case are presented below.

### 11.2.1 Bending Moment and Torsion

Bending moments exerted on a shaft produce a maximum stress, from Eq. (4.45), of

$$\sigma_x = \frac{Mc}{I}. \quad (11.1)$$

Similarly, the shear stress due to an applied torque is, from Eq. (4.33),

$$\tau_{xy} = \frac{Tc}{J}, \quad (11.2)$$

where, for a circular cross section,

$$c = \frac{d}{2} \quad I = \frac{\pi d^4}{64} \quad \text{and} \quad J = \frac{\pi d^4}{32}. \quad (11.3)$$

Substituting Eq. (11.3) into Eqs. (11.1) and (11.2) gives

$$\sigma_x = \frac{64Md}{2\pi d^4} = \frac{32M}{\pi d^3}, \quad (11.4)$$

$$\tau_{xy} = \frac{Td/2}{\pi d^4/32} = \frac{16T}{\pi d^3}. \quad (11.5)$$

Note that since  $\sigma_y = 0$ , these stresses result in a plane stress loading. Therefore, from Eq. (2.16),

$$\sigma_1, \sigma_2 = \frac{\sigma_x}{2} \pm \sqrt{\left(\frac{\sigma_x}{2}\right)^2 + \tau_{xy}^2}. \quad (11.6)$$

Substituting Eqs. (11.4) and (11.5) into Eq. (11.6) gives

$$\begin{aligned} \sigma_1, \sigma_2 &= \frac{16M}{\pi d^3} \pm \sqrt{\left(\frac{16M}{\pi d^3}\right)^2 + \left(\frac{16T}{\pi d^3}\right)^2} \\ &= \frac{16}{\pi d^3} \left[ M \pm \sqrt{M^2 + T^2} \right]. \end{aligned} \quad (11.7)$$

From Eq. (2.19), the principal shear stresses are

$$\tau_1, \tau_2 = \pm \sqrt{\tau_{xy}^2 + \left(\frac{\sigma_x}{2}\right)^2}. \quad (11.8)$$

Substituting Eqs. (11.4) and (11.5) into Eq. (11.8) gives

$$\tau_1, \tau_2 = \pm \frac{16}{\pi d^3} \sqrt{M^2 + T^2}. \quad (11.9)$$

### Distortion-Energy Theory

As shown in Section 6.7.1 and by Eqs. (6.11) and (6.12), the Distortion-Energy Theory (DET) predicts failure if the von Mises stress satisfies the following condition:

$$\sigma_e = (\sigma_1^2 + \sigma_2^2 - \sigma_1\sigma_2)^{1/2} = \frac{S_y}{n_s}, \quad (11.10)$$

where  $S_y$  is the yield strength of shaft material and  $n_s$  is the safety factor. Substituting Eq. (11.7) into Eq. (11.10), the DET predicts failure if

$$\frac{16}{\pi d^3} (4M^2 + 3T^2)^{1/2} = \frac{S_y}{n_s}. \quad (11.11)$$

Thus, the DET predicts the smallest diameter where failure will occur as

$$d = \left( \frac{32n_s}{\pi S_y} \sqrt{M^2 + \frac{3}{4}T^2} \right)^{1/3}. \quad (11.12)$$

If the shaft diameter is known and the safety factor is desired, Eq. (11.12) becomes

$$n_s = \frac{\pi d^3 S_y}{32 \sqrt{M^2 + \frac{3}{4}T^2}}. \quad (11.13)$$

### Maximum-Shear-Stress Theory

As shown in Section 6.7.1 and by Eq. (6.8), the Maximum-Shear-Stress Theory (MSST) predicts failure for a plane or biaxial stress state ( $\sigma_3 = 0$ ) if

$$|\sigma_1 - \sigma_2| = \frac{S_y}{n_s}. \quad (11.14)$$

Equation (11.7) gives

$$\frac{32\sqrt{M^2 + T^2}}{\pi d^3} = \frac{S_y}{n_s}. \quad (11.15)$$

Thus, the MSST predicts the smallest diameter where failure will occur as

$$d = \left( \frac{32n_s}{\pi S_y} \sqrt{M^2 + T^2} \right)^{1/3}. \quad (11.16)$$

If the shaft diameter is known and the safety factor is an desired, Eq. (11.16) becomes

$$n_s = \frac{\pi d^3 S_y}{32 \sqrt{M^2 + T^2}}. \quad (11.17)$$

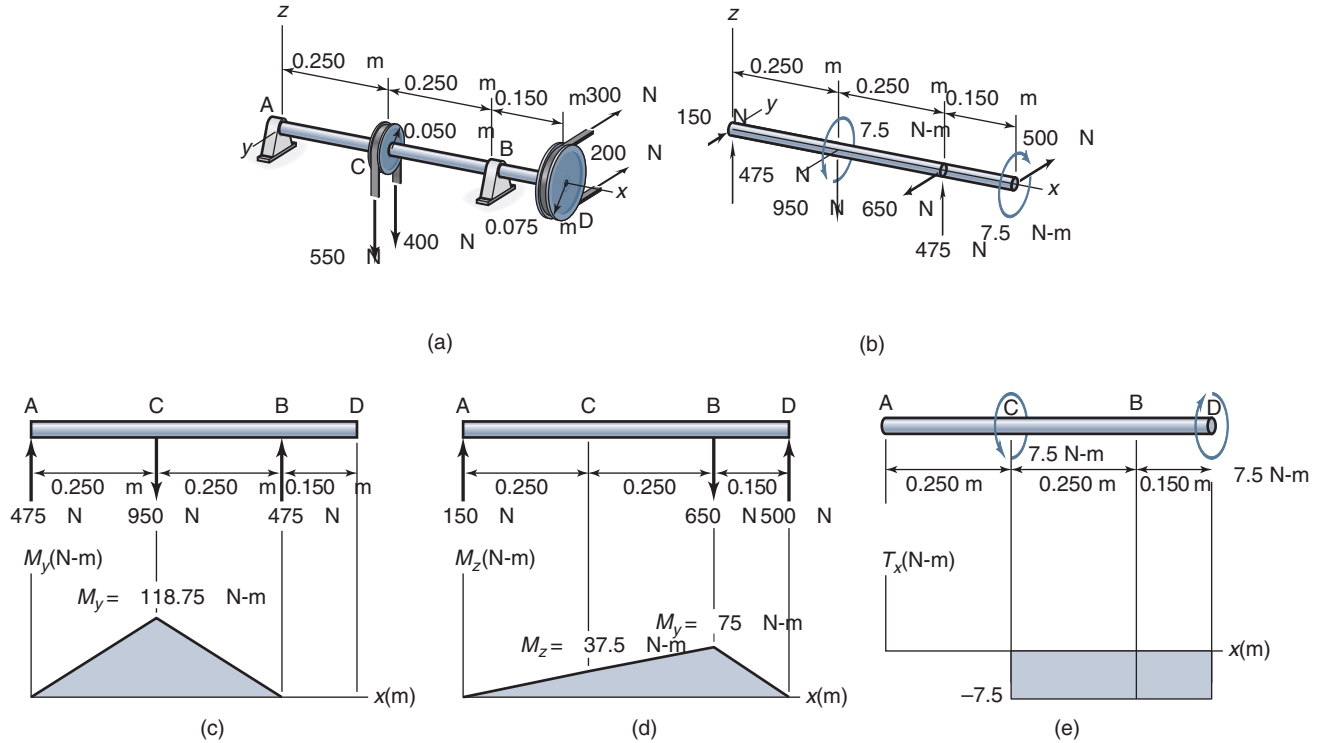


Figure 11.1: Figures used for Example 11.1. (a) Assembly drawing; (b) free-body diagram; (c) moment diagram in  $x$ - $z$  plane; (d) moment diagram in  $x$ - $y$  plane; (e) torque diagram.

### Example 11.1: Static Design of a Shaft

**Given:** A shaft with mounted belt drives has tensile forces applied as shown in Fig. 11.1a and frictionless journal bearings at locations A and B. The yield strength of the shaft material is 500 MPa.

**Find:** Determine the smallest safe shaft diameter by using both the DET and the MSST for a safety factor of 2.0. Also, provide a free-body diagram as well as moment and torque diagrams.

**Solution:** A free-body diagram is shown in Fig. 11.1b; a moment diagram in the  $x$ - $y$  plane, in Fig. 11.1c; and a moment diagram in the  $x$ - $z$  plane in Fig. 11.1d. These have been constructed using the approach described in Section 2.8. From the moment diagrams, the maximum moment is

$$M_{\max} = \sqrt{(118.75)^2 + (37.5)^2} = 124.5 \text{ N-m.}$$

Figure 11.1e gives the torque diagram. Using the DET, the smallest safe diameter is given by Eq. (11.12) as

$$\begin{aligned} d &= \left( \frac{32n_s}{\pi S_y} \sqrt{M^2 + \frac{3}{4}T^2} \right)^{1/3} \\ &= \left\{ \frac{32(2)}{\pi(500 \times 10^6)} \left[ 124.5^2 + \frac{3}{4}(7.5)^2 \right]^{1/2} \right\}^{1/3} \\ &= 17.2 \text{ mm.} \end{aligned}$$

Using the MSST as given in Eq. (11.16) gives

$$\begin{aligned} d &= \left( \frac{32n_s}{\pi S_y} \sqrt{M^2 + T^2} \right)^{1/3} \\ &= \left\{ \frac{32(2)}{\pi(500 \times 10^6)} [124.5^2 + 7.5^2]^{1/2} \right\}^{1/3} \\ &= 17.2 \text{ mm.} \end{aligned}$$

Since the torque is small relative to the moment, little difference exists between the DET and MSST predictions. This is not normally the case, although the results are usually close. Note that it is good design practice to specify a diameter that is rounded up to a convenient integer dimension. In this case, a diameter of 20 mm would be a good option.

### 11.2.2 Bending, Torsion, and Axial Loading

If, in addition to bending and torsion, an axial load is present, the normal stress is similar to Eq. (11.4) and is given by:

$$\sigma_x = \frac{32M}{\pi d^3} + \frac{4P}{\pi d^2}. \quad (11.18)$$

The shear stress is still expressed by Eq. (11.5); and the principal normal stresses, by Eq. (11.6). Substituting Eqs. (11.18) and (11.5) into Eq. (11.6) gives

$$\begin{aligned} \sigma_1, \sigma_2 &= \frac{16M}{\pi d^3} + \frac{2P}{\pi d^2} \pm \sqrt{\left( \frac{16M}{\pi d^3} + \frac{2P}{\pi d^2} \right)^2 + \left( \frac{16T}{\pi d^3} \right)^2} \\ &= \frac{2}{\pi d^3} \left[ 8M + Pd \pm \sqrt{(8M + Pd)^2 + (8T)^2} \right]. \end{aligned} \quad (11.19)$$



Substituting Eqs. (11.18) and (11.5) into Eq. (11.8) gives the principal shear stresses as

$$\tau_1, \tau_2 = \pm \frac{2}{\pi d^3} \sqrt{(8M + Pd)^2 + (8T)^2}. \quad (11.20)$$

### Distortion-Energy Theory

Substituting Eq. (11.19) into Eq. (11.10) shows that the DET predicts failure if

$$\frac{4}{\pi d^3} \sqrt{(8M + Pd)^2 + 48T^2} = \frac{S_y}{n_s}. \quad (11.21)$$

This equation is more complicated than Eq. (11.16), and an explicit expression for the diameter cannot be obtained. Numerical solutions of Eq. (11.21) are relatively easy to obtain, however.

### Maximum-Shear-Stress Theory

Substituting Eq. (11.19) into Eq. (11.14) shows that the MSST predicts failure if

$$\frac{4}{\pi d^3} \sqrt{(8M + Pd)^2 + 64T^2} = \frac{S_y}{n_s}. \quad (11.22)$$

Again, when an axial loading is included, an explicit expression for the diameter cannot be obtained.

## 11.3 Fatigue Design of Shafts

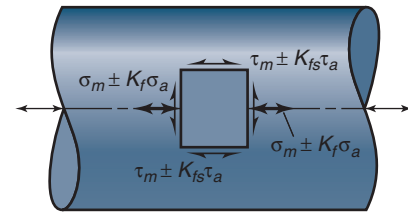
In cyclic loading, the stresses vary throughout a cycle and do not remain constant as in static loading. In this section, a general analysis is presented for the fluctuating normal and shear stresses for ductile materials, and appropriate equations are then given for brittle materials. Significant effort is expended in deriving the ultimate expressions for diameter and safety factor, as this makes simplifying assumptions readily apparent. However, the casual reader may wish to proceed to the end of this section where useful design expressions are summarized.

### 11.3.1 Ductile Materials

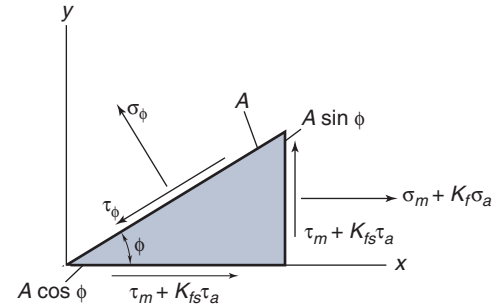
Figure 11.2 shows the normal and shear stresses acting on a shaft. In Fig. 11.2a, the stresses act on a rectangular element, and in Fig. 11.2b, they act on an oblique plane at an angle  $\phi$ . The normal stresses are denoted by  $\sigma$  and the shear stresses by  $\tau$ . Subscript  $a$  designates alternating and subscript  $m$  designates mean or steady stress. Also,  $K_f$  designates the fatigue stress concentration factor due to normal loading, and  $K_{fs}$  designates the fatigue concentration factor due to shear loading. On the rectangular element in Fig. 11.2a, the normal stress is  $\sigma = \sigma_m \pm K_f \sigma_a$  and the shear stress is  $\tau = \tau_m \pm K_{fs} \tau_a$ . This uses the approach presented in Section 7.7 that applies the stress concentration factor to the alternating stress and not the mean stress. This approximation has certain implications that will be discussed below.

The largest stress occurs when  $\sigma_a$  and  $\tau_a$  are in phase, or when the frequency of one is an integer multiple of the frequency of the other. Summing the forces tangent to the diagonal gives

$$\begin{aligned} 0 &= -\tau_\phi A + (\tau_m + K_{fs} \tau_a) A \cos \phi \cos \phi \\ &\quad - (\tau_m + K_{fs} \tau_a) A \sin \phi \sin \phi \\ &\quad + (\sigma_m + K_f \sigma_a) A \cos \phi \sin \phi. \end{aligned}$$



(a)



(b)

Figure 11.2: Fluctuating normal and shear stresses acting on shaft. (a) Stresses acting on rectangular element; (b) stresses acting on oblique plane at angle  $\phi$ .

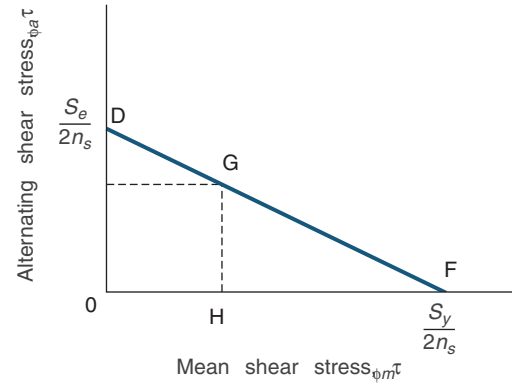


Figure 11.3: Soderberg line for shear stress.

Making use of double angle relations simplifies this expression to

$$\tau_\phi = (\tau_m + K_{fs} \tau_a) \cos 2\phi + \frac{1}{2} (\sigma_m + K_f \sigma_a) \sin 2\phi.$$

Separating the mean and alternating components of stress gives the stress acting on the oblique plane as

$$\begin{aligned} \tau_\phi &= \tau_{\phi m} + \tau_{\phi a} \\ &= \left( \frac{\sigma_m}{2} \sin 2\phi + \tau_m \cos 2\phi \right) \\ &\quad + \left( \frac{K_f \sigma_a}{2} \sin 2\phi + K_{fs} \tau_a \cos 2\phi \right). \end{aligned} \quad (11.23)$$

Recall the Soderberg line in Fig. 7.16 for tensile loading. For shear loading, the end points of the Soderberg line are  $S_{se} = S_e/2n_s$  and  $S_{sy} = S_y/2n_s$ . Figure 11.3 shows the Soderberg line for shear stress. From the proportional triangles GHF and D0F of Fig. 11.3,

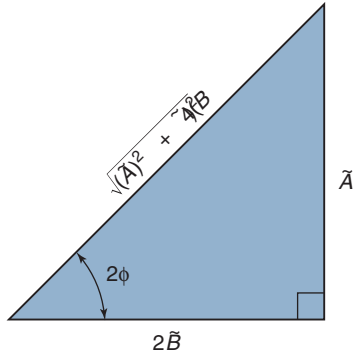


Figure 11.4: Illustration of relationship given in Eq. (11.28).

$$\frac{HF}{OF} = \frac{HG}{OD}, \quad \text{or} \quad \frac{S_y/2n_s - \tau_{\phi m}}{S_y/2n_s} = \frac{\tau_{\phi a}}{S_e/2n_s},$$

so that

$$\frac{1}{n_s} = \frac{\tau_{\phi a}}{S_e/2} + \frac{\tau_{\phi m}}{S_y/2}. \quad (11.24)$$

Substituting the expressions for  $\tau_{\phi a}$  and  $\tau_{\phi m}$  into Eq. (11.24) gives

$$\begin{aligned} \frac{1}{n_s} &= \frac{\frac{K_f \sigma_a}{2} \sin 2\phi + K_{fs} \tau_a \cos 2\phi}{S_e/2} \\ &+ \frac{\left(\frac{\sigma_m}{2} \sin 2\phi + \tau_m \cos 2\phi\right)}{S_y/2} \\ &= \tilde{A} \sin 2\phi + 2\tilde{B} \cos 2\phi, \end{aligned} \quad (11.25)$$

where

$$\tilde{A} = \frac{\sigma_m}{S_y} + \frac{K_f \sigma_a}{S_e}, \quad (11.26)$$

$$\tilde{B} = \frac{\tau_m}{S_y} + \frac{K_{fs} \tau_a}{S_e}. \quad (11.27)$$

The stress combination that produces the smallest safety factor is desired, since this corresponds to a maximum-stress situation. The minimum value of  $n_s$  corresponds to a maximum value of  $1/n_s$ . Differentiating  $1/n_s$  in Eq. (11.25) and equating the result to zero gives

$$\frac{d}{d\phi} \left( \frac{1}{n_s} \right) = 2\tilde{A} \cos 2\phi - 4\tilde{B} \sin 2\phi = 0.$$

Therefore,

$$\frac{\sin 2\phi}{\cos 2\phi} = \tan 2\phi = \frac{\tilde{A}}{2\tilde{B}}. \quad (11.28)$$

This relationship is illustrated in Fig. 11.4, which shows that

$$\sin 2\phi = \frac{\tilde{A}}{\sqrt{(\tilde{A})^2 + 4(\tilde{B})^2}}$$

and

$$\cos 2\phi = \frac{2\tilde{B}}{\sqrt{(\tilde{A})^2 + 4(\tilde{B})^2}}. \quad (11.29)$$

Substituting these into Eq. (11.25) gives

$$\begin{aligned} \frac{1}{n_s} &= \frac{(\tilde{A})^2}{\sqrt{(\tilde{A})^2 + 4(\tilde{B})^2}} + \frac{4(\tilde{B})^2}{\sqrt{(\tilde{A})^2 + 4(\tilde{B})^2}} \\ &= \sqrt{(\tilde{A})^2 + 4(\tilde{B})^2}. \end{aligned}$$

Substituting Eqs. (11.26) and (11.27) gives

$$\begin{aligned} \frac{1}{n_s} &= \sqrt{\left(\frac{\sigma_m}{S_y} + \frac{K_f \sigma_a}{S_e}\right)^2 + 4\left(\frac{\tau_m}{S_y} + \frac{K_{fs} \tau_a}{S_e}\right)^2}, \\ \frac{S_y}{n_s} &= \sqrt{\left(\sigma_m + \frac{S_y}{S_e} K_f \sigma_a\right)^2 + 4\left(\tau_m + \frac{S_y}{S_e} K_{fs} \tau_a\right)^2}. \end{aligned} \quad (11.30)$$

Setting  $\sigma_y = 0$ ,  $\sigma_x = \sigma$ , and  $\tau_{xy} = \tau$  in Eq. (2.19) for biaxial stresses, the maximum shear stress is

$$\tau_{\max} = \sqrt{\left(\frac{\sigma}{2}\right)^2 + \tau^2}, \quad (11.31)$$

and the safety factor is

$$\begin{aligned} n_s &= \frac{S_y/2}{\tau_{\max}} = \frac{S_y/2}{\sqrt{(\sigma/2)^2 + \tau^2}} = \frac{S_y}{\sqrt{\sigma^2 + 4\tau^2}}, \\ \frac{S_y}{n_s} &= \sqrt{\sigma^2 + 4\tau^2}. \end{aligned} \quad (11.32)$$

Equations (11.32) and (11.30) have the same form, and

$$\sigma = \sigma_m + \frac{S_y}{S_e} K_f \sigma_a \quad \text{and} \quad \tau = \tau_m + \frac{S_y}{S_e} K_{fs} \tau_a.$$

Note that the normal and shear stresses each contain a steady and an alternating component, the latter weighted for the effect of fatigue and stress concentration.

By making use of Eqs. (11.4) and (11.5), Eq. (11.30) becomes

$$n_s = \frac{\pi d^3 S_y}{32 \sqrt{\left(M_m + \frac{S_y}{S_e} K_f M_a\right)^2 + \left(T_m + \frac{S_y}{S_e} K_{fs} T_a\right)^2}}. \quad (11.33)$$

If the smallest safe diameter for a specified safety factor is desired, Eq. (11.33) can be rewritten as

$$d = \left[ \frac{32n_s}{\pi S_y} \sqrt{\left(M_m + \frac{S_y}{S_e} K_f M_a\right)^2 + \left(T_m + \frac{S_y}{S_e} K_{fs} T_a\right)^2} \right]^{1/3} \quad (11.34)$$

Equations (11.33) and (11.34) represent the general form of a shaft design equation using the Soderberg line and MSST. Note in Eq. (11.34) that  $S_y$ ,  $S_y/S_e$ ,  $K_f$ , and  $K_{fs}$  depend on the shaft diameter  $d$ . Thus, a numerical or iterative approach is needed to solve for the required diameter.

Peterson [1974] modified Eq. (11.30) by changing the coefficient of the shear stress term from 4 to 3, such that the DET is satisfied and gives

$$\frac{S_y}{n_s} = \sqrt{\left(\sigma_m + \frac{S_y}{S_e} K_f \sigma_a\right)^2 + 3\left(\tau_m + \frac{S_y}{S_e} K_{fs} \tau_a\right)^2}. \quad (11.35)$$

By making use of Eqs. (11.4) and (11.5), Eq. (11.35) becomes

$$n_s = \frac{\pi d^3 S_y}{32 \sqrt{\left(M_m + \frac{S_y}{S_e} K_f M_a\right)^2 + \frac{3}{4} \left(T_m + \frac{S_y}{S_e} K_{fs} T_a\right)^2}} \quad (11.36)$$

The smallest safe diameter corresponding to a specific safety factor can then be expressed as

$$d^3 = \frac{32 n_s}{\pi S_y} \sqrt{\left(M_m + \frac{S_y}{S_e} K_f M_a\right)^2 + \frac{3}{4} \left(T_m + \frac{S_y}{S_e} K_{fs} T_a\right)^2} \quad (11.37)$$

The distinction between Eqs. (11.33) and (11.34) and Eqs. (11.36) and (11.37) needs to be recognized. Equations (11.33) and (11.34) assume that the MSST is valid; Eqs. (11.36) and (11.37) assume that the DET is valid. All four equations are general equations applicable to ductile materials.

### Example 11.2: Fatigue Design of a Shaft

**Given:** When a rear-wheel-drive car accelerates around a bend at high speeds, the drive shafts are subjected to both bending and torsion. The acceleration torque,  $T$ , is reasonably constant at 400 N-m while the bending moment is varying due to cornering and is expressed in newton-meters as

$$M = 250 + 800 \sin \omega t.$$

Thus, the mean and alternating moments are  $M_m = 250$  N-m and  $M_a = 800$  N-m. Assume there is no notch that can produce a stress concentration. The reliability must be 99% and the safety factor is 4.5. The shaft is forged from high-carbon steel, so that it has equivalent mechanical properties as AISI 1080 steel that has been quenched and tempered at 800°C.

**Find:** The shaft diameter using the MSST.

**Solution:** From Eq. (7.7) and Table A.2 the bending endurance limit for AISI 1080 steel is

$$S'_e = 0.5 S_u = 0.5 (615) = 307.5 \text{ MPa}.$$

From Fig. 7.11, the surface finish factor for an as-forged surface at  $S_{ut} = 615$  MPa is  $k_f = 0.42$ . To evaluate the size factor, the shaft diameter needs to be chosen, and this value can be modified later if necessary. From Eq. (7.20), and assuming  $d = 30$  mm,

$$k_s = 1.248 d^{-0.112} = 1.248 (30)^{-0.112} = 0.853.$$

From Table 7.4, for 99% probability of survival, the reliability factor is 0.82. Substituting this value into Eq. (7.18) gives the endurance limit as

$$S_e = k_f k_s k_r S'_e = (0.42)(0.853)(0.82) (307.5 \times 10^6),$$

or  $S_e = 90.19$  MPa. Substituting into Eq. (11.34) with  $T_a = 0$  gives

$$\begin{aligned} d^3 &= \left\{ \frac{32 n_s}{\pi S_y} \sqrt{\left(M_m + \frac{S_y}{S_e} K_f M_a\right)^2 + T_m^2} \right\}^{1/3} \\ &= \frac{32(4.5)}{\pi (380 \times 10^6)} \\ &\quad \times \sqrt{\left(250 + \frac{(380 \times 10^6)}{(90.19 \times 10^6)} (1)(800)\right)^2 + (400)^2}. \end{aligned}$$

which is solved as  $d = 0.0760 \text{ m} = 76.0 \text{ mm}$ .

Note that this value is very different from the assumed shaft diameter of 30 mm, so at least one more iteration is required. Use the value of 76.0 mm as the new assumed value for diameter. From Eq. (7.20),

$$k_s = 1.248 d^{-0.112} = 1.248 (76.0)^{-0.112} = 0.768.$$

Therefore,

$$S_e = (0.42)(0.768)(0.82)(307.5 \times 10^6) = 81.33 \text{ MPa}.$$

From Eq. (11.34),

$$\begin{aligned} d^3 &= \frac{32(4.5)}{\pi (380 \times 10^6)} \\ &\quad \times \sqrt{\left[250 + \frac{(380 \times 10^6)}{(81.33 \times 10^6)} (1)(800)\right]^2 + (400)^2}, \end{aligned}$$

or  $d = 0.0785 \text{ m}$ . Note that the size factor was calculated based on a diameter of 76.0 mm, and the updated solution is 78.5 mm. Since these are very close, no further iterations are deemed necessary. A diameter of 78.5 mm is an awkward design specification; a reasonable dimension to specify for the shaft would be 80 mm or even larger, depending on such factors as stock availability and cost.

### Example 11.3: Fatigue Design of a Shaft Under Combined Loading

**Given:** The shaft made of AISI 1080 high-carbon steel (quenched and tempered at 800°C) shown in Fig. 11.5 is subjected to completely reversed bending and steady torsion. A standard needle bearing (see Fig. 13.1c) is to be placed on diameter  $d_2$  and this surface will therefore be ground to form a good seat for the bearing. The remainder of the shaft will be machined. The groove between the sections ensures that the large diameter section is not damaged by the grinding operation, and is called a *grinding relief*.

Assume that standard needle bearing bore sizes are in 5-mm increments in the range 15 to 50 mm. Design the shaft so that the relative sizes are approximately (within 1 mm)  $d_2 = 0.75 d_3$  and  $d_1 = 0.65 d_3$ . At this location, the loading involves completely reversed bending of 70 N-m, and steady torsion of 45 N-m. Design the shaft for infinite life.

**Find:** Determine the diameter  $d_2$  that results in a safety factor of at least 5.0.

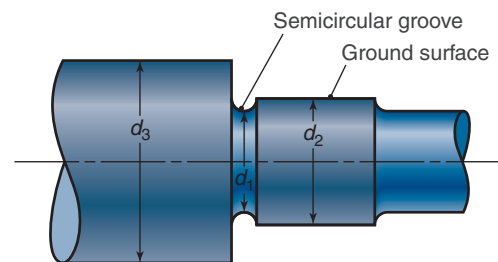


Figure 11.5: Section of shaft in Example 11.3.

**Solution:** The stress concentration factor can be obtained from the geometry using the ratios given. Not that some variation will occur due to rounding of the dimensions, but this has only a minor effect on the stress concentration. Therefore,

$$\frac{d_2}{d_1} = \frac{0.75d_3}{0.65d_3} = 1.154.$$

Since the grinding relief groove is semicircular,

$$\frac{r}{d} = \frac{(d_2 - d_1)/2}{d_1} = \frac{1}{2} \left( \frac{d_2}{d_1} - 1 \right) = 0.0769.$$

Therefore, from Fig. 6.6b,  $K_c = 2.05$ . From Table A2 for this steel,  $S_u = 615$  MPa and  $S_y = 380$  MPa. From Eq. (7.7) for bending,

$$S'_e = 0.5S_u = 307 \text{ MPa}.$$

For the shaft, one surface is ground, but the remainder is machined. An inspection of Fig. 11.5 suggests that the ground surface has no stress concentrations and has a larger diameter than the region of grinding relief. Therefore, failure is most likely at the relief, and a surface finish correction factor will be calculated based on a machined surface. Therefore, from Eq. (7.19),

$$k_f = eS_u^f = (4.51)(615)^{-0.265} = 0.822.$$

No yield criterion has been specified, so the MSST will be used. The problem states that the diameter  $d_2$  will be a seat for a bearing, and such bearings are available in 5-mm increments. Therefore,  $d_2$  will be arbitrarily assigned a value of 20 mm, and the safety factor will be calculated and compared to the required value using Eq. (11.33). If the safety factor is not sufficient, then  $d_2$  will be increased until a sufficiently high safety factor results. An alternative approach is to derive an expression for diameter based on Eq. (11.34), and then obtain a numerical solution using a mathematics software package. Either approach is valid and will produce the same results.

If  $d_2$  is 20 mm, then  $d_3$  is  $d_2/0.75 = 26.67$  mm, which is rounded up to  $d_3 = 27$  mm. Similarly,  $d_1 = 0.65d_3 = 17.55$  mm, so that  $d_1$  will be assigned a value of 18 mm. The size factor is obtained from Eq. (7.20) as

$$k_s = 1.248d^{-0.112} = 1.248(27)^{-0.112} = 0.863.$$

The selection of  $d_3$  for use in calculating the size factor should be discussed. No detailed information is given regarding the manufacture of the shaft. It is reasonable to assume that the shaft was machined from extruded bar stock slightly larger than the  $d_3$  dimension, thus justifying the approach in this solution. However, if the shaft were forged, roll forged, or swaged, and then machined to the final dimensions, it would be reasonable to use  $d_1$  to obtain the size factor. Also note that  $k_f$  and  $k_s$  are coincidentally equal in this case.

No other correction factors apply to this problem, so that the modified endurance limit is obtained from Eq. (7.18):

$$S_e = k_f k_s S'_e = (0.822)(0.863)(307.5) = 218.1 \text{ MPa}.$$

If  $d_1 = 18$  and  $d_2 = 20$ , then the notch radius is  $r = 1$  mm for a semicircular groove. Therefore, from Fig. 7.10 for  $S_u = 615$  MPa, the notch sensitivity factor is around  $q_n = 0.7$ . From Eq. (7.17),

Table 11.1: Summary of results for Example 11.3.

$d_2$ (mm)	$d_1$ (mm)	$d_3$ (mm)	$n_s$
20	18	27	1.32
25	22	34	2.50
30	26	40	4.26
35	31	47	6.65

$$K_f = 1 + (K_c - 1)q_n = 1 + (2.05 - 1)(0.7) = 1.735.$$

For completely reversed bending,  $M_m = 0$  and  $M_a = 70$  N-m, and for steady torsion,  $T_a = 0$  and  $T_m = 45$  N-m. Therefore, from Eq. (11.33),

$$n_s = \frac{\pi(0.020)^3(380 \times 10^6)}{32 \sqrt{\left[ \left( \frac{380}{218.1} \right) (1.735)(70) \right]^2 + 45^2}} = 1.38.$$

This safety factor is too low, since a minimum safety factor of 5.0 was prescribed. Thus, the diameter  $d_2$  is increased, and the procedure is repeated. Table 11.1 summarizes the results for a number of values of  $d_2$ . Therefore, the value of  $d_2 = 35$  mm,  $d_1 = 31$  mm, and  $d_3 = 47$  mm are used to design the shaft.

### 11.3.2 Brittle Materials

Although shafts are usually cold-worked metals that are machined to final desired dimensions, there are applications where castings, which are often brittle materials, are used as shafts. As discussed in Ch. 6, this requires a slightly different analysis approach than for ductile materials.

For brittle materials, the forces in Fig. 11.2b are assumed to be *normal* rather than tangent to the diagonal. Also, the design line for any failure theory relevant to brittle materials (see Section 6.7.2) extends from  $S_e/n_s$  to  $S_u/n_s$  instead of from  $S_e/2n_s$  to  $S_y/2n_s$  as was true for the ductile materials. Following procedures similar to those used in obtaining Eq. (11.30) gives

$$\begin{aligned} \frac{2S_u}{n_s} &= K_c \left( \sigma_m + \frac{S_u}{S_e} \sigma_a \right) \\ &+ \sqrt{K_c^2 \left( \sigma_m + \frac{S_u}{S_e} \sigma_a \right)^2 + 4K_{cs}^2 \left( \tau_m + \frac{S_u}{S_e} \tau_a \right)^2}. \end{aligned} \quad (11.38)$$

where  $K_c$  is the theoretical stress concentration factor. By making use of Eqs. (11.4) and (11.5), Eq. (11.38) can be written as

$$n_s = \frac{\pi d^3 S_u / 16}{K_c \Psi + \sqrt{K_c^2 \Psi^2 + K_{cs}^2 \left( T_m + \frac{S_u}{S_e} T_a \right)^2}}, \quad (11.39)$$

where  $\Psi$  is given by

$$\Psi = M_m + \frac{S_u}{S_e} M_a. \quad (11.40)$$

If the minimum safe diameter of the shaft is desired for a spe-

cific safety factor,

$$d = \left\{ \frac{16n_s}{\pi S_u} \left[ K_c \Psi + \sqrt{K_c^2 \Psi^2 + K_{cs}^2 \left( T_m + \frac{S_u}{S_e} T_a \right)^2} \right] \right\}^{1/3} \quad (11.41)$$

The important difference in the equations developed above for the safety factor and the smallest safe diameter is that Eqs. (11.33) and (11.34) are applicable for ductile materials while assuming the MSST, Eqs. (11.36) and (11.37) are also applicable for ductile materials but while assuming the DET, and Eqs. (11.39) and (11.41) are applicable for brittle materials. Note the major differences between the equations developed for brittle and ductile materials. For brittle materials [Eqs. (11.39) and (11.41)] the stress concentration factor  $K_c$  and the ultimate stress  $S_u$  are used, whereas for ductile materials [Eqs. (11.33), (11.34), (11.36), and (11.37)] the fatigue stress concentration factor  $K_f$  and the yield stress  $S_y$  are used.

## 11.4 Additional Shaft Design Considerations

Sections 11.2 and 11.3 described in detail the design approach for sizing or analyzing a shaft from a stress standpoint. Rotating shafts are very likely to encounter sufficient stress cycles to necessitate design based on an endurance limit (see Section 7.8). Therefore, the same concerns discussed in Ch. 7 hold for shafts. It needs to be recognized that the design approach in Ch. 7 is empirical in nature, but must be verified through experiments. Shafts are often spared from extensive test programs because of their inherently high safety factors, the reasons for which are discussed below.

A common cyclic stress variation that occurs in practical applications is reversed bending and steady torsion. From Section 7.3, note that reversed bending implies that  $\sigma_m = 0$ , or  $M_m = 0$ . Also, steady torsion implies that  $\tau_a = 0$ , or  $T_a = 0$ . Thus, reduced forms of Eqs. (11.33) and (11.34), (11.36) and (11.37), or (11.39) and (11.41) can be readily determined. For example, for such a loading, Eqs. (11.33) and (11.34) become

$$n_s = \frac{\pi d^3 S_y}{32 \sqrt{\left( \frac{S_y}{S_e} K_f M_a \right)^2 + T_m^2}}, \quad (11.42)$$

$$d = \left[ \frac{32n_s}{\pi S_y} \sqrt{\left( \frac{S_y}{S_e} K_f M_a \right)^2 + T_m^2} \right]^{1/3}. \quad (11.43)$$

Recall that Eqs. (11.42) and (11.43) are for the MSST and Soderberg line; similar expressions can be obtained for other criteria.

As mentioned previously, shafts usually display fairly large safety factors compared to other machine elements. There are a number of reasons for this, including:

1. Shafts are usually in difficult-to-access locations, and have many machine elements mounted onto them. Replacing a shaft requires significant time merely for exposure; removing machine elements, replacing the shaft, and remounting the machine elements (and aligning them) also requires significant time. Recognizing this, designers commonly assign large safety factors to avoid high costs associated with failure and replacement of shafts.

2. Shafts themselves are usually quite expensive, and protection of the shaft is one of the main reasons that keys or pins (Section 11.6) or slip clutches (Section 18.10) are used.
3. Deflection is a major concern, and often shaft size is specified to meet a deflection requirement, leading to low stress levels. Deflection includes lateral deflection of the shaft from bending moments (Ch. 5), as well as torsional deflection (see Section 4.4).
4. Certain machine elements, such as gears or connecting rods, require that the shaft provide load support with minimal deflection. For this reason, it is not unusual to place bearings immediately adjacent to such machine elements. Thus, the spans and bending moments encountered in practice problems and examples are not reflective of well-supported shafts in practice. However, it must be recognized that providing additional bearings is not a straightforward approach, and requires careful alignment and adjustment in order to evenly distribute loads.

### Design Procedure 11.1: Shafts

The general procedure for shaft design is as follows:

1. Develop a free-body diagram by replacing the various machine elements mounted on the shaft by their statically equivalent load or torque components. To illustrate this, Fig. 11.6a shows two gears exerting forces on a shaft, and Fig. 11.6b then shows a free-body diagram of the shaft.
2. Draw a bending moment diagram in the  $x$ - $y$  and  $x$ - $z$  planes as shown in Fig. 11.6c and d. The resultant internal moment at any section along the shaft may be expressed as
 
$$M_x = \sqrt{M_{xy}^2 + M_{xz}^2}. \quad (11.44)$$
3. Analyze the shaft based on lateral deflection due to bending using the approach in Ch. 5. If deflection is a design constraint, select a diameter that results in acceptable deflection, or else relocate supports to reduce the bending moments encountered.
4. Develop a torque diagram as shown in Fig. 11.6e. Torque developed from one power-transmitting element must balance that from other power-transmitting elements.
5. Analyze the shaft based on deflection due to torsion (Section 4.4). If torsional deflection is a design constraint, select a diameter that results in acceptable deflection.
6. Evaluate the suitability of the shaft from a stress standpoint:



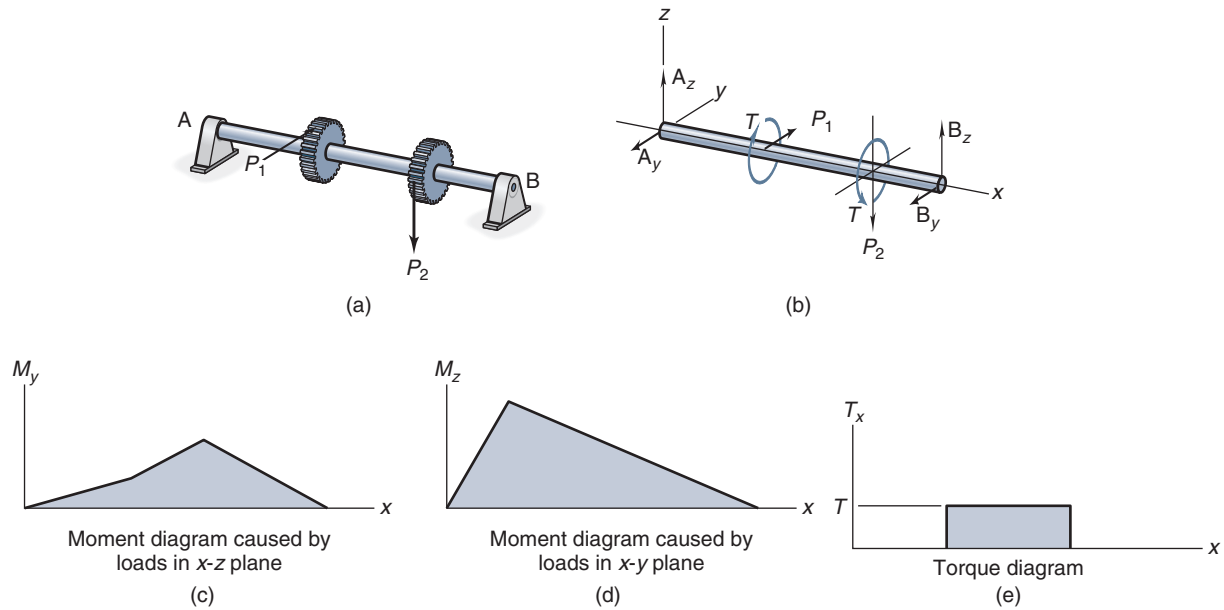


Figure 11.6: Shaft assembly. (a) Shaft with two bearings at A and B and two gears with resulting forces  $P_1$  and  $P_2$ ; (b) free-body diagram of torque and forces resulting from assembly drawing; (c) moment diagram in  $x-z$  plane; (d) moment diagram in  $x-y$  planes; (e) torque diagram.

- (a) Establish the location of the critical cross-section, or the  $x$  location where the torque and moment are the largest.
- (b) For ductile materials, use the MSST or the DET covered in Section 6.7.1.
- (c) For brittle materials, use the maximum-normal-stress theory (MNST), the internal friction theory (IFT), or the modified Mohr theory (MMT) (see Section 6.7.2).

7. Use keyways, set screws or pins (see Section 11.6), or slip clutches (Section 18.10) where appropriate to protect the shaft.
8. Compare the critical speed of the shaft (Section 11.5) to the operating conditions. Change shaft diameter or supports to avoid critical speeds if necessary.

## 11.5 Critical Speed of Rotating Shafts

All rotating shafts deflect during operation. The magnitude of the deflection depends on the stiffness of the shaft and its supports, the total mass of the shaft and its attached parts, and the amount of system damping. The **critical speed** of a rotating shaft, sometimes called the **natural frequency**, is the speed at which the rotating shaft becomes dynamically unstable and large deflections associated with vibration are likely to develop. For any shaft there are an infinite number of critical speeds, but only the lowest (first) and occasionally the second are generally of interest to designers. The others are usually so high as to be well out of the operating range of shaft speed. This text considers only the first critical speed

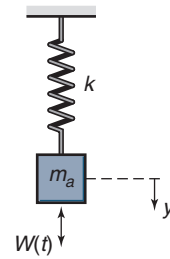


Figure 11.7: Simple single-mass system.

of the shaft. Two approximate methods of finding the first critical speed (or lowest natural frequency) of a system are given in this section, one attributed to Rayleigh and the other to Dunkerley.

### 11.5.1 Single-Mass System

The **first critical speed** (or **lowest natural frequency**) can be obtained by observing the rate of interchange between the kinetic (energy of motion) and potential (energy of position) energies of the system during its cyclic motion. A single mass on a shaft can be represented by the simple spring and mass shown in Fig. 11.7. The dashed line indicates the static equilibrium position. The potential energy of the system is

$$U = \int_0^{\delta} (m_a g + k\delta) d\delta - m_a g\delta,$$

where

- $m_a$  = mass, kg
- $g$  = gravitational acceleration, 9.807 m/s<sup>2</sup>
- $k$  = spring rate, N/m
- $\delta$  = deflection, m

Integrating gives

$$U = \frac{1}{2} k\delta^2. \quad (11.45)$$

The kinetic energy of the system with the mass moving with a velocity of  $\dot{\delta}$  is

$$K_e = \frac{1}{2} m_a (\dot{\delta})^2. \quad (11.46)$$

Observe the following about Eqs. (11.45) and (11.46):

1. As the mass passes through the static equilibrium position, the potential energy is zero and the kinetic energy is at a maximum and equal to the total mechanical energy of the system.
2. When the mass is at the position of maximum displacement and is on the verge of changing direction, its velocity is zero. At this point the potential energy is at a maximum and is equal to the total mechanical energy of the system.

The total mechanical energy is the sum of the potential and kinetic energies and is constant at any time. Therefore,

$$\frac{d}{dt} (U + K_e) = 0. \quad (11.47)$$

Substituting Eqs. (11.45) and (11.46) into Eq. (11.47) gives

$$\frac{d}{dt} \left[ \frac{1}{2} k \delta^2 + \frac{1}{2} m_a (\dot{\delta})^2 \right] = k \delta \dot{\delta} + m_a \dot{\delta} \ddot{\delta} = 0.$$

Factoring  $\dot{\delta}$  leads to

$$\dot{\delta} (m_a \ddot{\delta} + k \delta) = 0, \quad (11.48)$$

$$\ddot{\delta} + \omega^2 \delta = 0,$$

where

$$\omega = \sqrt{k/m_a}, \text{ rad/s.} \quad (11.49)$$

The general solution to this differential equation is

$$\delta = C_1 \sin(\omega t + \phi), \quad (11.50)$$

where  $C_1$  is an integration constant. The first critical speed (or lowest natural frequency) is  $\omega$ . Substituting Eq. (11.50) into Eqs. (11.45) and (11.46) gives

$$U = \frac{k}{2} C_1^2 \sin^2(\omega t + \phi), \quad (11.51)$$

$$K_e = \frac{m_a}{2} C_1^2 \omega^2 \cos^2(\omega t + \phi). \quad (11.52)$$

Note from Eq. (11.49) that, for static deflection, if  $k = W/\delta$  and  $m_a = W/g$ , then

$$\omega = \sqrt{\frac{k}{m_a}} = \sqrt{\frac{W/y}{W/g}} = \sqrt{\frac{g}{\delta}}. \quad (11.53)$$

## 11.5.2 Multiple-Mass System

From Eq. (11.46), the kinetic energy for  $n$  masses is

$$K_e = \frac{1}{2} m_{a1} (\dot{\delta}_1)^2 + \frac{1}{2} m_{a2} (\dot{\delta}_2)^2 + \cdots + \frac{1}{2} m_{an} (\dot{\delta}_n)^2. \quad (11.54)$$

If the deflection is represented by Eq. (11.50), then  $y_{\max} = C_1$ . Also,  $\dot{y}_{\max} = C_1 \omega = y_{\max} \omega$ . Therefore, the maximum kinetic energy is

$$K_{e,\max} = \frac{\omega^2}{2} \sum m_{an} (\delta_{n,\max})^2. \quad (11.55)$$

From Eq. (11.45), the potential energy for  $n$  masses is

$$U = \frac{1}{2} k_1 \delta_1^2 + \frac{1}{2} k_2 \delta_2^2 + \cdots + \frac{1}{2} k_n \delta_n^2, \quad (11.56)$$

and the maximum potential energy is

$$U_{\max} = \frac{1}{2} k_1 (\delta_{1,\max})^2 + \frac{1}{2} k_2 (\delta_{2,\max})^2 + \cdots + \frac{1}{2} k_n (\delta_{n,\max})^2. \quad (11.57)$$

The **Rayleigh method** assumes that  $K_{e,\max} = U_{\max}$  or

$$\frac{1}{2} \omega^2 \sum_{i=1,\dots,n} m_{ai} (\delta_{i,\max})^2 = \frac{1}{2} \sum_{i=1,\dots,n} k_i (\delta_{i,\max})^2.$$

Solving for angular velocity,

$$\omega^2 = \frac{\sum_{i=1,\dots,n} k_i (\delta_{i,\max})^2}{\sum_{i=1,\dots,n} m_{ai} (\delta_{i,\max})^2}, \quad (11.58)$$

but

$$k_i = \frac{W_i}{\delta_{i,\max}} \quad \text{and} \quad m_{ai} = \frac{W_i}{g}. \quad (11.59)$$

where  $W_i$  is the  $i$ th weight placed on the shaft and  $g$  is gravitation acceleration,  $9.807 \text{ m/s}^2$ . Substituting Eq. (11.59) into Eq. (11.58) gives

$$\omega_{cr} = \sqrt{\frac{g \sum_{i=1,\dots,n} W_i \delta_{i,\max}}{\sum_{i=1,\dots,n} W_i \delta_{i,\max}^2}}. \quad (11.60)$$

This is the first critical speed (first natural frequency) of a multiple-mass system when using the Rayleigh method. Equation (11.60) is known as the **Rayleigh equation**. Because the actual displacements are larger than the static displacements used in Eq. (11.60), the energies in both the denominator and the numerator will be underestimated by the Rayleigh formulation. However, the error in the underestimate will be larger in the denominator, since it involves the square of the approximated displacements. Thus, Eq. (11.60) *overestimates* (provides an upper bound on) the first critical speed.

The **Dunkerley equation** is another approximation to the first critical speed of a multiple-mass system; it is given as

$$\frac{1}{\omega_{cr}^2} = \frac{1}{\omega_1^2} + \frac{1}{\omega_2^2} + \cdots + \frac{1}{\omega_n^2}, \quad (11.61)$$

where

$\omega_1$  = critical speed if only mass 1 exists

$\omega_2$  = critical speed if only mass 2 exists

$\omega_n$  = critical speed if only the  $n$ th mass exists

Recall from Eq. (11.53) that  $\omega_i = \sqrt{g/\delta_i}$ .

The Dunkerley equation *underestimates* (provides a lower bound on) the first critical speed. The major difference between the Rayleigh and Dunkerley equations is in the deflections. In the Rayleigh equation, the deflection at a specific mass location takes into account the deflections due to all the masses acting on the system; in the Dunkerley equation, the deflection is due only to the individual mass being evaluated.

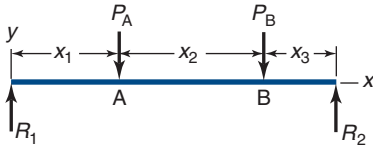


Figure 11.8: Simply supported shaft arrangement for Example 11.4.

### Example 11.4: Critical Shaft Speed

**Given:** Figure 11.8 shows a simply supported shaft arrangement. A solid shaft of 50 mm diameter made of AISI 1020 low-carbon steel is used. The following are given:  $x_1 = 0.750$  m,  $x_2 = 1.000$  m,  $x_3 = 0.500$  m,  $P_A = 300$  N, and  $P_B = 500$  N.

**Find:** Determine the first critical speed by using

- The Rayleigh method
- The Dunkerley method

**Solution:** From Table 5.1b, for simply-supported ends, the deflections are given by:

For  $0 \leq x \leq a$

$$\delta_y = \frac{Pbx}{6lEI} (l^2 - x^2 - b^2). \quad (a)$$

For  $a \leq x \leq l$

$$\delta_y = \frac{Pa(l-x)}{6lEI} (2lx - a^2 - x^2). \quad (b)$$

From Table 3.1, the modulus of elasticity for carbon steel is 207 GPa. For a solid, round shaft, the area moment of inertia is

$$I = \frac{\pi d^4}{64} = \frac{\pi (0.050)^4}{64} = 3.068 \times 10^{-7} \text{ m}^4.$$

The deflection at location A due to load  $P_A$  from Eq. (a) and  $a = x_1 = x = 0.750$  m and  $b = x_2 + x_3 = 1.5$  m is

$$\begin{aligned} \delta_{AA} &= \frac{P_A bx}{6lEI} (l^2 - x^2 - b^2) \\ &= \frac{(300)(1.5)(0.75) (2.25^2 - 0.75^2 - 1.5^2)}{6(2.25) (207 \times 10^9) (3.068 \times 10^{-7})} \\ &= -0.8857 \text{ mm.} \end{aligned}$$

Note that in Fig. 11.8, the  $y$ -direction is upward; thus,  $P_A$  and  $\delta_{AA}$  are negative. Also, the first subscript in  $\delta_{AA}$  designates the location where the deflection occurs, and the second subscript designates the loading that contributes to the deflection. The deflection at location A due to load  $P_B$  from Eq. (a) and  $a = x_1 + x_2$ ,  $x = x_1 = 0.750$  m, and  $b = 0.5$  m is

$$\begin{aligned} \delta_{AB} &= \frac{P_B bx}{6lEI} (l^2 - x^2 - b^2) \\ &= \frac{(500)(0.5)(0.75) (2.25^2 - 0.75^2 - 0.5^2)}{6(2.25) (207 \times 10^9) (3.068 \times 10^{-7})} \\ &= -0.9295 \text{ mm.} \end{aligned}$$

The total deflection at location A is

$$\delta_A = \delta_{AA} + \delta_{AB} = -0.8857 - 0.9295 = -1.815 \text{ mm.}$$

The deflection at location B due to load  $P_B$  from Eq. (a) and  $x = a = x_1 + x_2 = 1.75$  m and  $b = 0.5$  m is

$$\begin{aligned} \delta_{BB} &= \frac{P_B bx}{6lEI} (l^2 - x^2 - b^2) \\ &= \frac{(500)(0.5)(1.75) (2.25^2 - 1.75^2 - 0.5^2)}{6(2.25) (207 \times 10^9) (3.068 \times 10^{-7})} \\ &= -0.8930 \text{ mm.} \end{aligned}$$

The deflection at location B due to load  $P_A$  from Eq. (b) and  $a = x_1 = 0.75$  m,  $b = x_2 + x_3 = 1.5$  m, and  $x = x_1 + x_2 = 1.75$  m is

$$\begin{aligned} \delta_{BA} &= \frac{P_A a(l-x)}{6lEI} (2lx - a^2 - x^2) \\ &= \frac{(300)(0.75)(2.25 - 2.75)}{6(2.25) (207 \times 10^9) (3.068 \times 10^{-7})} \\ &\quad \times [2(2.25)(1.75) - 0.75^2 - 1.75^2], \end{aligned}$$

or  $\delta_{BA} = -0.5577$  mm. Thus, the total deflection at location B is

$$\delta_B = \delta_{BA} + \delta_{BB} = -0.5577 - 0.8930 = -1.451 \text{ mm.}$$

- Using the Rayleigh method, Eq. (11.60) gives the first critical speed as

$$\begin{aligned} \omega_{cr} &= \sqrt{\frac{g(P_A \delta_A + P_B \delta_B)}{P_A \delta_A^2 + P_B \delta_B^2}} \\ &= \sqrt{\frac{(9.81) [(300)(0.001815) + (500)(0.001451)]}{(300)(0.001815)^2 + (500)(0.001451)^2}}. \end{aligned}$$

$$\text{or } \omega_{cr} = 78.13 \text{ rad/s} = 746 \text{ rpm.}$$

- Using the Dunkerley method, Eq. (11.61) gives

$$\frac{1}{\omega_{cr}^2} = \frac{1}{\omega_{cr,A}^2} + \frac{1}{\omega_{cr,B}^2}.$$

where

$$\omega_{cr,A} = \sqrt{\frac{g}{\delta_{AA}}} = \sqrt{\frac{9.81}{0.0008857}} = 105.2 \text{ rad/s} = 1005 \text{ rpm,}$$

$$\omega_{cr,B} = \sqrt{\frac{g}{\delta_{BB}}} = \sqrt{\frac{9.81}{0.0008930}} = 104.8 \text{ rad/s} = 1001 \text{ rpm.}$$

Therefore, the critical speed is

$$\frac{1}{\omega_{cr}^2} = \frac{1}{\omega_{cr,A}^2} + \frac{1}{\omega_{cr,B}^2} = \frac{1}{1005^2} + \frac{1}{1001^2},$$

which is solved as  $\omega_{cr} = 709$  rpm.

In summary, the Rayleigh equation gives  $\omega_{cr} = 746$  rpm, which overestimates the first critical speed; the Dunkerley equation gives  $\omega_{cr} = 709$  rpm, which underestimates the first critical speed. Therefore, the actual first critical speed is between 709 and 746 rpm, and the shaft design should avoid this range of operation.

Table 11.2: Dimensions of selected plain parallel stock keys.

Shaft diameter $d$ , mm	Key width $w$ , mm	Key thickness $h$ , mm	Chamfer $s$ , mm	Available Lengths <sup>a</sup> $l$ , mm
6-8	2	2	0.16-0.25	6-20
8-10	3	3	0.16-0.25	6-36
10-12	4	4	0.16-0.25	8-45
12-17	5	5	0.25-0.40	10-56
17-22	6	6	0.25-0.40	14-70
22-30	8	7	0.25-0.40	18-90
30-38	10	8	0.40-0.60	22-110
38-44	12	8	0.40-0.60	28-140
44-50	14	9	0.40-0.60	36-160
50-58	16	10	0.40-0.60	45-180
65-75	20	12	0.60-0.80	50-200
75-85	22	14	0.60-0.80	56-220
85-95	25	14	0.60-0.80	63-250
95-110	28	16	0.60-0.80	70-280

<sup>a</sup> Standard lengths are 6, 8, 10, 12, 14, 16, 18, 20, 22, 25, 28, 32, 36, 40, 45, 50, 56, 63, 70, 80, 90, 100, 110, 125, 140, 160, 180, 200, 220, 250, 280.

## 11.6 Keys, Roll Pins, Splines, and Set Screws

A variety of machine elements, such as gears, pulleys, and cams, are mounted on rotating shafts. The portion of the mounted member in contact with the shaft is called the **hub**. This section describes methods of attaching the hub to the shaft. Press and shrink fits considered in Sections 10.5 and 10.6 are other options for attachment, as are using threaded hubs, or by welding or adhesively bonding the hub to the shaft (Ch. 16).

There is a great variety of **keys** and **pins**, as shown in Fig. 11.9. The simplest and most commonly used is the **parallel key**, which has a constant cross-section across its length. A **tapered key** has a constant width, but the height varies with a taper of  $0.597^\circ$ , and is driven into a tapered slot on the hub until it locks. A **Gib head** can be included on the key to facilitate removal. A **Woodruff key** has a constant width and a semicircular profile, and fits into a semicircular key seat machined onto the shaft. A Woodruff key is light-duty because it has a deep seat in the shaft, which can compromise strength, but it aligns itself readily against the hub. Selected standard key sizes are summarized in Tables 11.2 through 11.4. Keys are usually manufactured from low-carbon steel, but can be heat treated to obtain higher strengths. However, this is rare, as ductility in the key material is usually important.

**Roll pins** or **grooved pins** are alternatives to keys, as shown in Fig. 11.9i and 11.9j. Roll and grooved pins are used for light-duty service, and remain in place because of elastic recovery of the pin in the hole, so that it bears against the hole and is restrained by friction.

Consider the behavior of a simple square key, as shown in Fig. 11.9a. The main purpose of the key is to prevent rotation between the shaft and the connected machine element through which torque is being transmitted. The purpose of using the key is to transmit the *full* torque.

A key is also intended as a safety system. Most machines have an operating speed and torque that define the required size of the key. However, in the event of a drastic increase in the load conditions, the key will shear before the shaft or machine element (gear, cam, pulley, etc.) fails. Since keys are inexpensive and can be quickly replaced, designers use them to protect more expensive machinery components.

Note in Fig. 11.9 that if  $h = w$ , the key is square, a special case of a flat key. Keys should fit tightly so that key rotation

is not possible. In some applications, set screws may be required to restrict motion of the key.

Keyways result in stress concentrations in shafts. Figure 11.10 provides experimental measurements of stress concentrations associated with fitted keyways having a semicircular end. These stress concentrations should be applied to the shaft; any stress concentrations encountered by the key are generally incorporated into the key strength. It should further be noted that the data in Fig. 11.10 is conservative; actual stress concentrations associated with keyways are strongly dependent on the shaft diameter, keyway fillet radius, manufacturing tolerances, and key geometry. Stress concentration factors above 5 for bending have been reported for square keys near the key end. Fortunately, even with such a high stress concentration factor, failure for standard designs almost always occurs in the key instead of the shaft. Fatigue may be a concern, for which the stress concentration factors in Fig. 11.10 are considered reasonable.

### Design Procedure 11.2: Keys

Keys are designed to fail when an applied torque exceeds a critical value. Failure is due to shear or compressive bearing stresses, both of which are considered here. Depending on the design motivation, it is reasonable to design based on yield strength or ultimate strength. For example, if it is desired to design a keyway that will not plastically deform under a certain loading, then use of yield strength is proper. However, if it is desired to predict the maximum torque that can be supported by a key before failure, then ultimate strength is more appropriate. This Design Procedure arbitrarily uses yield strength, but could be easily adapted for determining the maximum torque that can be generated by a key. Similarly, fatigue considerations using the approaches of Ch. 7 could be applied; however, since a time-varying torque is not the more typically encountered loading, static design is usually sufficient.

1. Failure due to shear. The shear force applied to the key is given by:

$$P = \frac{T}{d/2} = \frac{2T}{d}. \quad (11.62)$$

The shear stress at yielding, recalling that  $S_{sy} = S_y/2$  (see Section 2.12), is

$$\tau = \frac{S_y}{2n_s} = \frac{P}{A_s}. \quad (11.63)$$

Therefore, the torque that causes plastic deformation of a key is obtained from Eqs. (11.62) and (11.63) as

$$T = \frac{S_y A_s d}{4n_s}. \quad (11.64)$$

The area for a key as shown in Fig. 11.9a–e is  $A_s = wl$ . For a round key (Fig. 11.9f),  $A_s = dl$ . For a Woodruff key, see Table 11.4.

2. Failure due to compressive or bearing stress. This failure mode is most commonly encountered with flat keys. The bearing stress for a key as shown in Fig. 11.9a–e is given by

$$\sigma = \frac{P}{A_c} = \frac{2T}{dlh/2} = \frac{4T}{dlh}. \quad (11.65)$$

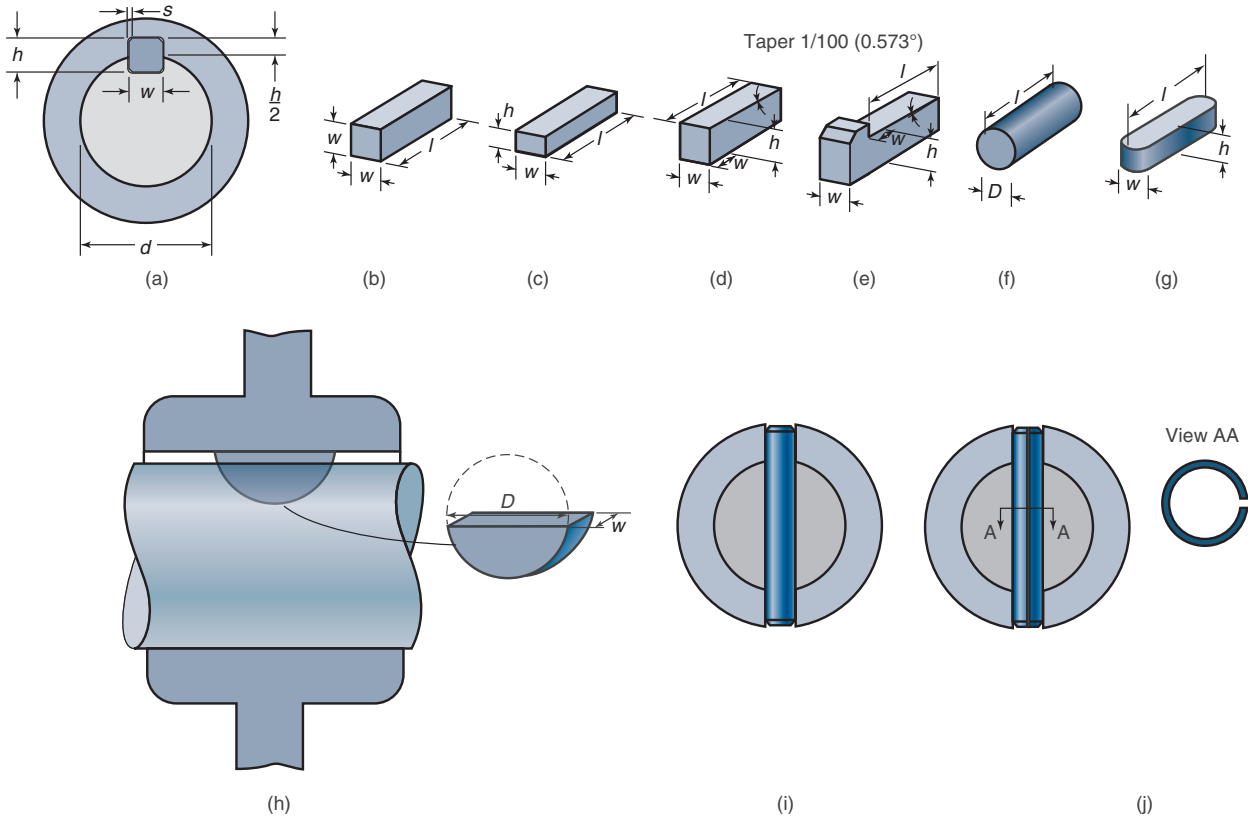


Figure 11.9: Illustration of keys and pins. (a) Dimensions of shaft with keyway in shaft and hub; (b) square parallel key; (c) flat parallel key; (d) tapered key; (e) tapered key with Gib head, or Gib-head key. The Gib head assists in key removal; (f) round key; (g) profile key; (h) Woodruff key with illustration of mounting; (i) pin, which is often grooved. The pin is slightly larger than the hole so that friction holds the pin in place; (j) roll pin. Elastic deformation of the pin in the smaller hole leads to friction forces that keep the pin in place.

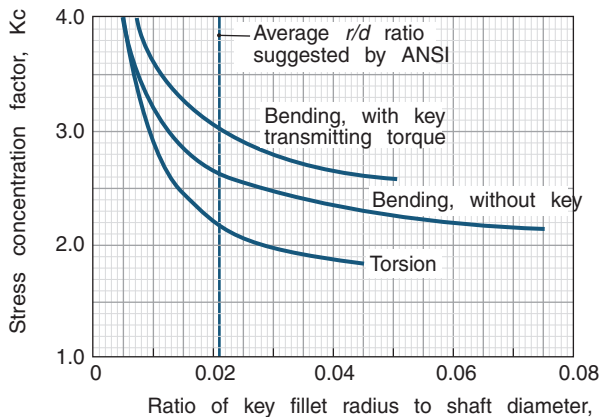


Figure 11.10: Stress concentrations for a standard profile key, where  $w = h = d/4$  (see Fig. 11.9g).

Therefore, the torque that results in excessive bearing stress is:

$$T = \frac{S_y d l h}{4 n_s} \quad (11.66)$$

Not surprisingly, Eq. (11.66) is independent of the width,  $w$ .

### Example 11.5: Key Design

**Given:** A 25-mm-diameter shaft and mating hub are both made of high-carbon steel. A standard Gib-head key made of AISI 1020 low-carbon steel with a yield strength of  $S_y = 295$  MPa is to be selected for this application, using  $n_s = 2.0$ .

**Find:**

- The required key length to transmit 500 Nm.
- The torque that can be transmitted without plastic deformation by a 25-mm-long key.
- The torque that can be transmitted by a Woodruff key without shearing.

**Solution:** From Table 11.3, the dimensions of a Gib-head key for use with a 25-mm diameter shaft are  $w = 6$  mm and  $h = 6$  mm.

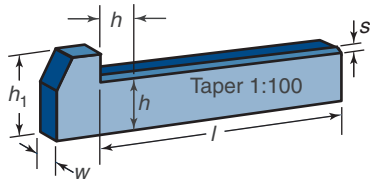
- Considering shearing of the key, Eq. (11.64) can be solved for the length to yield:

$$l = \frac{4 T n_s}{S_y w d} = \frac{4(500)(2)}{(295 \times 10^6)(0.025)(0.006)} = 0.090 \text{ m}$$

Similarly, for bearing stress, Eq. (11.66) gives



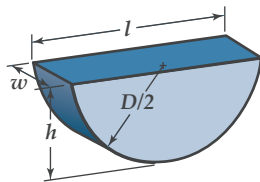
Table 11.3: Dimensions of plain and Gib-head taper stock keys.



Shaft diameter $d$ , mm	Key width $w$ , mm	Key thickness $h$ , mm	Available lengths <sup>a</sup> $l$ , mm	Chamfer $s$ , mm	Gib height $h_1$ , mm
10-12	4	4	8-45	0.16-0.25	7
12-17	5	5	10-56	0.25-0.40	8
22-30	6	6	14-70	0.25-0.40	10
30-38	8	7	18-90	0.25-0.40	11
38-44	10	8	22-110	0.40-0.60	12
44-50	12	8	28-140	0.40-0.60	12
50-58	14	9	36-160	0.40-0.60	14
58-65	16	10	45-180	0.40-0.60	16
65-75	18	11	50-200	0.40-0.60	18
75-85	20	12	56-220	0.60-0.80	20
85-95	22	14	63-250	0.60-0.80	22
95-110	25	14	70-280	0.60-0.80	22

<sup>a</sup> Standard lengths are 6, 8, 10, 12, 14, 16, 18, 20, 22, 25, 28, 32, 36, 40, 45, 50, 56, 63, 70, 80, 90, 100, 110, 125, 140, 160, 180, 200, 220, 250, 280.

Table 11.4: Dimensions of selected Woodruff keys.



Shaft diameter <sup>a</sup> $d$ , mm	Shaft diameter <sup>b</sup> $d$ , mm	Width $w$ , mm	Height $h$ , mm	Length $l$ , mm	Diameter $D$ , mm
4-6	—	1.5	2.6	6.75	7
6-8	10-12	2	2.6	6.75	7
		2	3.7	9.66	10
8-10	12-17	2	5	12.6	13
		2.5	3.7	9.66	10
		3	3.7	9.66	10
		3	5	12.65	13
10-12	17-22	3	7.5	18.57	19
		4	5	12.65	13
		4	6.5	15.72	16
12-17	22-30	4	9	21.63	22
		5	6.5	15.72	16
		5	7.5	18.75	19
17-22	—	6	7.5	18.75	19
		6	9	21.63	22
		6	10	24.49	25
—	30-38	6	11	27.35	28
22-30	—	8	9	21.63	22
	38+	8	11	27.35	28
30-38	—	10	11	27.35	28
	38+	10	13	31.43	32

<sup>a</sup> For torque transmission.

<sup>b</sup> For positioning only, torque must be transmitted through other means.

$$l = \frac{4Tn_s}{S_y d h} = \frac{4(500)(2)}{(295 \times 10^6)(0.025)(0.006)} = 0.090 \text{ m}$$

Table 11.3 shows that a 90-mm-long key is a standard size; however, this may be marginal and a 100-mm-long key may be necessary.

- (b) For a key with a length of 25 mm, the torque is given by Eq. (11.64) as

$$T = \frac{(295 \times 10^6)(0.006)(0.025)(0.025)}{4(2)} = 138 \text{ Nm}$$

- (c) For a Woodruff key, Table 11.4 suggests that a key with  $w = 8 \text{ mm}$  and  $h = 9 \text{ mm}$  be used; this key has a length of  $l = 21.63 \text{ mm}$  so that the shear area is approximately  $A = lw = (0.02163)(0.008) = 1.730 \times 10^{-4} \text{ m}^2$ . Therefore, from Eq. (11.64),

$$T = \frac{S_y A_s d}{4n_s} = \frac{(295 \times 10^6)(1.730 \times 10^{-4})(0.025)}{4(2)}$$

$$\text{or } T = 159 \text{ Nm.}$$

**Splines** are toothed sections that mate in a conformal toothed hub. While, in theory, almost any non-circular shape can serve as a spline when mated in a hub, spline profiles are standardized by the International Standards Organization, and are either *parallel-sided* or *involute*. Parallel-sided splines (Fig. 11.11) have a square cross-section with 4, 6, 10, or 16 teeth, and can be thought of as an arrangement of multiple keys. Involute splines use a geometry similar to gears, except that the pressure angle is  $30^\circ$  and the depth of the tooth is generally one-half that of an involute gear tooth (see Section 14.3). Involute splines are stronger than parallel-sided splines because stress concentrations are lower and better surface quality can be achieved in manufacturing. These splines have 6 to 50 teeth, and can utilize a flat root or fillet root profile (see Fig. 11.12). Splines are manufactured using similar approaches as for spur gears (see Section 14.8), although internal splines are commonly machined onto a hub

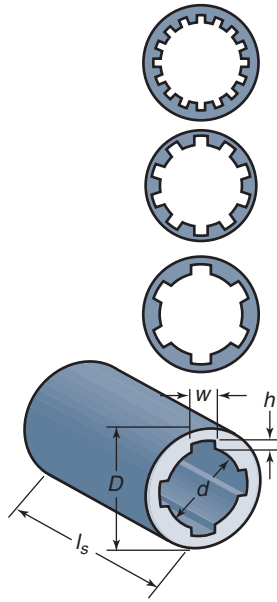


Figure 11.11: Standard parallel-sided splines hubs, showing (from top down) 16, 10, 6, and 4 teeth.

by broaching, wherein a constant or slightly tapered cross section is produced by a series of progressively larger cutters. Note that splines allow for axial motion of the hub on the shaft, which is beneficial for disassembly, but may require a retaining ring (Section 11.7) or similar device to secure the hub during operation.

Splines are produced directly from the shaft material, not from a softer metal as with a keyway, and so splines should be recognized as being suitable for transfer of large torques. The shear area of a spline is

$$A_s = \frac{\pi d_m l_s}{2}, \quad (11.67)$$

where  $d_m = (d_o + d)/2$  is the mean diameter of the spline,  $d$  is the root diameter (see Fig. 11.12), and  $l_s$  is the spline width. The Society of Automotive Engineers (SAE) recommends a spline width of

$$l_s = \frac{d^3 \left(1 - \frac{d_i}{d^4}\right)}{d_m^2}, \quad (11.68)$$

where  $d_i$  is the inner diameter in the case of a tubular shaft ( $d_i = 0$  for a solid shaft). SAE further notes that only around one-fourth of the shear area is stressed because of the unavoidable presence of manufacturing tolerances and/or bending loads. Therefore, the torque that can be withstood by a spline based on shear is given by

$$T = \tau_{\text{all}} \frac{d_m}{2} \left(\frac{A_s}{4}\right) = \tau_{\text{all}} \left(\frac{d_m}{2}\right) \left(\pi \frac{d_m}{2} \frac{l_s}{4}\right) = \frac{\pi \tau_{\text{all}} d_m^2 l_s}{16}, \quad (11.69)$$

where  $l_s$  is given by Eq. (11.68).

In addition to shearing, failure due to bearing stress is also a possibility, especially for parallel-sided splines. According to SAE, the torque that can be applied before bearing failure is

$$T = \frac{p n h d_m l_s}{8}, \quad (11.70)$$

Table 11.5: Holding force generated by set screws. Source: After Oberg et al. [2000].

Screw diameter, mm	Holding force, N
6.25	444
9.375	1110
12.5	2220
18.75	5780
25.0	11,100

where  $p$  is the allowable bearing pressure,  $n$  is the number of teeth,  $h$  is the tooth depth (see Fig. 11.12),  $d_m$  is the mean diameter, and  $l_s$  is given by Eq. (11.68). Note that the Eq. (11.70) also incorporates the SAE finding that essentially one-fourth of the contact length transfers the torque.

**Set screws** are threaded fasteners that are driven radially through a threaded hole in the hub. The point (which can be of a number of different geometries or materials) bears against the shaft, and torque is transmitted by frictional resistance of the set screw against the shaft and the shaft against the hub. It should be noted that set screws can only develop moderate forces, as summarized in Table 11.5. Alternatively, the holding force of a set screw can be approximated as

$$P_t = 2500 d_s^{2.31}, \quad (11.71)$$

where  $P_t$  is in pounds and  $d_s$  is the set screw diameter in inches. A suitable set screw diameter as a function of shaft diameter,  $d$ , is approximated by the empirical relationship:

$$d_s = \frac{d}{8} + \frac{5}{16}, \quad (11.72)$$

where  $d$  and  $d_s$  are in inches.

## 11.7 Retaining Rings and Pins

Keyways, set screws, and splines are used in situations where a torque needs to be transferred between a machine element and the shaft on which it is mounted. Some machine elements, such as rolling element bearings, compression rollers, or idler wheels need to be located on a shaft but do not need to transfer a torque. If axial (thrust) loads are limited, **retaining rings** are an economical and viable approach for locating such machine elements on shafts. Retaining rings, such as those shown in Fig. 11.13, are available in a wide variety of sizes and shapes.

Retaining rings are assembled onto a shaft by expanding or reducing their diameter depending on whether they will be located on an inner or outer groove. This is usually accomplished through the use of a special hand tool, although some retaining rings are snapped in place on a groove or use a spring-loaded fit that relies on friction (so-called *push-on* designs, since they may be located without the use of tools). Recall that a retaining ring groove, if required, causes a stress concentration, as shown in Fig. 6.7.

Table 11.6 summarizes properties of selected retaining rings. It should be noted that Table 11.6 is highly abstracted; there are many more types and sizes of these rings, and forces in excess of 100 kN can be developed. A retaining ring can fail due to shear or bearing failure of the shaft groove. The holding force that can be generated by shear of the ring is given by

$$P_t = \frac{\pi C_t d_t h S_{sy}}{n_s}, \quad (11.73)$$

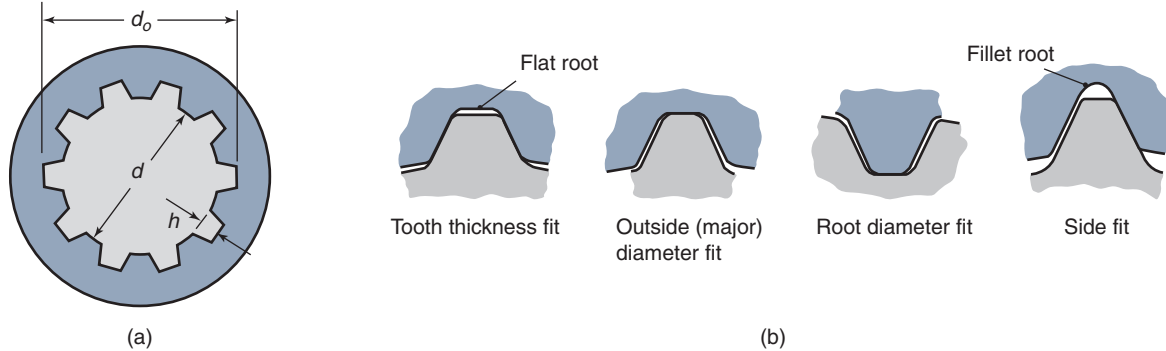


Figure 11.12: Involute splines. (a) Side view of a 10-toothed spline and hub; (b) types of fit between spline and hub.

while the holding force that can be withstood before bearing failure of the shaft groove is

$$P_t = \frac{\pi C_t d t_g S_{ut}}{n_s}, \quad (11.74)$$

where

$C_t$  = ring correction factor, as given in Table 11.6

$d$  = shaft diameter

$t_h$  = retaining ring thickness

$t_g$  = groove depth

$S_{sy}$  = shear strength of ring material

$S_{ut}$  = tensile strength of shaft material

$n_s$  = safety factor

There are a number of additional factors that can affect holding force of retaining rings, including:

- Chamfers and radii are commonly used on exterior shaft corners or grooves, in order to assist manufacture, assembly, and provide for proper seating. However, such design features can change the loading state of a retaining ring from pure shear to bending, and can significantly reduce the holding force.
- Impact loads and vibration can significantly reduce the holding force of some retaining rings. It should be noted that if there is clearance between the retaining ring and the part, then vibration often results in repeated impact.
- If the machine element is allowed to rotate, friction can lead to unseating of the retaining ring.

**Cotter pins** are also used to secure items onto a shaft, but develop much lower forces than carbon steel retaining rings. Cotter pins are metal fasteners with two prongs that are inserted through a hole; the prongs are then bent (plastically deformed) to secure them and hold a part in place. Alternatively, some cotter pins have geometric features that serve to anchor them. Cotter pins are available in a wide variety of materials and geometry, some of which are illustrated in Fig. 11.14.

## 11.8 Flywheels

Large variations in angular acceleration can cause large oscillations in torque, and vice-versa. For example, consider a mechanical power press that is used to produce coins from disk-shaped workpieces. The force exerted by the press is very low until the punch contacts the workpiece, and then the

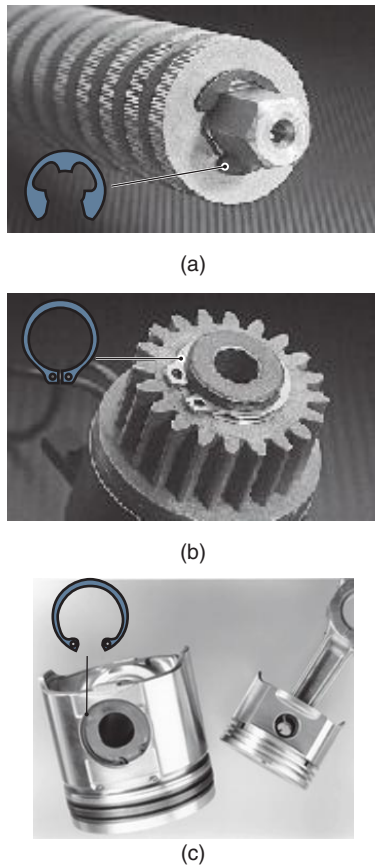









Figure 11.13: Examples of retaining rings. (a) An ME type snap ring, used to hold a series of cutters in place on a paper shredder shaft; (b) a general purpose MSH ring for locating a spur gear; (c) an internal retaining ring for securing a main piston bearing sleeve. *Source:* Courtesy of Rotor Clip Company, Inc.

Table 11.6: Properties of selected internal and external retaining rings. Ring nomenclature is manufacturer-specific; equivalent designs have other designations depending on supplier. *Source:* Courtesy of Rotor Clip Company, Inc.

Type	$C_t^a$	Shaft or hub diameter, mm	Groove diameter, mm	Ring width, mm	Notes
External rings					
 MSH	1.00	5	4.75	0.50	General purpose shoulder ring. Axial assembly required. Can accommodate up to 254.0-mm shaft diameter.
		15	14.15	1.00	
		25	23.50	1.20	
		50	47.20	1.75	
		75	71.20	2.55	
 ME	0.33	1	0.72	0.32	Popular snap-in-place retaining ring. Allows radial assembly. Can accommodate up to 34.9-mm shafts.
		5	3.90	0.70	
		10	8.00	1.00	
		20	16.00	1.40	
		25	20.00	1.40	
 MCR	1.30	12	11.34	1.00	Spiral shaft ring. Available up to 280-mm shaft diameter. Suitable for higher holding forces.
		25	23.88	1.17	
		50	47.70	1.73	
		75	71.54	2.62	
		100	95.40	3.05	
 LC	0.75	12.7	11.79	0.991	Two piece interlocking design, dynamically balanced when assembled. Suitable for high speeds. Allows radial assembly.
		25.4	22.15	1.422	
		50.8	46.43	2.184	
		76.2	70.97	2.616	
 DTX	—	5	4.90	0.40	Self-locking push-on type. Suitable only for small loads (< 300 N). Axial assembly required.
		10	9.85	0.6	
		20	19.75	1.0	
		25	24.75	1.0	
		45	44.75	1.5	
Internal rings					
 MHO	1.2	8	8.40	0.50	General purpose housing ring. Axial assembly required. Can accommodate up to 254.0-mm shaft diameter.
		12	12.65	0.70	
		25	26.60	1.20	
		50	53.10	1.75	
		75	79.70	2.55	
 DTI	—	8	8.10	0.40	Self-locking push-on type. For small loads only (< 200 N). Axial assembly required.
		15	15.10	0.5	
		25	25.20	1.0	
		35	35.20	1.0	
		50	50.20	1.0	

<sup>a</sup> See Eqs. (11.73) and (11.74).

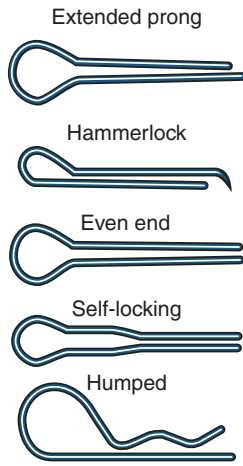


Figure 11.14: Illustration of common cotter pins. Cotter pins are often plastically deformed after insertion into a through-hole. An exception is the humped design, where the prong is inserted into a hole and the “hump” clips onto the round shaft. The hammerlock design is intended for use with castle nuts (see Table 16.3).

force becomes very high. After the coin is formed, perhaps in less than 1 mm of travel, the punch returns to the top dead center position. In such a circumstance, the peak torque can be used to select a motor, but this would be overly large and uneconomical. Clearly, the average torque over the cycle is much lower than the peak torque, a circumstance that is usually the case. To smooth out the velocity changes, and reduce the size of the motor needed, a **flywheel** is often attached to a shaft. The use of a flywheel will allow the following to occur:

1. Reduced amplitude of speed fluctuation
2. Reduced maximum torque required
3. Energy stored and released when needed during a cycle

A flywheel with driving (mean) torque  $T_m$  and load torque  $T_l$  is shown in Fig. 11.15. The flywheel in this figure is a flat circular disk, but it can also be a large gear. A motor supplies a torque  $T_m$ , which for design purposes should be as constant as possible. The load torque  $T_l$ , for such applications as crushing machinery, punch presses, and machine tools, varies considerably.

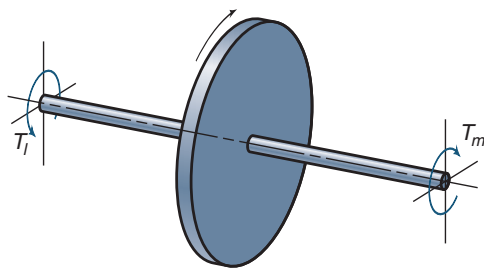


Figure 11.15: Flywheel with driving (mean) torque  $T_m$  and load torque  $T_l$ .

## 11.8.1 Dynamics

The kinetic energy in a rotating system like that shown in Fig. 11.15 is

$$K_e = \frac{I_m \omega^2}{2}, \quad (11.75)$$

where  $I_m$  is the mass moment of inertia and  $\omega$  is the angular velocity. The mass moments of inertia for six solids are given in Table 4.2, and mass moment of inertia is discussed in Section 4.2.6. From Newton's second law of motion as applied to the flywheel shown in Fig. 11.15,

$$-T_l + T_m = I_m \frac{d\omega}{dt}. \quad (11.76)$$

The design motor torque should be equivalent to the average torque, or  $T_m = T_{avg}$ . But

$$\frac{d\omega}{dt} = \frac{d\omega}{dt} \frac{d\theta}{d\theta} = \frac{d\theta}{dt} \frac{d\omega}{d\theta} = \omega \frac{d\omega}{d\theta}. \quad (11.77)$$

Substituting Eq. (11.77) into Eq. (11.76) gives

$$\begin{aligned} -T_l + T_{avg} &= I_m \omega \frac{d\omega}{d\theta}, \\ -(T_l - T_{avg}) d\theta &= I_m \omega d\omega. \end{aligned} \quad (11.78)$$

This equation can be written in terms of a definite integral as

$$-\int_{\theta_{\omega_{\min}}}^{\theta_{\omega_{\max}}} (T_l - T_{avg}) d\theta = \int_{\omega_{\min}}^{\omega_{\max}} I_m \omega d\omega$$

or

$$-\int_{\theta_{\omega_{\min}}}^{\theta_{\omega_{\max}}} (T_l - T_{avg}) d\theta = \frac{I_m}{2} (\omega_{\max}^2 - \omega_{\min}^2). \quad (11.79)$$

The left side of Eq. (11.79) represents the change in kinetic energy between the maximum and minimum shaft speeds and is equal to the area under the torque-angle diagram between the extreme values of speed. The far right side of Eq. (11.79) describes the change in energy stored in the flywheel. The only way to extract energy from the flywheel is to slow it down; adding energy will speed it up. Often it is a design constraint to achieve a desired speed variation ( $\omega_{\max} - \omega_{\min}$ ), which can be accomplished by providing a flywheel with a sufficiently large mass moment of inertia,  $I_m$ .

The location of minimum angular speed,  $\theta_{\omega_{\min}}$ , within a cycle of operation occurs after the maximum positive energy has been delivered from the motor. The location of maximum angular speed  $\theta_{\omega_{\max}}$  within a cycle of operation occurs after the maximum negative energy has been returned to the load, the point where the ratio of the energy summation to the area in the torque pulse is the largest negative value.

## 11.8.2 Flywheel Sizing

The size of a flywheel required to absorb the energy with an acceptable change in speed is a common design goal. The change in shaft speed during a cycle of operation is called the **fluctuation speed**,  $\omega_f$ , and is expressed as

$$\omega_f = \omega_{\max} - \omega_{\min}.$$

The **coefficient of fluctuation** is defined as

$$C_f = \frac{\omega_{\max} - \omega_{\min}}{\omega_{avg}} = \frac{2(\omega_{\max} - \omega_{\min})}{\omega_{\max} + \omega_{\min}}. \quad (11.80)$$



Table 11.7: Coefficient of fluctuation for various types of equipment.

Type of equipment	Coefficient of fluctuation, $C_f$
Crushing machinery	0.200
Electrical machinery	0.003
Electrical machinery, direct driven	0.002
Engines with belt transmissions	0.030
Flour milling machinery	0.020
Gear wheel transmission	0.020
Hammering machinery	0.200
Machine tools	0.030
Paper-making machinery	0.025
Pumping machinery	0.030-0.050
Shearing machinery	0.030-0.050
Spinning machinery	0.010-0.020
Textile machinery	0.025

Table 11.7 gives typical coefficients of fluctuation,  $C_f$ , for various types of equipment. Small values of  $C_f$  require relatively large flywheels. A larger flywheel will add more cost and weight to the system, factors that have to be considered along with the smoothness of the operation desired.

The far right side of Eq. (11.79) describes the kinetic energy fluctuation of the flywheel and can be rewritten as

$$K_e = \frac{I_m}{2} (\omega_{\max} + \omega_{\min}) (\omega_{\max} - \omega_{\min}). \quad (11.81)$$

Substituting Eq. (11.80) into Eq. (11.81) yields

$$K_e = I_m \omega_{\text{avg}}^2 C_f, \quad (11.82)$$

$$I_m = \frac{K_e}{C_f \omega_{\text{avg}}^2}. \quad (11.83)$$

Given the desired coefficient of fluctuation for a specific application, obtaining the change in kinetic energy,  $K_e$ , from the integration of the torque curve, and knowing the average angular velocity, the required mass moment of inertia,  $I_m$ , can be determined. By knowing  $I_m$ , the dimensions (i.e., the thickness and diameter) of the flywheel can be determined.

The most efficient flywheel design is obtained by maximizing  $I_m$  for the minimum volume of flywheel material used. Ideally, this design would take the shape of a ring supported by a thin disk, but thin cross-sections can be difficult to manufacture. Efficient flywheels have their masses concentrated at the largest radius (or in the rim) and their hubs supported on spokes, like bicycle wheels. This configuration places the greatest part of the mass at the largest radius possible and minimizes the weight for a given mass moment of inertia while making manufacturing problems tractable.

### Design Procedure 11.3: Flywheels

Flywheels are used to provide for smooth operation when the applied loading is not smooth. The design procedure for sizing a flywheel is as follows:

1. Select a material for the flywheel. Table 11.8 summarizes some common materials used for flywheels.
2. Select a coefficient of fluctuation,  $C_f$ , either from Table 11.7 or from design requirements.
3. Either from design constraints or analysis of the application, the load as a function of time needs to be determined. It is then useful to plot the load torque,  $T_l$ , versus position,  $\theta$ , for one cycle.

4. Determine the average load,  $T_{l,\text{avg}}$ , over one cycle.
5. Find the locations  $\theta_{\omega_{\max}}$  and  $\theta_{\omega_{\min}}$ . Often this is the most difficult task, and may require consideration of multiple intervals. The maximum velocity occurs after the interval where the energy contribution to the system is a maximum. Thus, the goal is to find the maximum value of the following expression over any interval in the load cycle:

$$\int_{\theta_{\omega_{\min}}}^{\theta_{\omega_{\max}}} (T_{\text{avg}} - T_l) d\theta.$$

6. Determine kinetic energy by integrating the torque curve as in Eq. (11.79).
7. Determine  $\omega_{\text{avg}}$  from Eq. (11.80).
8. Determine  $I_m$  from Eq. (11.83).
9. Find the dimensions of the flywheel. Table 4.2 provides useful expressions for  $I_m$  for common shapes.

### Example 11.6: Flywheel Design

**Given:** The output, or load torque, of a flywheel used in a punch press for each revolution of the shaft is 12 N-m from zero to  $\pi$  and from  $3\pi/2$  to  $2\pi$  and 144 N-m from  $\pi$  to  $3\pi/2$ . The coefficient of fluctuation is 0.05 about an average speed of 600 rpm. Assume that the flywheel's solid disk is made of low-carbon steel of constant 25 mm thickness.

**Find:** Determine the following:

- (a) The average load or output torque
- (b) The locations  $\theta_{\omega_{\max}}$  and  $\theta_{\omega_{\min}}$
- (c) The energy fluctuation required
- (d) The outside diameter of the flywheel

**Solution:**

- (a) By using the load or output torque variation for one cycle from Fig. 11.16, the average load torque is

$$2\pi T_{l,\text{avg}} = \pi(12) + \frac{\pi}{2}(144) + \frac{\pi}{2}(12);$$

$$T_{l,\text{avg}} = 6 + 36 + 3 = 45 \text{ N-m.}$$

- (b) From Fig. 11.16,

$$\theta_{\omega_{\max}} = \pi \quad \text{and} \quad \theta_{\omega_{\min}} = \frac{3\pi}{2}.$$

- (c) From the left side of Eq. (11.79), the kinetic energy for one cycle is

$$\begin{aligned} K_e &= - \int_{\theta_{\omega_{\min}}}^{\theta_{\omega_{\max}}} (T_l - T_{\text{avg}}) d\theta \\ &= (144 - 45) \frac{\pi}{2} \\ &= 155.5 \text{ N-m.} \end{aligned}$$

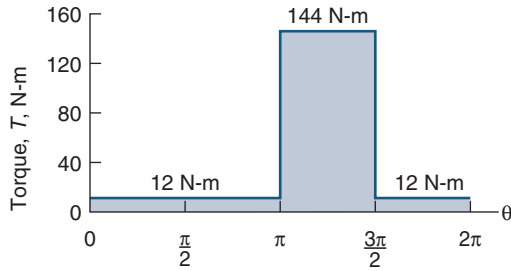


Figure 11.16: Load or output torque variation for one cycle used in Example 11.6.

(d) The average angular speed can be expressed as

$$\omega_{\text{avg}} = 600 \frac{\text{rev}}{\text{min}} \left( \frac{1 \text{ min}}{60 \text{ s}} \right) \left( \frac{2\pi}{1 \text{ rev}} \right) = 62.83 \text{ rad/s.}$$

From Eq. (11.83), the mass moment of inertia is

$$I_m = \frac{K_e}{C_f \omega_{\text{avg}}^2} = \frac{155.5}{(0.05)(62.83)^2} = 0.7879 \text{ kg-m}^2. \quad (a)$$

From Table 4.2 (also given on the inside back cover) the mass moment of inertia for a solid round disk is

$$I_m = \frac{m_a d^2}{8} = \frac{\pi d^2 t_h \rho}{4} \left( \frac{d^2}{8} \right) = \frac{\pi}{32} \rho t_h d^4.$$

From Table 3.1,  $\rho = 7860 \text{ kg/m}^3$  for low-carbon steel. Therefore,

$$I_m = \frac{\pi}{32} (7860)(0.025)d^4 = 19.29d^4. \quad (b)$$

Equating Eqs. (a) and (b) gives

$$d^4 = \frac{0.7879}{19.29} = 0.0408 \text{ m}^4,$$

which is solved as  $d = 0.4495 \text{ m}$ , or around 450 mm.

### 11.8.3 Stresses

The stresses in a flywheel are the sum of the rotational effects and the stresses associated with internal pressurization. Concepts introduced in Chapter 10 will be used here, in particular Section 10.4 for rotational effects and Section 10.3.2 for internal pressurization due to a press or shrink fit. The flywheel is assumed to be a disk with a central hole and constant thickness. The stresses in the flywheel due to rotational and press-fit effects can be written as

$$\sigma_\theta = \sigma_{\theta\omega} + \sigma_{\theta p}, \quad (11.84)$$

$$\sigma_r = \sigma_{r\omega} + \sigma_{rp}. \quad (11.85)$$

Making use of Eqs. (10.35) and (10.36) and Eqs. (10.23) and (10.24), respectively, and taking care to use consistent nomenclature, gives the tangential (hoop) and radial stresses

as

$$\sigma_\theta = \frac{3+\nu}{8} \rho \omega^2 \left( r_i^2 + r_o^2 + \frac{r_i^2 r_o^2}{r^2} - \frac{1+3\nu}{3+\nu} r^2 \right) + \frac{p_f r_f^2 \left( 1 + \frac{r_o^2}{r^2} \right)}{r_o^2 - r_f^2}, \quad (11.86)$$

$$\sigma_r = \frac{3+\nu}{8} \rho \omega^2 \left( r_i^2 + r_o^2 - \frac{r_i^2 r_o^2}{r^2} - r^2 \right) + \frac{p_f r_f^2 \left( 1 - \frac{r_o^2}{r^2} \right)}{r_o^2 - r_f^2}. \quad (11.87)$$

If the shaft is solid, then the stress at the inner flywheel radius simplifies to

$$\sigma_\theta = \frac{3+\nu}{8} \rho \omega^2 \left( r_o^2 - \frac{1+3\nu}{3+\nu} r_f^2 \right) + \frac{p_f (r_f^2 + r_o^2)}{r_o^2 - r_f^2}, \quad (11.88)$$

$$\sigma_r = \frac{3+\nu}{8} \rho \omega^2 (r_o^2 - r_f^2) - p_f. \quad (11.89)$$

Note that  $\sigma_\theta$  and  $\sigma_r$  are principal stresses since there is no shear stress associated with them. Usually,  $\sigma_\theta$  is larger than  $\sigma_r$ , implying that the maximum principal stress equals the tangential (hoop) stress ( $\sigma_1 = \sigma_\theta$ ). Also, the circumferential stress is largest at  $r = r_i$  for the flywheel. Thus, for brittle materials the design of the flywheel should be such that

$$\sigma_1 < S_u/n_s. \quad (11.90)$$

For ductile materials, a multiaxial failure theory, such as the DET, should be used. If  $\sigma_1 = \sigma_\theta$ ,  $\sigma_2 = \sigma_r$ , and  $\sigma_z = 0$ , from Eq. (6.12),

$$\sigma_e = \sqrt{\sigma_\theta^2 + \sigma_r^2 - \sigma_\theta \sigma_r}.$$

From Eq. (6.11), the DET predicts failure if

$$\sigma_e \geq \frac{S_y}{n_s}.$$

### Example 11.7: Flywheel Stresses

**Given:** A flywheel made of low-carbon steel has an outside radius of 150 mm and an inside radius of 25 mm. The flywheel is to be assembled (press fit) onto a shaft. The radial interference between the flywheel and shaft is 50  $\mu\text{m}$ , and the shaft will operate at a speed of 5000 rpm.

**Find:** Determine the following:

- The circumferential and radial stresses on the flywheel inner radius.
- The speed at which the flywheel will break loose from the shaft.

**Solution:**

- For steel, Table 3.1 gives  $E = 207 \text{ GPa}$ ,  $\nu = 0.3$ , and  $\rho = 7860 \text{ kg/m}^3$ . Solving Eq. (10.53) for the interference pressure yields

$$\begin{aligned} p_f &= \frac{\delta_r E (r_o^2 - r_i^2)}{2r_f r_o^2} \\ &= \frac{(50 \times 10^{-6}) (207 \times 10^9) (0.150^2 - 0.025^2)}{2(0.025) (0.150^2)} \\ &= 201.2 \text{ MPa.} \end{aligned}$$

Table 11.8: Materials for flywheels.

Material	Performance index, $M_f$ kJ/kg	Comment
Ceramics	200–2000 (compression only)	Brittle and weak in tension. Use is usually discouraged.
Reinforced polymers: Ceramic fiber Graphite fiber	200–500 100–400	The best performance; a good choice. Almost as good as CFRP and cheaper; an excellent choice.
Beryllium	300	Good but expensive, difficult to work, and toxic.
High-strength steel High-strength aluminum alloys High-strength magnesium alloys Titanium alloys	100–200 100–200 100–200 100–200	All about equal in performance; steel and Al-alloys less expensive than Mg and Ti alloys.
Lead alloys Cast iron	3 8–10	High density makes these a good (and traditional) selection when performance is velocity limited, not strength limited.

Note that  $\omega = 5000 \text{ rpm} = 523.6 \text{ rad/s}$ . For this case, the flywheel and shaft are both the same material, and the shaft is solid, so that the circumferential stress can be obtained from Eq. (11.88) as

$$\sigma_\theta = \left[ \frac{3 + 0.3}{8} (7860) (523.6)^2 \right] \times \left[ 0.15^2 - \frac{1 + 3(0.3)}{3 + 0.3} (0.025)^2 \right] + \frac{(201.2 \times 10^6) (0.15^2 + 0.025^2)}{0.15^2 - 0.025^2},$$

or  $\sigma_\theta = 233 \text{ MPa}$ . Similarly, the radial stress is obtained from Eq. (11.89) as

$$\sigma_r = \frac{3 + 0.3}{8} (7860) (523.6)^2 (0.15^2 - 0.025^2) - 201.2 \times 10^6.$$

or  $\sigma_r = -181.8 \text{ MPa}$ . The negative stress indicates that  $\sigma_r$  is compressive at the speed of 5000 rpm.

- (b) The flywheel breaks free when the radial stress at the inner radius is reduced to zero at an elevated speed. From Eq. (11.89),

$$\sigma_r = 0 = \frac{3 + 0.3}{8} (7860) \omega^2 (0.15^2 - 0.025^2) - 201.2 \times 10^6.$$

Solving for the angular velocity yields  $\omega = 1684 \text{ rad/s} = 16,080 \text{ rpm}$ . Thus, if the shaft speed exceeded this value, the flywheel would not be held onto the shaft. Note that the ability of the flywheel to transmit a torque would be compromised at far lower speeds, as suggested by Eq. (10.55).

### 11.8.4 Flywheel Materials

The main purpose of a flywheel is to store energy and then use it efficiently. Small flywheels, the type found in small appliances, are often made of lead, but steel and iron are preferred for health reasons. These flywheels operate at relatively low speeds so that a high density is the sole physical property that justifies these materials. Recently, flywheels

have been proposed for vehicle power storage and regenerative braking systems; high-strength steels and composites are of interest for these vehicular flywheels because they are more efficient at high speeds. Thus, a great diversity of materials is being used for flywheels. The obvious question is: What material is best suited for demanding high-speed flywheel applications?

Recall from Eqs. (11.86) and (11.87) that the speed effect is more significant than the pressurization effect. Thus, the maximum stress in a flywheel is

$$\sigma_{\max} = \left( \frac{3 + \nu}{8} \right) \rho \omega^2 f(r). \quad (11.91)$$

From Eq. (11.75), the kinetic energy is

$$K_e = \frac{1}{2} I_m \omega^2. \quad (11.92)$$

The mass moment of inertia,  $I_m$ , from Table 4.2 can be represented as

$$I_m = m_a g(r), \quad (11.93)$$

so that

$$K_e = \frac{1}{2} m_a g(r) \omega^2. \quad (11.94)$$

Assume that  $f(r)\omega^2 \approx g(r)\omega^2$ . From Eqs. (11.94) and (11.91)

$$\frac{K_e}{m_a} \propto \frac{\sigma_{\max}}{\rho}.$$

Thus, the best materials for a flywheel, namely those that store the most energy per mass, are those with high values of the performance index given by

$$M_f = \frac{\sigma_{\max}}{\rho}. \quad (11.95)$$

Note that the units for  $M_f$  are joules per kilogram (J/kg). Also, recall that a joule (J) is 1 newton-meter (N-m).

Table 11.8 gives performance indices for various materials. From this table observe that the best materials are ceramics, beryllium, and composites. Lead and cast iron do not perform as efficiently. This seems counter intuitive, mainly because lead and cast iron are suitable for low-speed applications where optimum performance is not critical.

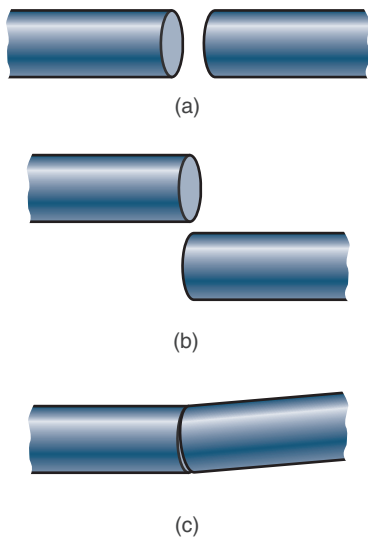


Figure 11.17: Types of shaft misalignment. (a) In-line; (b) parallel; (c) angular.

## 11.9 Couplings

**Couplings** are used to connect two shafts. This is a common need, for example, when connecting a motor to an input shaft, clutch, or transmission. If two shafts are aligned, then designing and installing a coupling is not difficult, and rigid couplings can be used. If there is some misalignment, either parallel, in-line, or angular (see Fig. 11.17), then the coupling needs to accommodate the misalignment and a *flexible coupling* may be required. Table 11.9 summarizes the most common types of couplings and their ability to accommodate misalignment, although it should be recognized that there are many variants within each classification.

Design of a coupling involves working closely with suppliers, and matching design requirements to coupling characteristics. Unless noted, the couplings discussed are available for a wide variety of torques and shaft sizes, and the design challenge is to match a coupling type with design constraints.

Whenever possible, shafts that need to be coupled should be arranged without misalignment of any form; this allows direct application of a rigid coupling. If misalignment is unavoidable, or if shock isolation is needed, Table 11.9 is a useful reference. In addition, it is not unusual to have high startup torques (compared to operating conditions). Fortunately, most electric motors have the largest torque available at zero speed. However, if this torque is insufficient to start motion, then compliant couplings may be an attractive alternative to the use of a speed reducer and its associated couplings.

### 11.9.1 Rigid Couplings

Examples of rigid couplings are shown in Fig. 11.18. Rigid couplings are commonly applied because of their low cost and high reliability. However, they do require close alignment and do not damp vibrations or provide electrical isolation between shafts. They have few size restrictions, although compression sleeve couplings have limited utility for large diameters; the mechanics of such couplings are discussed in Section 10.5. Rigid couplings have no backlash, making them useful for precision machines and servomechanisms. Their main downside is the inability to tolerate angular or paral-

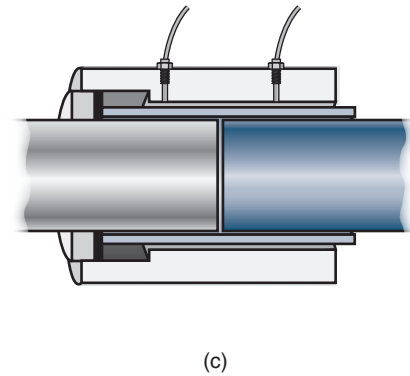
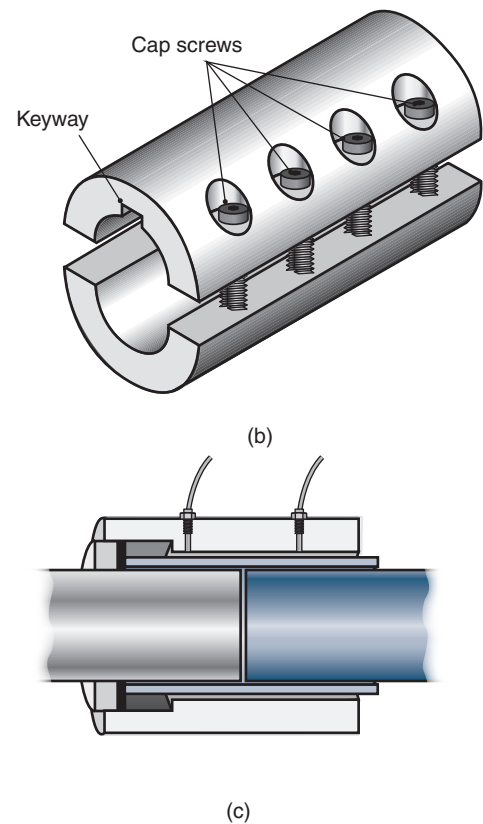
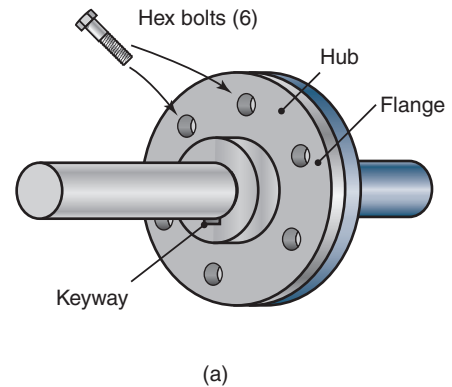


Figure 11.18: Types of rigid shaft couplings. (a) Flange coupling, consisting of a hub and flange and with a keyway for torque transmission; (b) two-piece sleeve couplings (one-piece designs are also available); (c) compression sleeve couplings, configured with hydraulic lines for installing the shaft; the hydraulic lines are not needed during the coupling's service life.

Table 11.9: General characteristics of shaft couplings.

Type	Misalignment tolerance <sup>a</sup>			Damping ability <sup>d</sup>	Notes
	In-line	Angular	Parallel		
<b>Rigid couplings</b>					
Flange	3	0	0	0	Useful when frequent uncoupling is required. Flanges must be installed in pairs and moved in pairs to maintain hole indexing. These couplings are usually keyed or splined to each shaft.
Sleeve	2	0	0	0	Similar to rigid flange coupling but easier to remove and install. Requires high-strength bolts and tight tolerances on sleeves and shafts.
Compression sleeve	2	0	0	0	Relies upon friction between shaft and coupling. Not practical for large diameter shafts or high torque applications.
<b>Flexible couplings</b>					
Elastomeric	1	1	0–2	4	Angular misalignment up to 3° and parallel misalignment up to 7.0 mm may be tolerated, depending on shaft diameter. Electrical isolation can be provided. Reduced torsional capacity compared to rigid coupling. Jaw designs can result in significant backlash.
Flexible metal	3	3	1	0–2	Can achieve higher torques for a given diameter and can withstand higher temperatures than elastomeric couplings.
Bellows	1	4	3	0	Lower capacity than rigid couplings, can be susceptible to fatigue failure. Tolerates moderate misalignment with no backlash.
Gear	4	2	0–2	0	Suitable for large torque applications. Parallel misalignment is tolerated only if space permits a pair of gear couplings with a spacer between them.
Helical	2	5	1	0	Suitable only for low torque applications, best able to accommodate angular misalignment.
Schmidt	0	0	5	1	Intended for parallel misalignment. Usually restricted to low power applications.
Universal	1	5	3–5	0	Popular rigid joint, ideal for high misalignment. Lubrication required, although can incorporate sealed bearings at higher cost.
Fluid	2	0	0	5	Intended for vibration and shock isolation. Can be provided with controlled filling to provide for soft start capability.

<sup>a</sup> 0 = none, 5 = high

lel misalignment, although limited in-line misalignment can be accounted for during assembly. Rigid couplings have essentially no energy loss, which can be a significant advantage compared to flexible couplings.

**Rigid flange couplings**, shown in Fig. 11.18a, consist of two hub and flange assemblies that are connected by bolts through the flanges. The hubs are keyed or splined (Section 11.6) onto their shafts. Special care must be taken with respect to the bolts on flange couplings. Details of bolt design are discussed in Ch. 16, but in general, it is important to make sure that the holes on the flanges are aligned carefully to ensure all of the bolts in the bolt circle are evenly loaded. This usually requires marking the holes to allow for proper realignment if the coupling is disassembled or moved to a new shaft. Tightening is usually performed in a set sequence of opposing bolts in order to ensure even load distribution.

**Sleeve couplings** (Fig. 11.18b) are also very popular, and can depend on a clamp or compression fit for assembly onto shafts. Some light to medium duty applications use keys for torque transmission and set screws to locate the sleeve. Clamp type designs can be one- or two-piece designs; the latter are especially useful for easy disassembly. **Compression sleeve couplings**, as shown in Fig. 11.18c, use the wedging action of a split conical section to provide a friction grip on the two shafts. Compression sleeve couplings accommodate higher torques, but require more expensive machining and have a larger diameter than equivalent capacity rigid

sleeve couplings. As with rigid flange couplings, bolts must be tightened carefully and in the correct order.

## 11.9.2 Flexible Couplings

Flexible couplings are needed to accommodate misalignment between shafts, and different designs are intended for the different types of misalignment that may occur. Flexible couplings are inherently more complex than rigid couplings, and therefore are invariably more expensive for a given shaft diameter or torque capability. However, flexible couplings often provide the additional benefit of damping vibrations and/or isolating the shafts electrically, as well as reducing shock loads. Some flexible couplings have significant backlash, however, which can be a concern for precision applications.

**Elastomeric couplings** transmit torque through a hard rubber component, and are able to accommodate some misalignment, but their main advantage is the adsorption of shock and vibration between two shafts. There are many types of elastomeric couplings, but common types are **jaw** and **flexible disk** couplings. A jaw coupling uses a rubber spacer, or *spider* between two jaws as shown in Fig. 11.19. The stiffness of the spider material can be tuned for specific applications and controlled backlash. Flexible disk couplings use a rubber or metal disc separating two flanges.



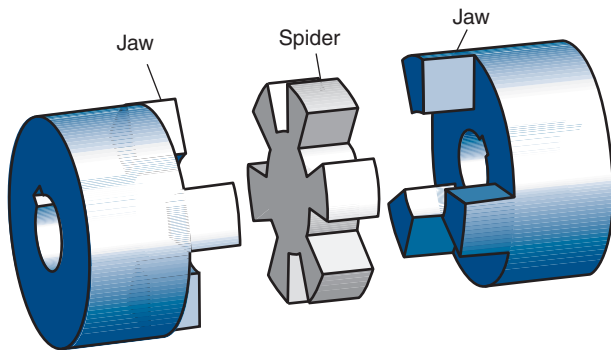


Figure 11.19: Schematic illustration of a jaw coupling.

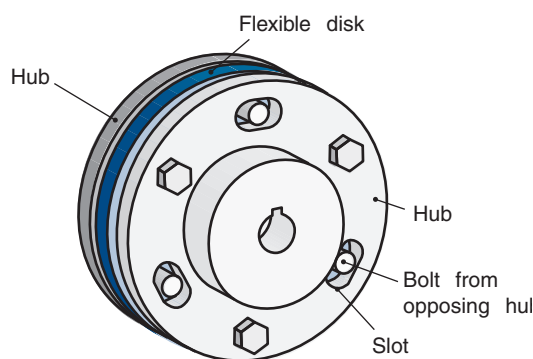


Figure 11.20: (a) An elastomeric disk coupling. Each hub is connected to the flexible disk with threaded fasteners that extend into slots on the opposing hub, allowing angular displacement between the hubs when a torque is applied. This reduces impact loads and increases damping.

The flexible disk coupling shown in Fig. 11.20 uses bolts to connect the flanges to the disk; in this case, alternating bolts connect each hub to the disk. That is, if six bolts are present in the disk, three connect it to each hub and are located in slots on the opposing side. This feature ensures that the coupling will still function (although its damping ability will be compromised) in the case of disk failure. Both jaw and flexible disk couplings are well-balanced and are suitable for high speed applications.

There are a number of **flexible metal coupling** designs, the simplest of which will be very similar to Fig. 11.20, but with a metal disk instead of a rubber one. Such couplings will be less compliant and not display the damping characteristics of elastomeric couplings, but are able to transmit much larger torques. A unique design of a flexible metal coupling is a **Falk coupling**, shown in Fig. 11.21. Falk couplings consist of a spring that is threaded through axial slots; the slots are tapered so that some deformation of the spring can occur. Under light loads, the slot grid bears near the outer edge of the hub teeth, providing for a long span, spring flexure and protection against shock. As the load increases, the distance between contact points on the hub teeth is shortened, although a span still exists.

High angular misalignment can be tolerated by **bellows** (Fig. 11.22) or **helical couplings** (Fig. 11.23). Their compliance does allow for limited in-line or parallel misalignment as well, and these couplings have no backlash. The main

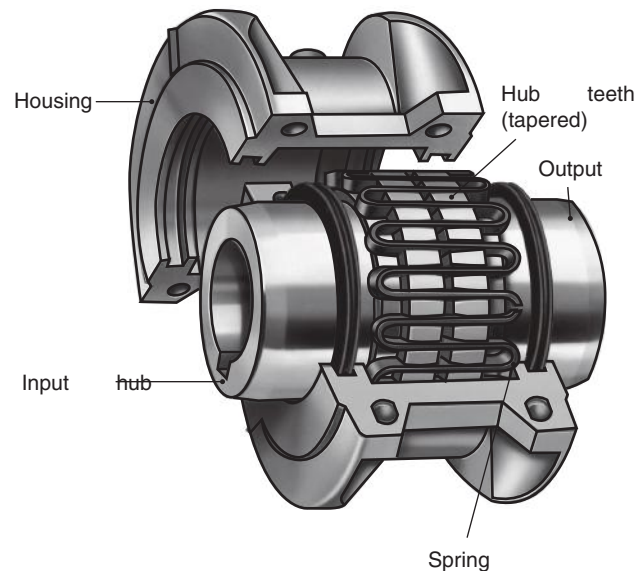


Figure 11.21: Schematic illustration of a Falk coupling, consisting of a metal spring threaded through a toothed hub. Source: Courtesy of Rexnord, Inc.

drawback is lower torque capacity than other couplings for a given shaft size. Bellows couplings are susceptible to fatigue failure.

When parallel misalignment occurs, **linkage** or **Schmidt couplings** can be used, as long as the shaft diameter is below 50 mm or so. Schmidt couplings, shown in Fig. 11.24, consist of three disks connected by six links. These links allow for very large parallel offsets, and some designs allow for limited angular and in-line misalignment as well. A unique feature of Schmidt couplings is that the parallel offset can be changed dynamically without removing and remounting the coupling. These couplings are useful for torque transmission at moderate speeds. The main disadvantage of these couplings is the need for proper lubrication, since the links are supported by journal or needle bearings.

**Universal couplings**, also known as *universal joints*, *U-joints*, or *Hooke couplings*, consist of two hinges that are axially oriented at  $90^\circ$  to each other, and connected by a cross shaft, as shown in Fig. 11.25. Universal joints allow for very high angular misalignment. They can also accommodate parallel misalignment if there is sufficient axial clearance. A peculiarity of universal joints is that if an input side has a uniform velocity, the output shaft will have a variable speed, which can result in excessive vibration and wear. A solution is to utilize two U-joints separated by a short spacer, so that the variations in speed are phased and a uniform output velocity can be achieved. This assembly, properly called a *double Cardan joint* or *CV joint*, is commonly employed in automotive drive axles.

**Fluid couplings**, as shown in Fig. 11.26, are intended for applications where significant shock loads exist, such as conveyors, crushing machines, and industrial scale mixers. Fluid couplings are also widely applied in automobiles, where they are the torque converter in automatic transmissions. Fluid couplings consist of an impeller and rotor, both enclosed in a casing. The impeller is attached to the input shaft; rotation causes hydraulic fluid to be pumped toward the rotor. If there is a velocity difference or *slip*, then the pumped fluid applies a torque to the rotor, which is directly connected to



Figure 11.22: A bellows coupling. *Source:* Courtesy of Lovejoy, Inc.



Figure 11.23: A helical coupling. *Source:* Courtesy of Lovejoy, Inc.



Figure 11.24: A Schmidt coupling. *Source:* Courtesy of Zero-Max, Inc.



Figure 11.25: A universal coupling. *Source:* Courtesy of Lovejoy, Inc.

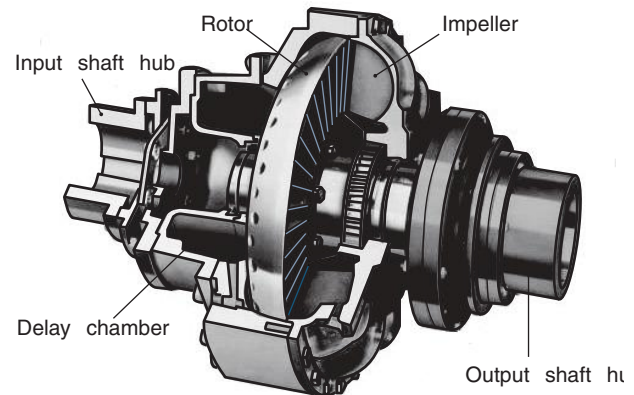


Figure 11.26: Schematic illustration of a fluid coupling. Note that a portion of the impeller and delay chamber have been removed for clarity. *Source:* Courtesy of Rexnord, Inc.

an output shaft. Thus, energy is transmitted through the hydrodynamic action of the fluid, and no direct contact between the two shafts occurs. The torque as a function of slip can be modified through use of a stator design in torque converters, or through delay chambers as shown.

**Gear couplings**, shown in Fig. 11.27, consist of two geared hubs connected by a sleeve with two internally geared sections. The in-line misalignment that can be tolerated depends on the width of the internal gear teeth. Further, some angular misalignment can be accommodated through the use of contoured teeth. These couplings have high torque capacity, but must be well lubricated to prevent wear.

## 11.10 Summary

A shaft is usually a circular cross-section rotating member that has such power-transmitting elements as gears, pulleys, flywheels, sprockets, and rolling-element bearings mounted on it. The loading on the shaft can be one or various combinations of bending, torsion, or axial or transverse shear. Furthermore, these types of loading can be either static or cyclic. A design procedure was presented that established the appropriate shaft diameter for specific conditions. If the shaft diameter is known, the safety factor (or the smallest diameter where failure first occurs) is often an important consideration. Three failure prediction theories considering important combinations of loading were presented. These theories are

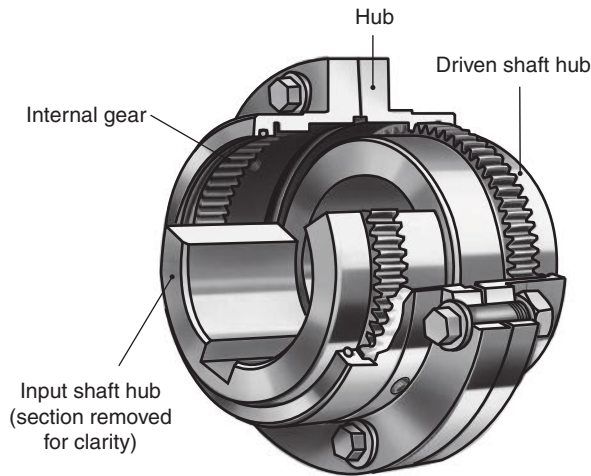


Figure 11.27: A gear coupling. *Source:* Courtesy of Rexnord, Inc.

by no means all-inclusive but should provide the essential understanding from which any other considerations can be easily obtained.

Shaft dynamics and in particular the first critical speed are important to design, since the rotating shaft becomes dynamically unstable and large vibrations are likely to develop at this speed. Both the Rayleigh and the Dunkerley equations for determining the first critical speed of a multiple-mass system were presented. The Rayleigh overestimates and the Dunkerley underestimates the exact solution, thus providing a range of operating speeds that the design should avoid.

A number of machine elements were presented for mounting parts onto shafts. These include design options that transmit a torque, such as keys, pins, and splines, as well as devices that only fix position on the shaft axis, such as retaining rings and cotter pins.

Flywheels were also discussed. In some applications, large variations in acceleration occur that can cause large oscillations in torque. The peak torque can be so high as to require an overly large motor. A flywheel is often used to smooth out the velocity changes and stabilize the back-and-forth energy flow of rotating equipment. A procedure for designing a flywheel was presented as well as flywheel dynamics, sizing, stresses, and material selection.

In the last section, some of the many types of shaft couplings were presented. Connecting two shafts is very common, such as when a motor is connected to a power transmitting shaft. The couplings all have their advantages and disadvantages, mostly associated with their ability to accommodate in-line, parallel, and/or angular misalignment. Another important capability of a coupling is damping of vibration and shock loads.

## Key Words

**coefficient of fluctuation** dimensionless speed range,  

$$\frac{\omega_{\max} - \omega_{\min}}{\omega_{\text{avg}}}$$

**critical speed** speed at which a rotating shaft becomes dynamically unstable

**coupling** a device used to connect two shafts; many forms are available

**Dunkerley equation** relation for first critical speed that underestimates frequency

**first critical speed** lowest frequency at which dynamic instability occurs

**flywheel** element that stores energy through rotational inertia

**hub** portion of member mounted onto shaft that directly contacts shaft

**key** element that transmits power from shaft to hub

**lowest natural frequency** same as first critical speed

**natural frequency** same as critical speed

**Rayleigh equation** relation for first critical speed that overestimates frequency

**retaining ring** elastically deformable stamped shape that usually seats in a flat groove to axially restrain a part on a shaft

**shaft** rotating or stationary member, usually of circular cross-section with small diameter relative to length and used to transmit power through such elements as gears, sprockets, pulleys, and cams

**spline** toothed profile for transmitting power from a shaft to a hub

## Summary of Equations

### Shaft design

$$\text{Static loading, DET: } d = \left( \frac{32n_s}{\pi S_y} \sqrt{M^2 + \frac{3}{4}T^2} \right)^{1/3},$$

$$n_s = \frac{\pi d^3 S_y}{32 \sqrt{M^2 + \frac{3}{4}T^2}}$$

$$\text{Static loading, MSST: } d = \left( \frac{32n_s}{\pi S_y} \sqrt{M^2 + T^2} \right)^{1/3},$$

$$n_s = \frac{\pi d^3 S_y}{32 \sqrt{M^2 + T^2}}$$

Static loading, DET, with axial loading:

$$\frac{4}{\pi d^3} \sqrt{(8M + Pd)^2 + 48T^2} = \frac{S_y}{n_s}$$

Static loading, MSST, with axial loading:

$$\frac{4}{\pi d^3} \sqrt{(8M + Pd)^2 + 64T^2} = \frac{S_y}{n_s}$$

Fatigue loading, DET and Soderberg:

$$d^3 = \frac{32n_s}{\pi S_y} \sqrt{(\Psi)^2 + \frac{3}{4} \left( T_m + \frac{S_y}{S_e} K_{fs} T_a \right)^2}$$

$$n_s = \frac{\pi d^3 S_y}{32 \sqrt{(\Psi)^2 + \frac{3}{4} \left( T_m + \frac{S_y}{S_e} K_{fs} T_a \right)^2}}$$

$$\text{where } \Psi = M_m + \frac{S_y}{S_e} K_f M_a.$$

Fatigue loading, MSST and Soderberg:

$$d^3 = \frac{32n_s}{\pi S_y} \sqrt{(\Psi)^2 + \left( T_m + \frac{S_y}{S_e} K_{fs} T_a \right)^2}$$

$$n_s = \frac{\pi d^3 S_y}{32 \sqrt{(\Psi)^2 + \left(T_m + \frac{S_y}{S_e} K_{fs} T_a\right)^2}}$$

Critical speed, single mass:  $\omega = \sqrt{\frac{g}{\delta}}$

Critical speed, Rayleigh equation:

$$\omega_{cr} = \sqrt{\frac{g \sum_{i=1, \dots, n} W_i \delta_{i, \max}}{\sum_{i=1, \dots, n} W_i \delta_{i, \max}^2}}$$

Critical speed, Dunkerley equation:

$$\frac{1}{\omega_{cr}^2} = \frac{1}{\omega_1^2} + \frac{1}{\omega_2^2} + \dots + \frac{1}{\omega_n^2}$$

### Keys

Failure due to shear:  $T = \frac{S_y A_s d}{4 n_s}$

Failure due to bearing stress:  $T = \frac{S_y d l h}{4 n_s}$

### Splines

Recommended spline width:  $l_s = \frac{d^3 \left(1 - \frac{d_i^4}{d^4}\right)}{d_m^2}$

Failure due to shear:  $T = \frac{\pi \tau_{all} d_m^2 l_s}{16}$

Failure due to bearing stress:  $T = \frac{p n h d_m l_s}{8}$

### Set screws

Holding force:  $P_t = 2500 d^{2.31}$

Approximate size:  $d_s = \frac{d}{8} + \frac{5}{16}$

### Retaining rings

Failure due to ring shear:  $P_t = \frac{\pi C_t d t_h S_{sy}}{n_s}$

Failure due to bearing failure:  $P_t = \frac{\pi C_t d t_g S_{ut}}{n_s}$

### Flywheels

Coefficient of fluctuation:

$$C_f = \frac{\omega_{\max} - \omega_{\min}}{\omega_{\text{avg}}} = \frac{2(\omega_{\max} - \omega_{\min})}{\omega_{\max} + \omega_{\min}}$$

Kinetic energy fluctuation:  $K_e = I_m \omega_{\text{avg}}^2 C_f$

## Recommended Readings

- Budynas, R.G., and Nisbett, J.K. (2011), *Shigley's Mechanical Engineering Design*, 9th ed., McGraw-Hill.
- Juvinall, R.C., and Marshek, K.M. (2012) *Fundamentals of Machine Component Design*, 5th ed., Wiley.
- Mott, R. L. (2014) *Machine Elements in Mechanical Design*, 5th ed., Pearson.
- Neale, M., Needham, P., and Horrell, R. (2005) *Couplings and Shaft Alignment*, Wiley.
- Norton, R.L. (2011) *Machine Design*, 4th ed., Prentice Hall.
- Oberg, E., and Jones, F.D. (2000) *Machinery's Handbook*, 26th ed., Industrial Press.
- Piotrowski, J. (1995) *Shaft Alignment Handbook*, 2nd ed., Marcel Dekker.

## References

- Oberg, E., et al. (2000) *Machinery's Handbook*, 26th ed., Industrial Press.
- Peterson, R.E. (1974) *Stress Concentration Factors*, Wiley.

## Questions

- 11.1** What is a shaft? How is it different from a beam?
- 11.2** Why is it important to consider both static and fatigue failure when designing shafts?
- 11.3** What is the consequence of including a thrust (axial) force on the shaft design equations?
- 11.4** What is meant by the critical speed of a shaft?
- 11.5** What is the Rayleigh equation? The Dunkerley equation?
- 11.6** What is the difference between a key and a pin?
- 11.7** What is a Gib head?
- 11.8** Is there an advantage to using a Woodruff key?
- 11.9** What should be harder, the hub or the key?
- 11.10** What is a flywheel?
- 11.11** What is the coefficient of fluctuation?
- 11.12** What is a rigid coupling? A flexible coupling?
- 11.13** What are retaining rings used for? What kind of retaining rings are there?
- 11.14** What is a spline?
- 11.15** What kind of shaft misalignments are there?

## Qualitative Problems

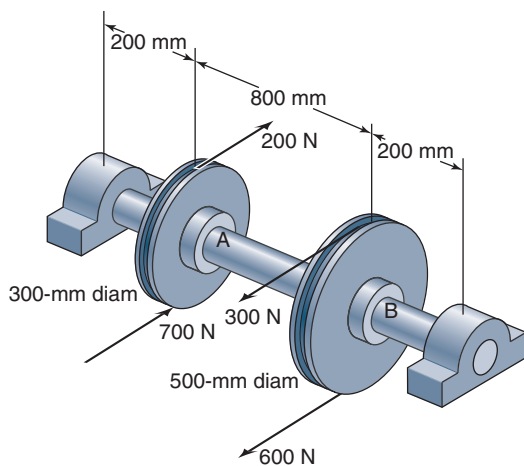
- 11.16** List reasons that shafts are designed with high safety factors.
- 11.17** What machine elements can be used to limit the torque encountered by a shaft during an overload or other malfunction?
- 11.18** Explain why rotating shafts vibrate when a concentrated mass is mounted on the shaft.
- 11.19** Describe the manufacturing processes that are used to produce shafts, and why.
- 11.20** Review Fig. 11.9 and explain the conditions when you would use one type of key compared to others.
- 11.21** List the similarities and differences between set screws and keys.
- 11.22** Plot the holding force for set screws predicted by Table 11.5 and Eqs. (11.71) and (11.72). Explain the reasons for any differences between the two predictions.
- 11.23** Under what conditions would you use a key instead of a spline? When would you use a spline instead of a key?
- 11.24** When would you advise using a press fit instead of a key?
- 11.25** Review Table 11.6 and list two applications for each type of retaining ring shown.



- 11.26** Explain the consequences of driving an automobile without a flywheel.
- 11.27** What consequences occur if a flywheel is operated at an excessively high speed?
- 11.28** What material characteristics are desirable for a flywheel?
- 11.29** List the advantages and disadvantages of (a) rigid couplings; (b) helical couplings; (c) Schmidt couplings; (d) fluid couplings.
- 11.30** For a circumstance where significant parallel shaft misalignment exists, which couplings would you consider? What coupling would be more suitable if the space available for a coupling is limited? Explain.

## Quantitative Problems

- 11.31** A 50-mm-diameter shaft is machined from AISI 1080 carbon steel (quenched and tempered at 800°C), and because of its rotation, encounters a bending moment that varies from  $-20$  to  $55$  N-m and a constant torque of  $25$  N-m. The shaft has a 5-mm hole drilled (machined) into it so that a roll pin can be inserted at that location. For a reliability of 99.5%, determine the safety factor for the shaft. Would the safety factor be larger or smaller if a retaining ring was used instead of the roll pin? Justify your answer. *Ans.  $n_s = 23.6$ .*
- 11.32** A shaft assembly shown in Sketch *a* is driven by a flat belt at location A and drives a flat belt at location B. The drive belt pulley diameter is 300 mm; the driven belt pulley diameter is 500 mm. The distance between sheaves is 800 mm, and the distance from each sheave to the nearest bearing is 200 mm. The belts are horizontal and load the shaft in opposite directions. Determine the size of the shaft and the types of steel that should be used. Assume a safety factor of 10. *Ans. For AISI 1080 steel,  $d = 35$  mm.*



Sketch *a*, for Problem 11.32

- 11.33** The gears in the shaft assembly shown in Fig. 11.1a transmit 100 kW of power and rotate at 4000 rpm. Gear wheel 1 is loaded against another gear such that the force  $P_1$  acts in a  $45^\circ$  direction at a radius of 80 mm from

the shaft center. The force  $P_2$  acts vertically downward at a radius of 110 mm from the shaft center. The distance from bearing A to gear 1 is 100 mm, that from gear 1 to gear 2 is 85 mm, and that from gear 2 to bearing B is 50 mm. Perform the following:

- Draw a free-body diagram with forces acting on the shaft when bearings A and B transmit only radial forces. *Ans.  $A_y = -750$  N,  $A_z = 1212$  N.*
- Find values of force components as well as the resultant force at locations A and B.
- Find the transmitted torque. *Ans.  $T = 238.7$  N-m.*
- Draw a bending moment diagram in the  $x$ - $y$  and  $x$ - $z$  planes along with a torque diagram; also, indicate the maximum bending moment and the maximum torque.
- Find the safety factor according to the distortion-energy theory (DET) and the maximum-shear-stress theory (MSST) if the shaft has a diameter of 35 mm and is made of high-carbon steel (AISI 1080, quenched and tempered at 800°C). *Ans.  $n_{s,MSST} = 5.75$ ,  $n_{s,DET} = 5.73$ .*

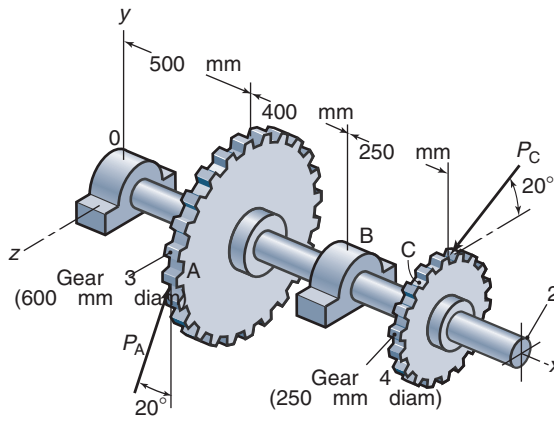
- 11.34** The shaft assembly given in Problem 11.32 has an extra loading from thermal expansion of the shaft. The bearings are assumed to be rigid in the axial direction, so that when the shaft heats up it cannot elongate but instead compressive stress builds up. Determine the thermal stress and find the safety factor by using the DET if the shaft heats up by

- $5^\circ\text{C}$ . *Ans.  $n_s = 5.69$ .*
- $15^\circ\text{C}$ . *Ans.  $n_s = 4.53$ .*

- 11.35** Given the shaft assembly in Problem 11.32 but calculating as if AISI 1080 steel, quenched and tempered at 800°C, was used and is considered to be brittle (using the MNST), find the safety factor  $n_s$  for fatigue by using the information in Problem 11.32. *Ans.  $n_{s,MNST} = 5.57$ .*

- 11.36** Gears 3 and 4 act on the shaft shown in sketch *b*. The resultant gear force,  $P_A = 2500$  N, acts at an angle of  $20^\circ$  from the  $y$ -axis. The yield stress for the shaft, which is made of cold-drawn steel, is 490 MPa and the ultimate stress is 580 MPa. The shaft is solid and of constant diameter. The safety factor is 3.0. Assume the DET throughout. Also, for fatigue loading conditions assume completely reversed bending with a bending moment amplitude equal to that used for static conditions. The alternating torque is zero. Determine the safe shaft diameter due to static and fatigue loading, rounding your answer to the next highest convenient dimension. Show shear and moment diagrams in the various planes. *Ans.  $d_{\text{static}} = 50$  mm,  $d_{\text{fatigue}} = 65$  mm.*



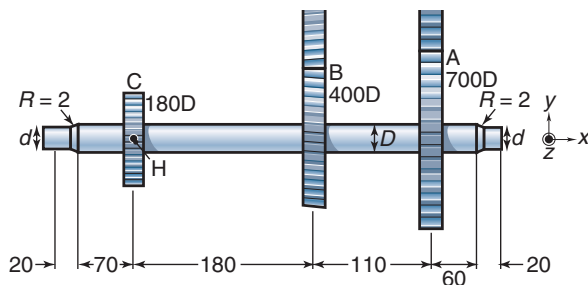


Sketch b, for Problem 11.36

**11.37** Derive Eq. (11.38). Start by showing the stresses acting on an oblique plane at angle  $\phi$ . The MNST should be used, implying that the critical stress line extends from  $S_e/n_s$  to  $S_u/n_s$ .

**11.38** The shaft shown in Sketch c rotates at 1000 rpm and transfers 6 kW of power from input gear A to output gears B and C. The spur gears A and C have pressure angles of  $20^\circ$ . The helical gear has a pressure angle of  $20^\circ$  and a helix angle of  $30^\circ$  and transfers 70% of the input power. All important surfaces are ground. All dimensions are in mm. The shaft is made of annealed carbon steel with  $S_{ut} = 636$  MPa and  $S_y = 365$  MPa.

- Draw a free-body diagram as well as the shear and moment diagrams of the shaft.
- Which bearing should support the thrust load and why? *Ans. The left bearing.*
- Determine the minimum shaft diameter for a safety factor of 3.0 and 99% reliability. *Ans.  $d = 20$  mm.*



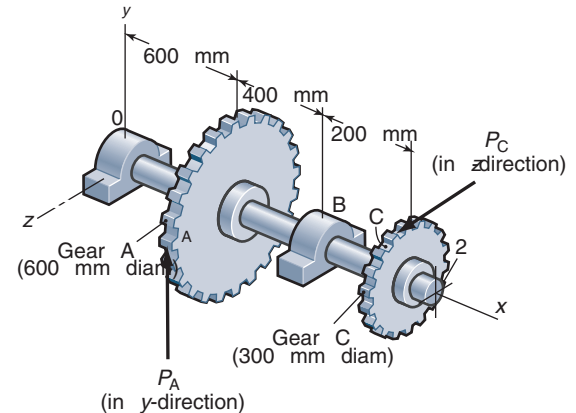
Sketch c, for Problem 11.38

**11.39** In Problem 11.38 if the shaft diameter is 30 mm and it is made of AISI 1030 steel, quenched and tempered at  $800^\circ\text{C}$ , what is the safety factor while assuming 90% reliability? *Ans.  $n_s = 4.09$ .*

**11.40** The shaft shown in Sketch d supports two gears. The shaft is made from high carbon steel (quenched and tempered AISI 1080), and is to be designed with a safety factor of 2.0. The gears transmit a constant torque caused

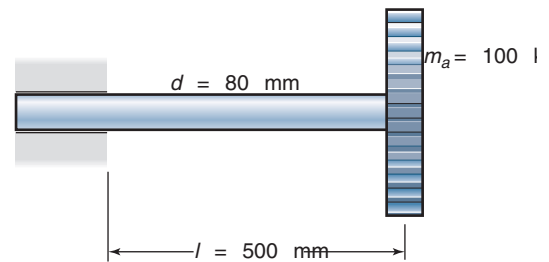
by  $P_A = 2000$  N acting vertically as shown. The shaft has a constant machined cross-section.

- What is the reaction force on gear C? *Ans.  $P_c = 4000$  N.*
- What is the critical location in the shaft? *Ans. At bearing B.*
- Using the Soderberg line, obtain the required shaft diameter. (Note: Ignore all endurance limit modification factors except the surface finish factor.) *Ans.  $d = 50$  mm.*
- One of the gears has been attached with a keyway, the other with a shrink fit. Which gear was attached with a keyway, and why?



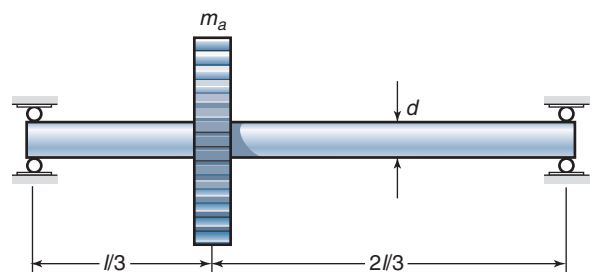
Sketch d, for Problem 11.40

**11.41** The rotor shown in Sketch e has a stiff bearing on the left. Find the critical speed when the shaft is made of steel with  $E = 207$  GPa. *Ans.  $N = 3018$  rpm.*



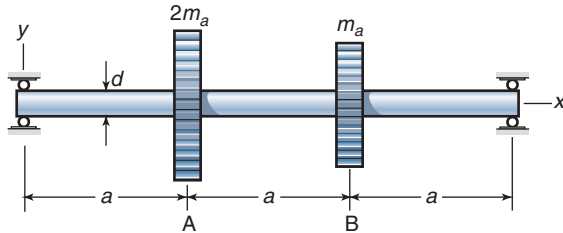
Sketch e, for Problem 11.41

**11.42** Determine the critical speed in bending for the shaft assembly shown in Sketch f. The modulus of elasticity of the shaft  $E = 207$  GPa, its length  $l = 350$  mm, its diameter  $d = 10$  mm, and the rotor mass  $m_a = 2.3$  kg. *Ans.  $\omega = 250$  rad/s.*

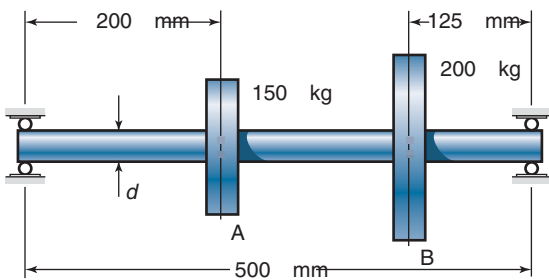


Sketch f, for Problem 11.42

- 11.43** Calculate the diameter of the shaft in the assembly shown in Sketch *g* so that the first critical speed is 9000 rpm. The shaft is made of steel with  $E = 207$  GPa. The distance  $a = 300$  mm and the mass  $m_a = 100$  kg; the mass of the shaft is neglected. Use both the Rayleigh and Dunkerley methods. *Ans.*  $d_R = 131$  mm,  $d_D = 133$  mm.

Sketch *g*, for Problem 11.43

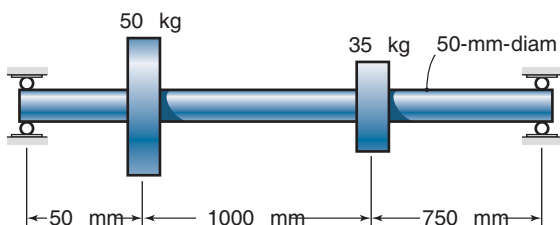
- 11.44** The simply-supported shaft shown in sketch *h* has two weights on it. Neglecting the shaft weight and using the Rayleigh method for the stainless steel ( $E = 193 \times 10^6$  GPa) shaft, determine the safe diameter to ensure that the first critical speed is no less than 3600 rpm. *Ans.*  $d_R = 62.6$  mm,  $d_D = 63.6$  mm

Sketch *h*, for Problems 11.44 and 11.50

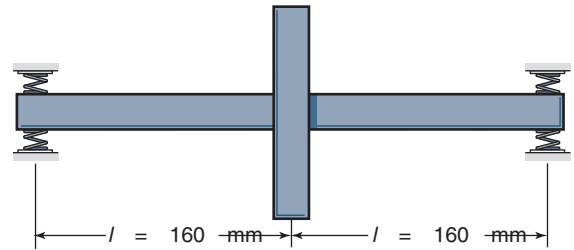
- 11.45** Determine the first critical speed by the Dunkerley and Rayleigh methods for the steel shaft shown in sketch *i*. Neglect the shaft mass. The area moment of inertia is  $I = \pi r^4/4$ , where  $r$  = shaft radius. The method of superposition may be used with the following given:

$$\delta = \frac{P}{6EI} \left[ \frac{bx^3}{l} \right] - \langle x-a \rangle^3 - \frac{xb(l^2 - b^2)}{l}$$

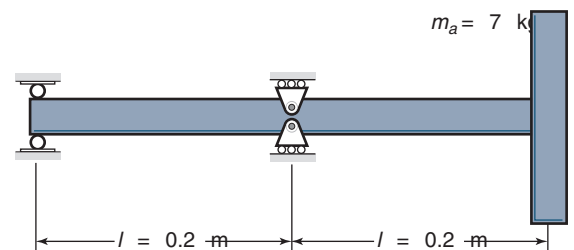
*Ans.*  $N_R = 765$  rpm,  $N_D = 783$  rpm.

Sketch *i*, for Problem 11.45

- 11.46** Calculate the diameter  $d$  of the shaft in Sketch *j* so that the lowest critical speed in bending becomes 9000 rpm. The modulus of elasticity  $E = 107$  GPa, the distance  $a = 300$  mm, and the mass  $m_a = 100$  kg. Neglect the mass of the shaft. Use the Rayleigh and Dunkerley methods. *Ans.*  $d_R = 155$  mm,  $d_D = 156$  mm.

Sketch *j*, for Problem 11.46

- 11.47** The shaft from Problem 11.43 transmits 200 kW at 3000 rpm. Design the shaft diameter so that the angular deflection between the two gears is  $0.75^\circ$ . At this diameter, what is the critical speed of the shaft? *Ans.*  $d = 31.1$  mm,  $\omega_{cr} = 504$  rpm.
- 11.48** The rotor in Sketch *k* has a shaft diameter of 32 mm, and the disk mass is 170 kg. Calculate the critical speed if the spring rates are 1668 and 3335 N/mm, respectively, and are the same in all directions. The elastic modulus  $E = 206$  GPa. For a shaft without springs the influence coefficient  $\alpha_{11} = l^3/(6EI)$ . *Ans.*  $N = 1360$  rpm.

Sketch *k*, for Problems 11.48 and 11.49

- 11.49** Calculate the critical speed for a rotor shown in Sketch *k* that has two moment-free bearings. The shaft has a diameter of 20 mm and is made of steel with  $E = 207$  GPa. *Ans.*  $N = 1993$  rpm.
- 11.50** The deflection at the center of the stainless steel shaft ( $E = 193$  GPa) shown in sketch *h* is equal to 1.875 mm. Find the diameter of the solid circular shaft and the first critical speed using both the Rayleigh and Dunkerley methods. *Ans.*  $d = 28.9$  mm,  $\omega_R = 80.4$  rad/s.
- 11.51** A flywheel has a hub made of aluminum alloy 2014-O. The hub is connected to a 20-mm-diameter annealed AISI 1040 steel shaft with a flat tapered key made of AISI 1020 steel, quenched and tempered at  $870^\circ\text{C}$ . Dimension the key so that a torque of 20 N-m can be transmitted with a safety factor of 4. *Ans.*  $w = 4.52$  mm,  $h = 12.2$  mm.
- 11.52** A jaw crusher is used to crush iron ore down to the particle size needed for iron ore pellet production. The pellets are later used in a blast furnace to make steel. If the ore pieces fed into the crusher are too large, the crusher

is protected by a torque-limiting key made of copper. The torque on the 400-mm-diameter shaft connecting the flywheel with the jaw mechanism should never go above 700 kN-m. Dimension a copper square tapered key so that the shaft is not damaged when an oversized ore particle comes into the crusher.

- 11.53** Given the sketch of the Woodruff key in Figure 11.9, show that the shear area is given by

$$A_s = 2w\sqrt{c(D - c)}$$

where  $c$  is the diametral clearance and  $D$  is the key diameter.

- 11.54** A punch press is to be driven by a constant torque electric motor that operates at 1200 rpm. A flywheel of constant thickness cut from 50 mm thick steel plate is to be used to ensure smooth operation. The punch press torque steps from 0 to 12,500 Nm, remaining constant for the first  $45^\circ$  of camshaft rotation, up to 80,000 Nm for the next  $45^\circ$ , and back to 0 for the remainder of the cycle. What is the minimum diameter of the flywheel?  
*Ans.  $d = 1.15$  m*

- 11.55** The output torque of a flywheel for each revolution of a shaft is 10 N-m from 0 to  $\pi$  and 120 N-m from  $\pi$  to  $2\pi$ . The coefficient of fluctuation is 0.04 at an average speed of 2000 rpm. Assume that the flywheel disk is an annealed AISI 1040 steel plate of 25-mm constant thickness. Determine the following:

- (a) Average load torque. *Ans. 65 Nm.*
- (b) Locations  $\theta_{\omega_{\max}}$  and  $\theta_{\omega_{\min}}$ . *Ans.  $\theta_{\omega_{\max}} = \pi$*
- (c) Energy required. *Ans.  $K_e = 172.8$  Nm.*
- (d) Outside diameter of flywheel. *Ans.  $d = 270$  mm.*

- 11.56** The output torque of a flywheel for each revolution of the shaft is 20 Nm from 0 to  $\pi/3$ , 100 Nm from  $\pi/3$  to  $2\pi/3$ , 40 Nm from  $2\pi/3$  to  $\pi$ , 90 Nm from  $\pi$  to  $5\pi/3$ , and 20 Nm from  $5\pi/3$  to  $2\pi$ . Input torque is assumed to be constant. The average speed is 860 rpm and the coefficient of fluctuation is 0.10. Find the diameter of the flywheel if it is to be cut from a 25-mm-thick steel plate. *Ans.  $d = 240$  mm.*

- 11.57** A 20-mm-thick flywheel is made of aluminum alloy 2014-O and runs at 9000 rpm in a racing car motor. What is the flywheel diameter if the aluminum alloy 2014 is stressed to a quarter of its yield strength at 9000 rpm? To decrease the flywheel outer diameter, higher density exotic materials are investigated. The flywheel is machined from a solid metal plate with no central hole, and the thickness cannot be larger than 20 mm. Which of the following is the best material that can be substituted for aluminum alloy 2014 but with the same safety factor?

- (a) pure copper
- (b) cartridge brass
- (c) annealed 5% phosphor bronze
- (d) magnesium alloy ZK61A
- (e) annealed Ti-6Al-4V

- 11.58** The aluminum alloy flywheel considered in Problem 11.57 has a mass moment of inertia of  $0.0025$  kg-m<sup>2</sup>. By mistake the motor is accelerated to 7000 rpm in neutral gear and the throttle sticks in the fully open position.

The only way to stop the motor is to disconnect the electric lead from the spark plug, and it takes 6 s before the motor is motionless. Neglecting the inertia of all movable parts in the motor except the flywheel, calculate the internal friction moment in the motor and the (mechanical part of the) friction losses in the motor at 5000 rpm. The friction moment is assumed to be constant at all speeds. *Ans.  $T_f = -0.305$  N-m.*

- 11.59** A one-cylinder ignition bulb motor to an old fishing boat has a flywheel that gives the motor a coefficient of fluctuation of 25% when it idles at 200 rpm. The mass moment of inertia for the flywheel is  $1.9$  kg-m<sup>2</sup>. Determine the coefficient of fluctuation at 500 rpm if the compression stroke consumes equally large energy at all speeds. Also, calculate the mass moment of inertia needed to obtain a 20% coefficient of fluctuation at 500 rpm. *Ans.  $C_f = 0.040$ ,  $I_m = 0.38$  kg-m<sup>2</sup>.*

- 11.60** A flywheel for a city bus drive should store as much energy as possible for a given flywheel weight. The diameter must be less than 1.5 m, and the mass must be smaller than 250 kg. Find which material from Tables A.1 and A.2 gives the highest possible stored energy for a safety factor of 4 assuming that the flywheel has constant thickness.

- 11.61** A flywheel on an AISI 1080 (Q&T at  $800^\circ\text{C}$ ) steel shaft is oscillating due to disturbances from a combustion engine. The engine is a four-stroke engine with six cylinders, so that the torque disturbances occur three times per revolution. The flywheel shaft has a diameter of 20 mm and is 1 m long, and the flywheel moment of inertia is  $0.5$  kg-m<sup>2</sup>. Find the engine speed at which the large torsional vibrations begin to appear. *Ans.  $N = 160$  rpm.*

- 11.62** An external retaining ring is to be stamped from quenched and tempered AISI 1080 steel and will be designed to secure a rolling element bearing against a shaft shoulder. The shaft is produced from annealed AISI 1040 steel and has a diameter of 25 mm. Calculate the restraining force that can be developed for MSH, ME, and MCR rings using a safety factor of 2. Also estimate the theoretical stress concentration factor that results in the shaft from the retaining ring groove if the radius of the groove corner radius is 0.5 mm. *Ans.  $P_{\text{MSH}} = 4.78$  kN.*

## Design and Projects

- 11.63** A front wheel for a riding lawnmower needs to be attached to a 20 mm diameter axle. The wheel has an integral hub that will be grease lubricated and can slide axially and rotate on the shaft (it is a steering wheel, not a drive wheel, so it only needs to idle). When the lawnmower turns, a force of up to 500 N can be applied in the axial direction. List design alternatives for securing the wheel to the axle. From your list, select the three most attractive designs for further analysis, and prescribe dimensions and restraining forces for these alternatives. Write a summary of your design analysis and select the approach you think is best suited for this application.

- 11.64** *Hydrodynamic braking* is used as an auxiliary brake in vehicles to prevent high speeds when undergoing a large change in elevation, such as with heavy vehicles on mountain roads. Explain how a fluid coupling can be used in this manner, and describe how braking torque

will vary with speed. Suggest how to dissipate the heat generated from this auxiliary brake.

- 11.65** Derive equivalent expressions to Eqs. (11.36) and (11.37) using the Goodman criterion and the MSST. Using a mathematics package, write a program that provides the diameter or safety factor if the modified Goodman criterion is used.
- 11.66** A hammer mill will be used to shred sugar cane to allow efficient extraction of sugar. Cane is fed into the hammer mill through a hopper, and impacted by cast iron hammers powered by a 8000 kW motor at 4000 rpm, so that around 10,000 tons of cane can be processed daily. When cane is struck by a hammer, it shatters, and the pulp is further reduced by repeated impacts until it is discharged. What kind of coupling would you use to connect the power source to the hammer mill? You may reference the technical literature or search the Internet for any further information you may require. Write a one-page memorandum outlining your design recommendation.
- 11.67** Would you recommend using a flywheel for the sugar cane shredder described in Problem 11.66? Explain.
- 11.68** Review Fig. 11.21, and derive an expression for the torsional stiffness of the Falk coupling from beam theory.

This page intentionally left blank



## Appendix A

# Physical and Mechanical Properties of Materials

### A.1 Mechanical Properties of Selected Alloy Steels

AISI Number	Condition <sup>a</sup>	Yield Strength, MPa	Ultimate Tensile Strength, MPa	Elongation in 50 mm, %	Reduction in Area, %	Brinell Hardness, HB
<b>Chromium-Molybdenum</b>						
4130	Annealed	361	560	28	56	156
	N 870- C	436	870	25	59	197
	Q&T 205- C	1460	1630	10	41	467
	Q&T 315- C	1380	1500	11	43	430
	Q&T 425- C	1190	1280	13	49	380
	Q&T 540- C	910	1030	17	57	315
4140	Q&T 650- C	703	814	22	64	245
	Annealed	417	655	26	57	200
	N 870- C	655	1020	18	47	300
	Q&T 205- C	1640	1770	8	38	510
	Q&T 315- C	1430	1550	9	43	445
	Q&T 425- C	1140	1250	13	49	370
	Q&T 540- C	834	951	18	58	285
	Q&T 650- C	655	758	22	63	230
<b>Nickel-Chromium-Molybdenum</b>						
4320	Annealed	425	580	29	50	160
	N 870- C	460	790	21	40	235
4340	Annealed	470	745	22	50	220
	Q&T 315- C	1590	1720	10	40	486
	Q&T 425- C	1360	1470	10	44	430
	Q&T 540- C	1080	1170	13	50	360
	Q&T 650- C	855	965	20	60	280
8620	A	357	536	31	60	150
	N 870- C	385	632	26	59	183
<b>Chromium-Vanadium</b>						
6150	Annealed	407	662	23	50	190
	N 870- C	615	940	22	50	270
	Q&T 540- C	1160	1200	15	20	350

Note: <sup>a</sup> N, normalized; Q&T, quenched and tempered

## A.2 Mechanical Properties of Selected Carbon Steels

AISI Number	Condition <sup>a</sup>	Yield Strength, MPa	Ultimate Tensile Strength, MPa	Elongation in 50 mm, %	Reduction in Area, %	Brinell Hardness, HB
1006	Hot Rolled	170	300	30	55	85
	Cold Drawn	280	330	20	45	95
1010	Cold Drawn	305	365	20	40	105
	Hot Rolled	180	325	28	50	95
1015	Cold Drawn	325	385	18	40	111
	Hot Rolled	190	340	28	50	100
1018	Cold Drawn	370	440	15	40	126
	Hot Rolled	220	400	25	50	116
1020	Q&T 870° C	295	395	37	60	100
	Cold Drawn	350	420	15	40	121
	Hot Rolled	205	380	25	50	110
1030	Annealed	317	430	30	60	130
	N 925° C	345	520	32	61	150
	Q&T 205° C	648	848	17	47	495
	Q&T 315° C	621	800	19	53	400
	Q&T 425° C	579	731	23	60	300
	Q&T 540° C	517	669	28	65	250
	Q&T 650° C	441	586	32	70	210
	Cold Drawn	440	525	12	35	149
	Hot Rolled	260	70	20	40	130
1040	Annealed	350	520	30	57	150
	N 900° C	374	590	28	55	170
	Q&T 205° C	593	779	19	48	262
	Q&T 425° C	552	758	21	54	240
	Q&T 650° C	434	634	29	65	192
	Cold Drawn	490	585	12	35	170
	Hot Rolled	290	525	18	40	149
1050	Annealed	365	636	24	40	190
	N 900° C	427	748	20	39	220
	Q&T 205° C	807	1120	9	27	514
	Q&T 425° C	793	1090	13	36	444
	Q&T 650° C	538	717	28	65	235
	Cold Drawn	580	690	10	30	197
	Hot Rolled	340	620	15	35	179
1060	Annealed	372	626	22	38	179
	N 900° C	421	776	18	37	230
	Q&T 425° C	765	1080	14	40	310
	Q&T 540° C	669	965	17	45	280
	Q&T 650° C	524	800	23	40	230
	Hot Rolled	370	680	12	30	201
1080	Q&T 800° C	380	615	25	30	255
	Hot Rolled	420	770	10	25	229
1095	Annealed	380	658	13	21	190
	N 900° C	500	1010	9	13	293
	Q&T 315° C	813	1260	10	30	375
	Q&T 425° C	772	1210	12	32	360
	Q&T 540° C	676	1090	15	37	320
	Q&T 650° C	552	896	21	30	269
	Hot Rolled	455	825	10	25	248
	Cold Drawn	525	680	10	20	197

Note: <sup>a</sup> N, normalized; Q&T, quenched and tempered

### A.3 Mechanical Properties of Selected Cast Irons

ASTM class	Condition <sup>a</sup>	Tensile yield strength MPa	Ultimate tensile strength MPa	Compressive strength MPa	Hardness HB
<b>Gray cast irons</b>					
20	As cast	—	152	572	156
25	As cast	—	179	669	174
30	As cast	—	214	752	210
35	As cast	—	252	855	212
40	As cast	—	293	965	235
50	As cast	—	362	1130	262
60	As cast	—	431	1293	302
<b>Ductile (nodular or spheroidal) cast irons</b>					
60-40-18	Annealed	324	448	359	160
65-45-12	Annealed	331	462	365	174
80-55-06	Annealed	365	565	385	228
120-90-02	Q&T	827	965	924	325

Note: <sup>a</sup> Q&T, quenched and tempered

### A.4 Mechanical Properties of Selected Stainless Steels

AISI no.	Manufacturing history <sup>c</sup>	Yield strength, MPa	Ultimate tensile strength, MPa	Elongation in 50 mm, %	Hardness
301	Annealed	205	515	40	85 HRB
	1/16-hard	310	620	40	95 HRB
	1/8-hard	380	690	40	20 HRC
	1/4-hard	515	860	25	25 HRC
	1/2-hard	758	1034	18	32 HRC
	3/4-hard	930	1205	12	37 HRC
	Full-hard	965	1276	9	41 HRC
302	Annealed	207	517	40	150 HB
	1/4-hard	517	860	10	310 HB
	1/2-hard	758	1034	9	320 HB
	Full-hard	965	1275	3	335 HB
304	Annealed	215	505	40	201 HB
304L	Annealed	170	485	40	201 HB
304H	Annealed	205	515	40	201 HB
316	Annealed	240	585	55	150 HB
316L	Annealed	207	538	55	145 HB
410	Annealed	275	485	20	95 HB
420	Annealed	345	655	25	241 HB
	Q&T 204°C	1360	1600	12	444 HB
	Q&T 427°C	1420	1620	10	461 HB
	Q&T 650°C	680	895	20	262 HB
431	Annealed	655	862	20	285 HB
	Q&T 204°C	1055	1345	20	388 HB
	Q&T 427°C	1080	1350	19	388 HB
	Q&T 650°C	695	960	20	277 HB
631	Cold rolled	1275	1030	6	41 HRC

<sup>a</sup> Q&T, quenched and tempered

## A.5 Mechanical Properties of Selected Aluminum Alloys

Alloy	Temper	Yield Strength MPa	Ultimate Tensile Strength MPa	Elongation in 50 mm, %
<b>Wrought</b>				
1100	O	35	90	40
	H14	120	125	25
1350	O	28	83	—
	H19	165	186	—
2011	T3	296	379	15
	T8	310	407	12
2014	O	97	186	18
	T4	290	427	20
	T6	414	483	13
2017	T4	276	427	22
2024	O	75	190	20
	T3	345	483	18
	T4	325	470	20
2219	O	76	179	20
	T87	393	476	10
3003	O	40	110	35
	H12	117	131	20
	H14	145	150	12
3004	H16	165	179	14
	O	69	179	20
	H34	186	234	6
3105	H38	234	276	6
	O	55	117	24
	H14	152	172	5
	H18	193	214	3
5005	H25	159	179	—
	H34	138	159	8
5052	O	90	190	25
	H32	186	234	62
	H34	215	260	12
	H36	234	269	10
5056	O	152	290	35
	H18	407	434	10
5083	O	145	290	22
	H321	228	317	16
5086	H32	207	290	12
	H34	255	324	10
5454	H112	131	269	14
	O	117	248	22
	H32	207	276	10
	H34	241	303	10
6061	H112	124	248	18
	O	55	125	25
	T4	145	241	22
6063	T6	275	310	15
	T5	145	186	12
	T6	214	241	12
7050	T7651	490	552	—
7075	O	105	230	16
	T6	500	570	11
<b>Cast</b>				
319.0	T6	165	248	2.0
333.0	T5	172	234	1.0
	T6	207	289	1.5
335.0	T6	172	241	3.0
	T7	248	262	0.5

## A.6 Mechanical Properties of Selected Magnesium Alloys

Alloy	Temper	Yield Strength MPa	Ultimate Tensile Strength MPa	Elongation in 50 mm, %	Hardness
<b>Sand and permanent-mold castings</b>					
AM100-A	T61	150	275	1.0	69 HB
AZ63A	T6	130	275	5.0	73 HB
EZ233A	T5	110	160	2.0	50 HB
HK31A	T6	105	220	8.0	55 HB
ZC63A	T6	125	210	3.5	62 HB
ZK61A	T6	195	310	10.0	70 HB
<b>Die castings</b>					
AS41A	F	150	220	4.0	—
AZ91A	F	150	230	3.0	63 HB
<b>Extrusions</b>					
AZ31B	F	200	260	15	—
AZ61A	F	230	310	16.0	60 HB
AZ80A	T5	275	380	7	—
ZK60A	T5	305	365	11.0	88 HB
<b>Sheet and Plate</b>					
AZ31B	H24	220	290	15.0	73 HB
HK31A	H24	200	255	9.0	68 HB
ZE10	F	163	263	16	—
ZEK199	F	308	311	19	—
ZK60A	T5	300	365	11	—

## A.7 Mechanical Properties of Selected Wrought Copper and Copper Alloys

Alloy	UNS No.	Temper	Yield Strength MPa	Ultimate Tensile Strength MPa	Elongation in 50 mm, %	Hardness
<b>Pure copper</b>						
0FHC	C10200	—	69-365	221-455	55-4	—
<b>High-copper alloys</b>						
Beryllium-copper	C17200	Annealed	—	490	35	60 HRB
		Hardened	1050	1400	2	42 HRC
<b>Brass</b>						
Gilding, 5% Zn	C21000	Annealed	77	245	45	52 HRF
		Hard	350	392	5	64 HRB
Red brass, 15% Zn	C23000	Annealed	91	280	47	64 HRF
		Hard	406	434	5	73 HRB
Cartridge brass, 30% Zn	C26000	Annealed	133	357	55	72 HRF
		Hard	441	532	8	82 HRB
Muntzmetal, 40% Zn	C28000	Annealed	119	378	45	80 HRF
		Hard	350	490	15	75 HRB
High lead brass, 36% Zn, 2% Pb	C35300	Annealed	119	350	52	68 HRF
		Hard	318	420	7	80 HRB
<b>Bronze</b>						
Phosphor bronze, 5% Sn	C51000	Annealed	175	350	55	40 HRB
		Hard	581	588	9	90 HRB
Phosphor bronze, 10% Sn	CS52400	Annealed	250	483	63	62 HRB
		Hard	658	707	16	96 HRB
Aluminum bronze	C60800	Annealed	175	420	66	49 HRB
		Cold rolled	441	700	8	94 HRB
	C63000	Extruded	414	690	15	96 HRB
		Half hard	517	814	15	98 HRB
High-silicon bronze	C65500	Annealed	210	441	55	66 HRB
		Hard	406	658	8	95 HRB
<b>Other alloys</b>						
Cupronickel, 30% Ni	C71500	Annealed	126	385	36	40 HRB
		Cold rolled	553	588	3	86 HRB
Nickel Silver	C75700	Annealed	196	427	35	55 HRB
		Hard	525	595	4	89 HRB



## A.8 Mechanical Properties of Selected Nickel-base Alloys at 25°C

Alloy	Yield Strength MPa	Ultimate Tensile Strength MPa	Elongation in 50 mm, %	Hardness
<b>Commercially pure and low-alloy nickels</b>				
Nickel 200	148	462	47	109 HB
Nickel 201	103	403	50	129 HB
Nickel 211	240	530	40	—
Duranickel 301	862	1170	25	30 HRC
<b>Nickel-copper alloys</b>				
Alloy 400	240	550	40	110 HB
Alloy K-500	790	1100	20	300 HB
Monel R-405	230	525	35	—
Monel K-500	750	1050	30	—
<b>Nickel-molybdenum and Nickel-silicon alloys</b>				
<b>Hastelloy B</b>				
As cast	345	586	10	93 HRB
Sheet	386	834	63	92 HRB
<b>Hastelloy C-4</b>				
As cast	400	785	54	—
Sheet	—	793	—	35 HRC
<b>Nickel-chromium-iron alloys</b>				
Inconel 600	310	655	40	75 HRB
Inconel 617	350	755	58	173 HB
Inconel 690	348	725	41	88 HRB
Inconel 751	976	1310	22	352 HB
Inconel 800	295	600	44	138 HB
<b>Other alloys</b>				
Hastelloy C-276	372	785	62	209 HB
Hastelloy G	320	690	50	79 HRB
Inconel 625	517	930	42.5	190 HB
Inconel 825	310	690	45	—

## A.9 Properties of Selected Nickel-based Superalloys at 870°C (1600°F)

Alloy	Condition	Ultimate tensile strength, MPa	Yield strength, MPa	Elongation in 50 mm, %
Astroloy	Wrought	770	690	25
Hastelloy X	Wrought	255	180	50
IN-100	Cast	885	695	6
IN-102	Wrought	215	200	110
Inconel 625	Wrought	285	275	125
Inconel 718	Wrought	340	330	88
MAR-M 200	Cast	840	760	4
MAR-M 432	Cast	730	605	8
René 41	Wrought	620	550	19
Udimet 700	Wrought	690	635	27
Waspaloy	Wrought	525	515	35

## A.10 Mechanical Properties of Selected Zinc Alloys

Alloy	Ultimate Tensile Strength MPa	Elongation in 50 mm, %	Hardness
<b>Die-casting alloys</b>			
Z35541	359	7	100 HB
Z33520	283	10	82 HB
Z33531	329	7	91 HB
Z33523	283	14	76 HB
Z35635	374	8	103 HB
Z35630	404	5	100 HB
Z35840	426	2	119 HB
<b>Wrought alloys (hot rolled)</b>			
Z21220	150	52	43 HB
Z44330	170	50	52 HB
Z41320	221	38	61 HB

## A.11 Mechanical Properties of Selected Titanium Alloys

Alloy	Condition	Temperature °C	Yield Strength MPa	Ultimate Tensile Strength MPa	Elongation in 50 mm, %
<b>Unalloyed grades</b>					
99.5% Ti	Annealed	25	240	330	30
		300	95	150	—
ASTM Grade 1	Annealed	25	170	240	—
ASTM Grade 4	Annealed	25	480	550	—
<b>Alpha and near-alpha alloys</b>					
Ti-5Al-2.5Sn	Annealed	25	810	860	16
		300	450	565	—
Ti-8Al-1Mo-1V	Annealed	25	830	900	—
Ti-2.25Al-11Sn-5Zr-1Mo	Annealed	25	900	1000	—
Ti-6Al-2Sn-4Zr-2Mo	Annealed	25	830	900	—
<b>Alpha-beta alloys</b>					
Ti-6Al-4V	Annealed	25	925	1000	10
		300	650	725	—
	Solution + age	25	1100	1175	10
		300	900	980	—
Ti-6Al-2Sn-4Zr-6Mo	Solution + age	25	1100	1170	—
<b>Beta alloys</b>					
Ti-3Al-8V-6Cr-4Mo-4Zr	Annealed	25	830	900	—
Ti-15V-3Cr-3Al-3Sn	Solution + age	25	965	1000	—
Ti-10V02Fe-3Al	Annealed	25	1100	1170	—
Ti-13V-11Cr-3Al	Solution + age	25	1210	1275	8
		300	830	1100	—

## A.12 Mechanical Properties of Selected Powder Metal Alloys

Material	Yield strength MPa	Ultimate Tensile strength MPa	Elastic modulus GPa	Hardness	Elongation in 25 mm (%)	Density (g/cm <sup>3</sup> )
<b>Ferrous</b>						
F-0008-20	170	200	85	35 HRB	< 1	5.8
F-0008-35	260	390	140	70 HRB	1	7.0
F-0008-55HT		450	115	22 HRC	< 1	6.3
F-0008-85HT		660	150	35 HRC	< 1	7.1
FC-0008-30	240	240	85	50 HRB	< 1	5.8
FC-0008-60	450	520	155	84 HRB	< 1	7.2
FC-0008-95		720	150	43 HRC	< 1	7.1
FN-0205-20	170	280	115	44 HRB	1	6.6
FN-0205-35	280	480	170	78 HRB	5	7.4
FN-0205-180HT		1280	170	78 HRB	< 1	7.4
FX-1005-40	340	530	160	82 HRB	4	7.3
FX-1005-110HT		830	160	38 HRC	< 1	7.3
<b>Stainless Steel</b>						
SS-303N1-38	310	470	115	70 HRB	5	6.9
SS-304N1-30	260	300	105	61 HRB	< 1	6.4
SS-316N1-25	230	280	105	59 HRB	< 1	6.4
SS-316N2-38	310	480	140	65 HRB	131	6.9
<b>Copper and Copper Alloys</b>						
CZ-1000-9	70	120	80	65 HRH	9	7.6
CZ-1000-11	80	160	100	80 HRH	12	8.1
CZP-3002-14	110	220	90	88 HRH	16	8.0
CT-1000-13	110	150	60	82 HRH	4	7.2
<b>Aluminum Alloys</b>						
Ax 123-T1	200	270	—	47 HRB	3	2.7
Ax 123-T6	390	400	—	72 HRB	< 1	2.7
Ax 231-T6	200	220	—	55 HRB	1	2.7
Ax 231-T6	310	320	—	77 HRB	< 1	2.7
Ax 431-T6	270	300	—	55 HRB	5	2.8s
Ax 431-T6	440	470	—	80 HRB	2	2.8
<b>Titanium Alloys</b>						
Ti-6Al-4V (HIP)	827	917	—	—	—	13
<b>Superalloys</b>						
Stellite 19	—	1035	—	—	49 HRC	< 1

### A.13 Mechanical Properties of Selected Engineering Plastics at Room Temperature

Material	Ultimate tensile strength MPa	Elastic modulus GPa	Elongation %	Poisson's ratio, $\nu$
<b>Thermoplastics:</b>				
Acrylonitrile-butadiene-styrene (ABS)	28-55	1.4-2.8	75-5	-
ABS, reinforced	100	7.5	-	0.35
Acetal	55-70	1.4-3.5	75-25	-
Acetal, reinforced	135	10	-	0.35-0.40
Acrylic	40-75	1.4-3.5	50-5	-
Cellulosic	10-48	0.4-1.4	100-5	-
Fluorocarbon	7-48	0.7-2	300-100	0.46-0.48
Nylon	55-83	1.4-2.8	200-60	0.32-0.40
Nylon, reinforced	70-210	2-10	10-1	-
Polycarbonate	55-70	2.5-3	125-10	0.38
Polycarbonate, reinforced	110	6	6-4	-
Polyester	55	2	300-5	0.38
Polyester, reinforced	110-160	8.3-12	3-1	-
Polyethylene	7-40	0.1-1.4	1000-15	0.46
Polypropylene	20-35	0.7-1.2	500-10	-
Polypropylene, reinforced	40-100	3.5-6	4-2	-
Polystyrene	14-83	1.4-4	60-1	0.35
Polyvinyl chloride	7-55	0.014-4	450-40	-
<b>Thermosets:</b>				
Epoxy	35-140	3.5-17	10-1	-
Epoxy, reinforced	70-1400	21-52	4-2	-
Phenolic	28-70	2.8-21	2-0	-
Polyester, unsaturated	30	5-9	1-0	-
<b>Elastomers:</b>				
Chloroprene (neoprene)	15-25	1-2	100-500	0.5
Natural rubber	17-25	1.3	75-650	0.5
Silicone	5-8	1-5	100-1100	0.5
Styrene-butadiene	10-25	2-10	250-700	0.5
Urethane	20-30	2-10	300-450	0.5

### A.14 Mechanical Properties of Selected Ceramics at Room Temperature

Material	Symbol	Transverse rupture strength MPa	Compressive strength MPa	Elastic modulus GPa	Hardness HK	Poisson's ratio, $\nu$
Aluminum oxide	Al <sub>2</sub> O <sub>3</sub>	140-240	1000-2900	310-410	2000-3000	0.26
Cubic boron nitride	cBN	725	7000	850	4000-5000	—
Diamond	—	1400	7000	830-1000	7000-8000	—
Silica, fused	SiO <sub>2</sub>	—	1300	70	550	0.25
Silicon carbide	SiC	100-750	700-3500	240-480	2100-3000	0.14
Silicon nitride	Si <sub>3</sub> N <sub>4</sub>	480-600	—	300-310	2000-2500	0.24
Titanium carbide	TiC	1400-1900	3100-3850	310-410	1800-3200	—
Tungsten carbide	WC	1030-2600	4100-5900	520-700	1800-2400	—
Partially stabilized zirconia	PSZ	620	—	200	1100	0.30

Note: These properties vary widely depending on the condition of the material.

## A.15 Mechanical Properties of Selected Materials used in Rapid Prototyping.

Material	Tensile strength MPa	Elastic modulus GPa	Elongation in 50 mm (%)	Characteristics
<b>Stereolithography</b>				
Accura 60	68	3.10	5	Transparent; good general-purpose material for rapid prototyping
Somos 9920	9	1.81	15	Transparent amber; good chemical resistance; good fatigue properties; used for producing patterns in rubber molding
WaterClear Ultra	55	2.9	6–9	Optically clear resin with ABS-like properties
WaterShed 11122	53	2.5	15	Optically clear with a slight green tinge; mechanical properties similar to those of ABS; used for rapid tooling
DMX-SL 100	32	2.4	12–28	Opaque beige; good general-purpose material for rapid prototyping
<b>Polyjet</b>				
FC720	60	2.9	20	Transparent amber; good impact strength, good paint adsorption and machinability
FC830	50	2.49	20	White, blue, or black; good humidity resistance; suitable for general-purpose applications
FC 930	1.4	0.185	218	Semiopaque, gray, or black; highly flexible material used for prototyping of soft polymers or rubber
<b>Fused-deposition modeling</b>				
Polycarbonate	52	2.0	3	White; high-strength polymer suitable for rapid prototyping and general use
Ultem 9085	72	2.2	5.9	Opaque tan, high-strength FDM material, good flame, smoke and toxicity rating.
ABS-M30i	36	2.4	4	Available in multiple colors, most commonly white; a strong and durable material suitable for general use; biocompatible
PC	68	2.28	4.8	White; good combination of mechanical properties and heat resistance
<b>Selective laser sintering</b>				
WindForm XT	78	7.32	2.6	Opaque black polyimide and carbon; produces durable heat- and chemical-resistant parts; high wear resistance.
Polyamide PA 3200GF	45	3.3	6	White; glass-filled polyamide has increased stiffness and is suitable for higher temperature applications
SOMOS 201	–	0.015	110	Multiple colors available; mimics mechanical properties of rubber
ST-100c	305	137	10	Bronze-infiltrated steel powder
<b>Electron-beam melting</b>				
Ti-6Al-4V	970	120	12–16	Can be heat-treated by hot isostatic pressing to obtain up to 600 MPa fatigue strength

This page intentionally left blank



# Appendix B

## Stress-Strain Relationships

### Symbols

$C$	elastic material coefficients, Pa
$E$	modulus of elasticity, Pa
$G$	shear modulus, Pa
$K$	bulk modulus, Pa
$x, y, z$	Cartesian coordinate system, m
$x', y', z'$	rotated Cartesian coordinate system, m
$\gamma$	shear strain
$\delta$	deformation, m
$\epsilon$	normal strain
$\lambda$	Lame's constant, Pa
$\nu$	Poisson's ratio
$\sigma$	normal stress, Pa
$\tau$	shear stress, Pa

### Subscripts

$x, y, z$	Cartesian coordinates
$x', y', z'$	rotated Cartesian coordinates
1, 2, 3	principal axes

### B.1 Introduction

This Appendix presents selected equations of elasticity, including derivations and definitions of terms that are of importance to the design of structures and machine elements. The derivations in this Appendix are much more mathematical than typical treatment elsewhere in the book, with much less effort expended to explain approaches. It is hoped that the statement and rapid derivation of equations will suffice to demonstrate their existence; the interested reader is encouraged to find far more in-depth treatment in the classic text by Timoschenko and Goodier [1970], as well as any of the other Recommended Readings at the end of the Appendix.

This appendix presents the laws of stress transformation that are used in Chapter 2, the Generalized Hooke's Law in three dimensions, defines elastic constants by their proper names, and gives generalized equations for stress and strain.

### B.2 Laws of Stress Transformation

Let a new orthogonal coordinate system  $0'x'y'z'$  be placed having origin  $P$ , having the  $z'$  axis coincident with the normal  $n$  to the plane, and having the  $x'$  and  $y'$  axes (which must parallel the plane with normal  $n$ ) coincident with the desired shear stresses directions. Such a coordinate system is shown in Fig. B.1, where the plane  $ABC$  is imagined to pass through point  $P$ , since the tetrahedron is very small. Figure B.1 also shows the three mutually perpendicular stress components

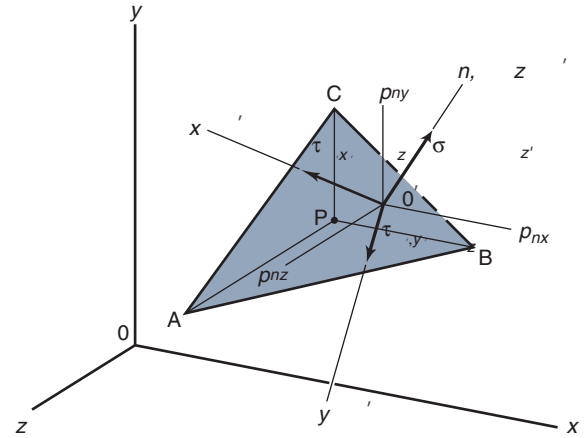


Figure B.1: Small tetrahedral element cut from body at point  $P$ . The three perpendicular stress components  $\sigma_{z'}$ ,  $\tau_{z'x'}$ , and  $\tau_{z'y'}$  acting on the inclined plane are shown.

$\sigma_{z'}$ ,  $\tau_{z'x'}$ , and  $\tau_{z'y'}$  acting on the inclined plane. The laws of stress transformation give these stresses in terms of  $\sigma_x$ ,  $\sigma_y$ ,  $\sigma_z$ ,  $\tau_{xy}$ ,  $\tau_{yz}$ , and  $\tau_{zx}$ . The previously established rules for shear stress subscripts are equally applicable here. For example,  $\tau_{z'x'}$  is the shear stress directed in the  $x'$  direction and acting in a plane through  $P$  whose normal is directed in the  $z'$  direction.

Because the normal direction coincides with the  $z'$  direction,

$$\begin{aligned} p_{nz} &= \sigma_z \cos(z', z) + \tau_{zx} \cos(z', x) + \tau_{yz} \cos(z', y) \\ p_{ny} &= \tau_{zx} \cos(z', z) + \sigma_x \cos(z', x) + \tau_{yx} \cos(z', y) \\ p_{nx} &= \tau_{zy} \cos(z', z) + \tau_{xy} \cos(z', x) + \sigma_y \cos(z', y) \end{aligned} \quad (B.1)$$

where

$$\cos(z', x) = \text{cosine of angle between } z' \text{ and } x$$

The stress  $\sigma_{z'}$  must equal the sum of the projections of  $p_{nz}$ ,  $p_{ny}$ , and  $p_{nx}$  onto the  $z'$  axis,

$$\sigma_{z'} = p_{nz} \cos(z', z) + p_{nx} \cos(z', x) + p_{ny} \cos(z', y) \quad (B.2)$$

Similarly,

$$\tau_{z'x'} = p_{nz} \cos(x', z) + p_{nx} \cos(x', x) + p_{ny} \cos(x', y) \quad (B.3)$$

By substituting Eqs. (B.1) into Eqs. (B.2) and (B.3) while also making use of the fact developed earlier that the shear

stresses are symmetrical (e.g.,  $\tau_{x'y'} = \tau_{y'x'}$ ), Eqs. (B.4) and (B.5) can be developed. Equations (B.6) to (B.9) can be derived in an entirely similar way by using two more tetrahedrons with inclined planes having outer normals parallel to the  $x'$  and  $y'$  axes. The result of all of the above is

$$\begin{aligned}\sigma_{z'} &= \sigma_z \cos^2(z', z) + \sigma_x \cos^2(z', x) + \sigma_y \cos^2(z', y) \\ &\quad + 2\tau_{zx} \cos(z', z) \cos(z', x) \\ &\quad + 2\tau_{xy} \cos(z', x) \cos(z', y) \\ &\quad + 2\tau_{yz} \cos(z', y) \cos(z', z)\end{aligned}\quad (\text{B.4})$$

$$\begin{aligned}\sigma_{x'} &= \sigma_x \cos^2(x', x) + \sigma_y \cos^2(x', y) + \sigma_z \cos^2(x', z) \\ &\quad + 2\tau_{xy} \cos(x', x) \cos(x', y) \\ &\quad + 2\tau_{xy} \cos(x', y) \cos(x', z) \\ &\quad + 2\tau_{zx} \cos(x', z) \cos(x', x)\end{aligned}\quad (\text{B.5})$$

$$\begin{aligned}\sigma_{y'} &= \sigma_y \cos^2(y', y) + \sigma_z \cos^2(y', z) + \sigma_x \cos^2(y', x) \\ &\quad + 2\tau_{yz} \cos(y', y) \cos(y', z) \\ &\quad + 2\tau_{zx} \cos(y', z) \cos(y', x) \\ &\quad + 2\tau_{xy} \cos(y', x) \cos(y', y)\end{aligned}\quad (\text{B.6})$$

$$\begin{aligned}\tau_{z'x'} &= \sigma_z \cos(z', z) \cos(x', z) + \sigma_x \cos(z', x) \cos(x', x) \\ &\quad + \sigma_y \cos(z', y) \cos(x', y) \\ &\quad + \tau_{zx} [\cos(z', z) \cos(x', x) + \cos(z', x) \cos(x', z)] \\ &\quad + \tau_{xy} [\cos(z', x) \cos(x', y) + \cos(z', y) \cos(x', x)] \\ &\quad + \tau_{yz} [\cos(z', y) \cos(x', z) + \cos(z', z) \cos(x', y)]\end{aligned}\quad (\text{B.7})$$

$$\begin{aligned}\tau_{x'y'} &= \sigma_x \cos(x', x) \cos(y', x) + \sigma_y \cos(x', y) \cos(y', y) \\ &\quad + \sigma_z \cos(x', z) \cos(y', z) \\ &\quad + \tau_{xy} [\cos(x', x) \cos(y', y) + \cos(x', y) \cos(y', x)] \\ &\quad + \tau_{yz} [\cos(x', y) \cos(y', z) + \cos(x', z) \cos(y', y)] \\ &\quad + \tau_{zx} [\cos(x', z) \cos(y', x) + \cos(x', x) \cos(y', z)]\end{aligned}\quad (\text{B.8})$$

$$\begin{aligned}\tau_{y'z'} &= \sigma_y \cos(y', y) \cos(z', y) + \sigma_z \cos(y', z) \cos(z', z) \\ &\quad + \sigma_x \cos(y', x) \cos(z', x) \\ &\quad + \tau_{yz} [\cos(y', y) \cos(z', z) + \cos(y', z) \cos(z', y)] \\ &\quad + \tau_{zx} [\cos(y', z) \cos(z', x) + \cos(y', x) \cos(z', z)] \\ &\quad + \tau_{xy} [\cos(y', x) \cos(z', y) + \cos(y', y) \cos(z', x)]\end{aligned}\quad (\text{B.9})$$

It is important to recognize the meaning of these equations. For example, Eq. (B.7) can be used to find the shear stress acting in the  $x'$  direction on a surface having an outer normal directed in the  $z'$  direction if the six Cartesian stress components  $\sigma_x, \sigma_y, \sigma_z, \tau_{xy}, \tau_{yz}$ , and  $\tau_{zx}$  at the point and the orientation of the coordinate system  $0x'y'z'$  are known.

### B.3 Laws of Strain Transformation

In the study of stresses we found that three normal stresses  $\sigma_x, \sigma_y$ , and  $\sigma_z$  and three shear stresses  $\tau_{xy}, \tau_{yz}$ , and  $\tau_{zx}$  act on planes parallel to the Cartesian planes. Similarly, three

normal strains  $\epsilon_x, \epsilon_y$ , and  $\epsilon_z$  and three shear strains  $\gamma_{xy}, \gamma_{yz}$ , and  $\gamma_{zx}$  characterize the behavior of line segments originally parallel to the Cartesian axes. From Durelli et al. (1958) the laws of strain transformation can be written directly from the laws of stress transformation given in Eqs. (B.4) to (B.9) if the following replacements are made to these equations:

$$\begin{aligned}\sigma_x &\leftarrow \epsilon_x, & \sigma_y &\leftarrow \epsilon_y, & \sigma_z &\leftarrow \epsilon_z, & 2\tau_{xy} &\leftarrow \gamma_{xy}, \\ 2\tau_{yz} &\leftarrow \gamma_{yz}, & 2\tau_{zx} &\leftarrow \gamma_{zx}\end{aligned}\quad (\text{B.10})$$

### B.4 Hooke's Law Generalized

What is the relationship between stresses and strains when the stress system is not in simple tension or compression as in Eq. (3.22)? The stress system can be defined by the six components  $\sigma_x, \sigma_y, \sigma_z, \tau_{xy}, \tau_{yz}$ , and  $\tau_{zx}$ ; and the strain system, by the six components  $\epsilon_x, \epsilon_y, \epsilon_z, \gamma_{xy}, \gamma_{yz}$ , and  $\gamma_{zx}$ . Thus, a generalization of Hooke's law is to make each stress component a linear function of the strain components or

$$\begin{aligned}\sigma_x &= C_{11}\epsilon_x + C_{12}\epsilon_y + C_{13}\epsilon_z + C_{14}\gamma_{xy} \\ &\quad + C_{15}\gamma_{yz} + C_{16}\gamma_{zx} \\ \sigma_y &= C_{21}\epsilon_x + C_{22}\epsilon_y + C_{23}\epsilon_z + C_{24}\gamma_{xy} \\ &\quad + C_{25}\gamma_{yz} + C_{26}\gamma_{zx} \\ \dots & \\ \dots & \\ \dots & \\ \tau_{zx} &= C_{61}\epsilon_x + C_{62}\epsilon_y + C_{63}\epsilon_z + C_{64}\gamma_{xy} \\ &\quad + C_{65}\gamma_{yz} + C_{66}\gamma_{zx}\end{aligned}\quad (\text{B.11})$$

where  $C_{11}, C_{12}, \dots, C_{66}$  = elastic material coefficients independent of stress or strain. Equation (B.11) is valid for many hard materials over a strain range of practical interest in designing machine elements.

The assumption of an isotropic material implies that the stress and strain components referred to a coordinate system  $0x'y'z'$  of any arbitrary orientation must be related by the same elastic material coefficients  $C_{11}, C_{12}, \dots, C_{66}$ . Thus, the six Eqs. (B.11) imply that the subscripts change,  $x \rightarrow x', y \rightarrow y'$ , and  $z \rightarrow z'$ , while the constants  $C_{11}, C_{12}, \dots, C_{66}$  remain the same. Thus,

$$\begin{aligned}\sigma_{x'} &= C_{11}\epsilon_{x'} + C_{12}\epsilon_{y'} + C_{13}\epsilon_{z'} + C_{14}\gamma_{x'y'} \\ &\quad + C_{15}\gamma_{y'z'} + C_{16}\gamma_{z'x'} \\ \sigma_{y'} &= C_{21}\epsilon_{x'} + C_{22}\epsilon_{y'} + C_{23}\epsilon_{z'} + C_{24}\gamma_{x'y'} \\ &\quad + C_{25}\gamma_{y'z'} + C_{26}\gamma_{z'x'} \\ \dots & \\ \dots & \\ \dots & \\ \tau_{z'x'} &= C_{61}\epsilon_{x'} + C_{62}\epsilon_{y'} + C_{63}\epsilon_{z'} + C_{64}\gamma_{x'y'} \\ &\quad + C_{65}\gamma_{y'z'} + C_{66}\gamma_{z'x'}\end{aligned}\quad (\text{B.12})$$

Recall that  $0x'y'z'$  is an arbitrary coordinate system.

First, obtaining a new coordinate system  $0x'y'z'$  by rotating  $0z$  through a  $180^\circ$  angle results in Fig. B.2. Recall that

$(x, y)$  = Angle between  $x$  and  $y$

From Fig. B.2 and the above notation

$$\begin{aligned}(x', x) &= 180^\circ, & (x', y) &= 90^\circ, & (x', z) &= 90^\circ \\ (y', y) &= 180^\circ, & (y', z) &= 90^\circ, & (y', x) &= 90^\circ \\ (z', z) &= 0^\circ, & (z', x) &= 90^\circ, & (z', y) &= 90^\circ\end{aligned}\quad (\text{B.13})$$

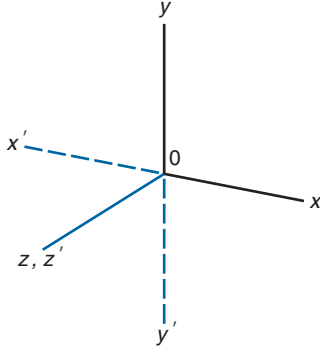


Figure B.2: Coordinate system  $0x'y'z'$  obtained by rotating  $0xz$  by  $180^\circ$ .

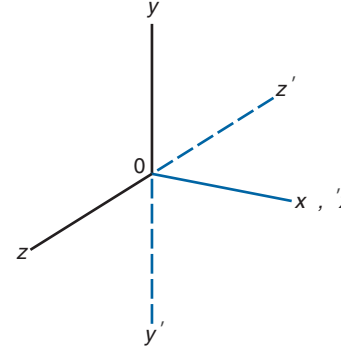


Figure B.3: Coordinate system  $0x'y'z'$  obtained by rotating  $0xz$  by  $180^\circ$ .

Making use of Eq. (B.13) reduces Eqs. (B.4) to (B.9) to

$$\begin{aligned}\sigma_{z'} &= \sigma_z, & \sigma_{x'} &= \sigma_x, & \sigma_{y'} &= \sigma_y, & \tau_{x'y'} &= \tau_{xy}, \\ \tau_{y'z'} &= -\tau_{yz}, & \tau_{z'x'} &= -\tau_{zx}\end{aligned}\quad (\text{B.14})$$

Similarly, for the strains

$$\begin{aligned}\epsilon_{z'} &= \epsilon_z, & \epsilon_{x'} &= \epsilon_x, & \epsilon_{y'} &= \epsilon_y, & \gamma_{x'y'} &= \gamma_{xy}, \\ \gamma_{y'z'} &= -\gamma_{yz}, & \gamma_{z'x'} &= -\gamma_{zx}\end{aligned}\quad (\text{B.15})$$

Substituting Eqs. (B.14) and (B.15) into Eq. (B.12) gives

$$\begin{aligned}\sigma_{x'} &= C_{11}\epsilon_x + C_{12}\epsilon_y + C_{13}\epsilon_z + C_{14}\gamma_{xy} \\ &\quad - C_{15}\gamma_{yz} - C_{16}\gamma_{zx} \\ \sigma_y &= C_{21}\epsilon_x + C_{22}\epsilon_y + C_{23}\epsilon_z + C_{24}\gamma_{xy} \\ &\quad - C_{25}\gamma_{yz} - C_{26}\gamma_{zx} \\ \dots & \\ \dots & \\ \dots & \\ \tau_{z'x'} &= -C_{61}\epsilon_x - C_{62}\epsilon_y - C_{63}\epsilon_z - C_{64}\gamma_{xy} \\ &\quad + C_{65}\gamma_{yz} + C_{66}\gamma_{zx}\end{aligned}\quad (\text{B.16})$$

Comparing Eqs. (B.11) and (B.16) shows that

$$C_{15} = -C_{15} \quad C_{16} = -C_{16}$$

implying that

$$\begin{aligned}C_{15} &= C_{16} = C_{25} = C_{26} = C_{35} = C_{36} = C_{45} = C_{46} = 0 \\ C_{51} &= C_{52} = C_{53} = C_{54} = C_{61} = C_{62} = C_{63} = C_{64} = 0\end{aligned}\quad (\text{B.17})$$

Substituting Eqs. (B.17) into Eqs. (B.11) gives

$$\begin{aligned}\sigma_x &= C_{11}\epsilon_x + C_{12}\epsilon_y + C_{13}\epsilon_z + C_{14}\gamma_{xy} \\ \sigma_y &= C_{21}\epsilon_x + C_{22}\epsilon_y + C_{23}\epsilon_z + C_{24}\gamma_{xy} \\ \sigma_z &= C_{31}\epsilon_x + C_{32}\epsilon_y + C_{33}\epsilon_z + C_{34}\gamma_{xy} \\ \tau_{xy} &= C_{41}\epsilon_x + C_{42}\epsilon_y + C_{43}\epsilon_z + C_{44}\gamma_{xy} \\ \tau_{yz} &= C_{55}\gamma_{yz} + C_{56}\gamma_{zx} \\ \tau_{zx} &= C_{65}\gamma_{yz} + C_{66}\gamma_{zx}\end{aligned}\quad (\text{B.18})$$

Thus, using the coordinate system of Fig. B.2 with the isotropic assumption reduces the 36 elastic material constants of Eqs. (B.11) to the 20 expressed in Eqs. (B.18).

Obtaining a new coordinate system by rotating  $0xz$  through a  $180^\circ$  angle results in Fig. B.3, giving

$$\begin{aligned}(x', x) &= 0^\circ, & (x', y) &= 90^\circ, & (z', z) &= 90^\circ \\ (y', y) &= 180^\circ, & (y', x) &= 90^\circ, & (y', z) &= 90^\circ \\ (z', z) &= 180^\circ, & (z', x) &= 90^\circ, & (z', y) &= 90^\circ\end{aligned}\quad (\text{B.19})$$

Making use of Eqs. (B.19) reduces Eqs. (B.4) to (B.9) to

$$\begin{aligned}\sigma_{z'} &= \sigma_z, & \sigma_{x'} &= \sigma_x, & \sigma_{y'} &= \sigma_y \\ \tau_{z'x'} &= -\tau_{zx}, & \tau_{x'y'} &= -\tau_{xy}, & \tau_{y'z'} &= \tau_{yz} \\ \epsilon_{x'} &= \epsilon_x, & \epsilon_{y'} &= \epsilon_y, & \epsilon_{z'} &= \epsilon_z \\ \gamma_{x'y'} &= -\gamma_{xy}, & \gamma_{y'z'} &= \gamma_{yz}, & \gamma_{z'x'} &= -\gamma_{zx}\end{aligned}\quad (\text{B.20})$$

The assumption of an isotropic material requires that the new coordinate system  $0x'y'z'$  shown in Fig. B.3 must be related to the same elastic material constants  $C_{11}, C_{12}, \dots, C_{66}$  expressed in Eqs. (B.18), implying that

$$\begin{aligned}\sigma_{x'} &= C_{11}\epsilon_{x'} + C_{12}\epsilon_{y'} + C_{13}\epsilon_{z'} + C_{14}\gamma_{x'y'} \\ \sigma_{y'} &= C_{21}\epsilon_{x'} + C_{22}\epsilon_{y'} + C_{23}\epsilon_{z'} + C_{24}\gamma_{x'y'} \\ \sigma_{z'} &= C_{31}\epsilon_{x'} + C_{32}\epsilon_{y'} + C_{33}\epsilon_{z'} + C_{34}\gamma_{x'y'} \\ \tau_{x'y'} &= C_{41}\epsilon_{x'} + C_{42}\epsilon_{y'} + C_{43}\epsilon_{z'} + C_{44}\gamma_{x'y'} \\ \tau_{y'z'} &= C_{55}\gamma_{y'z'} + C_{56}\gamma_{z'x'} \\ \tau_{z'x'} &= C_{65}\gamma_{y'z'} + C_{66}\gamma_{z'x'}\end{aligned}\quad (\text{B.21})$$

Substituting Eqs. (B.20) into Eqs. (B.21) gives

$$\begin{aligned}\sigma_x &= C_{11}\epsilon_x + C_{12}\epsilon_y + C_{13}\epsilon_z - C_{14}\gamma_{xy} \\ \sigma_y &= C_{21}\epsilon_x + C_{22}\epsilon_y + C_{23}\epsilon_z - C_{24}\gamma_{xy} \\ \sigma_z &= C_{31}\epsilon_x + C_{32}\epsilon_y + C_{33}\epsilon_z - C_{34}\gamma_{xy} \\ -\tau_{xy} &= C_{41}\epsilon_x + C_{42}\epsilon_y + C_{43}\epsilon_z - C_{44}\gamma_{xy} \\ \tau_{yz} &= C_{55}\gamma_{yz} - C_{56}\gamma_{zx} \\ -\tau_{zx} &= C_{65}\gamma_{yz} - C_{66}\gamma_{zx}\end{aligned}\quad (\text{B.22})$$

Equations (B.18) and (B.22) will agree only if

$$C_{14} = C_{24} = C_{34} = C_{41} = C_{42} = C_{43} = C_{56} = C_{65} = 0\quad (\text{B.23})$$

Substituting Eqs. (B.13) into Eqs. (B.8) gives

$$\begin{aligned}\sigma_x &= C_{11}\epsilon_x + C_{12}\epsilon_y + C_{13}\epsilon_z \\ \sigma_y &= C_{21}\epsilon_x + C_{22}\epsilon_y + C_{23}\epsilon_z \\ \sigma_z &= C_{31}\epsilon_x + C_{32}\epsilon_y + C_{33}\epsilon_z \\ \tau_{xy} &= C_{44}\gamma_{xy} \\ \tau_{yz} &= C_{55}\gamma_{yz} \\ \tau_{zx} &= C_{66}\gamma_{zx}\end{aligned}\quad (\text{B.24})$$

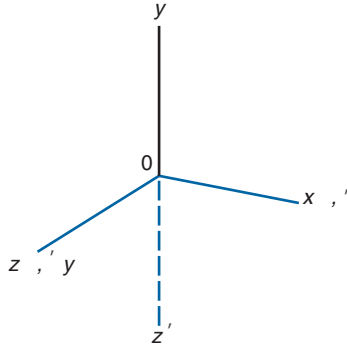


Figure B.4: Coordinate system  $0x'y'z'$  obtained by rotating  $0x$  by  $90^\circ$ .

Thus, using the coordinate system of Fig. B.3 with the isotropic assumption reduces the 20 elastic material constants of Eqs. (B.18) to the 12 expressed in Eqs. (B.24).

Third, rotating  $0x$  through a  $90^\circ$  angle results in Fig. B.4, implying that

$$\begin{aligned} (x', x) &= 0^\circ, & (x', y) &= 90^\circ, & (x', z) &= 90^\circ \\ (y', y) &= 90^\circ, & (y', x) &= 90^\circ, & (y', z) &= 0^\circ \\ (z', z) &= 90^\circ, & (z', x) &= 90^\circ, & (z', y) &= 180^\circ \end{aligned} \quad (\text{B.25})$$

Making use of Eqs. (B.25) reduces Eqs. (B.4) to (B.9) and Eq. (2.37) to

$$\begin{aligned} \sigma_{z'} &= \sigma_y, & \sigma_{x'} &= \sigma_x, & \sigma_{y'} &= \sigma_z \\ \tau_{z'x'} &= -\tau_{xy}, & \tau_{x'y'} &= \tau_{zx}, & \tau_{y'z'} &= -\tau_{yz} \\ \epsilon_{z'} &= \epsilon_y, & \epsilon_{x'} &= \epsilon_x, & \epsilon_{y'} &= \epsilon_z \\ \gamma_{z'x'} &= -\gamma_{xy}, & \gamma_{x'y'} &= \gamma_{zx}, & \gamma_{y'z'} &= -\gamma_{yz} \end{aligned} \quad (\text{B.26})$$

The assumption of an isotropic material requires that the new coordinate system  $0x'y'z'$  shown in Fig. B.4 must be related to the same elastic material constants expressed in Eqs. (B.24), implying that

$$\begin{aligned} \sigma_{x'} &= C_{11}\epsilon_{x'} + C_{12}\epsilon_{y'} + C_{13}\epsilon_{z'} \\ \sigma_{y'} &= C_{21}\epsilon_{x'} + C_{22}\epsilon_{y'} + C_{23}\epsilon_{z'} \\ \sigma_{z'} &= C_{31}\epsilon_{x'} + C_{32}\epsilon_{y'} + C_{33}\epsilon_{z'} \\ \tau_{x'y'} &= C_{44}\gamma_{x'y'} \\ \tau_{y'z'} &= C_{55}\gamma_{y'z'} \\ \tau_{z'x'} &= C_{66}\gamma_{z'x'} \end{aligned} \quad (\text{B.27})$$

Substituting Eqs. (B.26) into Eqs. (B.27) gives

$$\begin{aligned} \sigma_x &= C_{11}\epsilon_x + C_{12}\epsilon_y + C_{13}\epsilon_z \\ \sigma_y &= C_{21}\epsilon_x + C_{22}\epsilon_y + C_{23}\epsilon_z \\ \sigma_z &= C_{31}\epsilon_x + C_{32}\epsilon_y + C_{33}\epsilon_z \\ \tau_{xy} &= C_{44}\gamma_{xy} \\ \tau_{yz} &= C_{55}\gamma_{yz} \\ \tau_{zx} &= C_{66}\gamma_{zx} \end{aligned} \quad (\text{B.28})$$

Equations (B.24) and (B.28) will agree only if

$$\begin{aligned} C_{12} &= C_{13} & C_{21} &= C_{31} & C_{23} &= C_{32} \\ C_{22} &= C_{33} & C_{44} &= C_{66} \end{aligned} \quad (\text{B.29})$$

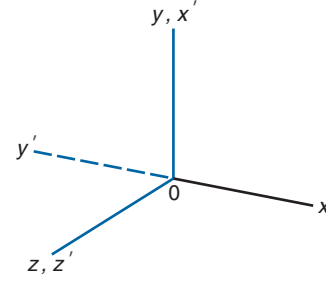


Figure B.5: Coordinate system  $0x'y'z'$  obtained by rotating  $0z$  by  $90^\circ$ .

Substituting Eqs. (B.29) into Eqs. (B.28) gives

$$\begin{aligned} \sigma_x &= C_{11}\epsilon_x + C_{12}(\epsilon_y + \epsilon_z) \\ \sigma_y &= C_{21}\epsilon_x + C_{22}\epsilon_y + C_{23}\epsilon_z \\ \sigma_z &= C_{21}\epsilon_x + C_{22}\epsilon_z + C_{23}\epsilon_y \\ \tau_{xy} &= C_{44}\gamma_{xy} \\ \tau_{yz} &= C_{55}\gamma_{yz} \\ \tau_{zx} &= C_{66}\gamma_{zx} \end{aligned} \quad (\text{B.30})$$

Thus, using the coordinate system of Fig. B.4 with the isotropic assumption reduces the 12 elastic material constants of Eqs. (B.24) to the 7 expressed in Eqs. (B.30).

Fourth, rotating  $0z$  through a  $90^\circ$  angle results in Fig. B.5, giving

$$\begin{aligned} (x', x) &= 90^\circ, & (x', y) &= 0^\circ, & (x', z) &= 90^\circ \\ (y', y) &= 90^\circ, & (y', x) &= 180^\circ, & (y', z) &= 90^\circ \\ (z', z) &= 0^\circ, & (z', x) &= 90^\circ, & (z', y) &= 90^\circ \end{aligned} \quad (\text{B.31})$$

Making use of Eqs. (B.31) reduces Eqs. (B.4) to (B.9) and Eq. (2.37) to

$$\begin{aligned} \sigma_{z'} &= \sigma_z, & \sigma_{x'} &= \sigma_y, & \sigma_{y'} &= \sigma_x \\ \tau_{z'x'} &= \tau_{yz}, & \tau_{x'y'} &= -\tau_{xy}, & \tau_{y'z'} &= -\tau_{zx} \\ \epsilon_{z'} &= \epsilon_z, & \epsilon_{x'} &= \epsilon_y, & \epsilon_{y'} &= \epsilon_x \\ \gamma_{z'x'} &= \gamma_{yz}, & \gamma_{x'y'} &= -\gamma_{xy}, & \gamma_{y'z'} &= -\gamma_{zx} \end{aligned} \quad (\text{B.32})$$

The assumption of an isotropic material requires that Eqs. (B.30) be written as

$$\begin{aligned} \sigma_{x'} &= C_{11}\epsilon_{x'} + C_{12}(\epsilon_{y'} + \epsilon_{z'}) \\ \sigma_{y'} &= C_{21}\epsilon_{x'} + C_{22}\epsilon_{y'} + C_{23}\epsilon_{z'} \\ \sigma_{z'} &= C_{21}\epsilon_{x'} + C_{22}\epsilon_{z'} + C_{23}\epsilon_{y'} \\ \tau_{x'y'} &= C_{44}\gamma_{x'y'} \\ \tau_{y'z'} &= C_{55}\gamma_{y'z'} \\ \tau_{z'x'} &= C_{66}\gamma_{z'x'} \end{aligned} \quad (\text{B.33})$$

Substituting Eqs. (B.32) into Eqs. (B.33) gives

$$\begin{aligned} \sigma_x &= C_{11}\epsilon_y + C_{12}(\epsilon_x + \epsilon_z) \\ \sigma_y &= C_{21}\epsilon_y + C_{22}\epsilon_x + C_{23}\epsilon_z \\ \sigma_z &= C_{21}\epsilon_y + C_{22}\epsilon_z + C_{23}\epsilon_x \\ \tau_{xy} &= C_{44}\gamma_{xy} \\ \tau_{yz} &= C_{55}\gamma_{yz} \\ \tau_{zx} &= C_{66}\gamma_{zx} \end{aligned} \quad (\text{B.34})$$

Equations (B.30) and (B.34) will agree only if

$$C_{22} = C_{11} \quad C_{21} = C_{12} \quad C_{23} = C_{12} \quad C_{55} = C_{44} \quad (\text{B.35})$$

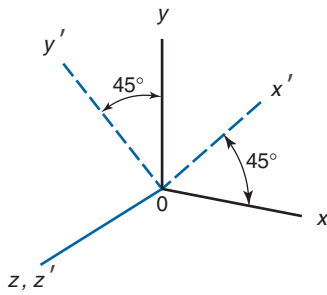


Figure B.6: Coordinate system  $0x'y'z'$  obtained by rotating  $0z$  by  $45^\circ$ .

Substituting Eqs. (B.37) into Eqs. (B.34) gives

$$\begin{aligned}\sigma_x &= C_{11}\epsilon_x + C_{12}(\epsilon_y + \epsilon_z) \\ \sigma_y &= C_{11}\epsilon_y + C_{12}(\epsilon_x + \epsilon_z) \\ \sigma_z &= C_{11}\epsilon_z + C_{12}(\epsilon_x + \epsilon_y) \\ \tau_{xy} &= C_{44}\gamma_{xy} \\ \tau_{yz} &= C_{55}\gamma_{yz} \\ \tau_{zx} &= C_{66}\gamma_{zx}\end{aligned}\quad (\text{B.36})$$

Thus, using the coordinate system of Fig. B.5 with the isotropic assumption reduces the seven elastic material constants of Eqs. (B.30) to the three expressed in Eqs. (B.36).

Fifth and finally, rotating  $0z$  through a  $45^\circ$  angle results in Fig. B.6, implying that

$$\begin{aligned}(x', x) &= 45^\circ, & (x', y) &= 45^\circ, & (x', z) &= 90^\circ \\ (y', y) &= 45^\circ, & (y', x) &= 135^\circ, & (y', z) &= 90^\circ \\ (z', z) &= 0^\circ, & (z', x) &= 90^\circ, & (z', y) &= 90^\circ\end{aligned}\quad (\text{B.37})$$

Making use of Eqs. (B.37) reduces Eqs. (B.4) to (B.9) and Eq. (2.37) to

$$\begin{aligned}\sigma_{z'} &= \sigma_z, \\ \sigma_{x'} &= \frac{1}{2}(\sigma_x + \sigma_y) + \tau_{xy}, \\ \sigma_{y'} &= \frac{1}{2}(\sigma_x + \sigma_y) - \tau_{xy}, \\ \tau_{z'x'} &= \frac{1}{\sqrt{2}}(\tau_{zx} + \tau_{yz}), \\ \tau_{x'y'} &= \frac{1}{2}(\sigma_y - \sigma_x), \\ \tau_{y'z'} &= \frac{1}{\sqrt{2}}(\tau_{yz} - \tau_{zx}), \\ \epsilon_{z'} &= \epsilon_z, \\ \epsilon_{x'} &= \frac{1}{2}(\epsilon_x + \epsilon_y + \gamma_{xy}), \\ \epsilon_{y'} &= \frac{1}{2}(\epsilon_x + \epsilon_y - \gamma_{xy}), \\ \gamma_{z'x'} &= \frac{1}{\sqrt{2}}(\gamma_{zx} + \gamma_{yz}), \\ \gamma_{x'y'} &= \frac{1}{2}(\epsilon_y - \epsilon_x), \\ \gamma_{y'z'} &= \frac{1}{\sqrt{2}}(\gamma_{yz} - \gamma_{zx})\end{aligned}\quad (\text{B.38})$$

The assumption of an isotropic material requires that Eqs. (B.37) be written as

$$\begin{aligned}\sigma_{x'} &= C_{11}\epsilon_{x'} + C_{12}(\epsilon_{y'} + \epsilon_{z'}) \\ \sigma_{y'} &= C_{11}\epsilon_{y'} + C_{12}(\epsilon_{x'} + \epsilon_{z'}) \\ \sigma_{z'} &= C_{11}\epsilon_{z'} + C_{12}(\epsilon_{x'} + \epsilon_{y'}) \\ \tau_{x'y'} &= C_{44}\gamma_{x'y'} \\ \tau_{y'z'} &= C_{55}\gamma_{y'z'} \\ \tau_{z'x'} &= C_{66}\gamma_{z'x'}\end{aligned}\quad (\text{B.39})$$

Substituting Eqs. (B.38) into the first of Eqs. (B.39) gives

$$\begin{aligned}\frac{1}{2}(\sigma_x + \sigma_y) + \tau_{xy} &= C_{11}\left(\frac{\gamma_{xy}}{2} + \frac{\epsilon_x + \epsilon_y}{2}\right) \\ &+ C_{12}\left(\frac{\epsilon_x + \epsilon_y}{2} - \frac{\gamma_{xy}}{2} + \epsilon_z\right)\end{aligned}$$

and substituting the expressions for  $\sigma_x$  and  $\sigma_y$  in Eqs. (B.36) into the above equation gives

$$\tau_{xy} = (C_{11} - C_{12})\frac{\gamma_{xy}}{2}\quad (\text{B.40})$$

Comparing Eq. (B.40) with the  $\tau_{xy}$  expression in Eqs. (B.36) gives

$$C_{11} = C_{12} + 2C_{44}\quad (\text{B.41})$$

Letting  $C_{12} = \lambda$  and  $C_{44} = G$  and making use of Eq. (B.41) gives Eqs. (B.36) as

$$\begin{aligned}\sigma_x &= (\lambda + 2G)\epsilon_x + \lambda(\epsilon_y + \epsilon_z) \\ \sigma_y &= (\lambda + 2G)\epsilon_y + \lambda(\epsilon_x + \epsilon_z) \\ \sigma_z &= (\lambda + 2G)\epsilon_z + \lambda(\epsilon_x + \epsilon_y) \\ \tau_{xy} &= G\gamma_{xy} \\ \tau_{yz} &= G\gamma_{yz} \\ \tau_{zx} &= G\gamma_{zx}\end{aligned}\quad (\text{B.42})$$

Thus, using Fig. B.6 with the isotropic assumption reduces the number of elastic material constants from the 36 expressed in Eqs. (B.11) to the 2 expressed in Eqs. (B.42).

Equation (B.42) can be solved for strains to give

$$\begin{aligned}\epsilon_x &= \frac{(\lambda + G)\sigma_x}{G(3\lambda + 2G)} - \frac{\lambda(\sigma_y + \sigma_z)}{2G(3\lambda + 2G)} \\ \epsilon_y &= \frac{(\lambda + G)\sigma_y}{G(3\lambda + 2G)} - \frac{\lambda(\sigma_x + \sigma_z)}{2G(3\lambda + 2G)} \\ \epsilon_z &= \frac{(\lambda + G)\sigma_z}{G(3\lambda + 2G)} - \frac{\lambda(\sigma_x + \sigma_y)}{2G(3\lambda + 2G)} \\ \gamma_{xy} &= \frac{\tau_{xy}}{G} \\ \gamma_{yz} &= \frac{\tau_{yz}}{G} \\ \gamma_{zx} &= \frac{\tau_{zx}}{G}\end{aligned}\quad (\text{B.43})$$

For isotropic but *nonhomogeneous* materials the constants  $\lambda$  and  $G$  are functions of the space coordinates  $x$ ,  $y$ , and  $z$  and vary from point to point. For isotropic and homogeneous materials these constants are not functions of the space coordinates and do not vary from point to point. They depend only on the particular material.

If the  $0x$ ,  $0y$ , and  $0z$  axes are chosen along the principal axes of stress,  $\tau_{xy} = \tau_{yz} = \tau_{zx} = 0$ . From Eqs. (B.43) it follows that  $\gamma_{xy} = \gamma_{yz} = \gamma_{zx} = 0$ . Thus, for isotropic materials the principal axes of stress and strain coincide.



## B.5 Physical Significance of Elastic Material Constants

The first elastic material constant is shear modulus, or modulus of rigidity,  $G$  in pascals. The second elastic material constant  $\lambda$ , known as Lamé's constant, is of no particular physical significance.

In a uniaxial stress state where  $\sigma_y = \sigma_z = \tau_{xy} = \tau_{yz} = \tau_{zx} = 0$  and  $\sigma_x$  is the applied uniaxial stress, Eqs. (B.43) give

$$\epsilon_x = \frac{(\lambda + G)\sigma_x}{G(3\lambda + 2G)} \quad (\text{B.44})$$

$$\epsilon_y = \epsilon_z = -\frac{\lambda\sigma_x}{2G(3\lambda + 2G)} \quad (\text{B.45})$$

Comparing Eq. (B.44) with Eq. (3.23) gives

$$\lambda = \frac{G(E - 2G)}{3G - E} \quad (\text{B.46})$$

where  $E$  = modulus of elasticity, the third elastic material constant, covered in Sec. 3.5.2. Relating the transverse strain in Eq. (B.45) to Poisson's ratio in Eq. (3.4) gives

$$\nu = \frac{\lambda}{2(\lambda + G)} \quad (\text{B.47})$$

or solving for  $\lambda$

$$\lambda = \frac{2G\nu}{1 - 2\nu} \quad (\text{B.48})$$

Thus, Eqs. (B.46) and (B.48) express  $\lambda$  in terms of two known elastic material constants. Equating Eqs. (B.46) and (B.48) gives

$$\nu = \frac{E - 2G}{2G} \quad (\text{B.49})$$

where Poisson's ratio  $\nu$  is the fourth elastic material constant. Equation (B.49) is equivalent to Eq. (3.6). The range of  $\lambda$  is between zero and 0.5. At  $\nu = 0$  no transverse deformation, but rather longitudinal deformation, occurs. At  $\nu = 0.5$  the material exhibits constant volume. The volume increase longitudinally is the same as the shrinkage in the transverse direction.

Besides the four elastic material constants  $G$ ,  $\lambda$ ,  $E$ , and  $\nu$  a fifth is provided by bulk modulus  $K$ , the ratio of applied hydrostatic pressure to observed volume shrinkage per unit volume, which is in pascals (pounds per square inch). The bulk modulus is obtained from hydrostatic compression or when

$$\sigma_x = \sigma_y = \sigma_z = -p \quad \text{for } p > 0$$

$$\tau_{xy} = \tau_{yz} = \tau_{zx} = 0$$

Substituting the above into Eqs. (B.43) gives

$$\epsilon_x = \epsilon_y = \epsilon_z = -\frac{p}{3\lambda + 2G} \quad (\text{B.50})$$

But the total strain is

$$\epsilon = \epsilon_x + \epsilon_y + \epsilon_z \rightarrow p = -\frac{(3\lambda + 2G)\epsilon}{3} = -K\epsilon \quad (\text{B.51})$$

where

$$K = \frac{3\lambda + 2G}{3} \quad (\text{B.52})$$

It is possible to express any of the elastic material constants ( $G$ ,  $\lambda$ ,  $E$ ,  $\nu$ , and  $K$ ) if two of these five constants are given. These relationships are expressed in Table B.1.

## B.6 Stress-Strain Equations in Terms of Modulus of Elasticity and Poisson's Ratio

From Table B.1,  $\lambda$  and  $G$  can be expressed in terms of  $E$  and  $\nu$  as

$$\lambda = \frac{\nu E}{(1 + \nu)(1 - 2\nu)} \quad \text{and} \quad G = \frac{E}{2(1 + \nu)} \quad (\text{B.53})$$

Substituting Eqs. (B.53) into Eqs. (B.43) gives

$$\begin{aligned} \epsilon_x &= \frac{1}{E} [\sigma_x - \nu(\sigma_y + \sigma_z)] \\ \epsilon_y &= \frac{1}{E} [\sigma_y - \nu(\sigma_z + \sigma_x)] \\ \epsilon_z &= \frac{1}{E} [\sigma_z - \nu(\sigma_x + \sigma_y)] \\ \gamma_{xy} &= \frac{2(1 + \nu)}{E} \tau_{xy} \\ \gamma_{yz} &= \frac{2(1 + \nu)}{E} \tau_{yz} \\ \gamma_{zx} &= \frac{2(1 + \nu)}{E} \tau_{zx} \end{aligned} \quad (\text{B.54})$$

Similarly, the stress components can be expressed in terms of strains as

$$\begin{aligned} \sigma_x &= \frac{E}{(1 + \nu)(1 - 2\nu)} [(1 - \nu)\epsilon_x + \nu(\epsilon_y + \epsilon_z)] \\ \sigma_y &= \frac{E}{(1 + \nu)(1 - 2\nu)} [(1 - \nu)\epsilon_y + \nu(\epsilon_x + \epsilon_z)] \\ \sigma_z &= \frac{E}{(1 + \nu)(1 - 2\nu)} [(1 - \nu)\epsilon_z + \nu(\epsilon_x + \epsilon_y)] \\ \tau_{xy} &= \frac{E}{2(1 + \nu)} \gamma_{xy} \\ \tau_{yz} &= \frac{E}{2(1 + \nu)} \gamma_{yz} \\ \tau_{zx} &= \frac{E}{2(1 + \nu)} \gamma_{zx} \end{aligned} \quad (\text{B.55})$$

Although the stress and strain equations given in Eqs. (B.54) and (B.55), respectively, are expressed in terms of  $E$  and  $\nu$ , by using Table B.1 these equations can be rewritten in terms of any two of the five elastic material constants ( $G$ ,  $\lambda$ ,  $E$ ,  $\nu$ , and  $K$ ). The reason for using  $E$  and  $\nu$  is that data for a particular material can be readily obtained for these constants as demonstrated in Tables 3.2 and 3.3. For rubber ( $\nu \rightarrow 0.5$ ) it is more accurate to use the bulk modulus  $K$  together with the shear modulus  $G$ , since  $1 - 2\nu$  appears in the denominator.

For the special case in which the  $x$ ,  $y$ , and  $z$  axes are coincidental with the principal axes 1, 2, and 3 (the *triaxial stress state*), Eqs. (B.54) and (B.55) are simplified by virtue of all shear stresses and shear strains being equal to zero:

$$\begin{aligned} \epsilon_1 &= \frac{1}{E} [\sigma_1 - \nu(\sigma_2 + \sigma_3)] \\ \epsilon_2 &= \frac{1}{E} [\sigma_2 - \nu(\sigma_1 + \sigma_3)] \\ \epsilon_3 &= \frac{1}{E} [\sigma_3 - \nu(\sigma_2 + \sigma_1)] \end{aligned} \quad (\text{B.56})$$

Table B.1: Relationships between elastic material constants for isotropic materials.

Constants involved	Lamé's constant, $\lambda$	Shear modulus, $G$	Modulus of elasticity, $E$	Poisson's ratio, $\nu$	Bulk modulus $K$
$\lambda \quad G$	—	—	$E = \frac{G(3\lambda + 2G)}{\lambda + G}$	$\nu = \frac{\lambda}{2(\lambda + G)}$	$K = \frac{3\lambda + 2G}{3}$
$\lambda \quad E$	—	$G = \frac{A^\dagger + (E - 3\lambda)}{4}$	—	$\nu = \frac{A - (E + \lambda)}{4\lambda}$	$K = \frac{A + (3\lambda + E)}{6}$
$\lambda \quad \nu$	—	$G = \frac{\lambda(1 - 2\nu)}{2\nu}$	$E = \frac{\lambda(1 + \nu)(1 - 2\nu)}{\nu}$	—	$K = \frac{\lambda(1 + \nu)}{3\nu}$
$\lambda \quad K$	—	$G = \frac{3(K - \lambda)}{2}$	$E = \frac{9K(K - \lambda)}{3K - \lambda}$	$\nu = \frac{\lambda}{3K - \lambda}$	—
$G \quad E$	$\lambda = \frac{G(2G - E)}{E - 3G}$	—	—	$\nu = \frac{E - 2G}{2G}$	$K = \frac{GE}{3(3G - E)}$
$G \quad \nu$	$\lambda = \frac{2G\nu}{1 - 2\nu}$	—	$E = 2G(1 + \nu)$	—	$K = \frac{2G(1 + \nu)}{3(1 - 2\nu)}$
$G \quad K$	$\lambda = \frac{3K - 2G}{3}$	—	$E = \frac{9KG}{3K + G}$	$\nu = \frac{3K - 2G}{2(3K + G)}$	—
$E \quad \nu$	$\lambda = \frac{\nu E}{(1 + \nu)(1 - 2\nu)}$	$G = \frac{E}{2(1 + \nu)}$	—	—	$K = \frac{E}{3(1 - 2\nu)}$
$E \quad K$	$\lambda = \frac{3K(3K - E)}{9K - E}$	$G = \frac{3EK}{9K - E}$	—	$\nu = \frac{3K - E}{6K}$	—
$\nu \quad K$	$\lambda = \frac{3K\nu}{1 + \nu}$	$G = \frac{3K(1 - 2\nu)}{2(1 + \nu)}$	$E = 3K(1 - 2\nu)$	—	—

$$^\dagger A = [(E + \lambda)^2 + 8\lambda^2]^{1/2}$$

$$\begin{aligned}\sigma_1 &= \frac{E}{(1 + \nu)(1 - 2\nu)} [(1 - \nu)\epsilon_1 + \nu(\epsilon_2 + \epsilon_3)] \\ \sigma_2 &= \frac{E}{(1 + \nu)(1 - 2\nu)} [(1 - \nu)\epsilon_2 + \nu(\epsilon_1 + \epsilon_3)] \\ \sigma_3 &= \frac{E}{(1 + \nu)(1 - 2\nu)} [(1 - \nu)\epsilon_3 + \nu(\epsilon_1 + \epsilon_2)]\end{aligned}\quad (\text{B.57})$$

For the commonly encountered *biaxial stress state*, one of the principal stresses (say,  $\sigma_3$ ) is zero and Eqs. (B.56) become

$$\begin{aligned}\epsilon_1 &= \frac{\sigma_1 - \nu\sigma_2}{E} \\ \epsilon_2 &= \frac{\sigma_2 - \nu\sigma_1}{E} \\ \epsilon_3 &= -\frac{\nu(\sigma_1 + \sigma_2)}{E}\end{aligned}\quad (\text{B.58})$$

For  $\sigma_3 = 0$  the third of Eqs. (B.57) gives

$$\epsilon_3 = -\frac{\nu(\epsilon_1 + \epsilon_2)}{1 - \nu}\quad (\text{B.59})$$

Substituting Eq. (B.59) into Eqs. (B.57) gives

$$\begin{aligned}\sigma_1 &= \frac{E(\epsilon_1 + \nu\epsilon_2)}{1 - \nu^2} \\ \sigma_2 &= \frac{E(\epsilon_2 + \nu\epsilon_1)}{1 - \nu^2} \\ \sigma_3 &= 0\end{aligned}\quad (\text{B.60})$$

For the *uniaxial stress state* Eqs. (B.58) and (B.60) must reduce to

$$\epsilon_1 = \frac{\sigma_1}{E} \quad \epsilon_2 = \epsilon_3 = -\frac{\nu\sigma_1}{E}\quad (\text{B.61})$$

$$\sigma_1 = E\epsilon_1 \quad \sigma_2 = \sigma_3 = 0\quad (\text{B.62})$$

These expressions for the uniaxial, biaxial, and triaxial stress states can be expressed in tabular form as shown in Table B.2.

Recall that we chose to express the stress and strain in terms of the modulus of elasticity and Poisson's ratio. Furthermore, we are considering the special case in which the  $x$ ,  $y$ , and  $z$  axes are coincidental with the principal axes 1, 2, and 3, thus implying that the shear stresses and strains are equal to zero. For this case the shear stress and strain are equal to zero.

## Example B.1: Hookian Material

**Given:** Equations (B.42) and (B.43).

**Find:** Determine the modulus of elasticity  $E$  as a function of  $G$  and  $\nu$ , where  $\nu$  is given by Hooke's law for uniaxial tension.

$$\epsilon_x = \frac{\sigma_x}{E}$$

$$\epsilon_y = -\frac{\nu\sigma_x}{E}$$

$$\epsilon_z = -\frac{\nu\sigma_x}{E}$$

**Solution:** Equation (B.43) gives

$$\epsilon_x = \frac{(\lambda + G)\sigma_x}{G(3\lambda + 2G)} - \frac{\lambda(\sigma_y + \sigma_z)}{2G(3\lambda + 2G)} = \frac{\sigma_x}{E} - \frac{\nu(\sigma_y + \sigma_z)}{E}$$

$$\epsilon_y = \frac{(\lambda + G)\sigma_y}{G(3\lambda + 2G)} - \frac{\lambda(\sigma_x + \sigma_z)}{2G(3\lambda + 2G)} = \frac{\sigma_y}{E} - \frac{\nu(\sigma_x + \sigma_z)}{E}$$

$$\epsilon_z = \frac{(\lambda + G)\sigma_z}{G(3\lambda + 2G)} - \frac{\lambda(\sigma_x + \sigma_y)}{2G(3\lambda + 2G)} = \frac{\sigma_z}{E} - \frac{\nu(\sigma_x + \sigma_y)}{E}$$

$$\left. \begin{aligned} \frac{\lambda + G}{G(3\lambda + 2G)} &= \frac{1}{E} \\ \frac{\lambda}{2G(3\lambda + 2G)} &= \frac{\nu}{E} \end{aligned} \right\} \frac{\lambda}{2(\lambda + G)} = \nu$$

Table B.2: Principal stresses and strains in terms of modulus of elasticity and Poisson's ratio for uniaxial, biaxial, and triaxial stress states. (It is assumed that the  $x$ ,  $y$ , and  $z$  axes are coincident with the principal axes 1, 2, and 3, thus implying that the shear stresses and strains are equal to zero.)

Type of stress	Principal strains	Principal stresses
Uniaxial	$\epsilon_1 = \frac{\sigma_1}{E}$	$\sigma_1 = E \epsilon_1$
	$\epsilon_2 = -\nu \epsilon_1$	$\sigma_2 = 0$
	$\epsilon_3 = -\nu \epsilon_1$	$\sigma_3 = 0$
Biaxial	$\epsilon_1 = \frac{\sigma_1}{E} - \frac{\nu \sigma_2}{E}$	$\sigma_1 = \frac{E(\epsilon_1 + \nu \epsilon_2)}{1 - \nu^2}$
	$\epsilon_2 = \frac{\sigma_2}{E} - \frac{\nu \sigma_1}{E}$	$\sigma_2 = \frac{E(\epsilon_1 + \nu \epsilon_2)}{1 - \nu^2}$
	$\epsilon_3 = -\frac{\nu \sigma_1}{E} - \frac{\nu \sigma_2}{E}$	$\sigma_3 = 0$
Triaxial	$\epsilon_1 = \frac{\sigma_1}{E} - \frac{\nu \sigma_2}{E} - \frac{\nu \sigma_3}{E}$	$\sigma_1 = \frac{E \epsilon_1 (1 - \nu) + \nu E (\epsilon_2 + \epsilon_3)}{1 - \nu - 2\nu^2}$
	$\epsilon_2 = \frac{\sigma_2}{E} - \frac{\nu \sigma_1}{E} - \frac{\nu \sigma_3}{E}$	$\sigma_2 = \frac{E \epsilon_2 (1 - \nu) + \nu E (\epsilon_1 + \epsilon_3)}{1 - \nu - 2\nu^2}$
	$\epsilon_3 = \frac{\sigma_3}{E} - \frac{\nu \sigma_1}{E} - \frac{\nu \sigma_2}{E}$	$\sigma_3 = \frac{E \epsilon_3 (1 - \nu) + \nu E (\epsilon_1 + \epsilon_2)}{1 - \nu - 2\nu^2}$

$$(\lambda + G)E = 3\lambda G + 2G^2$$

$$G(E - 2G) = \lambda(3G - E) \quad \lambda = \frac{G(E - 2G)}{3G - E}$$

$$\nu = \frac{G(E - 2G)}{2(3G - E) \left[ \frac{G(E - 2G)}{3G - E} + G \right]}$$

$$E = (\nu + 1)2G \quad \text{and} \quad G = \frac{E}{2(1 + \nu)}$$

The modulus of elasticity  $E = 2G(\nu + 1)$ , the shear modulus  $G = E/2(1 + \nu)$ , and Poisson's ratio  $\nu = E/2G - 1$ .

## References

- Durelli, A.J., Phillips, E.A., and Tsao, C.H. (1958) *Introduction to the Theoretical and Experimental Analysis of Stress and Strain*, McGraw-Hill.
- Timoshenko, S., and Goodier, J.N., (1970) *Theory of Elasticity*, McGraw-Hill.

## B.7 Summary

Hooke's law was generalized in this appendix. That is, the linear relationship between stress and strain in the elastic range was generalized for the six components of stress: three normal stresses and three shear stresses. By using the laws of stress and strain transformation, the 36 elastic material constants were reduced to 2 through five different coordinate orientations. It was also found that, for the isotropic and homogeneous materials assumed throughout this chapter, these elastic material constants are not functions of the space coordinates and do not vary from point to point. They depend only on the particular material.

Relationships were presented between the four elastic material constants (the shear modulus or modulus of rigidity  $G$ , the modulus of elasticity  $E$ , the bulk modulus  $K$ , and Poisson's ratio  $\nu$ ) and Lamé's constant  $\lambda$ , which has no particular physical significance. It was shown how any two of the five constants can be expressed in terms of the other constants. For the special case in which the  $x$ ,  $y$ , and  $z$  axes are coincidental with the principal axes, simplified equations were expressed where all shear stresses and shear strains were zero. For these situations uniaxial, biaxial, and triaxial principal stresses could be expressed. These equations serve as the foundation for the main text of this book.

## Appendix C

# Stress Intensity Factors for Some Common Crack Geometries

This appendix summarizes some stress intensity factors for common machine element configurations and test specimen geometries. Most of this appendix is taken from Suresh [1998], although Tada et al. [2000] was also used in the compilation.

### C.1 Internally-Cracked Tension Specimen

The stress intensity factor for a center crack of length  $l_c$  in a plate of width  $b$  is given by

$$K_I = \sigma \sqrt{\frac{\pi l_c}{2}} Y \quad (\text{C.1})$$

The geometry correction factor  $Y$  is shown in Fig. C.1. If the tensile stress is remote ( $h \gg b$ ), then the geometry factor is given by

$$Y = \sqrt{\sec \frac{\pi l_c}{2b}} \quad (\text{C.2})$$

If an internal crack of length  $l_c$  exists a distance  $d$  from the edge of the tension member of width  $b$ , the geometry correction factor is shown in Fig. C.2.

### C.2 Edge-Cracked Tension Specimen

For a single edge-cracked tension specimen of crack width  $l_c$  and width  $b$ , the stress intensity factor is given by

$$K_I = \sigma \sqrt{l_c} Y \quad (\text{C.3})$$

The geometry factor  $Y$  is shown in Fig. C.3. If the tensile stress is remote ( $h \gg b$ ), then the geometry factor is given by

$$Y = 1.99 - 0.41 \frac{l_c}{b} + 18.7 \left( \frac{l_c}{b} \right)^2 - 38.48 \left( \frac{l_c}{b} \right)^3 + 53.83 \left( \frac{l_c}{b} \right)^4 \quad (\text{C.4})$$

For a tensile specimen of width  $b$  with two edge cracks, each of length  $l_c$ , the geometry factor for use in Eq. (C.3) is given

by

$$Y = 1.99 + 0.76 \left( \frac{l_c}{b} \right) - 8.48 \left( \frac{l_c}{b} \right)^2 + 27.36 \left( \frac{l_c}{b} \right)^3 \quad (\text{C.5})$$

### C.3 Bending Specimen

The stress intensity factor for an edge-cracked bending specimen is given by

$$K_I = \left( \frac{6M}{w_t b^2} \right) \sqrt{\pi l_c} Y \quad (\text{C.6})$$

where

$M$  = applied moment, Nm (in.-lb)

$w_t$  = beam width, m (in.)

$b$  = beam height, m (in.)

$Y$  = a geometry correction factor, given by

$$Y = 1.122 - 1.4 \frac{l_c}{b} + 7.33 \left( \frac{l_c}{b} \right)^2 - 13.08 \left( \frac{l_c}{b} \right)^3 + 14.0 \left( \frac{l_c}{b} \right)^4 \quad (\text{C.7})$$

For a three-point bending specimen (see Fig. C.4), the stress intensity factor is given by

$$K_I = \left( \frac{3aF}{2w_t b^2} \right) \sqrt{\pi l_c} Y \quad (\text{C.8})$$

Two cases are available. Using the notation of  $\alpha = l_c/b$ ,

1. For  $a/b = 2$ ,

$$Y = \frac{1.99 - \alpha(1 - \alpha)(2.15 - 3.93\alpha + 2.7\alpha^2)}{(1 + 2\alpha)(1 - \alpha)^{3/2} \sqrt{\pi i}} \quad (\text{C.9})$$

2. For  $a/b = 4$ ,

$$Y = 1.106 - 1.552\alpha + 7.71\alpha^2 - 13.53\alpha^3 + 14.23\alpha^4 \quad (\text{C.10})$$

### C.4 Central Hole with Crack in Tension Specimen

A common occurrence when a central hole is placed in a tension specimen is that a crack will initiate at the locations of

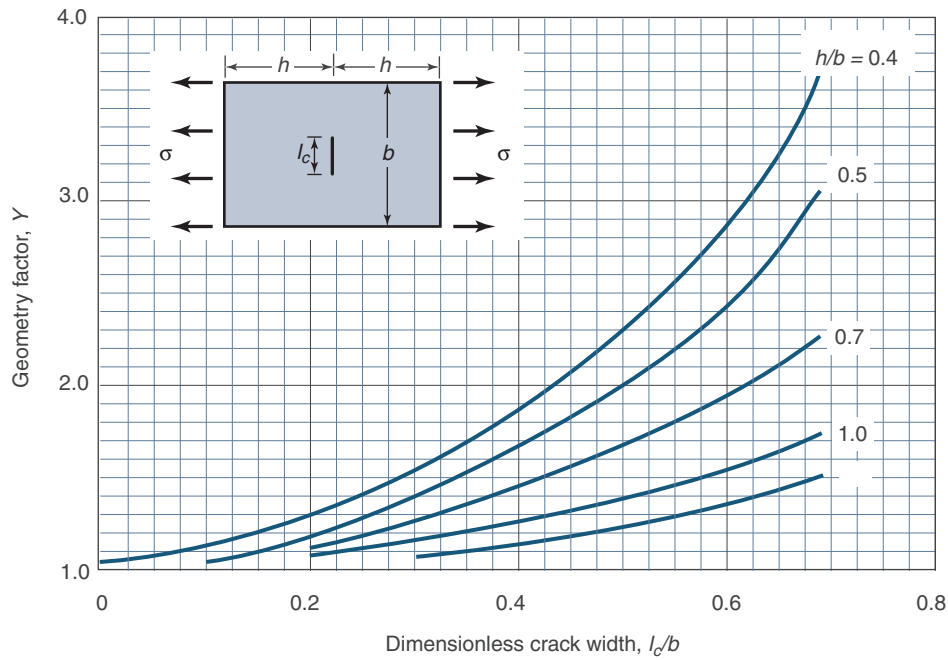


Figure C.1: Geometry factor for center-cracked tension specimen.

maximum stress. The effect on the stress state of the tension member can be quite significant, and a very large apparent crack can develop. This is treated as a center crack (the stress intensity factor is given by Eq. (C.1) but with a geometry correction factor as given in Fig. C.5.

## C.5 Crack in Wall of Pressure Vessel

In the circumstance where the internally applied pressure varies with time, a crack can develop and propagate within the wall of a pressure vessel. For such occurrences, the stress concentration factor is given by Eq. (C.1) with a geometry correction factor as given in Fig. C.6.

## References

- Suresh, S. (1998) *Fatigue of Materials*, 2nd. ed., Cambridge University Press.
- Tada, H., Paris, P.C., and Irwin, G.R. (2000), *The Stress Analysis of Cracks Handbook*, ASME Press.



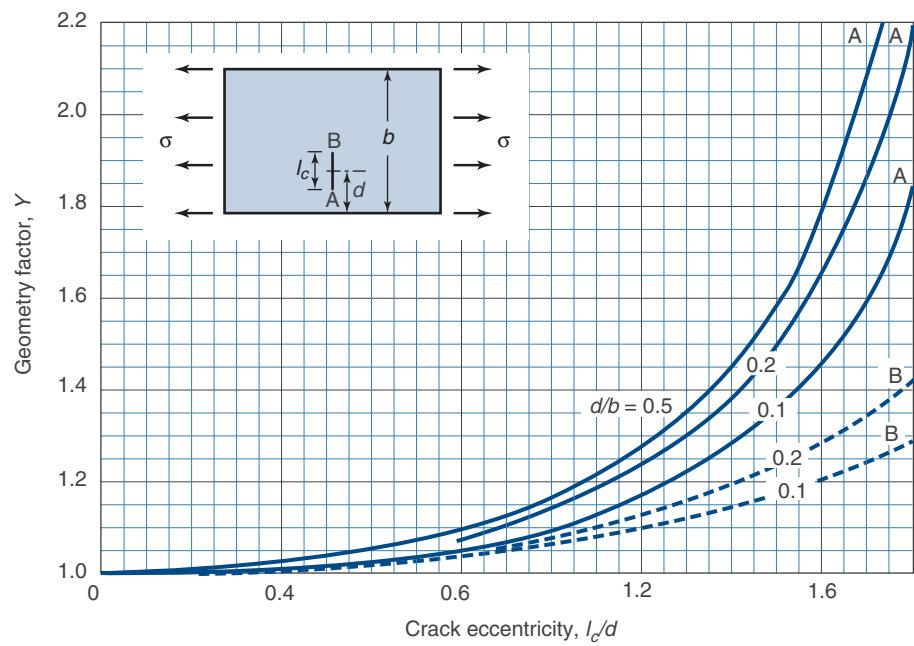


Figure C.2: Geometry factor for an non-centered internal crack.

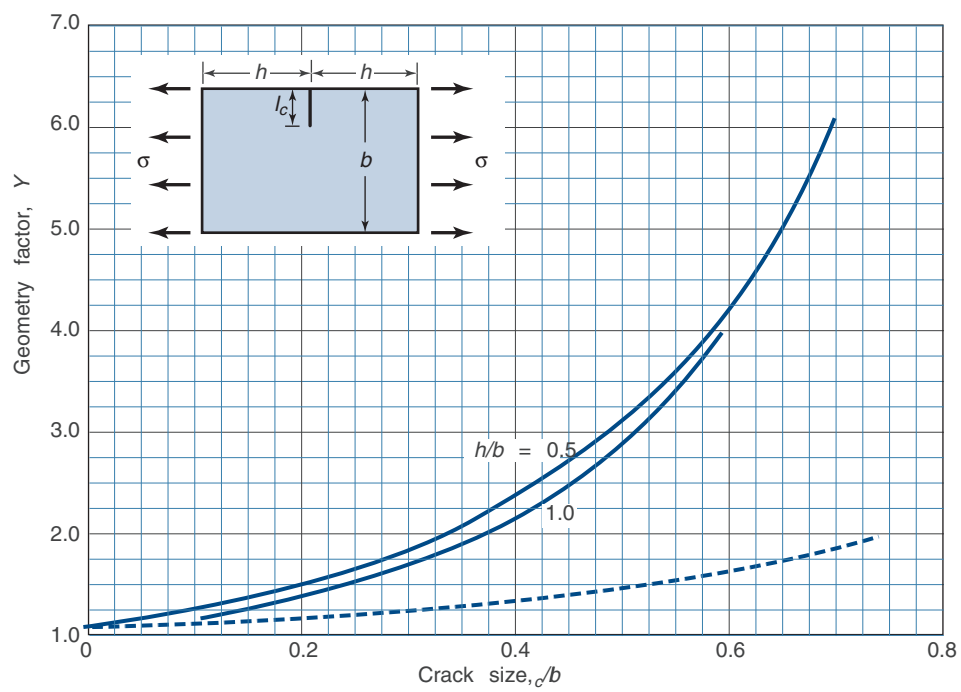


Figure C.3: Geometry factor for single edge-cracked tension specimen.

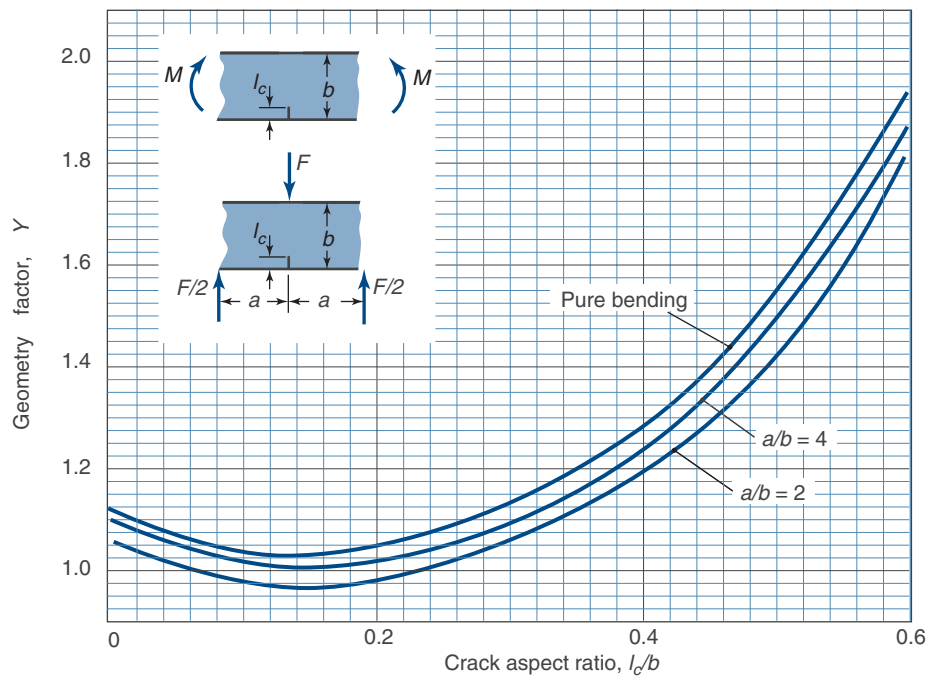


Figure C.4: Geometry factor for single edge-cracked tension specimen.

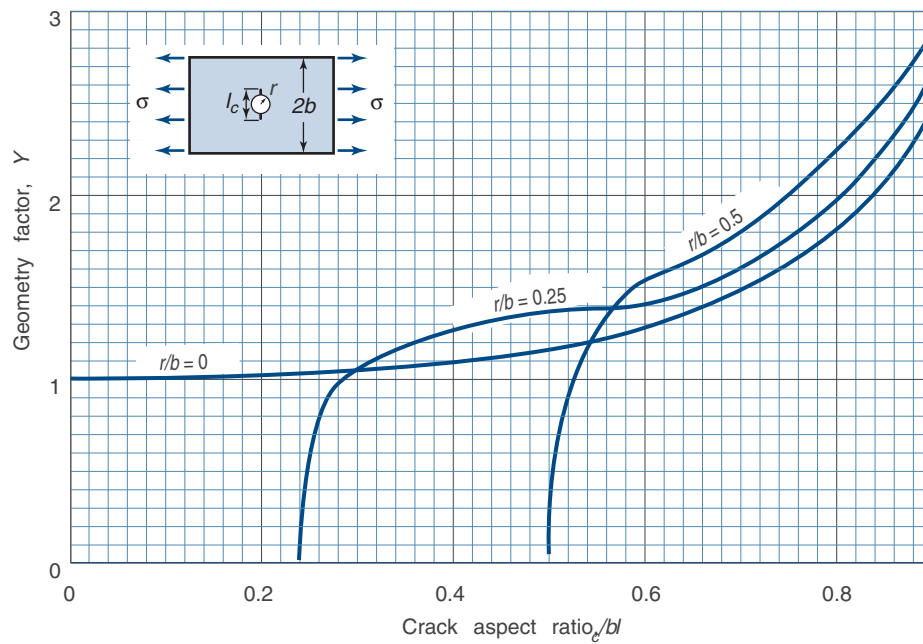


Figure C.5: Geometry factor for tension specimen with a central hole and cracks.

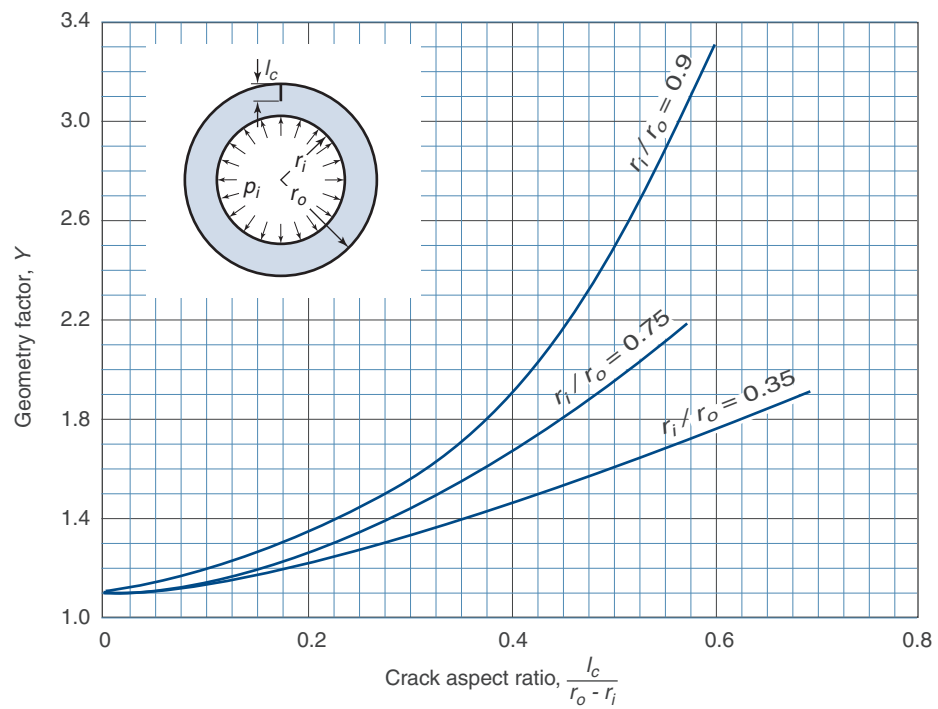


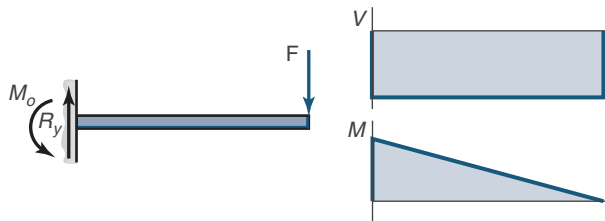
Figure C.6: Geometry factor for an internally pressurized cylinder.

This page intentionally left blank

## Appendix D

# Shear, Moment and Deflection of Selected Beams and Cantilevers

### D.1 Cantilever loaded at free end



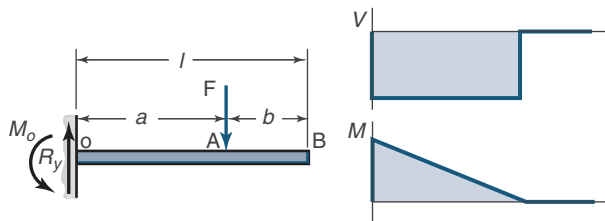
$$R_y = -V = F$$

$$M_o = F(l - x)$$

$$y = \frac{Fx^2}{6EI}(x - 3l)$$

$$y_{\max} = -\frac{Fl^3}{3EI}$$

### D.2 Cantilever loaded off-end



$$R_y = -V = F$$

$$M_{oA} = F(a - x)$$

$$M_{AB} = 0$$

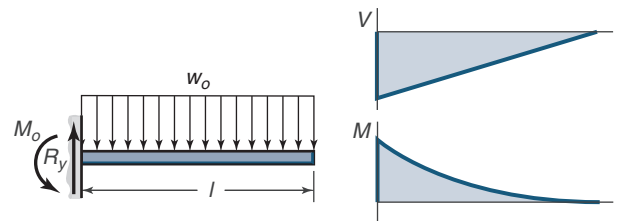
$$M_o = Fa$$

$$y_{oA} = \frac{Fx^2}{6EI}(x - 3a)$$

$$y_{AB} = \frac{Fa^2}{6EI}(a - 3x)$$

$$y_{\max} = \frac{Fa^2}{6EI}(a - 3l)$$

### D.3 Cantilever with uniform load



$$R_y = wl$$

$$M_o = \frac{wl^2}{2}$$

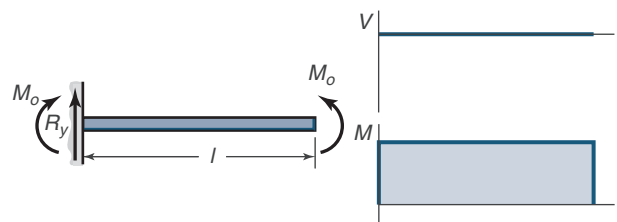
$$V = w(x - l)$$

$$M = \frac{1}{2}w(l - x)^2$$

$$y = \frac{wx^2}{24EI}(4lx - x^2 - 6l^2)$$

$$y_{\max} = -\frac{wl^4}{8EI}$$

### D.4 Cantilever with moment load



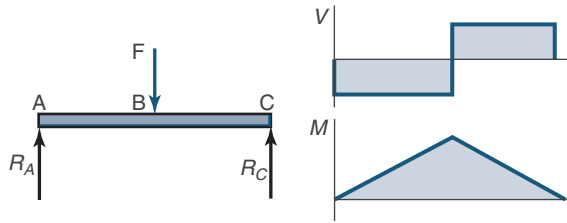
$$R_y = 0$$

$$y = \frac{M_o x^2}{2EI}$$

$$y_{\max} = \frac{M_o l^2}{2EI}$$



### D.5 Simply-supported beam with point load at mid-span



$$R_A = R_C = \frac{F}{2}$$

$$V_{AB} = -\frac{F}{2}$$

$$V_{BC} = \frac{F}{2}$$

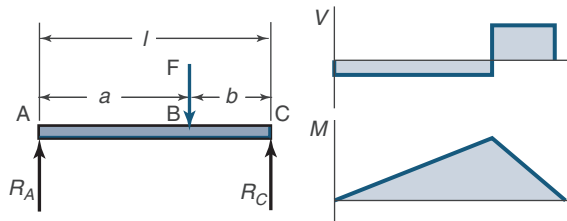
$$M_{AB} = \frac{Fx}{2}$$

$$M_{BC} = \frac{F(l-x)}{2}$$

$$y_{AB} = \frac{Fx(4x^2 - 3l^2)}{48EI}$$

$$y_{\max} = -\frac{Fl^3}{48EI}$$

### D.6 Simply-supported beam with intermediate point load



$$R_A = \frac{Fb}{l}$$

$$R_C = \frac{Fa}{l}$$

$$V_{AB} = -R_A$$

$$V_{BC} = R_B$$

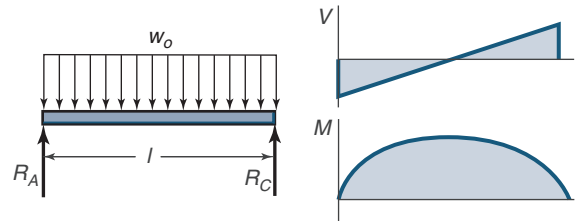
$$M_{AB} = \frac{Fbx}{l}$$

$$M_{BC} = \frac{Fa(l-x)}{l}$$

$$y_{AB} = \frac{Fbx(x^2 + b^2 - l^2)}{6EI}$$

$$y_{BC} = \frac{Fa(l-x)(x^2 + a^2 - 2lx)}{6EI}$$

### D.7 Simply-supported beam with uniform load



$$R_A = R_C = \frac{w_o l}{2}$$

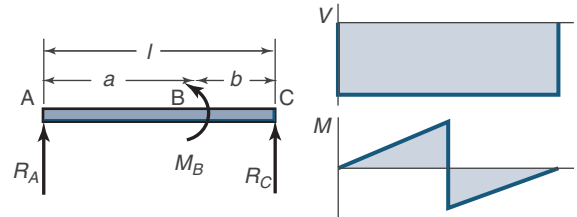
$$V = w_o x - \frac{w_o l}{2}$$

$$M = \frac{w_o x(l-x)}{2}$$

$$y = \frac{w_o x(2lx^2 - x^3 - l^3)}{24EI}$$

$$y_{\max} = -\frac{5w_o l^4}{384EI}$$

### D.8 Simply-supported beam with moment load



$$R_A = -R_C = \frac{M_B}{l}$$

$$V = -\frac{M_B}{l}$$

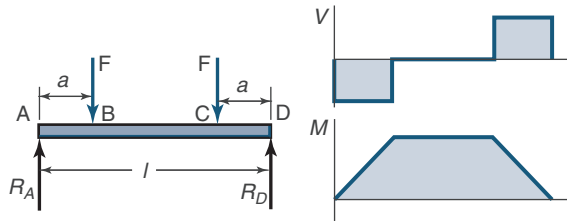
$$M_{AB} = \frac{M_B x}{l}$$

$$M_{BC} = \frac{M_B(x-l)}{l}$$

$$y_{AB} = \frac{M_B x(x^2 + 3a^2 - 6al + 2l^2)}{6EI}$$

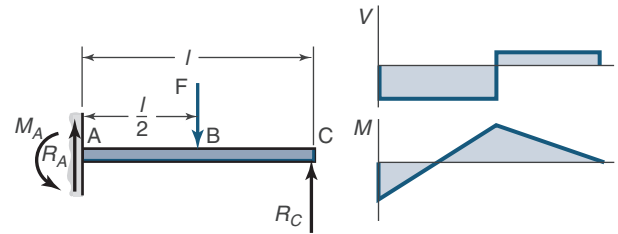
$$y_{BC} = \frac{M_B(x^3 - 3lx^2 + 2l^2x + 3a^2x - 3a^2l)}{6EI}$$

### D.9 Simply-supported beam with twin loads



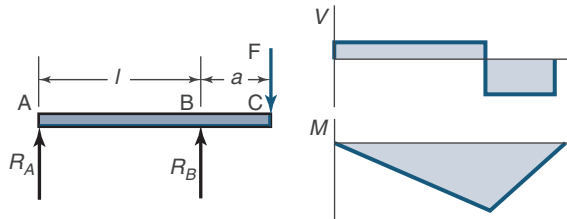
$$\begin{aligned}
 R_A &= R_D = F \\
 V_{AB} &= -F \\
 V_{BC} &= 0 \\
 V_{CD} &= F \\
 M_{AB} &= Fx \\
 M_{BC} &= Fa \\
 M_{CD} &= F(l-x) \\
 y_{AB} &= \frac{Fx(x^2 + 3a^2 - 3la)}{6EI} \\
 y_{BC} &= \frac{Fa(3x^2 + a^2 - 3lx)}{6EI} \\
 y_{\max} &= \frac{Fa(4a^2 - 3l^2)}{24EI}
 \end{aligned}$$

### D.11 Fixed-simply supported beam with point load at mid-span



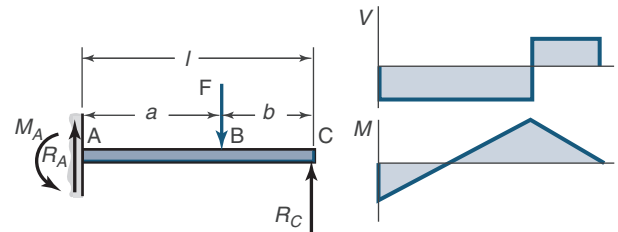
$$\begin{aligned}
 R_A &= \frac{11F}{16} \\
 R_C &= \frac{5F}{16} \\
 M_A &= \frac{3Fl}{16} \\
 V_{AB} &= -R_A \\
 V_{BC} &= R_C \\
 M_{AB} &= \frac{F(11x - 3l)}{16} \\
 M_{BC} &= \frac{5F(l-x)}{16} \\
 y_{AB} &= \frac{Fx^2(11x - 9l)}{96EI} \\
 y_{BC} &= \frac{F(l-x)(5x^2 + 2l^2 - 10lx)}{96EI}
 \end{aligned}$$

### D.10 Simply-supported beam with overhanging load



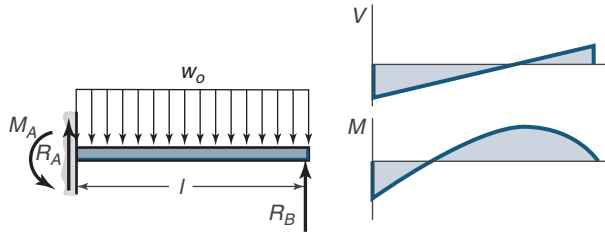
$$\begin{aligned}
 R_A &= -\frac{fa}{l} \\
 R_B &= \frac{F(l+a)}{l} \\
 V_{AB} &= \frac{Fa}{l} \\
 V_{BC} &= F \\
 M_{AB} &= -\frac{Fax}{l} \\
 M_{BC} &= F(x-l-a) \\
 y_{AB} &= \frac{Fax(l^2 - x^2)}{6EI} \\
 y_{BC} &= \frac{F(x-l)[(x-l)^2 - a(3x-l)]}{6EI} \\
 y_C &= -\frac{Fa^2(l+a)}{3EI}
 \end{aligned}$$

### D.12 Fixed-simply supported beam with intermediate point load



$$\begin{aligned}
 R_A &= \frac{Fb(3l^2 - b^2)}{2l^3} \\
 R_B &= \frac{Fa^2(3l-a)}{2l^3} \\
 M_A &= \frac{Fb(b^2 - l^2)}{2l^2} \\
 V_{AB} &= -R_A \\
 V_{BC} &= R_B \\
 M_{AB} &= \frac{Fb(b^2l - l^3 + 3l^2x - b^2x)}{2l^3} \\
 M_{BC} &= \frac{Fa^2(3l^2 - 3lx - al + ax)}{2l^3} \\
 y_{AB} &= \frac{Fbx^2[3l(b^2 - l^2) + x(3l^2 - b^2)]}{12EI l^3} \\
 y_{BC} &= y_{AB} - \frac{F(x-a)^3}{6EI}
 \end{aligned}$$

### D.13 Fixed-simply supported beam with uniform load



$$R_A = \frac{5w_o l}{8}$$

$$R_C = \frac{3w_o l}{8}$$

$$M_A = \frac{w_o l^2}{8}$$

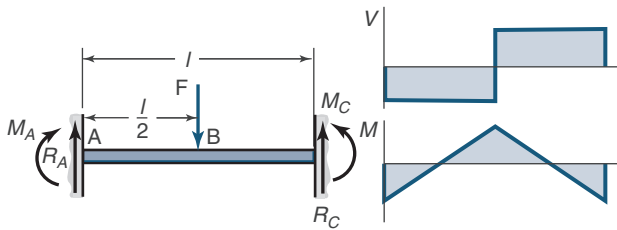
$$V = wx - \frac{5w_o l}{8}$$

$$M = \frac{w_o (-4x^2 + 5lx - l^2)}{8}$$

$$y = \frac{w_o x^2 (l - x)(2x - 3l)}{48EI}$$

$$y_{\max} = -\frac{wl^4}{185EI}$$

### D.14 Fixed-fixed beam with point load at mid-span



$$R_A = R_B = \frac{F}{2}$$

$$M_A = M_B = \frac{Fl}{8}$$

$$V_{AB} = -V_{BC} = -\frac{F}{2}$$

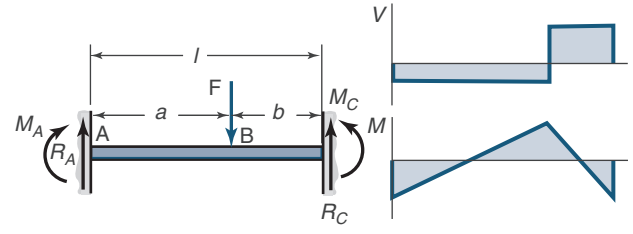
$$M_{AB} = \frac{F(4x - l)}{8}$$

$$M_{BC} = \frac{F(3l - 4x)}{8}$$

$$y_{AB} = \frac{Fx^2(4x - 3l)}{48EI}$$

$$y_{\max} = -\frac{Fl^3}{192EI}$$

### D.15 Fixed-fixed beam with intermediate point load



$$R_A = \frac{Fb^2(3a + b)}{l^3}$$

$$R_C = \frac{Fa^2(3b + a)}{l^3}$$

$$M_A = \frac{Fab^2}{l^2}$$

$$M_C = -\frac{Fa^2b}{l^2}$$

$$V_{AB} = -R_A$$

$$V_{BC} = R_C$$

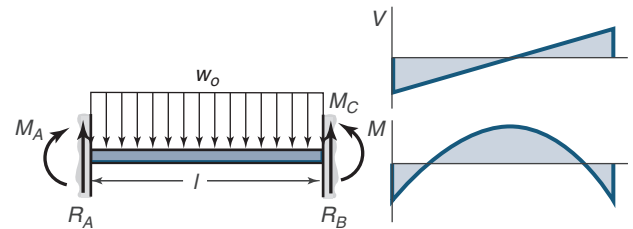
$$M_{AB} = \frac{Fb^2(3ax + bx - la)}{l^3}$$

$$M_{BC} = M_{AB} - F(x - a)$$

$$y_{AB} = \frac{Fb^2x^2(3ax + bx - 3al)}{6EI l^3}$$

$$y_{BC} = \frac{Fa^2(l - x)^2[(l - x)(3b + a) - 3bl]}{6EI l^3}$$

### D.16 Fixed-fixed beam with distributed load



$$R_A = R_B = \frac{w_o l}{2}$$

$$M_A = M_B = \frac{w_o l^2}{12}$$

$$V = -\frac{w_o(l - 2x)}{2}$$

$$M = \frac{w_o(6lx - 6x^2 - l^2)}{12}$$

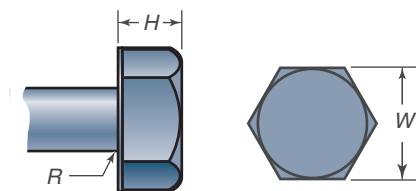
$$y = -\frac{w_o x^2}{24EI}(l - x)^2$$

$$y_{\max} = -\frac{w_o l^4}{384EI}$$

## Appendix E

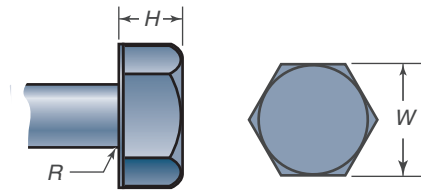
# Dimensions of Threaded Fasteners

### E.1 Dimensions of Selected Bolts



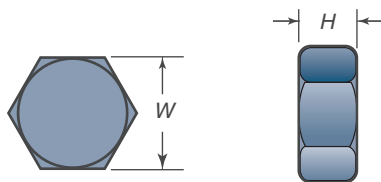
Nominal size	Hexagonal head type												
	Square		Regular			Heavy			Structural				
	W	H	W	H	R <sub>m</sub>	i	W	n	H <sub>m</sub>	i	W	R <sub>f</sub>	H <sub>m</sub>
Metric series – dimensions in mm													
5	8	3.58	8	3.58	0.2	—	—	—	—	—	—	—	—
6	—	—	10	4.38	0.3	—	—	—	—	—	—	—	—
8	—	—	13	5.68	0.4	—	—	—	—	—	—	—	—
10	—	—	16	6.85	0.4	—	—	—	—	—	—	—	—
12	—	—	18	7.95	0.6	21	7.95	0.6	—	—	—	—	—
14	—	—	21	9.25	0.6	24	9.25	0.6	—	—	—	—	—
16	—	—	24	10.75	0.6	27	10.75	0.6	27	10.75	0.6	—	—
20	—	—	30	13.40	0.8	34	13.40	0.8	34	13.40	0.8	—	—
24	—	—	36	15.90	0.8	41	15.90	0.8	41	15.90	0.8	—	—
30	—	—	46	19.75	1.0	50	19.75	1.0	50	19.75	1.0	—	—
36	—	—	55	23.55	1.0	60	23.55	1.0	60	23.55	1.0	—	—

## E.2 Dimensions of Hexagonal Cap Screws



Nominal size	Fillet radius, <i>R</i>	Type of Screw		Height, <i>H</i>
		Cap, <i>W</i>	Heavy, <i>W</i>	
Metric series – dimensions in mm				
5	0.2	8	—	3.65
6	0.3	10	—	4.15
8	0.4	13	—	5.50
10	0.4	16	—	6.63
12	0.6	18	21	7.76
14	0.6	21	24	9.09
16	0.6	24	27	10.32
20	0.8	30	34	12.88
24	0.8	36	41	15.44
30	1.0	46	50	19.48
36	1.0	55	60	23.38

## E.3 Dimensions of Hexagonal Nuts



Nominal size	Width, $W$	Height, $H$		
		Regular hexagonal	Thick or slotted	JAM
Metric series – dimensions in mm				
5	8	4.7	5.1	2.7
6	10	5.2	5.7	3.2
8	13	6.8	7.5	4
10	16	8.4	9.3	5
12	18	10.8	12.0	6
14	21	12.8	14.1	7
16	24	14.8	16.4	8
20	30	18.0	20.3	10
24	36	21.5	23.9	12
30	46	25.6	28.6	15
36	55	31.0	34.7	18



## E.4 Dimensions of Metric Washers. (Dimensions in millimeters.)

Washer Size	Minimum Inner Diameter	Maximum Outer Diameter	Maximum Thickness
1.6 N	1.95	4.00	0.70
1.6 R	1.95	5.00	0.70
1.6 W	1.95	6.00	0.90
2 N	2.50	5.00	0.90
2 R	2.50	6.00	0.90
2 W	3.50	8.00	0.90
2.5 N	3.00	6.00	0.90
2.5 R	3.00	8.00	0.90
2.5 W	3.00	10.00	1.20
3 N	3.50	7.00	0.90
3 R	3.50	10.00	1.20
3 W	3.50	12.00	1.40
3.5 N	4.00	9.00	1.20
3.5 R	4.00	10.00	1.40
3.5 W	4.00	15.00	1.75
4 N	4.70	10.00	1.20
4 R	4.70	12.00	1.40
4 W	4.70	16.00	2.30
5 N	5.50	11.00	1.40
5 R	5.50	15.00	1.75
5 W	5.50	20.00	2.30
6 N	6.65	13.00	1.75
6 R	6.65	18.80	1.75
6 W	6.65	25.40	2.30
8 N	8.90	18.80	2.30
8 R	8.90	25.40	2.30
8 W	8.90	32.00	2.80
10 N	10.85	20.00	2.30
10 R	10.85	28.00	2.80
10 W	10.85	39.00	3.50
12 N	13.30	25.40	2.80
12 R	13.30	34.00	3.50
12 W	13.30	44.00	3.50
14 N	15.25	28.00	2.80
14 R	15.25	39.00	3.50
14 W	15.25	50.00	4.00
16 N	17.25	32.00	3.50
16 R	17.25	44.00	4.00
16 W	17.25	56.00	4.60
20 N	21.80	39.00	4.00
20 R	21.80	50.00	4.60
20 W	21.80	66.00	5.10
24 N	25.60	44.00	4.60
24 R	25.60	56.00	5.10
24 W	25.60	72.00	5.60
30 N	32.40	56.00	5.10
30 R	32.40	72.00	5.60
30 W	32.40	90.00	6.40
36 N	38.30	66.00	5.60
36 R	38.30	90.00	6.40
36 W	38.30	110.00	8.50

Note: N = narrow; R = Regular; W = wide.

Mechanical Engineering

# Fundamentals of Machine Elements

Third Edition

SI Version

## New and Improved SI Edition—Uses SI Units Exclusively in the Text

Adapting to the changing nature of the engineering profession, this **third edition** of **Fundamentals of Machine Elements** aggressively delves into the fundamentals and design of machine elements with an SI version. This latest edition includes a plethora of pedagogy, providing a greater understanding of theory and design.

## Significantly Enhanced and Fully Illustrated

The material has been organized to aid students of all levels in design synthesis and analysis approaches, to provide guidance through design procedures for synthesis issues, and to expose the reader to a wide variety of machine elements. Each chapter contains a quote and photograph related to the chapter as well as case studies, examples, design procedures, an abstract, list of symbols and subscripts, recommended readings, a summary of equations, and end-of-chapter problems.

## What's New in This Edition:

- Covers life cycle engineering
- Provides a description of the hardness and common hardness tests
- Offers an inclusion of flat groove stress concentration factors
- Adds the staircase method for determining endurance limits and includes Haigh diagrams to show the effects of mean stress
- Discusses typical surface finishes in machine elements and manufacturing processes used to produce them
- Presents a new treatment of spline, pin, and retaining ring design, and a new section on the design of shaft couplings
- Reflects the latest International Standards Organization standards
- Simplifies the geometry factors for bevel gears
- Includes a design synthesis approach for worm gears
- Expands the discussion of fasteners and welds
- Discusses the importance of the heat affected zone for weld quality
- Describes the classes of welds and their analysis methods
- Considers gas springs and wave springs
- Contains the latest standards and manufacturer's recommendations on belt design, chains, and wire ropes

The text also expands the appendices to include a wide variety of material properties, geometry factors for fracture analysis, and new summaries of beam deflection.

 **CRC Press**  
Taylor & Francis Group  
an informa business  
[www.crcpress.com](http://www.crcpress.com)

6000 Broken Sound Parkway, NW  
Suite 300, Boca Raton, FL 33487  
711 Third Avenue  
New York, NY 10017  
2 Park Square, Milton Park  
Abingdon, Oxon OX14 4RN, UK

K23633

